UNIVERSITÀ DI SIENA 1240

Dipartimento di Scienze fisiche, della Terra e dell'ambiente

Dottorato in Scienze e tecnologie ambientali, geologiche e polari

34° Ciclo

Coordinatore: Prof. Simone Bastianoni

Provenance analysis of glaciogenic sedimentary formations: cases study from Late Paleozoic Ice Age rocks in Victoria Land (Antarctica) and from Cenozoic DSDP Leg 28 and IODP Expedition 374 cores in the Ross Sea (Antarctica)

Settore scientifico disciplinare: *GEO/02 – GEO/07*

Candidato
Luca Zurli
Università di Siena

Firma del candidato
Zurl. Luca

Tutore
Prof. Gianluca Cornamusini
Università di Siena

Firma del tutore

Co-tutore
Prof. Franco Maria Talarico
Università di Siena

Anno accademico di conseguimento del titolo di Dottore di ricerca
2020/21

Università degli Studi di Siena
Dottorato in Scienze e tecnologie ambientali, geologiche e polari
34° Ciclo

Data dell'esame finale

____

Commissione giudicatrice

____
____
____

Esperto/i

____
____

Supplenti

____
____

Table of Contents

ABSTRACT

This thesis focus on the provenance study with multidisciplinary approach of sediments and rocks deposited in glacial environments in Antarctica in two distinct temporal contests: the Late Paleozoic Ice Age (LPIA) which involved Gondwana, and the Cenozoic glacial-interglacial cycles. The common point between the two distinct context is the comparison of glacial depositional systems and the provenance study of different temporal, climatic, paleogeographic, and continental settings, whereas both in the Antarctic continent. The comparison could highlight differences between the two studied glacial settings, and it could be useful both for paleo-geographic and paleo-climatic reconstructions and for future previsions.

This work is focused on the study of the gravel fraction (clasts larger than 2 mm), constituting glacial sedimentological facies (i.e., diamictite and conglomerate), through petrographic analyses which allow the direct comparison between clasts and outcropping geology of the glacier's catchments. Other analytical technologies were used to constrain provenance hypothesis based on clast petrography; in particular, chemical analyses on selected mineralogical phases were carried out. These preliminary data seem to show variations in the chemical composition of biotite in intrusive rocks, and it could be used as a marker for the provenance discrimination of intrusive rocks constituting East and West Antarctica. Moreover, geochronological analyses on detrital zircons, from sand size, were carried out; this is an analytical technique largely used for provenance analysis. This technique allows, if applied on fossil systems, the indirect reconstruction of the paleo-tectonic and paleo-morphologic setting of the study region.

The methodologies described have been applied in two different cases study extremely different. The first concerns the glacial sediments deposited during the Late Paleozoic Ice Age which currently crop out in Victoria Land (Antarctica); the petrographic and geochronological analyses, coupled with sedimentological and stratigraphic investigations, allow to better define the distribution of the glacial cover across Gondwana in the early Permian, strengthening the hypothesis of multiple and diachronous ice sheets which developed one of the longest glacial phases of the Earth. The second case study is framed inside the IODP Expedition 374, which aims the understanding of the Antarctic Ice sheets dynamics in the Ross Sea (Antarctica) since early Miocene. Gravel sized clasts within sediment cores were identified and described. The clast petrology, compared with ongoing geochronological, geochemical and thermochronological analyses, allows the reconstruction of the paleo-ice flows in the Ross Sea in the early Miocene to Pliocene.

RIASSUNTO

Questo lavoro di tesi riguarda principalmente lo studio di provenienza di sedimenti e rocce deposti in ambienti glaciali nel continente antartico in due contesti temporali estremamente differenziati, ovvero durante la LPIA (Late Paleozoic Ice Age) che ha interessato il Gondwana, e durante i cicli glaciale-interglaciale del Cenozoico, attraverso un approccio multidisciplinare. Il filo conduttore tra due contesti così distanti è stato quello di confrontare sistemi di trasporto glaciali e di ricostruzione della provenienza dei sedimenti in frangenti temporali, climatici, paleogeografici e geodinamici estremamente diversi, seppure relativi sempre al continente antartico. Questo confronto può anche evidenziare affinità e differenze dei due sistemi glacigenici, che possono essere utili sia per ricostruzioni paleoclimatiche e paleogeografiche, che per la previsione di scenari futuri.

Il lavoro di tesi si è basato principalmente sullo studio della frazione grossolana (ciottoli > 2mm) di facies glaciali (diamictiti e conglomerati), attraverso analisi petrografiche, che permettono un confronto diretto con le litologie affioranti nel bacino di alimentazione dei ghiacciai. Alle analisi petrografiche sono state affiancate altre tecniche analitiche in modo da rafforzare le ipotesi di provenienza. In particolare, alla petrografia dei ciottoli sono state affiancate analisi chimiche di alcune fasi mineralogiche. Questi dati preliminari sembrano evidenziare il fatto che la composizione chimica delle biotiti che si trovano all'interno di rocce intrusive può essere un marker discriminante per la provenienza, con particolare riferimento alle rocce intrusive che costituiscono l'Antartide Orientale e Occidentale. Inoltre, sono state effettuate analisi geocronologiche sugli zirconi della frazione sabbiosa, una tecnica largamente utilizzata che fornisce ottimi risultati ai fini di discriminare la provenienza dei sedimenti. In particolare, quest'ultima tecnica permette, se applicata a sistemi fossili molto antichi, di ricostruire indirettamente il contesto tettono-morfologico nell'area di studio. Tali metodologie analitiche sono state applicate su due casi studio estremamente diversi tra di loro. Il primo ha riguardato i sedimenti glaciali deposti durante la Late Paleozoic Ice Age ed attualmente affioranti nella Terra Vittoria in Antartide; le analisi petrografiche e geocronologiche, unite ad indagini sedimentologico-stratigrafiche, hanno permesso di andare a dettagliare la distribuzione della copertura glaciale nel Gondwana durante il Permiano inferiore, rafforzando l'ipotesi che usa serie di calotte glaciali si fossero sviluppate asincronamente durante una delle più durature fasi glaciali della storia della Terra. Il secondo caso studio è inquadrato all'interno della IODP Expedition 374 che mira alla comprensione delle dinamiche delle calotte antartiche nel Mare di Ross (Antartide) dal Miocene Inferiore all'attuale. Sui carotaggi sono stati identificati e descritti dettagliatamente i ciottoli che, confrontando i dati di questo studio, con indagini geocronologiche, termocronologiche e geochimiche tuttora in corso, hanno permesso di avanzare ipotesi sui flussi glaciali presenti nel Mare di Ross negli ultimi 18 Milioni di anni, mettendo in luce la nascita della Calotta Antartica Occidentale marina nel Miocene Inferiore.

1. General introduction

In the last decades, geological studies largely contributed to the reconstruction of the climate evolution of the Earth, which is a key topic to understand the climate change currently in place in our Planet. In this prospective, glaciogenic deposits are one of the most intriguing materials because their understanding allows the reconstruction of the paleoclimate and paleo-ice dynamics in the geological record. Antarctica is the only world region that allow the study of both current and past glaciogenic rock and sediments because it discontinuously experienced extensive glacial conditions in its history. Glacial environments are currently recorded in the rocks and sediments that crop out in onshore and offshore Antarctica.

Following this common thread, for this thesis has been tried to compare multidisciplinary two important, but temporally very far away times of the Earth's history, particularly interesting Antarctica, as the Late Paleozoic Ice Age (LPIA) event, which is the most intense glaciation of the Phanerozoic, and the glaciations occurring during the Cenozoic. The comparison among the geological features of these so far different glaciation events, will be very useful for to better understand the differences occurring in the glaciation Earth's events, depending by different environmental, climate, paleogeographic and geodynamic conditions, so to furnish a proxy data set, that could be useful also for the elaboration of present and future climatic scenario.

The main operative aim of this thesis is the application of petrographic and geochronological techniques for the provenance analysis of glaciogenic rocks and sediments. Provenance study consists of compare the characteristics of the sediments with those of the rock outcrops and then to determinate the possible source region of the analyzed sediments. One of the most problematic issues of provenance study in the Antarctic region is the scarce knowledge of the onshore and offshore geology due to the wide ice cover and the inaccessibility of the outcrops.

Glacial sediments reflect a wide range of depositional environments, mainly linked with climatic, geographic, and tectonic settings. One of the most common glaciogenic sedimentary facies is the diamicton (diamictite when lithified), which include, in strongly varying percentage, wide variable granulometric fractions, ranging from mud to boulder. Moncrieff (1989) provided a non-genetic classification based on the percentage of each granulometric fraction.

Because the wide variability in the sediment size, the provenance study of glaciogenic sediments provides the opportunity to combine various methodologies, usually applicable on specific granulometric fractions (Licht and Hemming, 2017). Therefore, the multi-analytical approach which is applicable on every granulometric fraction of the glacial sediments provide a stronger provenance interpretation (Licht and Hemming, 2017). Multi-analytical provenance studies, applying geochronological, petrographic, thermochronological, and geochemical approaches, of glaciogenic sediments have been applied in

Antarctica yet. Most of them were applied on Cenozoic sediments (Talarico and Sandroni, 1998, 2009, 2009; Sandroni and Talarico, 2001, 2004, 2006, 2011; Licht et al., 2005; Farmer et al., 2006; Talarico, 2007; Licht and Palmer, 2013; Olivetti et al., 2013, 2015; Talarico et al., 2013; Anderson et al., 2014; Cornamusini and Talarico, 2016; Perotti et al., 2017, 2018; Perotti, 2018; Li et al., 2020) in order to constrain Antarctic Ice sheets behavior in response to climate changes that characterized the last 50 Ma. However, provenance analyses were also successfully carried out in older glaciogenic rocks that currently crop out in Antarctica, such us the Late Paleozoic Ice Age deposits (Elliot et al., 2015; Craddock et al., 2019), even though these rocks were poorly studied from this point of view.

In this thesis, two study cases have been investigated, applying petrographic, geochemical, and geochronological techniques, to constrain the provenance of the glacially transported sediments, and therefore the glacial setting in the past. The study cases are relative to two completely different situations: the first case concerns the rocks related with the Late Paleozoic Ice Age (LPIA) cropping out in Victoria Land along the Transantarctic Mountains; the second case concerns the sediments occurring offshore in the Ross Sea related with Cenozoic glaciations. The work aims to demonstrate that glaciogenic sediments are a good matrix where apply provenance technique and could be also used to reconstruct the bedrock geology in the region where outcrops lack, such as Antarctica. The thesis also aims to demonstrate that petrographic, geochronological, and geochemical techniques are applicable not only in young sediments, where the geological setting of the investigated area is similar to present day, but also in old sediments, where geodynamic setting was completely different.

Furthermore, the thesis intends to demonstrate the power of these proxy data regarding the possibility to integrate climatic scenario and numerical models.

Results and interpretations of the data collected in this thesis are documented through scientific articles here reported. The Chapter 2 of the thesis “Detrital zircons from Late Paleozoic Ice Age sequences in Victoria Land (Antarctica): new constraints on the glaciation of southern Gondwana” has been published in the Geological Society of America Bulletin (Zurli et al., 2022a).

Chapter 3 of the thesis encloses petrographic and mineral chemistry data that have been and will be jointed with other provenance techniques. The contribution and data from this thesis allow the publication of a high-impact scientific article (Marshaleck et al., 2021) and a data report (Zurli et al., 2022b). Other data will contribute to two other scientific articles (Mallery et al., in preparation; Olivetti et al., in preparation).

2. Detrital zircons from Late Paleozoic Ice Age sequences in Victoria Land (Antarctica): new constraints on the glaciation of southern Gondwana

2.1. Chapter Overview

This chapter is a paper accepted and published in the Volume 134, Number 1-2, pages 160-178 of the Geological Society of America Bulletin (Zurli et al., 2022a). Data were collected in collaboration with the Korea Polar Research Institute (KOPRI). Luca Zurli co-conceptualized the project, investigated samples and data, and wrote the original draft. Gianluca Cornamusini co-conceptualized the project, provided resources, reviewed and edited the manuscript, supervised and administrated the project. Jusun Woo provided resources for the sample analysis and reviewed and edited the manuscript. Giovanni Pio Liberato investigated samples and data and reviewed and edited the manuscript. Seung Hee Han investigated the samples. Yoonsup Kim provided resources for the sample analysis and reviewed and edited the manuscript. Franco Maria Talarico co-conceptualized the project, provided resources, reviewed and edited the manuscript, supervised and administrated the project, and provided founding.

2.2. Introduction

The Late Paleozoic Ice Age (LPIA) is one of the longest and most extensive cold intervals in Earth's history, lasting over 70 Ma from the Visean (Mississippian) to the Capitanian/Wuchiapingian (Isbell et al., 2003, 2012; Fielding et al., 2008a; Craddock et al., 2019). The LPIA and the ensuing transition from icehouse to greenhouse conditions had significant effects on the Earth's climate, in both hemispheres, as well as its physical, chemical, and biological development (Heckel, 1994, 2008; Falcon-Lang, 2004; Joachimski et al., 2006; Clapham and James, 2008; Grossman et al., 2008; Isbell et al., 2008b, 2012; Falcon-Lang and Di Michele, 2010; Craddock et al., 2019). The detailed study of LPIA glacial sequences is therefore important reconstructing the paleo-environments of the Gondwana supercontinent. The upper Paleozoic glaciogenic sedimentary sequences occur in most of the Carboniferous-Permian basins located in the southern part of Gondwana (Figure 1; Powell and Li, 1994; Isbell et al., 2003; Craddock et al., 2019), where their stratigraphic assemblage has been well studied (Fielding et al., 2008b, 2008c; Isbell et al., 2008b; Lopez-Gamundi and Buatois, 2010; Limarino et al., 2014). Their recognition in all Gondwana continental blocks led to a conclusion that a large ice sheet once covered the entire southern Gondwana for a long time (Lindsay, 1970; Veevers and Powell, 1987; Frakes and Francis, 1988; Barrett, 1991; Frakes et al., 1992; Ziegler et al., 1997; Hyde et al., 1999; Veevers, 2001; Blackey, 2008; Buggisch et al., 2011). However, more recent studies (Isbell et al., 2003, 2008a, 2012; Fielding et al., 2008b; Isbell, 2010; Koch and Isbell, 2013; Cornamusini et al., 2017) imply a different model for the glacial history, which suggest diachronous development of several distinct minor ice centers in different sectors of Gondwana, each displaying individual behaviors (Figure 1). According to this model, local and regional-scale glacial episodes reflect the relative migration of Gondwana across of the South Pole (Isbell et al., 2003, 2012; Lopez-Gamundi and Buatois, 2010; Craddock et al., 2019). Three major glacial episodes have been recognized (Isbell et al., 2003, 2012; Craddock et al., 2019): Glacial Episode I (360-342 Ma), Glacial Episode II (334-313 Ma), and Glacial Episode III (315-265 Ma). In Antarctica, as well as most of Gondwana, glacial deposits are related to the most intense Glacial Episode III of the LPIA (Isbell et al., 2003, 2012; Fielding et al., 2008a, 2008c). Within the Glacial Episode III Fielding et al. (2008b) further distinguished four discrete glacial intervals (P1 to P4) in Australia, which recorded grounded ice. The glaciogenic rocks in Victoria Land were mostly formed during the P1 glacial interval (Gzhelian to Sakmarian) while Antarctica experienced warmer conditions with the development of fluvial systems during the later glacial intervals (P2 to P4; Isbell et al., 2012).

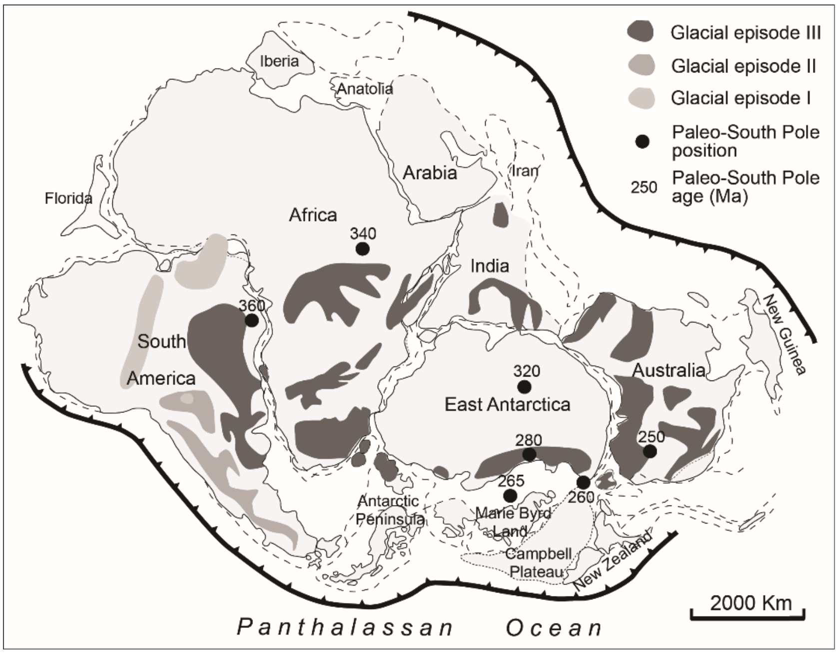

Figure 1. Distribution of Late Paleozoic Ice Age glaciogenic deposits in Gondwana. Continental block assemblage is after Sirevaag et al. (2018) and references therein; sediment distribution and Glacial episodes are adapted from Craddock et al. (2019) and Isbell et al. (2012) and references therein; South Pole positions are after Craddock et al. (2019).

The geochronological analysis of detrital zircons represents a key tool not only for the provenance study of LPIA glaciogenic sequences but also for paleo-environmental reconstructions of Gondwanan basins. Recently, a significant amount of detrital zircon U-Pb dating has been carried out on upper Paleozoic sedimentary sequences from Gondwana glacial basins (Elliot et al., 2015; Craddock et al., 2017, 2019; Griffis et al., 2018; Martin et al., 2019), but only few data were reported from Antarctica. Elliot et al. (2015) and Craddock et al. (2017) provided U/Pb ages of detrital zircons from two tillite samples of the Pagoda Formation in the Central Transantarctic Mountains (CTAM) region and one sample from the Whiteout Conglomerate in the Ellsworth Mountains. However, zircon U-Pb data are lacking in Victoria Land, despite it being a key region of the Transantarctic Mountains (TAM) that links the CTAM and Tasmania (Australia).

Here, the first detrital zircon U-Pb geochronological data from the Carboniferous(?)-Permian glaciogenic deposits of the Metschel Tillite in southern Victoria Land (SVL), and tillites in northern Victoria Land (NVL), are presented. The geochronological and petrographic characteristics of these tillites were compared to those of Transantarctic Mountains rocks, to establish the possible source areas of the glaciogenic clasts. The results provide new constraint on the ice covers and their catchment areas in Victoria Land during the LPIA.

2.3. Geological Setting and Regional Stratigraphy

Victoria Land represents the portion of the Transantarctic Mountains, a ca. 3000 km mountain range dividing East Antarctica from West Antarctica, which flanks the Ross Sea, north of the McMurdo Sound (Figure 2). The TAM represent the uplifted western shoulder of the West Antarctic Rift System, related to the Mesozoic?-Cenozoic extension (Cooper et al., 1991; Stump and Fitzgerald, 1992; Fitzgerald, 2002; Storti et al., 2007; Olivetti et al., 2018; Li et al., 2020). This uplift exposed a succession from the basement of late Precambrian to Ordovician in age and the overlying sedimentary strata (Stump, 1995; Goodge, 2020 and reference therein).

The TAM basement is characterized by igneous rocks of the Granite Harbour Intrusive Complex (Gunn and Warren, 1962) intruding several meta-sedimentary sequences during the Ross Orogeny (ca. 610 to 480 Ma; Stump, 1995; Talarico and Kleinschmidt, 2008; Goodge et al., 2012; Goodge, 2020). The basement rocks experienced a prolonged erosive phase, leading the formation of a flat or gently undulating surface: the Kukri Erosion Surface (McKelvey et al., 1977). Up to 2 km thick siliciclastic sequences of the Devonian to Lower Jurassic Beacon Supergroup deposited above the regional erosion surface (McKelvey, 1970; McKelvey et al., 1970; Barrett et al., 1972; Barrett, 1991; Elliot, 2013).

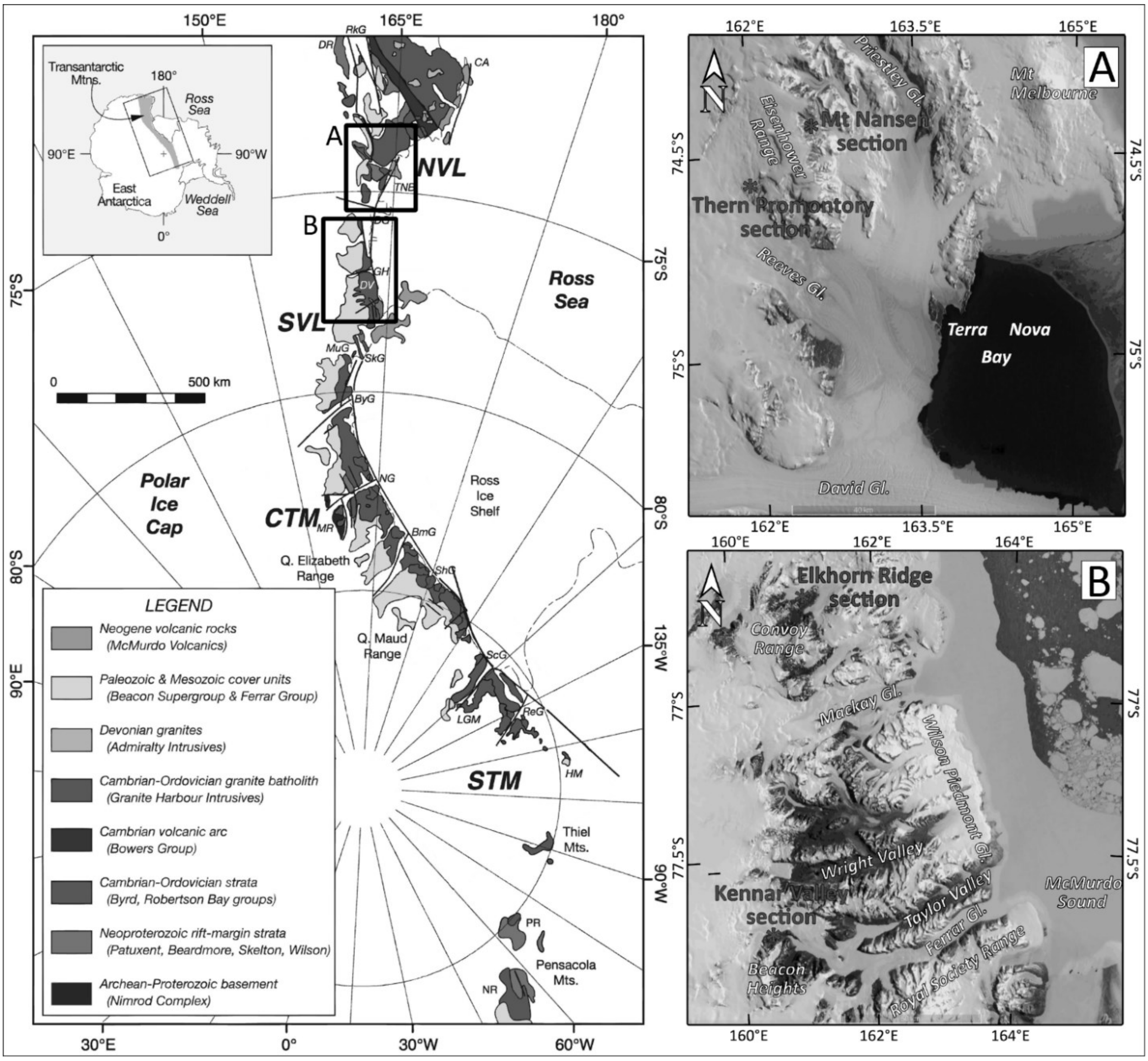

Figure 2. The left side shows a simplified geological map of the Transantarctic Mountains (modified from American Geographical Society, 1969 and Goodge, 2020). Boxes A and B indicate the study areas shown in detail on the right side (adapted from Perotti et al., 2018). NVL—northern Victoria Land; SVL—southern Victoria Land; CTM—central Transantarctic Mountains; STM—southern Transantarctic Mountains; Q.—Queen; Mt—Mount; Gl.—Glacier; DR—Daniels Range; RkG—Rennick Glacier; CA—Cape Adare; TNB—Terra Nova Bay; DG—Davis Glacier; GH—Granite Harbour; DV—Dry Valleys; MuG—Mulock Glacier; SkG—Skelton Glacier; ByG—Byrd Glacier; NG—Nimrod Glacier; MR—Miller Range; BmG—Beardmore Glacier; ShG—Shacketon Glacier; ScG—Scott Glacier; ReG—Reedy Glacier; LGM—La Gorge Mountains; HM—Horlick Mountains; PR—Patuxent Range; NR—Neptune Range.

In Victoria Land, the Beacon Supergroup is subdivided into two groups (Figure 3): the Devonian Taylor Group (Harrington, 1965) and the Carboniferous(?)/Permian to Lower Jurassic Victoria Group (Barrett, 1991; Cox et al., 2012 and references therein). The Taylor Group is bounded above by the Maya Erosion Surface (Harrington, 1965; McKelvey et al., 1977) which represents a hiatus spanning 109 to 86 Ma (Cox et al., 2012) and defines the paleo-morphology which the upper Paleozoic glacial sediments deposited. Another regional-scale surface, the Pyramid Erosion Surface, defines the upper boundary of the glacial deposits, separating them from the middle-upper part of the Victoria Group (Barrett, 1991). This latter erosion surface occurs in some areas of SVL (Cox et al., 2012), but poorly defined or potentially absent elsewhere including NVL (Bomfleur et al., 2014; Cornamusini et al., 2017) and the CTAM (Isbell et al., 1997). The Beacon Supergroup shows wide stratigraphic variations along the TAM (Figure 3). While in the CTAM and SVL the Victoria Group rests unconformably on the Devonian Taylor Group (Barrett, 1991; Collinson et al., 1994; Isbell et al., 2012), in NVL the Victoria Group directly lies on the Neoproterozoic-Ordovician crystalline basement as the Devonian deposits are absent (Laird and Bradshaw, 1981; Collinson et al., 1986).

The glacial beds, known as the Pagoda Formation in the CTAM (Lindsay, 1969, 1970; Barrett et al., 1986; Miller, 1989), the Metschel Tillite in SVL (McKelvey et al., 1970; Barrett and McKelvey, 1981; Barrett, 1991; Isbell, 2010), and the Lanterman Formation in NVL (Cornamusini et al., 2017), represent the base of the Victoria Group. There are significant lateral changes in the thickness of these glacial sediments along the TAM and they are completely absent in some localities (Barrett and McKelvey 1981; Isbell et al. 2008). In NVL these Permian strata occur sparsely lying onto the basement rocks and were mapped as Neall Massif tillite (Capponi et al., 2012; Casnedi et al., 2012; Pertusati et al., 2012). Cornamusini et al. (2017) suggested a formal stratigraphic unit, Lanterman Formation, with its type sections near Orr Glacier in the Lanterman Range. All the NVL tillites could be potentially correlated with the latter formation.

The age of the Metschel Tillite is not yet well constrained, but its equivalents in CTAM (Pagoda Formation) and in NVL (Lanterman Formation) yield early Permian palynomorphs (Kyle, 1977; Askin, 1998; Isbell et al., 2008b; Cornamusini et al., 2017). Moreover, a palynological assemblage from a lenticular horizon of a carbonaceous siltstone overlying basal conglomerates in the Eisenhower Range (NVL) indicates an early Permian age (Bomfleur et al. 2014). This datum constrains the basal diamictites in the Eisenhower Range to be no younger than early Permian, indicating these deposits can be correlatives of the Metschel Tillite in SVL and the Lanterman Formation in the Rennick Glacier area of NVL (Collinson et al., 1994; Isbell, 2010; Bomfleur et al., 2014; Cornamusini et al., 2017).

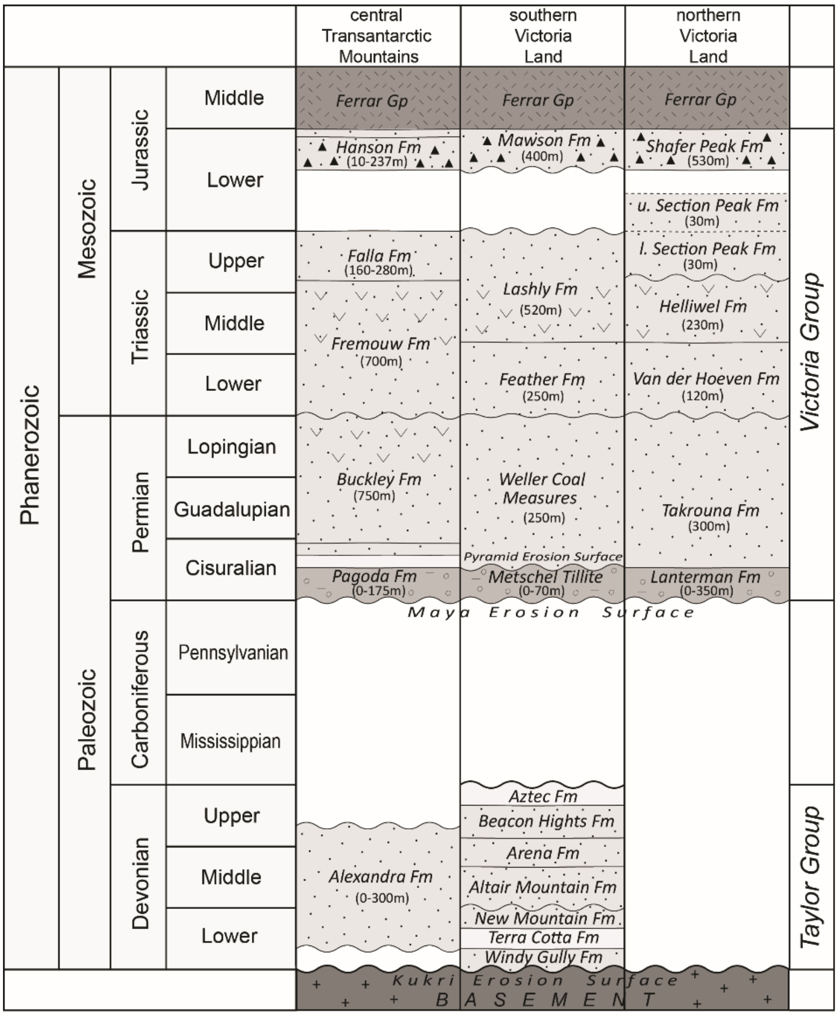

Figure 3. Simplified stratigraphy of the Beacon Supergroup along the Transantarctic Mountains. Numbers in brackets are estimated thickness of stratigraphic units (adapted from Elliot, 2013; Cornamusini et al., 2017; Liberato et al., 2017; Bomfleur et al., 2020; Gulbranson et al., 2020). Gp—Group; Fm—Formation; u.—upper; l.—lower.

2.4. Materials and Methods

Four sections of the LPIA sequences in Victoria Land were studied (Figure 2). From the South to North, they are Kennar Valley in the Beacon Heights (SVL), Elkhorn Ridge in the Convoy Range (SVL), Thern Promontory in the Eisenhower Range (NVL), and Mount Nansen in the Eisenhower Range (NVL). Field data and analyzed samples were collected during the 30th and 31st Italian PNRA expeditions (Table 1). The stratigraphic position of each sample is reported in Figure 4.

Table 1 Details of the Victoria Land samples, Antarctica

Sample ID	Section	Area	Region	Coordinates		Lithology
				Lat (°S)	Lon (°E)	
22-01-15C3	Kennar Valley	Beacon Heights	SVL	77.7733	160.357	clast-poor massive diamictite
03-01-15C3	Elkhorn Ridge	Convoy Range	SVL	76.6678	161.075	clast-poor massive diamictite
04-01-15C10	Thern Promontory	Eisenhower Range	NVL	74.5629	161.996	clast-rich massive diamictite
22-11-15C5	Mt Nansen	Eisenhower Range	NVL	74.4646	162.524	weakly stratified clast-poor diamictite

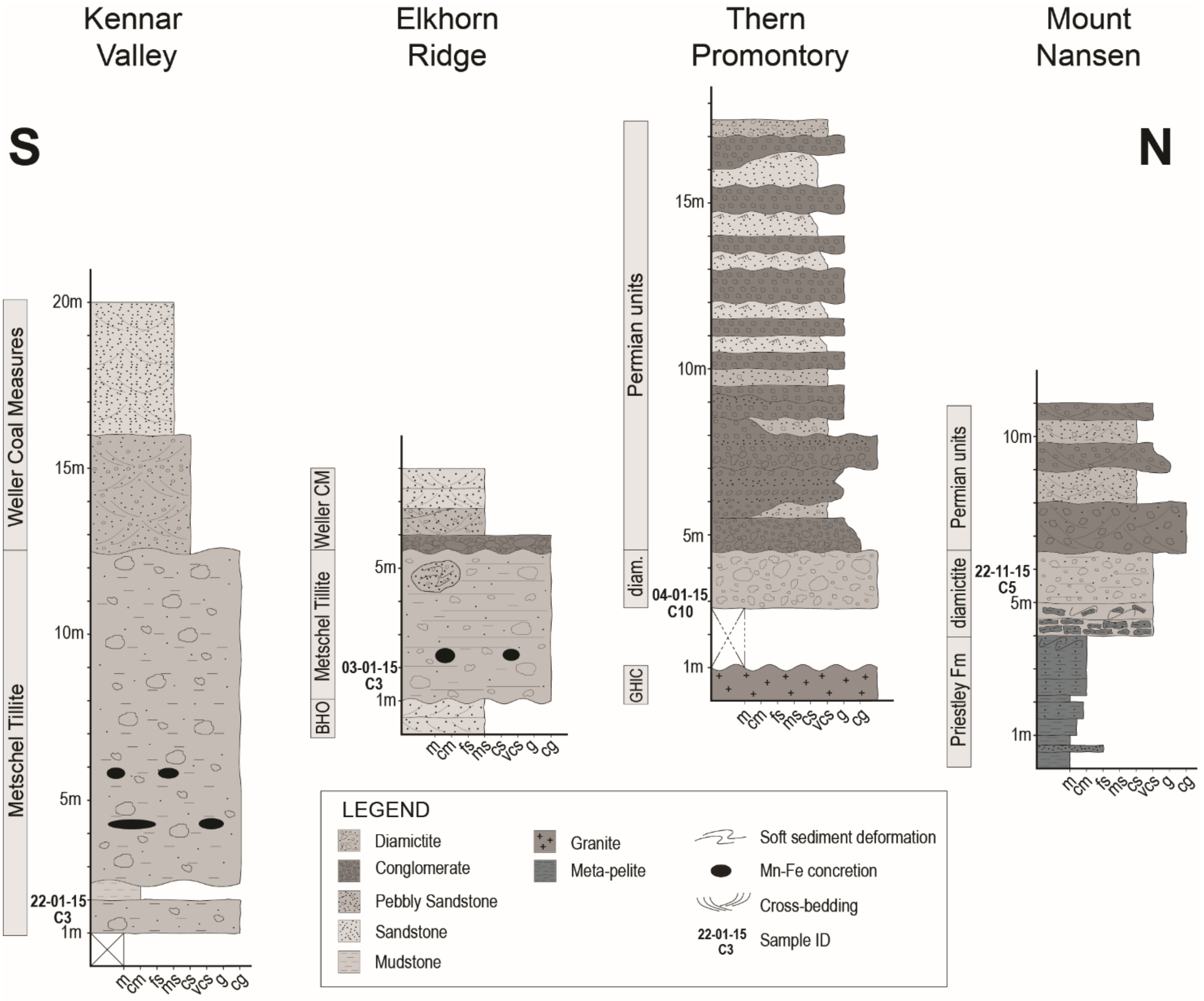

Figure 4. Stratigraphic logs of the studied sections. On the left side of the logs the name of the each lithostratigraphic unit is reported. BHO - Beacon Heights Orthoquartzite, GHIC - Granite Harbour Intrusive Complex; m - mud; cm - coarse mud; fs - fine sand; ms - medium sand; cs - coarse sand; vcs - very coarse sand; g - gravel; cg - coarse gravel.

The samples have been preliminarily characterized by qualitative petrographic examination using a polarized light microscope and standard thin sections to obtain basic mineralogical and textural information. This was coupled with geochronological data for provenance insights.

Zircon grains were separated from 1-2 kg of the whole rock using a modified heavy liquid technique (Cheong et al., 2013). The separated grains were mounted in epoxy with reference standard zircons - Plešovice (Sláma et al., 2008) for external standard and Z91500 (Wiedenbeck et al., 1995, 2004) for the primary standard. Back Scattered Electron (BSE) and Cathodoluminescence (CL) images were obtained using a JEOL JSM-6610 Scanning Electron Microscope (SEM) at the Korea Polar Research Institute (KOPRI). The BSE images were used to identify fractures and inclusions within each grain, whereas the CL images enabled evaluation of the internal structure and chemical zonation within the grains to determinate the best positions of analytical spots (Figure 5). SEM and stereomicroscope photomicrographs were also used to classify the shape of the grains, following categories of Zimmerman and Hall (2016), and Zoleikhaei et al. (2016). The grain shape classification is available in the Supplemental information.

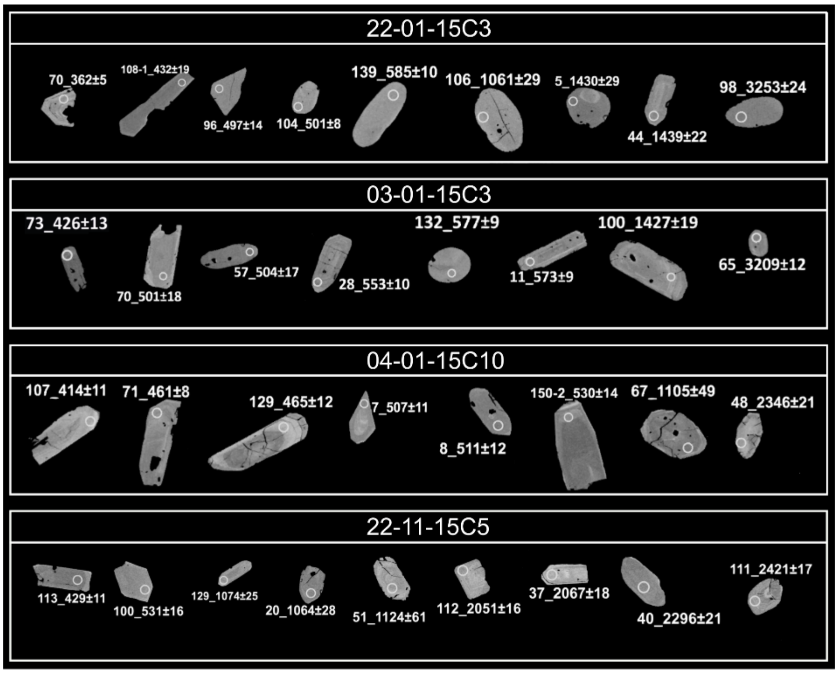

Figure 5. Back Scattered Electrons (BSE) images of analyzed zircon grains from the four samples. White circles indicate analyzed spot with diameter of 25 microns. The first number of the acronyms (e.g., 70_) represents the ID of the grain within the sample while the second number (e.g., 362±5) is the isotopic age and the associated error.

The U-Th-Pb isotopic analysis was carried out using a Laser Ablation-Inductively Coupled Plasma-Mass Spectrometer (LA-ICP-MS) at KOPRI laboratories. Each analysis consisted of 30 seconds of the background and data acquisition using a laser spot size of ca. 25 microns. During data collection an analysis of Z91500 standard was done every five unknown grains, as well as a Plešovice standard every ten unknown grains. Raw data were processed using the software IgroPro-Iolite. Tera-Wesserburg Concordia diagrams (Tera and Wasserburg, 1972) were obtained using Isoplot/Ex (Ludwig, 2003). Concordance of isotopic ages was determined following Spencer et al. (2016). Interpretations and data discussions are based on grains with a concordance between 85% and 105% (Elliot et al., 2015); non-concordant ages have been excluded from interpretations. The $^{206}Pb/^{238}U$ age has been selected for grains younger than 1 Ga while, for zircons older than 1 Ga, the $^{207}Pb/^{206}Pb$ age was used (Estrada et al., 2016). Based on these ages, zircons were split into eight groups. Groups with ages older than 450 Ma follow Estrada et al. (2016) classification: > 2500 Ma (Archean), 2500-1601 Ma (Paleoproterozoic), 1600-1301 Ma (early-middle Mesoproterozoic), 1300-901 Ma (middle Mesoproterozoic to early Neoproterozoic) corresponding to the Grenville Orogeny, 900-701 Ma (middle Neoproterozoic), 700-551 Ma (Late Neoproterozoic) corresponding to the Pan-African Orogeny, 550-451 Ma (late Neoproterozoic to Ordovician) corresponding to the Ross Orogeny. The group < 450 Ma (late Ordovician to Carboniferous) indicated as post-Ross, was introduced for the grains that fall in this age interval. The Th/U ratio of zircon has been used to determine the growth process of zircons:

grains with Th/U ratio < 0.1 are considered metamorphic growth (Williams and Claesson, 1987; Hanchar and Millar, 1993; Wysoczanski and Allibone, 2004), while when the ratio is higher than 0.1, the zircon is considered of magmatic origin. LA-ICP-MS raw data are available as Supplemental information.

2.5. Results

In the following sections we report the results of the detrital zircon age analysis, qualitative petrographic characterization, and sedimentological-stratigraphic studies of each glaciogenic sequences reported in the logs of Figure 4. Every sampled log (Figure 4) is individually described, from South to North.

2.5.1. Kennar Valley

At this outcrop, the contact of the Metschel Tillite with the underlying Devonian Taylor Group is covered by talus deposits (McKelvey et al., 1977; Isbell, 2010), whereas horizontal beds of Aztec Siltstone, representing the upper Taylor Group formation, crop out several meters below the diamictite. The Metschel Tillite is about 15-20 meters thick (Figure 4) and has a marked lenticular geometry with abrupt lateral facies changes. The diamictite is commonly clast-poor (Moncrieff, 1989), with abundant blueish/greenish sandy-mudstone matrix. It is mainly massive to weakly stratified in the upper part. Thin dark mudstone layers occur inside the diamictite, as well as massive sandstone pods and lenses in the upper portion (Figure 4 and Figure 6A). Clasts in the diamictite are rounded to sub-angular and range in size from granules to cobbles. Furthermore, the middle-upper part of the diamictite is locally rich in dark ovoidal-shape Mn-Fe concretions (decimeters in diameter), preferentially aligned along stratigraphic layers (Figure 6A). The diamictite is strongly affected by glacio-tectonic deformation, which led to the development of large-scale thrust faults which stacked tillite sheets (Isbell, 2010). The soft-sediment deformation structures including isoclinal and recumbent folds show vergences towards SE and SSW. The diamictite passes upwards, through a sharp irregular contact, to the undeformed trough-cross bedded sandstones of the Permian Weller Coal Measures, which show paleocurrent directions towards ca. NNE.

Table 2 Detrital zircon ages distribution in the Victoria Land samples, Antarctica

Sample ID	Concordant/ analysed grains	post-Ross <450 Ma	Ross 550-451 Ma	Pan-African 700-551 Ma	900-701 Ma	Grenville 1300-901 Ma	1600-1301 Ma	Paleo-Proterozoic 2500-1601 Ma	Archean >2500 Ma
22-01-15C3	136/149	3.70%	24.30%	26.50%	4.40%	16.20%	17.60%	4.40%	2.90%
03-01-15C3	146/149	0.70%	27.40%	31.50%	9.60%	15.10%	5.50%	8.20%	2.10%
04-01-15C10	130/150	10.00%	80.80%	0.80%	3.10%	3.80%	0.80%	0.80%	0%
22-11-15C5	98/130	1.00%	6.10%	8.20%	1.00%	37.80%	0%	38.80%	7.10%

Note: Age intervals are from Estrada et al. (2016)

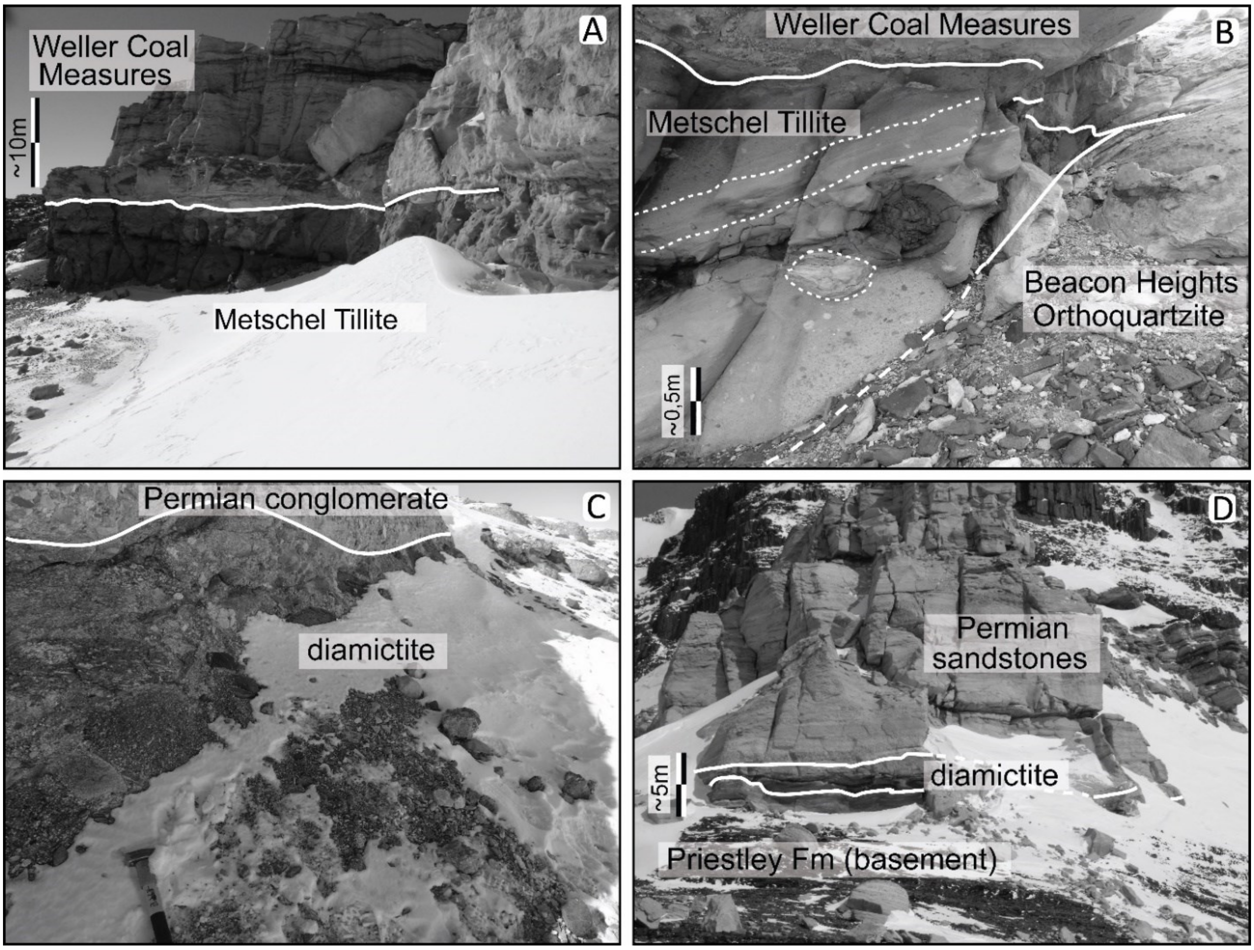

Figure 6. Field photographs of the studied outcrops. (A) Kennar Valley in the Beacon Heights (southern Victoria Land). (B) Elkhorn Ridge in the Convoy Range (southern Victoria Land); deformed sandstone pod is circled as well as the stratification is outlined by dotted lines. (C) Thern Promontory in the Eisenhower Range (northern Victoria Land) - hammer for scale. (D) Mt Nansen in the Eisenhower Range (northern Victoria Land).

The petrographic analysis shows that sample 22-01-15C3 is isotropic matrix-rich greywacke with ca. 40% mud-size matrix containing dispersed sand- to granule-size grains (Figure 7A). White mica fragments occur in the matrix, as well as zircon, brown and blue tourmaline, rare garnet, and opaque minerals. Clasts are either well-rounded or angular to sub-angular. Compositionally, they are mainly monocrystalline quartz, and minor altered K-feldspar, and lithic fragments of felsic volcanic, granitoid and metamorphic (quartzite, schist, and phyllite) rocks. The petrographic characterization of cobbles and pebbles sampled from diamictite level shows that they are constituted by quartzite, gneiss, schist, and meta-sandstone.

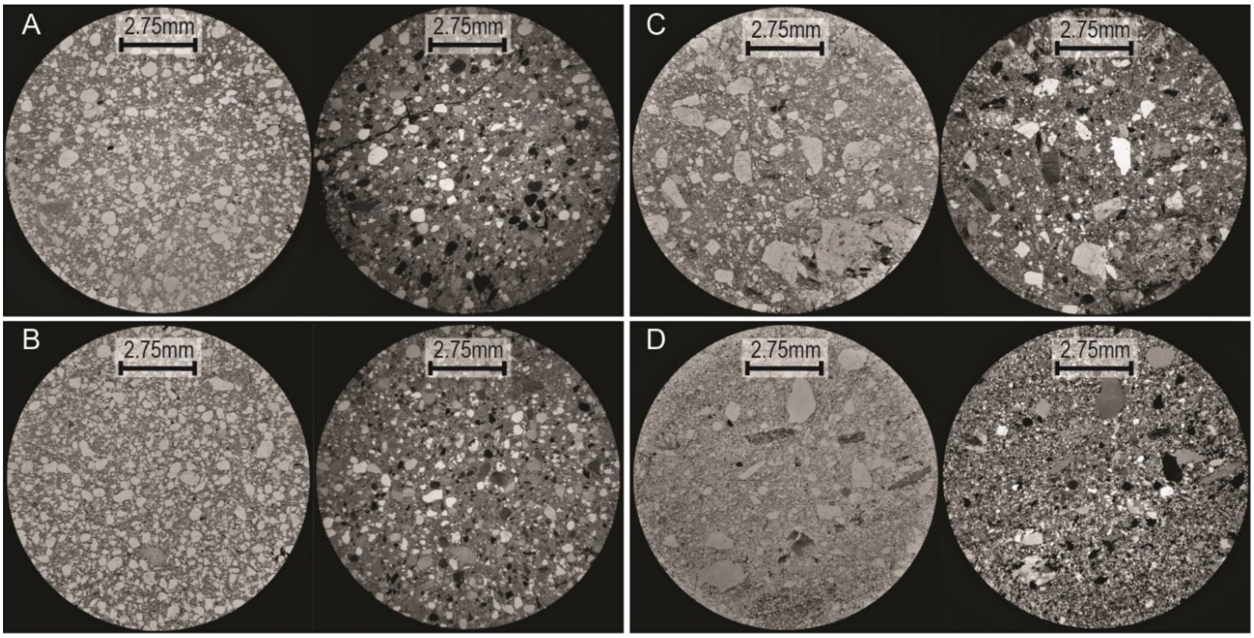

Figure 7. Microphotographs (PPL on the left and XPL on the right) of the analyzed diamictite samples. A) 22-01-15C3 – Kennar Valley (southern Victoria Land); B) 03-01-15C3 - Elkhorn Ridge (southern Victoria Land); C) 04-01-15C10 - Thern Promontory (northern Victoria Land); D) 22-11-15C5 - Mt Nansen (northern Victoria Land).

In sample 22-01-15C3, 149 zircon grains were analyzed, of which 136 were concordant (Table 2). Ages range from the Paleoarchean (3253±24 Ma) to the Late Devonian (362±5 Ma). Most of the analyzed zircons are rounded to sub-rounded (87%), whereas the remaining 13% of the grains, mainly found in the youngest age groups, are euhedral to subhedral (Figure 8). Half of the zircons show late Neoproterozoic to early Cambrian ages (Table 2), with four main peaks at ca. 527 Ma, ca. 583 Ma, ca. 552 Ma, and ca. 501 Ma (Figure 8). About 26% of these are in the Ross – Pan-African age interval (700-551 Ma), while 24% fit in the Ross age (550-451 Ma) interval (Table 2). Rounded to sub-rounded grains constitute 97% of the Ross-Pan-African age group and 76% of the Ross age group (Figure 9). A secondary population (ca. 17%) has a peak at ca. 1445 Ma; Meso to Neoproterozoic (1300-901 Ma) zircons are common (ca. 15%), with the main peak at ca. 1085 Ma, and Paleoproterozoic to Archean grains are relatively rare (Figure 8). A Silurian age is recorded (432±19 Ma) in only one zircon grain of subhedral shape for which the Th/U ratio indicates a magmatic growth (Th/U = 0.71). Four euhedral to subhedral zircon grains recorded Late Devonian age in the range of 382-365 Ma (Figure 9). On the basis of the Th/U ratio (Figure 8), most of the analyzed zircons have a magmatic origin, whereas only five grains show clear metamorphic growth.

2.5.2. Elkhorn Ridge

In this outcrop, the Metschel Tillite fills a depression in the Maya Erosional Surface (Burgess et al., 1981; Cox et al., 2012; Figure 6B). The diamictite horizon has a maximum thickness of 5-6 meters (Figure 4 and Figure 6B), and it is lenticular with lateral continuity of few tens of meters. It overlies the Beacon Heights

Orthoquartzite and it is overlain by the Weller Coal Measures (Burgess et al., 1981; Cox et al., 2012). The clast-poor diamictite (Moncrieff, 1989) is made up of a greenish/blueish sandy-mudstone matrix with dispersed granules to cobbles, characterizing a massive to weakly stratified facies. Near the top of the sequence, some deformed pods of medium grained, massive, or weakly stratified pebbly sandstone occur (Figure 6B). At the top, the diamictite is bounded by the Pyramid Erosion Surface, which is overlain by a matrix-supported conglomerate, ranging in thickness from 20 to a few cm, passing upwards to trough cross-bedded pebbly sandstones and coarse sandstones (Figure 4 and Figure 6B). This diamictite, consistent with the one in the Kennar Valley, is characterized by the presence of dark brownish Mn-Fe oxides concretions forming sub-circular shapes. These are few decimeters in diameter and usually preferentially aligned along the layers (Figure 6B). The conglomerates and pebbly sandstones on the top of the diamictite, mainly indicate northward paleocurrents through pebble imbrication and trough cross-stratification, but the diamictite does not contain clear indicators of transport direction. The thin section analysis revealed that sample 03-01-15C3 is an isotropic greywacke where the mud-size matrix constitutes ca. 40% of the rock (Figure 7B). Clasts are both well-rounded and angular to sub-angular and they mainly consist of monocrystalline quartz; altered K-feldspar is less common. Lithic fragments are scattered and made up of metamorphic, granitoid and sedimentary rocks. Accessory minerals include white mica, pinkish garnet, apatite, zircon, blue tourmaline, rutile, and opaque minerals (Figure 7B). Pebbles and cobbles collected within the diamictite, which are sub-rounded and weathered, consist of schist, gneiss, felsic porphyry, and quartz sandstone (comparable with the lithologies of the Upper Devonian Taylor Group formations).

In the sample 03-01-15C3 from Elkhorn Ridge, 149 grains were analyzed with 146 (98%) falling in the concordance range (Table 2); zircon ages fall between Silurian (423 ± 13 Ma) and Meso/Paleo-Archean (3209 ± 12 Ma). Most of the analyzed zircons are rounded to sub-rounded (86%); the subhedral ones occur most frequently in the youngest population (Figure 9). The age spectrum is quite similar to sample 22-01-15C3 from Kennar Valley (Figure 8 and Table 2). About 27% of the zircons fall in the Ross age interval (550-451 Ma) with 33% subhedral grains. About 32% of grains fall in the Ross-Pan-African age interval (700-551 Ma) with only 13% subhedral grains (Figure 9). Three main age peaks occur at ca. 518 Ma, ca. 583 Ma and ca. 554 Ma (Figure 8). Smaller populations have peaks at ca. 1457 Ma mainly, ca.1098 Ma and ca. 2244 Ma (Figure 8). The sample gave only one grain of late Silurian age, and no Carboniferous-Devonian ages were found. The Th/U ratio primarily indicates magmatic growth with a few grains having a metamorphic origin (Figure 8).

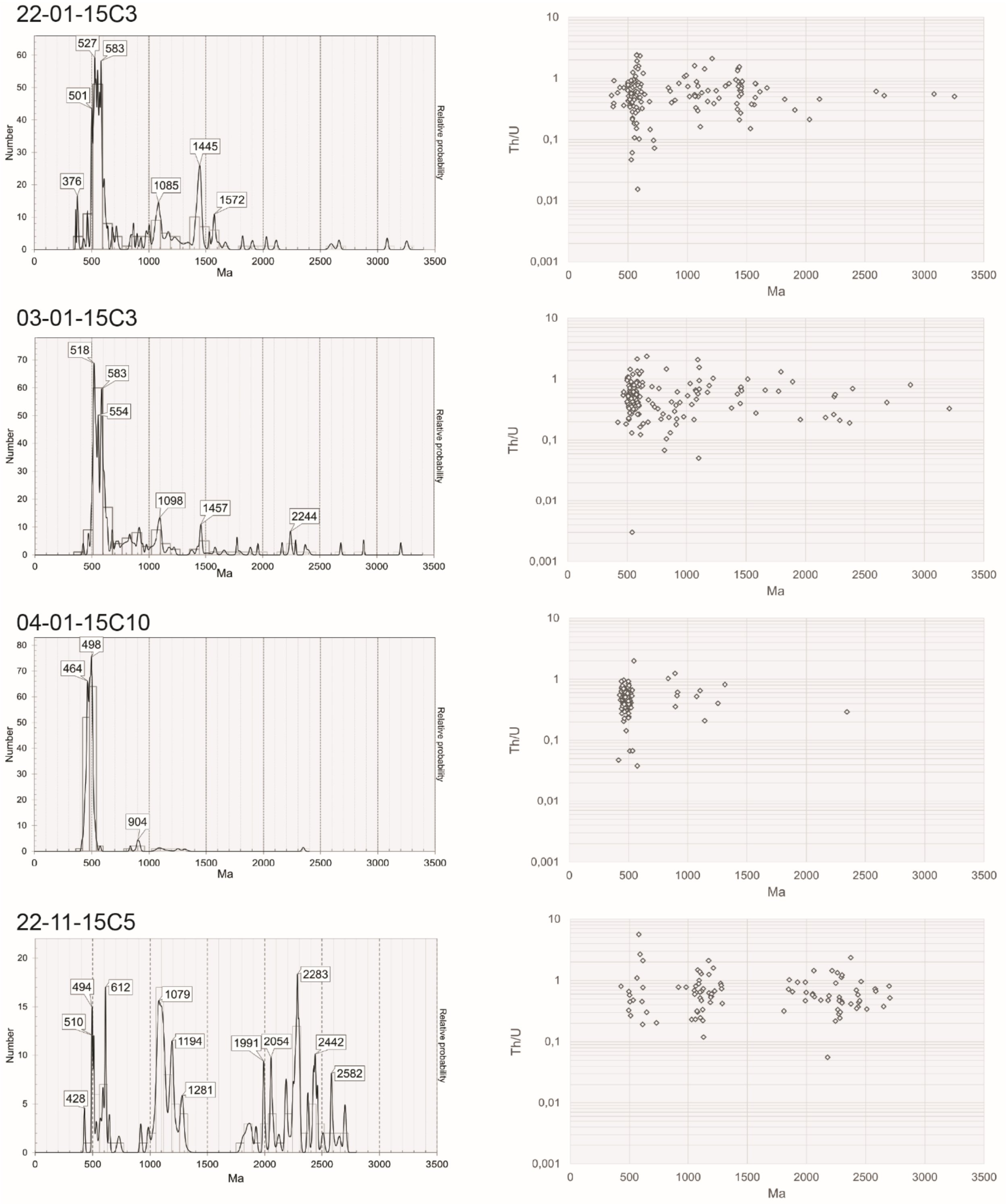

Figure 8. U-Pb age histograms and probability density plots of the U-Pb geochronological analysis, with peak values shown in the left column. Th/U ratio scatter diagrams are given in the right column.

2.5.3. Thern Promontory

At Thern Promontory, at least 2 m of diamictite crops out in a gently slope above the glacier (Figure 6C); the contact with the basement, which consist of granitoids of the Granite Harbour Intrusive Complex cropping out few meters below, was not directly observable because of snow cover (Figure 4 and Figure

6C). The diamictite is overlain by conglomerates attributed to the Section Peak Fm. It was formerly named as Neall Massif Tillite (Casnedi et al., 2012) that could be tentatively correlated with the Lanterman Formation in the Rennick Glacier area of NVL (Cornamusini et al., 2017). The massive or faintly bedded diamictite is greenish/brownish in color, greatly heterogeneous and clast-rich (Moncrieff, 1989), and contains angular to sub-rounded granules to boulders dispersed in a sandy-mudstone matrix (Figure 6C). The diamictite lacks any soft-sediment deformational structures, deformed sandstone pods, and transport indicators. The upper boundary of the diamictite is a sharp, irregular surface with minor channelization structures. It is directly overlain by a discontinuous, few centimeters thick, matrix-poor conglomerate lag that sharply passes upward into alternated beds of light grey clast-supported conglomerate and pebbly sandstone (Figure 4 and Figure 6C). Petrographic analysis shows that sample 04-01-15C10 is an isotropic greywacke made up of mud-size matrix with angular to sub-angular sand to granule size clasts (Figure 7C). Clasts are mainly quartz, K-feldspar, and granitoid and metamorphic lithic fragments. Large palish lamellae of biotite commonly occur within the diamictite matrix, while white mica crystals are rare (Figure 7C). Macroscopically, the clasts within the diamictite (pebble and cobble size) mainly consist of medium/coarse grained pink granite alongside a few metamorphic (dark phyllite/schist), fine-grained (meta-) sedimentary rocks and rare red porphyry (Figure 6C). Casnedi et al. (2012) also reported the occurrence of granite, deformed metamorphic rocks, felsic porphyry, black shale, sandstone, limestone, and quartzite clasts for the same diamictite outcrop.

In the sample 04-01-15C10, the U/Pb geochronological analysis performed on 150 detrital zircon grains; 20 analysis (13%) were excluded because they were not concordant (Table 2). The youngest grain is Silurian in age (414±11 Ma), while the oldest is early Paleoproterozoic (2346±21 Ma). In this sample, 33% of grains are rounded to sub rounded, while 58% are subhedral and 8% euhedral (Figure 9). About 81% of zircons have a Ross age (550-451 Ma), 10% a post-Ross age (<450 Ma), and less than 9% are older than 550 Ma (Table 2); the latter have a rounded to sub-rounded shape (Figure 9). The probability density diagram (Figure 8) shows two age peaks at ca. 498 Ma and ca. 464 Ma, as well as a minor peak of Grenvillian age (ca. 904 Ma). The Th/U ratios are indicative of igneous origin (Figure 8).

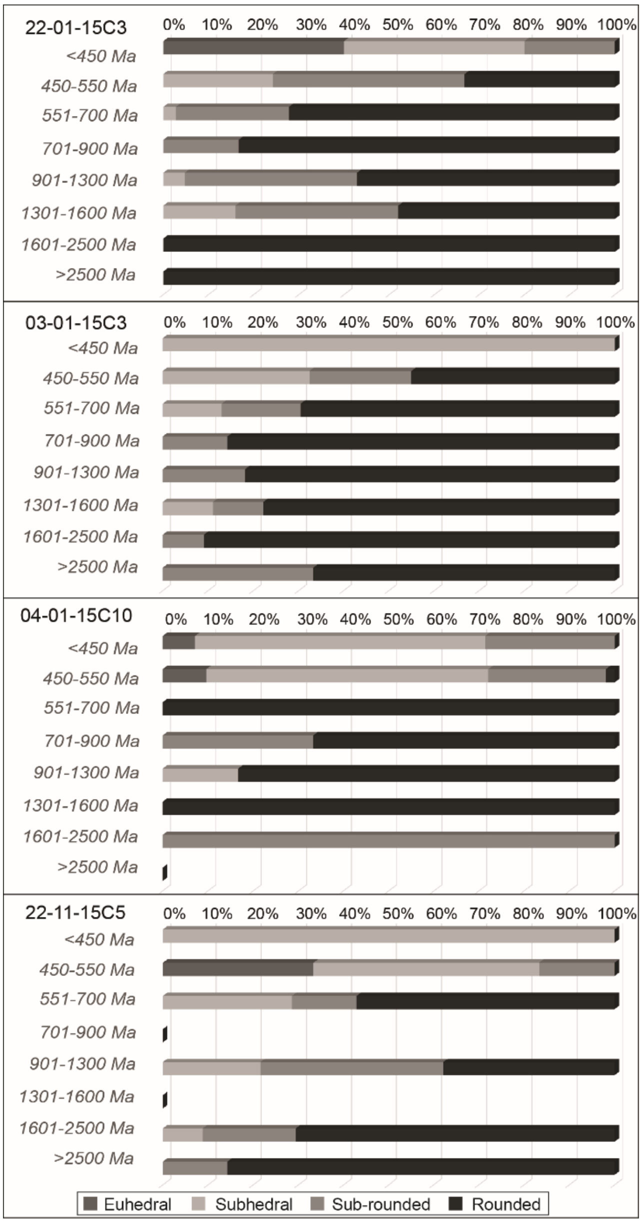

Figure 9. Bar chart representing proportion of the analyzed zircon grain shapes in relation with age ranges of the Victoria Land samples.

2.5.4. Mt. Nansen

A few meters thick, lenticular, weakly stratified, clast-poor, sandy diamictite (Moncrieff, 1989) crops out along the steep cliff north of Mt. Nansen in the Eisenhower Range. It lies above the low-grade meta-sedimentary rocks of the Priestley Formation, which is intruded by granitoids of the Granite Harbour Intrusive Complex (Figure 4 and Figure 6D). The diamictite horizon shows a lenticular bedding with abrupt lateral pinch-out. It contains sub-angular clasts in a greenish muddy-sandstone matrix. At the base, whitish quartz-rich fine sandstone blocks form a breccia with fold structures. Within the weakly stratified diamictite, soft sediment deformation structures, such as isoclinal folds, show vergence toward WSW. The top of the diamictite is defined by a sharp boundary, with occasional gentle scours, overlain by clast-supported conglomerates with southward dipping cross-stratification (Figure 6D). The overlying thick succession of pebbly sandstones and very coarse sandstones shows well-developed trough cross-bedding and clast-imbrication indicating north directed paleocurrents. Petrographically, the lowermost diamictite sample (22-11-15C5) is a pebbly sandstone with a low developed grain fabric (Figure 7D). The matrix is made up of fine sand angular to sub-rounded monocrystalline quartz. Clasts have a sub-angular to sub-rounded shape and they are made up of monocrystalline and polycrystalline quartz, rare and altered K-feldspar, and lithic fragments mainly comprised of quartzite with minor schist and phyllite (Figure 7D).

In sample 22-11-15C5, 130 zircon grains were analyzed (Table 2). About 78% of grains are rounded to sub-rounded and the roundness increase with the age of zircons (Figure 9). This sample shows a wide range of ages (Figure 8), spanning the Silurian (429±11 Ma) to Neoarchean (2705±21Ma). The main population (39%) is Paleoproterozoic in age and shows numerous peaks with the most prominent one at ca. 2283 Ma

(Figure 8 and Table 2). Grenville-age zircons represent 38% of all zircon grains, with the main age peak at ca. 1079 Ma (Figure 8 and Table 2). About 8% of grains are in the Pan-African age range (700-551 Ma), while 6% fall in the Ross one (550-451 Ma). Only one Silurian zircon was found (429±11 Ma), which had a subhedral shape (Figure 5 and Figure 8) and a magmatic origin based on the Th/U ratio of 0.66. Almost all the other zircons from this sample also appear to have a magmatic origin (Figure 9).

2.6. Discussion and Provenance Implications

2.6.1. Glacial and Environmental Inferences

Massive to stratified diamictites form both in polar and temperate, proximal to distal, glaciomarine settings through the rain-out of debris from icebergs or floating ice, meltwater plumes, and subaqueous debris flows (Eyles et al., 1983, 1985; Dowdeswell et al., 1994; Woodworth-Lynas and Dowdeswell, 1994; Powell and Domack, 2002; Isbell, 2010; Henry et al., 2012). The presence of sandstone lenses and pods are usually interpreted as the result of tractive flows, hyper-concentrated density flows, and gravity flows under subaqueous conditions (Isbell, 2010; Henry et al., 2012), which develop in the proximal proglacial setting of temperate glaciers (Powell and Domack, 2002; Isbell, 2010; Henry et al., 2012).

In agreement with previous work, sedimentological-stratigraphic features, thickness and lateral extent of the outcrop discussed here suggest that glaciogenic diamictites of NVL and SVL formed under quite different depositional settings. Isbell (2010), and Koch and Isbell (2013) proposed deposition in a subaqueous, probably glaciomarine environment for diamictite in SVL and the CTAM, although Barrett (1981, 1991), Barrett and McKelvey (1981) and Woolfe (1994) suggested a glacio-continental depositional setting in SVL. Sedimentary facies of diamictite in NVL, coupled with the absence of definite marine features, indicate that deposition occurred in a glacio-continental environment, shifting from subaerial to glacio-lacustrine settings (Collinson et al., 1986; Cornamusini et al., 2017).

2.6.1.1. Southern Victoria Land

Massive to weakly stratified clast-poor diamictite is the most common sedimentary facies. This facies is usually associated with deformed sandstone pods and mudstone intervals in the upper part of the sequences. Moreover, glaciotectonic structures described by Isbell (2010) in SVL are indicative of deposition near the glacial front. According to Isbell (2010), facies associations and glaciotectonic deformation indicate that deposition of the Metschel Tillite at Kennar Valley occurred in an ice-proximal to ice-distal setting of a marine tidewater glacier. The thinner diamictite at Elkhorn Ridge, closely matches with the facies association of the Kennar Valley diamictite, suggesting a similar depositional setting. The glacio-tectonic structures in the Kennar Valley section (Isbell, 2010), were used to define the ice flow direction from E-NE to the westward sectors (N252°), implying a possible provenance from Marie Byrd Land (MBL) or Ross Sea, towards East Antarctica. Petrographically, both diamictites contain common, well-rounded, mono-crystalline quartz grains, together with angular ones. Well-rounded monocrystalline quartz grains are the main mineralogical constituent of the Devonian Taylor Group sandstones, which are mostly quartzarenite and secondary subarkose (Shaw, 1962; Korsch, 1974; Mcpherson, 1978; Barrett et al., 1986; Cornamusini and Talarico, 2016). This, in accordance with the occurrence of quartz-sandstone clasts in the Elkhorn Ridge diamictite, is a clear evidence that the Metschel Tillite also reworked the older underlying Taylor Group deposits, such as the Aztec Siltstone and the Beacon Heights Orthoquartzite. The glacial sequence in SVL which is close to the margin of the elongated Transantarctic Basin (Isbell et al., 1997) is thinner than those in CTAM, NVL, and Tasmania. Post-glacial erosion, marked by the Pyramid Erosion Surface, played only a minor role in the thinning of the glaciogenic deposits because the sedimentation occurred predominantly in continuity, as recorded by the interfingering of the Metschel Tillite and the overlying Weller Coal Measures at Mount Ritchie (Isbell, 2010).

2.6.1.2. Northern Victoria Land

At Thern Promontory, as well as at Mt. Nansen in the Eisenhower Range, the facies associations, together with the absence of sedimentological features indicative of subaqueous environment, are suggestive of subaerial depositional conditions. This is in agreement with the northernmost NVL diamictites of Rennick Glacier area as the Lanterman Formation of Cornamusini et al. (2017) and the Neall Massif Tillite (Collinson et al. 1986; John, 2014). The clast-rich massive diamictite facies of Thern Promontory can be interpreted as glacial till (Sudgen and John, 1988), resulting from either subglacial deposition (Eyles and Eyles, 1992; Miller, 1996) or ice-influenced debris flows (Visser, 1997; Koch and Isbell, 2013; Limarino et al., 2014). However, the occurrence of clast-rich para-conglomerate and the absence of glacial striae and other glacial features could also imply a glacio-fluvial deposition within a periglacial environment. This depositional setting has been hypothesized to be the case for the clast-supported conglomerates comprising the glaciogenic succession in the Rennick Glacier area (Laird and Bradshaw, 1981; Cornamusini et al., 2017), or part of the Neall Massif Tillite (Collinson et al., 1986; John, 2014; Schöner and John, 2014). Massive diamictites of similar thickness with different features, formed subglacially both in temperate alpine continental glaciers and polythermal terrestrial glaciers (Glasser and Hambrey, 2001; Eyles and Lazorek, 2007; Hambrey and Glasser, 2012).

At Mt. Nansen, the tillite is a massive to stratified, internally deformed sandy diamictite. This facies can develop with comparable thickness in a subglacial to ice-marginal depositional environment beneath temperate to polythermal terrestrial glacier (Glasser and Hambrey, 2001; Eyles and Lazorek, 2007; Hambrey and Glasser, 2012). Both Eisenhower Range diamictites show no such glacial features, as striated clasts, and Schöner et al. (2011) suggested that a glacial origin cannot be fully proven for these sections. However, the absence or scarcity of striated clasts can be also justified by the fact that Hambrey and Glasser (2012) recorded relatively few (6-14%) striated clasts in the subglacial diamictite deposited by temperate and polythermal terrestrial glaciers. Furthermore, striae are delicate features with low preservation potential in the rock record during burial and diagenesis, so the percentages may be much lower in old glacial diamictites.

The physiography and morphology of the substratum which the glacial sediments were deposited is irregular. This led to marked differences in paleo-environment, as stated above, varying from possible glaciomarine environments in CTAM and SVL to glacio-continental environment in NVL. In particular, there are significant differences in the thickness of the diamictite beds. The data presented herein, as well as previous publications (Barrett et al., 1986; Collinson et al., 1986; Barrett, 1991; Isbell et al., 1997; Isbell, 2010; Schöner et al., 2011; Cox et al., 2012; Koch and Isbell, 2013; Cornamusini et al., 2017), and unpublished reports by Barrett then elaborated in Zurli (2018), all show LPIA glaciogenic deposits throughout Victoria Land contain marked changes in the diamictite thickness. This is consistent with the CTAM data (Isbell et al., 1997, 2008b). The diamictite thicknesses in SVL and overall, in the Eisenhower Range of NVL are markedly thinner compared to those in the CTAM, northernmost NVL (Rennick Glacier area) and Tasmania. In SVL, the thickness is lowest in the northern area (Elkhorn Ridge) and increases southward to the Dry Valleys area (Kennar Valley) and mainly to the Darwin Mountains, while areas with very thin or no diamictite are interspersed along this transect. This configuration suggests glacial sediments deposited on an irregular topography, represented by the Maya Erosion Surface, with trough-shape glacial valleys or basins located between morphological highs. This interpretation agrees with the model proposed for the CTAM, where the glacial basins are located between the Byrd and the Shackleton glaciers, and in the Ohio Range, where diamictite beds are up to 450m thick (Isbell et al., 1997, 2008b).

Post-glacial erosion, represented by the Pyramid Erosion Surface, had a minimal role in the thinning of the glaciogenic sediments. Deposition occurred substantially in continuity, as recorded in the Rennick Glacier where the Lanterman Formation passes upwards without significant break into the Takrouna Formation (Cornamusini et al., 2017), and as evidenced at Mt. Ritchie in SVL (Isbell, 2010).

2.6.2. Geochronology

2.6.2.1. Southern Victoria Land

The detrital geochronology of the two investigated Metschel Tillite samples (Kennar Valley, 22-01-15C3 and Elkhorn Ridge, 03-01-15C3) reveals quite similar detrital age compositions (Figure 8), providing new constraints for LPIA evolution in SVL. The zircon age signatures of the tillite deposits involved in the discussions are showed and summarized in the Figure 10.

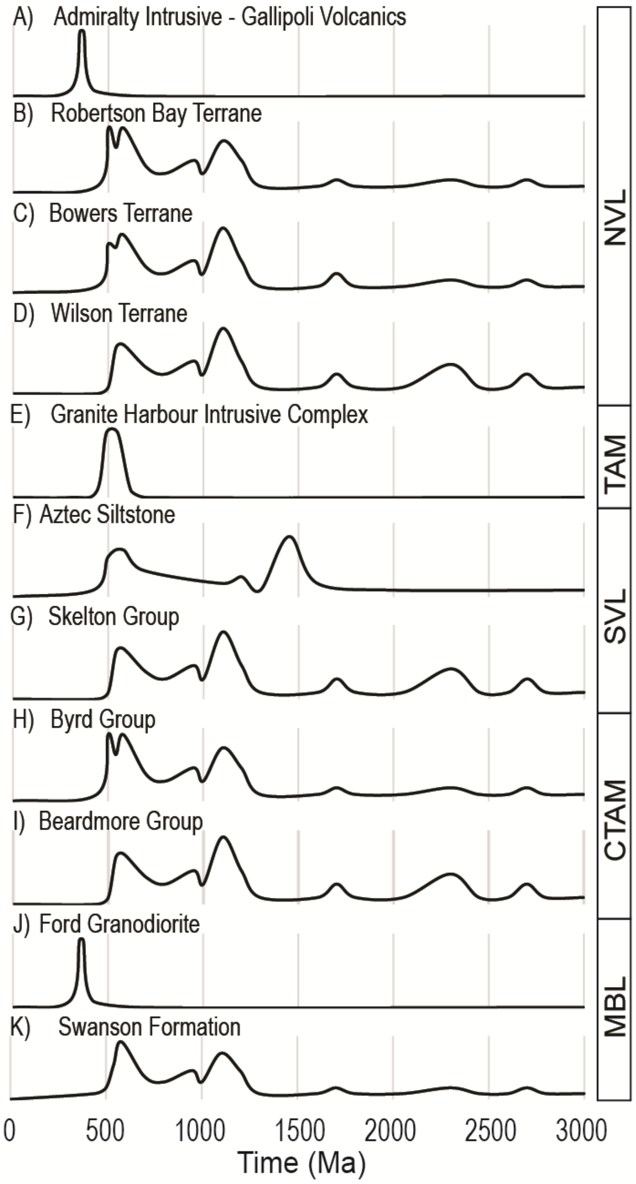

Figure 10. Compilation of zircon U-Pb ages from the possible source units of the diamictite: (A) Fioretti et al. (1997); Grindley and Oliver (1983); Henjes-Kunst and Kreuzer (2003); Kreuzer et al. (1987, 1981); Stump (1995); Vetter et al. (1983). (B), (C), and (D) Estrada et al. (2016) and Paulsen et al. (2016); (E) Cox et al. (2012) and reference therein, Goodge et al. (2012), and Goodge (2020) and reference therein; (F) Paulsen et al. (2017); (G) Wysoczanski and Allibone (2004) and Cooper et al. (2011); (H), and (I) Goodge (2002) and Goodge et al. (2004a, 2004b, 2012); (L), and (M) Pankhurst et al. (1998) and Yakymchuk et al. (2013, 2015). MBL—Marie Byrd Land; CTAM—central Transantarctic Mountains; SVL—southern Victoria Land; TAM—Transantarctic

Mountains; NVL— northern Victoria Land.

Archean (>2.5 Ga) and Paleoproterozoic (2500-1601 Ma) populations are minor in both samples. The most likely source of these grains are the Devonian sandstones of the Beacon Supergroup (Savage, 2005; Elliot et al., 2015; Paulsen et al., 2017) and/or the Neoproterozoic and/or Cambro-Ordovician meta-sedimentary units of the Ross Orogen (Goodge et al., 2004a, 2004b, 2012; Cooper et al., 2011; Estrada et al., 2016; Paulsen et al., 2016; Goodge, 2020). These grains usually show a high degree of roundness, consistent with a polycyclic depositional history (Zoleikhaei et al., 2016).

The 1600-1301 Ma age interval is widely represented in the samples, with a major peak at ca. 1450 Ma. Most of these grains are rounded to sub-rounded, might indicating a polycyclic history (Zoleikhaei et al., 2016), long transport distance or increased time in the surface environment. Differently, the other ca. 15% of these zircons are subhedral. These grains can be most likely be sourced by the Devonian Taylor Group strata, particularly the Aztec Siltstone which are dominated by the ca. 1450 Ma population in the Dry Valleys area (Paulsen et al., 2017).

Zircon dating to the Grenville Orogeny (1300-901 Ma) reflect the contribution from three possible different sources: i) Neoproterozoic metamorphic rocks, ii) Cambro-Ordovician metamorphic rocks, and iii) Devonian Taylor Group sedimentary strata. Neoproterozoic metamorphic rocks (Beardmore, Skelton and Wilson groups) have additional major populations, such as Paleoproterozoic one (2500-1601 Ma; Goodge et al., 2004a, 2004b; Wysoczanski and Allibone, 2004; Cooper et al., 2011; Estrada et al., 2016; Paulsen et al., 2016), which are, on the contrary, poorly represented in the here analyzed sample. Nevertheless, these units may have partially contributed to the tillite composition, especially the Skelton Group which constitutes part of the basement in the Dry Valley region (Cox et al., 2012). Cambro-Ordovician meta-sedimentary strata such as the Byrd Group in the CTAM (Goodge et al., 2004b) and the Swanson Formation in MBL (Pankhurst et al., 1998; Yakymchuk et al., 2013, 2015) contain Grenville ages as a secondary population. Grenville ages are also dominant in meta-sedimentary rocks from the Robertson Bay and Bowers terranes in NVL (Estrada et al., 2016; Paulsen et al., 2016). Reworking of older Taylor Group strata or direct erosion of Grenvillian basement units are less apparent in our data. Geochronological analysis of sandstones and conglomerates has revealed that the Grenvillian population is a very minor in Devonian strata (Savage, 2005; Gilmer, 2008; O'Toole, 2010; Elliot et al., 2015; Paulsen et al., 2017). The general high roundness of Grenvillian zircons, indicative of multiple reworking cycles (Zoleikhaei et al., 2016), is not consistent with a direct erosion of an inland Grenville igneous or metamorphic source (Cooper et al., 2011), which is restricted to only a few occurrences in NVL (Kim and Kim, 2019) and in CTAM (Goodge et al., 2010).

The zircon age population spanning 700-551 Ma is one of the most dominant in our samples. These ages can be linked to the evolution of the proto-Pacific margin of Gondwana during initial extensional rift-related processes and subsequent late Pan-African age or early-Ross contraction tectonics (Cawood, 2005; Cooper et al., 2011; Goodge et al., 2010, 2012; Goodge, 2020). Zircon grains of this age interval are documented in 590-565 Ma granitoid glacial erratics close to the Nimrod Glacier in the CTAM (Goodge et al., 2010, 2012; Goodge, 2020), as well as in granitoids and metamorphic rocks in the Koettlitz Glacier area of SVL (Hagen-Peter and Cottle, 2016). Zircon showing 700-551 Ma ages are also present in several Neoproterozoic and Cambro-Ordovician meta-sedimentary rocks of the Wilson, Bowers, and Robertson Bay terranes in NVL, the Skelton Group in SVL, the Beardmore and Byrd groups in CTAM, and the Swanson Formation in MBL (Pankhurst et al., 1998; Goodge et al., 2004a, 2004b, 2010, 2012; Wysoczanski and Allibone, 2004; Cooper et al., 2011; Yakymchuk et al., 2015; Estrada et al., 2016; Paulsen et al., 2016; Goodge, 2020). Moreover, Ross – Pan-African zircons widely occur in the upper units of the Devonian Taylor Group (Elliot et al., 2015; Paulsen et al., 2017). The rounded to sub-rounded grain shape is probably indicative of a polycyclic history (Zoleikhaei et al., 2016) and the main sources are most likely represented by both Cambro-Ordovician rocks (meta-sedimentary rocks of the Byrd Group, Robertson Bay, and Bowers terranes) and the Devonian strata of the Beacon Supergroup (e.g., Aztec Siltstone Formation). An additional secondary or minor contribution from Ross – Pan-African magmatic rocks not cropping out today, but possibly occurring in a subglacial unexposed inner belt on the inland side of the TAM in SVL needs to be taken in consideration.

Zircons dating 550-451 Ma are consistent with a direct and indirect provenance from the predominantly igneous rocks comprising the Ross Orogenic belt. This population is widely represented in the SVL diamictites with rounded to sub-rounded zircons, with a minor proportion of subhedral grains. The possible sources of these grains are the Granite Harbour Intrusive Complex, which was emplaced in SVL between 520 and 480 Ma, with a peak at 515-505 Ma (Hagen-Peter and Cottle, 2016; Allibone et al., 1993a, 1993b) and in particular, the Koettlitz Glacier Alkali Province, which represents an older suite of alkaline plutons emplaced in SVL between 550 and 530 Ma (Rowell et al., 1993; Hall et al., 1995; Encarnación and Grunow, 1996; Read et al., 2002; Cottle and Cooper, 2006; Cooper et al., 2011; Cox et al., 2012; Hagen-Peter and Cottle, 2016). Another possible source of the Ross age zircons are the Cambro-Ordovician meta-sedimentary successions occurring along the TAM, such as the Robertson Bay and Bowers terranes meta-sedimentary rocks in NVL (Estrada et al., 2016; Paulsen et al., 2016) and the Byrd Group in CTAM (Goodge et al., 2004a, 2004b; Goodge, 2020). A few published data suggest that the Swanson Formation in MBL is unlikely to be a possible source, owing to the near absence of Ross age grains (Pankhurst et al., 1998; Yakymchuk et al., 2015). Similarly, the Ross age population is not widely represented in the younger strata of the Devonian Beacon Supergroup sandstones, both in Dry Valleys and Beardmore Glacier areas (Elliot et al., 2015; Paulsen et al., 2017), whereas differently, the older Taylor Group strata (New Mountain and Altar Mountain formations) in SVL are dominated by this population (Savage, 2005; Gilmer, 2008). However, Permian glacial erosion involved only the Devonian uppermost formations such as the Aztec Siltstone and the Beacon Heights Orthoquartzite (McKelvey et al., 1977); no evidence of erosion of lower Taylor Group strata has been recorded, and these deposits can thus be excluded as source of Ross age grains. The most likely source of these zircons is therefore the Cambro-Ordovician meta-sedimentary rocks, together with the Devonian sandstones of the upper part of the Taylor Group and the plutons of the Granite Harbour Intrusive Complex.

Moreover, rare subhedral Silurian zircons grains were recorded in SVL samples. This age fits the time window of the Lachlan Orogeny of eastern Australia, and is recorded in the Robertson Bay Terrane and the Swanson Formation in MBL (Bradshaw et al., 1983; Bradshaw, 2007; Crispini et al., 2014). The moderate numbers of zircons recording the Ross Orogeny ages in SVL (520-480 Ma) indicates that either (i) this source was, to a large extent, not exposed during the early Permian deposition of the Metschel Tillite, or (ii) the catchment area of the glaciers did not extend into this source rock, which form most of the present TAM geology in SVL (Figure 2).

Four Devonian-Carboniferous zircons, with a peak at ca. 376 Ma have been recorded in the 22-01-15C3 sample from the Kennar Valley. Possible sources for these zircons are: i) the Admiralty Intrusives and the Gallipoli Volcanic Group in NVL, ii) the Ford Granodiorite and the Fosdick Migmatite-Granite Complex in MBL, and iii) unexposed equivalents. The Admiralty Intrusive Complex is a series of I-type granitoid plutons cropping out in the Wilson, Bowers, and Robertson Bay terranes in NVL. Geochronological dating indicates an intrusion age of 370-350 Ma (Vetter et al., 1983; Kreuzer et al., 1981, 1987; Fioretti et al., 1997; Henjes-Kunst and Kreuzer, 2003). Confined volcanic episodes occurred in relation to this magmatic activity; calc-alkaline volcanic rocks of the Gallipoli Volcanics, such as andesitic and dacitic lavas and welded rhyolitic ignimbrites, occur in the Wilson, Bowers, and Robertson Bay terranes in NVL (Grindley and Oliver, 1983; Stump, 1995). In the Wilson Terrane, rhyolites of the Gallipoli Volcanic Group were dated using Rb/Sr method to ca. 382 Ma (Grindley and Oliver, 1983), while at Mt Black Prince, K-Ar and Ar-Ar dating of biotite from the Gallipoli Volcanics gave an age of ca. 369 Ma (Henjes-Kunst and Kreuzer, 2003). During the Devonian, the Ross Province of MBL was also affected by magmatic activity; the Ford Granodiorite suite shows an U/Pb isotopic age of 375-345 Ma (Pankhurst et al., 1998; Yakymchuk et al., 2013, 2015), whereas zircons from the Fosdick Migmatite-Granite Complex yield ages of 370-335 Ma (Siddoway and Fanning, 2009; Korhonen et al., 2010). Only one grain (382±8 Ma) of this group shows a certain magmatic origin based on the Th/U ratio (Figure 8).

On the basis of paleo-ice flow directions (Isbell, 2010), the tillite composition of Kennar Valley should reflect the geology to the east of the TAM (Figure 11). This includes rocks adjacent to and beneath the Ross Sea, as well as MBL, a region geologically poorly constrained due to the extensive present-day ice cover (Pankhurst et al., 1998; Mukasa and Dalziel, 2000; Siddoway and Fanning, 2009; Yakymchuk et al., 2013, 2015; Jordan et al., 2020). The geology of the Ross Sea region, currently covered by Cenozoic glacial sediments, is largely unknown apart from indirect insights (Tinto et al., 2019) and a short core-log recovered by the DSDP_leg28 site 270 drillhole (Shipboard Scientific Party, 1975). The cored calc-silicate gneiss and marble were initially correlated with the Skelton Group of SVL on the base of lithology (Ford and Barrett, 1975) and later with the Bowers Terrane of NVL on the basis of the 437±6 Ma U-Pb ages of titanite (Mortimer et al., 2011). Interpretations of the DSDP_leg28 Site 270 basement core constrain the prolongation of the NVL terranes into the Ross Sea region (Mortimer et al., 2011).

The detrital zircon composition of the SVL diamictites, together with the roundness of the grains that indicate a polycyclic history (Zoleikhaei et al., 2016), appear to be mainly sourced from a mixing of reworked Devonian upper Taylor Group strata, Cambro-Ordovician meta-sedimentary rocks, Neoproterozoic metamorphic rocks, and subordinately from Granite Harbour Intrusive Complex granitoids. Devonian-Carboniferous ages, although rare, are of notable importance because they suggest the possible presence of Devonian-Carboniferous magmatic rocks in the glaciers' catchment area. Based on the known outcrops of these rocks, those zircons were sourced either from i) NVL, or ii) MBL, or iii) NVL or MBL extension in the current Ross Sea basin. The latter hypothesis constrains the extent in the Ross Sea of the Neoproterozoic metamorphic units (Skelton Group and Wilson Terrane), the Cambro-Ordovician meta-sedimentary strata (Bowers and Robertson Bay terranes and Swanson Formation), as well as the Devonian-Carboniferous magmatism, so far only constrained in NVL and MBL (Figure 11). The petrography of the diamictite matrix highlights the presence of scattered felsic volcanic clasts, which are possibly comparable with the volcanic rocks of the Gallipoli Volcanics (Barrett and McKelvey, 1981; Stump, 1995). Additionally, the petrography of the diamictite reveals clues suggesting the partial reworking of Taylor Group strata, as well as the lithology of pebbles and cobbles indicates the predominance of metamorphic source rocks, although these experienced prolonged reworking based on their sub-rounded shape.

The source rocks comprising the Elkhorn Ridge diamictite in the Convoy Range are the same or similar to those discussed for the Kennar Valley diamictite. A SSE provenance from SVL and/or from MBL, including a local reworking of the Devonian Beacon Supergroup strata, seems likely (Figure 11).

2.6.2.2. Thern Promontory (NVL)

The sample 04-01-15C10 shows different detrital zircon age populations with respect to the SVL samples. The source of zircons older than 550 Ma is likely the Neoproterozoic to Cambro-Ordovician metamorphic rocks of the Ross Supergroup (Henjes-Kunst et al., 2004; Estrada et al., 2016; Paulsen et al., 2016), which represent the local regional basement in the proposed catchment area of the diamictites (Skinner and Ricker, 1968; Casnedi et al., 2012; Pertusati et al., 2012).

The Ross age zircons (550-451 Ma), which comprise the largest population, are predominantly sourced from the plutons of the Cambro-Ordovician Granite Harbour Intrusive Complex cropping out in the Eisenhower Range (Skinner and Ricker, 1968; Casnedi et al., 2012; Pertusati et al., 2012). The diamictite-basement contact in the studied outcrop is covered by ice (Figure 4 and Figure 6). However, Skinner and Ricker (1968) mapped the granitoid rocks in the area as the Larsen Granodiorite and the Irizar Granite. The age spectrum analysis indicates a low detrital zircon age variability, in accordance with petrographic data. The Irizar Granite is a pink, non-porphyritic, coarse grained granite (Skinner and Ricker, 1968). In the type locality of Cape Irizar, the granite shows $^{206}Pb/^{238}U$ ages comprised 450±1 Ma and 497±2 Ma and a $^{207}Pb/^{206}Pb$ age of 490±4 Ma (Rocchi et al., 2009). Moreover, the macroscopic analysis of the diamictite clast composition reveals that most of the pebbles are made up of pink medium/coarse grained granitoid rocks (sub-rounded to sub-angular pebbles) and few pebbles of metamorphic rocks (rounded to sub-rounded). The low variability in the clast composition indicates a local source for this diamictite and further suggests that the diamictite formed by a glacier with a limited catchment area.

2.6.2.3. Mt. Nansen (NVL)

The sample collected near Mt. Nansen (22-11-15C5) in the Eisenhower Range (NVL) shows a very different detrital zircon spectrum compared to that of the sample in the Thern Promontory sequence. It also differs to samples from SVL, with a wide range of age populations. The source of the Paleoproterozoic zircons (2500-1601 Ma), which are mainly rounded to sub-rounded, is probably the Neoproterozoic-Cambrian metamorphic rocks, which constitute most of the Wilson Terrane. In particular, quartzites of both the

Priestley Formation and Rennick Schist show quite similar age spectra, both in the age of peaks and abundance of most age populations. Elsner et al. (2013) proposed that the Paleoproterozoic population in the Triassic sandstones could be sourced both from East Antarctica and from western terranes.

Grenville age zircons (1300-901 Ma), as well as the Paleoproterozoic populations, imply contribution from the Neoproterozoic-Cambrian metamorphic units constituting the Wilson Terrane, which shows the same age range (Estrada et al., 2016; Paulsen et al., 2016). Bowers and Robertson Bay terranes meta-sedimentary rocks could be potential sources. However, no local sources of those units are present. The direct erosion of Grenvillian age units (Cooper et al., 2011), as recorded in another outcrop in NVL (Kim and Kim, 2019) and in the CTAM (Goodge et al., 2010), is less likely as testify by the high roundness of grains.

The Ross – Pan-African grains (700-551 Ma) were probably sourced from Neoproterozoic to Cambro-Ordovician metamorphic units; this population comprises 5-20% of total grains in these units (Estrada et al., 2016; Paulsen et al., 2016). An alternative source of this population could be the plutons emplaced along the TAM in the initial stages of the Ross Orogeny (Goodge, 2002, 2020,; Goodge et al., 2004a, 2004b, 2012; Hagen-Peter and Cottle, 2016; Hagen-Peter et al., 2016).

The source of the Ross age zircons (550-451 Ma) is uncertain because they can be provided by the Neoproterozoic-Cambrian Wilson Group (Paulsen et al., 2016) and/or by local Cambro-Ordovician Granite Harbour Intrusive Complex plutons (Irizar Granite and Larsen Granodiorite plutons) with comparable ages (Skinner and Ricker, 1968; Rocchi et al., 2009; Casnedi et al., 2012; Pertusati et al., 2012). Elsner et al. (2013) showed two important peaks at ca. 600 Ma and ca. 1100-1000 Ma revealed by samples from the Triassic-Jurassic sandstones of the Section Peak Formation, similarly to the here recorded data for the stratigraphically underlying Mt. Nansen diamictite, indicating at least a partially similar provenance for the Permian tillite and the overlying Mesozoic fluvial sandstones of the NVL.

Whereas the diamictite sample shows a wide isotopic age distribution, the clastic source seems to be quite restricted to the metamorphic rocks of the Wilson Terrane. In particular, the quartzites of the Priestley Formation and the Rennick Schist are the most probable source rocks for the diamictite because of their similar zircon U-Pb age spectra (Estrada et al., 2016; Paulsen et al., 2016). Moreover, petrographic analysis of the diamictite shows the predominance of quartz grains and the few lithic fragments are mainly made up of quartzites and minor granitoids and phyllites/schists. However, the local basement, lying just below the diamictite is constituted by low-grade meta-sedimentary fine-grained strata, intruded by Granite Harbour Intrusive Complex plutons.

2.6.3. Glacial Extent and Regional Inferences

The extent of the ice cap which led to the deposition of the Metschel Tillite in SVL, namely SVL ice cap, is unknown. The small thickness of the diamictite is not consistent with large-scale ice cover, but large-scale glaciotectonic structures at Mount Ritchie and Kennar Valley (Isbell, 2010) were produced by a significant ice cover. Moreover, the almost identical petrographic and geochronological composition of the Metschel Tillite at Kennar Valley and Elkhorn Ridge indicates a wide and homogeneous catchment basin of the ice cover that produced those tillites. The geochronological assemblage of the Metschel Tillite is, however, different from the Pagoda Formation (Elliot et al., 2015), indicating that the formation was probably sourced from at least two different catchment areas (Figure 11). The presence of an ice center situated on the interior East Antarctica (Figure 11) flowing eastward (Fielding et al., 2008c; Isbell et al., 2012) is not well constrained on the basis of the geochronological and petrographic composition carried out by this study; however, Isbell (2010) recorded evidence of glacio-tectonic structures indicating eastward ice flow in two localities of SVL.

The features of the LPIA deposits in the Eisenhower Range suggest a motif of land-terminating ice covers, with a restricted catchment area (Figure 11). Such tillites show no compositional or sedimentological link or affinity with the southern Metschel Tillite, which was deposited in a glacio-marine environment (Isbell, 2010) by the SVL ice cap that had completely different catchment area (Figure 11). The glacio-continental environment suggested for the Eisenhower Range diamictites is comparable with the NVL diamictites of Lanterman Formation in the Rennick Glacier area, deposited in a glacio-lacustrine and glacio-fluvial settings (Cornamusini et al., 2017). Preliminary provenance studies of NVL tillites in the Lanterman Range (Cornamusini et al., 2017) and Neall Massif (Collinson et al., 1986) indicate generalized paleo-ice flow directions toward N-NW, even though the overlying Permian-Triassic sandstones indicate paleocurrent directions towards W-SW (Schöner and John, 2014). The NVL data are in contrast with those of the Metschel Tillite in SVL, where provenance data indicate a main west-directed ice movement, oblique-transversal with respect to the current orientation of the TAM (Isbell, 2010).

This study highlights the differences between SVL and NVL, which is consistent with the view that the LPIA glaciation was characterized by multiple and diachronous ice centers across Gondwana (Isbell et al., 2003, 2008a, 2012; Fielding et al., 2008b; Isbell, 2010; Koch and Isbell, 2013; Cornamusini et al., 2017). The SVL ice cap (Figure 11) led to the deposition of the Metschel Tillite in a possible glacio-marine setting (Isbell, 2010), which has a detrital zircon assemblage only partially comparable with that of the Pagoda Formation in the CTAM (Elliot et al., 2015). Differently, the Eisenhower Range tillites record deposition in a continental environment as revealed by facies analysis, and also conceivable by the focused compositional and geochronological assemblage. This differences in the depositional environment highlight that the Transantarctic Basin closed north of the Convoy Range in the late Carboniferous/early Permian, where the Metschel Tillite is thinner than the southernmost SVL but contains a comparable geochronological and compositional assemblage. Northwards, thicker glacial sequences are recovered in the Lanterman Range (Collinson et al., 1986; Cornamusini et al., 2017) and Neall Massif (Collinson et al., 1986), where an ice cover, probably extending to Tasmania (NVL-Tas ice cap) led to the deposition of the Lanterman

Formation in NVL (Cornamusini et al., 2017). The Lanterman Formation contains evidence for north to north-westward paleo-ice flow directions (Cornamusini et al., 2017), towards the Tasman Basin, where the deposition of the Wynyard Tillite, and its correlative, occurred in a glacio-marine environment during the Pennsylvanian to Asselian (Fielding et al., 2010; Henry et al., 2012; Reid et al., 2014). However, the sediment thickness of Tasman tillites (ranging from 0 to 550 m; Reid et al., 2014 and references therein) is not compatible with a small ice center; it was probably related to a wide ice cover, even if Tasman tillites also show high reduction in thickness and bottom irregularity (Henry et al., 2012; Reid et al., 2014). Despite inhomogeneities due to local conditions, the generalized northward paleo-ice flow directions of the Tasman tillite (Reid et al., 2014) (Figure 11), is consistent with a source from the NVL-Tas ice cap centered in NVL and the northern Ross Sea (Figure 11). The NVL-Tas ice cap was subaerial in NVL with glaciers occupying valleys; in contrast, its Tasman Basin front developed in a fjordal glacio-marine setting. A present-day analogy could be represented by the Greenland Ice Cap with its terminus located in both fjordal glacimarine and continental settings.

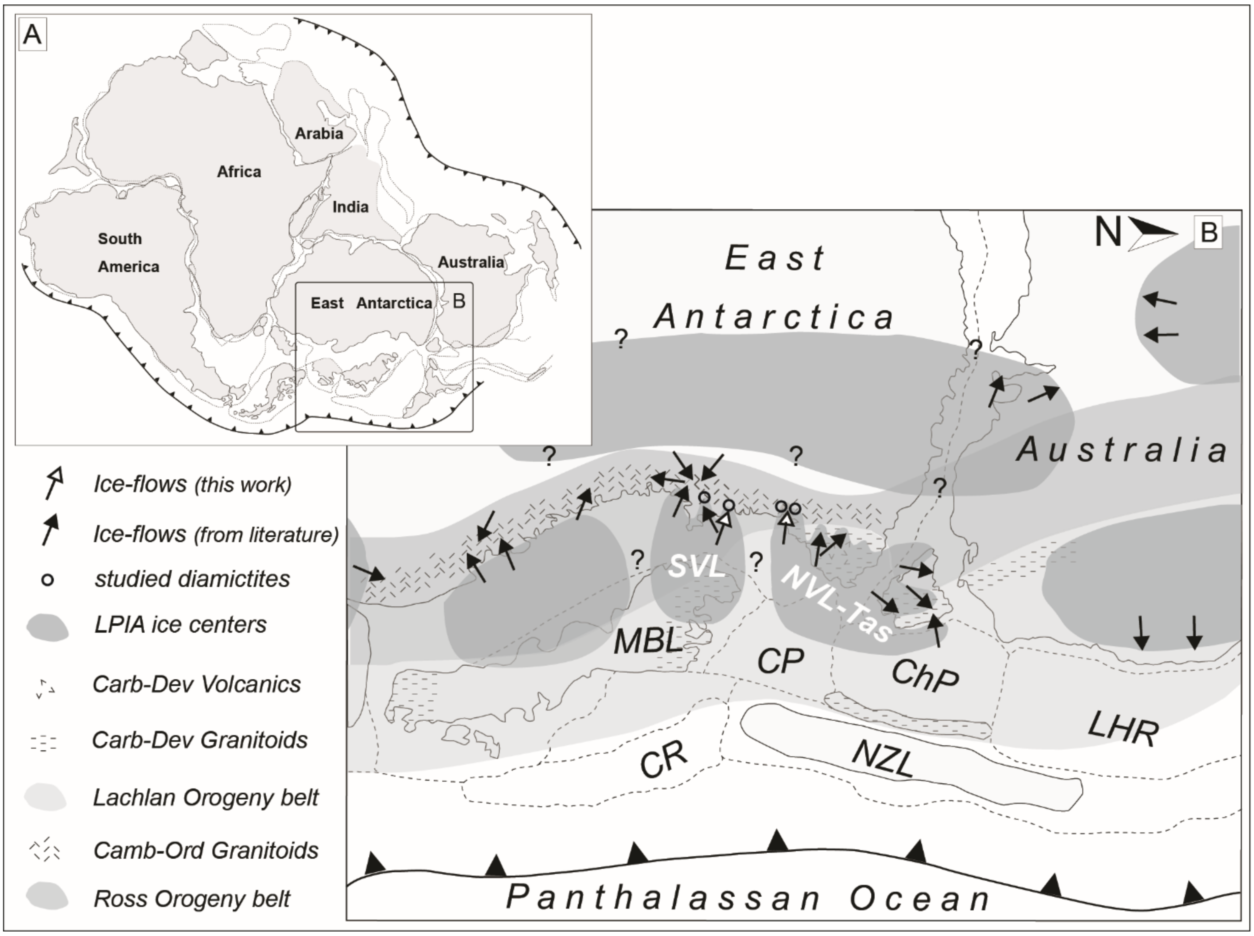

Figure 11. (A) Gondwana assemblage during the Late Paleozoic Ice Age (after Sirevaag et al., 2018). (B) Reconstruction of the Late Paleozoic Ice Age setting during the early Permian in the southern Gondwana sector. Continental block assemblage and orogenic belts are modified from Elliot and Fanning (2008) and Elliot (2013); ChP: Challenge Plateau; CR: Chatham Rise; CP: Campbell Plateau; LHR: Lord Howe Rise; MBL: Marie Byrd Land; NZL: New Zealand. Ice flow directions are after Barrett and McKelvey

(1981); Barrett (1991); Collinson et al. (1994); Isbell et al. (1997, 2012); Fielding et al. (2008a, 2008b); Isbell (2010); Reid et al. (2014); Cornamusini et al. (2017); Craddock et al. (2019). Ice extension in eastern Australia is after Fielding et al. (2008a).

2.7. Conclusion

This study focuses on the geochronological, petrographic, and sedimentological characterization of less understood Late Paleozoic Ice Age diamictites in southern and northern Victoria Land (Antarctica), to establish the regional paleo-geographical interpretation to compare with CTAM and Tasman glacial basins.

Large differences in the geochronological-petrographic composition and in depositional settings are apparent between these glaciogenic sequences. The SVL Metschel Tillite was deposited by the SVL ice cap in a sub-glacial to ice-distal marine environment. No evidence of this type of deposition occurred in the Eisenhower Range diamictites in NVL which was characterized by glacio-continental conditions, accordingly to the diamictite of the Lanterman Formation in the Rennick Glacier area.

Detrital zircon ages and petrographic composition of the two Eisenhower Range diamictites in NVL, indicate a clear difference in the source of these deposits. The Thern Promontory diamictite was mainly sourced from the local plutons of the Granite Harbour Intrusive Complex, whereas the main source of the Mount Nansen diamictite most likely was the metamorphic rocks of the Wilson Terrane. In contrast, U-Pb age determinations of detrital zircons reveal that the Metschel Tillite of SVL was mainly sourced from the reworking of Devonian Beacon Supergroup sandstones, the Neoproterozoic-early Paleozoic metamorphic basement rocks, and granitoids of the Cambro-Ordovician Granite Harbour Intrusive Complex. The small Carboniferous-Devonian population implies that ice catchment includes rocks of this age, which are currently reported in NVL and Marie Byrd Land. Compositional characterization carried out by this study in conjunction with previous work on paleo-ice flow directions, reveal that the most probable source region of the Metschel Tillite is the area east of the current Transantarctic Mountains, i.e., the present-day Ross Sea (Figure 11). This points to the occurrence of Cambro-Ordovician meta-sedimentary rocks, which constitute the Bowers and Robertson Bay terranes in NVL, the Byrd Group in CTAM, and the Swanson Formation in MBL, forming basement beneath the present-day Ross Sea. Moreover, Carboniferous-Devonian magmatic rocks, referred to the Admiralty Intrusives and Gallipoli Volcanics in NVL and Ford Granodiorite in MBL, are also likely to be present beneath the Ross Sea. The tillite compositional patterns linked with source areas, and the stratigraphic-sedimentological features support the emerging view of a LPIA characterized by discrete ice centers developing in the southern sector of the Gondwana. The SVL ice cap deposited the Metschel Tillite while the NVL-Tas ice cap is responsible of the glaciogenic sediments in NVL and Tasmania with continental and coastal marine settings respectively.

3. Provenance of Cenozoic glacial sediments in the Central Ross Sea (Antarctica): insights from IODP_exp374 and DSDP_leg28 drillcores

3.1. Overview

In this chapter the Cenozoic glaciogenic sediments and rocks were analyzed, applying petrographic methods on gravel size clasts recovered from drillcores in the Ross Sea. The IODP Site U1521 clasts distribution data were jointed with geochemical, geochronological, and palynological data obtained by the other IODP Expedition 374 scientists in a paper published in Volume 600, Number 7889, pages 450-455 of Nature (Marschalek et al., 2021); detailed data report of petrological and minero-geochemical analyses were published as chapter in the chapter in the Ross Sea West Antarctic Ice Sheet History - Proceedings of the International Ocean Discovery Program, 374 (Zurli et al., 2022b). IODP Site U1522 data presented here will be joined with geochronological and geochemical data (Mallery et al., in prep.). DSDP Site 270 data presented here will be joined with geochronological and thermochronological data (Olivetti et al., in prep.). Luca Zurli performed clast counts, petrographic characterization, and mineral chemistry analyses.

3.2. Introduction

During Cenozoic Antarctica was settled in polar latitude, allowing formation of glacial covers during cold phases (Figure 12). In the Phanerozoic (Mesozoic to Cenozoic), extensive ice made its appearance in Antarctica during the late Eocene with mountain glaciers (Rose et al., 2013), while continental-scale glaciation started after the Eocene-Oligocene Transition (EOT; ca. 34 Ma; Miller et al., 1991; Zachos et al., 1992), coincident with CO_2 concentration felt below 750 ppm (Galeotti et al., 2016).

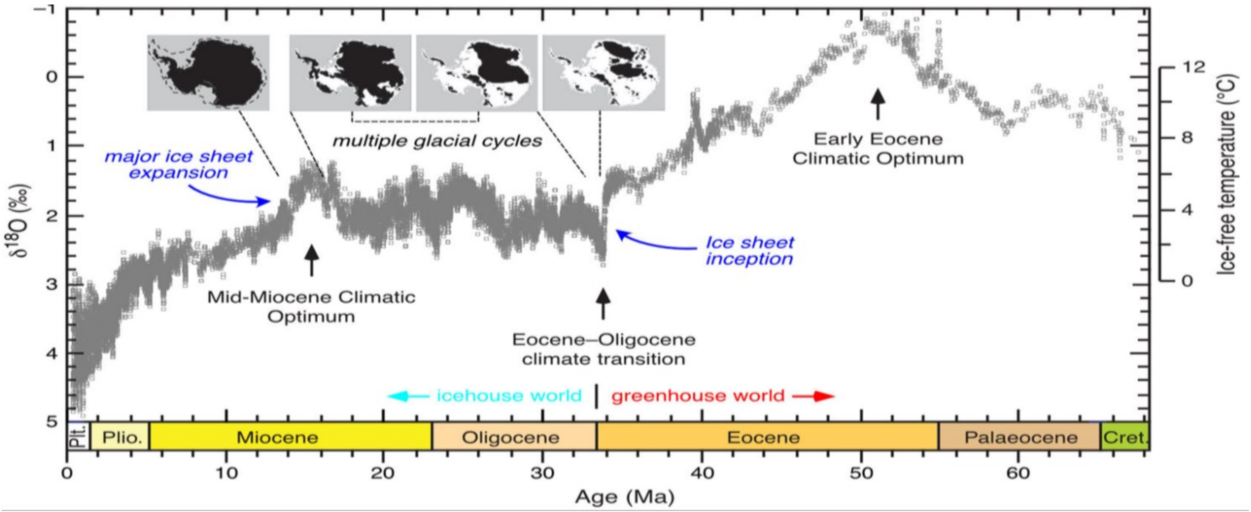

Figure 12 δ¹⁸O and temperature variations in the Cenozoic (from Paxman, 2021 and reference therein).

Since ca. 32.8 Ma a stable, continental-scale ice sheet developed in Antarctica and reached the Ross Sea coast and the expansion was revealed in the Cape Roberts Project (CRP) drillcores (Galeotti et al., 2016). During the Oligocene and Miocene, the Antarctic ice expanded and retreated (Gasson and Keisling, 2020), mainly driven by orbital and climate forcing (Levy et al., 2016, 2019). The Miocene was characterized by wide fluctuations of CO_2 and ^{18}O concentration, that emphasized variations in the atmospheric and ocean temperatures; in warmest periods, usually associated with high CO_2 concentration (> 500 ppm), ice sheets retreated and vegetation grew in the Antarctic coasts, while in the coldest intervals, usually when CO_2 was lower than 300 ppm, ice sheets advanced across continental shelves (Levy et al., 2016). The Middle Miocene Climate Optimum (MMCO) was the most intensive and long warm period in the Miocene, when Antarctic ice sheets strongly retreated (Warny et al., 2009; Lear et al., 2010; Feakins et al., 2012; Levy et al., 2016; Pierce et al., 2017; Sangiorgi et al., 2018). After the MMCO, the Middle Miocene Climate Transition (MMCT) marked an expansion of ice sheets, which became more stable (Shevenell et al., 2004, 2008; Holbourn et al., 2005; Lewis et al., 2008), whereas warm period, and then ice retreat, occurred during the middle Miocene and the Pleistocene (Gasson and Keisling, 2020).

The reconstruction of the changes that involved the Antarctic ice sheets in the past, help predictions of their future behavior under climate changes and of the contribution that Antarctic ice masses loss could provide to sea level rise (Masson-Delmotte et al., 2013; Kennicutt et al., 2015). First studies of Cenozoic paleo-climate evolution of Antarctica using sediment cores started in the 70's with the DSDP_leg28 cruise (Shipboard Scientific Party, 1975), and intensified later with CIROS Project (Barrett, 1989), ODP_leg119 (Hambrey et al., 1991), Cape Roberts Project (CRP; Cape Roberts Science Team, 1998a, 1998b, 2000b, 2000a), and Antarctic DRILLing project (ANDRILL) (Naish et al., 2007; Harwood et al., 2009). However, first occurrence of marine-based West Antarctic Ice Sheet (WAIS) is still strongly debated (Paxman, 2021). IODP Expedition 374 aims to understand the past behavior, and the ocean-ice interaction of the WAIS during Neogene and Quaternary (McKay et al., 2019). In this scenario, provenance study of gravel size glacially transported clasts aims to evaluate the source region of them, and therefore the paleo-ice flows pattern, and its changes throughout time, that could reflect changes in the glacial setting in response to climate and orbital forcing. The petrographic approach on gravel was previously successfully adopted in the coastal drillholes of the Ross Sea and onshore (Cape Roberts Science Team, 1998b, 1998a; Talarico and Sandroni, 1998, 2009, 2011; Talarico et al., 2000; Sandroni and Talarico, 2001, 2011; Cornamusini and Talarico, 2016; Perotti et al., 2017, 2018).

In this thesis, gravel size clasts from three drillholes (IODP Site U1521, Site U1522 and DSDP Site 270) in the Central Ross Sea (Figure 13) were analyzed from a petrographic point of view.

The studied sediments span in age from Oligocene to Pliocene and they recorded the major climatic changes throughout the Cenozoic.

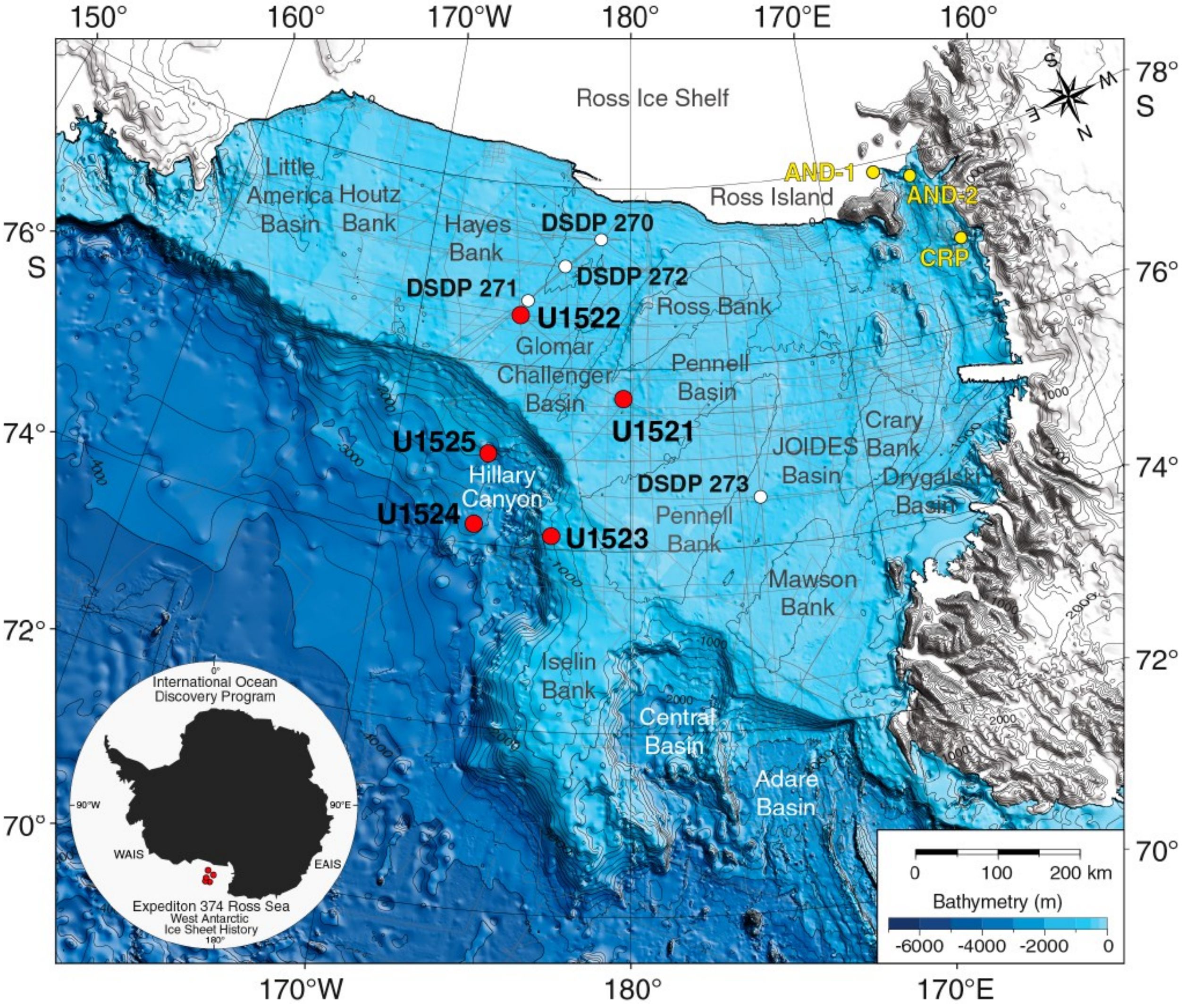

Figure 13 Map of the Ross Sea with reported location of the main drilling sites of IODP Expedition 374, DSDP leg 28, ANDRILL, and Cape Roberts Project (CRP; McKay et al., 2019)

3.3. Geological Setting and Regional Stratigraphy

3.3.1. Basement Geology

The Antarctic continent is constituted by old cratons, limited to East Antarctica, and younger orogenic belts that encircle the shields (Figure 14; Kleinschmidt, 2021). The Ross Sea is an expression of the West Antarctic Rift System (WARS), a sector of thinned crust, associated with active volcanism, dividing East and West Antarctica since Cretaceous (Siddoway, 2021 and reference therein). The Ross Sea Embayment is bordered by the Transantarctic Mountains to the West and the Marie Byrd Land to the East. These regions are geologically well differentiated, and they are deeply described separately in the following sub-chapters.

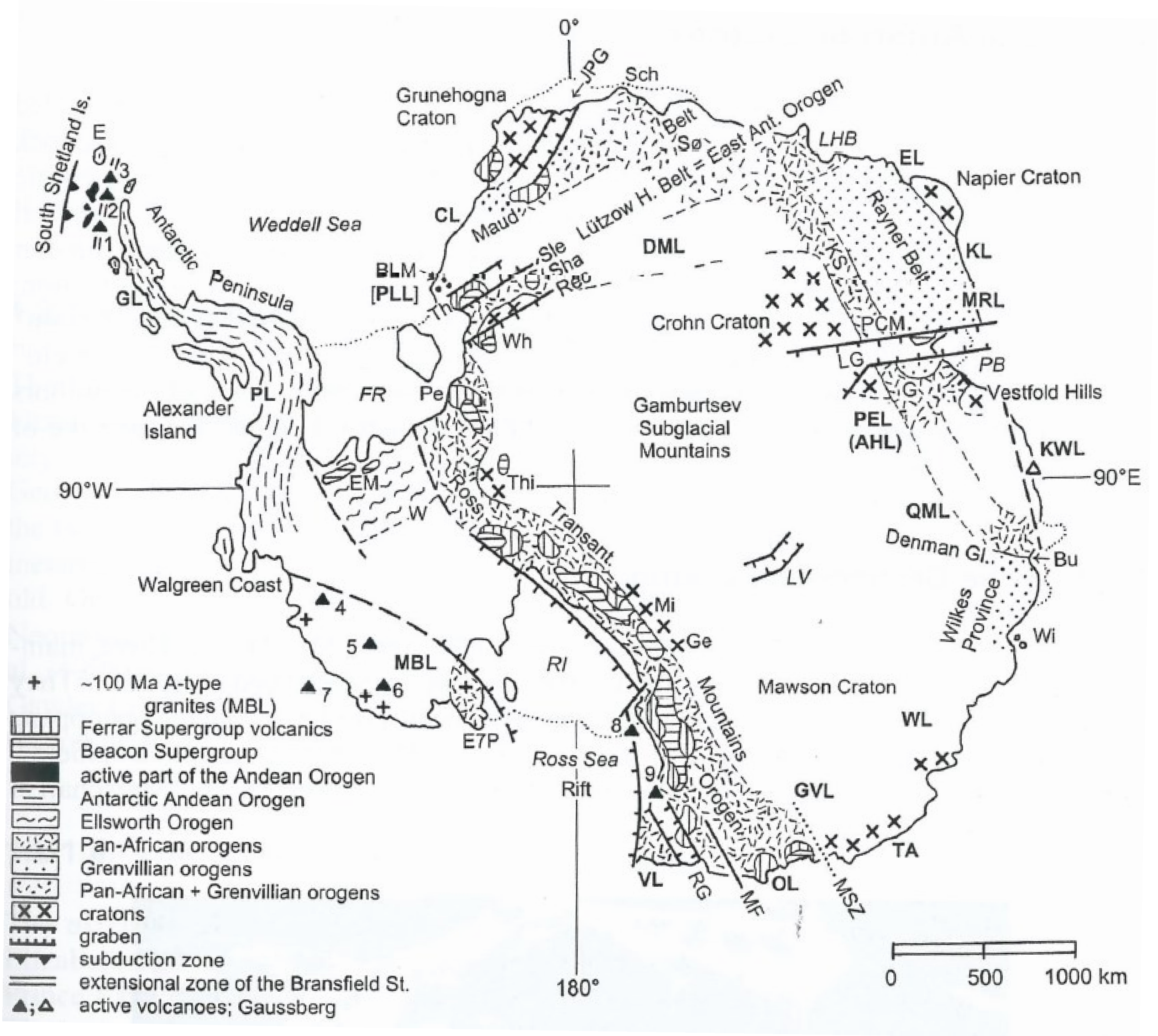

Figure 14 Schematic geological map of Antarctica (from Kleinschmidt, 2021)

3.3.1.1. Transantarctic Mountains

The Transantarctic Mountains (TAM) are a mountain belt that extend over 3000 Km from northern Victoria Land (NVL) to the Weddell Sea and they physiographically divide East and West Antarctica. The TAM uplift is related with the development of the WARS that led the crustal thinning and the widening of the Ross Sea basins. Thermochronological studies revealed that TAM experienced episodic and localized uplift events (Olivetti et al., 2018) from the Cretaceous through the Cenozoic (Fitzgerald, 2002 and reference therein; Olivetti et al., 2018).

Rock units exposed along the TAM (Figure 15) record the geological evolution of the continent from the Precambrian to the Holocene (Figure 16).

The oldest geological unit recognized is represented by portions of the Mawson Craton, one of the cratons that constitute East Antarctica, that crops out in the Geologists and Miller ranges in the upper Nimrod Glacier. The metamorphic rock of the Nimrod Group (Goodge and Fanning, 2016) recorded Mesoarchean magmatic events, magmatism and metamorphism during the Nimrod Orogeny (Figure 16; ca. 1700 Ma), and metamorphic overprint during the Ross Orogeny in the Neoproterozoic-Ordovician (Goodge, 2020). Lithologically, the Nimrod Group is upper-amphibolite to lower-granulite facies interlayering of schist, quartzite, amphibolite, banded quartz-feldspatic to mafic gneiss, granitic to gabbroid orthogneiss, calc-silicate gneiss, migmatite, and eclogite (Grindley et al., 1964; Grindley, 1972; Goodge et al., 1991, 1993; Goodge and Peacock, 1995; Stump, 1995). These rocks experienced a medium to high metamorphic grade (kyanite-zone mineral assemblage) during the Ross Orogeny (Grindley, 1972; Goodge et al., 1992; Goodge, 2007).

During the Neoproterozoic sedimentary successions were deposited, locally associated with magmatism, in the passive margin of Gondwana (Figure 16); these successions constitute part of the Wilson Group (Priestley Formation and Rennick Schist) in NVL, the Skelton Group in SVL, and the Beardmore Group (Cobham and inboard Goldie formations) in central and southern TAM (Goodge, 2020 and reference therein). The sedimentary protoliths, consisting of greywacke, shale, sandstone, and limestone, were affected by metamorphism during the Ross Orogeny. While in northern and southern Victoria Land the metamorphism varies from greenschist to granulite facies, the Beardmore Group experienced the regional low-grade metamorphism (Stump, 1995 and reference therein; Goodge, 2020 and reference therein).

Above the Neoproterozoic (meta-)sedimentary and magmatic units unconformably lie the Cambrian-Ordovician meta-sediments, which were deposited in the active margin of Gondwana (Figure 16) and then weakly affected by the Ross Orogeny deformation (Goodge, 2020 and reference therein). In NVL Cambrian syn-orogenic siliciclastic sequences, metamorphosed during the Ross Orogeny, constitute part of the Wilson Terrane, while the Bowers Terrane is characterized by weakly metamorphosed volcanic, volcanoclastic, and siliciclastic; the Robertson Bay Terrane is therefore constituted by Cambrian-

Ordovician siliciclastic strata, metamorphosed up to greenschist facies (Goodge, 2020 and reference therein). The early Paleozoic rocks in the CTAM constitute the Byrd Group. Between Byrd and Nimrod glaciers the Lower Cambrian Shackleton Limestone, a mainly carbonate platform with interbedded meta-siliciclastic units, crops out (Stump, 1995 and reference therein; Goodge, 2020 and reference therein). Carbonates are unconformably overlay by clastic sequences that constitute the Douglas Conglomerate (mainly made up of Shackleton Limestone clasts) and the weakly metamorphosed Starshot, Dick and outboard Goldie formations (Stump, 1995; Goodge, 2020). Southward, in the Shackleton Glacier area, the early Paleozoic rocks are the undated siliciclastic Greenlee Formation, probably correlative of the Starshot Formation of the Byrd Group (Goodge, 2020 and reference therein), the Middle Cambrian Taylor Formation is made up of ashfall and pyroclastic tuff, felsic and mafic volcanic rocks and limestone, and the Henson Marble. In the southern Transantarctic Mountains (STAM), the Lower Paleozoic units are the siliciclastic meta-sediments of the La Gorce and Duncan formations and the felsic volcanic rocks of the Liv Group, which is widely diffused in the region. The siliciclastic formations are greywacke, mudstone and siltstone with a low-grade metamorphic overprint (Stump, 1995). The Cambrian Liv Group rocks are quartz- and plagioclase phyric dacitic porphyries, basalts and rhyolites (Borg, 1980; Stump, 1995; Goodge, 2020).

The Ross-Delamerian Orogeny affected the proto-Pacific margin of Gondwana from at least 615 Ma to ca. 470 Ma (Figure 16; Goodge, 2020); the orogenic mechanism led to the emplacement of large granitic batholiths that are currently exposed along the TAM (Figure 15) and they constitute the Granite Harbour Intrusive Complex (GHIC). Most of the intrusions are calc-alkaline and mainly took place between 520 and 480 Ma, whereas older alkaline suites (i.e., Koettlitz Alkali Suite) emplaced in SVL between 550 and 530 Ma (Goodge, 2020 and reference therein). In the STAM the intrusive bodies are associated with widespread coeval felsic volcanic rocks (Van Schmus et al., 1997; Encarnación et al., 1999; Wareham et al., 2001). Intrusive rocks vary from isotropic to foliated, biotite ± hornblende granite, granodiorite, and tonalite (Stump, 1995 and reference therein).

After the orogenic phase, the proto-Pacific margin of Gondwana, that occupied equatorial to sub-tropical paleolatitudes (Torsvik and Cocks, 2017) was affected by a prolonged erosion interval, that generates a low-relief regional-scale erosion surface, named Kukri Erosion Surface (Barrett, 1991). Above that lies the Devonian to Jurassic Beacon Supergroup (Figure 16), a thick siliciclastic sedimentary sequence deposited in the Gondwana basins (Barrett, 1991). The Beacon Supergroup is divided in the Devonian Taylor Group, mainly constituted by quartzose sandstone to mudstone, and the Permian to Jurassic Victoria Group, that includes diamictite, quartzo-feldspatic sandstone, quartz-arenite, mudstone, coal, and volcanoclastic sandstone (Barrett, 1991 and reference therein).

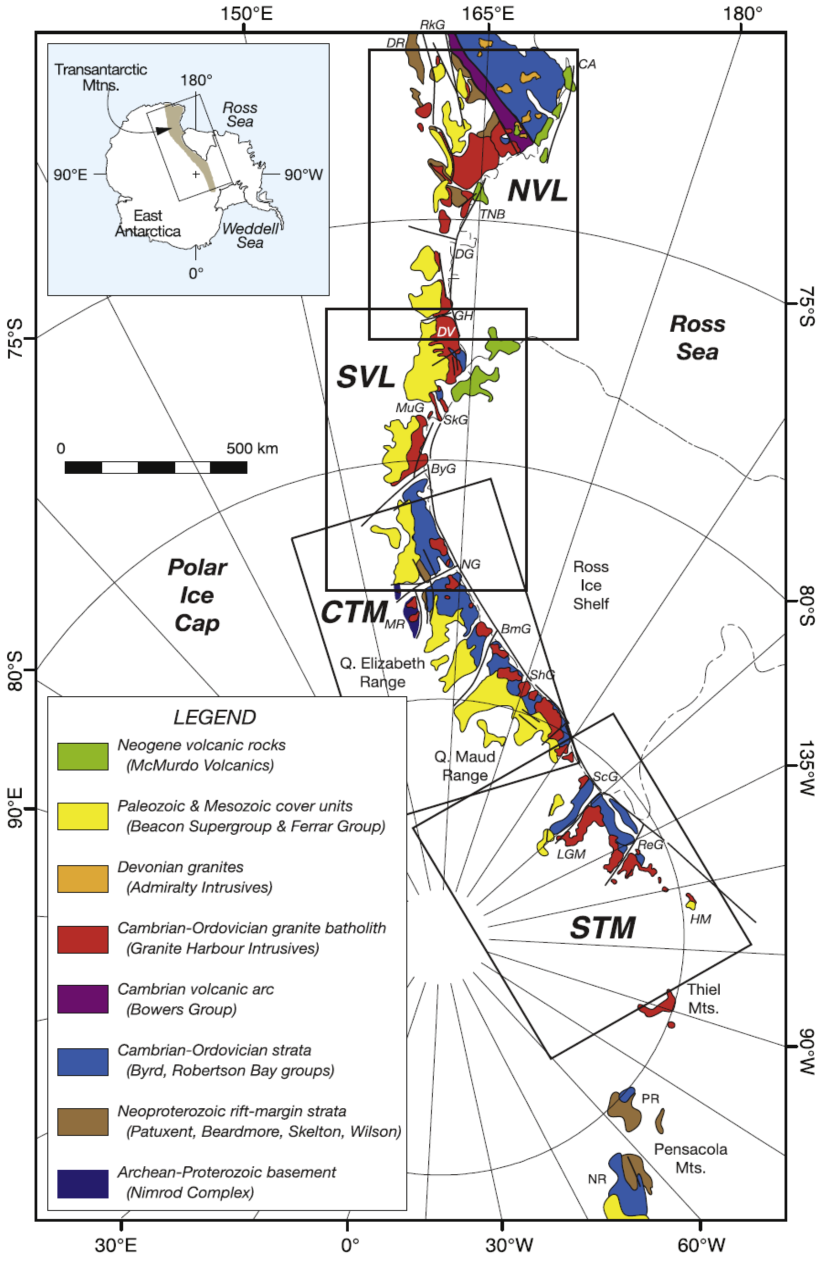

Figure 15 Simplified geological map of the Transantarctic Mountains (from American Geographical Society, 1969; Goodge, 2020)

In the late Devonian to early Carboniferous the proto-Pacific margin of Gondwana was affected by magmatism (Figure 16), that was explicit in the Admiralty Intrusive Complex and volcanism of the Gallipoli Volcanics of NVL (Stump, 1995) and Ford Granodiorite in MBL (see 3.3.1.2). The Beacon Supergroup strata, and minorly the crystalline basement, were intruded by sills and dikes of the Ferrar Group in the Jurassic, linked with the Gondwana breakup (Figure 16). Sills are tholeiitic dolerite, and their thickness widely vary from less than 1 m to hundreds of meters (Elliot and Fleming, 2008). Sub-volcanic magmatism was also associated with large effusions of tholeiitic basalt (Kirkpatrick Basalt) in the Gondwana basins (Elliot and Fleming, 2008).

Furthermore, since latest Oligocene (Figure 16), linked with the WARS development, portions of the TAM were affected by alkaline basaltic volcanism, expressed by the McMurdo Volcanic Group. Volcanic centers are mainly located in southern and northern Victoria Land coasts, whereas small edifices occur in the Queen Maud Mountains (STAM; Smellie et al., 2021 and reference therein).

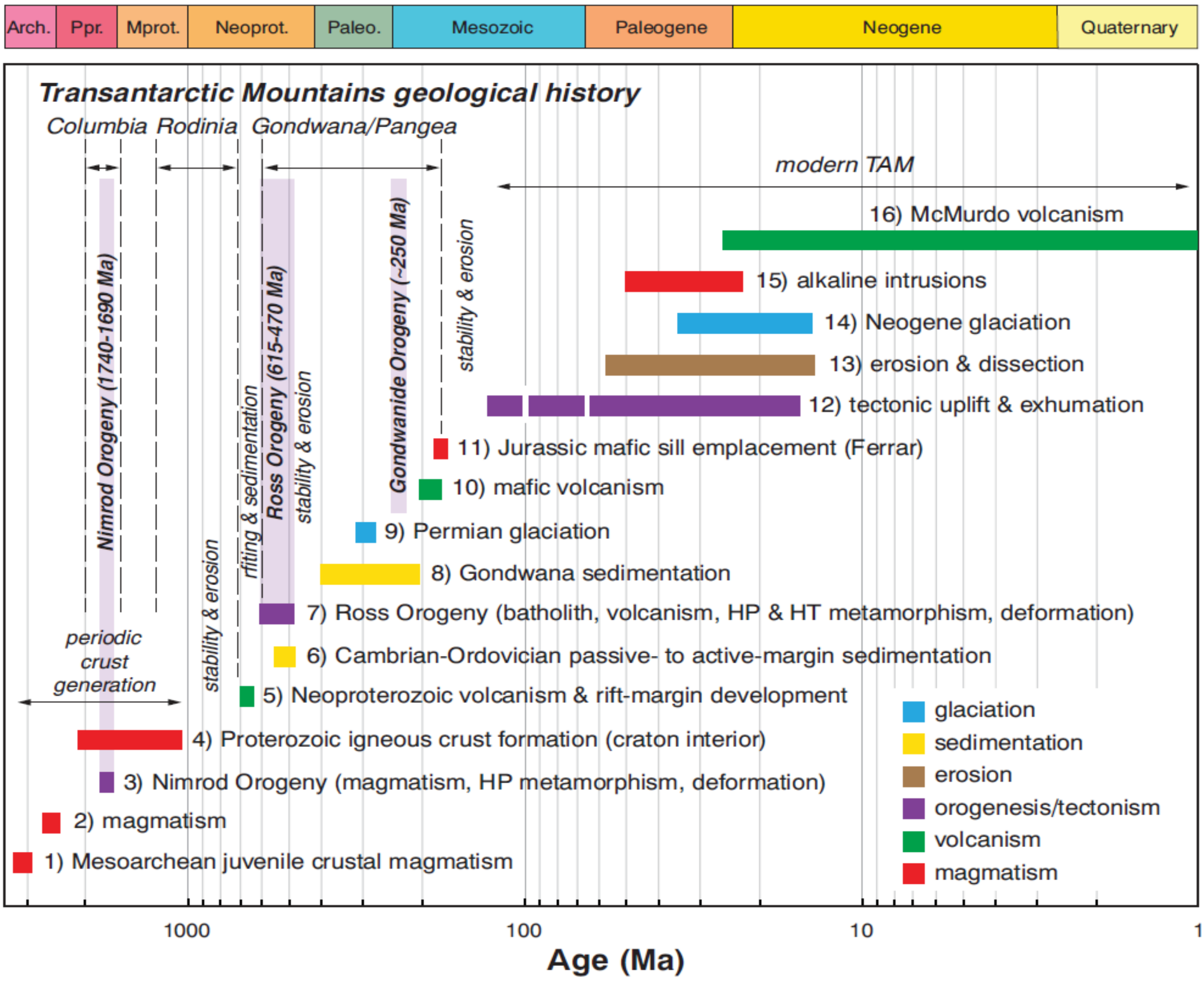

Figure 16 Timeline of the major geological events that involved the Transantarctic Mountains (from Goodge, 2020)

3.3.1.2. West Antarctica

West Antarctica can be divided in three separate physiographic regions (Jordan et al., 2020); in this thesis the Ross Sea region (Figure 17), comprising Marie Byrd Land (MBL) and the WARS, is taken into account. The best rock exposures are limited to the Marie Byrd Land coast (Figure 17), although the geological knowledge is poor due to the large ice cover and the limited accessibility for scientists.

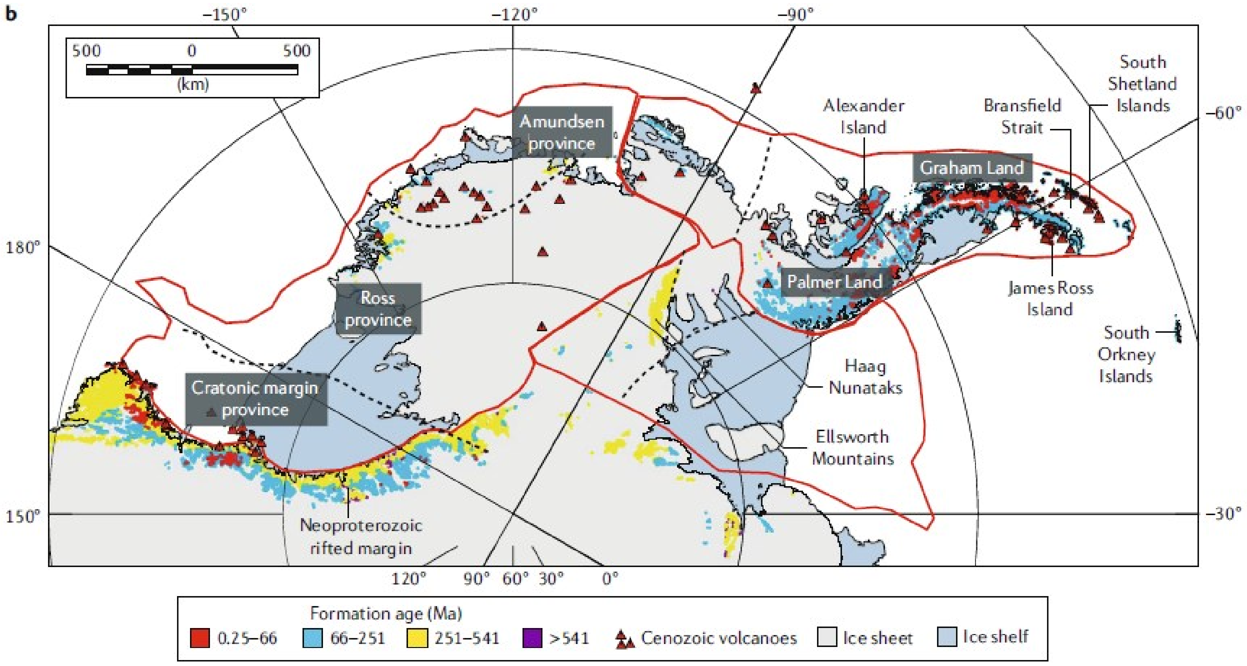

Figure 17 Simplified geological map of West Antarctica with indicated the provinces (modified from Jordan et al., 2020)

Rocks constituting MBL ranges from early Paleozoic to Cenozoic. The oldest rock units are represented by the Cambrian-Ordovician meta-sedimentary rocks of the Swanson Formation (Bradshaw et al., 1983; Adams, 1986). The sedimentary protoliths are turbidites deposited during the Ross-Delamerian Orogeny in the proto-Pacific margin of Gondwana, and they are considered equivalent of the Robertson Bay Group in northern Victoria Land (Ireland et al., 1998; Adams et al., 2014). Lithologically, turbidites are mainly greywackes which were affected by (sub-)greenschist metamorphism (Adams, 1986).

During the late Devonian to early Carboniferous (375-345 Ma), the Swanson Formation was intruded by calc-alkaline magmatism (Pankhurst et al., 1998; Siddoway and Fanning, 2009; Yakymchuk et al., 2015). The expression of the mid-Paleozoic magmatism is the Ford Granodiorite suite, that crops out in the Ford Ranges coast. The Ford Granodiorite lithologies are grey, metaluminous to peraluminous, biotite ± hornblende granodiorite and tonalite (Weaver et al., 1991).

Subsequent to the mid-Paleozoic magmatism, there is a gap in the geological record of MBL, until the development of middle Cretaceous magmatism (Pankhurst et al., 1998; Mukasa and Dalziel, 2000; Siddoway, 2021). Indeed, between 115 and 95 Ma (Siddoway et al., 2004a; McFadden et al., 2010; Yakymchuk et al., 2013; Brown et al., 2016) the Byrd Coast Granite emplaced in Ruppert and Hobbs coasts, Ford Range, and Edward VII Peninsula. The suite is a pinkish, coarse, equigranular to porphyritic leucogranites and monzogranites. The granitic intrusion is also associated with mafic dikes (dolerite) emplacement in the Ross Province, spanning in age from 142 to 94 Ma (Siddoway et al., 2005; Saito et al., 2013).

The mid-Paleozoic and Cretaceous magmatism was also coupled with metamorphic events that are mainly recorded in the Fosdick Mountains. The Fosdick Granite-Migmatite Complex is constituted by para- and ortho-gneisses that experienced at least two high-grade metamorphic events (Siddoway et al., 2004b; Korhonen et al., 2010b, 2010a, 2012; Yakymchuk et al., 2015). Gneisses present granulite facies mineralogical assemblage. Migmatitic orthogneisses are made up of quartz + plagioclase + alkali feldspar + biotite + iron oxides ± garnet (Korhonen et al., 2010b, 2010a). Migmatitic paragneisses show melanosome domains, with cordierite + sillimanite + biotite + quartz + plagioclase + alkali feldspar ± garnet, and coarse grained leocosome containing quartz + alkali feldspar + anti-perthite + biotite ± garnet (Korhonen et al., 2010b, 2010a). Moreover, other migmatite outcrops are reported in the Edward VII Peninsula and eastern MBL (Smith, 1996; Mukasa and Dalziel, 2000).

In the Cenozoic the MBL uplifted and experienced extended volcanism. The first volcanic event is dated at late Eocene (36.6 Ma), whereas the most intensive volcanic activity started in the middle Miocene (Wilch et al., 2021). Volcanic rocks composition ranges from mafic basanite to felsic trachyte and phonolite (Wilch et al., 2021); moreover, volcanic rocks are usually associated with varieties of volcaniclastic deposits formed during the lava eruptions (Wilch et al., 2021). Within West Antarctica, 19 major volcanic edifices, and numerous minor ones, were documented, even though geophysical surveys documented widespread volcanoes and magmatic intrusions beneath the West Antarctic Ice Sheet (Blankenship et al., 1993; Behrendt, 2013).

3.3.2. Ross Sea Stratigraphy

The opening of the Ross Sea is the result of the WARS that led to the development of sedimentary basins (Figure 18; Cooper et al., 1991), which are filled by Cenozoic sediments. Geographically the Ross Sea is divided by the Ross and Iselin banks into two separate domains: the Eastern and Western Ross Sea; the boundary also marks the geological limit between East and West Antarctica asthenosphere (Tinto et al., 2019).

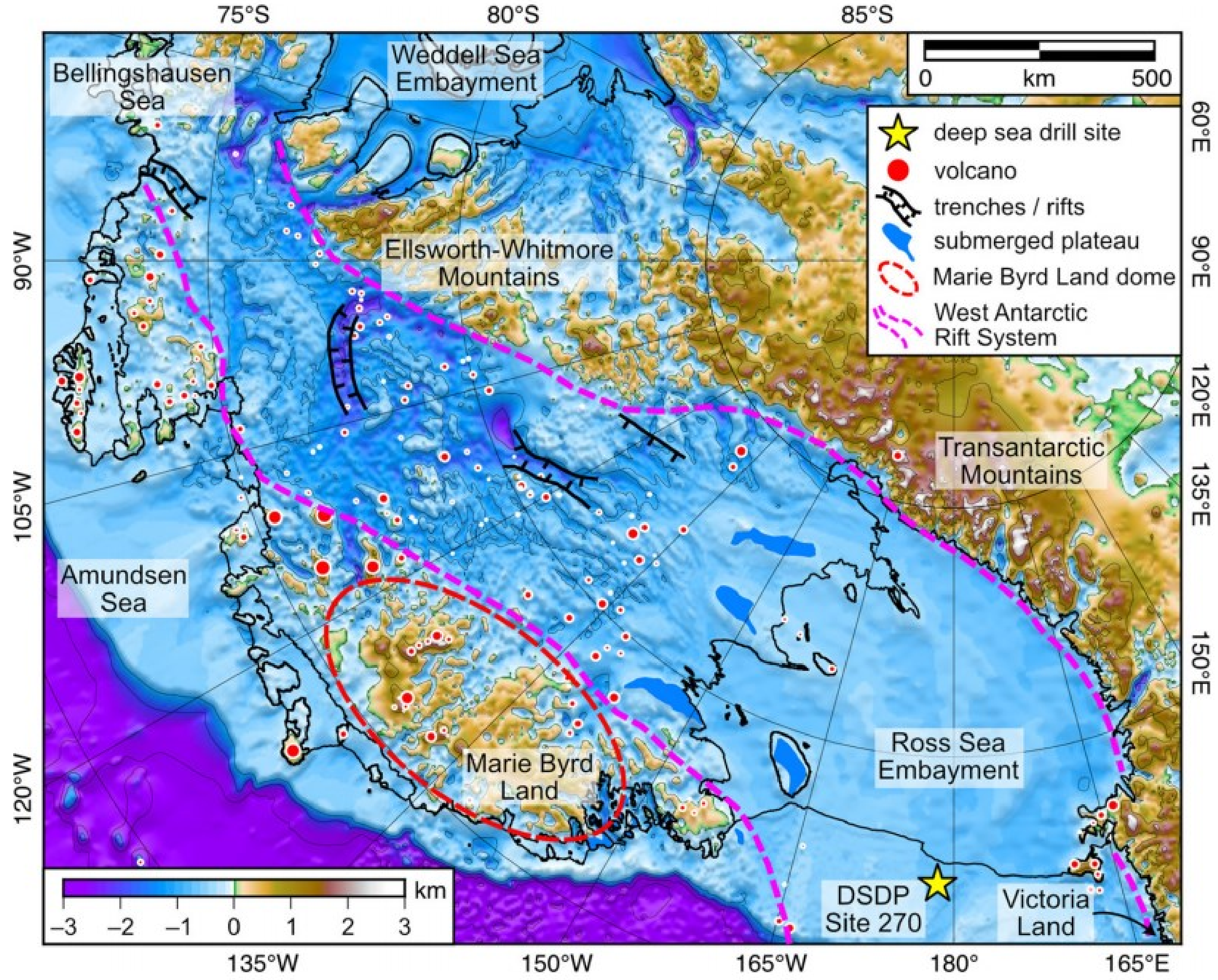

Figure 18 Present day tophography of the Ross Embayment (from Paxman, 2021)

In the western Ross Sea, Pennell, Joides, and Drygalski basins are separated by Pennell and Crary-Mawson banks (Figure 13); southward Pennel and Joides basins jointed into the Central Basin which is separated from the Victoria Land Basin by the McMurdo Sound. In the eastern Ross Sea, the Little America, Whales, and Glomar Challenger basins are separated by the Houtz and Hayes banks (Figure 13).

The sedimentary filling of the Ross Sea basins is strongly influenced by periodical advances and retreats of the EAIS and WAIS, which were drained by ice flows during the Cenozoic.

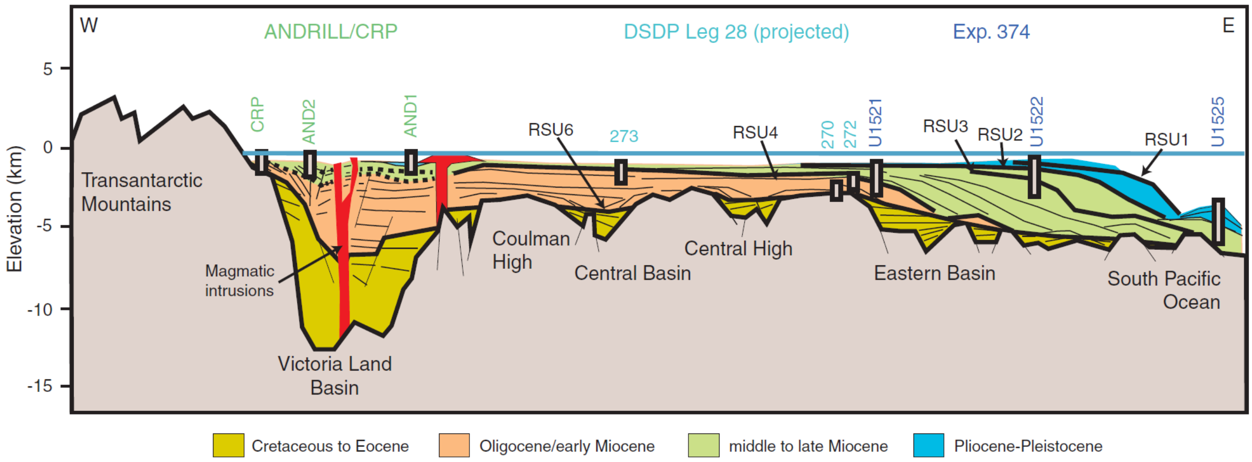

Figure 19 Ross Sea seismic stratigraphy in a ca. E-W transect (from McKay et al., 2019)

The stratigraphic framework of the Cenozoic Ross Sea sediments is mainly based on geophysical surveys which are locally constrained by drilling (Figure 19). The Antarctic Offshore Stratigraphy Project (ANTOSTRAT) defines eight seismic units (RSS-1 to RSS-8), which are bounded by six regional scale seismic unconformities (RSU-6 to RSU-1; Brancolini et al., 1995; De Santis et al., 1995). The rock package of the RSS-1, internally divided by the RSU-7, is the oldest and poorly constrained one. The lowest, which are inferred to be late Cretaceous to Paleocene (Wilson and Luyendyk, 2009), have never been reached by drillings; on the contrary the upper part of the RSS-1, drilled by CIROS and CRP projects, are upper Eocene to Oligocene and they consist of fluvial, deltaic, and shallow-shelf rift-fill, that, in the uppermost part, are glacially influenced (Fielding et al., 2000; Galeotti et al., 2016). The RSS-1 is upper bounded by the RSU-6, above that lie the upper Oligocene to lower Miocene deposits of the RSS-2. This rock package consists of alternate sequence of grounding zone prograding wedges and sub-horizontal strata (McKay et al., 2019 and reference therein). This interval has been intercepted by ANDRILL, CRP and DSDP_leg28 cores (Figure 20); DSDP Site 270, that is taken into account in this thesis, completely fall in this rock package. Above the RSU-5 the early Miocene grounding zone prograding wedges and sub-horizontal strata sequences (RSS-3; McKay et al., 2019 and reference therein) were drilled by ANDRILL, CRP and DSDP_leg28 projects (Figure 20) and this latter strata package is one of the main targets of the IODP Site U1521 (McKay et al., 2019), here studied. Above RSU-4a lie the strata of the RSS-4, that are early Miocene (Figure 20), which are upper bounded by the RSU-4, that is in turn overlain by the middle Miocene RSS-5. RSU-3 marks the first evidence of an expanded marine WAIS and this event, and the overlying late Miocene strata, are among the main targets of the IODP Site U1522 (McKay et al., 2019).

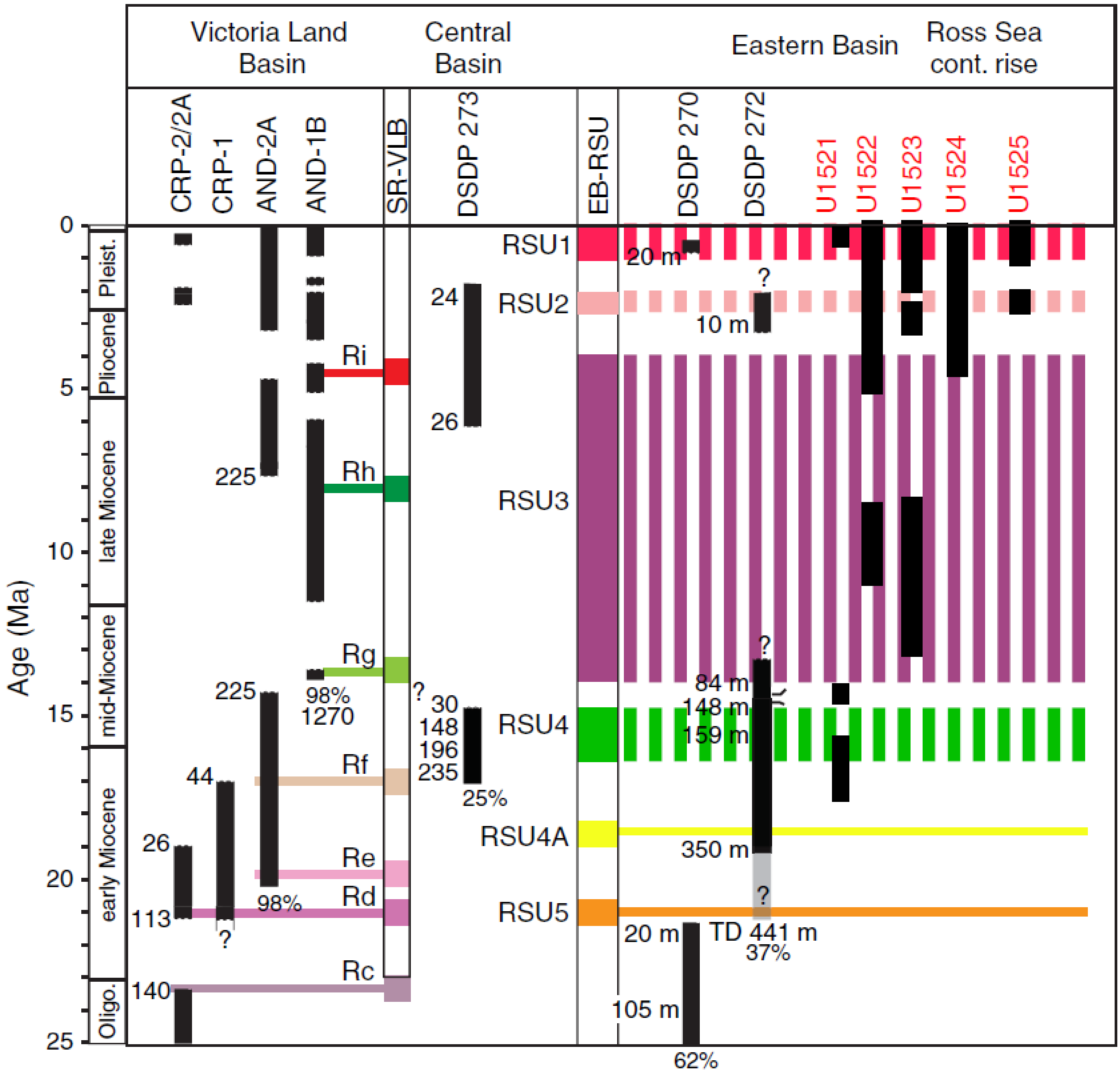

Figure 20 Seismic stratigraphy of the Ross Sea (modified from (McKay et al., 2019)

3.4. Materials and Methods

The petrology and relative abundance of clasts >2 mm were evaluated on the archive half sections of IODP Site U1521, U1522, and DSDP Site 270 cores at the IODP Gulf Coast Repository in Texas A&M University, College Station (USA).

DSDP Site 270 (Shipboard Scientific Party, 1975), located in the Central High in the Central Ross Sea (Figure 13; 77°26.48’S, 178°30.19’W), cored 422,5 m bsf, reached the basement, and recovered Oligocene to early Miocene sediments (Shipboard Scientific Party, 1975; Kulhanek et al., 2019). IODP Site U1521 is located in the Pennell Basin (Figure 13; 75°41.0351’S, 179°40.3108’W) and 650.1 m bsf (DSF) was cored, 411.5 m of which were recovered (McKay et al., 2019); the sedimentary record was divided into 7

Lithostratigraphic Units (LSU), and 3 sub-units, on the basis of sedimentological features (McKay et al., 2019). Recovered sediments span from early Miocene to Pleistocene (McKay et al., 2019), whereas the Miocene interval is the most represented in the record. IODP Site U1522 is located in the Glomar Challenger Basin (Figure 13; 76°33.2262'S, 174°45.4652'W). The hole was 701.8 m bsf (DSF) depth and 279.57 m of sediments were recovered (40%); the sedimentary record was divided into 4 LSU and 3 sub-units, spanning from late Miocene to Pleistocene (McKay et al., 2019).

Sampling, macroscopic observations and preliminary petrographic analyses were performed following the same methods for the Cape Roberts and ANDRILL projects (Cape Roberts Science Team, 1998b, 1998a; Talarico and Sandroni, 1998, 2009; Talarico et al., 2000; Sandroni and Talarico, 2001; Panter et al., 2008). Thus, each clast >2 mm (granule to cobble granulometric fraction) was macroscopically classified into 8 broad lithological groups:

i. Intrusive rocks with either isotropic and foliated varieties of felsic to intermediate granitoids and mafic intrusive rocks.
ii. Volcanic rocks with aphyric or porphyritic, vesicular and/or amygdale bearing varieties ranging in composition from mafic to felsic.
iii. Metamorphic rocks with schistose or gneissic varieties marked by minerals orientation and various low-grade metasedimentary rocks (meta-limestone, meta-siltstone, meta-sandstone, meta-greywacke).
iv. Sedimentary rocks with clastic lithologies (sandstone and micro-conglomerate with visible clastic texture), limestone, and chert.
v. Intraclasts with intrabasinal sedimentary clasts, ranging from granules to cobbles, of reworked diamictite and mud clasts.
vi. Dolerites with fine- to medium-grained holocrystalline, mafic sub-volcanic rock with sub-ophitic to ophitic texture.
vii. Quartz grains consist of grey vitreous single and usually monocrystalline grains.
viii. Felsic porphyry group includes felsic porphyritic rocks, with fine grained to microscrystalline groundmass with dispersed millimetric euhedral to subhedral porphyritic crystals.

Data processing involved counting and classifying each clast in the different lithological groups for each 10 cm of the entire archive half core. A total amount of 15691 clasts was counted and classified in the IODP Site U1521A, 19414 Clasts for IODP Site U1522A, and 3099 clasts for DSDP Site 270. Distribution of different lithologies has been registered for each logged core.

In addition, representative pebbles and cobbles were sampled from the working half core to produce standard petrographic thin sections and analyze them by optical microscopy. Lists of sampled clasts are shown in Table 3 for IODP Site U1521, Table 4 for IODP Site U1522, and Table 5 for DSDP Site 270. For each thin section, photomicrographs and a petrographic description were made (available in Appendix III, V, and VII). Moreover, 10 diamictite bulk samples were taken, dried and sieved following the procedures described in Perotti et al. (2018): the granulometric fraction >2 mm was mounted in epoxy and made into thin section for petrographic analysis. The latter was aimed to identify grain lithologies present also in the bulk samples where pebbles and cobbles are rare. Classification of lithic grains followed the method adopted in Licht et al. (2005) for metamorphic and intrusive clasts and Pompilio et al. (2007) and Panter et al. (2008) for volcanic clasts.

The sample ID joins the IODP/DSDP expedition/leg number (i.e., 374-), the site and hole names (i.e., U1521A-), the core number and type (i.e., 29R-; R: rotary), the section number and the section half (i.e., 6W-; W: working half), and the depth interval of the sample within the section (i.e., 59-63 cm).

Table 3 List of thin sections made from sampled clasts and bulk sediments of Site U1521 core. Position of clasts in each section is also shown. Samples marked with an asterisk (*) are diamictite bulk samples dried, sieved, and mounted on thin sections (granulometric fraction >2mm). Sect. – section; LSU - lithostratigraphic units are from McKay et al. (2019).

Sample ID	**Exp**	**Site**	**Hole**	**Core**	**Type**	**Section**	**Sect. half**	**Top Offset** (cm)	**Bottom Offset** (cm)	**Depth** (m bsf)	**LSU**
374-U1521A-29R-6W, 59-63 cm	374	U1521	A	29	R	6	W	59	63	272,77	IV
374-U1521A-30R-3W, 85-89 cm	374	U1521	A	30	R	3	W	85	89	279,34	IV
374-U1521A-35R-3W, 65-72 cm	374	U1521	A	35	R	3	W	65	72	326,27	VI A
374-U1521A-36R-1W, 67-70 cm*	374	U1521	A	36	R	1	W	67	70	333,97	VI A
374-U1521A-36R-1W, 80-90 cm*	374	U1521	A	36	R	1	W	80	90	334,10	VI A
374-U1521A-36R-3W, 45-55 cm*	374	U1521	A	36	R	3	W	45	55	336,59	VI A
374-U1521A-37R-3W, 110-113 cm	374	U1521	A	37	R	3	W	110	113	346,79	VI A
374-U1521A-38R-1W, 110-113 cm	374	U1521	A	38	R	1	W	110	113	353.61	VI A
374-U1521A-38R-2W, 134-140 cm	374	U1521	A	38	R	2	W	134	140	355,34	VI A
374-U1521A-38R-3W, 24-28 cm	374	U1521	A	38	R	3	W	24	28	355,72	VI A
374-U1521A-39R-CCW, 10-12 cm	374	U1521	A	39	R	CC	W	10	12	359.53	VI A
374-U1521A-43R-2W, 80-85 cm*	374	U1521	A	43	R	2	W	80	85	378,78	VI A
374-U1521A-43R-2W, 94-98 cm*	374	U1521	A	43	R	2	W	94	98	378,92	VI A
374-U1521A-43R-2W, 100-105 cm*	374	U1521	A	43	R	2	W	100	105	378,98	VI A
374-U1521A-44R-4W, 85-88 cm	374	U1521	A	44	R	4	W	85	88	386,46	VI B
374-U1521A-48R-6W, 38-40 cm	374	U1521	A	48	R	6	W	38	40	427,30	VI B
374-U1521A-49R-8W, 31-36 cm*	374	U1521	A	49	R	8	W	31	36	438,51	VI B
374-U1521A-50R-4W, 133-136 cm	374	U1521	A	50	R	4	W	133	136	444.55	VI C
374-U1521A-55R-4W, 2-5 cm	374	U1521	A	55	R	4	W	2	5	491,04	VI C
374-U1521A-60R-4W, 125-128 cm	374	U1521	A	60	R	4	W	125	128	539.85	VI C
374-U1521A-60R-5W, 62-65 cm	374	U1521	A	60	R	5	W	62	65	541,08	VI C
374-U1521A-60R-7W, 90-93 cm	374	U1521	A	60	R	7	W	90	93	543,64	VI C
374-U1521A-61R-5W, 26-30 cm	374	U1521	A	61	R	5	W	26	30	550.17	VI C
374-U1521A-62R-4W, 120-125 cm	374	U1521	A	62	R	4	W	120	125	559,14	VI C
374-U1521A-63R-5W, 8-17 cm	374	U1521	A	63	R	5	W	8	17	568,89	VII
374-U1521A-63R-CCW, 10-13 cm	374	U1521	A	63	R	cc	W	10	13	569,98	VII
374-U1521A-64R-3W, 28-31 cm	374	U1521	A	64	R	3	W	28	31	576,32	VII
374-U1521A-64R-3W, 109-112 cm	374	U1521	A	64	R	3	W	109	112	577.18	VII

374-U1521A-64R-6W, 20-24 cm	374	U1521	A	64	R	6	W	20	24	579,95	VII
374-U1521A-66R-4W, 63-67 cm	374	U1521	A	66	R	4	W	63	67	597,03	VII
374-U1521A-67R-6W, 115-120 cm	374	U1521	A	67	R	6	W	115	120	610,17	VII
374-U1521A-68R-2W, 58-61 cm	374	U1521	A	68	R	2	W	58	61	613,70	VII
374-U1521A-69R-1W, 120-125 cm	374	U1521	A	69	R	1	W	120	125	622,50	VII
374-U1521A-69R-5W, 119-122 cm	374	U1521	A	69	R	5	W	119	122	627.96	VII
374-U1521A-69R-6W, 40-45 cm	374	U1521	A	69	R	6	W	40	45	628,65	VII
374-U1521A-69R-6W, 63-66 cm	374	U1521	A	69	R	6	W	63	66	628,88	VII
374-U1521A-70R-1W, 55-58 cm	374	U1521	A	70	R	1	W	55	58	631,45	VII
374-U1521A-70R-4W, 120-125 cm	374	U1521	A	70	R	4	W	120	125	636,10	VII
374-U1521A-70R-5W, 112-115 cm	374	U1521	A	70	R	5	W	112	115	637,53	VII
374-U1521A-71R-1W, 87-90 cm	374	U1521	A	71	R	1	W	87	90	641,37	VII

Table 4 List of thin sections made from sampled clasts of Site U1522 core. Position of clasts in each section is also shown. Sect. – section. Samples marked with an asterisk (*) are diamictite bulk samples dried, sieved, and mounted on thin sections (granulometric fraction >2mm); LSU - lithostratigraphic units are from McKay et al. (2019).

Sample ID	**Exp**	**Site**	**Hole**	**Core**	**Type**	**Section**	**Sect. half**	**Top Offset** (cm)	**Bottom Offset** (cm)	**Depth (m bsf)**	**LSU**
374-U1522A-55R-2W, 17-20 cm	374	1522	A	55	R	2	W	17	20	493.29	IIIB
374-U1522A-55R-3W, 52-56 cm	374	1522	A	55	R	3	W	52	56	494.9	IIIB
374-U1522A-56R-1W, 48-51 cm	374	1522	A	56	R	1	W	48	51	504.88	IIIB
374-U1522A-56R-4W, 44-46 cm	374	1522	A	56	R	4	W	44	46	504.83	IIIB
374-U1522A-57R-1W, 0-3 cm	374	1522	A	57	R	1	W	0	3	510.91	IIIB
374-U1522A-57R-2W, 120-123 cm	374	1522	A	57	R	2	W	120	123	513.45	IIIB
374-U1522A-57R-5W, 1-6 cm	374	1522	A	57	R	5	W	1	6	516.52	IIIB
374-U1522A-57R-5W, 37-41 cm	374	1522	A	57	R	5	W	37	41	516.88	IIIB
374-U1522A-58R-1W, 68-71 cm	374	1522	A	58	R	1	W	68	71	521.18	IIIB
374-U1522A-58R-3W, 120-121 cm	374	1522	A	58	R	3	W	120	121	524.51	IIIB
374-U1522A-58R-4W, 4-7 cm	374	1522	A	58	R	4	W	4	7	524.78	IIIB
374-U1522A-58R-6W, 131-133 cm	374	1522	A	58	R	6	W	131	133	528.56	IIIB
374-U1522A-59R-7W, 22-24 cm	374	1522	A	59	R	7	W	22	24	537.07	IIIB
374-U1522A-59R-7W, 91-93 cm	374	1522	A	59	R	7	W	91	93	537.86	IIIB
374-U1522A-60R-3W, 64-66 cm	374	1522	A	60	R	3	W	64	66	543.15	IIIB
374-U1522A-60R-3W, 87-91 cm	374	1522	A	60	R	3	W	87	91	543.38	IIIB
374-U1522A-60R-5W, 36-40 cm	374	1522	A	60	R	5	W	36	40	545.71	IIIB
374-U1522A-61R-1W, 0-2 cm	374	1522	A	61	R	1	W	0	2	549.3	IIIC
374-U1522A-61R-1W, 29-32 cm	374	1522	A	61	R	1	W	29	32	549.59	IIIC
374-U1522A-61R-1W, 44-47 cm	374	1522	A	61	R	1	W	44	47	549.74	IIIC
374-U1522A-61R-CCW, 38-40 cm	374	1522	A	61	R	CC	W	38	40	550.9	IIIC
374-U1522A-61R-CCW, 67-70 cm	374	1522	A	61	R	CC	W	67	70	551.19	IIIC
374-U1522A-62R-1W, 12-15 cm	374	1522	A	62	R	1	W	12	15	558.92	IIIC
374-U1522A-62R-1W, 65-68 cm	374	1522	A	62	R	1	W	65	68	559.46	IIIC
374-U1522A-62R-2W, 8-10 cm	374	1522	A	62	R	2	W	8	10	560.1	IIIC
374-U1522A-62R-2W, 49-52 cm	374	1522	A	62	R	2	W	49	52	560.52	IIIC
374-U1522A-62R-2W, 52-55 cm	374	1522	A	62	R	2	W	52	55	560.55	IIIC
374-U1522A-62R-CCW, 17-20 cm	374	1522	A	62	R	CC	W	17	20	562.33	IIIC

374-U1522A-63R-2W, 112-115 cm	374	1522	A	63	R	2	W	112	115	570.79	IIIC
374-U1522A-64R-1W, 1-5 cm	374	1522	A	64	R	1	W	1	5	557.83	IIIC
374-U1522A-64R-4W, 86-89 cm	374	1522	A	64	R	4	W	86	89	582.95	IIIC
374-U1522A-64R-4W, 89-92 cm	374	1522	A	64	R	4	W	89	92	583	IIIC
374-U1522A-65R-3W, 77-80 cm	374	1522	A	65	R	3	W	77	80	590.9	IIIC
374-U1522A-65R-3W, 89-92 cm	374	1522	A	65	R	3	W	89	92	591.03	IIIC
374-U1522A-66R-1W, 56-59 cm	374	1522	A	66	R	1	W	56	59	597.36	IIIC
374-U1522A-66R-CCW, 19-22 cm	374	1522	A	66	R	CC	W	19	22	601.19	IIIC
374-U1522A-67R-1W, 53-58 cm*	374	1522	A	67	R	1	W	53	58	606.85	IIIC
374-U1522A-67R-2W, 72-75 cm	374	1522	A	67	R	2	W	72	75	608.48	IIIC
374-U1522A-67R-2W, 105-108 cm	374	1522	A	67	R	2	W	105	108	608.81	IIIC
374-U1522A-67R-3W, 71-72 cm	374	1522	A	67	R	3	W	71	72	609.88	IIIC
374-U1522A-67R-4W, 6-8 cm	374	1522	A	67	R	4	W	6	8	610.45	IIIC
374-U1522A-67R-6W, 21-24 cm	374	1522	A	67	R	6	W	21	24	612.79	IIIC
374-U1522A-68R-1W, 71-86 cm	374	1522	A	68	R	1	W	71	86	616.51	IIIC
374-U1522A-68R-2W, 78-80 cm	374	1522	A	68	R	2	W	78	80	617.81	IIIC
374-U1522A-68R-4W, 86-89 cm	374	1522	A	68	R	4	W	86	89	619.92	IIIC
374-U1522A-68R-6W, 56-60 cm	374	1522	A	68	R	6	W	56	60	622.83	IIIC
374-U1522A-69R-1W, 0-4 cm	374	1522	A	69	R	1	W	0	4	625.33	IIIC
374-U1522A-69R-1W, 3-5 cm	374	1522	A	69	R	1	W	3	5	625.33	IIIC
374-U1522A-70R-1W, 57-60 cm	374	1522	A	70	R	1	W	57	60	635.37	IIIC
374-U1522A-70R-2W, 73-74 cm	374	1522	A	70	R	2	W	73	74	636.93	IIIC
374-U1522A-70R-2W, 134-137 cm	374	1522	A	70	R	2	W	134	137	637.54	IIIC
374-U1522A-71R-4W, 45-48 cm	374	1522	A	71	R	4	W	45	48	648.86	IV
374-U1522A-72R-1W, 34-37 cm	374	1522	A	72	R	1	W	34	37	654.15	IV
374-U1522A-72R-1W, 108-111 cm	374	1522	A	72	R	1	W	108	111	654.90	IV
374-U1522A-72R-3W, 71-74 cm	374	1522	A	72	R	3	W	71	74	657.24	IV
374-U1522A-75R-1W, 25-28 cm	374	1522	A	75	R	1	W	25	28	682.85	IV
374-U1522A-75R-2W, 9-12 cm	374	1522	A	75	R	2	W	9	12	684.11	IV
374-U1522A-75R-6W, 42-45 cm	374	1522	A	75	R	6	W	42	45	690.18	IV
374-U1522A-76R-1W, 109-111 cm	374	1522	A	76	R	1	W	109	111	693.3	IV
374-U1522A-76R-2W, 7-10 cm	374	1522	A	76	R	2	W	7	10	693.78	IV
374-U1522A-76R-3W, 42-45 cm	374	1522	A	76	R	3	W	42	45	695.37	IV

Table 5 List of thin sections made from sampled clasts and basement of DSDP Site 270 core. Position of clasts in each section is also shown. Samples marked with an asterisk (*) are diamictite bulk samples dried, sieved, and mounted on thin sections (granulometric fraction >2mm); LSU - lithostratigraphic units are from Kraus (2016)

Sample ID	**Leg**	**Site**	**Core**	**Type**	**Section**	**Sect. Half**	**Top Offset** (cm)	**Bottom Offset** (cm)	**Depth** (m bsf)	**LSU**
28-270-2R-2W,91-106 cm	28	270	2	R	2	W	91	106	2.50	I
28-270-13R-3W, 99-113 cm	28	270	13	R	3	W	99	113	105.05	II
28-270-14R-1W, 39-41 cm	28	270	14	R	1	W	39	41	110.40	II
28-270-19R-2W, 50-54 cm	28	270	19	R	2	W	50	54	160.00	III
28-270-24R-2W*	28	270	24	R	2	W				IV
28-270-27R-1W, 102-107 cm	28	270	27	R	1	W	102	107	235.00	IV

28-270-27R-4W, 41-44 cm	28	270	27	R	4	W	41	44	238.90	IV
28-270-27R-4W, 103-105 cm	28	270	27	R	4	W	103	105	239.50	IV
28-270-27R-2W*	28	270	27	R	2	W				IV
28-270-38R-3W, 130-133 cm	28	270	38	R	3	W	130	133	342.75	V
28-270-38R-3W, 141-143 cm	28	270	38	R	3	W	141	143	342.85	V
28-270-39R-1W, 122-123 cm	28	270	39	R	1	W	122	123	349.20	VI
28-270-47R-2W	28	270	47	R	2	W			411.50	ND
28-270-47R-3W, 110-116 cm	28	270	47	R	3	W	110	116	413.60	ND
28-270-48R-1W, 100-105 cm	28	270	48	R	1	W	100	105	415.50	ND
28-270-49R-1W	28	270	49	R	1	W			422.70	ND

Table 6 List of thin sections of Polar Rock Repository samples. MBL: Marie Byrd Land; SVL: southern Victoria Land; CTM: Central Transantarctic Mountains; GHIC: Granite Harbour Intrusive Complex.

Sample ID	Region	Area	Coordinates		Formation	Lithology
			Latitude (°S)	Longitude (°)		
PRR-18760	MBL	Rockefeller Mountains	77° 55'	155° 12.4' W	Byrd Coast Granite	Biotite leucogranite
PRR-18768	MBL	Rockefeller Mountains	78° 6.5'	155° 13.3' W	Byrd Coast Granite	Biotite leucogranite
PRR-18783	MBL	Rockefeller Mountains	78° 3.7'	155° 11.9' W	Byrd Coast Granite	Biotite leucogranite
PRR-18792	MBL	Rockefeller Mountains	78° 5.3'	155° 18.1' W	unknown	Biotite schist
PRR-18812	MBL	Rockefeller Mountains	78° 5.3'	155° 18.1' W	unknown	Biotite gneissic schist
PRR-18853	MBL	Rockefeller Mountains	78° 4.9'	155° 27.1' W	unknown	Biotite gneissic schist
PRR-33877	MBL	Phillips Mountains	76° 18'	145° 21' W	Ford Granodiorite	Biotite-Hornblende granodiorite
PRR-33917	MBL	Fosdick Mountains	76° 30'	144° 36' W	Fosdick Migmatite	Biotite migmatite
PRR-33918	MBL	Fosdick Mountains	76° 30'	144° 36' W	Fosdick Migmatite	Biotite-Sillimanite migmatite
PRR-33926	MBL	Phillips Mountains	76° 13.6'	143° 51.5' W	Byrd Coast Granite	Biotite leucogranite
PRR-33991	MBL	Ford Ranges	76° 56'	144° 40' W	Ford Granodiorite	Biotite-Hornblende granodiorite
PRR-34146	MBL	Ford Ranges	77° 11'	144° 26' W	Byrd Coast Granite	Biotite leucogranite
PRR-34164	MBL	Fosdick Mountains	76° 29'	146° 6.4' W	Fosdick Migmatite	Biotite-Sillimanite-Garnet gneiss
PRR-34188	MBL	Phillips Mountains	76° 18	145° 21' W	Ford Granodiorite	Biotite-Hornblende granodiorite
PRR-34205	MBL	Fosdick Mountains	76° 30'	144° 36' W	Fosdick Migmatite	Biotite schist
PRR-34207	MBL	Fosdick Mountains	76° 31'	145° 50' W	Fosdick Migmatite	Biotite schist
PRR-34239	MBL	Ford Ranges	77° 9.7'	145° 16.7' W	Swanson Formation	Biotite phyllite
PRR-34385	MBL	Fosdick Mountains	76° 31'	145° 50' W	Swanson Paragneiss	Biotite gneiss
PRR-4604	TAM	Brown Hills (SVL)	79° 36’	158°40’ E	GHIC	Biotite-Hornblende monzogranite
PRR-21042	TAM	Brown Hills (SVL)	79° 44.8’	159° 32.5’ E	GHIC	Biotite-Hornblende granite
PRR-15282	TAM	Miller Range (CTM)	82° 51.4’	157° 43.2’ E	GHIC	Biotite monzogranite
PRR-15321	TAM	Miller Range (CTM)	83° 29’	157° 52’ E	GHIC	Biotite monzogranite
PRR-15790	TAM	Miller Range (CTM)	83° 13’	157° 54’ E	GHIC	Biotite monzonite

Representative metamorphic and intrusive rock samples have been selected for mineral-chemistry analyses. Chemical analyses were carried out with an energy-dispersive X-ray system (Bruker Quantax 200 EDX) coupled with an Electron Scanning Microscope (Tescan Vega3) at the Department of Physical, Earth and Environmental Sciences - University of Siena. Analytical conditions were 20 kV of accelerating voltage, 15 µA of emission current, and a beam spot size of 0.2 µm. Natural mineral standards were used for calibration. Chemical analyses were carried out on 1 to 15 grains of biotite, white mica, amphibole, pyroxene, and garnet within each sample; crystals were selected based on the absence of alteration and/or inclusions. Biotite and white mica cations were recalculated on the basis of 22 oxygens, amphibole cations were recalculated on the basis of 23 oxygens, pyroxene on the basis of 6 oxygens, garnet on the basis of 12 oxygens.

Moreover, in order to compare the petrology and mineral-chemistry of clasts with Ross Embayment outcrops, 18 igneous and metamorphic rock samples from Marie Byrd Land and 5 intrusive rock samples from TAM, were analyzed (Table 6). Samples were provided by the Polar Rock Repository (PRR) at Byrd Polar and Climate Research Centre of the Ohio State University, and previously partially investigated by Perotti et al., 2017 and Perotti, 2018. SEM-EDS chemical analyses of biotite, pyroxene, and garnet were carried out on 15 samples (Appendix IX).

3.5. Results

3.5.1. IODP Site U1521A

3.5.1.1. Clast Petrology

Here general petrological features of logged and sampled clasts from Site U1521 are provided. For a detailed description of each thin section see Appendix III. Figure 21 shows photomicrographs of representative lithologies found in gravel sized clasts.

Granitoid rocks are in general hetero-granular, fine- to coarse-grained, with hypidiomorphic to allotriomorphic texture. Grey granitoids are more common than pinkish to reddish varieties. In some cases, they are isotropic granites (i.e., Samples 374-U1521A-35R-3W, 65-72 cm; 55R-4W, 2-5 cm; 68R-2W, 58-61 cm), in others they show a weakly foliated texture (i.e., Samples 29R-6W, 59-63 cm; 69R-6W, 63-66 cm). Few samples show a slightly porphyritic texture with orthoclase as the main porphyritic mineral (i.e., Samples 48R-6W, 38-40 cm; 55R-4W, 2-5 cm). In general, femic minerals are represented by biotite, which always occurs but usually is replaced by chlorite and secondary white mica. Hornblende is rarer and often chloritized (i.e., Sample 4W, 2-5 cm). In some cases white mica is directly associated with biotite (i.e., Sample 29R-6W, 59-63 cm). The color index ranges from 2% to 12%. Plagioclases form subhedral to euhedral laths that are in general very altered and replaced by aggregates of saussurite (sericite ± albite ± epidote ± calcite), whereas alkali feldspars (orthoclase and/or microcline) are often replaced by kaolinite and/or sericite microaggregates. Quartz is anhedral and usually interstitial, with undulose extinction in some cases (i.e., Samples 29R-6W, 59-63 cm; 69R-6W, 63-66 cm). One sample (Sample 64R-3W, 28-31 cm) shows a mortar texture with fine-grained quartz intergrowth rimming coarser crystals. Accessory phases are in general apatite, zircon/monazite, opaque minerals, and allanite. Modal compositions range from monzogranite to granodiorite.

Metamorphic rocks include meta-graywackes, schists, biotite ± white mica gneisses, and phyllites. Gneiss (i.e., Sample 374-U1521A-60R-5W, 62-65 cm) is heterogranular (fine- to medium- grained) and has a grano-lepidoblastic texture with granoblastic domains defined by plagioclase and fine-grained quartz and biotite flakes that define the rock foliation. Another gneiss (i.e., Sample 64R-6W, 20-24 cm) has a lepidoblastic texture defined by iso-orientation of biotite and white mica flakes and a granoblastic domain with quartz and microcline. Schists are prevalently fine- to medium-grained (i.e., Samples 69R-6W, 40-45 cm; 70R-4W, 120-125 cm), with a weak foliation defined by orientation of biotite and rare white mica (i.e., Samples 69R-6W, 40-45 cm; 70R-4W, 120-125 cm). Phyllites (i.e., Samples 62R-4W, 120-125 cm; 63R-5W, 8-17 cm) show very fine-grained schistosity with lepidoblastic layers defined by biotite, opaque minerals and quartz boudins (i.e., Sample 62R-4W, 120-125 cm), chlorite and quartz (i.e., Sample 63R-5W, 8-17 cm), and chlorite, quartz, and opaque minerals alternations (i.e., Sample 69R-1W, 120-125 cm). Meta-graywackes (i.e., Samples 38R-2W, 134-140 cm; 64R-3W, 109-112 cm) have a very fine- to medium-grained heterogranular clastic texture with biotite crystals that define a weak foliation; clasts are mainly composed of quartz and minorly altered feldspar grains (plagioclase more common than alkali feldspar), set up in an abundant argillaceous matrix and sometimes calcite cement. In general, metamorphic grade of sampled clasts is low, with paragenesis typical of greenschists/sub-greenschists facies. Only in a few cases (i.e., Samples 64R-6W, 20-24 cm; 69R-6W, 40-45 cm; 70R-4W, 120-125 cm) mineral paragenesis points to a medium grade.

Sampled sedimentary rocks are mudstone, siltstone, sandstone, greywacke, and limestone. Siltstone (i.e., Sample 374-U1521A-63R-CCW, 10-13 cm) has mainly quartzo-feldspathic silt-sized grains with isotropic texture. Sandstones are laminated mature quartz-arenites made up by sub-rounded to well-rounded quartz grains, usually with quartz overgrowth, and minor slightly altered feldspars (i.e., Sample 38R-3W, 24-28 cm), and an isotropic heterogranular (medium- to very coarse-grained) matrix-rich arkosic sandstone made of monocrystalline and polycrystalline quartz and feldspar grains (i.e., Sample 71R-1W, 87-90 cm). Carbonate rocks comprise heterogranular micrite to microsparites (i.e., Samples 37R-3W, 110-113 cm; 66R-4W, 63-67 cm; 67R-6W, 115-120 cm) and a clast-supported coarse-grained conglomerate with clasts made of sparitic limestone, oolitic limestone, heterogranular quartz-bearing meta-limestone, quartzite, and meta-sandstone (i.e., Sample 44R-4W, 85-88 cm). Greywacke (i.e., Sample 60R-7W, 90-93 cm) is composed of heterogranular (fine- to medium-grained) angular to sub-angular clasts made of monocrystalline quartz, minor feldspars and felsic sub-volcanic rock lithic grains.

Volcanic and sub-volcanic rocks are represented by one sample (Sample 374-U1521A-30R-3W, 85-89 cm) of altered basalt with holocrystalline very fine-grained sub-ophitic texture made of plagioclase and clinopyroxene, with minor interstitial quartz.

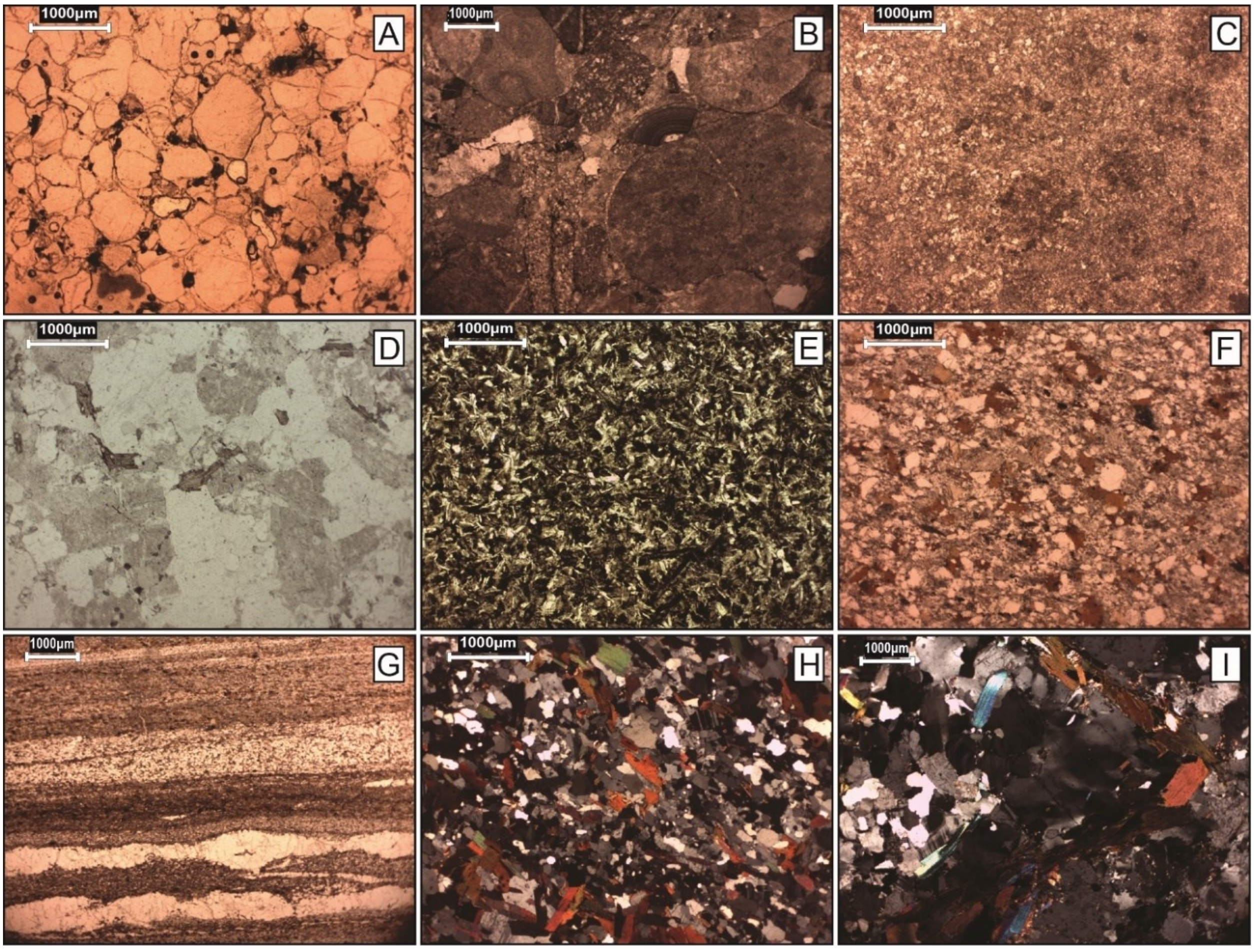

Figure 21 Photomicrographs of the main gravel size clast lithologies from IODP Site U1521 core (from Zurli et al., 2022b). A) Quartz-arenite, PPL, magnification 2.5X (355.72 m CSF-A); B) Carbonate conglomerate, PPL, magnification 1.6X (386.46 m CSF-A); C) Limestone, PPL, magnification 2.5X (610.17 m CSF-A); D) Granite, PPL, magnification 2.5X (326.27 m CSF-A); E) Basalt, PPL, magnification 2.5X (279.34 m CSF-A); F) Biotite meta-greywacke, PPL, magnification 2.5X (577.18 m CSF-A); G) Phyllite with quartz boudins, PPL, magnification 1.6X (559.14 m CSF-A); H) Biotite schist, XPL, magnification 2.5X (636.10 m CSF-A); I) Biotite ± white mica gneiss, XPL, magnification 1.6X (579.95 m CSF-A).

3.5.1.2. Mineral chemistry

Analyzed biotite crystals do not have any intra-crystalline chemical variability; biotite representative compositions are shown in Table 7. Full dataset of EDS analyses is provided in the Appendix IV.

Figure 22 shows biotite composition in terms of X_{Fe} (Fe/(Fe+Mg)) versus Al^{IV}. In the analyzed biotites, Al^{IV} ranges between 2.12 and 2.72 a.p.f.u., whereas X_{Fe} ranges from 0.40 and 0.76. In each sample, analyzed biotites usually show small compositional range. Two main compositional groups can be identified: i) the first has X_{Fe} between 0.40 and 0.53 and Al^{IV} that varies between 2.12 and 2.58 a.p.f.u.; ii) the second group has X_{Fe} that ranges between 0.56 and 0.76, and Al^{IV} varying from 2.27 and 2.72 a.p.f.u.

Table 7 Representative composition of biotite crystals from IODP Site U1521 clasts. Sample ID (e.g. 374-U1521A-29R-6W, 59-63 cm), and crystal ID (e.g. Bt3) are reported. Top (Wt%) EDS data are reported as values in normalized percentage of oxides weight; bottom (APFU): recalculated cations, on the basis of 22 oxygens, are shown, values are in atoms per formula unit (a.p.f.u.).

	374-U1521A-29R-6W, 59-63 cm	**374-U1521A-60R-5W, 62-65 cm**	**374-U1521A-64R-3W, 109-112 cm**	**374-U1521A-64R-6W, 20-24 cm**	**374-U1521A-68R-2W, 58-61 cm**	**374-U1521A-69R-6W, 40-45 cm**	**374-U1521A-70R-4W, 120-125 cm**
Wt%	**Bt3**	**Bt5**	**Bt3c**	**Bt11**	**Bt4**	**Bt1**	**Bt6**
SiO2	37,59	36,21	37,85	36,53	35,43	36,47	37,38
TiO2	3,20	3,35	2,29	2,14	3,47	3,27	3,46
Al2O3	19,33	18,07	19,05	16,91	18,98	17,38	16,43
FeO	17,12	21,50	15,45	22,62	22,29	19,19	19,03
MnO							
MgO	10,38	8,36	12,37	9,44	7,99	10,81	11,40
CaO							
Na2O							
K2O	8,95	8,90	8,85	9,09	8,53	9,01	9,18
Cl							
F							
TOTAL	96,57	96,39	95,85	96,73	96,69	96,12	96,87
APFU							
Si	5,53	5,47	5,56	5,54	5,35	5,48	5,57
AlIV	2,47	2,53	2,44	2,46	2,65	2,52	2,43
AlVI	0,87	0,69	0,85	0,57	0,73	0,55	0,45
Ti	0,35	0,38	0,25	0,24	0,39	0,37	0,39
Fe(ii)	2,10	2,72	1,90	2,87	2,82	2,41	2,37
Mn	0,00	0,00	0,00	0,00	0,00	0,00	0,00
Mg	2,27	1,88	2,71	2,14	1,80	2,42	2,53
Ca	0,00	0,00	0,00	0,00	0,00	0,00	0,00
Na	0,00	0,00	0,00	0,00	0,00	0,00	0,00
K	1,68	1,72	1,66	1,76	1,64	1,73	1,74
Cl	0,00	0,00	0,00	0,00	0,00	0,00	0,00
F	0,00	0,00	0,00	0,00	0,00	0,00	0,00
TOTAL	15,29	15,39	15,37	15,58	15,39	15,48	15,48
XFe	0,48	0,59	0,41	0,57	0,61	0,50	0,48

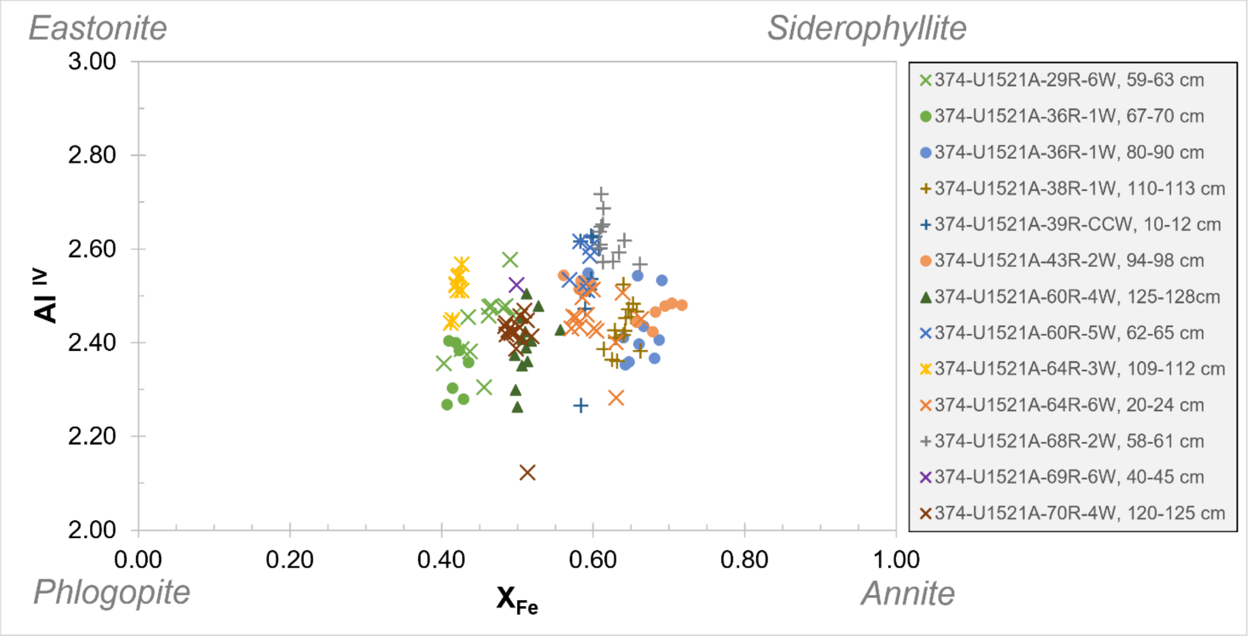

Figure 22 Biotite composition in terms of Al^{IV} versus X_{Fe} (Fe/(Fe+Mg)) for IODP Site U1521 clasts. Compositional end-members are shown in the edges of the diagram. Cross symbol represents metamorphic clasts, asterisk represents low-grade meta-sedimentary clasts; plus symbols represents intrusive clasts; triangle represents volcanic and sub-volcanic clasts; circle represents intrusive clasts within bulk diamictite samples.

Amphibole were analyzed in three samples: an intrusive clast (i.e., Sample 374-U1521A-38R-1W, 110-113 cm), and three grains within two samples of bulk diamictite (i.e., samples 374-U1521A-36R-1W, 80-90cm and 43R-2W, 94-98 cm). In Figure 23 calcic amphiboles were classified on the basis of (Leake et al., 1997). Samples show quite similar composition: silica content varies from 6.28 to 6.60 a.p.f.u., while X_{Mg} (Mg/(Mg+Fe)) ranges from 0.33 to 0.54.

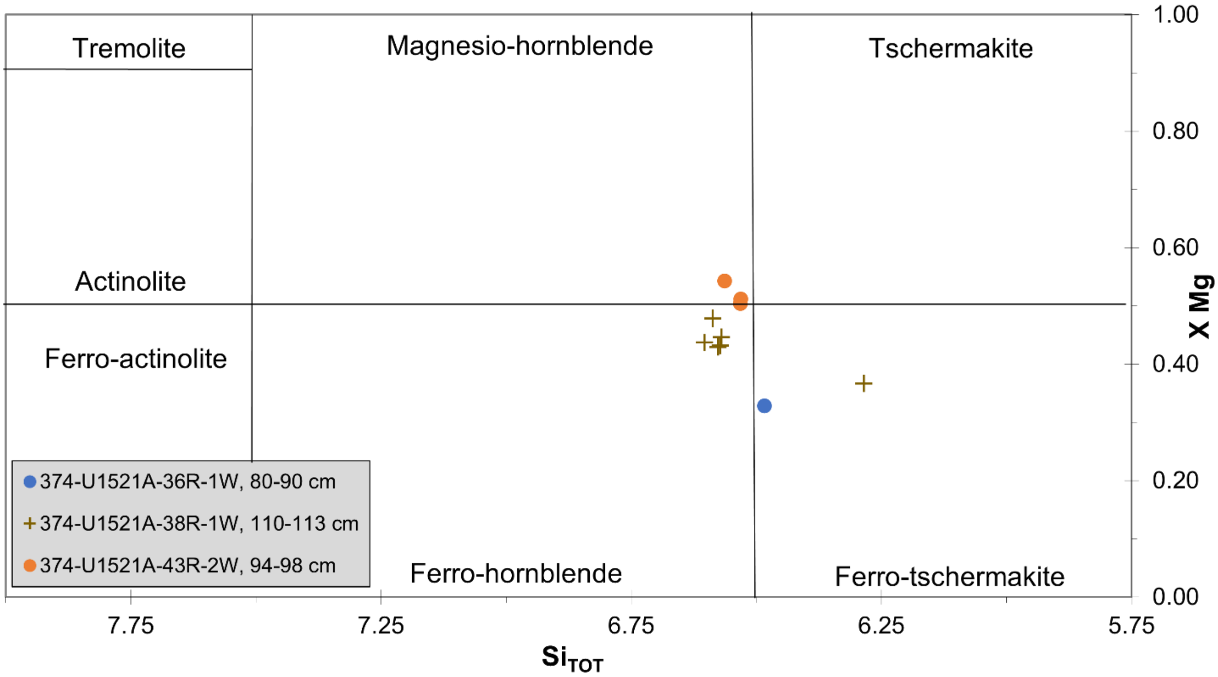

Figure 23 Amphibole composition in terms of Si versus X_{Mg} (Mg/(Mg+Fe)) for IODP Site U1521 clasts. Classification of calcic amphibole follow (Leake et al., 1997). Plus symbol represents intrusive clasts; circle represent intrusive grains within bulk diamictite sample.

3.5.1.3. Clast Distribution

Figure 24 shows the total number of clasts per 1 m along the Site U1521 core, which highlights variations in clast content and composition by lithostratigraphic unit. The clast lithology distribution along the core allows the identification of three main petrofacies (PF; Table 8).

Table 8 Petrofacies classification on the basis of clast lithology assemblage of IODP Site U1521

Petrofacies ID	Main lithological groups	Other features	Occurrence
PF21-1	meta-sedimentary ≈ felsic intrusive >> dolerite	basalt quite absent	U1521: 648-568 m CSF-A
PF21-2	meta-sedimentary ≥ felsic intrusive >> basalt	dolerite rare; mud intraclast present	U1521: 568-380 m CSF-A
PF21-3	meta-sedimentary ≈ felsic intrusive >> dolerite	basalt present	U1521: 380-324 m CSF-A

LSU I includes the top 7.4 m of the core and consists of diatom-rich mud to diatom bearing mud with dispersed clasts and two intervals of diatom-bearing sandy mud (McKay et al., 2019). This unit was not investigated for clasts identification.

LSU II (7.4-85.34 m CSF-A) is characterized by interbedded lithified clast-poor diamictite, diatomite and mudstone (McKay et al., 2019) but the recovery is very low (25%). Here the number of clasts varies between 0 to 30 per each meter interval. Within this unit, clasts lithologies are dominated by granitoid rocks and metamorphic rocks (on average 30.3% and 33.9% of the total amount of counted clasts, respectively). Dolerites are widely represented (16.7%), whereas other groups are present in minor amount: quartz fragments (9.9%), volcanic rocks (5.2%), mud intraclasts (3.7%) and sedimentary rocks (0.4%).

LSU III (85.34-209.17 m CSF-A) is a bioturbated diatom-bearing/rich mudstone sequence (McKay et al., 2019). This lithostratigraphic unit is characterized by the near absence of pebbles and cobbles; the number of gravel-size clasts ranges from 0 to 10 for each m interval in most of the logged cores, from 10R to 22R (Figure 24D). In LSU III clasts were counted but not classified because they are very rare, altered and too small in size to be accurately classified.

LSU IV (209.17-280.72 m CSF-A) is a diatom-bearing sandy diamictite (McKay et al., 2019) and clast numbers range from 20 to 60/meter. Clast assemblage is characterized by a high number of metamorphic rocks (45.9% on average), whereas granitoids are the second most abundant lithology (19.4%); other groups represented are volcanic rock (10.6%), quartz fragments (8.9%), dolerite (8.4%), mud intraclasts (5.9%), and sedimentary rock (0.9%). The amount of metamorphic and intrusive rocks is homogeneous throughout this LSU; on the other hand, dolerite clasts increase down core, whereas volcanic rocks decrease (Figure 24E).

LSU V (280.72-324.20 m CSF-A) was not logged because of poor recovery (16%), drilling disturbance and its composition of mainly chert nodules and silica-cemented mudstone lacking gravel size clasts (McKay et al., 2019).

LSU VI has been subdivided into three sub-units (McKay et al., 2019) which are treated separately.

LSU VI subunit A (324.20-380.04 m CSF-A) is an interbedded sequence of clast-rich to clast-poor diamictite and mudstone (McKay et al., 2019): here number of clasts are generally high but wide variations occur along the subunit with intervals with 20 clasts/m (i.e., Section 38R-1) and intervals with up to 160 clasts/m (i.e., Section 43R-2 and 3). Clast lithology distribution also varies along the subunit. Granitoid rocks range from 26.3% to 45.0% of the total amount of clasts, with an average value of 36.7%. Metamorphic rocks range from 36.4% to 55.2% with an average of 44.8% and they are the most represented group. Dolerites are quite homogeneous, ranging from 5.3 to 14.2%, with an average of 9.2%. Other groups are less represented (quartz fragments average 3.9%, volcanic rocks 3.3%, mud intraclasts 1.8%, sedimentary clasts 0.3%). Six of the bulk samples from diamictites are all from this LSU (see Table 3 for sample position): percentages of counted lithic grains >2mm from analyzed thin sections are shown in Appendix III. Overall, percentage composition of gravel-sized lithics counted in thin sections mostly reflects that of clasts logged macroscopically. Indeed, metamorphic lithics (gneisses, schists, phyllites, meta-sandstones, marbles) are the dominant group ranging from 41% to 50% in the 6 analyzed samples, followed by granitoid rocks (ranging from 8% to 23%) and dolerites (ranging from 10% to 23%). Sedimentary lithic fragments are present in minor numbers, but microscopic analysis allowed us to discriminate between clastic sedimentary lithics (sandstones, siltstones, conglomerates, ranging from 0% to 14%) and carbonate rocks (limestones, ranging from 0% to 8% of the total amount). Basaltic volcanic lithics range from 1% to 5%, whereas felsic porphyries range from 0% to 6%.

Subunit VIB (380.04-440.58 m CSF-A) consists of massive to stratified clast-poor to clast-rich diamictite (McKay et al., 2019). Generally, the number of clasts is lower than in Subunit VIA but wide variations occur, from 20 clasts/m (i.e., Section 48R-1) to 85 clasts/m (i.e. core 47R section 4). Subunit VIB is characterized by a decreasing down core number of dolerites (ranging from 0.6 to 4.3% and averaging 2.8%) and by an increasing down core number of volcanic rocks, ranging from 1.5 to 7.5% (average value of 4.9%). Most of the clasts are represented by metamorphic rocks (49.8% on average) and intrusive rocks (38.3% on average). Other groups are scarcely represented (<5%). One sample of bulk diamictite from this LSU (see Table 3) was analyzed. Generally, clast composition of this sample (Appendix III) reflects the macroscopic classification of clasts in this LSU. The metamorphic rocks group is the most represented (42%); whereas others are low in percentage (intrusive - 11%, basalt - 3%, felsic porphyry - 9%, and clastic sedimentary - 7%). Moreover, dolerites are nearly absent (1%), and carbonate sedimentary rocks are completely absent.

In Subunit VIC (440.58-567.95 m CSF-A), constituted by interbedded clast-poor diamictite and mudstone (McKay et al., 2019), the number of clasts is generally lower than in Subunit VIA and varies between less than 10/m in clast-poor intervals to more than 90/m in clast-rich intervals with most of the unit characterized by clasts ranging in number from 20 to 60/m. Subunit VIC is similar in composition to Subunit VIB. Metamorphic rocks are most abundant (50.1% on average) and the intrusive rock group is the second (37.2% on average) most represented. Similar to Subunits VIB, dolerite occurrence is very low (2.2% on average). The volcanic rock group is scarcely represented (2.4% on average) as are the other groups (<5%). Volcanic clasts do not occur continuously along the subunit: they are quite rare in the lowermost portion of the subunit (from 568.8 m to 504.2 m CSF-A in Cores 63R to 57R), whereas they increase in the uppermost portion of the subunit (from 504.2 m to 438.9 m CSF-A in Cores 57R to 50R).

LSU VII (567.95-648.17 m CSF-A) consists of interbedded clast-poor sandy to clast-rich muddy diamictite (McKay et al., 2019) and characterized by a generally high number of clasts, ranging from 20/m in clast-poor intervals up to 120/m in clast-rich intervals. LSU VII is characterized by high abundance of metamorphic (47.3% on average) and intrusive (39.3% on average) rocks. In comparison with sub-units VIB and VIA, in the LSU VII dolerites amount abruptly increase, representing, on average, 9.9% of the whole gravel fraction. The volcanic rocks group is almost absent in this unit; moreover, the other groups are poorly represented within the clast assemblage (Figure 24E).

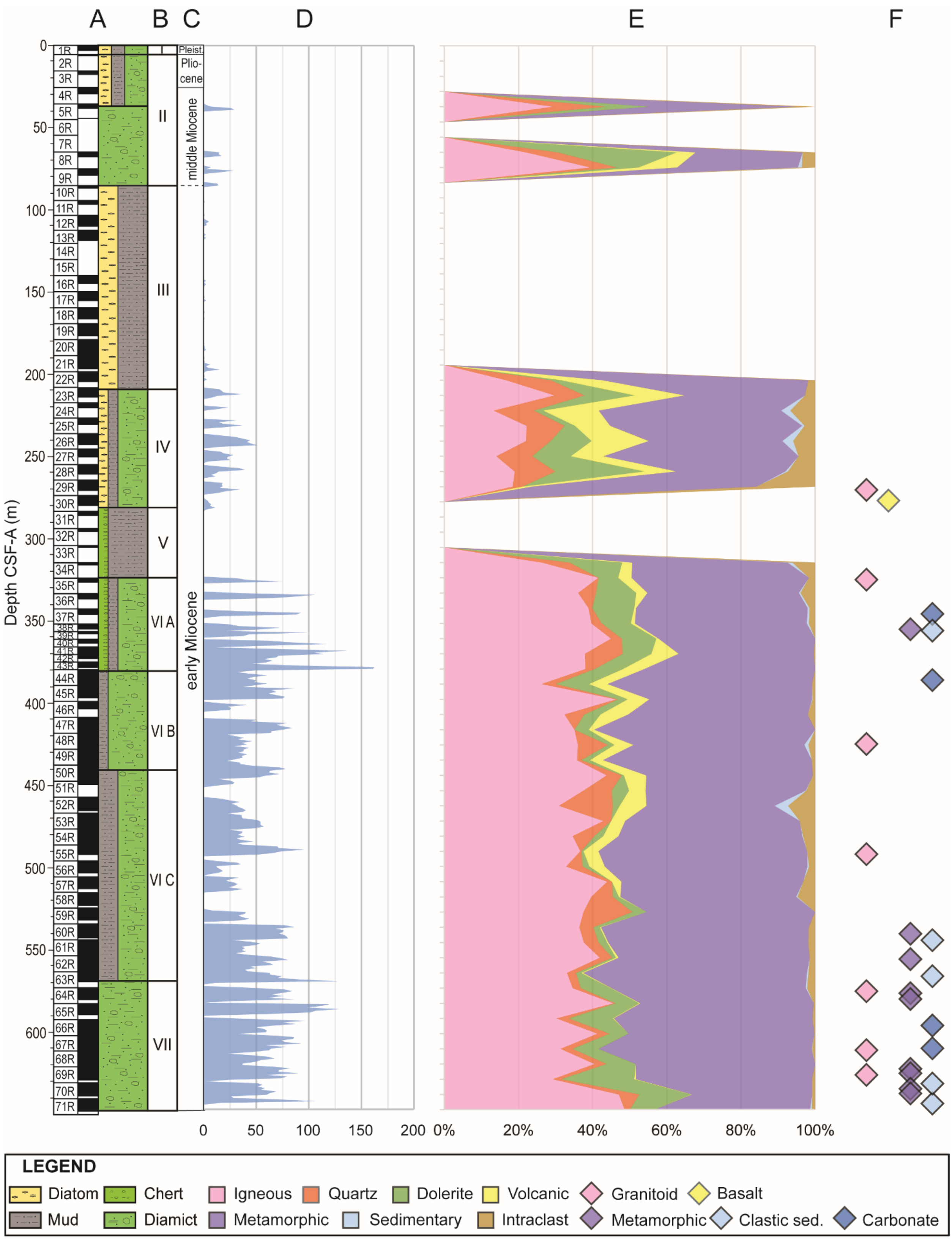

Figure 24 Clasts lithology distribution along the IODP Site U1521 core (from Zurli et al., 2022b) A) Stratigraphic log of the IODP Site U1521 with core number and recovery (from McKay et al., 2019); B) Lithostratigraphic Unit (from McKay et al., 2019); C) age (from McKay et al., 2019); D) number of clasts/meter; E) occurrence in percentage of each lithological group all along the core. Percentage is calculated for each logged core; squares in the legend identify rock lithologies (modified after (Marschalek et al., 2021); F) Position of sampled pebbles and cobbles and classification on the basis of thin section analysis (diamonds in the legend, see Appendix III for detailed petrographic descriptions and mineral assemblage).

3.5.2. IODP Site U1522

3.5.2.1. Clast Petrography

The main petrographic features, based both on macroscopic and microscopic analysis, of each identified lithological group are reported in this section; the detailed microscopic description of each clast is in the Appendix V. Figure 25 shows photomicrographs of representative clasts of each lithological group.

Macroscopically, most of the intrusive rock clasts are felsic, whereas mafic and intermediate varieties commonly occur along the core. Felsic varieties are usually grey, while rarely pinkish ones were recognized. In general, granitoid rocks are slightly hetero-granular, fine- to medium/coarse-grained, with hypidiomorphic to allotriomorphic texture. Some samples (i.e. 374-U1522A-57R-5W, 1-6 cm; 374-U1522A-58R-4W, 4-7 cm; 374-U1522A-60R-5W, 36-40 cm; 374-U1522A-76R-1W, 109-111 cm) usually show a metamorphic overprint, marked by undulose extinction and partial recrystallization of quartz, weak schistose to gneissic structure. Samples are usually isotropic but sometimes weakly foliated structure occurs (i.e. 374-U1522A-67R-2W, 105-108 cm); slightly porphyritic texture is rare (i.e. 374-U1522A-58R-1W, 68-71 cm; 374-U1522A-69R-1W, 0-4 cm; 374-U1522A-69R-1W, 0-4 cm). Microgranitoid varieties rarely occur (i.e. 374-U1522A-62R-2W, 49-52 cm; 374-U1522A-76R-1W, 109-111 cm). In the felsic granitoids, the mafic mineralogical phase is usually biotite (i.e. 374-U1522A-58R-1W, 68-71 cm), hornblende (i.e. 374-U1522A-70R-2W, 134-137 cm) or commonly both (i.e. 374-U1522A-67R-2W, 105-108 cm; 374-U1522A-69R-1W, 0-4 cm). The main mineralogical phases are usually quartz, plagioclase and alkali feldspar. Quartz crystals are usually anhedral and interstitial, with homogeneous to weakly undulose extinction (i.e. 374-U1522A-67R-2W, 105-108 cm). Plagioclase forms anhedral to subhedral twinned crystals, and sometimes shows chemical zonation (i.e. 374-U1522A-58R-1W, 68-71 cm; 374-U1522A-67R-2W, 105-108 cm). Alkali feldspars, that form anhedral to subhedral crystals, are usually present both as microcline and orthoclase. Feldspars usually show a great degree of alteration, and they are partially or nearly completely replaced by sericite and phyllosilicate aggregates. Modal compositions range from tonalite/granodiorite to monzogranite.

Mafic intrusive rocks are recognized macroscopically and then confirmed by thin section analysis. They vary from fine- to coarse-grained, with usually weakly developed sub-ophitic texture. The main mineralogical constituent is plagioclase, that sometimes is almost completely replaced by sericite and phyllosilicate aggregates. Mafic mineral are pyroxenes, usually clinopyroxene (i.e., 374-U1522A-60R-3W, 87-91 cm; 374-U1522A-62R-2W, 8-10 cm; 374-U1522A-69R-1W, 3-5 cm; 374-U1522A-76R-3W, 42-45 cm) or amphiboles, usually hornblende (i.e., 374-U1522A-61R-1W, 29-32 cm). Rarely samples show the sub-ophitic texture typical of dolerite (i.e., 374-U1522A-76R-3W, 42-45 cm). Accessory minerals are quartz or olivine (i.e., 374-U1522A-60R-3W, 87-91 cm). Clinopyroxene sometimes forms crystal with pecilitic texture (374-U1522A-69R-1W, 3-5 cm).

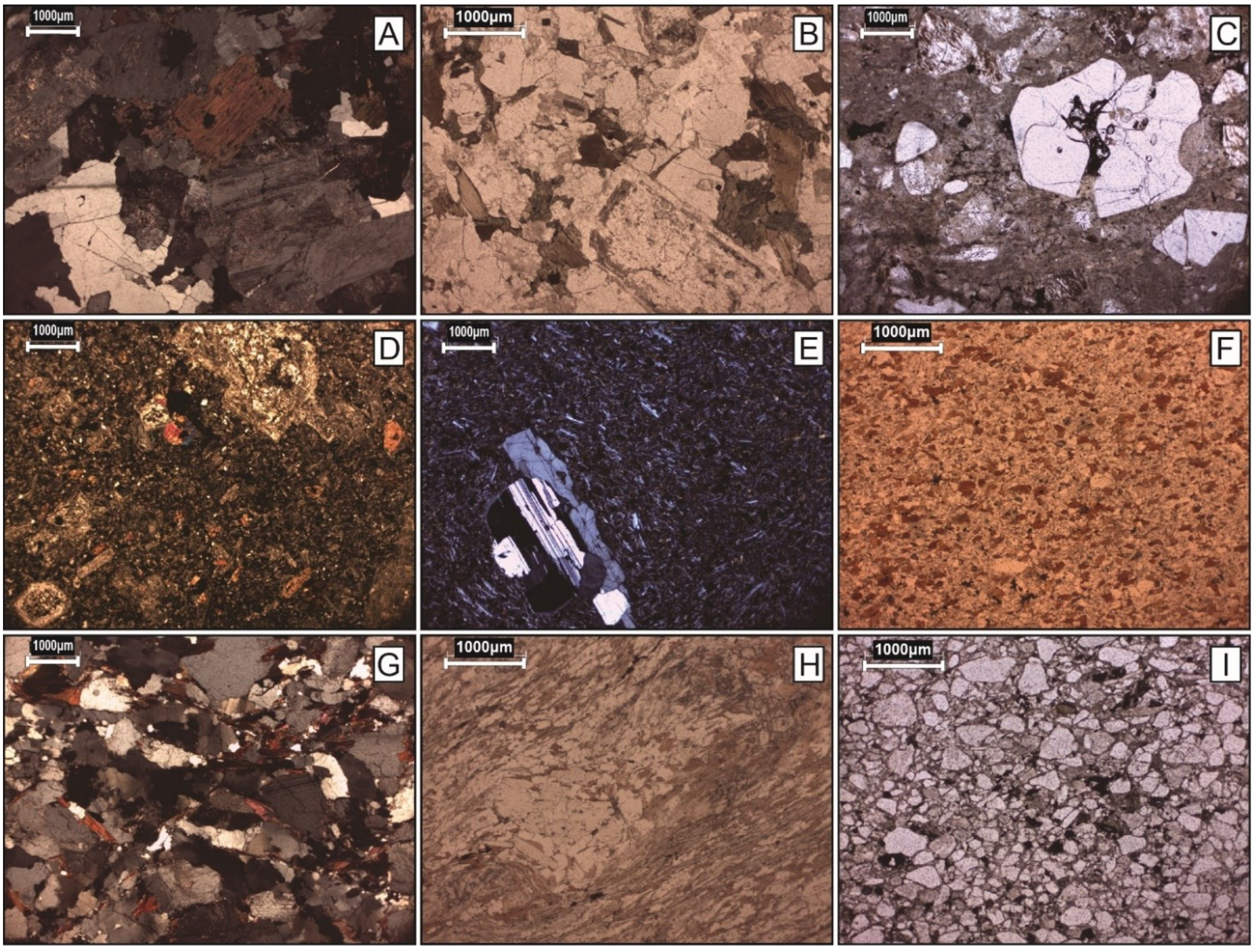

Figure 25 Photomicrographs of the main gravel size clast lithologies from IODP Site U1522. A) Biotite monzogranite, XPL, magnification 1.6X (521.18 m CSF-A); B) Biotite - Hornblende granodiorite, PPL, magnification 2.5X (625.33 m CSF-A); C) Felsic porphyry, PPL, magnification 1.6X (562.33 m CSF-A); D) Porphyry, XPL, magnification 1.6X (582.95 m CSF-A); E) Basalt, XPL, magnification 1.6X (549.30 m CSF-A); F) Biotite meta-greywacke, PPL, magnification 2.5X (493.29 m CSF-A); G) Biotite gneiss, XPL, magnification 1.6X (597.36 m CSF-A); H) Aluminum silicate – Garnet mica-schist, PPL, magnification 2.5X (617.81 m CSF-A); I) Sandstone, PPL, magnification 12.5X (560.55 m CSF-A).

Felsic porphyritic rocks commonly occur in the core. Macroscopically they are made up of a microcrystalline groundmass with millimeters-scale euhedral to subhedral porphyritic crystals. Clasts are yellowish/greyish to pinkish, and sometimes fluidal structure is recognizable. Thin section analysis confirm that groundmass is microcrystalline to hypoialine, with a quartzofeldspatic composition. Porphyritic crystals, that vary from 10 to 40% in volume, are sometimes glomerophorphyric (i.e., 374-U1522A-57R-2W, 120-123 cm), euhedral to subhedral. They are feldspars (both plagioclase and alkali feldspar) and quartz; the latter usually shows reabsorption rims. Rarely metamorphic overprint occurs (i.e., 374-U1522A-61R-1W, 44-47 cm). Sometimes mafic, where amphibole and olivine crystals are present (i.e., 374-U1522A-64R-4W, 86-89 cm), and intermediate (i.e., 374-U1522A-72R-1W, 34-37 cm) varieties occur. Volcanic rocks are basaltic varieties with holocrystalline very fine-grained, usually porphyritic texture. The samples are usually strongly altered, and mafic minerals, as well as plagioclase, are abundantly replaced by secondary phases. Groundmass is mainly made up of plagioclase, sometimes coupled with pyroxene and/or olivine (i.e., 374-U1522A-61R-1W, 0-2 cm; 374-U1522A-62R-1W, 12-15 cm; 374-U1522A-67R-3W, 71-72 cm). Porphyritic crystals are plagioclase ± olivine ± pyroxene. Olivine is usually strongly altered and almost completely replaced by secondary phases, as serpentine (i.e., 374-U1522A-59R-7W, 91-93 cm;) or bowlingite (i.e., 374-U1522A-62R-1W, 12-15 cm). Opaque minerals are always present, sometimes in abundant percentage. In the sample 374-U1522A-67R-1W, 53-58 cm few trachytic basalt grains were recognized. Moreover, a volcanoclastic clast (lapilli tuff) was found (i.e., 374-U1522A-67R-2W, 72-75 cm).

Metamorphic rocks group comprises meta-sandstone, hornfels, schist, and gneiss. Macroscopically meta-sandstone, greyish to blackish, and meta-pelites, blackish, do not show marked schistosity. Meta-sandstones are mainly biotite spotted ± white mica meta-greywacke (i.e., 374-U1522A-55R-2W, 17-20 cm, 374-U1522A-56R-1W, 48-51 cm; 374-U1522A-57R-1W, 0-3 cm), sometimes with a calcite-rich matrix. Schists are fine- to medium-grained, more or less schistose. Mineralogical assemblage comprises quartz, plagioclase and biotite (i.e., 374-U1522A-66R-CCW, 19-22 cm) ± white mica (i.e., 374-U1522A-63R-2W, 112-115 cm; 374-U1522A-75R-2W, 9-12 cm) ± amphibole (i.e., 374-U1522A-68R-1W, 56-59 cm) ± Al-silicate and garnet (i.e., 374-U1522A-68R-2W, 78-80 cm); sometimes calcite crystals are abundant (i.e., 374-U1522A-68R-6W, 56-60 cm). A granofelsic, amphibole rich (actinolite) meta-sedimentary clast occurs (i.e., 374-U1522A-72R-3W, 71-74 cm). Very fine-grained biotite hornfels rarely occurs (i.e., 374-U1522A-61R-CCW, 38-40 cm). Gneissic rocks are rarer; a biotite orthogneiss occurs (i.e., 374-U1522A-57R-5W, 37-41 cm). Most of the samples are composed of quartz, plagioclase, biotite (i.e., 374-U1522A-66R-1W, 56-59 cm) ± diopside (i.e., 374-U1522A-67R-4W, 6-8 cm). Only one meta-carbonate rock was found in the studied clasts (i.e., 374-U1522A-55R-3W, 52-56 cm). The paragenesis of sampled clasts vary from greenschist/sub-greenschist to amphibolite facies, indicating that clasts came from rocks that experience low- to medium-grade metamorphism.

Sedimentary rocks are mainly sandstone, mudstone, and carbonate. Sandstone varies from sub-arkosic varieties (i.e., 374-U1522A-62R-2W, 52-55 cm; 374-U1522A-68R-4W, 86-89 cm) with angular grains, to laminated quartzarenite ones (i.e., 374-U1522A-65R-3W, 77-80 cm) that are made up by sub-rounded grains.

The mudstone shows planar lamination marked by oxides and carbonates thin laminae (i.e., 374-U1522A-58R-3W, 120-121 cm). Sample 374-U1522A-70R-2W, 73-74 cm is a brecciate carbonate.

3.5.2.2. Mineral Chemistry

Analyzed mineralogical phases are biotite, white mica, amphibole, pyroxene, and garnet. Full dataset of EDS analysis is provided in Appendix VI. Biotite crystals were analyzed from metamorphic and intrusive lithologies. Figure 26 shows the biotite composition in terms of X_{Fe} (Fe/(Fe+Mg)) versus Al^{IV}. Analyzed biotites do not have any intra-crystalline chemical variability. The Al^{IV} value varies from 2.25 and 2.67 a.p.f.u., whereas X_{Fe} ranges between 0.37 and 0.54. All the samples have a quite similar composition, and any significant difference occurs between intrusive and metamorphic samples. Every biotite crystal composition is homogeneous in each sample.

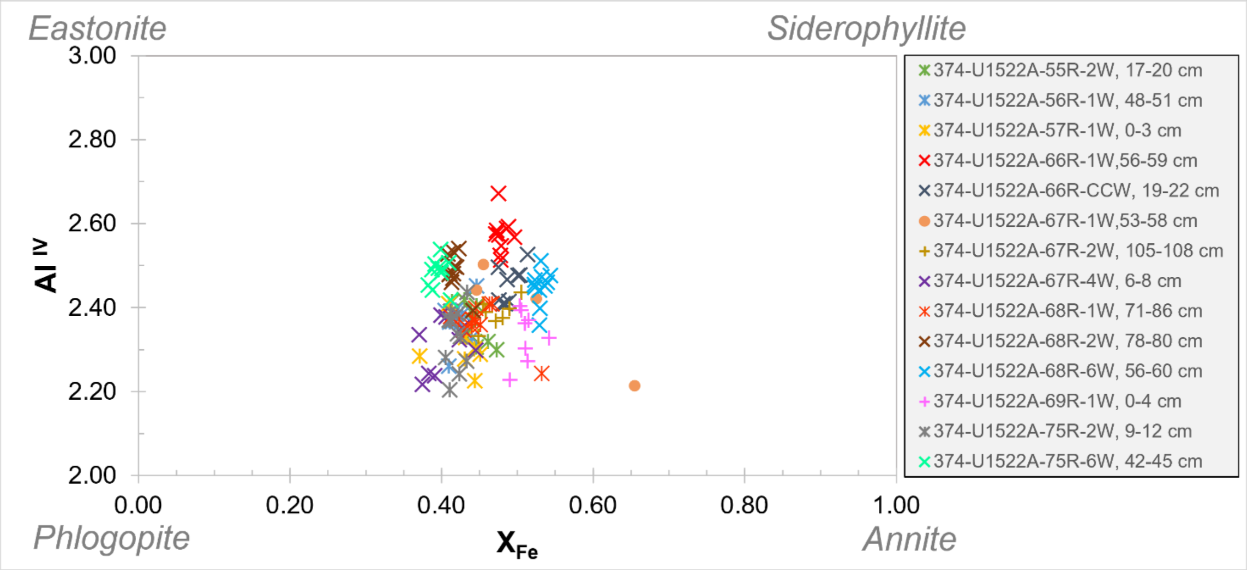

Figure 26 Biotite composition in terms of Al^{IV} versus X_{Fe} (Fe/(Fe+Mg)) for IODP Site U1522 clasts. Compositional end-members are shown at the edges of the diagram. Cross symbol represents metamorphic clasts, asterisk represents low-grade meta-sedimentary clasts; plus symbols represents intrusive clasts; circle represents intrusive clasts within bulk diamictite samples.

Amphiboles were analyzed from intrusives (i.e. Sample 374-U1522A-61R-1W, 29-32 cm; 67R-2W, 105-108 cm; 69R-1W, 0-4 cm), volcanic and sub-volcanic rocks (i.e. Sample 374-U1522A-64R-4W, 86-89 cm; 67R-2W, 72-75 cm), and metamorphic rocks (i.e. 374-U1522A-68R-1W, 71-86 cm; 72R-3W, 71-74 cm). Analyzed amphiboles were classified based on Leake et al. (1997) and classification diagrams are shown in Figure 27 in terms of Si_{TOT} versus X_{Mg}. Analyzed crystals fall in the calcic amphibole field, however two different classifications have been adopted due to differences in the $(Na+K)_A$ value. Most of the samples have $Ca_B \geq 1.50$ and $(Na+K)_A < 0.50$ (see Appendix VI) and the classification of Figure 27A has been adopted. In this case samples are quite compositionally inhomogeneous. Crystals in the intrusive rocks fall in the magnesio-hornblende field; however, samples 374-U1522A-61R-1W, 29-32 cm and 67R-2W, 105-108 cm show strongly inhomogeneous composition, probably due to alteration, previously seen with petrographic analysis, while sample 374-U1522A-69R-1W, 0-4 cm shows small variations. Amphibole crystals analyzed in a sub-volcanic rock (Sample 374-U1522A-64R-4W, 86-89 cm) mainly fall in the tschermakite field. Crystals from meta-sedimentary rocks mainly fall in the actinolite filed, whereas amphiboles from sample 374-U1522A-68R-1W, 71-86 cm ranges from actinolite to magnesio-hornblende. Only one sample (374-U1522A-67R-2W, 72-75 cm) have $Ca_B \geq 1.50$, $(Na+K)_A \geq 0.50$, $Ti < 0.50$, and $Al^{VI} < Fe^{3+}$ (see Appendix VI) and the classification is shown in Figure 27B, where the crystals fall in the magnesio-hastingsite field.

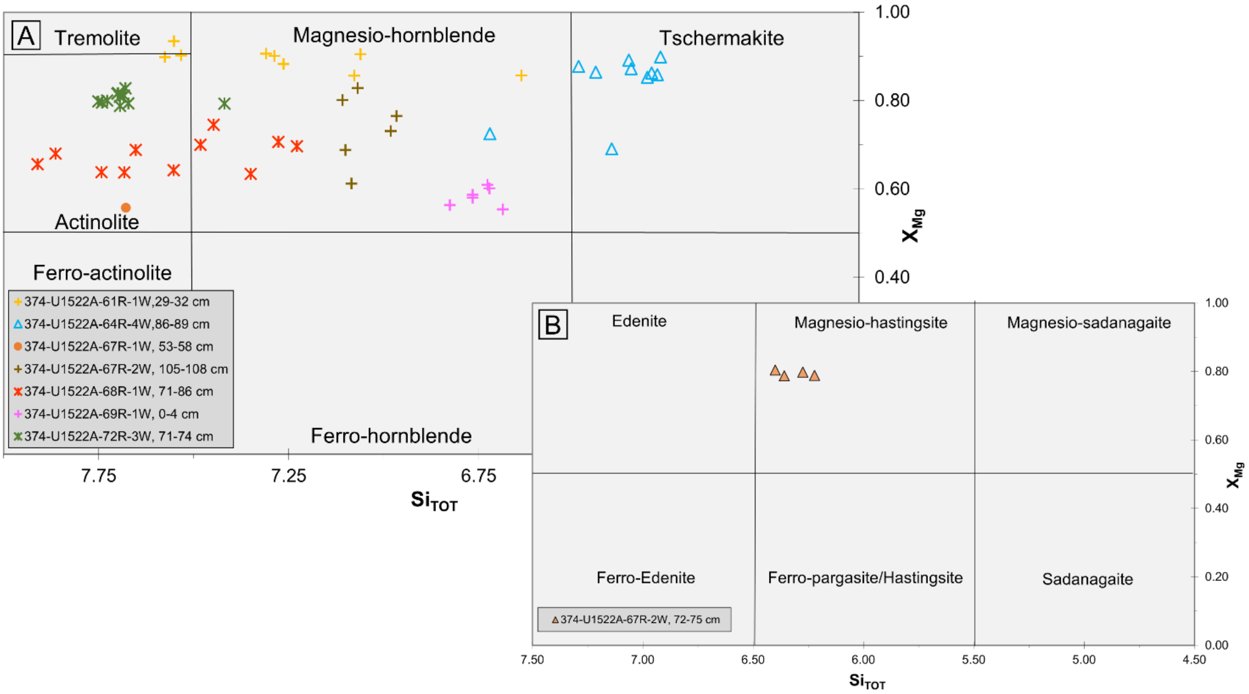

Figure 27 Amphibole composition in terms of Si_{TOT} versus X_{Mg} for IODP Site U1522 clasts. A) Classification for calcic amphibole with $Ca_B \geq 1.50$ and $(Na+K)_A < 0.50$ (Leake et al., 1997); B) Classification for calcic amphibole with $Ca_B \geq 1.50$, $(Na+K)_A \geq 0.50$, $Ti < 0.50$, and $Al^{VI} < Fe^{3+}$ (Leake et al., 1997). Cross symbol represents metamorphic clasts, asterisk represents low-grade meta-sedimentary clasts; plus symbols represents intrusive clasts; empty triangle represents volcanic and sub-volcanic clasts; filled triangle represents volcanoclastic clasts; circle represents intrusive clasts within bulk diamictite samples.

White mica rarely occurs within samples and were analyzed only from 3 clasts of metamorphic origin. Figure 28 shows the white mica composition in terms of Si versus Al. Total Si varies between 6.09 and 6.41 a.p.f.u. while Al ranges from 5.17 to 5.63 a.p.f.u. Whereas the number of grains is low, samples form two separate populations: the first is represented by samples 374-U1522A-66R-1W, 56-59 cm and 68R-2W, 78-80 cm with grains that show Al-Muscovite composition; the second is represented by sample 374-U1522A-75R-2W, 9-12 cm that shows a more phengitic-muscovite composition.

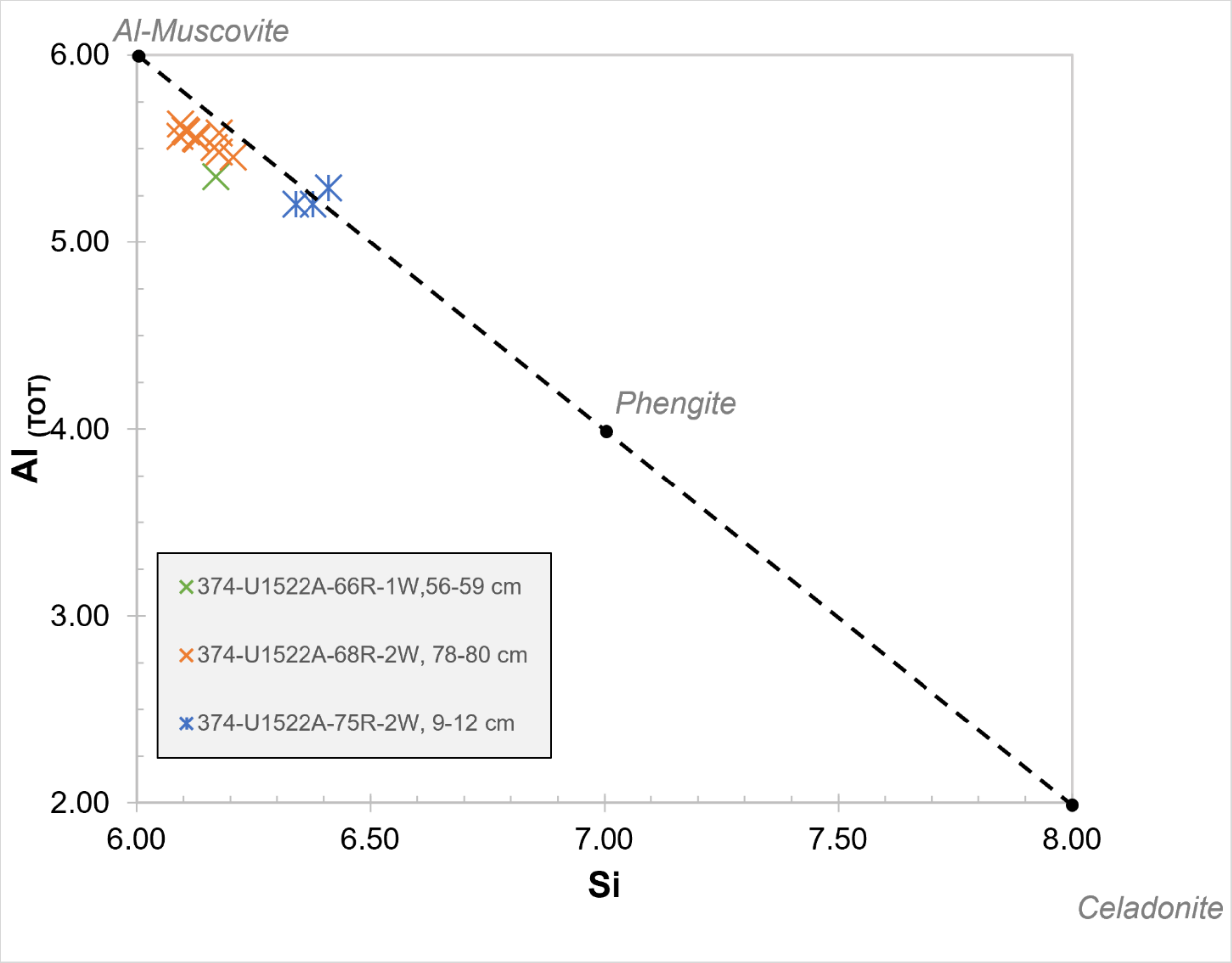

Figure 28 White mica composition in terms of Si versus Al for IODP Site U1522 clasts. Compositional end-members are shown within the graph

Pyroxenes occur only in two samples, one of volcanic origin (374-U1522-67R-2W, 72-75 cm) and one metamorphic (374-U1522-67R-4W, 6-8 cm). Pyroxene grains from volcanic clast have augite composition, while grains from metamorphic clast have diopside composition (Figure 29).

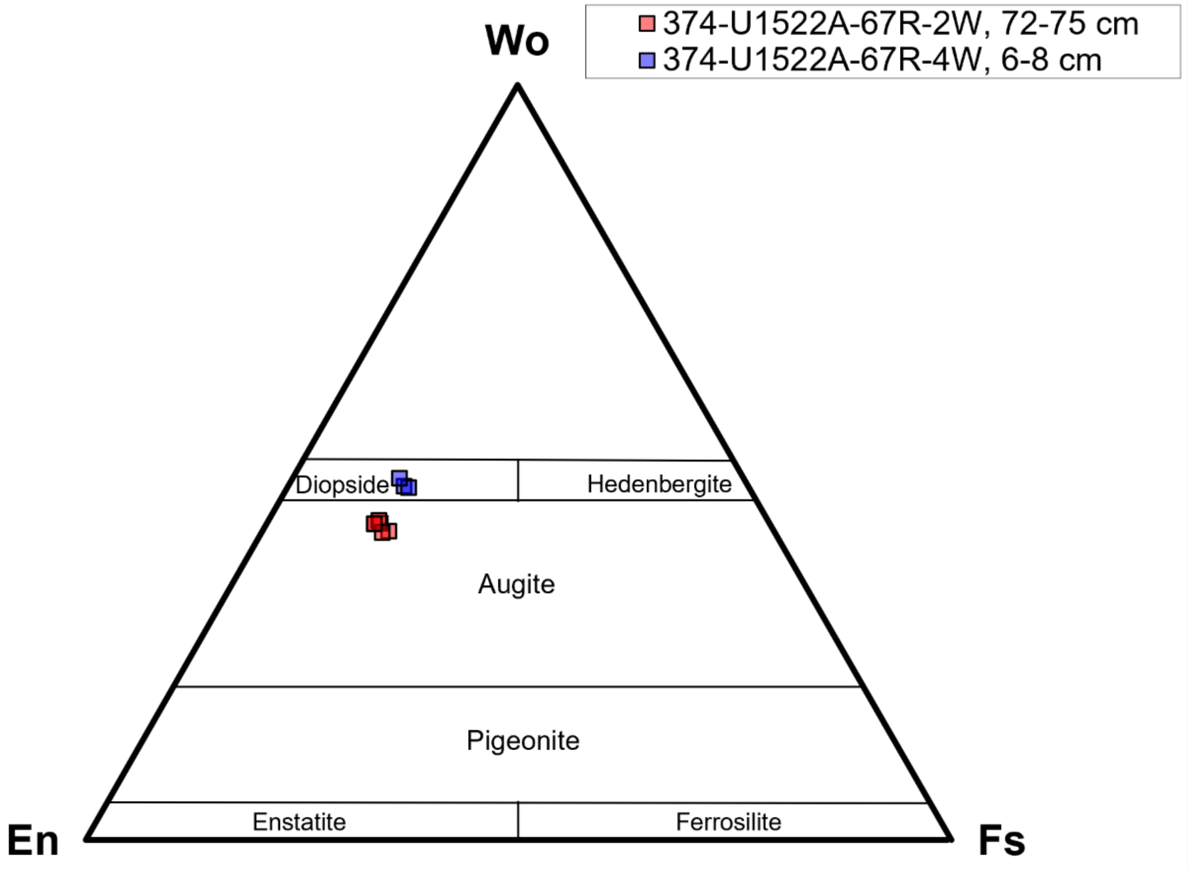

Figure 29 Pyroxene composition for IODP Site U1522 clasts. En – Enstatite, Fs – Ferrosilite, Wo - Wollastonite

Garnet was found only in one clast of Al-silicate mica-schist (Sample 374-U1522A-68R-2W, 78-80 cm). Figure 30 show the classification diagram for garnet in terms of spessartine, almandine, and pyrope (Aubrecht et al., 2009) and where classification fields are reported (Aubrecht et al., 2009; Krippner et al., 2014). Analyzed grains fall in the field of garnets derived from gneisses which recorded amphibolite facies metamorphic conditions (Krippner et al., 2014). The classification fits with the petrographic characterization of the clast (see Appendix V).

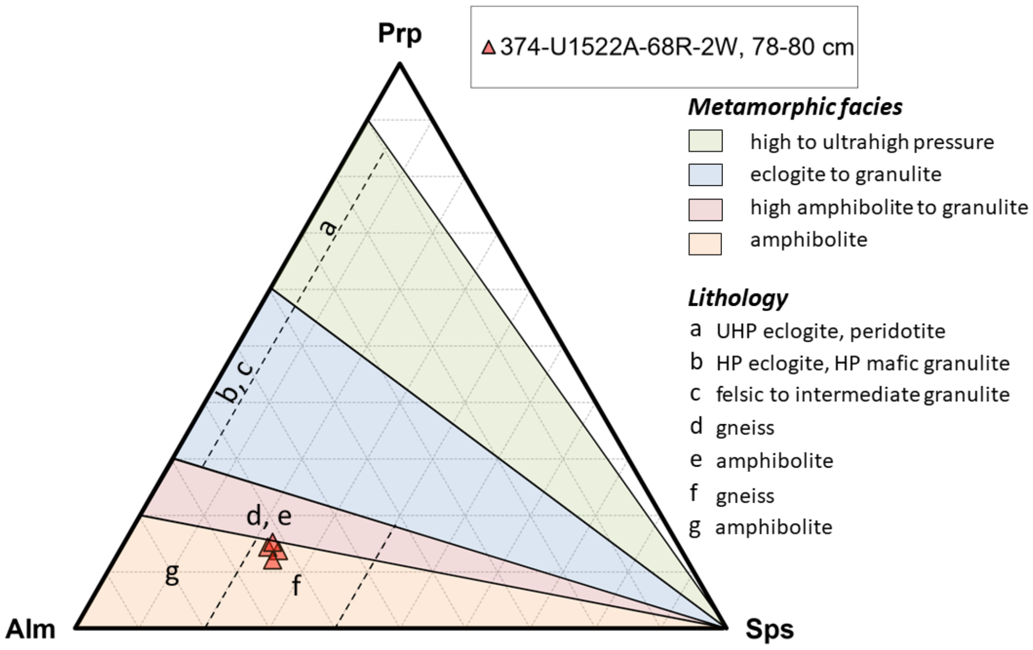

Figure 30 Ternary diagram used for garnet classification in terms of almandine spessartine, and pyrope (Aubrecht et al., 2009) for IODP Site U1522 clasts. Fields are from Aubrecht et al. (2009) and Krippner et al. (2014). Alm – Almandine, Prp – Pyrope, Sps - Spessartine

3.5.2.3. Clast Distribution

In the Miocene-Pliocene interval of the IODP Site U1522A a total number of 19414 clasts was counted and logged within the core; wide variations in the number of clasts distribution occur along the core (Figure 31D). The clast lithology distribution was described based on the lithostratigraphic unit division of McKay et al. (2019). Based on the occurrence of lithological groups along the core, three main petrofacies occur (Table 9).

Table 9 Petrofacies classification on the basis of clast lithology assemblage of IODP Site U1522.

Petrofacies ID	Main lithological groups	Other features	Occurrence
PF22-1	meta-sedimentary > felsic intrusive >> basalt ≥ felsic porphyry	dolerite quite absent	U1522: 696-505 m CSF-A
PF22-2	meta-sedimentary >> felsic intrusive	Mud intraclast common; basalt and felsic porphyry rare; dolerite absent	U1522: 505-398 m CSF-A)
PF22-3	meta-sedimentary > felsic intrusive >> basalt	Felsic porphyry present; dolerite absent	U1522: 398-203 m CSF-A)

LSU II (203.20–397.58 m CSF-A) consists of massive dark greenish gray to greenish gray diatom-bearing/rich sandy and muddy diamictite (McKay et al., 2019). Only 32% of the drilling was recovered, and in the interval comprised between ca. 350 and 400 m there is not any recovery (McKay et al., 2019).

The clasts number is 10 clast/10 cm on average, ranging from 0 to 23 clasts/10 cm. In this LSU, the most common lithological group is represented by the metamorphic rocks one (70% on average); intrusive rocks group represent 25% on average of the whole number of clasts. Other groups represent overall the 5%. Within the interval, the clasts distribution is not homogeneous (Figure 31E): between cores 22R and 28R (ca. 265 m CSF-A) an increase of basaltic rocks and dolerite is recorded, representing 3% and 1% on average respectively, as well as of mud intraclasts (1% on average) while these groups are less represented in the lower portion of the LSU II. Inverse proportionality is shown by felsic porphyry group behavior because it is more common between core 29R and 45R, while it weakly decreases in the cores 22R-28R.

LSU III (397.58–646.93 m CSF-A) is dived into three subunits (Figure 31B) based on the style of interbedding and lithologic accessories (McKay et al., 2019); each subunit is treated separately.

Subunit III A (397.58–465.08 m CSF-A) is a massive bioturbated greenish gray muddy diatomite with glauconite and interbedded massive dark greenish gray diatom-bearing/rich sandy and muddy diamictite with variable clast abundance (McKay et al., 2019). LSU III A have an average value of 5 clasts/10 cm, ranging from 0 to 19 clasts/10 cm. Clast lithology assemblage is quite homogenous along the interval (Figure 31E). The most common clasts are metamorphic ones (80% on average), while intrusive ones are 8% on average. Basaltic rocks are less than 1%, few dolerite clasts occur (ca. 1% on average), while felsic porphyry clasts are quite absent. The subunit is characterized by an elevated number of mud intraclasts that represent 8% on the whole, but they range between 2 and 14%. The higher concentration of mud intraclasts correspond to the interval where the total number of clasts is lowest (i.e. core 48R, 49R, 50R).

Subunit III B (465.08–548.37 m CSF-A) consists of interbedded very dark to dark greenish gray diatom-bearing sandy and muddy diamictite (McKay et al., 2019). On average, the clast number is 8 clasts/10 cm, with variability comprised between 0 and 26 clasts/10cm. The clast lithology distribution is not homogeneous and two distinct clasts assemblages could be identified (Figure 31E): one from core 52R to 56R (ca. 460-505 m CSF-A), and one from core 57R to 60R (ca. 505-550m CSF-A). The upper clasts assemblage is completely similar to those of the subunit IIIA, with metamorphic clasts that are ca. 70% on average, intrusive ca. 17% on average, basalts 2%, dolerite ca. 1%, felsic porphyry quite absent, and an elevated number of mud intraclasts (8% on average) that reached 19% in the core 54R. The lower clasts assemblage is quite similar to those of the LSU II. It is dominated by metamorphic rock clasts (54% on average) and intrusive ones (36% on average). Quartz fragments are ca. 4% of the whole, felsic porphyry 2%, while other lithological groups are quite rare.

Subunit III C (548.37–646.93 m CSF-A) consists of dark to very dark greenish gray diatom-bearing sandy to muddy diamictite (McKay et al., 2019). The clast number along the interval vary between 0 and 26 clasts/10 cm, with an average of 9 clasts/10 cm. The clast lithology distribution is homogenous along the interval (Figure 31E); metamorphic clasts are the most common (50% on average), followed by intrusive ones (32% on average), mainly felsic and minor mafic in composition. Basaltic rocks represent ca. 7% of the total number of clasts, quartz fragment 6%, and felsic porphyry ca. 2%; other groups are less than 1%. LSU IV (646.93–695.74 m CSF-A) is a massive to stratified diatom-bearing diamictite, diatom-rich mudstone, muddy diatomite (McKay et al., 2019). On average, 8 clasts/10 cm occur within the LSU, varying from 0 to 23 clasts/10cm. The clast lithology distribution is quite homogenous along the core (Figure 31E), and it is compositionally comparable with those of the LSU III B. Metamorphic rocks group represent 57% and intrusive rocks group, mainly represented by felsic varieties and minor by mafic ones, are ca. 32%. Quartz fragments represent 4%, basaltic rock clasts ca. 3%, and felsic porphyry ones ca. 2%; other lithological groups are less than 1%.

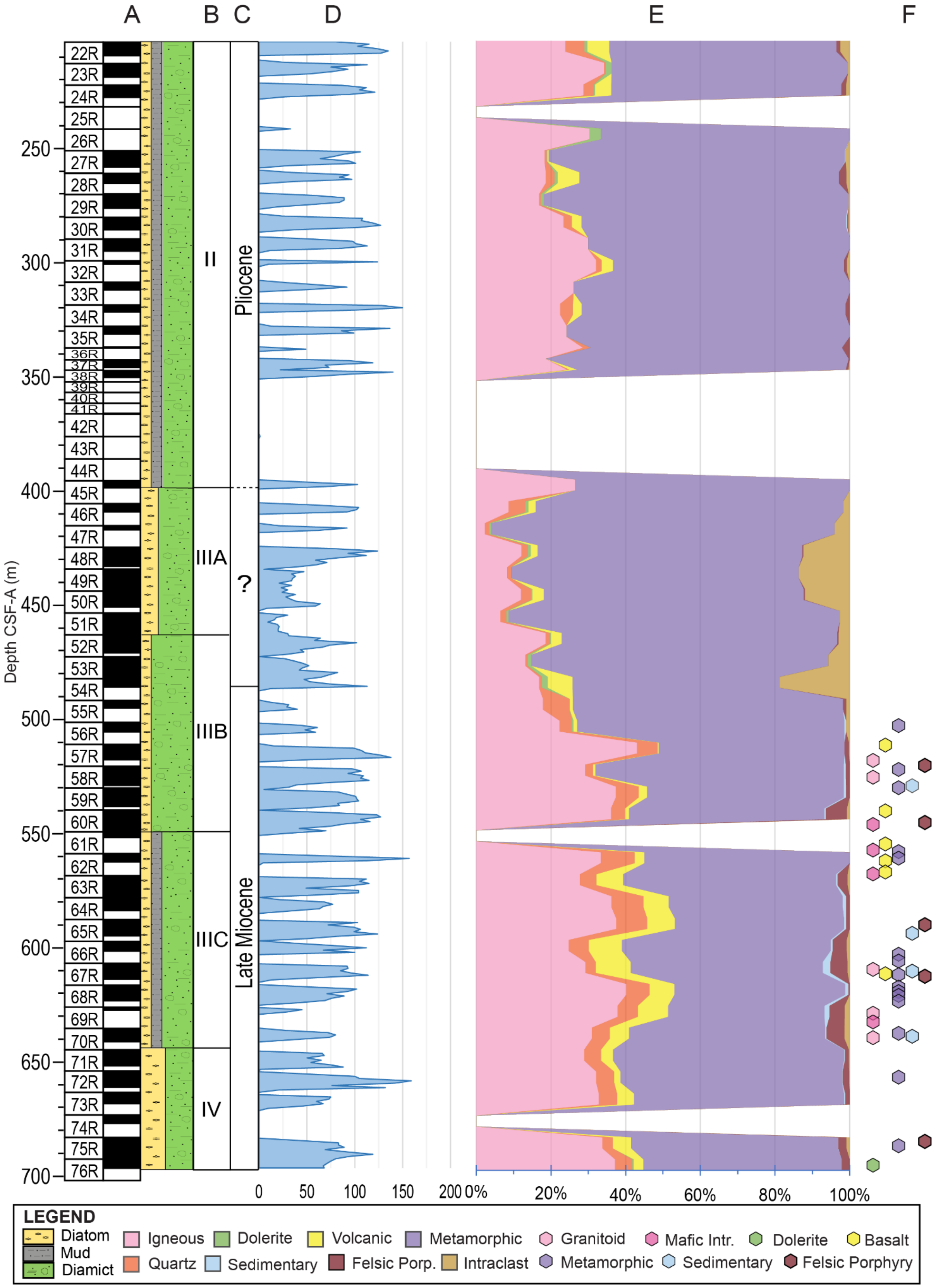

Figure 31 A) Stratigraphic log of the IODP_exp374 Site U1522A with core number and percentage of recovery (from McKay et al., 2019); B) Lithostratigraphic Unit (from McKay et al., 2019); C) age interval (from McKay et al., 2019); D) number of clasts >2mm/meter; E) occurrence in percentage of each lithological group all along the core. Percentage is calculated for each logged

core; squares in the legend identify rock lithologies; F) Position of sampled pebbles and cobbles and classification on the basis of thin section analysis (diamonds in the legend, see Appendix V for detailed petrographic descriptions and mineral assemblage).

3.5.3. DSDP Site 270

3.5.3.1. Clast Petrography

The number of large pebbles and cobble in the working half of the DSDP Site 270 core is very low and only few samples have been analyzed in thin section. Photomicrographs of representative clasts and of the basement rocks are shown in Figure 32, while detailed petrographic analysis are in the Appendix VII.

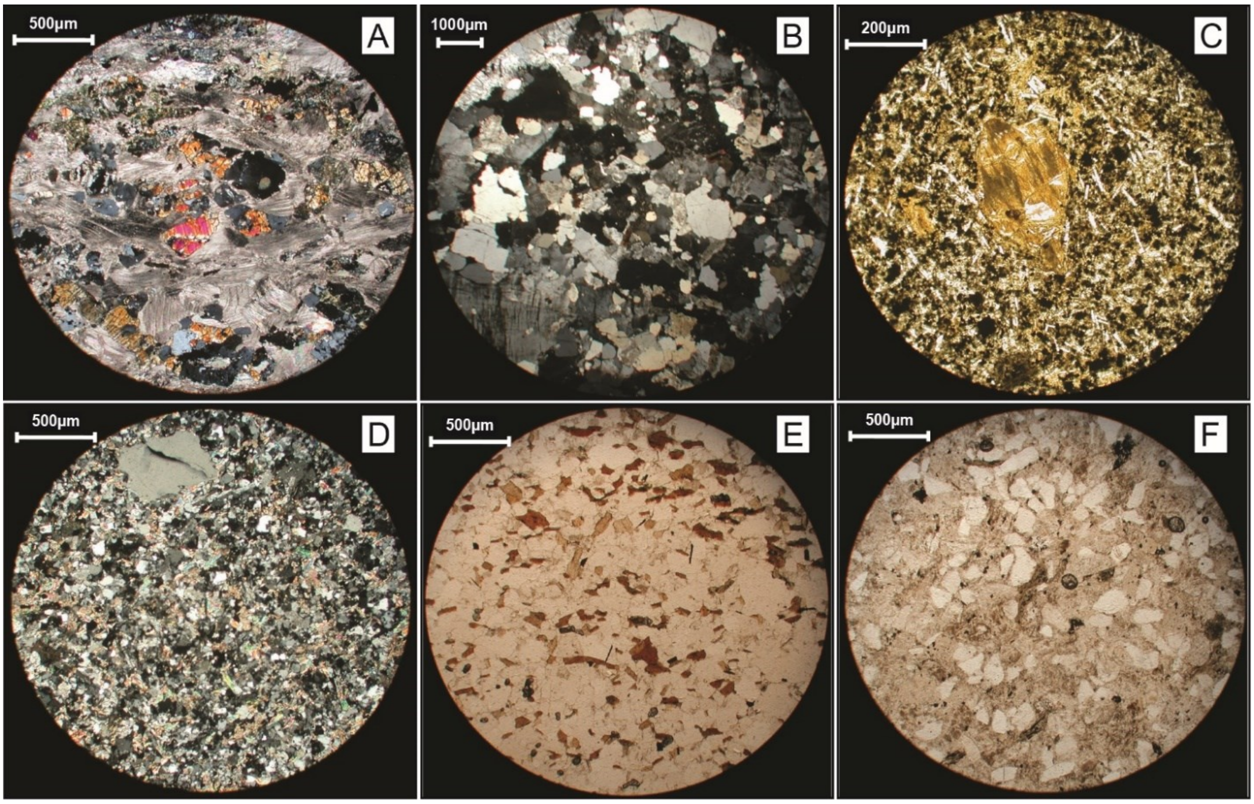

Figure 32 Photomicrographs of the main gravel size clast lithologies from DSDP Site 270 core. A) Calc-silicate gneiss constituting the basement at DSDP Site 270, XPL, magnification 4X (sample 28-270-49R-1W); B) Leucogranite, XPL, magnification 1X (sample 28-270-47R-2W); C) Basalt, PPL, magnification 10X (sample 28-270-19R-2W, 50-54 cm); D) Meta-sandstone, XPL, magnification 4X (sample 28-270-14R-1W, 39-41 cm); E) Biotite schist, PPL, magnification 4X (sample 28-270-38R-3W, 141-143 cm); F) Sandstone, PPL, magnification 4X (sample 28-270-38R-3W, 130-133 cm)

The rocks that constitute the basement at the DSDP Site 270 are alternations of calc-silicate gneiss and marble. The mineralogical phases recognized in the gneiss indicate an amphibolite metamorphic facies, with a retrograde greenschist and zeolite facies overprint (Ford and Barrett, 1975).

The macroscopic characterization of the cores reveals that most of the clasts are small (<5mm) and their identification is not clear. Intrusive clasts are mainly felsic grey granitoid rocks, whereas pink and reddish varieties occur. Granitoid rocks are medium grained with isotropic texture. The only intrusive clast analyzed in thin section was collected in the breccia overlying the basement (sample, 28-270-47R-2W), revealing a monzogranite composition. Mafic varieties commonly occur within the core, although they are a minority.

Volcanic rocks are poorly represented along the core whereas few clasts have been recognized. The microscopic analysis shows the presence of both microcrystalline isotropic olivine bearing basalt (i.e., sample 28-270-19R-2W, 50-54 cm) and trachytic varieties (i.e., sample 28-270-27R-2W).

Felsic sub-volcanic rocks, such as rhyolitic porphyry, commonly occurs within the core (i.e., sample 28-270-27R-2W).

Most of the clasts that characterize the core are meta-sedimentary. They appear grey to very dark grey/black, usually elongated shape related with metamorphic foliation which is not almost visible. Microscopic analysis reveals that most of the sample are quartzo-feldspatic meta-sandstone and meta-siltstone, with schistose texture (i.e., sample 28-270-27R-1W, 102-107 m) usually marked by grano-lepidoblastic biotite (i.e., samples 28-270-13R-3W, 99-113 cm; 38R-3W, 141-143 cm). Rarely white mica hornfels occurs (i.e., sample 27-270-14R-1W, 39-41 cm).

Sedimentary rock clasts were poorly recognized in the macroscopic analysis of the core; however, the thin section analysis reveals that they are more common that thought. This discrepancies between macro and microscopic analysis are probably due to the difficulty to discriminate between pure sedimentary and weakly schistose varieties at macroscopic scale for these small and mostly altered type of clasts. Most of the sedimentary clasts are sandstone mainly constituted by quartz and feldspars (i.e., sample 28-270-39R-1W, 122-123 cm), sometimes with volcanic lithic fragments (i.e., sample 28-270-38R-3W, 130-133 cm). Minorly represented are the mudstone clasts (i.e., sample 28-270-27R-4W, 41-44 cm).

3.5.3.2. Mineral Chemistry

Mineral chemistry analysis was performed in five thin sections, four clasts and one basement sample. Biotite crystals were analyzed within clasts (i.e., 28-270-13R-3W, 99-113; 38R-3W, 141-143 cm; 47R-2W) as well as white mica (sample 28-270-14R-1W, 39-41 cm), while pyroxene was analyzed in the basement thin section (Sample 28-270-49R-1W). Full dataset of EDS analyses is available on Appendix VIII.

Figure 33 shows biotite composition in terms of X_{Fe} (Fe/(Fe+Mg)) versus Al^{IV}. X_{Fe} varies from 0.50 to 0.64 while Al^{IV} ranges between 2.14 a.p.f.u. and 2.63 a.p.f.u. Analyzed crystals do not show chemical zonation, and, within each sample, crystals show a very similar composition; on the contrary, the three samples show small compositional differences between each other.

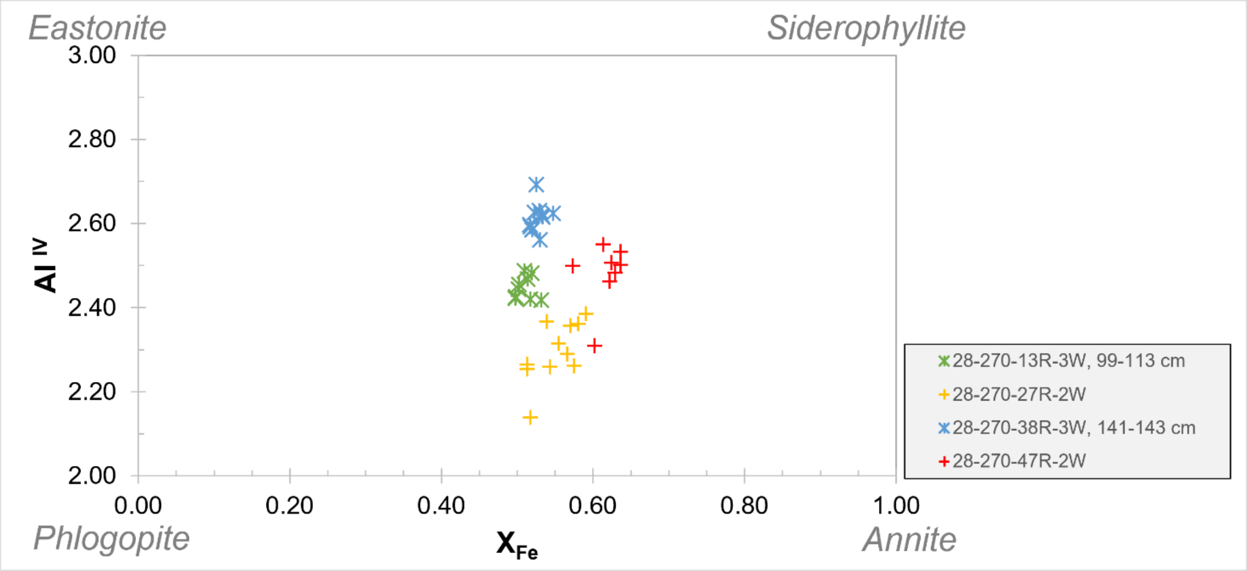

Figure 33 Biotite composition in terms of Al^{IV} versus X_{Fe} (Fe/(Fe+Mg)) for DSDP Site 270 clasts. Compositional end-members are shown at the edges of the diagram. Asterisk represents low-grade meta-sedimentary clasts; plus symbols represents intrusive clasts.

Figure 34 shows the white mica composition in terms of Si versus Al; this mineralogical phase was found only in one sample, showing a phengitic muscovite composition. Al value ranges between 4.94 and 5.29 a.p.f.u.; silica content varies from 6.28 to 6.54 a.p.f.u. Analyzed crystals do not show any internal chemical zonation.

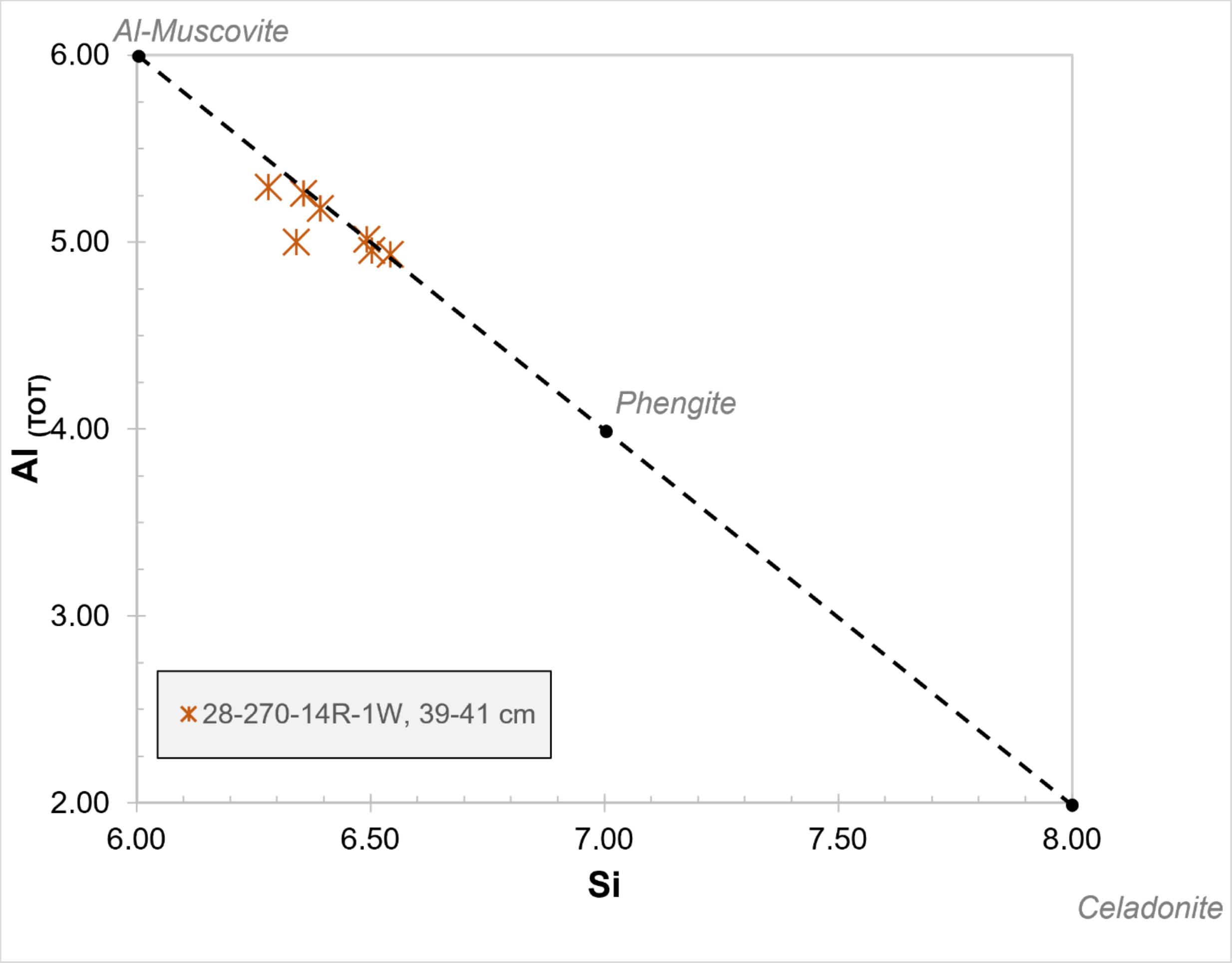

Figure 34 White mica composition in terms of Si versus Al for DSDP Site 270 clast. Compositional end-members are shown within the graph

The calc-silicate gneiss constituting the basement of the DSDP Site 270 has clinopyroxene crystals (see Appendix VII for detailed petrographic description). Figure 35 show that analyzed clinopyroxene crystals are diopside ($CaMgSi_2O_6$), consistent with what was observed in the petrographic analysis, as well as from the expedition report of Ford and Barrett (1975) and that all crystals have similar chemical composition.

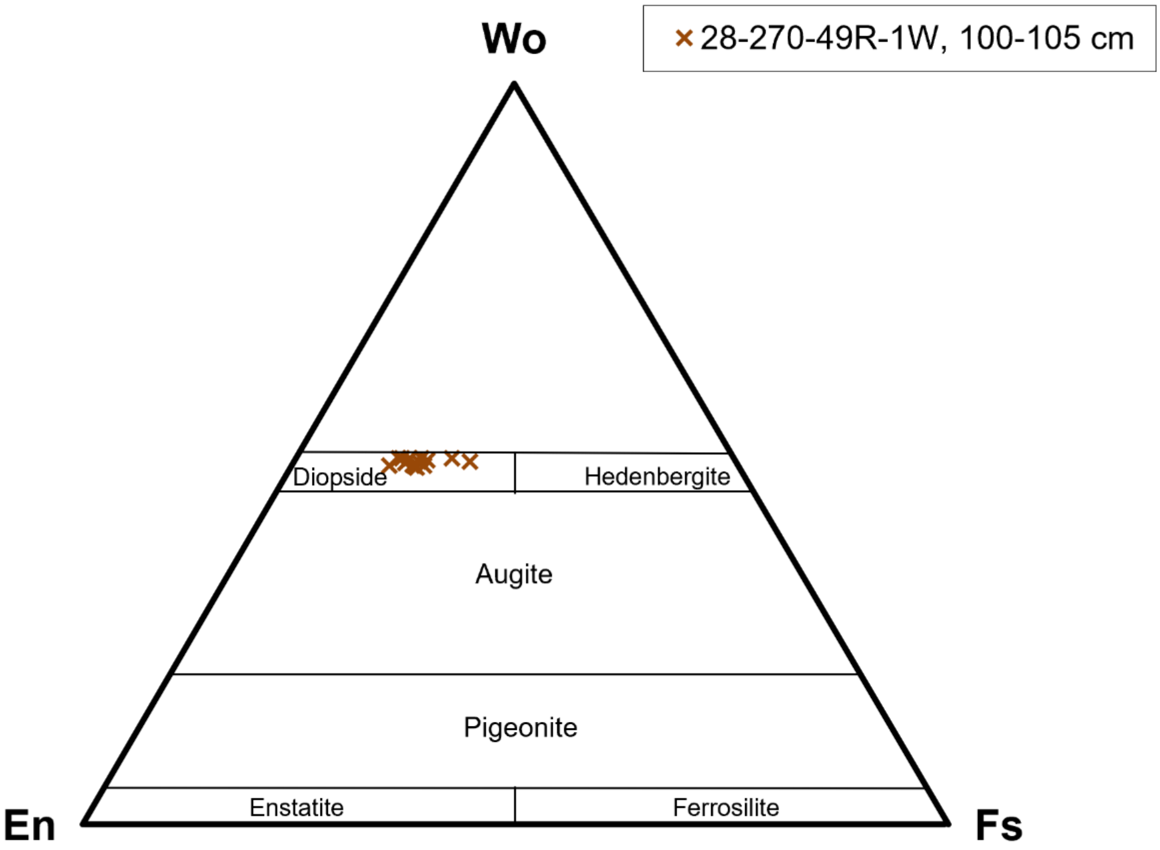

Figure 35 Pyroxene composition for DSDP Site 270 basement rock. En – Enstatite, Fs – Ferrosilite, Wo - Wollastonite

3.5.3.3. Clast Distribution

In the Oligocene-Pleistocene interval of the DSDP Site 270 core a total of 3099 gravel size clasts were counted and logged in continuum along the core. The clast associations description is based on the lithostratigraphic units division proposed by Kraus (2016) and adopted by Kulhanek et al. (2019), where six LSU have been identified (Figure 36). The clast lithology distribution along the core allows the identification of two main petrofacies (Table 10).

Table 10 Petrofacies classification on the basis of clast lithology assemblage of DSDP Site 270.

Petrofacies ID	Main lithological groups	Other features	Occurrence
PF270-1	meta-sedimentary >> felsic intrusive	felsic porphyry common; basalt rare	270: 385-202 m bsf
PF270-2	meta-sedimentary >> felsic intrusive	basalt, felsic porphyry, and dolerite rare	270: 202-3 m bsf

LSU I (0-20 m CSF-A) consists of Pleistocene sediments. The recovered percentage is very low and only few clast lithology data have been collected.

LSU II (20-124 m CSF-A) consists of mudstone with dropstones and minor clast-poor diamictite interbeds (Kraus, 2016). Clasts number varies between 0 and 14 clasts/10 cm with an average of 1.5 clasts/10 cm. The lithology of clasts is quite homogeneous along the interval: the most represented lithological group is the meta-sedimentary one (73% on average), while intrusive rocks group represent the 18% of clasts on average. Dolerite clasts vary between 0% and 11% (5% on average) of the whole. Moreover, basaltic clasts occur in the core 5R.

LSU III (124-202 m CSF-A) mainly consists of mudstone with rare dispersed dropstones (Kraus, 2016). The clasts amount ranges between 0 and 3 clasts/10 cm, with an averaged value of 0.19 clasts/10 cm. The most represented lithological group is the meta-sedimentary one (87% on average) that ranges from 67% and 100% of the clasts. The second population is represented by intrusive clasts (8% on average), which vary between 0% and 20%. Whereas other lithological groups are poorly represented (<3% on average), in this lithostratigraphic unit few dolerite (i.e., in the core 17R, section 2A) and basalts were recorded (i.e., in the core 19R, section 2A). The lithological distribution is quite homogeneous along the interval.

LSU IV (202-252 m CSF-A) is made up of massive to stratified diamictite, interlayered with mudstone with dropstones, and minor with sandstone/siltstone and mudstone (Kraus, 2016). This LSU records the highest clasts amount of the entire drillhole: 2.9 clasts/10 cm on average, with values varying between 0 and 14 clasts/10 cm. Clast's lithology assemblage is not homogeneous along the LSU: at ca. 230 m bsf a variation in the percentage amount is recorded; this change corresponds with the boundary between the diamictite dominated interval and the mudstone dominated one. Between ca. 230 and 252 m most of the clasts are metamorphic (69% on average), followed by intrusives (24% on average), while minor are quartz fragments (3% on average), and felsic porphyry (2% on average). In the upper interval (202-230 m CSF-A) the percentage of intrusive rocks decreases (2% on average), while the metamorphic rock clasts strongly increase (96% on average).

LSU V (252-348 m CSF-A) consists of mudstone with dispersed dropstones (Kraus, 2016). The clasts amount is on average 1.8 clasts/10 cm and ranges between 0 and 7 clasts/10 cm. In this LSU, the main lithological group is the metamorphic rock one, that constitute the 68% on average, and it ranges between 47% and 88%. Intrusive rocks represent the 22% of clasts in average, ranging from 11% and 38%. Other lithological groups (i.e. quartz fragments and porphyries) are minoritarian (2-3%). Mud intraclasts number is quite homogeneous along the LSU and they constitute the 3% of the total clasts amount.

LSU VI (348-385 m CSF-A) is characterized by sandstone beds interlayered with mudstone with dropstones (Kraus, 2016). In this lithostratigraphic unit, clasts amount ranges from 0 to 8 clasts/10cm, with a mean value of 0.8 clasts/10cm. Clasts are dominated by meta-sedimentary lithologies (73% on average, ranging from 47% to 100%); secondary lithological groups are intrusives (9% on average, ranging from 0% to 21%), sedimentary rocks (7% on average, ranging from 0% to 36%), and porphyries (4% on average, ranging from 0% to 18%). Mud intraclasts commonly (5% on average) occur within the LSU.

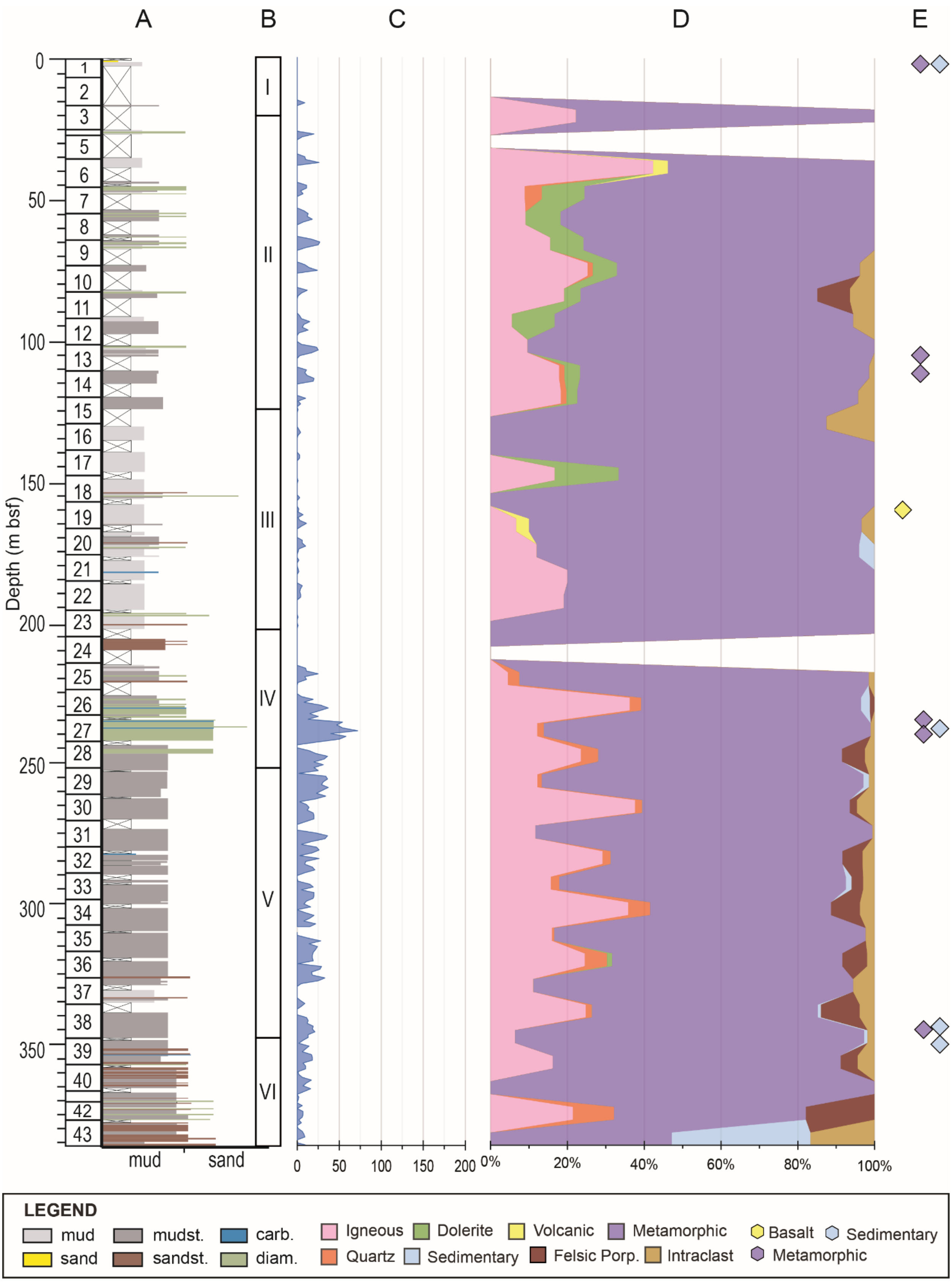

Figure 36 A) Stratigraphic log of the DSDP Site 270 with core number (Kulhanek et al., 2019); B) Lithostratigraphic Unit (from Kraus, 2016); C) number of clasts >2mm/meter; D) occurrence in percentage of each lithological group all along the core. Percentage is calculated for each logged core; squares in the legend identify rock lithologies; E) Position of sampled pebbles and

cobbles and classification on the basis of thin section analysis (diamonds in the legend, see Appendix VII for detailed petrographic descriptions and mineral assemblage).

3.6. Discussion and provenance inferences

3.6.1. Clast petrography and distribution

3.6.1.1. IODP Site U1521

The provenance analysis is limited to the early Miocene interval of the core, below ca. 200 m bsf (LSU IV to VII) due to the scarcity of data in the overlying interval, as well as in LSU V where data are absent.

The clast abundance strongly varies along the core and Figure 24D shows the cyclic variation of them. In particular, where the core recovery is continuum (i.e. LSU VI C), their fluctuation is strongly linked with astronomical cycles (Sullivan et al., 2021; Marschalek et al., 2021). Clast distribution strongly responses to precession/eccentricity of WAIS during a 2.4 Ma eccentricity forcing minimum and an obliquity response during a 2.4 Ma eccentricity forcing maximum (Sullivan et al., 2021).

The clast lithology assemblage allows to divide the core into three main petrofacies (Table 8) which reflect changes in the sediment supply (Figure 24). The stratigraphically lowermost petrofacies (PF21-1) characterizes the LSU VII, the petrofacies PF21-2 is found in the sub-LSU VI C and VI B, while the petrofacies PF21-3 involves sub-LSU VI A and LSU IV. Even though the main lithological groups (i.e. meta-sedimentary and granitoid rocks groups) do not record any relevant variation along the studied interval, other minor lithological groups suffer wide variation in the three petrofacies.

The PF21-1 shows relative abundance of dolerite clasts that suggests a provenance from the TAM region, where dolerite sills of the Jurassic Ferrar Group largely crop out all along the mountain belt. Dolerite is also recorded in Marie Byrd Land as dikes related with Cretaceous magmatism (Siddoway et al., 2005; Saito et al., 2013); however, the high abundance of dolerite clasts is less consistent with WA provenance where the occurrence of this lithology is scattered. Moreover, the lack of basaltic clasts in this petrofacies is consistent with TAM source of these sediments because CTAM and STAM lack of Cenozoic eruptive centers, while WA is rich of volcanic edifices (Wilch et al., 2021). The most possible source of the meta-sedimentary clasts are the Cambro-Ordovician units that largely crop out in the STAM and CTAM (i.e. La Gorge and Starshot formations respectively) which are mainly made up of meta-greywacke and meta-pelites affected by low-grade metamorphism (Stump, 1995). The occurrence of marbles is consistent with the formations previously described. The most probable source of granitoid rock are the plutons of the Granite Harbour Intrusive Complex, that occurs all along the TAM (Stump, 1995). However, the small amount of (meta-)porphyry in the clast assemblage, that largely crops out in the STAM (i.e., Liv Group), is less consistent with a provenance from this sector of the TAM. The provenance of these sediments from East Antarctica sectors is also constrained by geochronological (zircon U-Pb), thermochronological (hornblende Ar/Ar), geochemical (Nd and Sr isotopes), palynological, and clay mineralogical analysis of this sediment package (Marschalek et al., 2021). In particular, the absence of Cretaceous zircons leads to exclude a provenance from WA sectors (Marschalek et al., 2021). Marschalek et al. (2021) speculate that these sediments should derive from the erosion, caused by ice caps, of local high (i.e. Pennel and Ross banks) that in the Early Miocene were subaerial (Paxman, 2021) and then able to host ice cover; this interpretation fits with seismic data (Pérez et al., 2021). The compositional difference is consistent with the hypothesis that PF21-1 has East Antarctica affinity. The PF21-1 characterizes LSU VII (Sequence 1 of Pérez et al. 2021) that is interpreted as ice-proximal, possibly subglacial, sedimentation (Marschalek et al., 2021); the LSU upper boundary is constituted by the RSU 5 (Pérez et al., 2021). The LSU VII shows sediments older than 18 Ma (Marschalek et al., 2021). Previously, in the Ross Sea, this stratigraphic interval was intercepted by ANDRILL 2A core (Levy et al., 2016) at the depth of ca. 780 m bsf, where a regional-scale erosion surface (U2 of Levy et al. (2016) is reported. However, the glacial processes in the near cost site eroded the sediment that could be possibly correlated with LSU VII of IODP Site U1521.

Petrofacies 21-2 is characterized by an abrupt decrease of dolerite clasts, while basaltic rock clasts appear (Figure 24). The decrease of clast lithologies typical of the TAM (i.e., dolerite) is indicative of a shift in the sediment supply that is now centered in WA sectors. The appearance of basaltic clasts, also marked by an increase of Fe/Ti ratio from XRF analysis (McKay et al., 2019; Marschalek et al., 2021) is also consistent with a provenance from WA, where subglacial volcanoes are testified and inferred by geophysical surveys (Wilch et al., 2021). Moreover, the dolerite decrease is coupled with the limestone disappearance. Limestones, although occurring in the Swanson Formation of MBL, are more common in the TAM (Stump, 1995). Most of the sediments of the PF21-2 are very low grade meta-sedimentary rocks (i.e. 374-U1521A-62R-4W, 120-125 cm and 63R-5W, 8-17 cm), sometimes unmetamorphosed (i.e. 374-U1521A-60R-7W, 90-93 cm); the most likely source of these clasts is the Swanson Formation. The biotite gneissic clasts (i.e. 374-U1521A-60R-5W, 62-65 cm) are likely sourced from the Fosdick Complex or its equivalent beneath ice sheet. Intrusive rocks could be sourced from both the Ford Granodiorite and Byrd Coast Granite plutons that crops out in MBL; the two analyzed samples (i.e. 374-U1521A-48R-6W, 38-40 cm and 55R-4W, 2-5 cm) show granodioritic composition and it is consistent with a source from these plutons. Geochronological analysis (zircon U-Pb) testifies that the sediment source was located in WA, where Cretaceous zircons have been found in abundance (Marschalek et al., 2021). Moreover, sediments geochemistry (Nd and Sr isotopes) is consistent with WA provenance on the basis of negative correlation in the Nd/Sr ratio and its similarity with Last Glacial Maximum tills with a constrained WA provenance (Licht et al., 2014; Marschalek et al., 2021). This petrofacies is recognized in sub-LSU VI C and VI B (Sequence 2 of Pérez et al. 2021) that shows sedimentary facies typical of ice-proximal deposition to a more ice-distal prograding wedge (Marschalek et al., 2021). The age model of the Site U1521 core indicate that deposition occurred between 17.95 and 17.40 Ma (Marschalek et al., 2021); the interval is delimited by the RSU 5 at the base and D-b surface at its bottom (Pérez et al., 2021). ANDRILL 2A core recovered a continuous section of this time interval (Levy et al., 2016); the provenance of clasts for this time interval is mainly in the region between Skelton and Mulock glaciers and minorly in the region between Mulock and Byrd glaciers (Zattin et al., 2010, 2012; Talarico and Sandroni, 2011; Cornamusini and Talarico, 2016; Levy et al., 2016). A provenance from south of the drilling site of ANDRILL 2A sediment implies that Ross Sea was largely filled by WAIS and that EAIS ice flows were flattened along the present-day TAM alignment (Talarico and Sandroni, 2011; Cornamusini and Talarico, 2016). This scenario is consistent with what observed in the Central Ross Sea at the Site U1521 core, where, in the same time interval, WAIS expansion has been documented (Marschalek et al., 2021).

PF21-3 shows the reappearance of dolerite clasts, while basaltic ones are also present. The abundance of dolerite clasts is indicative of a provenance from TAM sectors rather than WA and then the Ferrar Group is the most likely source of this lithology. Most of the clasts are low- to medium-grade meta-sedimentary rocks that were likely sourced from the Neoproterozoic or the Cambro-Ordovician meta-sedimentary sequences that crop out all along the TAM (i.e., La Gorce Formation, Beardmore, and Byrd groups). Granite Harbour Intrusive Complex plutons are the likely source of the felsic intrusive clasts, that are the second main lithology. Sedimentary rocks are also indicative of TAM provenance: the quartzarenite sample (374-U1521A-38R-3W, 24-28 cm) is likely attributable to the Beacon Supergroup sandstones (Cornamusini and Talarico, 2016), while limestone (374-U1521A-37R-3W, 110-113 cm) was probably sourced from Byrd Group formations (Stump, 1995). Moreover, reworked Permian palynomorphs that typically characterize Beacon Supergroup, were found in the LSU 4 (Marschalek et al., 2021) testifying that Beacon sandstones contribute to sediment supply. Geochronological and geochemical analysis are also consistent with TAM source for those sediments (Marschalek et al., 2021). The PF21-3 occurred for sediments of the sub-LSU VI A and LSU IV (Sequences 3A and 4A respectively of Pérez et al. 2021); LSU VI A represents sedimentation in ice-proximal environment, while LSU IV sedimentation varies from ice-proximal to ice-distal depositional setting (Marschalek et al., 2021). LSU VI A spans in age from 17.40 to ca. 16.50 Ma (Marschalek et al., 2021). In ANDRILL 2A core the same time interval recorded clast provenance from the coast in front of the drilling site (Royal Society Range) that implies eastward paleo-ice flows and therefore that Ross Sea was not filled by an expanded WAIS (Talarico and Sandroni, 2011; Cornamusini and Talarico, 2016). This hypothesis is consistent with Site U1521 record that is characterized by EAIS sediment provenance and then that WAIS was not expanded in the Ross Sea in this time interval. LSU IV, base of which is the RSU4a (Pérez et al., 2021), deposited between ca. 16.30 and 16.20 Ma (Marschalek et al., 2021). In this time interval in ANDRILL 2A a mixed provenance from Skelton Glacier and Royal Society Range is recorded (Talarico and Sandroni, 2011; Cornamusini and Talarico, 2016); thus imply that ice flows from TAM were not barred by expanded WAIS in the Ross Sea and this is consistent with data from Site U1521 for which an EAIS provenance has been recorded.

The clast petrology and their distribution along the core allows to individuate change in the sediment supply which are strongly linked with climate forcing (Levy et al., 2019; Marschalek et al., 2021). Compared to coastal cores (i.e., ANDRILL and CRP), IODP Site U1521 recorded dynamics of both WAIS and EAIS, and this allows to corroborate past dynamics proposed on the basis of previous drilling project in the Ross Sea. In particular Site U1521 records the first grown of marine-based WAIS, occurred 17.95 Ma (Marschalek et al., 2021); this expansion of WAIS is documented on the basis of provenance study, where clast petrology led a key role, together with geochronology, geochemistry, and thermochronology, in the determination of sediment source region.

3.6.1.2. IODP Site U1522

Clast lithology assemblage varies along the investigated interval of the core (Figure 31) and two main changes occur, which define three petrofacies (Table 8). The petrofacies 22-1 is dominated by metamorphic (most of them from low-grade meta-sedimentary rocks) and intrusive clasts; moreover, basalts and felsic porphyries are common while dolerite is rare or absent. Petrofacies 22-2 is dominated by metamorphic clasts, while intrusives are subordinated; moreover, basalts and felsic porphyries strongly decrease while dolerite, although very poorly represented, occurs. Another feature of this petrofacies is the abundance of mud intraclast. The third petrofacies (PF22-3) is dominated by metamorphic and minorly intrusive clasts; basalts and felsic porphyries occur whereas in less abundance than PF22-1. Dolerite is rare but sometimes occurs. One of the most important features of the clast lithology assemblages of this core is the almost total absence of dolerite clasts (which source rock is abundant in TAM) and clasts also abundantly present in IODP Site U1521 core intervals (see previous paragraph), together with the relative abundance of basalts.

Petrofacies 22-1 characterizes the lowermost part of the core (cores 76R to 57R, ca. 700-510 m CSF-A) that is late Miocene in age (McKay et al., 2019). PF22-1 lithologies are comparable with West Antarctica geology. In particular, the lack of dolerite makes East Antarctica provenance unlikely. Most of the clast are from low-grade metasedimentary rocks, and the most likely source is the Cambro-Ordovician Swanson Formation, which largely crops out in MBL, and it should be inferred under West Antarctica. Schists and gneisses could also be sourced from the Fosdick Complex or its correlative beneath ice cover. Granitoids rocks, the second lithological group in abundance, should be sourced from the Carboniferous-Devonian Ford Granodiorite suite and the Cretaceous Byrd Coast Granite suite. Intrusive clasts analyzed in thin section are mainly biotite ± hornblende granodiorite (i.e., Sample 374-U1522A-67R-2W, 105-108 cm; 69R-1W, 0-4 cm; 70R-2W, 134-137 cm) and their lithology is consistent with the Ford Granodiorite suite petrography (Weaver et al., 1991). The presence of both those age (Carboniferous-Devonian and Cretaceous) intervals in the detrital zircons (Mallery et al., 2021) is coherent with the proposed source; the abundance of Cretaceous zircons in this interval is consistent with WA provenance (Mallery et al., 2021). Mafic intrusive rocks are not abundant but their presence is constant within the petrofacies, and their most likely source are the Cretaceous dolerite and mafic dikes, cropping out in MBL (Siddoway et al., 2005; Saito et al., 2013). Sub-volcanic felsic clasts, which commonly occur within the PF, should not be linked with any known source region. Similar lithologies are usually associated with Ross Orogeny granitoids all along the TAM, and they are more widespread in the STAM (Stump, 1995), but this source should be likely excluded because: i) their abundance in the PF is not consistent with the amount of STAM outcrops, ii) they are not associated with other STAM lithologies, such as the dolerite of the Ferrar Group and the sandstone of the Beacon Supergroup, and iii) they are in association with basaltic rocks which are very rare in these sectors of the TAM. The source of this lithology should be likely found beneath the WAIS cover. A possibility is that these rocks are related with a Permo-Triassic arc, which do not crops out in this sector of Antarctica but only in Antarctic Peninsula, however its occurrence in MBL/Ross sea is inferred by provenance study of the Beacon Supergroup (Elliot, 2013). Petrographic analysis of the Beacon sandstones in SVL reveal the abundance of felsic (rhyolite) to intermediate (trachyte) lithic fragments in the intervals where the 200-250 Ma zircons dominates (Liberato 2021, personal communication); these lithologies are consistent with the clasts found in the IODP Site U1522. Moreover, in the detrital zircons the Permo-Triassic population is abundant (Mallery et al., 2021) and this is consistent with the work hypothesis proposed for the clast source. Moreover, the geochronological studies of detrital zircons in the LGM sediments in the Ross Sea reveal the presence of Permian-Triassic zircons which are usually associated with Cretaceous ages (Licht et al., 2014; Perotti et al., 2017), supporting the hypothesis of an unexposed source of Permian-Triassic age (Elliot and Fanning, 2008; Elliot, 2013; Elliot et al., 2015, 2017, 2019). The most likely source of the basalts are the Cenozoic volcanoes which are inferred beneath WA (Wilch et al., 2021). The clast composition that characterizes the PF and biotite chemistry, together with ongoing geochronological data (Mallery et al., 2021), suggest that the provenance of these sediments are the terranes of West Antarctica.

Petrofacies 22-2 characterizes the interval between core 56R and 45R (ca. 510-395 m CSF-A), which is inferred to be latest Miocene to Pliocene but it does not have a strong age constrain (McKay et al., 2019). Rather that PF22-1, PF22-2 shows the decrease of intrusive and basaltic rocks, while felsic porphyries quite disappear. The clast lithology assemblage change is also coupled with changes in the detrital zircon signature, where Cretaceous and Permo-Triassic grains strongly decrease and they are quite absent, indicating a more East Antarctic derived composition (Mallery et al., 2021). However, clast composition is indicative of a West Antarctica derived source, although different from the PF22-1; in particular, the absence of dolerite seems to be unlikely with TAM source, where dolerite is abundant. The decrease of intrusive clast indicates that the source region had limited outcrops of these rocks or that they have been partially eroded previously. Moreover, the presence of basalts, although less than in PF22-1, is not consistent with a STAM/CTM provenance. The quite disappear of felsic sub-volcanic rocks strengthens the hypothesis that they are sourced by the Permo-Triassic arc, because in this PF the Permo-Triassic zircons strongly decrease (Mallery et al., 2021), supporting the strong direct proportionality between this lithology and the zircon age population. The abundance of mud intraclasts is probably related with the sedimentary processes linked with sediment deposition; sediments with high mud intraclasts number are observed at the boundary between subglacial and ice-proximal glacimarine environment (Robinson et al., 2021). This aspect needs to be deepened by sedimentological and seismic studies in order to constrain the depositional processes and the paleo-environment. Therefore, the source region of these sediments should be likely West Antarctica, probably where currently are the ice stream (i.e., Whillans Ice Stream, Kamb Ice Stream), although a mixed source (from both West Antarctica and possibly TAM) can not be excluded.

Petrofacies 22-3 characterizes core 38R to core 22R (ca. 200-350 m CSF-A), a core section that is Pliocene in age (McKay et al., 2019). The clast composition is similar to that observed in PF22-1, although basaltic rocks and felsic porphyries are less common; however, a similar source region is the most likely hypothesis. The detrital zircon signature (Mallery et al., 2021) confirm the similarity between PF22-3 and PF22-1 sediments, with a well-developed WA signature.

3.6.1.3. DSDP Site 270

The petrographic analysis of the basement cored at DSDP 270 site is useful to compare the local basement lithology with the glacially transported clasts. Basement rocks affinity is consistent both with Skelton Group (Ford and Barrett, 1975) and Bowers Terrane (Mortimer et al., 2011), suggesting a general similarity with TAM rocks.

Lithologies similar to those observed in the basement were not recognized in the glaciomarine sediments, although it is reported on the clasts that make up the basal breccia (Ford and Barrett, 1975), consistent with the talus nature of the strata, with local provenance of the clasts (Ford and Barrett, 1975; Kraus, 2016). Moreover, the analysis of the breccia clasts could help to understand the nature of the Central High (CH) basement on which the core was drilled. On the basis of the lithologies found in the breccia, the basement in the CH results to be formed mainly by biotite ± hornblende ± garnet schist and gneiss, dark argillite and hornfels, orthogneiss, calc-silicate gneiss and marble (the same of the drilled basement interval), and granite (Ford and Barrett, 1975); this highlights the coexistence of low- to medium-grade metamorphic and intrusive rocks. The petrographic analysis of a fine-grained biotite leucogranite (sample 28-270-47R-2W) confirms the macroscopic characterization (Ford and Barrett, 1975), but does not provide any regional affinity. The absence of dolerite and sandstone (i.e., Beacon Supergroup) seems to exclude similarity with inboard TAM geology; however, their absence does not exclude that these rocks are the correlative of pre-Devonian basement forming the TAM.

The clast lithology distribution in the glaciogenic sedimentary sequence allows the identification of two main petrofacies (Table 8). The PF270-1, which characterizes the lowermost part of the core (LSU VI, V, and IV; ca. 385 to 200 m bsf), is dominated by meta-sedimentary clasts and minorly by felsic intrusive and sub-volcanic ones. The absence of dolerite indicates an unlikely provenance linked with EAIS which drains from the TAM, where the Ferrar Dolerite largely crops out. The presence of meta-sedimentary and intrusive clasts means that it can not be excluded that the sediment source was both West Antarctica sector and local (i.e., Central High). In the view of a local provenance the clast lithology should reflect the breccia composition; most of the lithologies found in the glacial sediments were also described in the breccia (i.e., biotite ± hornblende schist, hornfels, argillite, and granite). However, some lithologies constituting the breccia (i.e., gneiss and marble) rarely occur in the PF270-1. Moreover, felsic porphyry, recognized both with the macroscopic analysis and through thin section analysis (i.e., sample 28-270-27R-2W), were not reported as breccia constituent (Ford and Barrett, 1975). However, a local provenance of these clasts cannot be excluded, also because the glacier(s) catchment area was probably wider than those of the talus, which is supposed to be very local (Kraus, 2016); therefore, felsic sub-volcanic rock outcrops in the CH cannot be excluded. On the contrary, clast lithologies could also be provided by West Antarctica terranes. The low-grade meta-sedimentary clasts could be sourced from the Swanson Formation, which largely crops out in MBL, while gneiss constitutes the Fosdick Migmatite Complex (and its correlative beneath the ice cover). Ford Granodiorite and Byrd Coast Granite could provide the felsic intrusive varieties, while mafic dikes associated with Cretaceous magmatism could be the source of mafic intrusive clasts. Felsic porphyry outcrops are not reported in MBL; however, their occurrence was inferred to explain the late Miocene sediments in the IODP Site U1522 site (see 3.6.1.2). The few volcanic clasts (mainly trachyte) found within the PF are consistent with the Cenozoic volcanic edifices which occurred in the eastern side of the WARS (Wilch et al., 2021). Sedimentary clasts do not have any corresponding in the outcropping geology of MBL. They may represent unmetamorphosed portion of the Swanson Formation, occurring beneath WAIS, or unknown sedimentary sequences, occurring beneath WAIS or in the CH; similar lithologies were also found in the LGM tills from the CRS (Perotti et al., 2017). The clast lithology association of the PF270-1 does not provide clear indication of provenance because both the local (CH) and WA source cannot be excluded, while the influence of EAIS seems to be unlikely. Comparison with other provenance tools (i.e., geochronology and apatite fission track), which are in progress, is needed to improve the knowledge of these sediments. PF270-1 is also similar with PF22-2 which occurs in the IODP Site U1522.

PF270-2 characterizes the uppermost part of the core (LSU III and II; ca. 200 to 3 m bsf) and it not strongly differs from PF270-1 whereas the number of felsic intrusive and sub-volcanic clasts decreases, while mafic intrusive and dolerite weakly increases. While meta-sedimentary and intrusive rocks can be sourced both from the local CH and MBL, the common presence of mafic varieties could be indicative of WA provenance because they likely be sourced by the Cretaceous mafic dikes of MBL (Siddoway et al., 2005; Saito et al., 2013). The quite absence of felsic porphyry is also indicative of a change in the sediment supply, that could also be linked with changes in the glacial setting. However, the comparison of petrographic data with other provenance tools (i.e., geochronology) is needed to better constrain the origin of these sediments.

3.6.2. Mineral Chemistry

Mineral chemistry analysis provides a huge amount on data to compare clasts with outcropping geology. Biotite is the most analyzed mineralogical phase in this study, both from glacially transported clasts and onshore geology. Biotite chemistry can be found in the literature both from other drilling sites and onshore (Biagini et al., 1991; Talarico and Sandroni, 1998; Talarico et al., 2000, 2013; Sandroni and Talarico, 2001, 2006; Perotti et al., 2017, 2018), as well as amphibole (Talarico et al., 2011; Perotti et al., 2017).

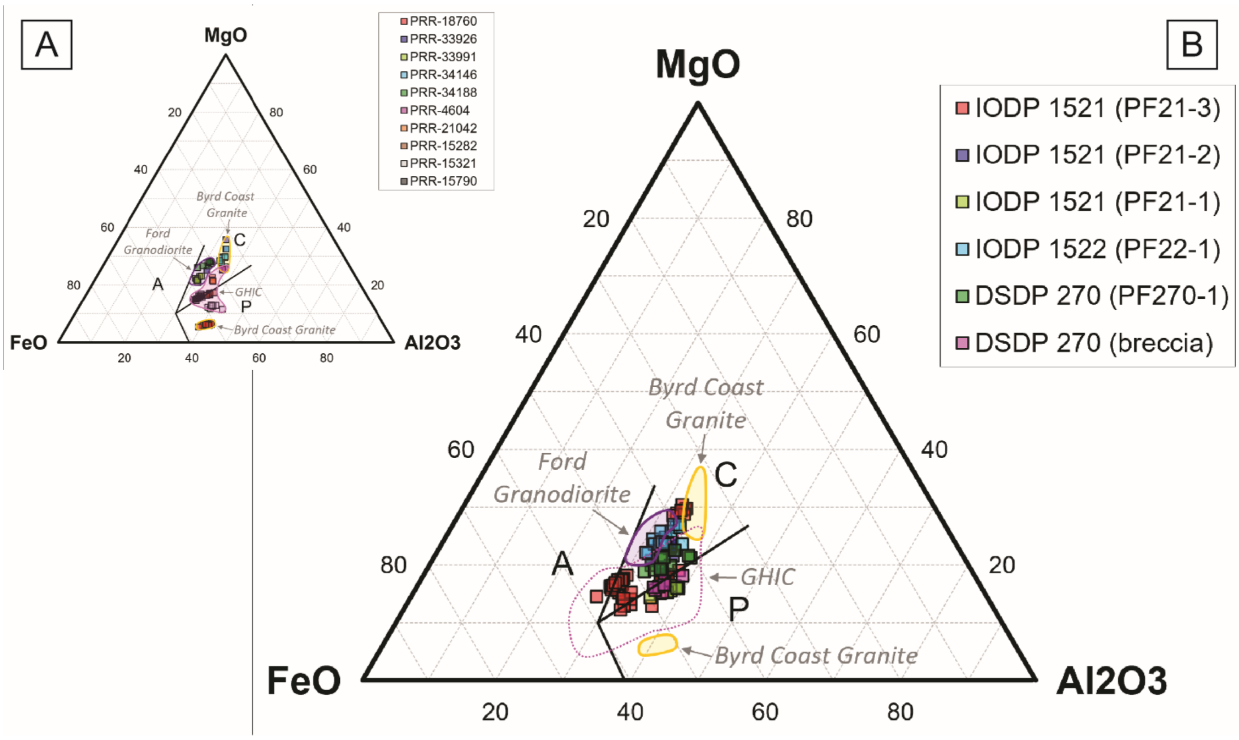

Figure 37 Ternary plot in terms of FeO (total), Al_2O_3, and MgO of biotites from granitoid rocks (Abdel-Rahman, 1994). A) Classification of the Polar Rock Repository samples; data were grouped on the basis of formations and the same fields were shown in B); B) classification of biotite from IODP Site U1521 and U1522 and DSDP Site 270. Dotted pink line represents biotite in Granite Harbour Intrusive Complex (GHIC) from northern Victoria Land outcrops (Biagini et al., 1991), from Southern Victoria Land and Central Transantarctic Mountains (this study), and from intrusive clasts collected in CIROS-1, CIROS-2, CRP-1, CRP-2, and CRP-3 cores which are interred to be sourced from Granite Harbour Intrusive Complex (GHIC) outcrops (Talarico and Sandroni, 1998; Talarico et al., 2000; Sandroni and Talarico, 2001, 2004, 2006). A: alkaline anorogenic field; C: calc-alkaline field; P: peraluminous field.

Whereas biotite was analyzed from few intrusive clasts, Figure 37 shows that data form two distinctive populations in the ternary plot. Moreover, intrusive suites from MBL and TAM have distinct geochemical signatures, with Ford Granodiorite and Byrd Coast Granite that fall in the calcalkaline field of Abdel-Rahman (1994) and Bell et al. (2017); GHIC field is reconstructed based on PRR samples from CTM e SVL, on intrusive clasts from CIROS and CRP drillcores which have inferred TAM provenance (Talarico and Sandroni, 1998; Talarico et al., 2000; Sandroni and Talarico, 2001, 2004, 2006), and on NVL granitoids (Biagini et al., 1991). Biotite from one Byrd Coast Granite sample also fall in the lowermost part of the peraluminous field (Figure 37). These differences could be explained because the Byrd Coast Granite originated both from melting of the Swanson Formation and Ford Granodiorite, and the whole rock chemistry highlights the compositional differences (Korhonen et al., 2010b). Analyzed clast from PF21-1, which is supposed to be sourced from the TAM, falls at the boundary between peraluminous and calcalkaline fields and it resembles with GHIC rocks, consistent with the inferred TAM provenance. The sample collected in the basal breccia of the DSDP Site 270 core is strongly similar to the U1521 sample, and they are both resembling to GHIC granitoid field. This result provides a strong implication about the composition of the basement in the Central High and in the entire Central Ross Sea because the basal breccia at the DSDP Site 270 is interpreted as a talus (Ford and Barrett, 1975; Kraus, 2016) and then a local provenance is supposed. The breccia is mainly composed by calc-silicate gneiss, the same of the underlying cored basement, and granitoids (Ford and Barrett, 1975). Ford and Barrett (1975) supposed the basement in the CH is correlative of the metamorphic rocks of SVL; U-Pb dating on titanite suggests a correlation with rocks of the Bowers and Robertson Bay terranes of NVL (Mortimer et al., 2011). The data obtained from SEM-EDS analysis of biotite from this sample is consistent with a similarity of the CH basement with the TAM. On the contrary, analysis of the granitoids from PF22-1, which is inferred to have West Antarctica signature, strongly differs from IODP Site U1521 and DSDP Site 270 clasts, falling in the I-Type calcalkaline field (Figure 37; Abdel-Rahman, 1994; Bell et al., 2017). Moreover, data well fit in the Ford Granodiorite, mainly I-Type calcalkaline (Pankhurst et al., 1998; Siddoway and Fanning, 2009; Yakymchuk et al., 2015), and Byrd Coast Granite composition (the facies directly derived from melting of Ford Granodiorite), supporting the hypothesis that these clasts were sourced from terranes that have affinity with MBL geology. In addition, Figure 38 tentatively compares biotite composition in terms of Al^{IV} versus X_{Fe} in glacially transported clasts with some MBL outcropping formations. In Figure 38A reference fields were built based on Polar Rock Repository samples which were collected both in MBL and TAM (CTM and SVL) outcrops. Moreover, intrusive clasts from CIROS-1, CIROS-2, CRP-1, CRP-2, and CRP-3 drillcores, which are inferred to be sourced in the TAM (Talarico and Sandroni, 1998; Talarico et al., 2000; Sandroni and Talarico, 2001, 2004, 2006), were used to improve the database of GHIC rocks. In Figure 38B any clear trend can be observed due to the wide variability in the biotite composition. However, biotite from clasts supposed to have WA provenance (those from PF21-2, PF22-1, PF270-1) usually show X_{Fe} lower than biotite from clasts supposed to have EA provenance; the latter usually have Al^{IV} content higher than WA derived clasts. On the contrary, in Figure 38C, that considers only granitoid rocks, data form two well distinct group. Here, the clast from PF21-1, which is supposed to have TAM provenance, has composition that does not fit with MBL rocks, while it well fits in the GHIC granitoids; this is consistent with a TAM source of these clasts. Similarly, the granite clasts from the DSDP 270 breccia is comparable with GHIC granitoids, supporting the hypothesis that the CH basement reflect the TAM geology rather than the MBL geology.

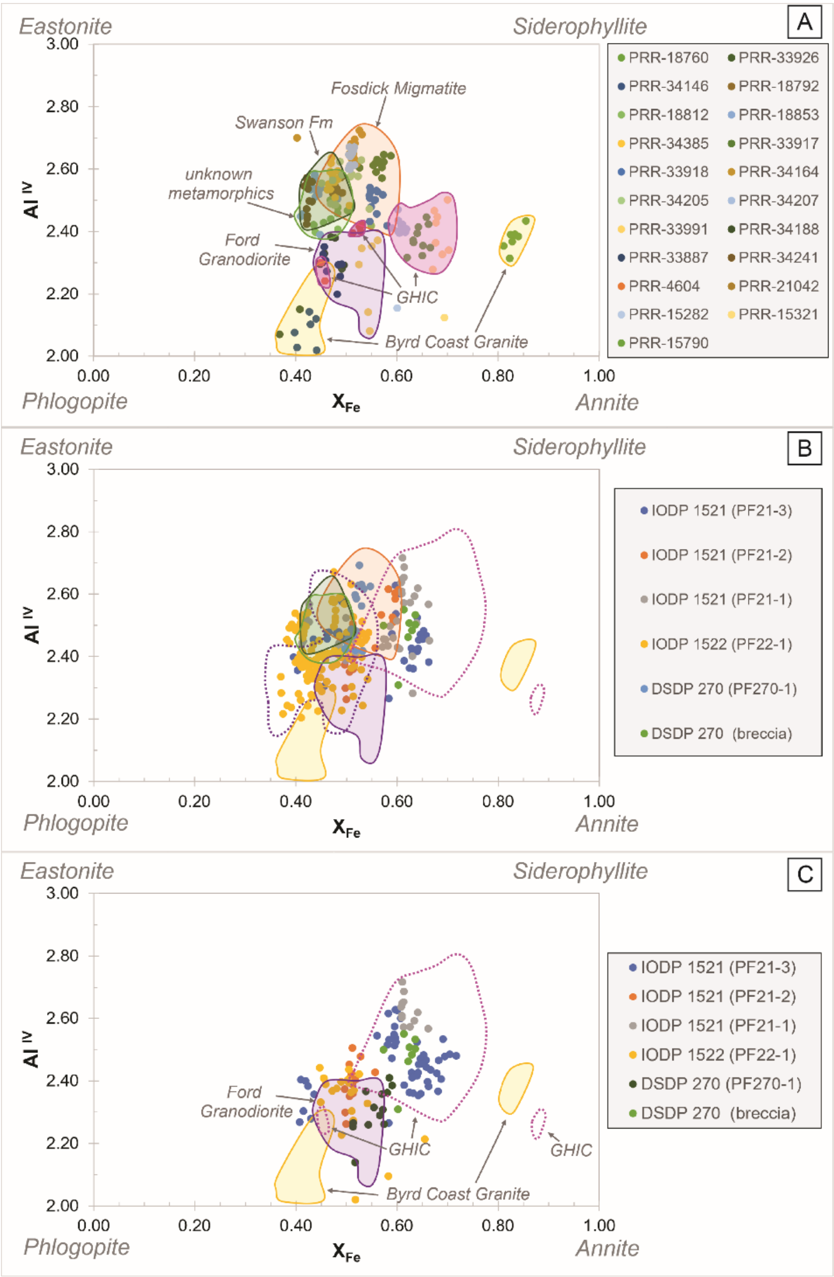

Figure 38 Biotite composition in terms of Al^{IV} versus X_{Fe} (Fe/(Fe+Mg)); compositional end-members are shown at the edges of the diagram. A) Classification of the Polar Rock Repository samples. Rocks were grouped on the basis of formations and the same fields were shown in B) and C). Fm: Formation; B) Classification of biotite from IODP Site U1521, Site U1522, and DSDP Site 270 igneous and metamorphic clasts. Samples were grouped and named on the basis of the petrofacies (PF) where they were collected; C) Classification of biotite in granitoid clasts from IODP Site U1521, Site U1522, and DSDP Site 270. Samples were grouped and named on the basis of the petrofacies (PF) where they were collected. Dotted violet line represents biotite composition of Eastern Ross Sea pebbles (Perotti et al., 2017), dotted pink line represents Granite Harbour Intrusive Complex (GHIC) from northern Victoria Land outcrops (Biagini et al., 1991), from Southern Victoria Land and Central Transantarctic Mountains (this study), and from intrusive clasts collected in CIROS-1, CIROS-2, CRP-1, CRP-2, and CRP-3 cores which are interred to be sourced from Granite Harbour Intrusive Complex (GHIC) outcrops (Talarico and Sandroni, 1998; Talarico et al., 2000; Sandroni and Talarico, 2001, 2004, 2006).

Figure 38C also shows that biotite of clasts from PF22-1, supposed to have WA signature, strongly fit with both Eastern Ross Sea tills, which have MBL signature (Perotti et al., 2017), and Ford Granodiorite. This result offers another evidence that sediments deposited within the PF22-1, were linked with an ice cover that drained terranes comparable with MBL geology. These data show that biotite from GHIC rocks is mainly more ferriferous ($X_{Fe} > 0.60$), while biotite crystals from MBL generally more magnesium rich ($X_{Fe} < 0.60$). Although databases, of both outcrop rocks and transported clasts, need to be improved, the preliminary data presented here tentatively offer a discrimination for the clast source identification.

The comparison of amphiboles in igneous clasts from the IODP Site U1522 with onshore geology (Figure 39) provides other indications of a West Antarctica provenance of the PF22-1. Whereas amphibole analysis within each sample strongly varies, probably due to alteration, in Figure 39 can be observed that, in general, Site U1522 amphiboles have X_{Mg} value higher than 0.5, comparable with Eastern Ross Sea intrusive clasts with inferred MBL provenance (Perotti et al., 2017) and with amphiboles from Ford Granodiorite samples analyzed in this study (PRR-33991 and PRR-34188). On the contrary, calcic amphiboles of the GHIC, based on analysis of intrusive gravel size clasts from CIROS and CRP cores, Eocene erratics collected at Minna Bluff (SVL), and Ross Sea Drift I collected in the Dry Valleys (SVL) which are inferred to be sourced from GHIC (Talarico and Sandroni, 1998; Talarico et al., 2000, 2013; Sandroni and Talarico, 2001, 2004, 2006; Perotti et al., 2018), usually show X_{Mg} value lower than 0.5. Therefore, whereas no strong fit exists between PF22-1 and MBL amphiboles, they are more comparable with MBL rocks rather than TAM ones, supporting the hypothesis of WA provenance of these sediments. The hypothesis proposed here needs further investigations improving chemical analyses of outcropping rocks and of glacially transported clasts.

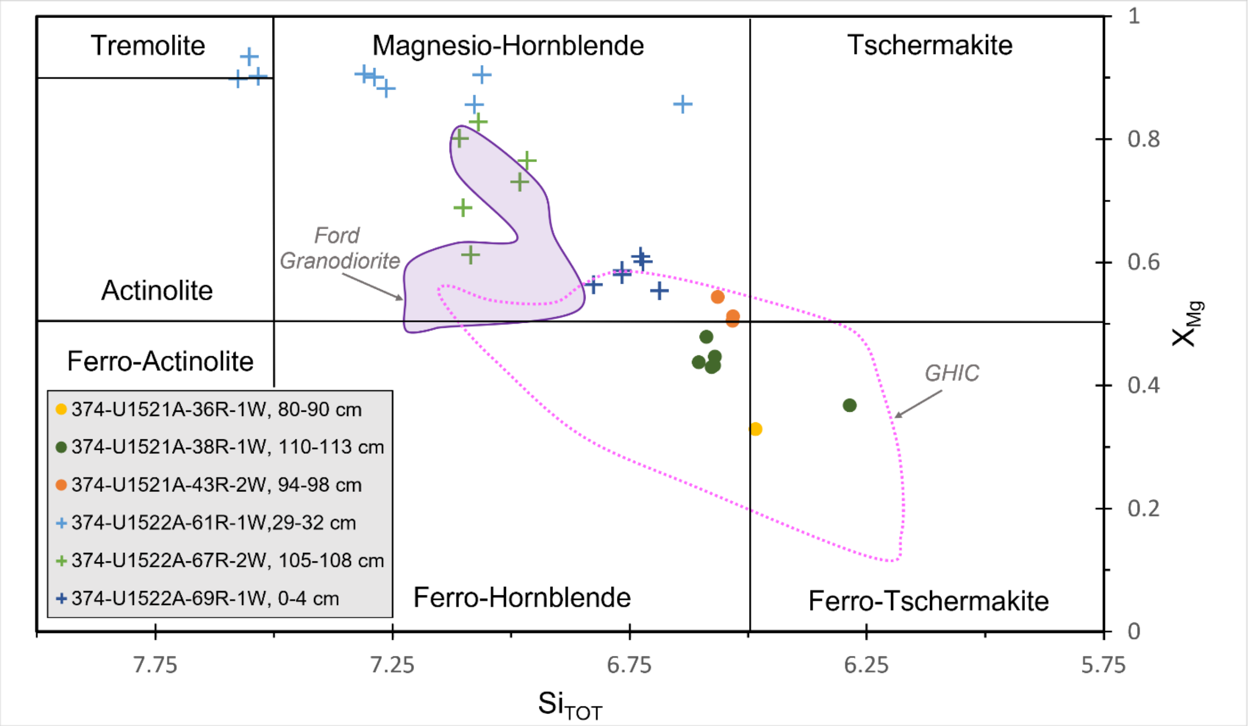

Figure 39 Calcic amphibole composition in terms of Si_{TOT} versus X_{Mg} (Leake et al., 1997) of granitoid clasts from IODP Site U1522. Grains from sample 374-U1522A-67R-2W, 72-75 cm are in the magnesio-hastingsite field (see Figure 27). Ford Granodiorite field (filled with violet) is on the basis of PRR-33991 and PRR-34188 (Perotti et al., 2017). Dotted pink line represents literature of amphiboles from glacially transported intrusive gravel-size clasts, which are inferred to have been sourced from Granite Harbour Intrusive Complex in the Transantarctic Mountains (Talarico and Sandroni, 1998; Talarico et al., 2000, 2013; Sandroni and Talarico, 2001, 2004, 2006; Perotti et al., 2018). Plus symbols represents intrusive clasts; circle represents intrusive clasts within bulk diamictite samples.

Chemical data from biotite and amphibole of intrusive clasts are also comparable because both recorded magnesium variation. Both mineralogical phases highlight those crystals from MBL rocks are usually more magnesiferous that TAM ones, which instead are more iron-rich.

3.7. Conclusion about provenance of Cenozoic glacial sediments

The petrographic and minero-chemical characterization of gravel size clasts collected in the CRS cores provides useful information about the Antarctic Ice Sheets dynamics during Cenozoic.

The analysis of IODP Site U1521 clasts, compared with geochronological and geochemical analyses of the diamictite matrix (Marschalek et al., 2021), allows the identification of two main shift in the sediment composition, revealing the first advance in the Central Ross Sea of a marine-based West Antarctic Ice Sheet in the early Miocene (ca. 18 Ma), long before it was thought (during the MMCT).

The lithologies of the clasts in the IODP Site U1522 indicate that the lower Miocene sediments were likely sourced in relationship with West Antarctic Ice Sheet dynamic because clast composition, primarily linked with the absence of dolerite and sandstone which largely crops out in the TAM, resembles rock outcrops in Marie Byrd Land rather than other surrounding areas. Moreover, chemical analysis on biotite and hornblende within intrusive clasts reveal a strong affinity of those clasts with intrusive rock outcrops in Marie Byrd Land. The comparison of gravel petrography with other provenance proxies, such us mineral chemistry and geochronology, is needed to confirm the main hypothesis of this thesis work.

DSDP Site 270 provides insights of the basement composition of the Central High in the Central Ross Sea. Chemical analysis on biotite from intrusive clast in the breccia overlying the basement, shows affinity with Granite Harbour Intrusive Complex rocks which extensively characterize the Transantarctic Mountains. The analysis of glacially transported clasts leaves the door open to both a local provenance and a distal one from Marie Byrd Land sectors, of the gravel. The multi-analytical approach, which combines clast petrography, mineral chemistry and geochronology, is needed to better constrain the sediment source.

Whereas the database of chemical analysis of biotite and amphibole need to be improved, data presented here show, for the first time, that these common mineralogical phases can be promising as a valid provenance tool, coupled with other proxies, in region, like Antarctica, where the geological knowledge of the onshore and offshore geology is limited and not totally adequate. Indeed, preliminary analysis reveal difference in the chemical composition between East Antarctica granitoids (i.e., Granite Harbour Intrusive Complex) and West Antarctica ones (i.e., Ford Granodiorite and Byrd Coast Granite). However, these preliminary observations must necessarily be implemented with additional analyses from outcrops geology of the Ross Sea region in order to implement the database. However, despite the needed data to be implemented, the obtained results of this thesis relative to the petrographic provenance studies, show and fix some fundamental points because they allow to highlight changes in the clast composition through time and it is fundamental to recognized provenance changes.

4. General conclusions

This thesis aims to carry out provenance study through a multianalytical approach on glaciogenic sediments and rocks involving the Antarctica continent, but comparing very different time lapses, as late Paleozoic (late Carboniferous to Permian) and late Cenozoic (Neogene). The study of glaciogenic material allow the reconstruction of the glacial settings in the past and the response of the system to the paleo climate changes that afflicted the Earth in the past. Antarctica is a privileged place to study glaciogenic rocks because the continent, in its current continental setting, holds ice sheets since the Paleogene (ca. 35 Ma), allowing the study of the evolution of the Antarctic ice sheets through time. Moreover, in the sedimentary rocks deposited in the Late Paleozoic, when Antarctica was part of the Gondwana supercontinent, remote past glacial events are recorded. The work considers two distinct cases study in order to provide that these techniques are successfully applicable in every contest of glaciogenic material. The first case study concerns the glaciogenic rocks deposited during the Late Paleozoic Ice Age, that currently crop out in Victoria Land, a northern sector of the Transantarctic Mountains. These rocks were initially analyzed with a sedimentological approach to define the depositional processes and to reconstruct the paleo-environment for this sector of Gondwana. Sedimentological features allow to confirm that the studied sequences were deposited mainly sub-aqueously near the ice front. The provenance analysis of diamictite facies of four outcrops in Victoria Land, is based both in the petrographic characterization of diamictite matrix and gravel and in the geochronological analysis of the detrital zircons contained within them. This study is the first led extensively for the whole region, with this kind of approach of Late Paleozoic glaciogenic rocks in this sector of Gondwana. The join of geochronological and petrographic analyses allows to highlight difference between the northern Victoria Land tillites and the southern Victoria Land ones which are proposed to be related with two possibly distinct ice caps, the NVL-Tas Ice Cap and the SVL Ice Cap respectively. These results fit with the emerging view of a Late Paleozoic Ice Age characterized by local ice caps which diachronously developed within Gondwana, instead of a unique wide glacial sheet as noted by “classical” view. Furthermore, the provenance evidence, emphasize a clast source from the west, where currently in settled the Ross Sea and the Marie Byrd Land, to east, according to paleo-currents and paleo-geographic reconstructions (Isbell et al., 2008a; Isbell, 2010; Ives and Isbell, 2021).

The second case study regards Oligocene to Pliocene glaciogenic sediments recovered by cores during the IODP Expedition 374 and DSDP Leg 28 in the Ross Sea. These sediments recorded the dynamics of the East and West Antarctic Ice sheets during the Cenozoic. The understanding of the dynamics of the Antarctic Ice sheets in response to climate forcing of the past is a key tool for predicting the response of the Antarctic Ice cover to the present-day climate changes. The main goal of this study is the characterization, by the minero-petrographic point of view, of the gravel size clasts occurring in three cores in the Central

Ross Sea that recorded the sedimentary history since the Oligocene. The petrographic analysis of the clasts allows the identification of different clasts assemblages both in the three cores and along each core, indicating changes in the sediment supply, likely linked with ice setting changes. In particular, a main provenance shift is recognized in the early Miocene and recorded in the IODP Site U1521, where the change in clast lithology composition, marked by the disappear of TAM lithologies, such as the dolerite, and the appearance of West Antarctica ones, such as basalt, coupled with geochemical, geochronological, sedimentological, and seismic indicators (Marschalek et al., 2021), is used to constrain the first advance of the West Antarctic Ice Sheet in the continental shelf of the Ross Sea. Preliminary mineral chemistry analysis of biotite and amphibole seems to show difference between East and West Antarctica intrusive rocks; the comparison of chemical analyses of biotite and amphibole in the intrusive clasts with ones from the outcrops confirms the inferred provenance based on the clast assemblages. If further analysis will confirm the trend observed in this thesis, SEM-EDS chemical analysis of biotite and amphibole, which are cheap and fast, could provide a new useful tool in the provenance study in the Ross Sea region. The characterization of gravel is also compared with geochronological and geochemical analyses of the diamictite matrix to constrain the work hypothesis.

Both cases study demonstrates that the provenance study, in particular of glaciogenic sediments which are strongly heterometric, need a multianalytical approach to have more robust constrains. Furthermore, this study highlights as so different time deposits with glacial influence can be approached with similar techniques and methodologies. The petrographic characterization of the glacially transported gravel size clasts allows to characterize the sediments composition and the comparison of them with the bedrock outcrops throughout the glaciers catchment areas to define the possible source regions. The comparison of petrographic data with geochronological (U-Pb on detrital zircons) and mineral chemistry analyses allow to constrain the sediments provenance. This thesis enabled to demonstrate that so different glaciations could be modelized collecting important proxy data useful to strengthen the predictive models for the study of the development of the current Antarctica ice sheets.

Acknowledgments

This work was supported by the Italian National Antarctic Research Program - PNRA [PNRA18-00233 and AZ2.08 PNRA PEA2013]. I wish to thank Dr Rosaria Palmeri and Dr Sonia Sandroni of the National Museum of Antarctica (MNA) – Siena Section (http://www.mna.it/siena/siena-sede-espositiva), where the Late Paleozoic Ice Age samples are stored. I wish also to thank the Korea Polar Research Institute (KOPRI) and its staffs who helped me during the geochronological analyses and the Chungbuk National University laboratory for the samples preparation.

I wish to thank the International Ocean Discovery Project (IODP) and the Gulf Coast Repository staff at Texas A&M University, College Station (USA) for their support and useful help during core logging and for having provided samples on the basis of our requests. We wish to also thank all IODP Expedition 374 Science Party members and in particular Laura De Santis, Rob McKay, and Denise Kulhanek for their useful comments and the support they always provided. I also thank the Polar Rock Repository in the Byrd Polar Research Centre, Ohio State University, for providing useful samples of rocks from the study area.

My acknowledgement also goes to Matteo Perotti for his precious contribution and Prof Claudio Ghezzo with whom I have had fruitful discussions.

In memory of our friend and colleague Franco Talarico, who highly contributed to this research, who suddenly passed away.

REFERENCES

Abdel-Rahman, A.-F.M., 1994, Nature of Biotites from Alkaline, Calc-alkaline, and Peraluminous Magmas: Journal of Petrology, v. 35, p. 525–541, doi:10.1093/petrology/35.2.525.

Adams, C.J., 1986, Geochronology of granite terranes in the Ford Ranges, Marie Byrd Land, West Antarctica: New Zealand Journal of Geology and Geophysics, v. 30, p. 51–76.

Adams, C.J., Bradshaw, J.D., and Ireland, T.R., 2014, Provenance connections between late Neoproterozoic and early Palaeozoic sedimentary basins of the Ross Sea region, Antarctica, south-east Australia and southern Zealandia: Antarctic Science, v. 26, p. 173–182, doi:10.1017/S0954102013000461.

Allibone, C.J., Cox, S.C., Graham, I.J., Smillie, R.W., Johnstone, R.D., Ellery, S.G., and Palmer, K., 1993a, Granitoids of the Dry Valleys area, southern Victoria Land, Antarctica: plutons, field relationships, and isotopic dating: New Zealand Journal of Geology and Geophysics, v. 36, p. 281–297.

Allibone, C.J., Cox, S.C., and Smillie, R.W., 1993b, Granitoids of the Dry Valleys area, southern Victoria Land: geochemistry and evolution along the early Palaeozoic Antarctic craton margin: New Zealand Journal of Geology and Geophysics, v. 36, p. 299–316.

American Geographical Society, 1969, GeologicMap of Antarctica: AntarcticMap Folio Series, Folio 12 geological map.

Anderson, J.B. et al., 2014, Ross Sea paleo-ice sheet drainage and deglacial history during and since the LGM: Quaternary Science Reviews, v. 100, p. 31–54, doi:10.1016/j.quascirev.2013.08.020.

Askin, R.A., 1998, Floral trends in the high latitudes: Palynological evidence from the Transantarctic Mountains: Journal of African Earth Sciences, v. 27, p. 12–13.

Aubrecht, R., Méres, Š., Sýkora, M., and Mikuš, T., 2009, Provenance of the detrital garnets and spinels from the Albian sediments of the Czorsztyn Unit (Pieniny Klippen Belt, Western Carpathians, Slovakia): Geologica Carpathica, v. 60, p. 463–483, doi:10.2478/v10096-009-0034-z.

Barrett, P.J., 1989, Antarctic Cenozoic History from theCIROS- 1Drillhole, McMurdo Sound, Antarctica: Wellington, Barret, P.J., New Zealand Department of Scientific and Industrial Research Bulletin, v. 245, 254 p.

Barrett, P.J., 1981, History of the Ross Sea region during the deposition of the Beacon Supergroup 400-180 million years ago: Journal of the Royal Society of New Zealand, v. 11, p. 447–458, doi:10.1080/03036758.1981.10423334.

Barrett, P.J., 1991, The Devonian to Jurassic Beacon Supergroup of the Transantarctic Mountains and correlatives in other parts of Antarctica, *in* The Geology of Antarctica, Oxford, Tingey, R.J., p. 120–152.

Barrett, P.J., Elliot, D.H., and Lindsay, J.F., 1986, The Beacon Supergroup (Devonian-Triassic) and Ferrar Group (Jurassic) in the Beardmore Glacier area, Antarctica, *in* Geology of the Central Transantarctic Mountains: Antarctic Research Series, American Geophysical Union, Turner, M.D., Splettstoesser, J.F., v. 36, p. 339–428.

Barrett, P.J., Grindley, G.W., and Webb, P.N., 1972, The Beacon Supergroup of East Antarctica, *in* Antarctic Geology and Geophysics, Universitetsforslaget, Oslo, Adie, R.J., p. 319–332.

Barrett, P.J., and McKelvey, B.C., 1981, Permian tillites of south Victoria Land, Antarctica: Earth's pre-Pleistocene glacial record, p. 233–236.

Behrendt, J.C., 2013, The aeromagnetic method as a tool to identify Cenozoic magmatism in the West Antarctic Rift System beneath the West Antarctic Ice Sheet — A review; Thiel subglacial volcano as possible source of the ash layer in the WAISCORE: Tectonophysics, v. 585, p. 124–136, doi:10.1016/j.tecto.2012.06.035.

Bell, E.A., Boehnke, P., and Mark Harrison, T., 2017, Applications of biotite inclusion composition to zircon provenance determination: Earth and Planetary Science Letters, v. 473, p. 237–246, doi:10.1016/j.epsl.2017.06.012.

Biagini, R., Di Vincenzo, G., and Ghezzo, C., 1991, Petrology and geochemistry of peraluminous granitoids from Priestley and Aviator glaciers region, Northern Victoria Land, Antarctica: Memorie della Società Geologica Italiana, v. 46205–230.

Blackey, R.C., 2008, Gondwana paleogeography from assembly to breakup - a 500m.y. odyssey: Resolving the Late Paleozoic Ice Age in Time and Space: Geological Society of America Special Paper, v. 441, p. 1–28.

Blankenship, D.D., Bell, R.E., Hodge, S.M., Brozena, J.M., Behrendt, J.C., and Finn, C.A., 1993, Active volcanism beneath the West Antarctic ice sheet and implications for ice-sheet stability: Nature, v. 361, p. 526–529, doi:10.1038/361526a0.

Bomfleur, B., Mörs, T., Unverfärth, J., Liu, F., Läufer, A., Castillo, P., Oh, C., Park, T.S., Woo, J., and Crispini, L., 2020, Uncharted Permian to Jurassic continental deposits in the far north of Victoria Land, East Antarctica: Journal of the Geological Society, v. 178, doi:https://doi.org/10.1144/jgs2020-062.

Bomfleur, B., Schöner, R., John, N., Schneider, J.W., Elsner, M., Viereck-Goette, L., and Kerp, H., 2014, New Palaeozoic deposits of the Victoria Group in the Eisenhower range, northern Victoria Land, Antarctica: Antarctic Science, v. 26, p. 277–278.

Borg, S.G., 1980, Petrology and geochemistry of the Wyatt Formation and the Queen Maud batholith, upper Scott Glacier area, Antarctica [PhD thesis]: Arizona State University.

Bradshaw, J.D., 2007, The Ross Orogen and Lachlan Fold Belt in Marie Byrd Land, northern Victoria Land and New Zealand: implication for the tectonic setting of the Lachlan Fold Belt in Antarctica: U. S. Geological Survey and the National Academies, v. 59, https://doi.org/10.3133/of2007-1047.srp059.

Bradshaw, J.D., Andrews, P.B., and Field, B.D., 1983, Swanson Formation and related rocks of Marie Byrd Land and a comparison with the Robertson Bay Group of northern Victoria Land, *in* Antarctic Earth Science: Australian Academy of Science, Canberra, Oliver, R. L., James, P. R. and Jago, J. B., p. 274–279.

Brancolini, G. et al., 1995, Descriptive text for the Seismic Stratigraphic Atlas of the Ross Sea, *in* Geology and Seismic Stratigraphy of the Antarctic Margin, Washington, DC, Cooper, A., Barker, P.F., and Brancolini, G., Antarctic Research Series, v. 68, p. A271–A268.

Brown, C.R., Yakymchuk, C., Brown, M., Fanning, C.M., Korhonen, F.J., Piccoli, P.M., and Siddoway, C.S., 2016, From Source to Sink: Petrogenesis of Cretaceous Anatectic Granites from the Fosdick Migmatite–Granite Complex, West Antarctica: Journal of Petrology, v. 57, p. 1241–1278, doi:10.1093/petrology/egw039.

Buggisch, W., Wang, X., Alekseev, A.S., and Joachimski, M.M., 2011, Carboniferous–Permian carbon isotope stratigraphy of successions from China (Yangtze platform), USA (Kansas) and Russia (Moscow Basin and Urals): Palaeogeography, Palaeoclimatology, Palaeoecology, v. 301, p. 18–38.

Burgess, C.J., Palmer, A., and Anderson, J.M., 1981, The geology of the Fry Glacier area, South Victoria Land, Antarctica, with particular reference to the Taylor Group: New Zealand Journal of Geology and Geophysics, v. 24, p. 373–388, doi:https://doi.org/10.1080/00288306.1981.10422727.

Cape Roberts Science Team, 2000a, Initial Report of CRP-3: Siena, Barret, P.J., Sart, M., Wise, S., Studies from the Cape Roberts Project, Ross Sea, Antarctica, v. 7 (1/2).

Cape Roberts Science Team, 1998a, Miocene strata in CRP-1, Cape Roberts Project, Antarctica: Terra Antartica, v. 5, p. 63–124.

Cape Roberts Science Team, 1998b, Quaternary strata in CRP-1, Cape Roberts Project, Antarctica: Terra Antartica, v. 5, p. 31–62.

Cape Roberts Science Team, 2000b, Scientific Results of CRP-2/2A: Siena, Barret, P.J., Ricci, C.A., Studies from the Cape Roberts Project, Ross Sea, Antarctica, v. 7 (4/5).

Capponi, G., Meccheri, M., Pertusati, P.C., Carosi, R., Crispini, L., Musumeci, M., Oggiano, G., Roland, N.W., and Tessensohn, F., 2012, Antarctic Geological Map Series 1 : 250000 - Freyberg Mountains Quadrangle (Victoria Land): Petrusati, P.C. and Tessensohn, F.

Casnedi, R., Pertusati, P.C., Salvini, F., Carosi, R., Meccheri, M., Musumeci, M., Oggiano, G., and Ricci, C.A., 2012, Antarctic Geological Map Series 1 : 250000 - Reeves Névé Quadrangle (Victoria Land): Petrusati, P.C. and Tessensohn, F.

Cawood, P.A., 2005, Terra Australis Orogen: Rodinia breakup and developement of the Pacific and Iapetus margins of Gondwana during the Neoproterozoic and Paleozoic: Earth-Science Reviews, v. 69, p. 249–279.

Cheong, W., Cho, M., and Kim, Y., 2013, An Efficient Method for Zircon Separation Using the Gold Pan: The Journal of the Petrological Society of Korea, v. 22, p. 63–70, doi:http://dx.doi.org/10.7854/JPSK.2013.22.1.063.

Clapham, M.E., and James, N.P., 2008, Paleoecology of Early–Middle Permian marine communities in eastern Australia; response to global climate change in the aftermath of the late Paleozoic ice age: Palaios, v. 23, p. 738–750.

Collinson, J.W., Isbell, J.L., Elliot, D.H., Miller, M.F., and Miller, J.M.G., 1994, Permian-Triassic Transantarctic basin, *in* Permian-Triassic Pangean basins and foldbelt along the Panthalassan marfin of Gondwanaland, Boulder, Colorado, Veevers, J., Powell, C., Geological Society of America Memoir, v. 184.

Collinson, J.W., Pennington, D.C., and Kemp, N.R., 1986, Stratigraphy and petrology of Permian and Triassic fluvial deposits in Northern Victoria Land, Antarctica: Antarctic Research Series, v. 46, p. 211–242.

Cooper, A.K.., Barrett, P.J., Hinz, K., Traube, V., Letichenkov, G., and Stagg, H.M., 1991a, Cenozoic prograding sequences of the Antarctic continental margin: a record of glacio-eustatic and tectonic events: Marine Geology, v. 102, p. 175–213, doi:https://doi.org/10.1016/0025-3227(91)90008-R.

Cooper, A.K.., Davey, F.J., and Hinz, K., 1991b, Crustal extension and origin of sedimentary basins beneath the Ross Sea and Ross Ice Shelf, Antarctica, *in* Geological evolution of Antarctica, Cambridge, Thomson, M.R.A., Crame, J.A., Thomson, J.W., p. 285–291.

Cooper, A.F., Maas, R., Scott, J.M., and Barber, A.J.W., 2011, Dating of volcanism and sedimentation in the Skelton Group, Transantarctic Mountains: Implications for the Rodinia-Gondwana transition in southern Victoria Land, Antarctica: GSA Bulletin, v. 123, p. 681–702, doi:10.1130/B30237.1.

Cornamusini, G., and Talarico, F.M., 2016, Miocene Antarctic ice dynamics in the Ross Embayment (Western Ross Sea, Antarctica): Insights from provenance analyses of sedimentary clasts in the AND-2A drill core: Global and Planetary Change, v. 146, p. 38–52, doi:http://dx.doi.org/10.1016/j.gloplacha.2016.09.001.

Cornamusini, G., Talarico, F.M., Cirilli, S., Spina, A., and Woo, J., 2017, Upper Paleozoic glacigenic deposits of Gondwana: Stratigraphy and paleoenvironmental significance of a tillite succession in Northern Victoria Land (Antarctica): Sedimentary Geology, v. 358, p. 51–69, doi:http://dx.doi.org/10.1016/j.sedgeo.2017.07.002.

Cottle, J.M., and Cooper, A.F., 2006, The Fontaine Pluton; an early Ross Orogeny calc-alkaline gabbro from southern Victoria Land, Antarctica: New Zealand Journal of Geology and Geophysics, v. 49, p. 177–189.

Cox, S.C., Turnbull, I.M., Isaac, M.J., Townsend, D.B., and Smith Lyttle, B., 2012, Geology of Southern Victoria Land, Antarctica: Institute of Geological & Nuclear Sciences 22. 135 geological map.

Craddock, J.P. et al., 2019, Detrital zircon provenance of Permo-Carboniferous glacial diamictites across Gondwana: Earth-Science Reviews, v. 192, p. 285–316, doi:https://doi.org/10.1016/j.earscirev.2019.01.014.

Craddock, J.P., Fitzgerald, P., Konstantinou, A., Nereson, A., and Thomas, R.J., 2017, Detrital Zircon provenance of upper Cambrian-Permian Strata and Tectonic evolution of the Ellsworth Mountains, West Antarctica: Gondwana Research, v. 45, p. 191–207, doi:http://dx.doi.org/10.1016/j.gr.2016.11.011.

Crispini, L., Federico, L., and Capponi, G., 2014, Structure of the Millen Schist Belt (Antarctica): Clues for the tectonics of northern Victoria Land along the paleo-Pacific margin of Gondwana: Tectonics, v. 33, p. 420–440, doi:10.1002/2013TC003414.

De Santis, L., Anderson, J.B., Brancolini, G., and Zayatz, I., 1995, Seismic Record of Late Oligocene Through Miocene Glaciation on the Central and Eastern Continental Shelf of the Ross Sea, *in* Geology and Seismic Stratigraphy of the Antarctic Margin, Washington, DC, Cooper, A., Barker, P.F., and Brancolini, G., Antarctic Research Series, v. 68.

Dowdeswell, J.A., Whittington, R.J., and Marienfeld, P., 1994, The origin of massive diamicton facies by iceberg rafting and scouring, Scoresby Sund, East Greenland: Sedimentology, v. 41, p. 21–35, doi:doi: 10.1111/j.1365-3091.1994.tb01390.x.

Elliot, D.H., 2013, The geological and tectonic evolution of the Transantarctic Mountains: a review: Hambrey, M. J., Barker, P. F., Barrett, P. J., Bowman, V., Davies, B., Smellie, J. L. & Tranter, M. (eds) Antarctic Palaeoenvironments and Earth-Surface Processes. Geological Society, London, Special Publications, v. 381, doi:http://dx.doi.org/10.1144/SP381.14.

Elliot, D.H., and Fanning, C.M., 2008, Detrital zircons from upper Permian and lower Triassic Victoria Group sandstones, Shackleton Glacier region, Antarctica: Evidence for multiple sources along the Gondwana plate margin: Gondwana Research, v. 13, p. 259–274, doi:10.1016/j.gr.2007.05.003.

Elliot, D.H., Fanning, C.M., and Hulett, S.R.W., 2015, Age provinces in the Antarctic craton: Evidence from detrital zircons in Permian strata from the Beardmore Glacier region, Antarctica: Gondwana Research, v. 28, p. 152–164, doi:https://doi.org/10 .1016 /j.gr.2014.03.013.

Elliot, D.H., Fanning, C.M., Isbell, J.L., and Hulett, S.R.W., 2017, The Permo-Triassic Gondwana sequence, central Transantarctic Mountains, Antarctica: Zircon geochronology, provenance, and basin evolution: Geosphere, v. 13, p. 155–178, doi:https:// doi .org /10 .1130 /GES01345 .1.

Elliot, D.H., Fanning, C.M., Mukasa, S.B., and Millar, I.L., 2019, Hf- and O-isotope data from detrital and granitoid zircons reveal characteristics of the Permian–Triassic magmatic belt along the Antarctic sector of Gondwana: Geosphere, v. 15, doi:https://doi.org/10.1130/GES02011.1.

Elliot, D.H., and Fleming, T.H., 2008, Physical volcanology and geological relationships of the Jurassic Ferrar Large Igneous Province, Antarctica: Journal of Volcanology and Geothermal Research, v. 172, p. 20–37, doi:10.1016/j.jvolgeores.2006.02.016.

Elsner, M., Schoner, R., Gerdes, A., and Gaupp, R., 2013, Reconstruction of the early Mesozoic plate margin of Gondwana by U–Pb ages of detrital zircons from northern Victoria Land, Antarctica, *in* Antarctica and Supercontinent Evolution, London, Harley, S. L., Fitzsimons, I. C.W., Zhao, Y., Geological Society: Special Publications, v. 383, p. 211–232.

Encarnación, J., and Grunow, A., 1996, Changing magmatic and tectonic styles along the paleo- Pacific margin of Gondwana and the onset of early Paleozoic magmatism in Antarctica: Tectonics, v. 15, p. 1325–1341.

Encarnación, J., Rowell, A.J., and Grunow, A., 1999, A U-Pb age for the Cambrian Taylor Formation, Antarctica: Implications for the Cambrian time scale: Journal of Gology, v. 107, p. 497–504, doi:10.1086/314361.

Estrada, S., Läufer, A., Eckelmann, K., Gärtner, A., and Linnemann, U., 2016, Continuous Neoproterozoic to Ordovician sedimentation at the East Gondwana margin - Implications from detrital zircons of the Ross Orogen in northern Victoria Land, Antarctica: Gondwana Research, v. 37, p. 426–448.

Eyles, N., and Eyles, C.H., 1992, Glacial depositional systems, *in* Facies Models: Response to Sea Level Change, St. Johns, NF, Walker, R.G., James, N.P., p. 73–100.

Eyles, N., Eyles, C.H., and Miall, A.D., 1983, Lithofacies types and vertical profile models; an alternative approach to the description and environmental interpretation of glacial diamict and diamictite sequences: Sedimentology, v. 30, p. 393–410.

Eyles, C.H., Eyles, N., and Miall, A.D., 1985, Models of glaciomarine sedimentation and their application to the interpretation of ancient glacial sequences: Palaeogeography, Palaeoclimatology, Palaeoecology, v. 51, p. 15–84.

Eyles, N., and Lazorek, M., 2007, Glacial Landsforms, sediments - Glacigenic Lithofacies: Encyclopedia of Quaternary Science, p. 920–932, doi:https://doi.org/10.1016/B0-44-452747-8/00085-5.

Falcon-Lang, H.J., 2004, Pennsylvanian tropical rain forests responded to glacial–interglacial rhythms: Geology, v. 32, p. 689–692.

Falcon-Lang, H.J., and Di Michele, W.A., 2010, What happened to the coal forest during Penssylvanian glacial phases? Palaios, v. 25, p. 611–617.

Farmer, G.L., Licht, K., Swope, R., and Andrews, J., 2006, Isotopic constraints on the provenance of fine-grained sediment in LGM tills from the Ross Embayment, Antarctica: Earth and Planetary Science Letters, v. 249, p. 90–107, doi:10.1016/j.epsl.2006.06.044.

Feakins, S.J., Warny, S., and Lee, J.-E., 2012, Hydrologic cycling over Antarctica during the middle Miocene warming: Nature Geoscience, v. 5, p. 557–560, doi:10.1038/ngeo1498.

Fielding, C.R., Frank, T.D., Birgenheier, L.P., Rygel, M.C., Jones, A.T., and Roberts, J., 2008a, Stratigraphic imprint of the Late Paleozoic Ice Age in eastern Australia: a record of alternating glacial and nonglacial climate regime: Journal of the Geological Society, v. 165, p. 129–140.

Fielding, C.R., Frank, T.D., Birgenheier, L.P., Rygel, M.C., Jones, A.T., and Roberts, J., 2008b, Stratigraphic record and facies associations of the late Paleozoic ice age in eastern Australia (New South Wales and Queensland), *in* Resolving the Late Paleozoic Ice Age in Time and Space, Fielding, C.R., Frank, T.D., and Isbell, J.L., Special Paper, v. 441, p. 41–57.

Fielding, C.R., Frank, T.D., and Isbell, J.L., 2008c, The late Paleozoic ice age - A review of current understanding and synthesis of global climate patterns, *in* Resolving the Late Paleozoic Ice Age in Time and space, Fielding, C.R., Frank, T.D., and Isbell, J.L, Geological Society of America Special Paper, v. 441, p. 343–354, doi: 10.1130/2008.2441(24).

Fielding, C.R., Frank, T.D., Isbell, J.L., Henry, L.C., and Domack, E.W., 2010, Stratigraphic signature of the late Palaeozoic Ice Age in the Parmeener Supergroup of Tasmania, SE Australia, and inter-regional comparisons: Palaeogeography, Palaeoclimatology, Palaeoecology, v. 298, p. 70–90, doi:10.1016/j.palaeo.2010.05.023.

Fielding, C.R., Naish, T., Woolfe, K.J., and Lavelle, M.A., 2000, Facies Analysis and Sequence Stratigraphy of CRP-2/2A, Victoria Land Basin, Antarctica: Terra Antartica, v. 7, p. 323–338.

Fioretti, A.M., Cavazzini, G., and Visonà, D., 1997, Admiralty intrusives in the southern Bowers Terrane: The Collis Peak Pluton. Comparison with the Salamander Granite Complex, Northern Victoria Land, Antarctica, *in* The Antarctic Region: Geological Evolution and Processes, Siena, C.A. Ricci, p. 287–292.

Fitzgerald, P., 2002, Tectonics and landscape evolution of the Antarctic plate since the breakup of Gondwana, with an emphasis on the West Antarctic Rift System and the Transantarctic Mountains, *in* Proceedings of the 8th International Symposiumon Antarctic Earth Science, Wellington, Gamble, J., Skinner, D.A., Henrys, S., Royal Society of New Zealand Bulletin, v. 35, p. 453–469.

Ford, A.B., and Barrett, P.J., 1975, Basement rocks of the south-central Ross Sea, Site 270, *in* Initial Reports, Deep Sea Drilling Project 28, Washington, DC, Hayes, D.E., p. 861–868.

Frakes, L.A., and Francis, J.E., 1988, A guide to Phanerozoic cold polar climates from high latitude ice-rafting in the Cretaceous: Nature, v. 333, p. 547–549.

Frakes, L.A., Francis, J.E., and Syktus, J.I., 1992, Climate Modes of the Phanerozoic: Cambridge University Press, v. 274.

Galeotti, S. et al., 2016, Antarctic Ice Sheet variability across the Eocene-Oligocene boundary climate transition: Science, v. 352, p. 76–80, doi:10.1126/science.aab0669.

Gasson, E.G.W., and Keisling, B., 2020, The Antarctic Ice Sheet: A Paleoclimate Modeling Perspective: Oceanography, v. 33, p. 90–100, doi:https://doi.org/10.5670/oceanog.2020.208.

Gilmer, G.J., 2008, Paleoenvironmental Interpretations of the Lower Taylor Group, Olympus Range Area, southern Victoria Land, Antarctica [Ms'C Thesis]: University of Canterbury, 2001 p.

Glasser, N.F., and Hambrey, M.J., 2001, Styles of sedimentation beneath Svalbard valley glaciers under changing dynamic and thermal regimes: Journal of the Geological Society, v. 158, p. 697–707.

Goodge, J.W., 2002, From Rodinia to Gondwana: Supercontinent evolution in the Transantarctic Mountains, *in* Antarctica at the Close of a Millennium, Wellington, Gamble, J., Skinner, D.A., Henrys, S, v. 35, p. 61–74.

Goodge, J.W., 2020, Geological and tectonic evolution of the Transantarctic Mountains, from ancient craton to recent enigma: Gondwana Research, v. 80, p. 51–122, doi:https://doi.org/10.1016/j.gr.2019.11.001.

Goodge, J.W., 2007, Metamorphism in the Ross orogen and its bearing on Gondwana margin tectonics: Cloos, M., Carlson, W.D., Gilbert, M.C., Liou, J.G., and Sorensen, S.S., eds., Convergent Margin Terranes and Associated Regions: A Tribute to W.G. Ernst: Geological Society of America Special Paper, v. 419, p. 185–203, doi:10.1130/2006.2419(10).

Goodge, J.W., Borg, S.G., Smith, B.K., and Bennett, V.C., 1991, Tectonic significance of Proterozoic ductile shortening and translation along the Antarctic margin of Gondwana: Earth and Planetary Science Letters, v. 102, p. 58–70.

Goodge, J.W., and Fanning, C.M., 2016, Mesoarchean and Paleoproterozoic history of the Nimrod Complex, central Transantarctic Mountains, Antarctica: Stratigraphic revisions and relation to the Mawson Continent in East Gondwana: Precambrian Research, v. 285, p. 242–271, doi:10.1016/j.precamres.2016.09.001.

Goodge, J.W., Fanning, C.M., Brecke, D.M., Licht, K.J., and Palmer, E.F., 2010, Continuation of the Laurentian Grenville province across the Ross Sea margin of East Antarctica: Journal of Geology, v. 118, p. 601–619.

Goodge, J.W., Fanning, C.M., Norman, M.D., and Bennett, V.C., 2012, Temporal, isotopic and spatial relations of Early Paleozoic Gondwana-margin arc magmatism, central Transantarctic Mountains, Antarctica: Journal of Petrology, v. 53, p. 2027–2065, doi:10.1093/petrology/egs043.

Goodge, J.W., Hansen, V.L., and Peacock, S.M., 1992, Multiple petrotectonic events in high-grade metamorphic rocks of the Nimrod Group, central Transantarctic Mountains, Antarctica: Recent Progress in Antarctic Earth Science, p. 203–209.

Goodge, J.W., Hansen, V.L., Peacock, S.M., Smith, B.K., and Walker, N.W., 1993, Kinematic evolution of the Miller Range Shear Zone, Central Transantarctic Mountains, Antarctica, and implications for Neoproterozoic to Early Paleozoic tectonics of the East Antarctic Margin of Gondwana: Tectonics, v. 12, p. 1460–1478, doi:10.1029/93TC02192.

Goodge, J.W., Myrow, P., Phillips, D., Fanning, C.M., and Williams, I.S., 2004a, Siliciclastic record of rapid denudation in response to convergent-margin orogenesis, Ross Orogen, Antarctica, *in* Detrital

Thermochronology—Provenance Analysis, Exhumation, and Landscape Evolution of Mountain Belts, Colorado, Bernet, M., Spiegel, C, Geological Society of America Special Paper, v. 378, p. 101–122.

Goodge, J.W., and Peacock, S.M., 1995, Eclogite-facies metamorphism preserved in tectonic blocks from a lower crustal shear zone, central Transantarctic Mountains, Antarctica: Lithos, v. 36, p. 1–13, doi:https://doi.org/10.1016/0024-4937(95)00006-2.

Goodge, J.W., Williams, I.S., and Myrow, P., 2004b, Provenance of Neoproterozoic and lower Paleozoic siliciclastic rocks of the central Ross orogen, Antarctica: Detrital record of rift-, passive-, and active-margin sedimentation: GSA Bulletin, v. 116, p. 1253–1279.

Griffis, N.P. et al., 2018, Isotopes to ice: constraining provenance of glacial deposits and ice centres in west-central Gondwana: Palaeogeography, Palaeoclimatology, Palaeoecology, v. 531, doi:https://doi.org/10.10167j.palaeo.2018.04.020.

Grindley, G.W., 1972, Polyphase deformation of the Precambrian Nimrod Group, central Transantarctic Mountains: Antarctic geology and geophysics, p. 313–318.

Grindley, G.W., McGregor, V.R., and Walcott, R.I., 1964, Outline of the geology of the Nimrod-Beardmore-Axel Heiberg glaciers region, Ross Dependency: Antarctic Geology, p. 2016–2019.

Grindley, G.W., and Oliver, P.J., 1983, Post-Ross orogeny cratonization of Northern Victoria Land: Antarctic Earth Science, p. 133–139.

Grossman, E.L., Yancey, T.E., Jones, T.E., Bruckschen, P., Chuvashov, B., Mazzullo, S.J., and Mii, H.S., 2008, Glaciation, aridification, and carbon sequestration in the Permo- Carboniferous; the isotopic record from low latitudes: Palaeogeography, Palaeoclimatology, Palaeoecology, v. 268, p. 222–233.

Gulbranson, E., Cornamusini, G., Ryberg, P.E., and Corti, V., 2020, When does large woody debris influence ancient rivers? Dendrochronology applications in the Permian and Triassic, Antarctica: Palaeogeography, Palaeoclimatology, Palaeoecology, v. 541.

Gunn, B.M., and Warren, G., 1962, Geology of Victoria Land between the Mawson and Mulock Glaciers, Antarctica: New Zealand Geological Survey Bulletin, v. 71, p. 157.

Hagen-Peter, G., and Cottle, C., 2016, Synchronous alkaline and subalkaline magmatism during the late Neoproterozoic–early Paleozoic Ross orogeny, Antarctica: Insights into magmatic sources and processes within a continental arc: Lithos, v. 262, p. 677–698.

Hagen-Peter, G., Cottle, C., Smit, M., and Cooper, A.F., 2016, Coupled garnet Lu–Hf and monazite U–Pb geochronology constrain early convergent margin dynamics in the Ross orogen, Antarctica: Journal of Metamorphic Geology, v. 34, p. 293–319.

Hall, C.E., Cooper, A.F., and Parkinson, D.L., 1995, Early Cambrian carbonatite in Antarctica: Journal of the Geological Society of London, v. 152, p. 721–728.

Hambrey, M.J., Ehrmann, W.U., and Larsen, B., 1991, Cenozoicglacial record of the Prydz Bay continental shelf, East Antarctica, *in* Proceeding ODP Scientific Results, Ocean Drilling Program, Proceedings of the Ocean Drilling Program, v. 119, p. 77–132, doi:10.2973/odp.proc.sr.119.1991.

Hambrey, M.J., and Glasser, N.F., 2012, Discriminating glacier thermal and dynamic regimes in the sedimentary record: Sedimentary Geology, v. 251–252, p. 1–33, doi:10.1016/j.sedgeo.2012.01.008.

Hanchar, J.M., and Millar, C.F., 1993, Zircon zonation patterns as revealed by cathodoluminescence and backscattered electron images: implications for interpretation of complex crustal histories: Chemical Geology, v. 110, p. 1–13.

Harrington, H.J., 1965, Geology and morphology of Antarctica, *in* Biogeography and ecology in Antarctica, Van Oye P., Van Mieghen J., p. 1–71.

Harwood, D.M., Florindo, F., Talarico, F.M., and Levy, R.H. (Eds.), 2009, Southern McMurdo Sound Project, Antarctica. Initial science report on AND-2A.: Siena, v. 15, 235 p.

Heckel, P.H., 1994, Evaluation of evidence for glacio-eustatic control over marine Pennsylvanian cyclothems in North America and consideration of possible tectonic effects, *in* Tectonic and eustatic controls on sedimentary cycles. Tulsa, Oklahoma, SEPM (Society for Sedimentary Geology): Concepts in Sedimentology and Paleontology, Dennison, J.M., Ettensohn, F.R, v. 4, p. 65–87.

Heckel, P.H., 2008, Pennsylvanian cyclothems in midcontinent North America as far-field effects of waxing and waning of Gondwana ice sheets, *in* Resolving the Late Paleozoic Ice Age in Time and Space: Geological Society of America Special, Fielding, C.R., Frank, T., Isbell, J.L, Special Paper 441, p. 275–289.

Henjes-Kunst, F., and Kreuzer, H., 2003, Mid-Paleozoic igneous activity in Northern Victoria Land, Antarctica: implications of new geochronological data: Geologisches Jahrbuch, v. B85, p. 271–302.

Henjes-Kunst, F., Roland, N.W., Dunphy, J.M., and Fletcher, I.R., 2004, SHRIMP U-Pb Dating of High-Grade Migmatites and Related Magmatites from Northwestern Oates Land (East Antarctica): Evidence for a Single High-Grade Event of Ross-Orogenic Age: Terra Antartica, v. 11, p. 67–84.

Henry, L.C., Isbell, J.L., Fielding, C.R., Domack, E.W., Frank, T.D., and Fraiser, M.L., 2012, Proglacial deposition and deformation in the Upper Carboniferous to Lower Permian Wynyard Formation, Tasmania: A process analysis: Palaeogeography, Palaeoclimatology, Palaeoecology, v. 315–316, p. 142–157, doi:10.1016/j.palaeo.2011.11.020.

Holbourn, A., Kuhnt, W., Schulz, M., and Erlenkeuser, H., 2005, Impacts of orbital forcing and atmospheric carbon dioxide on Miocene ice-sheet expansion: Nature, v. 438, p. 483–487, doi:10.1038/nature04123.

Hyde, W.T., Crowley, T.J., Tarasov, L., and Paltier, W.R., 1999, The Pangean ice age: studies with a coupled climate-ice sheet model: Climate Dynamics, v. 15, p. 619–629.

Ireland, T.R., Flöttmann, T., Fanning, C.M., Gibson, G.M., and Preiss, W.V., 1998, Development of the early Paleozoic Pacific margin of Gondwana from detrital-zircon ages across the Delamerian orogen: Geology, v. 26, p. 243–246.

Isbell, J.L., 2010, Environmental and paleogeographic implications of glaciotectonic deformation of glaciomarine deposits within Permian strata of the Metschel Tillite, southern Victoria Land, Antarctica, *in* Late Paleozoic Glacial Events and Postglacial Transgressions in Gondwana. Geological Society of America Special Papers 468, López-Gamundí, O.R., Buatois, L.A., v. 468, p. 81–100.

Isbell, J.L., Fraiser, M.L., and Henry, L.C., 2008a, Examining the complexity of environmental change during the late Paleozoic and early Mesozoic: Palaios, v. 23, p. 267–269.

Isbell, J.L., Gelhar, G.A., and Seegers, G.M., 1997, Reconstruction of preglacial topography using a postglacial flooding surface: upper Paleozoic deposits, Central Transantarctic Mountains, Antarctica: Journal of Sedimentary Research, v. 67, p. 264–273, doi:10.1306/D426854A-2B26-11D7-8648000102C1865D.

Isbell, J.L., Henry, L.C., Gulbranson, E., Limarino, C.O., Fraiser, M.L., Koch, Z.J., Ciccioli, P.L., and Dineen, A.A., 2012, Glacial paradoxes during the late Paleozoic ice age: evaluating the equilibrium line altitude as a control on glaciation: Earth Science Reviews, v. 22, p. 1–19.

Isbell, J.L., Koch, Z.J., Szablewski, G.M., and Lenaker, P.A., 2008b, Permian glacigenic deposits in the Transantarctic Mountains, Antarctica, *in* Resolving the Late Paleozoic Ice Age in Time and Space. Geological Society of America Special Paper 441, Fielding, C.R., Frank, T.D., Isbell, J.L., v. 441.

Isbell, J.L., Miller, M.F., Wolfe, K.L., and Lenaker, P.A., 2003, Timing of late Paleozoic glaciation in Gondwana: was glaciation responsible for the development of northern hemisphere cyclothems?, *in* Extreme depositional environments: mega end members in geologic time: Geological Society of America Special Paper, 370, Chan, M.A., Archer, A.W., v. 370, p. 5–24.

Ives, L.R.W., and Isbell, J.L., 2021, A lithofacies analysis of a South Polar glaciation in the Early Permian: Pagoda Formation, Shackleton Glacier region, Antarctica: Journal of Sedimentary Research, v. 91, p. 611–635, doi:10.2110/jsr.2021.004.

Joachimski, M.M., Bitter, P.H., and Buggisch, W., 2006, Constraints on Pennsylvanian glacioeustatic sea-level changes using oxygen isotopes of conodont apatite: Geology, v. 34, p. 277–280.

John, N., 2014, Sedimentology and composition of the Takrouna Formation, northern Victoria Land, Antarctica - Provenance and depositional evolution of a Permian Gondwana basin [PdD Thesis]: University of Jena, 375 p.

Jordan, T.A., Riley, T.R., and Siddoway, C.S., 2020, The geological history and evolution of West Antarctica: Nature Rewiews Earth & Environment, v. 1, p. 117–133, doi:https://doi.org/10.1038/s43017-019-0013-6.

Kennicutt, M.C. et al., 2015, A roadmap for Antarctic and Southern Ocean science for the next two decades and beyond: Antarctic Science, v. 27, p. 3–18, doi:10.1017/S0954102014000674.

Kim, Y., and Kim, T., 2019, Preliminary reconnaissance of the Grenville basement and its Ross perturbation: contrasting zircon and monazite ages in a migmatitic gneiss from the Priestley Schist, northern Victoria Land, Antarctica, *in* Incheon.

Kleinschmidt, E.: G. (Ed.), 2021, The Geology of the Antarctic Continent: Stuttgart, Germany, Schweizerbart Science Publishers, http://www.schweizerbart.de//publications/detail/isbn/9783443110345/Kleinschmidt_ed_The_Geology_of_the_A.

Koch, Z.J., and Isbell, J.L., 2013, Processes and products of grounding-line fans from the Permian Pagoda Formation, Antarctica: insight into glacigenic conditions in polar Gondwana: Gondwana Research, v. 24, p. 161–172.

Korhonen, F.J., Brown, M., Grove, M., Siddoway, C.S., Baxter, E.F., and Inglis, J.D., 2012, Separating metamorphic events in the Fosdick migmatite-granite complex, West Antarctica: POLYMETAMORPHISM IN THE FOSDICK MOUNTAINS: Journal of Metamorphic Geology, v. 30, p. 165–192, doi:10.1111/j.1525-1314.2011.00961.x.

Korhonen, F.J., Saito, S., Brown, M., and Siddoway, C.S., 2010a, Modeling multiple melt loss events in the evolution of an active continental margin: Lithos, v. 116, p. 230–248, doi:10.1016/j.lithos.2009.09.004.

Korhonen, F.J., Saito, S., Brown, M., Siddoway, C.S., and Day, J.M.D., 2010b, Multiple generations of granite in the Fosdick Mountains, Marie Byrd kLand, West Antarctica: implications for polyphase intracrustal differentiation in a continental margin setting: Journal of Petrology, v. 51, p. 627–670, doi:doi:10.1093/petrology/egp093.

Korsch, R.J., 1974, Petrographic comparison of the Taylor and Victoria Groups (Devonian to Triassic) in South Victoria Land, Antarctica: New Zealand Journal of Geology and Geophysics, v. 17, p. 523–541.

Kraus, C., 2016, Oligocene to early Miocene glacimarine sedimentation of the central Ross Sea, and implications for the evolution of the West Antarctic Ice Sheet [MsC]: Antarctic Research Centre - Victoria University of Wellington, 164 p.

Kreuzer, H., Höhndorf, A., Lenz, H., Muller, P., and Vetter, U., 1987, Radiometric ages of Pre-Mesozoic rocks from Northern Victoria Land, Antarctica: Gondwana Six: Structure, Tectonics and Geophysics, p. 31–47.

Kreuzer, H., Höhndorf, A., Lenz, H., Vetter, U., Tessensohn, F., Muller, P., Jordan, H., Harre, W., and Besang, C., 1981, K/Ar and Rb/Sr dating of igneous rocks from north Victoria Land, Antarctica: Geologisches Jahrbuch, v. B41, p. 267–273.

Krippner, A., Meinhold, G., Morton, A.C., and von Eynatten, H., 2014, Evaluation of garnet discrimination diagrams using geochemical data of garnets derived from various host rocks: Sedimentary Geology, v. 306, p. 36–52, doi:10.1016/j.sedgeo.2014.03.004.

Kulhanek, D.K. et al., 2019, Revised chronostratigraphy of DSDP Site 270 and late Oligocene to early Miocene paleoecology of the Ross Sea sector of Antarctica: Global and Planetary Change, v. 178, p. 46–64, doi:10.1016/j.gloplacha.2019.04.002.

Kyle, R.A., 1977, Processes and products of grounding-line fans from the Permian Pagoda Formation, Antarctica: insight into glacigenic conditions in polar Gondwana: New Zealand Journal of Geology and Geophysics, v. 20, p. 1081–1102.

Laird, M.G., and Bradshaw, J.D., 1981, Permian tillites of North Victoria Land: In: Hambrey, M.J., Harland, W.B. eds., Earth’s pre-Pleistocene Glacial Record. Cambridge University Press, Cambridge, p. 237–240.

Leake, B.E. et al., 1997, Nomenclature of amphiboles: report of the subcommittee on amphiboles of the international mineralogical association, commissiion on new minerals and mineral names: The Canadian Mineralogist, v. 35, p. 219–246.

Lear, C.H., Mawbey, E.M., and Rosenthal, Y., 2010, Cenozoic benthic foraminiferal Mg/Ca and Li/Ca records: Toward unlocking temperatures and saturation states: OCEAN TEMPERATURES AND SATURATION STATE: Paleoceanography, v. 25, doi:10.1029/2009PA001880.

Levy, R. et al., 2016, Antarctic ice sheet sensitivity to atmospheric CO $_2$ variations in the early to mid-Miocene: Proceedings of the National Academy of Sciences, v. 113, p. 3453–3458, doi:10.1073/pnas.1516030113.

Levy, R.H. et al., 2019, Antarctic ice-sheet sensitivity to obliquity forcing enhanced through ocean connections: Nature Geoscience, v. 12, p. 132–137, doi:10.1038/s41561-018-0284-4.

Lewis, A.R. et al., 2008, Mid-Miocene cooling and the extinction of tundra in continental Antarctica: Proceedings of the National Academy of Sciences, v. 105, p. 10676–10680, doi:10.1073/pnas.0802501105.

Li, X., Zattin, M., and Olivetti, V., 2020, Apatite Fission Track Signatures of the Ross Sea Ice Flows During the Last Glacial Maximum: Geochemistry, Geophisics, Geosystems, v. 21, doi:https://doi.org/10.1029/2019GC008749.

Liberato, G.P., Cornamusini, G., Perotti, M., Sandroni, S., and Talarico, F.M., 2017, Stratigraphy of a Permian-Triassic fluvial-dominated succession in Southern Victoria Land (Antarctica): preliminary data: Journal of Mediterranean Earth Sciences, v. 9, p. 167–171.

Licht, K.J., and Hemming, S.R., 2017, Analysis of Antarctic glacigenic sediment provenance through geochemical and petrologic applications: Quaternary Science Reviews, v. 164, p. 1–24, doi:10.1016/j.quascirev.2017.03.009.

Licht, K.J., Hennessy, A.J., and Welke, B.M., 2014, The U-Pb detrital zircon signature of West Antarctic ice stream tills in the Ross embayment, with implications for Last Glacial Maximum ice flow reconstructions: Antarctic Science, v. 26, p. 687–697, doi:10.1017/S0954102014000315.

Licht, K.J., Lederer, J.R., and Jeffrey Swope, R., 2005a, Provenance of LGM glacial till (sand fraction) across the Ross embayment, Antarctica: Quaternary Science Reviews, v. 24, p. 1499–1520, doi:0.1016/j.quascirev.2004.10.017.

Licht, K.J., Lederer, J.R., and Jeffrey Swope, R., 2005b, Provenance of LGM glacial till (sand fraction) across the Ross embayment, Antarctica: Quaternary Science Reviews, v. 24, p. 1499–1520, doi:10.1016/j.quascirev.2004.10.017.

Licht, K.J., and Palmer, E.F., 2013, Erosion and transport by Byrd Glacier, Antarctica during the Last Glacial Maximum: Quaternary Science Reviews, v. 62, p. 32–48, doi:10.1016/j.quascirev.2012.11.017.

Limarino, C.O., Césari, S.N., Spalletti, L.A., Taboada, A.C., Isbell, J.L., Geuna, S., and Gulbranson, E., 2014, A paleoclimatic review of southern South America during the late Paleozoic: A record from icehouse to extreme greenhouse conditions: Gondwana Research, v. 25, p. 1396–1421, doi:http://dx.doi.org/10.1016/j.gr.2012.12.022.

Lindsay, J.F., 1970, Depositional environment of Paleozoic glacial rocks in the central Transantarctic Mountains: Geological Society of America Bulletin, v. 81, p. 1149–1172.

Lindsay, J.F., 1969, Stratigraphy and sedimentation of Lower Beacon rocks in the central Transantarctic Mountains, Antarctica: Institute of Polar Studies Report 33. Ohio State University Research Foundation,.

Lopez-Gamundi, O.R., and Buatois, L.A., 2010, Introduction: Late Paleozoic glacial events and postglacial transgressions in Gondwana, *in* Late Paleozoic Glacial Events and Postglacial Transgressions, Gondwana: Geological Society of America Special Paper 468, Lopez-Gamundi, O.R., Buatois, L.A., v. 468, p. V–VIII.

Ludwig, K.R., 2003, Isoplot/Ex version 3.0: A geochronological toolkit for Microsoft Excel: Special Publication, No. 4. Berkeley Geochronology Center, 2455 Ridge Road, Berkeley CA 94709, USA.,.

Mallery, C., Licht, K.J., Thomson, S.N., van de Flierdt, T., Perotti, M., Marschalek, J., and Zurli, L., 2021, Detrital Zircons as a Tracer of Paleo-Ice Sheet Dynamics and Subglacial Geology in the Central Ross Sea, Antarctica, *in* AGU Fall Meeting, New Orleans, LA.

Marschalek, J.W. et al., 2021, A large West Antarctic Ice Sheet explains early Neogene sea-level amplitude: Nature, v. 600, p. 450–455, doi:10.1038/s41586-021-04148-0.

Martin, J.R., Redfern, J., Horstwood, M.S.A., Mory, A.J., and Williams, B.P.J., 2019, Detrital zircon age and provenance constraints on late Paleozoic ice-sheet growth and dynamics in Western and Central Australia: Australian Journal of Earth Sciences, v. 66, p. 183–207, doi:10.1080/08120099.2019.1531925.

Masson-Delmotte, V. et al., 2013, Information from Paleoclimate Archives, *in* Climate Change 2013: The Physical Science Basis. Contribution of Working Group I to the Fifth Assessment Report of the Intergovernmental Panel on Climate Change, Cambridge, United Kingdom and New york, NY, USA, Stocker, T.F., D. Qin, G.-K. Plattner, M. Tignor, S.K. Allen, J. Boschung, A. Nauels, Y. Xia, V. Bex and P.M. Midgley, p. 82.

McFadden, R.R., Teyssier, C., Siddoway, C.S., Whitney, D.L., and Fanning, C.M., 2010, Oblique dilation, melt transfer, and gneiss dome emplacement: Geology, v. 38, p. 375–378, doi:10.1130/G30493.1.

McKay, R.M. et al., 2019, Ross Sea West Antarctic Ice Sheet History: College Station, Texas, Proceedings of the International Ocean Discovery Program, v. 374.

McKelvey, B.C., 1970, Recent discoveries of Devonian fish in Antarctica: Polar Record, v. 15, p. 216–217.

McKelvey, B.C., Webb, P.N., Gorton, M.P., and Kohn, B.P., 1970, Stratigraphy of the Beacon Supergroup between the Olympus and Boomerang ranges, south Victoria Land, Antarctica: Nature, v. 227, p. 1126–1128.

McKelvey, B.C., Webb, P.N., and Kohn, B.P., 1977, Stratigraphy of the Taylor and lower Victoria Groups (Beacon Supergroup) between the Mackay Glacier and Boomerang Range, Antarctica: New Zealand Journal of Geology and Geophysics, v. 20, p. 813–863.

Mcpherson, J.G., 1978, Stratigraphy and sedimentology of the Upper Devonian Aztec Siltstone, southern Victoria Land, Antarctica: New Zealand Journal of Geology and Geophysics, v. 21, p. 667–683.

Miller, J.M.G., 1989, Glacial advance and retreat sequences in a Permo-Carboniferous section, central Transantarctic Mountains: Sedimentology, v. 36, p. 419–430.

Miller, J.M.G., 1996, Glacial sediments, *in* Sedimentary Environments: Processes, Facies and Stratigraphy, Oxford, Reading, H.G., p. 454–484.

Miller, K.G., Wright, J.D., and Fairbanks, R.G., 1991, Unlocking the Ice House: Oligocene-Miocene oxygen isotopes, eustasy, and margin erosion: Journal of Geophysical Research: Solid Earth, v. 96, p. 6829–6848, doi:10.1029/90JB02015.

Moncrieff, A.C.M., 1989, Classification of poorly-sorted sedimentary rocks: Sedimentary Geology, v. 65, p. 191–194.

Mortimer, N., Palin, J.M., Dunlap, W.J., and Hauff, F., 2011, Extent of the Ross Orogen in Antarctica: new data from DSDP 270 and Iselin Bank: Antarctic Science, v. 23, p. 297–306, doi:10.1017/S0954102010000969.

Mukasa, S.B., and Dalziel, I.W.D., 2000, Marie Byrd Land, West Antarctica: Evolution of Gondwana's Pacific margin constrained by U-Pb geochronology and feldspar common-Pb isotopic compositions: Geological Society of America Bulletin, v. 112, p. 611–627.

Naish, T.R., Powell, R.D., Levy, R.H., Henrys, S., Krissek, L., Niessen, F., Pompilio, M., Scherer, R., and Wilson, G.S., 2007, Synthesis of the Initial Scientifi c Results of the MIS Project (AND-1B Core), Victoria Land Basin, Antarctica: Terra Antartica, v. 14, p. 317–327.

Olivetti, V., Balestrieri, M.L., Rossetti, F., and Talarico, F.M., 2013, Tectonic and climatic signals from apatite detrital fission track analysis of the Cape Roberts Project core records, South Victoria Land, Antarctica: Tectonophysics, v. 594, p. 80–90, doi:10.1016/j.tecto.2013.03.017.

Olivetti, V., Balestrieri, M.L., Rossetti, F., Thomson, S.N., Talarico, F.M., and Zattin, M., 2015, Evidence of a full West Antarctic Ice Sheet back to the early Oligocene: insight from double dating of detrital apatites in Ross Sea sediments.: Terra Nova, v. 27, p. 238–246, doi:10.1111/ter.12153.

Olivetti, V., Rossetti, F., Balestrieri, M.L., Pace, D., Cornamusini, G., and Talarico, F.M., 2018, Variability in uplift, exhumation and crustal deformation along the Transantarctic Mountains front in southern Victoria Land, Antarctica: Tectonophysics, v. 745, p. 229–244, doi:https://doi.org/10.1016/j.tecto.2018.08.017.

O'Toole, T.F., 2010, The lower Taylor Group: Taylor and Wright Valleys, southern Victoria Land, Antarctica; Paleoenvironmental Interpretations and Sequence Stratigraphy [Ms'C Thesis]: University of Canterbury, 220 p.

Pankhurst, R.J., Weaver, S.D., Bradshaw, B.C., Storey, B.C., and Ireland, T.R., 1998, Geochronology and geochemistry of pre-Jurassic superterranes in Marie Byrd Land, Antarctica: Journal of Geophysical Research, v. 103, p. 2529–2547.

Panter, K. et al., 2008, Petrologic and Geochemical Composition of the AND-2A Core, ANDRILL Southern McMurdo Sound Project, Antarctica: Terra Antartica, v. 15.

Paulsen, T., Deering, C., Sliwinski, J., Bachmann, O., and Guillong, M., 2016, Detrital zircon ages from the Ross Supergroup, north Victoria Land, Antarctica: Implications for the tectonostratigraphic evolution of the Pacific-Gondwana margin: Gondwana Research, v. 35, p. 79–96, doi:http://dx.doi.org/10.1016/j.gr.2016.04.001.

Paulsen, T., Deering, C., Sliwinski, J., Bachmann, O., and Guillong, M., 2017, New detrital zircon age and trace element evidence for 1450 Ma igneous zircon sources in East Antarctica: Precambrian Research, v. 300, p. 53–58, doi:http://dx.doi.org/10.1016/j.precamres.2017.07.011.

Paxman, G.J.G., 2021, Antarctic palaeotopography: Geological Society, London, Memoirs, p. M56-2020–7, doi:10.1144/M56-2020-7.

Pérez, L.F. et al., 2021, Early and middle Miocene ice sheet dynamics in the Ross Sea: Results from integrated core-log-seismic interpretation: GSA Bulletin, doi:10.1130/B35814.1.

Perotti, M., 2018, Provenance of late-Quaternary sediments from Ross Sea region (Antarctica) [PhD thesis]: University of Siena, 256 p.

Perotti, M., Andreucci, B., Talarico, F., Zattin, M., and Langone, A., 2017, Multianalytical provenance analysis of Eastern Ross Sea LGM till sediments (Antarctica): Petrography, geochronology, and thermochronology detrital data: PROVENANCE OF EASTERN ROSS SEA LGM TILLS: Geochemistry, Geophysics, Geosystems, v. 18, p. 2275–2304, doi:10.1002/2016GC006728.

Perotti, M., Zurli, L., Sandroni, S., Cornamusini, G., and Talarico, F., 2018, Provenance of Ross Sea Drift in McMurdo Sound (Antarctica) and implications for middle-Quaternary to LGM glacial transport: New evidence from petrographic data: Sedimentary Geology, v. 371, p. 41–54, doi:10.1016/j.sedgeo.2018.04.009.

Pertusati, P.C. et al., 2012, Antarctic Geological Map Series 1 : 250000 - Mt. Melbourne Quadrangle (Victoria Land): Petrusati, P.C. and Tessensohn, F. Antarctic Geological 1:250,000 Map Series.

Pierce, E.L., van de Flierdt, T., Williams, T., Hemming, S.R., Cook, C.P., and Passchier, S., 2017, Evidence for a dynamic East Antarctic ice sheet during the mid-Miocene climate transition: Earth and Planetary Science Letters, v. 478, p. 1–13, doi:10.1016/j.epsl.2017.08.011.

Pompilio, M. et al., 2007, Petrology and geochemistry of AND-1B Core, ANDRILL McMurdo Sound ice shelf project, Antarctica: Terra Antartica, v. 14, p. 255–288.

Powell, R.D., and Domack, E., 2002, Modern glaciomarine environments, *in* Modern and Past Glacial Environments, Oxford, UK, Menzies, J, p. 361–389.

Powell, R.D., and Li, Z.X., 1994, Reconstruction of the Panthalassan margin of Gondwanaland, *in* Permian–Triassic Transantarctic Basin, Permian–Triassic Pangea Basins and Foldbelts Along the Panthalassan Margin of Gondwanaland: Geologic Society of America Memoir, 184, Veevers, J., Powell, C., v. 184, p. 5–9.

Read, S.E., Cooper, A.F., and Walker, N.W., 2002, Geochemistry and U-Pb geochronology of the Neoproterozoic-Cambrian Koettlitz Glacier alkaline province, Royal Society Range, Transantarctic Mountains, Antarctica, *in* Antarctica at the Close of a Millennium, Wellington, Gamble, J.A., Skinner, D.N.B., Henrys, S.A., p. 143–151.

Reid, C.M., Forsyth, S.M., Clarke, M.J., and Bacon, C., 2014, The Parmeener Supergroup - Late Carboniferous to Triassic, *in* Geological Evolution of Tasmania, Corbett, K.D., Quilty, P.G., Calver, C.R., Geological Society of Australia Special Publication, v. 24, p. 363–384.

Robinson, D.E., Menzies, J., Wellner, J.S., and Clark, R.W., 2021, Subglacial sediment deformation in the Ross Sea, Antarctica: Quaternary Science Advances, v. 4, p. 100029, doi:10.1016/j.qsa.2021.100029.

Rocchi, S., Di Vincenzo, G., Ghezzo, C., and Nardini, I., 2009, Granite-lamprophyre connection in the latest stages of the early Paleozoic Ross Orogeny (Victoria Land, Antarctica): GSA Bulletin, v. 121, p. 801–819, doi:10.1130/B26342.1.

Rose, K.C., Ferraccioli, F., Jamieson, S.S.R., Bell, R.E., Corr, H., Creyts, T.T., Braaten, D., Jordan, T.A., Fretwell, P.T., and Damaske, D., 2013, Early East Antarctic Ice Sheet growth recorded in the landscape of the Gamburtsev Subglacial Mountains: Earth and Planetary Science Letters, v. 375, p. 1–12, doi:10.1016/j.epsl.2013.03.053.

Rowell, A.J., Rees, M.N., Duebendorfer, E.M., Wallin, E.T., Van Schmus, W.R., and Smith, E.I., 1993, An active Neoproterozoic margin: evidence from the Skelton Glacier area. Transantarctic Mountains: Journal of the Geological Society of London, v. 150, p. 677–682.

Saito, S., Brown, M., Korhonen, F.J., McFadden, R.R., and Siddoway, C.S., 2013, Petrogenesis of Cretaceous mafic intrusive rocks, Fosdick Mountains, West Antarctica: Melting of the sub-continental arc mantle along the Gondwana margin: Gondwana Research, v. 23, p. 1567–1580, doi:10.1016/j.gr.2012.08.002.

Sandroni, S., and Talarico, F.M., 2006, Analysis of clast lithologies from CIROS-2 core, New Harbour, Antarctica — Implications for ice flow directions during Plio-Pleistocene time: Palaeogeography, Palaeoclimatology, Palaeoecology, v. 231, p. 215–232, doi:10.1016/j.palaeo.2005.07.031.

Sandroni, S., and Talarico, F., 2001, Petrography and Provenance of Basement Clasts and Clast Variability in CRP-3 Drillcore (Victoria Land Basin, Antarctica): Terra Antartica, v. 8, p. 449–467.

Sandroni, S., and Talarico, F.M., 2004, Petrography and Provenance of Basement Clasts in CIROS-1 Core, McMurdo Sound, Antarctica: Terra Antartica, v. 11, p. 93–114.

Sandroni, S., and Talarico, F.M., 2011, The record of Miocene climatic events in AND-2A drill core (Antarctica): Insights from provenance analyses of basement clasts: Global and Planetary Change, v. 75, p. 31–46, doi:10.1016/j.gloplacha.2010.10.002.

Sangiorgi, F. et al., 2018, Southern Ocean warming and Wilkes Land ice sheet retreat during the mid-Miocene: Nature Communications, v. 9, p. 317, doi:10.1038/s41467-017-02609-7.

Savage, J.E., 2005, Provenance analysis of the Sperm Bluff Formation, Southern Victoria Land, Antarctica [Ms'C Thesis]: University of Canterbury, 206 p.

Schöner, R., Bomfleur, B., Schneider, J.W., and Viereck-Götte, L., 2011, Systematic Description of the Triassic to Lower Jurassic Section Peak Formation in North Victoria Land (Antarctica): Polarforschung, v. 80, p. 71–87.

Schöner, R., and John, N., 2014, Sedimentological Field Investigations on the Takrouna Formation (Permian, Beacon Supergroup) in Northern Victoria Land, Antarctica: Polarforschung, v. 84, p. 49–58.

Shaw, S.E., 1962, Petrography of Beacon Sandstone Samples from Beacon Height West, Upper Taylor Glacier, Antarctica: New Zealand Journal of Geology and Geophysics, v. 5, p. 733–739.

Shevenell, A.E., Kennett, J.P., and Lea, D.W., 2008, Middle Miocene ice sheet dynamics, deep-sea temperatures, and carbon cycling: A Southern Ocean perspective: MIDDLE MIOCENE ICE VOLUME AND TEMPERATURE: Geochemistry, Geophysics, Geosystems, v. 9, p. n/a-n/a, doi:10.1029/2007GC001736.

Shevenell, A.E., Kennett, J.P., and Lea, D.W., 2004, Middle Miocene Southern Ocean Cooling and Antarctic Cryosphere Expansion: Science, v. 305, p. 1766–1770, doi:10.1126/science.1100061.

Shipboard Scientific Party, 1975, Sites 270, 271, 272: In: Hayes, D.E., Frakes, L.A. (Eds.), Initial Reports of the Deep Sea Drilling Project, v. 28, p. 211–334.

Siddoway, C.S., 2021, The Geology of West Antarctica, *in* The Geology of the Antarctic Continent, Tubinger - Germany, Georg Kleinschmidt, Beiträge zur Regionalen Geologie der Erde, v. 33, p. 613.

Siddoway, C.S., Baldwin, S.L., Fitzgerald, P.G., Fanning, C.M., and Luyendyk, B.P., 2004a, Ross Sea mylonites and the timing of intracontinental extension within the West Antarctic rift system: Geology, v. 32, p. 57, doi:10.1130/G20005.1.

Siddoway, C.S., and Fanning, C.M., 2009, Oaleozoic tectonism on the East Gondwana margin: evidence from SHRIMP U-Pb zircon geochronology of a migmatite-granite complex in West Antarctica: Tectonophysics, v. 477, p. 262–277.

Siddoway, C.S., Richard, S.M., Fanning, C.M., and Luyendyk, B.P., 2004b, Origin and emplacement of a middle Cretaceous gneiss dome, Fosdick Mountains, West Antarctica, *in* Gneiss Domes in Orogeny, Geological Society of America, doi:10.1130/0-8137-2380-9.267.

Siddoway, C.S., Sass, L.C., and Esser, R.P., 2005, Kinematic history of western Marie Byrd Land, West Antarctica: direct evidence from Cretaceous mafic dykes: Geological Society, London, Special Publications, v. 246, p. 417–438, doi:10.1144/GSL.SP.2005.246.01.17.

Sirevaag, H., Ksienzyk, A.K., Jacobs, J., Dunkl, I., and Läufer, A., 2018, Tectono-Thermal Evolution and Morphodynamics of the Central Dronning Maud Land Mountains, East Antarctica, Based on New Thermochronological Data: Geosciences, v. 8, doi:doi:10.3390/geosciences8110390.

Skinner, D.N.B., and Ricker, J., 1968, The geology of the region between the Mawson and Priestley Glaciers, North Victoria Land, Antarctica: New Zealand Journal of Geology and Geophysics, v. 11, p. 1009–1040, doi:10.1080/00288306.1968.10420767.

Sláma, J. et al., 2008, Plešovice zircon — A new natural reference material for U–Pb and Hf isotopic microanalysis: Chemical Geology, v. 249, p. 1–35, doi:https://doi.org/10.1016/j.chemgeo.2007.11.005.

Smellie, J.L., Panter, K.S., and Geyer, A., 2021, Volcanism in Antarctica: 200 Million Years of Subduction, Rifting and Continental Break-up: London, Smellie J.L., Panter K.S., and Gayer A., Geological Society, London, Memoirs, v. 55.

Smith, C.H., 1996, Migmatites of the Alexandra Mountains, West Antarctica: Pressure-temperature conditions of formation and regional context: Geologisches Jarhbuch, v. B52, p. 169–178.

Spencer, C.J., Kirkland, C.L., and Taylor, R.J.M., 2016, Strategies towards statistically robust interpretations of in situ U-Pb zircon geochronology: Geoscience Frontiers, v. 7, p. 581–589, doi:http://dx.doi.org/10.1016/j.gsf.2015.11.006.

Storti, F., Salvini, F., Rossetti, F., and Phipps, M.J., 2007, Intraplate termination of transform faulting within the Antarctic continent: Earth and Planetary Science Letters, v. 260, p. 115–126.

Stump, E., 1995, The Ross orogen of the Transantarctic Mountains: Cambridge, 284 p.

Stump, E., and Fitzgerald, P.J., 1992, Episodic uplift of the Transantarctic Mountains: Geology, v. 20, p. 161–164.

Sudgen, D.E., and John, B.S., 1988, Glaciers and landscape: a geomorphological approach: London, Arnold, E., 376 p.

Sullivan, N.B. et al., 2021, Astronomical pacing of the Antarctic Cryosphere: Terrestrial vs. Marine-based Ice Sheet Responses during the Early Miocene, *in* AGU Fall Meeting, New Orleans, LA.

Talarico, F., and ANDRILL-MIS Science Team, 2007, Clast provenance and variability in MIS (AND-1B) core and their implications for the paleoclimatic evolution recorded in the Windless Bight - southern McMurdo Sound area (Antarctica), *in* ANDRILL Research and Publications.

Talarico, F.M., and Kleinschmidt, G., 2008, The Antarctic Continent in Gondwanaland: A Tectonic Review and Potential Research Targets for Future Investigations Developments: Earth & Environmental Sciences, v. 8, doi:10.1016/S1571-9197(08)00007-4.

Talarico, F.M., Pace, D., and Levy, R.H., 2013, Provenance of basement erratics in Quaternary coastal moraines, southern McMurdo Sound, and implications for the source of Eocene sedimentary rocks: Antarctic Science, v. 25, p. 681–695, doi:10.1017/S0954102013000072.

Talarico, F.M., Pace, D., and Sandroni, S., 2011, Amphibole-bearing metamorphic clasts in ANDRILL AND-2A core: A provenance tool to unravel the Miocene glacial history in the Ross Embayment (western Ross Sea, Antarctica): Geosphere, v. 7, p. 922–937, doi:doi: 10.1130/GES00653.1.

Talarico, F.M., and Sandroni, S., 2011, Early Miocene basement clasts in ANDRILL AND-2A core and their implications for paleoenvironmental changes in the McMurdo Sound region (western Ross Sea, Antarctica): Global and Planetary Change, v. 78, p. 23–35, doi:10.1016/j.gloplacha.2011.05.002.

Talarico, F.M., and Sandroni, S., 1998, Petrography, Mineral Chemistry and Provenance of Basement Clasts in thee CRP-1 Drillcore (Victoria Land Basin, Antarctica): Terra Antartica, v. 5, p. 601–610.

Talarico, F.M., and Sandroni, S., 2009, Provenance signatures of the Antarctic Ice Sheets in the Ross Embayment during the Late Miocene to Early Pliocene: The ANDRILL AND-1B core record: Global and Planetary Change, v. 69, p. 103–123, doi:10.1016/j.gloplacha.2009.04.007.

Talarico, F., Sandroni, S., Fielding, C.R., and Atkins, C., 2000, Variability, Petrography and Provenance of Basement Clasts in Core from CRP-2/2A, Victoria Land Basin, Antarctica: Terra Antartica, v. 7, p. 529–544.

Tera, F., and Wasserburg, G.J., 1972, U-Th-Pb systematics in lunar highland samples from the Luna 20 and Apollo 16 missions: Earth and Planetary Science Letters, v. 17, p. 36–51, doi:https://doi.org/10.1016/0012-821X(72)90257-9.

Tinto, K.J. et al., 2019, Ross Ice Shelf response to climate driven by the tectonic imprint on seafloor bathymetry: Nature Geoscience, v. 12, p. 441–449, doi:10.1038/s41561-019-0370-2.

Torsvik, T.H., and Cocks, L.R., 2017, Earth History and Palaeogeography: 317 p.

Van Schmus, W.R., McKenna, L.W., Gonzales, D.A., Fetter, A.H., and Rowell, A.J., 1997, U-Pb geochronology of parts of the Pensacola, Thiel, and Queen Maud mountains, Antarctica, *in* The Antarctic Region: Geological Evolution and Processes, Siena, C.A. Ricci.

Veevers, J.J., 2001, Atlas of Billion-Year Earth History of Australia and Neighbours in Gondwanaland: Sydney, National Key Center for Geochemical Evolution and Metallogeny of Continents (GEMOC), 76 p.

Veevers, J.J., and Powell, C.M., 1987, Late Paleozoic glacial episodes in Gondwanaland reflected in transgressive-regressive depositional sequences in Euramerica: Geological Society of America Bulletin, v. 98, p. 475–487.

Vetter, U., Roland, N., Kreuzer, H., HoHndorf, A., Lenz, H., and Besang, C., 1983, Geochemestry, petrography and geochronology of the Cambro-Ordovician and Devonian-Carboniferous granitoids of northern Victoria Land, Antarctica: Antarctic Earth Science, p. 140–143.

Visser, J.N.J., 1997, A review of the Permo-Carboniferous glaciation in Africa, *in* Late Glacial and Postglacial Environmental Changes: Quaternary, Carboniferous–Permian, and Proterozoic, Oxford, Martini, I.P., p. 169–191.

Wareham, C.D., Stump, E., Storey, B.C., Millar, I.L., and Riley, T.R., 2001, Petrogenesis of the Cambrian Liv group, a bimodal volcanic rock suite from the Ross orogen, Transantarctic Mountains: GSA Bulletin, v. 113, p. 360–372, doi:10.1130/0016-7606(2001)113<0360:POTCLG>2.0.CO;2.

Warny, S., Askin, R.A., Hannah, M.J., Mohr, B.A.R., Raine, J.I., Harwood, D.M., Florindo, F., and the SMS Science Team, 2009, Palynomorphs from a sediment core reveal a sudden remarkably warm Antarctica during the middle Miocene: Geology, v. 37, p. 955–958, doi:10.1130/G30139A.1.

Weaver, S.D., Bradshaw, J.D., and Adams, C.J., 1991, Granitoids of the Ford Ranges, Marie Byrd Land, Antarctica, *in* Geological Evolution of Antarctica, Cambridge, M. R. A. Thompson et al., p. 345–351.

Wiedenbeck, M. et al., 2004, Further Characterisation of the 91500 Zircon Crystal: Geostandards and Geoanalytical Research, v. 28, p. 9–39, doi:https://doi.org/10.1111/j.1751-908X.2004.tb01041.x.

Wiedenbeck, M., Allé, P., Corfu, F., Griffin, W.L., Meier, M., Oberli, F., von Quadt, A., Roddick, J.C., and Spiegel, W., 1995, Three natural zircon standards for U-Th-Pb, Lu-Hf, trace element and REEb analyses: Geostandards and Geoanalytical Research, v. 19, p. 1–23, doi:https://doi.org/10.1111/j.1751-908X.1995.tb00147.x.

Wilch, T.I., McIntosh, W.C., and Panter, K.S., 2021, Chapter 5.4a Marie Byrd Land and Ellsworth Land: volcanology: Geological Society, London, Memoirs, v. 55, p. 515–576, doi:10.1144/M55-2019-39.

Williams, I.S., and Claesson, S., 1987, . Isotopic evidence for the Precambrian provenance and Caledonian metamorphism of high grade paragneisses from the Seve Nappes, Scandinavian Caledonides. II. Ionmicroprobe zircon U-Th-Pb: Contrib. Mineral. Petrol, v. 97, p. 205–217.

Wilson, D.S., and Luyendyk, B.P., 2009, West Antarctic paleotopography estimated at the Eocene-Oligocene climate transition: Geophysical Research Letters, v. 36, p. L16302, doi:10.1029/2009GL039297.

Woodworth-Lynas, C.M.T., and Dowdeswell, J.A., 1994, Soft-sediment striated surfaces and massive diamicton facies produced by floating ice., *in* Earth's Glacial Record, Cambridge, Deynoux, M., Miller, J.M.G., Domack, E.W., Eyles, N., Fairchild, I.J., Young, G.M., p. 241–259.

Woolfe, K.J., 1994, Cycles of erosion and deposition during the Permo-Carboniferous glaciation in the Transantarctic Mountains: Antarctic Science, v. 6, p. 93–104.

Wysoczanski, R.J., and Allibone, A.H., 2004, Age, correlation, and provenance of the Neoproterozoic Skelton Group, Antarctica: Grenville age detritus on the margin of East Antarctica: The Journal of Geology, v. 112, p. 401–416, doi:http://dx.doi.org/10.1086/421071.

Yakymchuk, C., Brown, C.R., Brown, M., Siddoway, C.S., Fanning, C.M., and Korhonen, F.J., 2015, Paleozoic evolution of western Marie Byrd Land, Antarctica: GSA Bulletin, v. 127, p. 1464–1484.

Yakymchuk, C., Siddoway, C.S., Fanning, C.M., McFadden, R., Korhonen, F.J., and Brown, M., 2013, Anatectic reworking and differentiation of continental crust along the active margin of Gondwana: a zircon Hf–O perspective from West Antarctica: Harley, S.L., Fitzsimons, I.C.W., and Zhao, Y., eds., Antarctica and Supercontinent Evolution, v. 383, doi:10 .1144 /SP383 .7.

Zachos, J.C., Breza, J.R., and Wise, S.W., 1992, Early Oligocene ice-sheet expansion on Antarctica: Stable isotope and sedimentological evidence from Kerguelen Plateau, southern Indian Ocean: Geology, v. 20, p. 569–573, doi:10.1130/0091-7613(1992)020<0569:EOISEO>2.3.CO;2.

Zattin, M., Andreucci, B., Thomson, S.N., Reiners, P.W., and Talarico, F.M., 2012, New constraints on the provenance of the ANDRILL AND-2A succession (western Ross Sea, Antarctica) from apatite triple dating: APATITE TRIPLE DATING IN ANTARCTICA: Geochemistry, Geophysics, Geosystems, v. 13, doi:10.1029/2012GC004357.

Zattin, M., Talarico, F.M., and Sandroni, S., 2010, Integrated provenance and detrital thermochronology studies on the ANDRILL AND-2A drill core: Late Oligocene-Early Miocene exhumation of the Transantarctic Mountains (southern Victoria Land, Antarctica): Provenance and thermochronology on the AND-2A drill core: Terra Nova, v. 22, p. 361–368, doi:10.1111/j.1365-3121.2010.00958.x.

Ziegler, A.M., Hulver, M.L., and Rowley, D.B., 1997, Permian World topography and climate, *in* Late Glacial and Postglacial Environmental Changes: Quaternary Carboniferous–Permian, and Proterozoic, Oxford University Press, Oxford, U.K., Martini, I.P., p. 67–80.

Zimmerman, S., and Hall, R., 2016, Provenance of Triassic and Jurassic sandstones in the Banda Arc: Petrography, heavy minerals and zircon geochronology: Gondwana Research, v. 37, p. 1–19, doi:http://dx.doi.org/10.1016/j.gr.2016.06.001.

Zoleikhaei, Y., Frei, D., Morton, A., and Zamanzadeh, S.M., 2016, Roundness of heavy minerals (zircon and apatite) as a provenance tool for unraveling recycling: A case study fromthe Sefidrud and Sarbaz rivers in N and SE Iran: Sedimentary Geology, v. 342, p. 106–117, doi:http://dx.doi.org/10.1016/j.sedgeo.2016.06.016.

Zurli, L., 2018, Caratterizzazione e studio di provenienza di successioni glacigeniche tardo-Paleozoiche del Beacon Supergroup in Terra Vittoria (Antartide): stratigrafia, petrografia e geocronologia [Ms'C Thesis]: University of Siena, 179 p.

Zurli, L., Cornamusini, G., Woo, J., Liberato, G.P., Han, S., Kim, Y., and Talarico, F.M., 2022a, Detrital zircons from Late Paleozoic Ice Age sequences in Victoria Land (Antarctica): New constraints on the glaciation of southern Gondwana: GSA Bulletin, v. 134, p. 160–178, doi:10.1130/B35905.1.

Zurli, L., Perotti, M., and Talarico, F.M., 2022b, Data Report: Petrology of gravel-sized clasts from Site U1521 core, IODP Expedition 374, Ross Sea West Antarctic Ice Sheet History, *in* Ross Sea West Antarctic Ice Sheet History, College Station, TX (International Ocean Discovery Program), McKay, R.M., De Santis, L., Kulhanek, D.K., and the Expedition 374 Scientists, Proceeding of the International Ocean Discovery Program 374, https://doi.org/10.14379/iodp.proc.374.201.2021.

APPENDIX

APPENDIX I

LA-ICP-MS raw data

Appendix I contains raw laser ablation–inductively coupled plasma–mass spectrometry (LA-ICP-MS) analysis of the late Paleozoic diamictite samples from Victoria Land, Antarctica. Crossed out data represent not concordant ages which were excluded from the interpretations.

Table 11 LA-ICP-MS raw data of sample 22-01-15C3

Grain ID	Final Age ^{207}Pb/^{235}U	Final Age ^{207}Pb/^{235}U 2σ	Final Age ^{206}Pb/^{238}U	Final Age ^{206}Pb/^{238}U 2σ	Final Age ^{208}Pb/^{232}Th	Final Age ^{208}Pb/^{232}Th 2σ	Final Age ^{207}Pb/^{206}Pb	Final Age ^{207}Pb/^{206}Pb 2σ	^{232}Th/^{238}U	% Concordance (^{206}Pb/^{238}U)/(^{207}Pb/^{235}U)	% Concordance (^{206}Pb/^{238}U)/(^{207}Pb/^{206}Pb)	Preferred age (Ma)	Preferred age 2σ (Ma)
C3-1_1	550	24	557	10	530	20	467	47	0.59647836	102	118	557	10
C3-1_2	528	18	538	10	529	36	517	55	0.2245098	103	103	538	10
C3-1_3	736	27	722	22	1030	75	783	54	0.07207447	99	92	723	22
C3-1_4	522	14	524	10	512	15	514	31	0.45287356	101	101	524	10
C3-1_5	1442	27	1450	20	1427	44	1425	29	0.88485966	101	101	1430	29
C3-1_6	578	16	566	10	541	18	614	60	0.61107314	99	91	567	10
C3-1_7	590	11	609	13	586	18	549	37	0.80179422	104	110	610	13
C3-1_8	983	22	973	15	928	29	963	31	1.0631769	99	101	975	15
C3-1_9	999	13	1002	12	961	22	983	19	0.73525668	101	102	1004	12
C3-1_10	499	15	498.5	7.7	478	13	488	50	0.73104693	100	101	500	8
C3-1_11	586	27	590	13	539	18	563	62	1.58963585	101	104	590	13
C3-1_12	983	26	992	20	941	28	931	46	1.11515152	101	106	991	20
C3-1_13	602	22	583	10	473	24	587	61	0.29700599	97	98	582	10
C3-1_14	516	22	519	8.1	494	18	526	53	0.83547696	100	98	518	8
C3-1_15	1475	28	1499	23	1438	47	1439	29	0.63687151	101	104	1443	29
C3-1_16	1451	25	1474	26	1409	39	1446	25	0.60684411	101	101	1451	25
C3-1_17	620	22	625	12	617	27	613	52	0.32197943	100	100	620	12
C3-1_18	1103	24	1105	17	1049	38	1068	24	0.3309816	99	102	1072	24
C3-1_19	573	17	576.2	8.2	556	13	548	30	0.91109514	99	103	570	8
C3-1_20	530	20	541	13	621	59	528	33	0.06093458	101	100	535	13
C3-1_21	1463	30	1474	28	1457	51	1453	40	0.86496454	100	100	1457	40
C3-1_22	1120	16	1147	15	1176	30	1085	18	0.2948874	102	105	1089	18
C3-1_23	599	29	596	14	610	82	650	71	0.10197269	99	91	594	14
C3-1_24	595	18	609.3	9.1	605	21	546	41	0.41149212	102	111	610	9

C3-1_25	1391	54	1385	28	1498	55	1424	72	1.4488189	100	97	1428	72
C3-1_26	1827	16	1829	19	1913	39	1817	15	0.4556597	101	102	1821	15
C3-1_27	1090	16	1102	19	1127	35	1088	27	0.50448654	102	102	1093	27
~~C3-1_28~~	~~1426~~	~~38~~	~~1178~~	~~35~~	~~1547~~	~~58~~	~~1798~~	~~44~~	~~1.24310118~~	~~84~~	~~67~~		
C3-1_29	1086	23	1100	19	1111	41	1065	32	0.50724138	103	105	1069	32
C3-1_30-2	611	14	623.1	9.3	651	14	554	30	0.54607407	104	115	641	10
C3-1_31	673	18	675	14	697	29	658	40	0.41758242	101	103	681	14
C3-1_32	1341	26	1346	28	1387	47	1348	45	0.82166667	100	100	1352	45
~~C3-1_33~~	~~985~~	~~58~~	~~815~~	~~22~~	~~1040~~	~~180~~	~~1300~~	~~130~~	~~0.23639344~~	~~82~~	~~62~~		
C3-1_34	618	15	618	12	625	19	619	34	0.6012024	99	98	612	12
C3-1_35	1624	32	1618	26	1562	53	1609	30	0.60169492	98	99	1612	30
C3-1_36	551	25	547	14	552	45	627	64	0.21374046	97	85	537	14
C3-1_37	389	17	387	16	401	20	453	59	0.38983051	98	83	381	16
C3-1_38	1394	27	1352	35	1300	66	1434	22	0.20994624	96	93	1438	22
C3-1_39	877	40	854	17	860	35	1014	93	0.50513347	96	83	1017	93
C3-1_40	875	26	867	20	855	32	921	39	0.62025316	98	93	856	20
C3-1_41	502	37	468	12	510	38	680	110	0.35948361	93	67	465	12
C3-1_42	491	21	504	10	453	23	510	65	0.42780749	102	98	501	10
C3-1_43	1503	19	1441	19	1359	42	1573	22	0.81127733	96	91	1577	22
C3-1_44	1375	37	1376	26	1298	64	1436	22	0.51299246	100	95	1439	22
C3-1_45	542	21	543.8	9.2	532	16	542	56	1.24682652	100	99	542	9
C3-1_46	1083	26	1095	26	1075	42	1119	37	0.58174905	101	97	1122	37
C3-1_47	1169	20	1176	19	1166	30	1170	26	0.63218391	100	100	1174	26
C3-1_48	1346	32	1270	26	1110	69	1419	37	0.31230083	94	89	1422	37
C3-1_49	553	15	558	10	530	14	572	41	0.88808901	100	96	553	10
C3-1_50	535	15	541	10	506	22	534	39	0.28164868	100	100	536	10
C3-1_51	453	15	466.1	9.4	453	17	480	51	0.70243205	102	96	464	9
C3-1_52	523	21	499	13	414	23	629	60	0.81496599	95	79	499	13
~~C3-1_53~~	~~1372~~	~~48~~	~~936~~	~~27~~	~~999~~	~~69~~	~~2131~~	~~82~~	~~0.69021739~~	~~68~~	~~44~~		
C3-1_54	574	14	577.8	9.2	574	18	586	34	0.59200508	101	99	580	9
C3-1_55	499	19	503.8	9.6	485	23	487	53	0.51232033	102	103	507	10
C3-1_56-1	1524	22	1544	35	1545	78	1561	30	0.36996736	102	100	1564	30
C3-1_57	500	16	508	13	501	15	516	48	0.44489796	103	99	513	13
C3-1_58	1172	46	1154	31	1097	33	1206	79	2.10914454	99	96	1209	79
C3-1_59	1406	42	1416	38	1478	57	1452	49	0.74009509	101	98	1455	49
C3-1_60	615	14	624	11	610	14	584	30	1.2050257	102	107	629	11
C3-1_61	626	15	570	13	884	33	881	33	0.15142315	91	65	571	13
C3-1_62	625	32	540	16	617	52	996	85	0.71232877	86	54	540	16
C3-1_63	568	41	565	13	548	28	566	86	1.08034188	99	99	564	13
C3-1_64	2578	40	2532	57	2620	130	2592	36	0.61115385	98	97	2594	36
C3-1_65	535	12	540.2	8	559	19	536	38	0.43173943	100	100	538	8
C3-1_66-1	574	29	579	14	587	19	589	78	1.92368839	100	97	576	14
C3-1_67	1467	28	1500	32	1563	55	1435	32	1.54592363	102	104	1438	32
C3-1_68	873	13	868	11	919	29	853	27	0.40138768	99	101	867	10

C3-1_69	383	12	374.8	5.3	383	18	411	49	0.34505607	98	91	375	5
C3-1_70	388	12	361.1	5.1	386	11	523	61	0.52560647	93	69	362	5
C3-1_71-2	926.8	9.6	932	12	948	19	894	13	0.43989071	101	104	896	13
C3-1_72	598	31	581	19	1380	260	696	82	0.01535533	97	83	582	19
C3-1_73	834	32	839	19	901	36	822	55	0.70217918	101	102	840	19
C3-1_74	590.3	9.2	582.3	5.3	595	17	578	26	0.29642974	98	100	582	5
C3-1_75	1314	40	1292	29	1409	63	1319	58	0.74418605	98	98	1321	58
C3-1_76	569	13	565.2	9.5	585	23	543	37	0.27357651	99	103	564	10
C3-1_77	544	25	547	10	559	18	534	80	0.94621027	100	102	545	10
C3-1_78-1	530	16	526.4	9.7	559	23	508	38	0.47882455	99	103	525	10
C3-1_79	560	25	546	16	607	44	618	66	0.5083632	97	88	545	16
C3-1_80	1600	22	1618	21	1655	46	1571	29	0.82287449	101	103	1573	29
C3-1_81	1131	26	1128	20	1172	34	1144	43	1.42462845	102	100	1145	43
C3-1_82	496	13	494.6	7.3	499	15	514	41	0.51275168	102	98	505	7
C3-1_83	598	23	517.5	7	615	26	909	90	0.50717703	88	58	528	7
C3-1_84	570.3	9.7	576	7.4	576	14	564	28	0.48518519	103	104	587	8
C3-1_85	513	11	518.9	6.6	520	11	492	37	0.57494692	103	107	528	7
~~C3-1_86~~	~~844~~	~~21~~	~~747~~	~~17~~	~~1008~~	~~38~~	~~1112~~	~~37~~	~~0.33730632~~	~~89~~	~~68~~		
C3-1_87	657	27	588	16	619	39	969	68	0.84308365	90	61	589	16
C3-1_88	513	27	516	11	523	34	521	81	0.35971223	100	98	514	11
C3-1_89	1390	14	1403	20	1375	30	1408	20	0.94591029	100	99	1409	20
C3-1_90	941	29	945	18	899	37	949	51	0.83135392	99	98	929	18
C3-1_91	590	23	587	13	567	17	628	58	1.5140665	96	90	567	13
C3-1_92	1610	31	1613	29	1572	59	1670	28	0.6961367	97	93	1671	28
C3-1_93	2598	42	2602	56	2421	98	2662	22	0.52354049	97	95	2662	22
~~C3-1_94~~	~~1472~~	~~51~~	~~1394~~	~~49~~	~~1446~~	~~88~~	~~1650~~	~~49~~	~~0.81481481~~	~~92~~	~~82~~		
C3-1_95	1395	36	1399	30	1367	56	1454	26	0.55252606	97	93	1455	26
C3-1_96	509	25	510	14	460	27	534	76	0.63505747	98	93	497	14
C3-1_97	560	13	563	9.3	585	28	567	39	0.18281718	99	97	553	9
C3-1_98	3224	34	3223	82	3040	190	3252	24	0.504662	99	98	3253	24
C3-1_99-1	585	16	588	10	568	13	579	49	1.42243437	100	101	584	10
C3-1_100	547	12	547.8	8.5	504	15	611	29	0.34955752	100	90	549	9
C3-1_101	562	24	572	12	540	15	585	70	2.38429752	102	98	573	12
C3-1_102	531	33	525	13	475	21	578	96	0.92371476	99	91	526	13
C3-1_103	1181	28	1184	31	1175	61	1243	57	0.62825955	100	95	1243	57
C3-1_104	504	13	503.5	8.4	466	13	504	42	0.87004548	99	99	501	8
~~C3-1_105~~	~~1309~~	~~34~~	~~1243~~	~~39~~	~~1358~~	~~49~~	~~1485~~	~~32~~	~~0.57~~	~~94~~	~~83~~		
C3-1_106	1061	15	1064	15	1035	25	1061	29	0.54283548	99	99	1061	29
C3-1_107	1459	20	1472	23	1478	36	1462	21	0.89025326	100	100	1462	21
C3-1_108-1	444	36	436	19	430	33	558	91	0.70562771	97	77	432	19
C3-1_109	513	29	527	17	504	30	545	76	0.9239905	103	96	526	17
C3-1_110	1032	34	992	29	838	35	1061	35	1.60803059	96	93	1061	35
C3-1_111	1019	39	1028	31	1016	51	1064	74	0.51284585	101	97	1064	74
C3-1_112	1552	21	1565	21	1587	49	1530	12	0.15089672	101	103	1531	12

C3-1_113-1	1459	24	1494	36	1463	74	1449	24	0.27065868	103	104	1449	24
C3-1_114	570	23	570	13	600	41	556	61	0.18331479	101	103	573	13
C3-1_115	682	27	685	23	816	66	700	45	0.14547677	101	98	687	23
~~C3-1_116~~	~~3301~~	~~18~~	~~3473~~	~~43~~	~~3550~~	~~130~~	~~3188~~	~~15~~	~~0.09539711~~	~~105~~	~~109~~		
C3-1_117	547	21	539	17	560	37	629	50	0.40813559	98	85	536	17
C3-1_118	578	17	561	11	629	23	596	42	0.10671642	96	93	555	10
~~C3-1_119~~	~~767~~	~~34~~	~~609~~	~~14~~	~~1610~~	~~150~~	~~1284~~	~~82~~	~~0.11220657~~	~~79~~	~~47~~		
C3-1_120	625	16	609	11	637	24	668	53	0.48431457	96	90	601	10
C3-1_121	1481	29	1483	24	1540	55	1432	36	0.74322169	100	103	1431	36
C3-1_122	1599	16	1597	16	1647	38	1573	15	0.48403977	100	101	1573	15
C3-1_123	524	25	526	17	750	130	533	72	0.04661836	101	99	528	17
C3-1_124	1085	14	1084	12	1094	22	1090	18	0.74649407	101	100	1090	18
C3-1_125	563	13	552.2	9.4	571	15	564	33	0.74888227	99	99	557	10
C3-1_126	1966	16	1901	26	1909	59	2029	16	0.21251752	98	95	2029	16
C3-1_128	1246	41	1247	48	1310	120	1267	56	0.47345133	101	99	1267	56
C3-1_129	418	19	381.5	7.7	398	17	618	45	0.91287129	91	62	382	8
C3-1_130	3038	27	3025	70	3137	92	3082	18	0.55225893	99	98	3082	18
C3-1_131	1456	15	1455	18	1441	26	1454	16	0.68529257	99	99	1453	16
C3-1_132	2128	30	2145	40	2222	66	2114	22	0.45607613	100	100	2114	22
C3-1_133	1106	13	1102	15	1101	37	1109	14	0.16160164	98	98	1109	14
~~C3-1_134~~	~~610~~	~~19~~	~~517~~	~~15~~	~~639~~	~~27~~	~~941~~	~~47~~	~~0.34138889~~	~~84~~	~~54~~		
C3-1_135	594	16	535	12	583	19	858	44	0.56686542	89	61	527	12
C3-1_136	523	47	506	18	524	50	680	150	0.77891156	96	74	501	18
C3-1_137	577	17	575	13	597	23	658	27	0.33443609	99	87	571	13
C3-1_138	531	24	518	13	549	35	591	81	0.33936652	98	88	517	13
C3-1_139	584	18	586	10	582	21	584	44	0.76899463	100	100	585	10
C3-1_140-1	1412	21	1412	22	1434	40	1424	28	1.3377724	100	99	1423	28
C3-1_141	700	18	709	12	689	51	706	34	0.09634571	102	101	715	13
C3-1_142	1041	38	1040	35	993	39	1079	53	0.88127854	101	97	1078	53
C3-1_143	598	37	594	19	575	34	597	81	0.71489971	100	101	600	19
C3-1_144	517	22	509	13	508	22	565	47	0.45012788	100	91	515	13
C3-1_145	1139	29	1131	31	1159	54	1224	36	0.38876404	100	93	1223	36
C3-1_146	1809	21	1774	41	2023	70	1907	23	0.30333988	99	94	1906	23
C3-1_147	1153	23	1156	28	1186	46	1172	35	0.41929499	101	100	1171	35
C3-1_148	1063	49	892	20	1340	110	1450	100	~~0.33882353~~	~~85~~	~~62~~		
C3-1_149	540	16	548.1	9.4	553	19	516	58	0.49072753	103	108	554	10
C3-1_150	551	15	546.7	8.9	526	19	602	42	0.44501542	100	92	551	9

Table 12 LA-ICP-MS raw data of sample 03-01-15C3

Grain ID	Final Age ^{207}Pb/^{235}U	Final Age ^{207}Pb/^{235}U 2σ	Final Age ^{206}Pb/^{238}U	Final Age ^{206}Pb/^{238}U 2σ	Final Age ^{208}Pb/^{232}Th	Final Age ^{208}Pb/^{232}Th 2σ	Final Age ^{207}Pb/^{206}Pb	Final Age ^{207}Pb/^{206}Pb 2σ	^{232}Th/^{238}U	% Concordance (^{206}Pb/^{238}U)/ (^{207}Pb/^{235}U)	% Concordance (^{206}Pb/^{238}U)/ (^{207}Pb/^{206}Pb)	Preferred age (Ma)	Preferred age 2σ (Ma)
C3-2_1	1026	23	978	19	1105	23	1083	17	0.467403315	95	90	1083	17
C3-2_2	1214	24	1203	22	1244	30	1224	22	1.029605263	99	98	1224	22
C3-2_3	596	15	584.9	9.2	578	13	620	18	0.919042189	98	94	585	9
C3-2_4	515	17	512	12	506	22	527	30	0.350102669	99	97	512	12
C3-2_5	879	43	851	20	853	36	975	27	0.236775819	97	87	851	20
C3-2_6	543	29	523	12	534	18	645	42	0.649616368	96	81	523	12
C3-2_7	528	24	515	13	515	21	587	28	0.218411552	98	88	515	13
C3-2_8	546	43	526	14	525	31	635	41	0.799591002	96	83	526	14
C3-2_9	857	42	786	25	1036	57	1054	32	0.221467391	92	75	786	25
C3-2_10	637	34	630	16	630	24	690	30	0.877669903	99	91	630	16
C3-2_11	571	13	572.7	9.4	593	15	564	22	0.492625369	100	102	573	9
C3-2_12	838	40	814	23	790	130	898	68	0.06812933	97	91	814	23
C3-2_13	542	13	534.2	9.5	579	14	562	25	0.503614458	99	95	534	10
C3-2_14	563	34	548	15	609	33	646	84	1.20326087	97	85	548	15
C3-2_15	571	15	572	12	547	14	577	26	0.323394495	100	99	572	12
C3-2_16	567	22	555	11	559	20	638	29	0.39185336	98	87	555	11
C3-2_17	529	37	525	16	553	31	573	42	0.609090909	99	92	525	16
C3-2_18	670	44	666	32	726	43	698	72	2.366197183	99	95	666	32
C3-2_19-1	1438	32	1436	27	1419	34	1452	16	0.39800995	100	99	1452	16
C3-2_20	587	16	586	10	588	16	601	17	0.845953003	100	98	586	10
C3-2_21	579	20	583.8	9.4	571	13	583	36	2.129461907	101	100	584	9
C3-2_22	947	25	944	16	930	26	950	30	0.413709285	100	99	944	16
C3-2_23	2223	36	2219	64	2142	72	2238	22	0.261612903	100	99	2238	22
C3-2_24	1114	19	1118	17	1131	28	1107	18	0.683718642	100	101	1107	18
C3-2_25	922	22	917	17	902	38	968	33	0.222293814	99	95	917	17
C3-2_26	2391	42	2391	45	2320	120	2371	16	0.191428571	100	101	2371	16
C3-2_27	519	41	505	19	490	32	586	75	0.397272727	97	86	505	19
C3-2_28	553	15	553	10	539	16	563	21	0.485061511	100	98	553	10
C3-2_29	890	32	831	21	936	59	1036	33	0.10434322	93	80	831	21
C3-2_30-1	523	19	527	11	521	18	532	29	0.755656109	101	99	527	11
C3-2_31	1451	30	1465	34	1438	44	1454	22	0.7136	101	101	1454	22
C3-2_32	2882	24	2902	39	2958	54	2883	10	0.800589391	101	101	2883	10
C3-2_33-2	551	13	557.4	7.2	551	15	549	30	0.501446759	101	102	557	7
C3-2_34	592	16	600	16	608	24	586	23	0.2654102	101	102	600	16
C3-2_35	584	13	583	11	579	16	579	52	0.911330049	100	101	583	11
C3-2_36	600	23	608	15	613	25	612	65	0.515640767	101	99	608	15

C3-2_37	1891	27	1916	39	1995	40	1892	19	0.906785981	101	101	1892	19
C3-2_38	1094	57	1092	29	1093	42	1094	80	2.074074074	100	100	1094	80
C3-2_39	587	17	590.5	9.7	602	22	586	38	0.77753304	101	101	591	10
C3-2_40	596	27	602	12	617	22	630	60	1.201096892	101	96	602	12
C3-2_41	625	13	635	12	631	20	612	24	0.185691318	102	104	635	12
C3-2_42	966	18	976	16	1075	36	963	26	0.241008403	101	101	976	16
C3-2_43	535	27	515	17	516	25	652	61	0.783737024	96	79	515	17
C3-2_44	526	26	515	12	527	27	643	75	0.487027027	98	80	515	12
C3-2_45	542	32	514	15	548	38	656	46	0.228938907	95	78	514	15
C3-2_46	1580	23	1579	40	1640	39	1583	20	0.275783476	100	100	1583	20
C3-2_47	543	11	536.2	8.2	548	14	579	28	0.270136519	99	93	536	8
C3-2_48	588	21	586	14	587	16	603	41	1.349854227	100	97	586	14
C3-2_49	899	22	899	14	854	28	908	23	0.295064378	100	99	899	14
C3-2_50	1379	51	1315	52	1300	64	1514	79	1	95	87	1514	79
C3-2_51	1784	18	1796	22	1727	24	1773.6	9.6	0.632796781	101	101	1774	10
C3-2_52	993	22	991	14	1006	30	1009	37	0.533923304	100	98	1009	37
C3-2_53	1045	27	1058	24	1049	40	1030	55	0.845977011	101	103	1030	55
C3-2_54	1096	27	1092	15	1051	28	1077	30	0.662222222	100	101	1077	30
C3-2_55	508	12	468	11	499	10	684	28	0.542642924	92	68	468	11
C3-2_56	1058	18	1039	22	1002	23	1096	16	0.572533849	98	95	1096	16
C3-2_57	519	26	504	17	516	19	582	73	1.022834117	97	87	504	17
C3-2_58	707	20	709	19	709	23	721	46	0.751716247	100	98	709	19
C3-2_59	694	18	679	13	681	27	744	46	0.458405546	98	91	679	13
C3-2_60	597	12	594	10	583	11	588	23	0.414659686	99	101	594	10
C3-2_61	529	25	523	17	531	28	545	53	0.714839961	99	96	523	17
C3-2_62	570	19	540	13	587	23	668	48	0.354558824	95	81	540	13
C3-2_63	620	11	613	10	602	15	617	16	0.122512648	99	99	613	10
C3-2_64	1434	30	1407	39	1424	54	1457	16	0.739919893	98	97	1457	16
C3-2_65	3213	19	3200	58	3443	71	3209	12	0.328369906	100	100	3209	12
C3-2_66	554	16	512	12	531	16	697	42	0.56351626	92	73	512	12
C3-2_67	540	21	539	17	531	27	557	49	0.131372549	100	97	539	17
C3-2_68	1106	26	1101	29	1060	31	1106	30	0.948543689	100	100	1106	30
C3-2_69	727	24	715	25	658	28	727	45	0.391304348	98	98	715	25
C3-2_70	500	28	501	18	511	32	480	66	0.426869806	100	104	501	18
C3-2_71	836	16	831	16	837	20	839	26	1.466307278	99	99	831	16
C3-2_72-1	533	14	524	11	527	15	571	39	0.512661252	98	92	524	11
C3-2_73	452	11	423	13	388	14	521	39	0.195620438	94	81	423	13
C3-2_74	547	23	551	11	532	27	554	59	0.394148244	101	99	551	11
C3-2_75	496	11	491.4	8.9	476	16	515	28	0.183270677	99	95	491	9
C3-2_76	555	15	548	13	556	25	591	39	0.299447514	99	93	548	13
C3-2_77	772	24	758	28	740	41	828	33	0.326783868	98	92	758	28

C3-2_78	510	20	506	14	481	11	534	57	1.07827476	99	95	506	14
C3-2_79	532	15	532	12	524	13	533	31	0.542772861	100	100	532	12
C3-2_80	926	27	913	33	854	33	960	31	0.179387417	99	95	913	33
~~C3-2_81~~	~~-990~~	~~240~~	~~46~~	~~49~~	~~228~~	~~27~~	~~4183~~	~~18~~	~~0.467400881~~	~~-5~~	~~1~~		
C3-2_83	1458	18	1459	26	1405	32	1464	15	0.642991239	100	100	1464	15
C3-2_84	555.4	9.8	554.2	9.7	540	13	569	27	0.399412012	100	97	554	10
C3-2_85	1143	27	1126	23	1121	32	1191	41	0.781954887	99	95	1191	41
C3-2_86	614	35	621	15	634	19	625	79	1.336252189	101	99	621	15
C3-2_87	902	25	864	37	854	43	956	55	0.131775701	96	90	864	37
C3-2_88	828	43	802	26	760	46	897	57	0.268229167	97	89	802	26
C3-2_89	1322	44	1282	31	1242	88	1378	29	0.335597826	97	93	1378	29
C3-2_90	556	11	558	11	549.1	8.8	575	27	0.718152866	100	97	558	11
C3-2_91	527	10	523.7	8	526	15	551	30	0.278193833	99	95	524	8
C3-2_92	556.8	9.9	563.2	9.1	553	12	553	20	0.482278481	101	102	563	9
C3-2_93	580	25	581	14	574	24	571	72	0.57612782	100	102	581	14
C3-2_94	497	11	501	9.6	481	11	498	26	0.542421354	101	101	501	10
C3-2_95	1659	33	1582	32	1605	45	1793	36	1.316151203	95	88	1793	36
C3-2_96	551.6	9	552.5	9.7	520	11	553	16	0.321318373	100	100	553	10
C3-2_97	511	14	516	9.1	502	12	508	49	1.059701493	101	102	516	9
C3-2_98	550	17	546	10	537	21	585	49	0.426985482	99	93	546	10
C3-2_99	2121	18	1997	29	2080	43	2242	13	0.518777293	94	89	2242	13
C3-2_100	1423	17	1427	30	1389	28	1427	19	0.569915254	100	100	1427	19
~~C3-2_101~~	~~1541~~	~~33~~	~~1421~~	~~29~~	~~1679~~	~~75~~	~~1717~~	~~36~~	~~0.835214447~~	~~92~~	~~83~~		
C3-2_102	519.9	8.7	517.5	7.9	521	10	516	25	0.331693364	100	100	518	8
C3-2_103	1893	14	1849	28	1784	58	1957	13	0.216073479	98	94	1957	13
C3-2_104	713	59	603	15	800	120	980	240	0.367804878	85	62	603	15
C3-2_105	576	15	580	11	594	19	557	38	0.452380952	101	104	580	11
C3-2_106	2246	22	2233	45	2205	39	2249	19	0.556958393	99	99	2249	19
C3-2_107	940	27	883	27	928	31	1043	40	0.383282091	94	85	1043	40
C3-2_108	605	12	610	12	580	12	589	25	0.164266487	101	104	610	12
C3-2_109	565	31	558	20	573	20	586	78	0.795427196	99	95	558	20
C3-2_110	614	19	618	23	605	20	618	44	0.746666667	101	100	618	23
C3-2_111	530	16	526	13	515	12	543	57	1.442379182	99	97	526	13
C3-2_112	535	13	534	10	537	10	531	25	0.904761905	100	101	534	10
C3-2_113	893	21	874	21	1070	28	922	29	0.423327306	98	95	874	21
C3-2_114	1043	27	1031	28	1046	64	1063	28	0.216283406	99	97	1063	28
C3-2_115	1659	27	1657	35	1657	46	1661	31	0.660071942	100	100	1661	31
C3-2_116	529	12	522.4	9.5	522	14	549	29	0.56028813	99	95	522	10
C3-2_117	1175	22	1174	21	1155	36	1175	32	0.605945946	100	100	1175	32
C3-2_118	527	15	519.5	8.9	513	15	555	48	0.511081263	99	94	520	9
C3-2_119	534	14	534.5	9.7	527	14	512	34	0.478738791	100	104	535	10

C3-2_120	480	35	472	17	518	38	550	120	0.617100372	98	86	472	17
C3-2_121	733	16	731	16	879	39	726	33	0.348190876	100	101	731	16
C3-2_122	581	13	578	12	579	15	578	27	0.620584653	99	100	578	12
C3-2_123	622	26	606	20	656	43	690	84	0.81809872	97	88	606	20
C3-2_124	606	13	604.5	9.1	614	13	602	36	1.231631864	100	100	605	9
C3-2_125	586	16	583	11	632	19	576	44	0.406223717	99	101	583	11
C3-2_126	545	14	541.8	8.8	870	300	537	38	0.003026482	99	101	542	9
C3-2_127	515	10	514	8.4	501	10	512	24	0.541932436	100	100	514	8
C3-2_128	512	22	510	20	512	30	512	55	0.52659176	100	100	510	20
~~C3-2_129~~	~~724~~	~~66~~	~~577~~	~~39~~	~~658~~	~~59~~	~~1190~~	~~140~~	~~0.2156013~~	~~80~~	~~48~~		
C3-2_130	2186	32	2174	58	2036	45	2169	12	0.234945706	99	100	2169	12
C3-2_131	693	13	676	14	671	18	749	20	0.197966963	98	90	676	14
C3-2_132	583	16	577.2	8.9	576	15	587	27	0.630608696	99	98	577	9
C3-2_133	800	33	768	35	821	63	835	76	0.703333333	96	92	768	35
C3-2_134	2409	22	2381	60	2383	50	2396	28	0.696078431	99	99	2396	28
C3-2_135	591	27	579	20	580	24	637	61	0.870503597	98	91	579	20
C3-2_136	926	29	922	23	897	30	961	58	0.615204678	100	96	922	23
C3-2_137	2577	19	2416	39	2454	34	2684	12	0.415407407	94	90	2684	12
C3-2_138	568	16	570	12	529	16	564	37	0.591297591	100	101	570	12
C3-2_139	2297	17	2276	29	2220	57	2287.9	9.8	0.211235955	99	99	2288	10
C3-2_140	613	16	629	15	625	23	559	33	0.773981603	103	113	629	15
C3-2_141	587	22	579	13	556	23	589	53	0.558457711	99	98	579	13
C3-2_142	913	19	911	16	942	29	915	39	0.373056995	100	100	911	16
C3-2_143	1113	27	1122	27	1143	33	1106	31	1.554054054	101	101	1106	31
C3-2_144	603	14	587	11	609	17	647	30	0.409311741	97	91	587	11
C3-2_145	1106	17	1114	18	1064	31	1081	27	0.633709981	101	103	1081	27
C3-2_146	579.7	9.8	588.1	9.9	592	17	571	36	0.264253394	101	103	588	10
C3-2_147	1093	16	1079	23	1472	92	1102	22	0.05059733	99	98	1102	22
C3-2_148	517	32	501	16	509	25	544	88	0.952830189	97	92	501	16
C3-2_149	604	14	596.8	8.4	544	16	633	28	0.371735791	99	94	597	8
C3-2_150	552	9.6	553.4	9.7	540	11	544	23	0.620955316	100	102	553	10

Table 13 LA-ICP-MS raw data of sample 04-01-15C10

Grain ID	Final Age ^{207}Pb/^{235}U	Final Age ^{207}Pb/^{235}U 2σ	Final Age ^{206}Pb/^{238}U	Final Age ^{206}Pb/^{238}U 2σ	Final Age ^{208}Pb/^{232}Th	Final Age ^{208}Pb/^{232}Th 2σ	Final Age ^{207}Pb/^{206}Pb	Final Age ^{207}Pb/^{206}Pb 2σ	^{232}Th/^{238}U	% Concordance (^{206}Pb/^{238}U)/ (^{207}Pb/^{235}U)	% Concordance (^{206}Pb/^{238}U)/ (^{207}Pb/^{206}Pb)	Preferred Age (Ma)	Preferred Age 2σ (Ma)
C10_1	509	27	511	15	501	22	555	84	0.55372807	100	92	511	15
C10_2	493	28	485	16	508	23	776	78	0.686684073	98	63	485	16
C10_3	501	29	498	12	511	28	585	58	0.48277446	99	85	498	12
C10_4	509	34	460	19	599	34	940	54	0.386206897	90	49	460	19
C10_5-1	500	23	495.8	9.9	492	16	577	45	0.565960355	99	86	496	10
C10_6	862	57	894	31	978	71	1100	65	1.244318182	104	81	894	31
C10_7	500	22	507	11	499	19	511	49	0.5309626	101	99	507	11
C10_8	489	26	511	12	490	30	506	63	0.447463768	104	101	511	12
~~C10_9~~	~~439~~	~~22~~	~~468~~	~~14~~	~~493~~	~~30~~	~~601~~	~~42~~	~~0.362756953~~	~~107~~	~~78~~		
~~C10_10~~	~~467~~	~~20~~	~~494~~	~~11~~	~~479~~	~~22~~	~~480~~	~~55~~	~~0.526048285~~	~~106~~	~~103~~		
C10_11	488	19	483	10	453	16	520	30	0.501199041	99	93	483	10
C10_12	496	20	497.8	9.3	509	18	584	42	0.663527397	100	85	498	9
C10_13	497	24	466.5	8.7	530	25	817	42	0.402169378	94	57	467	9
C10_14	486	15	489	7.7	503	15	508	41	0.664550781	101	96	489	8
C10_15	482	20	477.7	9	502	16	581	43	0.709198813	99	82	478	9
C10_16	1205	55	1202	36	1284	58	1314	40	0.816623822	100	91	1314	40
C10_17	522	43	510	12	527	29	609	45	0.375555556	98	84	510	12
C10_18	502	39	506	14	556	35	683	57	0.544162437	101	74	506	14
~~C10_19~~	~~422~~	~~43~~	~~483~~	~~21~~	~~505~~	~~39~~	~~506~~	~~53~~	~~0.262755102~~	~~114~~	~~95~~		
~~C10_20~~	~~496~~	~~37~~	~~405.9~~	~~9.3~~	~~559~~	~~34~~	~~898~~	~~42~~	~~0.342288557~~	~~82~~	~~45~~		
C10_21-1	493	23	497	11	550	18	567	77	0.851851852	101	88	497	11
C10_22	525	33	499	18	571	61	648	76	0.366144201	95	77	499	18
C10_23	491	25	494	12	542	22	624	59	0.315955766	101	79	494	12
C10_24	941	26	916	20	1078	28	1168	26	0.612195122	97	78	916	20
C10_25	566	28	573	15	608	61	662	37	0.03793911	101	87	573	15
C10_26	489	28	463.9	9.3	480	24	549	40	0.702643172	95	84	464	9
C10_27	482	37	484	14	503	26	641	66	0.592771084	100	76	484	14
C10_28	477	51	473	19	508	27	750	110	0.529179031	99	63	473	19
C10_29	494	20	490.7	8.4	501	19	553	36	0.493296089	99	89	491	8
~~C10_30~~	~~441~~	~~31~~	~~474~~	~~18~~	~~475~~	~~27~~	~~526~~	~~79~~	~~0.714285714~~	~~107~~	~~90~~		
C10_31-1	508	45	505	14	500	46	550	100	0.442234848	99	92	505	14
C10_32	511	33	518	15	516	26	675	72	0.587912088	101	77	518	15
C10_33	860	33	836	15	814	24	929	40	1.027385159	97	90	836	15
C10_34	502	25	500.3	9.6	465	17	535	28	0.634183673	100	94	500	10
C10_35	492	60	487	28	508	61	740	130	0.569780854	99	66	487	28
C10_36	491	44	468	18	432	34	678	46	0.442760943	95	69	468	18
C10_37	501	25	503.6	9.8	503	25	531	40	0.37818025	101	95	504	10
C10_38	529	23	515.2	8.9	508	21	585	33	0.41991342	97	88	515	9
C10_39	528	29	488.6	8.8	488	25	633	51	0.481349911	93	77	489	9

~~C10_40~~									~~0.452941176~~				
C10_41	499	35	480	16	534	49	633	33	0.142857143	96	76	480	16
C10_42	438	46	431	16	480	45	860	120	0.456170213	98	50	431	16
C10_43	508	22	513	13	502	24	592	60	0.671665351	101	87	513	13
~~C10_44~~	~~480~~	~~180~~	~~377~~	~~65~~	~~890~~	~~230~~	~~1720~~	~~520~~	~~0.406015038~~	~~79~~	~~22~~		
C10_45	477	30	479	14	513	27	614	37	0.310447761	100	78	479	14
C10_46	461	30	423	15	418	23	570	56	0.548523207	92	74	423	15
C10_47	484	28	478.2	9.6	489	19	616	35	0.446539379	99	78	478	10
C10_48	2140	100	2090	81	2240	150	2346	21	0.291873964	98	89	2346	21
C10_49	494	39	481	17	504	35	605	49	0.401546392	97	80	481	17
C10_50	467	31	464	12	462	22	596	29	0.394409938	99	78	464	12
C10_51	509	28	520	14	560	30	557	35	0.410117435	102	93	520	14
C10_52	498	23	482.5	8.7	526	16	567	28	0.384359401	97	85	483	9
C10_53-2	506	26	500.7	7.1	529	18	533	50	0.544885177	99	94	501	7
C10_54	513	23	500.6	9.8	519	22	557	36	0.607786171	98	90	501	10
C10_55	902	33	898	15	961	45	958	34	0.355263158	100	94	898	15
C10_56	445	34	452	16	461	26	653	62	0.479069767	102	69	452	16
C10_57	452	35	437	12	463	27	776	44	0.63559322	97	56	437	12
C10_58	547	31	544	10	536	22	660	49	1.986628462	99	82	544	10
C10_59	461	31	443	15	509	38	677	60	0.274183976	96	65	443	15
C10_60	458	31	459	12	444	20	608	44	0.622928177	100	75	459	12
C10_61	460	25	459	8.6	448	19	650	61	0.533231084	100	71	459	9
C10_62	461	39	465	17	454	38	690	75	0.431836735	101	67	465	17
C10_63	453	23	459	11	458	16	574	33	0.967320261	101	80	459	11
~~C10_64~~	~~460~~	~~200~~	~~375~~	~~62~~	~~700~~	~~280~~	~~2140~~	~~340~~	~~0.496296296~~	~~82~~	~~18~~		
C10_65	470	22	465.1	9.7	465	18	540	34	0.328730512	99	86	465	10
C10_66	482	25	479	12	461	24	565	47	0.388131516	99	85	479	12
C10_67	1085	48	1041	29	1007	37	1105	49	0.650070126	96	94	1105	49
C10_68	478	19	471.4	8.5	478	16	528	38	0.345342254	99	89	471	9
C10_69	466	23	463.2	8.5	467	24	540	40	0.391925466	99	86	463	9
C10_70	1003	40	1008	19	1012	47	1076	45	0.521267723	100	94	1076	45
C10_71	472	20	460.5	8.1	464	18	556	40	0.454504505	98	83	461	8
C10_72	506	49	467	15	514	36	815	42	0.544811321	92	57	467	15
C10_73	442	61	453	24	480	45	740	53	0.432	102	61	453	24
C10_74	499	39	448	16	559	48	950	40	0.459770115	90	47	448	16
C10_75	440	43	441	19	455	29	671	77	0.701538462	100	66	441	19
C10_76-1	520	43	498	19	501	38	567	87	0.924028269	96	88	498	19
C10_77	462	28	470	16	497	30	672	58	0.384816754	102	70	470	16
C10_78	455	28	464	14	472	21	510	57	0.477233429	102	91	464	14
C10_79	430	34	439	18	471	39	660	120	0.629200463	102	67	439	18
C10_80-1	488	25	478	11	476	19	548	44	0.527607362	98	87	478	11
C10_81	436	19	442	11	430	18	525	54	0.737616099	101	84	442	11
C10_82	519	26	481	12	470	29	675	79	0.486725664	93	71	481	12
C10_83	441	22	439	15	443	20	598	57	0.925327952	100	73	439	15

C10_84	526	19	506	12	510	31	519	55	0.497472194	96	97	506	12
C10_85	531	13	503.8	8.5	497	13	549	31	0.348605578	95	92	504	9
C10_86	473	20	470	10	444	14	504	48	0.530110263	99	93	470	10
C10_87	453	19	452.2	9.3	451	12	521	34	0.402331606	100	87	452	9
C10_88	508	27	468.8	9.9	493	33	587	65	0.392337165	92	80	469	10
~~C10_89~~	~~547~~	~~23~~	~~423~~	~~11~~	~~634~~	~~26~~	~~1047~~	~~35~~	~~0.267901235~~	~~77~~	~~40~~		
C10_90-2	478	23	467.9	9.2	462	22	471	45	0.416666667	98	99	468	9
C10_91	476	27	487	14	484	20	565	39	0.716097561	102	86	487	14
C10_92	460	19	458	14	475	22	572	47	0.204159132	100	80	458	14
C10_93	943	47	911	20	1007	54	1076	32	0.534441805	97	85	911	20
C10_94	457	45	460	26	460	37	710	110	0.634558824	101	65	460	26
C10_95	1190	51	1242	38	1170	61	1255	32	0.401772526	104	99	1255	32
~~C10_96~~	~~587~~	~~25~~	~~290~~	~~11~~	~~767~~	~~42~~	~~2011~~	~~97~~	~~0.313868613~~	~~49~~	~~14~~		
C10_97	474	34	461	18	505	41	667	79	0.39704142	97	69	461	18
C10_98	511	18	509.6	8.2	503	25	544	21	0.066924686	100	94	510	8
C10_99	459	25	481	13	475	29	533	75	0.573913043	105	90	481	13
C10_100	571	26	506.3	9.6	513	27	826	55	0.408152174	89	61	506	10
C10_101	494	24	485.2	9.6	480	22	480	32	0.588162762	98	101	485	10
C10_102	568	19	533	8.8	702	41	622	42	0.067021277	94	86	533	9
C10_103	486	18	481.9	8.2	474	18	481	34	0.381355932	99	100	482	8
C10_104	457	36	462	15	467	25	631	81	0.6308	101	73	462	15
C10_105	500	19	500	15	485	17	567	30	0.426048565	100	88	500	15
C10_106	507	22	498.9	9.8	487	21	513	25	0.242682927	98	97	499	10
C10_107	445	22	414	11	999	73	813	32	0.047286822	93	51	414	11
C10_108	479	25	448	15	464	22	771	45	0.779487179	94	58	448	15
~~C10_109~~	~~556~~	~~26~~	~~390.3~~	~~9.2~~	~~664~~	~~32~~	~~1311~~	~~33~~	~~0.363120567~~	~~70~~	~~30~~		
~~C10_110~~	~~434~~	~~34~~	~~474~~	~~22~~	~~475~~	~~22~~	~~561~~	~~74~~	~~0.402121212~~	~~109~~	~~84~~		
C10_111	477	26	482	13	464	25	597	72	0.625984252	101	81	482	13
C10_112	492	20	495	11	517	16	585	47	0.74	101	85	495	11
C10_113	469	30	466	26	509	21	621	67	0.293067227	99	75	466	26
C10_114	478	39	440	20	514	31	919	41	0.327442827	92	48	440	20
C10_115-1	480	27	496	11	494	20	481	63	0.508943089	103	103	496	11
C10_116	483	45	483	13	522	39	529	82	0.447916667	100	91	483	13
C10_117	498	17	495	10	516	16	531	30	0.509782609	99	93	495	10
C10_118	530	22	448.1	9.4	611	23	1000	47	0.363543441	85	45	448	9
C10_119	492	14	496.7	6.4	505	13	539	23	0.232179931	101	92	497	6
~~C10_120~~	~~587~~	~~20~~	~~490.8~~	~~9.8~~	~~625~~	~~29~~	~~965~~	~~47~~	~~0.394115209~~	~~84~~	~~51~~		
C10_121	957	53	1001	39	1103	67	1144	85	0.209302326	105	88	1144	85
C10_122	495	20	508.5	7.7	512	18	522	36	0.458116883	103	97	509	8
C10_123	546	26	520.4	9.8	607	31	606	55	0.341509434	95	86	520	10
C10_124	467	21	492.1	9.8	498	18	530	39	0.391610738	105	93	492	10
C10_125	467	34	468	18	469	31	651	78	0.587136929	100	72	468	18
~~C10_126~~	~~626~~	~~59~~	~~412~~	~~14~~	~~618~~	~~54~~	~~1650~~	~~180~~	~~0.519047619~~	~~66~~	~~25~~		
C10_127	478	21	488	10	504	26	572	46	0.431219512	102	85	488	10

C10_128	479	22	481	11	503	19	582	51	0.473460722	100	83	481	11
C10_129	476	24	465	12	480	18	555	24	0.22704918	98	84	465	12
C10_130	527	19	527.7	7.5	534	15	534	42	0.531482079	100	99	528	8
C10_131	485	14	504	10	502	15	488	33	0.788686022	104	103	504	10
~~C10_132~~	~~452~~	~~13~~	~~487.1~~	~~8.7~~	~~456~~	~~16~~	~~530~~	~~39~~	~~0.477137177~~	~~108~~	~~92~~		
~~C10_133~~	~~572~~	~~24~~	~~464~~	~~11~~	~~543~~	~~21~~	~~1016~~	~~62~~	~~0.701208981~~	~~81~~	~~46~~		
C10_134	508	18	493	11	462	21	515	35	0.462809917	97	96	493	11
~~C10_135~~	~~463~~	~~16~~	~~495~~	~~11~~	~~466~~	~~18~~	~~483~~	~~44~~	~~0.81443299~~	~~107~~	~~102~~		
C10_136	489	24	488	10	486	29	486	88	0.455723542	100	100	488	10
C10_137	507	24	474	15	559	37	870	87	0.607773852	93	54	474	15
C10_138	509	39	477	20	511	36	650	130	0.477393617	94	73	477	20
C10_139	498	14	498.6	9.1	521	24	501	35	0.276190476	100	100	499	9
C10_140	489	20	491	12	487	21	531	52	0.506422018	100	92	491	12
C10_141	460	35	492	25	514	39	700	110	0.583105023	107	70	492	25
C10_142	458	14	456.6	6.8	459	12	488	24	0.699579832	100	94	457	7
~~C10_143~~	~~340~~	~~430~~	~~286~~	~~93~~	~~720~~	~~270~~	~~3340~~	~~570~~	~~0.447852761~~	~~84~~	~~9~~		
C10_144	469	21	472.2	8.8	482	22	604	60	0.508940853	101	78	472	9
~~C10_145~~	~~529~~	~~15~~	~~401~~	~~9.1~~	~~591~~	~~17~~	~~1215~~	~~42~~	~~0.354187689~~	~~76~~	~~33~~		
~~C10_146~~	~~595~~	~~16~~	~~383.8~~	~~9.3~~	~~827~~	~~32~~	~~1487~~	~~38~~	~~0.241656366~~	~~65~~	~~26~~		
C10_147	499	13	500.4	8.4	481	15	500	34	0.392486583	100	100	500	8
C10_148	466	14	462.6	6.8	475	13	504	33	0.387809779	99	92	463	7
C10_149	536	24	498	20	491	21	628	71	0.437711864	93	79	498	20
C10_150-2	527	25	530	14	542	24	538	54	0.662105263	101	99	530	14

Table 14 LA-ICP-MS raw data of sample 22-11-15C5

Grain ID	Final Age ^{207}Pb/^{235}U	Final Age ^{207}Pb/^{235}U 2σ	Final Age ^{206}Pb/^{238}U	Final Age ^{206}Pb/^{238}U 2σ	Final Age ^{208}Pb/^{232}Th	Final Age ^{208}Pb/^{232}Th 2σ	Final Age ^{207}Pb/^{206}Pb	Final Age ^{207}Pb/^{206}Pb 2σ	^{232}Th/^{238}U	% Concordance (^{206}Pb/^{238}U)/ (^{207}Pb/^{235}U)	% Concordance (^{206}Pb/^{238}U)/ (^{207}Pb/^{206}Pb)	Preferred Age (Ma)	Preferred Age 2σ (Ma)
~~C5_1~~	~~-75~~	~~73~~	~~-120~~	~~120~~	~~7.03~~	~~0.21~~	~~1384~~	~~37~~	~~0.437068966~~	~~84~~	~~62~~		
C5_2	-180	110	-132	79	1.947	0.037	2705	21	0.517745303	99	99	2705	21
~~C5_3~~	~~-61~~	~~61~~	~~-170~~	~~170~~	~~6.61~~	~~0.23~~	~~1090~~	~~110~~	~~0.843771921~~	~~84~~	~~84~~		
C5_4	-57	31	-320	170	4.99	0.11	1213	55	1.591397849	98	97	1213	55
C5_5	-28	45	-43	79	9.52	0.21	936	60	0.302458548	90	69	645	13
C5_6	-250	280	-600	710	2.77	0.063	2261	25	1.331557923	93	88	2261	25
C5_7	-1	90	2	83	3.13	0.16	1810	36	0.315789474	98	100	1810	36
C5_8	-11	23	-16	26	8.44	0.37	1110	77	0.202733485	84	66	728	30
C5_9	-510	390	-500	380	2.77	0.072	2191	16	0.561649319	91	91	2191	16
~~C5_10~~	~~-6~~	~~-6~~	~~-9.3~~	~~-9.3~~	~~2~~	~~2~~			~~0.62745098~~	~~72~~			
C5_11	-290	170	-840	490	2.862	0.057	2216	32	1.441838867	93	87	2216	32
C5_12	60	580	80	500	2.028	0.038	2581	11	0.727943643	99	100	2581	11
~~C5_13~~	~~-70~~	~~140~~	~~-40~~	~~110~~	~~3.704~~	~~0.096~~	~~2506~~	~~60~~	~~0.609230769~~	~~77~~	~~62~~		
~~C5_14~~	~~222~~	~~29~~	~~93.1~~	~~9.6~~	~~5.05~~	~~0.17~~	~~3051~~	~~17~~	~~1.272727273~~	~~58~~	~~39~~		
~~C5_15~~	~~71~~	~~55~~	~~320~~	~~230~~	~~5.77~~	~~0.17~~	~~1370~~	~~330~~	~~1.003539823~~	~~97~~	~~75~~		

C5_16	-83	42	-390	200	5.363	0.075	1110	25	1.28342246	97	100	1110	25
C5_17	-4	17	-14	46	5.45	0.1	1052	62	0.684310019	100	104	1052	62
C5_18	29	83	70	180	2.66	0.17	2062	38	1.440806045	100	100	2062	38
C5_19	-292	94	-1460	490	5.476	0.087	1081	24	1.480235492	100	100	1081	24
C5_20	-12	16	-34	50	5.667	0.079	1064	28	0.808104887	99	99	1064	28
C5_21	22	25	55	65	12.59	0.23	915	34	0.65648517	86	54	494	9
C5_22	160	280	130	220	2.887	0.04	2054	11	0.603225806	96	93	2054	11
C5_23	-9	65	-90	340	10.98	0.43	860	200	1.095022624	96	66	564	21
C5_24	16	45	40	110	3.011	0.044	1855	34	1.025125628	100	100	1855	34
C5_25	276	60	298	66	2.503	0.05	2184	18	0.472250771	100	99	2184	18
C5_26	-90	460	-20	130	2.826	0.049	2274	10	0.282714055	93	86	2274	10
~~C5_27~~	~~189~~	~~46~~	~~145~~	~~36~~	~~2.94~~	~~0.12~~	~~2694~~	~~26~~	~~0.741176471~~	~~82~~	~~71~~		
~~C5_28~~	~~32~~	~~2.3~~	~~100.6~~	~~7~~	~~10.22~~	~~0.31~~	~~2209~~	~~19~~	~~1.594815825~~	~~57~~	~~27~~		
C5_29	-210	190	-540	480	5.61	0.17	1127	57	0.730538922	92	94	1127	57
C5_30	-9	27	-14	46	12.6	0.25	488	79	0.324338086	100	101	494	9
C5_31	-2	24	-2	61	5.496	0.079	1113	42	0.668252081	100	97	1113	42
C5_32	-3	16	-60	140	4.99	0.14	1173	80	2.10663199	100	101	1173	80
~~C5_33~~	~~-190~~	~~120~~	~~-540~~	~~350~~	~~3.768~~	~~0.094~~	~~1809~~	~~25~~	~~1.020864382~~	~~93~~	~~84~~		
C5_34	-1.21E+07	3.80E+06	-1.70E+07	5.40E+06	4.896	0.071	1188	26	0.438172043	100	101	1188	26
~~C5_35~~	~~370~~	~~180~~	~~850~~	~~420~~	~~3.41~~	~~0.12~~	~~1974~~	~~55~~	~~0.909836066~~	~~92~~	~~84~~		
C5_36	-24	15	-58	35	10.12	0.36	720	66	0.450980392	93	84	606	18
C5_37	-330	420	-390	510	2.776	0.092	2067	18	0.54011065	99	96	2067	18
C5_38	-90	120	-80	100	2.34	0.045	2296	11	0.456392887	101	100	2296	11
~~C5_39~~	~~-32~~	~~66~~	~~-120~~	~~230~~	~~5.58~~	~~0.18~~	~~1356~~	~~45~~	~~1.126005362~~	~~87~~	~~79~~		
C5_40	-480	230	-980	470	2.339	0.075	2296	21	1.123260437	100	100	2296	21
C5_41	-670	380	-370	210	2.342	0.026	2264	10	0.332684825	100	101	2264	10
C5_42	-960	480	-1490	760	2.956	0.099	1882	28	0.654185022	100	100	1882	28
C5_43	1.6	8.8	-20	270	10.74	0.54	860	120	5.63583815	90	67	579	29
C5_44	-55	30	-56	30	5.255	0.085	1103	35	0.246036524	101	102	1103	35
C5_45	-1000	750	-940	720	2.017	0.046	2586	18	0.665687919	100	101	2586	18
~~C5_46~~	~~28~~	~~58~~	~~29~~	~~53~~	~~8.77~~	~~0.27~~	~~1229~~	~~49~~	~~0.199397071~~	~~82~~	~~56~~		
~~C5_47~~	~~-63~~	~~36~~	~~-220~~	~~120~~	~~5.33~~	~~0.13~~	~~1047~~	~~46~~	~~0.836024845~~	~~100~~	~~106~~		
C5_48	-20	36	-24	41	5.239	0.097	1079	28	0.30358505	100	105	1079	28
C5_49	-70	260	-100	360	2.138	0.028	2462.5	9.5	0.95631068	100	101	2463	10
C5_50	-27	27	-78	78	12.44	0.39	750	140	0.576556777	91	67	501	15
C5_51	-73	86	-57	70	5.79	0.14	1124	61	0.221674877	88	92	1124	61
C5_52	-320	290	-310	280	2.392	0.076	2435	48	0.584558824	90	93	2435	48
C5_53	-100	40	-340	130	6.57	0.13	924	43	0.776957164	102	99	918	17
C5_54	-35	25	-103	78	10.07	0.32	595	96	0.765356265	101	103	614	19
~~C5_55~~	~~39.2~~	~~8.2~~	~~95~~	~~26~~	~~6.04~~	~~0.15~~	~~1906~~	~~41~~	~~0.518581081~~	~~75~~	~~52~~		
C5_56	-67	33	-200	110	6.06	0.12	969	41	0.777954005	101	101	983	21
C5_57	-40	39	-85	76	4.848	0.067	1197	20	0.546777547	100	101	1197	20
C5_58	-310	200	-260	160	2.553	0.058	2376	17	0.41322314	94	90	2376	17
C5_59	-180	190	-110	120	2.186	0.052	2436	17	0.36997539	98	100	2436	17

~~C5_60~~	~~-41~~	~~42~~	~~-52~~	~~55~~	~~8.43~~	~~0.25~~	~~1606~~	~~76~~	~~1.445859873~~	~~73~~	~~45~~		
C5_61	-43	35	-89	77	5.65	0.2	1175	50	0.62320442	89	90	1175	50
C5_62	-190	320	-370	600	3.14	0.12	1849	44	0.715982721	100	97	1849	44
C5_63	-11	44	-30	110	5.629	0.092	1069	33	0.63291966	100	99	1069	33
C5_64	-71	59	-130	110	5.59	0.22	1100	100	0.646699267	100	97	1100	100
C5_65	-48	45	-55	48	5.87	0.17	1029	41	0.229864253	100	99	1029	41
C5_66	-400	440	-150	160	2.426	0.053	2245	18	0.216483516	100	99	2245	18
C5_67	-11	12	-24	28	12.39	0.42	595	91	0.449949444	94	85	504	17
~~C5_68~~	~~-13~~	~~84~~	~~-6~~	~~44~~	~~8.81~~	~~0.32~~	~~1420~~	~~81~~	~~0.262068966~~	~~78~~	~~49~~		
~~C5_69~~	~~-0.2~~	~~1.4~~	~~-0.6~~	~~1.6~~	~~8.8~~	~~2~~	~~2790~~	~~270~~	~~0.610328638~~	~~69~~	~~30~~		
C5_70	177	58	141	40	2.428	0.059	2596	33	0.66927593	91	86	2596	33
C5_71	-58	57	-190	180	4.969	0.075	1223	35	0.890697674	100	97	1223	35
C5_72	-20	160	-200	1200	4.86	0.12	1275	36	2.357251908	92	95	1275	36
C5_73	-260	280	-290	310	2.449	0.043	2374	16	0.601521636	93	93	2374	16
C5_74	-27	78	-50	140	4.945	0.096	1197	20	0.518440905	99	99	1197	20
C5_75	-15	38	-50	140	5.366	0.066	1102	23	0.995249406	100	100	1102	23
C5_76	-27	56	-100	240	5.53	0.13	1093	49	1.220689655	100	98	1093	49
C5_77	-410	210	-310	160	2.367	0.052	2301	19	0.429292929	99	99	2301	19
~~C5_78~~	~~38~~	~~61~~	~~48~~	~~77~~	~~3.657~~	~~0.076~~	~~2462~~	~~19~~	~~0.545679012~~	~~78~~	~~64~~		
C5_79	330	140	165	71	3.065	0.061	2122	27	0.474576271	86	86	2122	27
~~C5_80~~	~~36.6~~	~~4.8~~	~~55.9~~	~~7.1~~	~~13.01~~	~~0.39~~	~~1948~~	~~56~~	~~0.903638151~~	~~58~~	~~24~~		
C5_81	-51	64	-63	79	4.77	0.16	1288	62	0.419323671	96	95	1288	62
C5_82	-4	17	-40	210	10.5	0.21	645	46	2.668010753	93	91	589	11
C5_83	-360	210	-190	110	2.357	0.03	2286	13	0.30406291	100	100	2286	13
~~C5_84~~	~~-13~~	~~41~~	~~-50~~	~~160~~	~~9.04~~	~~0.16~~	~~1231~~	~~38~~	~~1.403252944~~	~~82~~	~~55~~		
C5_85	-130	110	-280	230	2.872	0.055	1924	19	0.936602871	97	100	1924	19
C5_86	-148	51	-209	72	2.743	0.035	1998	21	0.634730539	99	101	1998	21
C5_87	-2	62	0	210	5.42	0.14	1089	28	0.881643836	95	101	1089	28
C5_88	-660	590	-380	340	2.269	0.063	2425	13	0.349021241	97	97	2425	13
C5_89	-260	160	-260	170	2.786	0.034	1990	14	0.466475096	100	100	1990	14
~~C5_90~~	~~55.3~~	~~6~~	~~85~~	~~11~~	~~6.56~~	~~0.16~~	~~2356~~	~~30~~	~~0.94721826~~	~~61~~	~~39~~		
C5_91	70	45	67	45	10.08	0.11	605	33	0.191988131	98	101	611	7
~~C5_92~~	~~357~~	~~63~~	~~240~~	~~47~~	~~3.006~~	~~0.031~~	~~2391~~	~~10~~	~~0.473801285~~	~~87~~	~~77~~		
~~C5_93~~	~~124~~	~~26~~	~~123~~	~~25~~	~~3.79~~	~~0.12~~	~~2380~~	~~45~~	~~0.414081886~~	~~79~~	~~64~~		
C5_94	-43	33	-101	77	5.334	0.094	1055	41	0.597210113	99	105	1055	41
C5_95	-88	53	-143	90	2.398	0.046	2248	17	0.902741852	100	100	2248	17
C5_96	-128	74	-590	350	5.059	0.067	1176	23	1.247240618	100	99	1176	23
C5_97	23	28	62	79	4.431	0.072	1279	32	0.830543933	99	103	1279	32
C5_98	-220	180	-430	360	2.72	0.047	1990	13	0.931677019	99	102	1990	13
C5_99	-88	72	-38	32	5.35	0.14	1130	23	0.118626431	94	98	1130	23
C5_100	-3.1	5	-7	13	11.75	0.37	573	95	0.474940334	101	93	531	16
C5_101	5600	1700	5500	1700	2.331	0.03	2278	13	0.532972973	100	101	2278	13
C5_102	-120	230	-80	140	2.24	0.1	2510	25	0.34051144	98	95	2510	25
C5_103	-30	110	-3	15	2.696	0.036	2178	17	0.055527211	96	94	2178	17

~~C5_104~~	~~20.5~~	~~5.9~~	~~62~~	~~12~~	~~9.36~~	~~0.42~~	~~2356~~	~~72~~	~~1.039426523~~	~~55~~	~~29~~		
~~C5_105~~	~~-3~~	~~24~~	~~-5~~	~~67~~	~~5.94~~	~~0.15~~	~~1432~~	~~57~~	~~1.001560062~~	~~83~~	~~70~~		
C5_106	-16	84	-4	42	1.92	0.043	2651	30	0.37431694	100	102	2651	30
C5_107	-240	200	-170	180	1.989	0.057	2698	18	0.804761905	98	98	2698	18
C5_108	-200	110	-240	130	5.206	0.087	1123	31	0.332577132	101	101	1123	31
~~C5_109~~	~~-43~~	~~41~~	~~-38~~	~~38~~	~~4.788~~	~~0.079~~	~~1473~~	~~23~~	~~0.31555783~~	~~91~~	~~83~~		
C5_110	-17	6.6	-168	65	10.05	0.19	600	58	2.101265823	99	102	613	11
C5_111	-430	420	-500	470	2.199	0.044	2421	17	0.694949495	99	100	2421	17
C5_112	-2200	1000	-2400	1100	2.635	0.032	2051	16	0.579820318	100	101	2051	16
C5_113	-28	16	-131	76	14.66	0.39	612	68	0.802469136	91	70	429	11
~~C5_114~~	~~-61~~	~~82~~	~~-210~~	~~290~~	~~10.41~~	~~0.3~~	~~1419~~	~~76~~	~~1.15916955~~	~~71~~	~~42~~		
C5_115	-93	45	-166	84	4.851	0.092	1191	31	0.533096927	100	102	1191	31
C5_116	-270	180	-190	130	2.173	0.025	2442	11	0.44048583	100	100	2442	11
C5_117	-76	47	-130	79	5.36	0.1	1112	34	0.468654434	100	99	1112	34
~~C5_118~~	~~-0.3~~	~~2.5~~	~~-2.4~~	~~6~~	~~8.2~~	~~1.9~~	~~3050~~	~~320~~	~~0.798245614~~	~~63~~	~~29~~		
~~C5_119~~	~~0~~	~~23~~	~~-3~~	~~42~~	~~9.28~~	~~0.24~~	~~1158~~	~~58~~	~~0.494623656~~	~~82~~	~~57~~		
~~C5_120~~	~~138~~	~~29~~	~~100~~	~~24~~	~~2.61~~	~~0.041~~	~~2484~~	~~15~~	~~0.457489879~~	~~89~~	~~84~~		
C5_121	-140	110	-130	85	2.213	0.034	2450	15	0.46721044	99	98	2450	15
~~C5_122~~	~~-96~~	~~71~~	~~-110~~	~~81~~	~~4.258~~	~~0.08~~	~~1644~~	~~28~~	~~0.381570997~~	~~88~~	~~83~~		
~~C5_123~~	~~-80~~	~~79~~	~~-230~~	~~220~~	~~5.419~~	~~0.087~~	~~1314~~	~~36~~	~~0.741391427~~	~~92~~	~~83~~		
C5_124	-210	310	-180	260	2.415	0.043	2277	29	0.468023256	97	98	2277	29
C5_125	-141	64	-130	58	5.537	0.07	1061	25	0.231060606	97	101	1061	25
C5_126	-132	51	-185	72	12.19	0.16	506	27	0.267027027	97	101	510	7
C5_127	-1020	520	-460	240	2.357	0.029	2283.4	7.6	0.243154762	99	100	2283	8
C5_128	-21	13	-139	88	5.34	0.12	1099	50	1.388235294	97	101	1099	50
C5_129	-179	59	-212	71	5.67	0.089	1074	24	0.315315315	97	98	1074	24
C5_130	56	80	130	210	4.574	0.073	1283	24	0.731648031	98	100	1283	24

APPENDIX II

Detrital zircon grain shape

Appendix II contains detrital zircon grain shape characterization of the late Paleozoic diamictite samples from Victoria Land, Antarctica. Crossed out data represent not concordant ages which were excluded from the interpretations; for those data the grain shape was not determined

Table 15 Grain shape in relation with ages of the sample 22-01-15C3

Grain ID	Preferred age (Ma)	2σ (Ma)	Grain shape
C3-1_1	557	10	Subhedral
C3-1_2	538	10	Sub-Rounded
C3-1_3	723	22	Rounded
C3-1_4	524	10	Rounded
C3-1_5	1430	29	Rounded
C3-1_6	567	10	Rounded
C3-1_7	610	13	Rounded
C3-1_8	975	15	Rounded
C3-1_9	1004	12	Rounded
C3-1_10	500	8	Sub-Rounded
C3-1_11	590	13	Rounded
C3-1_12	991	20	Rounded
C3-1_13	582	10	Rounded
C3-1_14	518	8	Rounded
C3-1_15	1443	29	Rounded
C3-1_16	1451	25	Sub-Rounded
C3-1_17	620	12	Rounded
C3-1_18	1072	24	Rounded
C3-1_19	570	8	Rounded
C3-1_20	535	13	Sub-Rounded
C3-1_21	1457	40	Rounded
C3-1_22	1089	18	Sub-Rounded
C3-1_23	594	14	Rounded
C3-1_24	610	9	Rounded
C3-1_25	1428	72	Sub-Rounded
C3-1_26	1821	15	Rounded
C3-1_27	1093	27	Rounded
~~C3-1_28~~			
C3-1_29	1069	32	Sub-Rounded
C3-1_30-2	641	10	Sub-Rounded
C3-1_31	681	14	Sub-Rounded
C3-1_32	1352	45	Rounded
~~C3-1_33~~			
C3-1_34	612	12	Rounded
C3-1_35	1612	30	Rounded
C3-1_36	537	14	Rounded
C3-1_37	381	16	Euhedral
C3-1_38	1438	22	Subhedral
C3-1_39	1017	93	Sub-Rounded
C3-1_40	856	20	Sub-Rounded
C3-1_41	465	12	Sub-Rounded
C3-1_42	501	10	Subhedral
C3-1_43	1577	22	Sub-Rounded
C3-1_44	1439	22	Subhedral
C3-1_45	542	9	Rounded
~~C3-1_46~~			
C3-1_47	1174	26	Rounded
C3-1_48	1422	37	Rounded
C3-1_49	553	10	Rounded
~~C3-1_50~~			
C3-1_51	464	9	Rounded
C3-1_52	499	13	Rounded
~~C3-1_53~~			
C3-1_54	580	9	Rounded
C3-1_55	507	10	Sub-Rounded
C3-1_56-1	1564	30	Rounded
C3-1_57	513	13	Sub-Rounded
C3-1_58	1209	79	Sub-Rounded
C3-1_59	1455	49	Sub-Rounded
C3-1_60	629	11	Rounded
C3-1_61	571	13	Rounded
C3-1_62	540	16	Sub-Rounded
C3-1_63	564	13	Rounded
C3-1_64	2594	36	Rounded
C3-1_65	538	8	Rounded
C3-1_66-1	576	14	Rounded
C3-1_67	1438	32	Sub-Rounded
C3-1_68	867	10	Rounded
C3-1_69	375	5	Subhedral
C3-1_70	362	5	Euhedral
C3-1_71-2	896	13	Rounded
C3-1_72	582	19	Rounded
C3-1_73	840	19	Rounded
C3-1_74	582	5	Rounded
C3-1_75	1321	58	Rounded
C3-1_76	564	10	Rounded
C3-1_77	545	10	Sub-Rounded
C3-1_78-1	525	10	Sub-Rounded
C3-1_79	545	16	Subhedral
C3-1_80	1573	29	Subhedral
C3-1_81	1145	43	Sub-Rounded
C3-1_82	505	7	Rounded
C3-1_83	528	7	Subhedral
C3-1_84	587	8	Rounded
C3-1_85	528	7	Sub-Rounded
~~C3-1_86~~			
C3-1_87	589	16	Sub-Rounded
C3-1_88	514	11	Subhedral
C3-1_89	1409	20	Sub-Rounded
C3-1_90	929	18	Sub-Rounded
C3-1_91	567	13	Sub-Rounded
C3-1_92	1671	28	Rounded
C3-1_93	2662	22	Rounded
~~C3-1_94~~			
C3-1_95	1455	26	Rounded
C3-1_96	497	14	Subhedral
C3-1_97	553	9	Rounded
C3-1_98	3253	24	Rounded
C3-1_99-1	584	10	Rounded
C3-1_100	549	9	Rounded
C3-1_101	573	12	Rounded
C3-1_102	526	13	Subhedral
C3-1_103	1243	57	Sub-Rounded

C3-1_104	501	8	Rounded
~~C3-1_105~~			
C3-1_106	1061	29	Rounded
C3-1_107	1462	21	Subhedral
C3-1_108-1	432	19	Subhedral
C3-1_109	526	17	Rounded
C3-1_110	1061	35	Sub-Rounded
C3-1_111	1064	74	Sub-Rounded
C3-1_112	1531	12	Rounded
C3-1_113-1	1449	24	Sub-Rounded
C3-1_114	573	13	Rounded
C3-1_115	687	23	Rounded
~~C3-1_116~~			
C3-1_117	536	17	Subhedral
C3-1_118	555	10	Rounded
~~C3-1_119~~			
C3-1_120	601	10	Sub-Rounded
C3-1_121	1431	36	Rounded
C3-1_122	1573	15	Rounded
C3-1_123	528	17	Sub-Rounded
C3-1_124	1090	18	Rounded
C3-1_125	557	10	Sub-Rounded
C3-1_126	2029	16	Rounded
C3-1_128	1267	56	Subhedral
C3-1_129	382	8	Sub-Rounded
C3-1_130	3082	18	Rounded
C3-1_131	1453	16	Sub-Rounded
C3-1_132	2114	22	Rounded
C3-1_133	1109	14	Rounded
~~C3-1_134~~			
C3-1_135	527	12	Subhedral
C3-1_136	501	18	Sub-Rounded
C3-1_137	571	13	Rounded
C3-1_138	517	13	Sub-Rounded
C3-1_139	585	10	Rounded
C3-1_140-1	1423	28	Rounded
C3-1_141	715	13	Rounded
C3-1_142	1078	53	Rounded
C3-1_143	600	19	Sub-Rounded
C3-1_144	515	13	Sub-Rounded
C3-1_145	1223	36	Rounded
C3-1_146	1906	23	Rounded
C3-1_147	1171	35	Rounded
~~C3-1_148~~			
C3-1_149	554	10	Sub-Rounded
C3-1_150	551	9	Sub-Rounded

Table 16 Grain shape in relation with ages of the sample 03-01-15C3

Grain ID	Preferred age (Ma)	2σ (Ma)	Grain shape
C3-2_1	1083	17	Rounded
C3-2_2	1224	22	Rounded
C3-2_3	585	9	Rounded
C3-2_4	512	12	Sub-Rounded
C3-2_5	851	20	Rounded
C3-2_6	523	12	Subhedral
C3-2_7	515	13	Subhedral
C3-2_8	526	14	Rounded
C3-2_9	786	25	Rounded
C3-2_10	630	16	Rounded
C3-2_11	573	9	Subhedral
C3-2_12	814	23	Rounded
C3-2_13	534	10	Subhedral
C3-2_14	548	15	Rounded
C3-2_15	572	12	Subhedral
C3-2_16	555	11	Subhedral
C3-2_17	525	16	Sub-Rounded
C3-2_18	666	32	Rounded
C3-2_19-1	1452	16	Sub-Rounded
C3-2_20	586	10	Rounded
C3-2_21	584	9	Rounded
C3-2_22	944	16	Rounded
C3-2_23	2238	22	Sub-Rounded
C3-2_24	1107	18	Rounded
C3-2_25	917	17	Sub-Rounded
C3-2_26	2371	16	Rounded
C3-2_27	505	19	Sub-Rounded
C3-2_28	553	10	Sub-Rounded
C3-2_29	831	21	Sub-Rounded
C3-2_30-1	527	11	Rounded
C3-2_31	1454	22	Rounded
C3-2_32	2883	10	Rounded
C3-2_33-2	557	7	Subhedral
C3-2_34	600	16	Rounded
C3-2_35	583	11	Rounded
C3-2_36	608	15	Rounded
C3-2_37	1892	19	Rounded
C3-2_38	1094	80	Rounded
C3-2_39	591	10	Sub-Rounded
C3-2_40	602	12	Rounded
C3-2_41	635	12	Rounded
C3-2_42	976	16	Rounded
C3-2_43	515	17	Rounded
C3-2_44	515	12	Subhedral
C3-2_45	514	15	Rounded
C3-2_46	1583	20	Rounded
C3-2_47	536	8	Sub-Rounded
C3-2_48	586	14	Rounded
C3-2_49	899	14	Sub-Rounded
C3-2_50	1514	79	Rounded
C3-2_51	1774	10	Rounded
C3-2_52	1009	37	Rounded
C3-2_53	1030	55	Rounded
C3-2_54	1077	30	Rounded
C3-2_55	468	11	Subhedral
C3-2_56	1096	16	Rounded
C3-2_57	504	17	Rounded
C3-2_58	709	19	Rounded
C3-2_59	679	13	Rounded
C3-2_60	594	10	Rounded
C3-2_61	523	17	Subhedral
C3-2_62	540	13	Sub-Rounded
C3-2_63	613	10	Rounded
C3-2_64	1457	16	Rounded
C3-2_65	3209	12	Sub-Rounded
C3-2_66	512	12	Subhedral
C3-2_67	539	17	Rounded
C3-2_68	1106	30	Rounded
C3-2_69	715	25	Rounded
C3-2_70	501	18	Subhedral
C3-2_71	831	16	Rounded
C3-2_72-1	524	11	Subhedral
C3-2_73	423	13	Subhedral

C3-2_74	551	11	Rounded
C3-2_75	491	9	Sub-Rounded
C3-2_76	548	13	Rounded
C3-2_77	758	28	Rounded
C3-2_78	506	14	Rounded
C3-2_79	532	12	Subhedral
C3-2_80	913	33	Rounded
~~C3-2_81~~			
C3-2_83	1464	15	Rounded
C3-2_84	554	10	Rounded
C3-2_85	1191	41	Rounded
C3-2_86	621	15	Sub-Rounded
C3-2_87	864	37	Rounded
C3-2_88	802	26	Rounded
C3-2_89	1378	29	Rounded
C3-2_90	558	11	Rounded
C3-2_91	524	8	Rounded
C3-2_92	563	9	Rounded
C3-2_93	581	14	Rounded
C3-2_94	501	10	Sub-Rounded
C3-2_95	1793	36	Rounded
C3-2_96	553	10	Rounded
C3-2_97	516	9	Rounded
C3-2_98	546	10	Rounded
C3-2_99	2242	13	Rounded
C3-2_100	1427	19	Subhedral
~~C3-2_101~~			
C3-2_102	518	8	Rounded
C3-2_103	1957	13	Rounded
C3-2_104	603	15	Sub-Rounded
C3-2_105	580	11	Rounded
C3-2_106	2249	19	Rounded
C3-2_107	1043	40	Sub-Rounded
C3-2_108	610	12	Rounded
C3-2_109	558	20	Rounded
C3-2_110	618	23	Sub-Rounded
C3-2_111	526	13	Rounded
C3-2_112	534	10	Rounded
C3-2_113	874	21	Rounded
C3-2_114	1063	28	Sub-Rounded
C3-2_115	1661	31	Rounded
C3-2_116	522	10	Subhedral
C3-2_117	1175	32	Rounded
C3-2_118	520	9	Sub-Rounded
C3-2_119	535	10	Rounded
C3-2_120	472	17	Rounded
C3-2_121	731	16	Rounded
C3-2_122	578	12	Rounded
C3-2_123	606	20	Sub-Rounded
C3-2_124	605	9	Rounded
C3-2_125	583	11	Rounded
C3-2_126	542	9	Rounded
C3-2_127	514	8	Subhedral
C3-2_128	510	20	Subhedral
~~C3-2_129~~			
C3-2_130	2169	12	Rounded
C3-2_131	676	14	Sub-Rounded
C3-2_132	577	9	Rounded
C3-2_133	768	35	Rounded
C3-2_134	2396	28	Rounded
C3-2_135	579	20	Rounded
C3-2_136	922	23	Sub-Rounded
C3-2_137	2684	12	Rounded
C3-2_138	570	12	Sub-Rounded
C3-2_139	2288	10	Rounded
C3-2_140	629	15	Rounded
C3-2_141	579	13	Rounded
C3-2_142	911	16	Rounded
C3-2_143	1106	31	Rounded
C3-2_144	587	11	Subhedral
C3-2_145	1081	27	Rounded
C3-2_146	588	10	Rounded
C3-2_147	1102	22	Rounded
C3-2_148	501	16	Sub-Rounded
C3-2_149	597	8	Rounded
C3-2_150	553	10	Subhedral

Table 17 Grain shape in relation with ages of the sample 04-01-15C10

Grain ID	Preferred age (Ma)	2σ (Ma)	Grain shape
C10_1	511	15	Subhedral
C10_2	485	16	Subhedral
C10_3	498	12	Sub-Rounded
C10_4	460	19	Subhedral
C10_5-1	496	10	Subhedral
C10_6	894	31	Rounded
C10_7	507	11	Euhedral
C10_8	511	12	Sub-Rounded
~~C10_9~~			
~~C10_10~~			
C10_11	483	10	Sub-Rounded
C10_12	498	9	Sub-Rounded
C10_13	467	9	Sub-Rounded
C10_14	489	8	Subhedral
C10_15	478	9	Subhedral
C10_16	1314	40	Rounded
C10_17	510	12	Subhedral
C10_18	506	14	Euhedral
~~C10_19~~			
~~C10_20~~			
C10_21-1	497	11	Subhedral
C10_22	499	18	Sub-Rounded
C10_23	494	12	Subhedral
C10_24	916	20	Rounded
C10_25	573	15	Rounded
C10_26	464	9	Subhedral
C10_27	484	14	Sub-Rounded
C10_28	473	19	Sub-Rounded
C10_29	491	8	Sub-Rounded
~~C10_30~~			
C10_31-1	505	14	Subhedral
C10_32	518	15	Subhedral
C10_33	836	15	Rounded
C10_34	500	10	Subhedral
C10_35	487	28	Euhedral
C10_36	468	18	Euhedral
C10_37	504	10	Subhedral
C10_38	515	9	Subhedral
C10_39	489	9	Subhedral
~~C10_40~~			
C10_41	480	16	Subhedral
C10_42	431	16	Subhedral
C10_43	513	13	Subhedral
~~C10_44~~			

C10_45	479	14	Subhedral
C10_46	423	15	Sub-Rounded
C10_47	478	10	Euhedral
C10_48	2346	21	Sub-Rounded
C10_49	481	17	Sub-Rounded
C10_50	464	12	Subhedral
C10_51	520	14	Sub-Rounded
C10_52	483	9	Euhedral
C10_53-2	501	7	Sub-Rounded
C10_54	501	10	Subhedral
C10_55	898	15	Sub-Rounded
C10_56	452	16	Sub-Rounded
C10_57	437	12	Subhedral
C10_58	544	10	Rounded
C10_59	443	15	Subhedral
C10_60	459	12	Subhedral
C10_61	459	9	Subhedral
C10_62	465	17	Subhedral
C10_63	459	11	Subhedral
~~C10_64~~			
C10_65	465	10	Subhedral
C10_66	479	12	Subhedral
C10_67	1105	49	Rounded
C10_68	471	9	Sub-Rounded
C10_69	463	9	Sub-Rounded
C10_70	1076	45	Rounded
C10_71	461	8	Subhedral
C10_72	467	15	Sub-Rounded
C10_73	453	24	Subhedral
C10_74	448	16	Sub-Rounded
C10_75	441	19	Subhedral
C10_76-1	498	19	Subhedral
C10_77	470	16	Subhedral
C10_78	464	14	Subhedral
C10_79	439	18	Sub-Rounded
C10_80-1	478	11	Sub-Rounded
C10_81	442	11	Subhedral
C10_82	481	12	Subhedral
C10_83	439	15	Subhedral
C10_84	506	12	Subhedral
C10_85	504	9	Subhedral
C10_86	470	10	Subhedral
C10_87	452	9	Euhedral
C10_88	469	10	Sub-Rounded
~~C10_89~~			
C10_90-2	468	9	Sub-Rounded
C10_91	487	14	Sub-Rounded
C10_92	458	14	Subhedral
C10_93	911	20	Rounded
C10_94	460	26	Subhedral
C10_95	1255	32	Rounded
~~C10_96~~			
C10_97	461	18	Subhedral
C10_98	510	8	Subhedral
C10_99	481	13	Subhedral
C10_100	506	10	Sub-Rounded
C10_101	485	10	Subhedral
C10_102	533	9	Sub-Rounded
C10_103	482	8	Subhedral
C10_104	462	15	Sub-Rounded
C10_105	500	15	Subhedral
C10_106	499	10	Subhedral
C10_107	414	11	Subhedral
C10_108	448	15	Subhedral
~~C10_109~~			
~~C10_110~~			
C10_111	482	13	Sub-Rounded
C10_112	495	11	Subhedral
C10_113	466	26	Subhedral
C10_114	440	20	Sub-Rounded
C10_115-1	496	11	Subhedral
C10_116	483	13	Subhedral
C10_117	495	10	Sub-Rounded
C10_118	448	9	Subhedral
C10_119	497	6	Euhedral
~~C10_120~~			
C10_121	1144	85	Subhedral
C10_122	509	8	Subhedral
C10_123	520	10	Subhedral
C10_124	492	10	Euhedral
C10_125	468	18	Euhedral
~~C10_126~~			
C10_127	488	10	Subhedral
C10_128	481	11	Subhedral
C10_129	465	12	Subhedral
C10_130	528	8	Subhedral
C10_131	504	10	Sub-Rounded
~~C10_132~~			
~~C10_133~~			
C10_134	493	11	Euhedral
~~C10_135~~			
C10_136	488	10	Subhedral
C10_137	474	15	Subhedral
C10_138	477	20	Subhedral
C10_139	499	9	Rounded
C10_140	491	12	Subhedral
C10_141	492	25	Subhedral
C10_142	457	7	Sub-Rounded
~~C10_143~~			
C10_144	472	9	Subhedral
~~C10_145~~			
~~C10_146~~			
C10_147	500	8	Subhedral
C10_148	463	7	Subhedral
C10_149	498	20	Subhedral
C10_150-2	530	14	Subhedral

Table 18 Grain shape in relation with ages of the sample 22-11-15C5

Grain ID	Preferred age (Ma)	2σ (Ma)	Grain shape
~~C5_1~~			
C5_2	2705	21	Rounded
~~C5_3~~			
C5_4	1213	55	ND*
C5_5	645	13	ND*
C5_6	2261	25	ND*
C5_7	1810	36	ND*
C5_8	728	30	ND*
C5_9	2191	16	ND*
~~C5_10~~			
C5_11	2216	32	Rounded
C5_12	2581	11	Sub-Rounded
~~C5_13~~			
~~C5_14~~			

~~C5_15~~			
C5_16	1110	25	Subhedral
C5_17	1052	62	Subhedral
C5_18	2062	38	Rounded
C5_19	1081	24	Subhedral
C5_20	1064	28	Sub-Rounded
C5_21	494	9	Euhedral
C5_22	2054	11	Sub-Rounded
C5_23	564	21	Subhedral
C5_24	1855	34	Sub-Rounded
C5_25	2184	18	Subhedral
C5_26	2274	10	Sub-Rounded
~~C5_27~~			
~~C5_28~~			
C5_29	1127	57	Subhedral
C5_30	494	9	Subhedral
C5_31	1113	42	Rounded
C5_32	1173	80	Rounded
~~C5_33~~			
C5_34	1188	26	Sub-Rounded
~~C5_35~~			
C5_36	606	18	Rounded
C5_37	2067	18	Sub-Rounded
C5_38	2296	11	Rounded
~~C5_39~~			
C5_40	2296	21	Rounded
C5_41	2264	10	Rounded
C5_42	1882	28	Rounded
C5_43	579	29	Subhedral
C5_44	1103	35	Sub-Rounded
C5_45	2586	18	Rounded
~~C5_46~~			
~~C5_47~~			
C5_48	1079	28	Subhedral
C5_49	2463	10	Sub-Rounded
C5_50	501	15	Subhedral
C5_51	1124	61	Sub-Rounded
C5_52	2435	48	Rounded
C5_53	918	17	Subhedral
C5_54	614	19	Rounded
~~C5_55~~			
C5_56	983	21	Sub-Rounded
C5_57	1197	20	Subhedral
C5_58	2376	17	Rounded
C5_59	2436	17	Rounded
~~C5_60~~			
C5_61	1175	50	Sub-Rounded
C5_62	1849	44	Sub-Rounded
C5_63	1069	33	Rounded
C5_64	1100	100	Sub-Rounded
C5_65	1029	41	Sub-Rounded
C5_66	2245	18	Rounded
C5_67	504	17	Sub-Rounded
~~C5_68~~			
~~C5_69~~			
C5_70	2596	33	Rounded
C5_71	1223	35	Sub-Rounded
C5_72	1275	36	Sub-Rounded
C5_73	2374	16	Rounded
C5_74	1197	20	Sub-Rounded
C5_75	1102	23	Rounded
C5_76	1093	49	Rounded
C5_77	2301	19	Rounded
~~C5_78~~			
C5_79	2122	27	Rounded
~~C5_80~~			
C5_81	1288	62	Rounded
C5_82	589	11	Sub-Rounded
C5_83	2286	13	Subhedral
~~C5_84~~			
C5_85	1924	19	Rounded
C5_86	1998	21	Rounded
C5_87	1089	28	Rounded
C5_88	2425	13	Rounded
C5_89	1990	14	Rounded
~~C5_90~~			
C5_91	611	7	Rounded
~~C5_92~~			
~~C5_93~~			
C5_94	1055	41	Rounded
C5_95	2248	17	Rounded
C5_96	1176	23	Sub-Rounded
C5_97	1279	32	Sub-Rounded
C5_98	1990	13	Sub-Rounded
C5_99	1130	23	Rounded
C5_100	531	16	Euhedral
C5_101	2278	13	Rounded
C5_102	2510	25	Rounded
C5_103	2178	17	Rounded
~~C5_104~~			
~~C5_105~~			
C5_106	2651	30	Rounded
C5_107	2698	18	Rounded
C5_108	1123	31	Rounded
~~C5_109~~			
C5_110	613	11	Rounded
C5_111	2421	17	Rounded
C5_112	2051	16	Subhedral
C5_113	429	11	Subhedral
~~C5_114~~			
C5_115	1191	31	Sub-Rounded
C5_116	2442	11	Rounded
C5_117	1112	34	Rounded
~~C5_118~~			
~~C5_119~~			
~~C5_120~~			
C5_121	2450	15	Rounded
~~C5_122~~			
~~C5_123~~			
C5_124	2277	29	Rounded
C5_125	1061	25	Rounded
C5_126	510	7	Subhedral
C5_127	2283	8	Rounded
C5_128	1099	50	Rounded
C5_129	1074	24	Subhedral
C5_130	1283	24	Subhedral

*N.D. = not determined.

APPENDIX III

Petrology of IODP Site U1521 clasts

This section shows the petrographic descriptions of gravel-sized clasts sampled from IODP Site U1521 core. List of analyzed clasts and their position along the core is shown in Table 3. Petrographic analysis was carried out with Leica DMLP polarizer microscopy equipped with a Leica ICC50 HD camera on polished thin sections. Each description is coupled with photomicrographs underlying representative features and microstructures. At the end of the appendix Table 20 summarizes clasts classification and Table 37 shows lithological percentages of lithic grains composing the > 2mm sieved fraction from bulk diamictite samples.

Sample 374-U1521A-29R-6W, 59-63 cm - Meta-granite

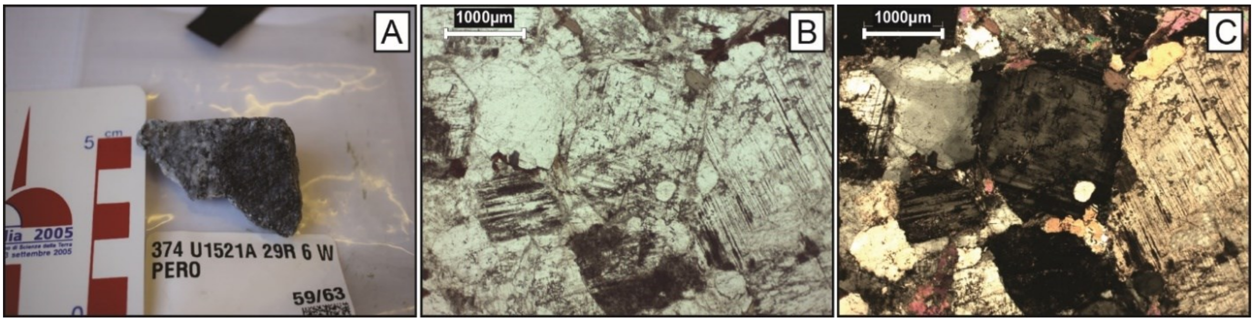

Figure 40 A) Macroscopic picture of the clast; B) PPL photomicrograph (2.5x); C) XPL photomicrograph (2.5x).

The clast is sub-angular. The rock is medium-grained, heterogranular, and it is characterized by a weak gneissic texture. The main mineralogical constituents are anhedral quartz, which usually shows undulose extinction and broad orientation, and subhedral plagioclase, slightly replaced by sericite aggregates; sometimes chemical zonation occurs within plagioclase crystals. K-feldspar, both orthoclase and microcline, occurs. Biotite represents 10-12% of the rocks; white mica is common.

Sample 374-U1521A-30R-3W, 85-89 cm - Basalt

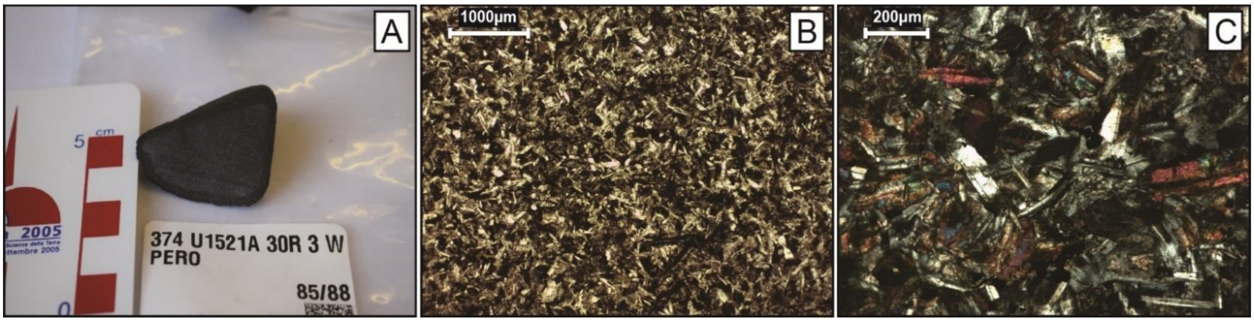

Figure 41 A) Macroscopic picture of the clast; B) PPL photomicrograph (2.5x); C) XPL photomicrograph (10x).

The sample is rounded. The rock is holocrystalline, with isotropic, very fine grained sub-ophitic texture. The main components are plagioclase and clinopyroxene. Opaque minerals are common.

Sample 374-U1521A-35R-3W, 65-72 cm - Granite

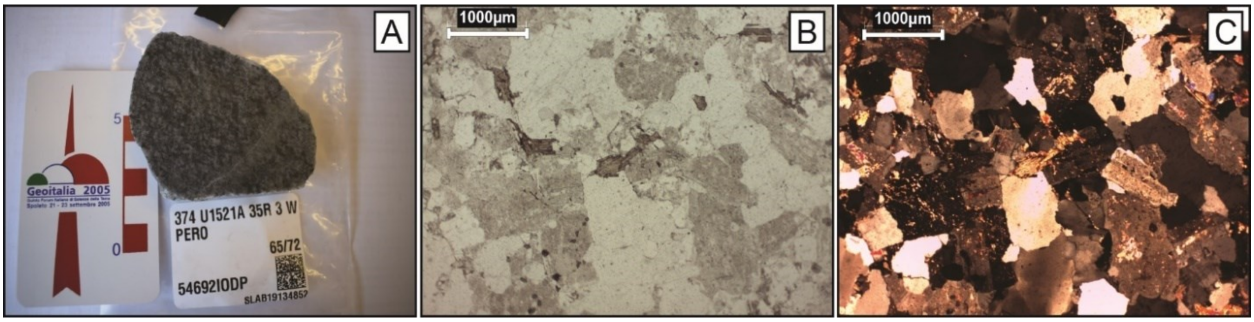

Figure 42 A) Macroscopic picture of the clast; B) PPL photomicrograph (2.5x); C) XPL photomicrograph (2.5x).

Sub-rounded clast of isotropic, fine-grained holocrystalline igneous rock with hypidiomorphic to allotriomorphic texture. Anhedral quartz with marked undulose extinction is the most abundant mineral (ca. 45%). Orthoclase (ca. 25%) is more common than plagioclase (ca. 15%); both feldspars are lightly altered by sericite/clay minerals aggregates. Mafic minerals are rare (<5%): chlorite replaces biotite (and/or hornblende); secondary white mica crystals are present, usually coupled with chlorite and sometimes as K-feldspar alteration.

Sample 374-U1521A-37R-3W, 110-113 cm - Limestone

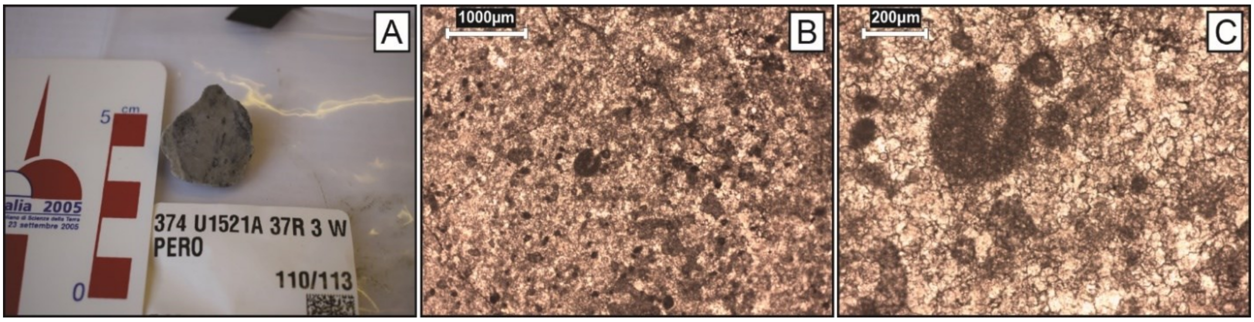

Figure 43 A) Macroscopic picture of the clast; B) PPL photomicrograph (2.5x); C) PPL photomicrograph (10x).

Sub-rounded clast of carbonate rock, with isotropic texture, fine to medium grained, mud-supported heterogranular from micrite to sparite grain size. The main mineralogical component is calcite, that has euhedral to anhedral habitus. Some portions of the sample contain peloids that are almost completely superimposed by newly formed microsparite but in some cases they are preserved. Accessory minerals are oxides and opaque minerals.

Sample 374-U1521A-38R-1W, 110-113 cm – Biotite-Hornblende granite

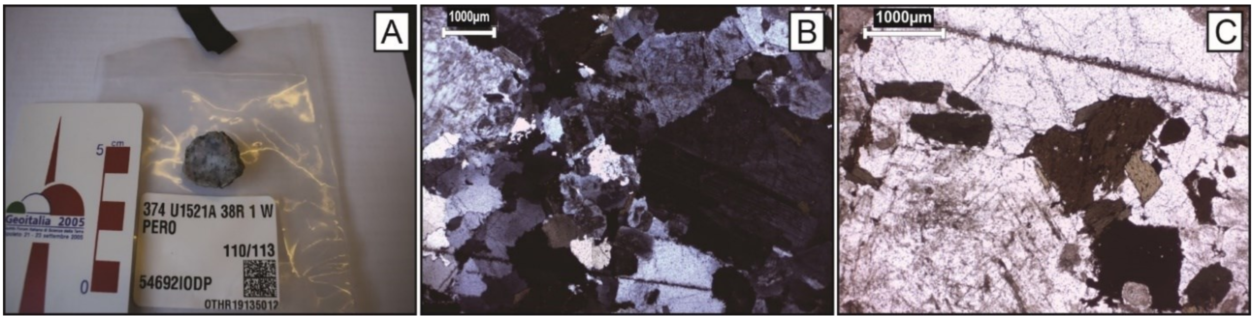

Figure 44 A) Macroscopic picture of the clast; B) XPL photomicrograph (1.6x); C) XPL photomicrograph (2.5x).

The sample is medium-grained, slightly porphyritic, holocrystalline intrusive rock with isotropic texture. The main constituent is quartz (ca. 40%) which usually form anhedral crystals with weak undulose extinction. Plagioclase represents ca. 30% of the whole volume and usually subhedral, sometimes slightly porphyritic crystals which sometimes show chemical zonation; plagioclase is partially replaced by sericite and clay minerals aggregates. Alkali feldspar (orthoclase) forms subhedral, sometimes slightly porphyritic, crystals which represent ca. 20% of the whole. Orthoclase is partially replaced by sericite and clay minerals aggregates. Mafic minerals are ca. 10% of the whole and they are in the same proportionality biotite and green hornblende. Titanite is a common accessory mineral phase.

Sample 374-U1521A-38R-2W, 134-140 cm - (Meta)-Graywacke

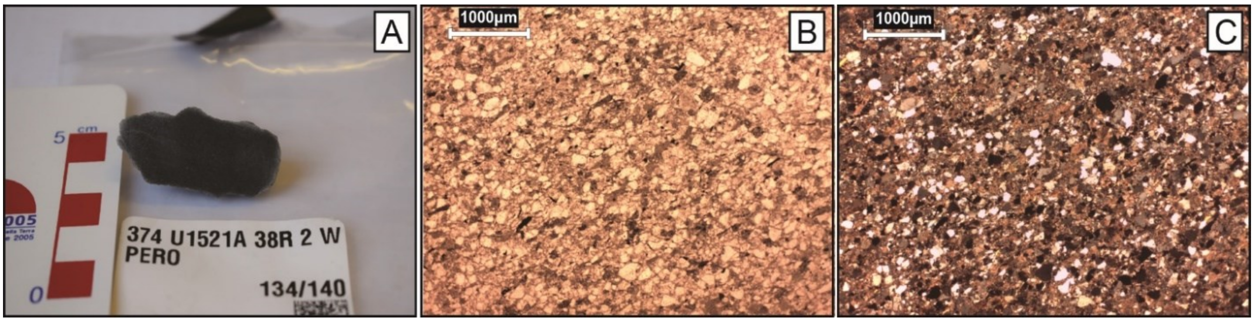

Figure 45 A) Macroscopic picture of the clast; B) PPL photomicrograph (2.5x); C) XPL photomicrograph (2.5x).

The sample has sub-angular shape. Fine-grained siliciclastic rock showing weak isorientation, with abundance of mud-size matrix; carbonate cement is abundant, too. Clasts are sub-angular to sub-rounded and they are mainly made up of mono-crystalline quartz, with normal and undulose extinction; plagioclase clasts are less than 10%; lithic fragments are prevalently micaceous phyllites and minor quartzites. White mica crystals are common as well as graphite; opaque minerals and zircons are accessory phases.

Sample 374-U1521A-38R-3W, 24-28 cm - Quartz-arenite

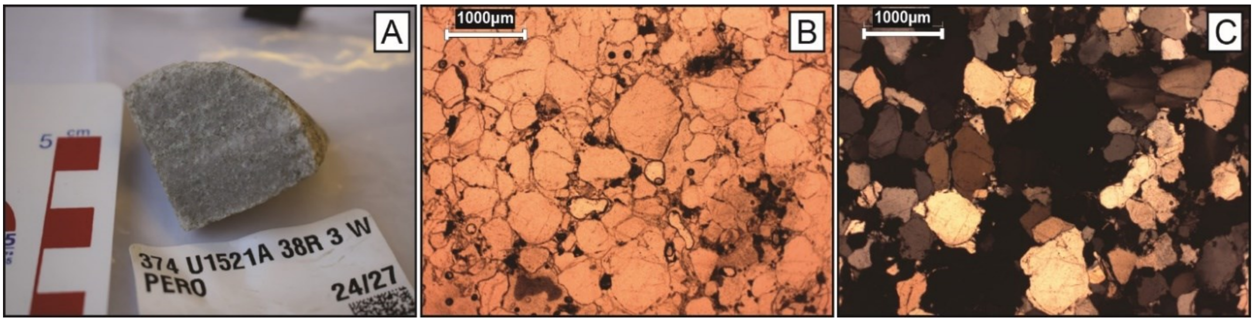

Figure 46 A) Macroscopic picture of the clast; B) PPL photomicrograph (2.5x); C) XPL photomicrograph (2.5x).

Sub-angular clast of laminated sandstone, with coarse-grained laminae and fine-grained ones. The grains are of sub-rounded to well-rounded shape, and they are mainly made up of monocrystalline quartz with homogeneous extinction, rarely with undulose ones. Intragranular spaces are filled mainly by quartz overgrowth; phyllosilicatic matrix and pseudo-matrix are less common. Lithic fragments are rare (quartzites) as well as feldspars, both plagioclase and K-feldspar, partially replaced by sericite aggregates. Accessory minerals are mainly white mica and zircons.

Sample 374-U1521A-39R-CCW, 10-12 cm – Two micas granite

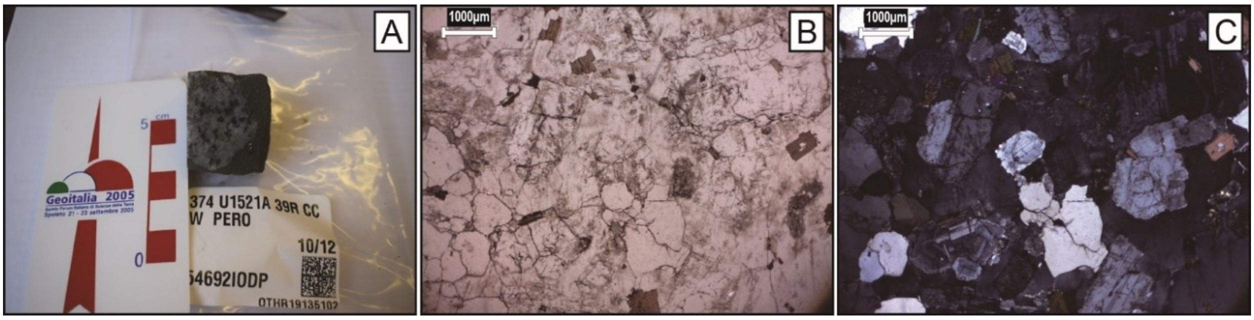

Figure 47 A) Macroscopic picture of the clast; B) PPL photomicrograph (1.6x); C) XPL photomicrograph (1.6x).

The sample is medium-grained, porphyritic rock with isotropic texture. Pecilitic mega-crystals of alkali feldspar (orthoclase) occur. Plagioclase forms both fine-grained, subhedral crystals and medium-grained subhedral ones. Plagioclase crystals sometimes have chemical zonation, and they usually are partially replaced by sericite and clay minerals aggregates. Quartz is usually anhedral and show weakly undulose extinction. Mafic minerals constitute ca. 10-12% of the whole and they are represented by biotite, which is sometime replaced by chlorite. Primary white mica crystals commonly occur within the rock.

Sample 374-U1521A-44R-4W, 85-88 cm - Carbonate conglomerate

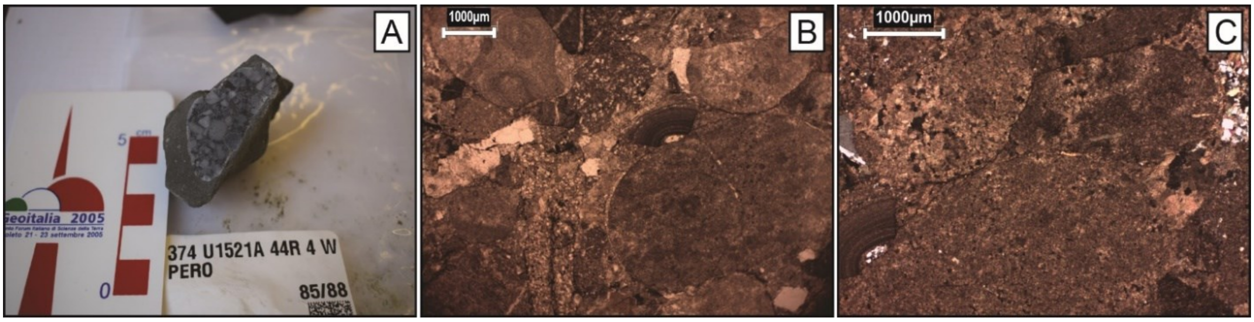

Figure 48 A) Macroscopic picture of the clast; B) PPL photomicrograph (1.6x); C) XPL photomicrograph (2.5x).

Rounded sample of clast-supported conglomerate with abundant matrix, made up of sparitic calcite and quartz fragments. Clasts are plurimillimetric, with sub-rounded to well-rounded shape; they are mainly constituted by: sparitic limestone, quartz bearing fine- to medium-grained meta-limestone, medium/coarse grained marble, quartzite, and weakly schistose meta-sandstone. In the examined thin section there is an ooid/pisoid fragments and a limestone clast with peloids as main allochem type.

Sample 374-U1521A-48R-6W, 38-40 cm - Granodiorite

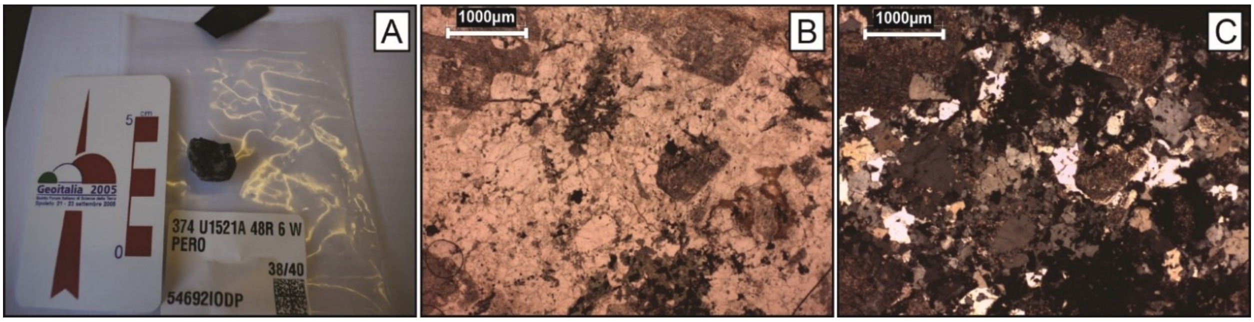

Figure 49 A) Macroscopic picture of the clast; B) PPL photomicrograph (2.5x); C) XPL photomicrograph (2.5x).

The clast is sub-angular. Holocrystalline intrusive rock, with heterogranular, hypidiomorphic, slightly porphyritic texture, showing a high grade of alteration. The rock is composed of fine- to coarse-grained quartz crystals with homogeneous extinction (ca. 50%), K-feldspar (orthoclase) anhedral crystals (ca. 10%), subhedral plagioclase crystals (ca. 30%); both feldspars are strongly altered and replaced by sericite aggregates and clay minerals. Secondary magnesian chlorite is also present (ca. 9%), associated with epidote (ca. 1%) and opaque minerals; those minerals probably replaced biotite (and/or hornblende).

Sample 374-U1521A-50R-4W, 133-136 cm – Leuco syeno-granite

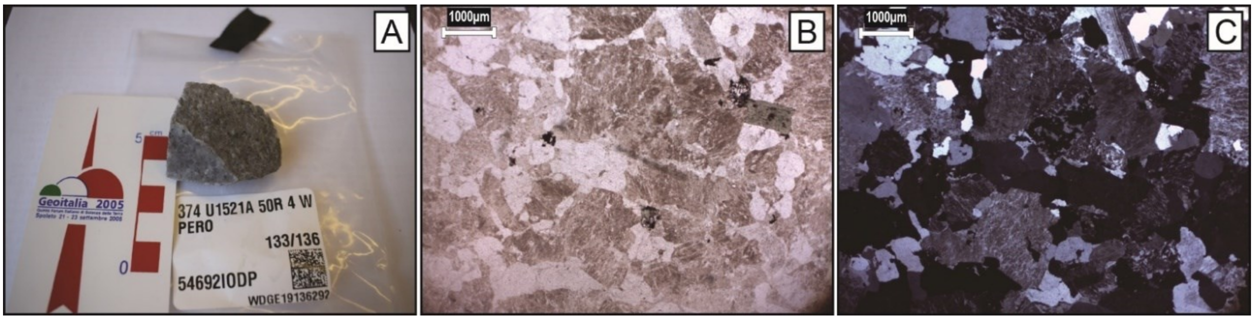

Figure 50 A) Macroscopic picture of the clast; B) PPL photomicrograph (1.6x); C) XPL photomicrograph (1.6x).

Fine- to medium-grained holocrystalline leucocratic intrusive rock with isotropic texture. The main mineralogical phase (> 50%) is alkali feldspar (pertitic orthoclase) which form both subhedral and anhedral crystals. Alkali felspar is commonly replaced by sericite and clay minerals aggregates. Quartz shows homogeneous extinction and represent ca. 30% of the whole. Plagioclase, weakly replaced by sericite, represents ca. 10% of the whole and forms anhedral to subhedral crystals. Mafic minerals are less than 3% and they are completely replaced by Mg-rich chlorite.

Sample 374-U1521A-55R-4W, 2-5 cm - Granodiorite/Granite

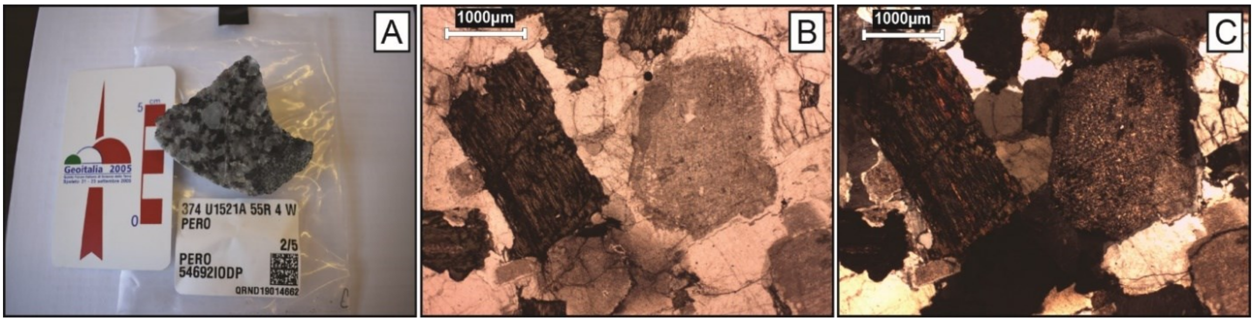

Figure 51 A) Macroscopic picture of the clast; B) PPL photomicrograph (2.5x); C) XPL photomicrograph (2.5x).

Sub-angular clast of medium to coarse grained, holocrystalline, hypidiomorphic to allotriomorphic intrusive rock, isotropic with porphyritic texture. Subhedral porphyritic crystals of feldspar, probably plagioclase (ca. 38%), are almost completely replaced by sericite aggregates; the rock also presents perthitic K-feldspars (ca. 24%) and rare microcline (<1%). Quartz crystals are fine grained and mainly interstitial (ca. 30%). Secondary magnesian chlorite, sometimes associated with white mica, is also present (ca. 8%), probably replacing biotite (and/or hornblende). Accessory minerals are opaques and apatite.

Sample 374-U1521A-60R-4W, 125-128 cm – Rhyolitic Porphyry

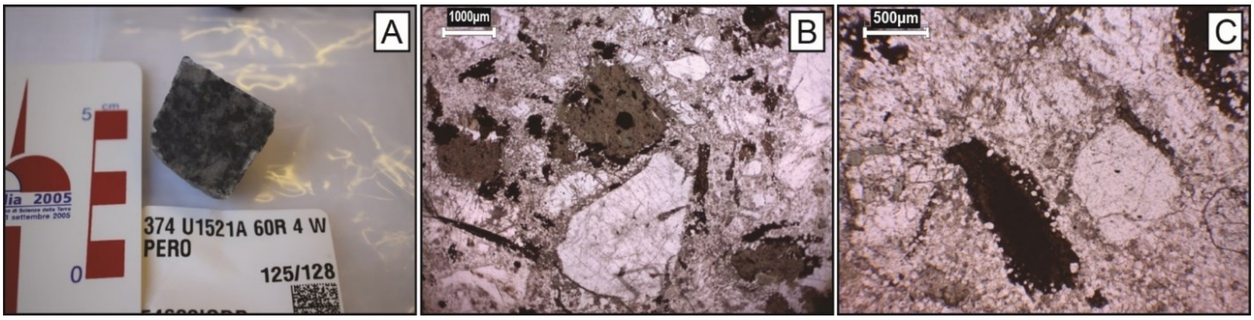

Figure 52 A) Macroscopic picture of the clast; B) PPL photomicrograph (1.6x); C) PPL photomicrograph (4x).

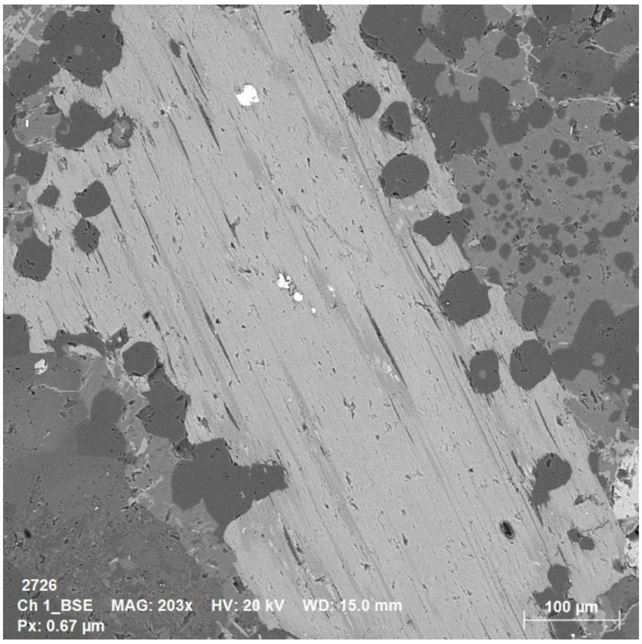

Figure 53 SEM - Back-Scattered Electrons image of the sample

The sample is holocrystalline porphyritic rock with isotropic texture. Groundmass is holocrystalline and fine-grained, mainly constituted by quartz and feldspars. The latter are partially replaced by sericite. Porphyritic crystals represent ca. 50% of the volume. They are constituted by quartz which form anhedral crystals with homogeneous extinction and sometimes show reabsorption rims; subhedral to anhedral plagioclase, sometimes with chemical zonation and poikilitic texture (small quartz inclusions); anhedral to subhedral alkali feldspar (pertitic orthoclase) crystals with poikilitic texture (small quartz inclusions in the rims), almost completely replaced by sericite and clay minerals aggregates; biotite crystals, partially replaced by chlorite, with poikilitic texture (small quartz inclusions in the rims). Another mineralogical phase of porphyritic crystals, forming prismatic crystals, occurs; however, this phase is completely replaced by chlorite, and it can not be certain identified.

Sample 374-U1521A-60R-5W, 62-65 cm - Biotite Gneiss

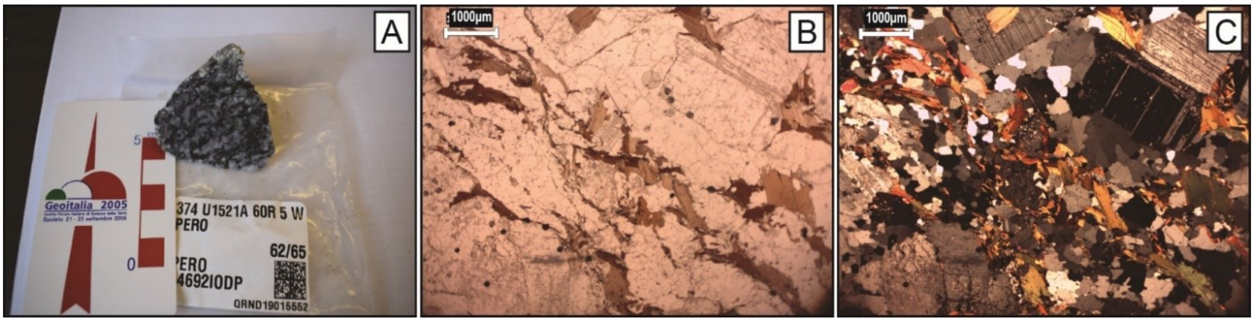

Figure 54 A) Macroscopic picture of the clast; B) PPL photomicrograph (1.6x); C) XPL photomicrograph (1.6x).

The clast is sub-angular. Heterogranular, fine- to medium-grained rock with gneissic granolepidoblastic texture. Biotite lepidoblasts (10-12%) show isorientation that marks the rock's foliation. Plagioclase crystals (43-45%) have anhedral to sub-euhedral habitus, they are medium-sized and sometimes show chemical zonation; quartz is fine-grained (ca. 45%). White mica rarely occurs. Apatite and zircons are accessory minerals.

Sample 374-U1521A-60R-7W, 90-93 cm - Greywacke

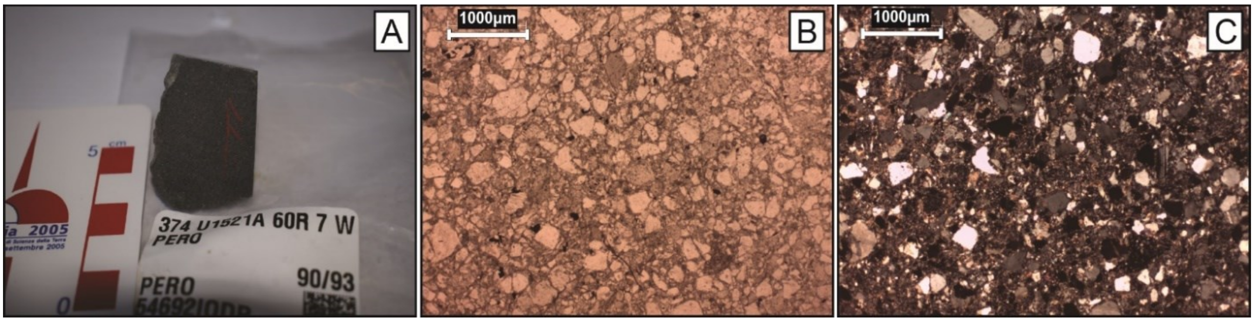

Figure 55 A) Macroscopic picture of the clast; B) PPL photomicrograph (2.5x); C) XPL photomicrograph (2.5x).

Angular clast of medium- to fine-grained siliciclastic rock with an isotropic texture; the mud-sized matrix is more than 20% and carbonate cement is also present. Grains are angular to sub-angular, made up of mono-crystalline quartz with undulose extinction; plagioclase is less common, instead K-feldspar is rare. Lithic fragments are mainly sub-volcanic felsic rocks. Accessory minerals are white mica, graphite, chlorite, tourmaline, zircon, and opaques.

Sample 374-U1521A-61R-5W, 26-30 cm – Meta-granite

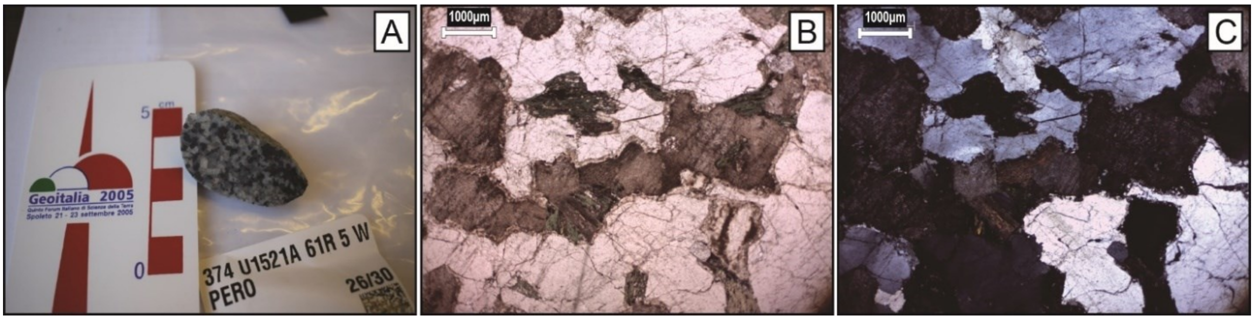

Figure 56 A) Macroscopic picture of the clast; B) PPL photomicrograph (1.6x); C) XPL photomicrograph (1.6x).

The sample is medium-grained, heterogranular, slightly schistose rock with mortar texture. The main constituent is quartz that show marked undulose extinction. Feldspars are almost completely replaced by sericite and clay minerals aggregates; however, plagioclase twinning is sometimes recognizable. Alkali feldspars may occur. Mafic minerals were completely replaced by magnesium-rich chlorite.

Sample 374-U1521A-62R-4W, 120-125 cm - Biotite phyllitic schist

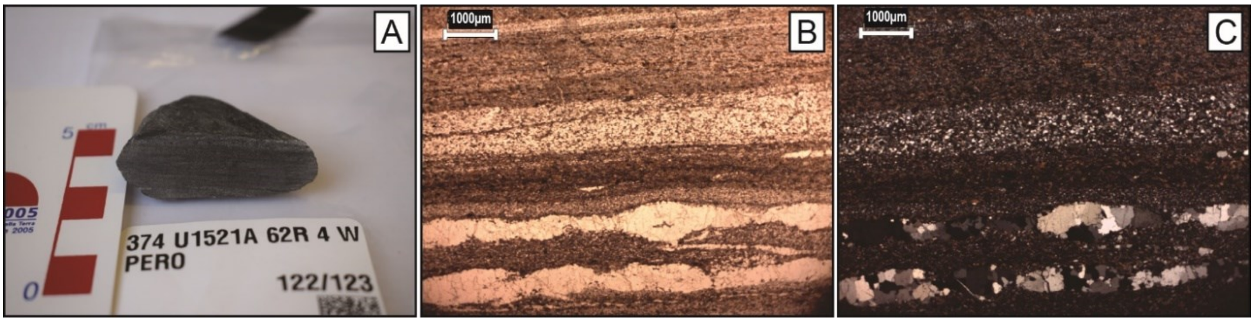

Figure 57 A) Macroscopic picture of the clast; B) PPL photomicrograph (1.6x); C) XPL photomicrograph (1.6x).

Rounded clast of fine-grained, schistose metamorphic rock. The rock shows some different grano-lepidoblastic layers: boudin layers of medium-grained recrystallized quartz; very fine-grained quartz-dominated layers with biotite and opaque minerals; fine-grained biotite dominated layers with quartz. Biotite texture indicates a weak thermo-metamorphic overprint.

Sample 374-U1521A-63R-5W, 8-17 cm – Chlorite graphitic phyllite

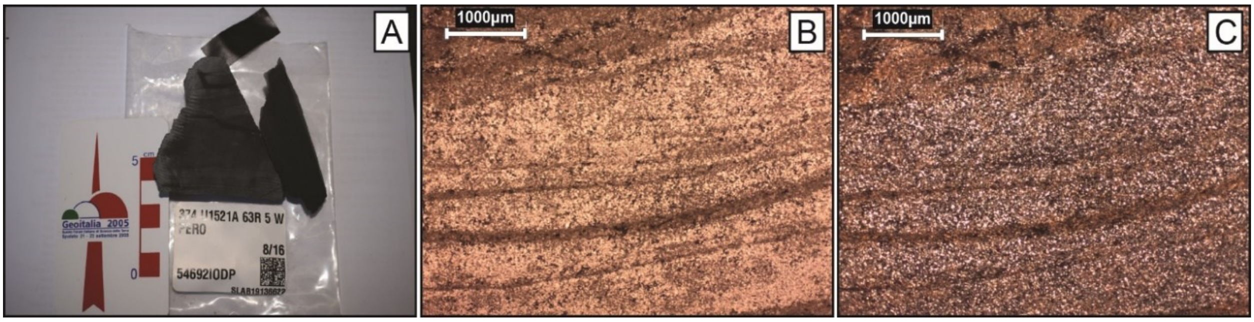

Figure 58 A) Macroscopic picture of the clast; B) PPL photomicrograph (2.5x); C) XPL photomicrograph (2.5x).

The clast is sub-angular. Very fine-grained schistose metamorphic rock made up of quartz-rich lenticular layers and chlorite dominated lepidoblastic layers that show a weak thermo-metamorphic overprint. Graphite chips are common throughout the rock.

Sample 374-U1521A-63R-CCW, 10-13 cm - Siltstone

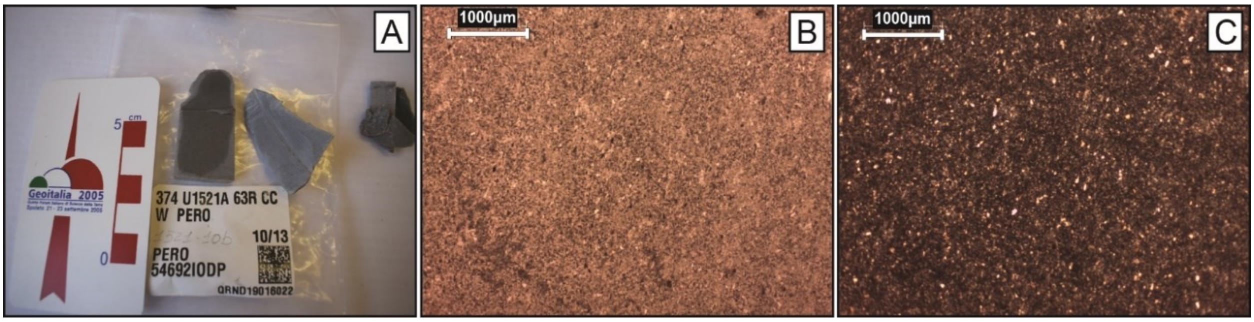

Figure 59 A) Macroscopic picture of the clast; B) PPL photomicrograph (2.5x); C) XPL photomicrograph (2.5x).

Angular clast of silt-grained clastic rock with isotropic texture. The rock shows very fine, angular, sandy clasts of monocrystalline quartz and plagioclase; the rock has a quartz-feldspatic composition. Accessory minerals are opaque and zircons.

Sample 374-U1521A-64R-3W, 28-31 cm - Meta-granite

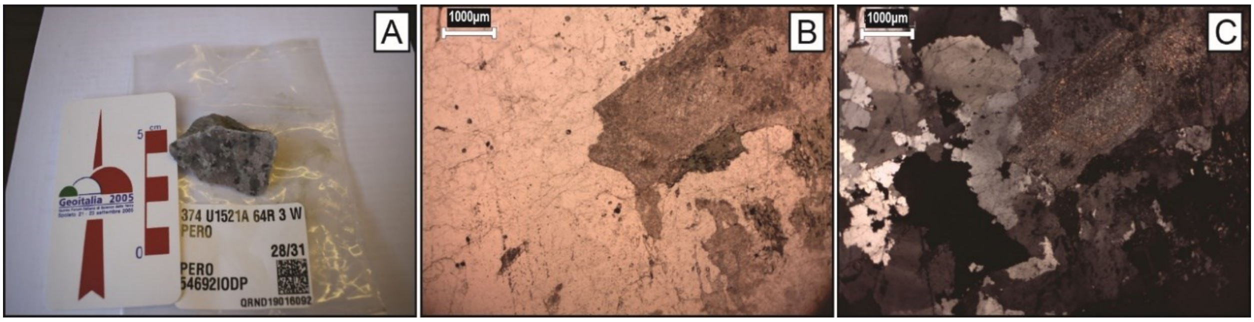

Figure 60 A) Macroscopic picture of the clast; B) PPL photomicrograph (1.6x); C) XPL photomicrograph (1.6x).

Sub-rounded clast of fine- to coarse-grained, hypidiomorphic holocrystalline meta-igneous rock with mortar texture. The rock has a very low colour index (<3%) with the mafic mineral constituted by secondary chlorite. Quartz is the main component (50-55%) and shows strong undulose extinction and medium-size crystal rims with very fine quartz granules (mortar texture). 20-25% of grains are made up of subhedral plagioclase, partially replaced by sericite aggregates, and 20-25% of K-feldspar (microperthitic orthoclase) with anhedral habitus.

Sample 374-U1521A-64R-3W, 109-112 cm - Biotite meta-greywacke

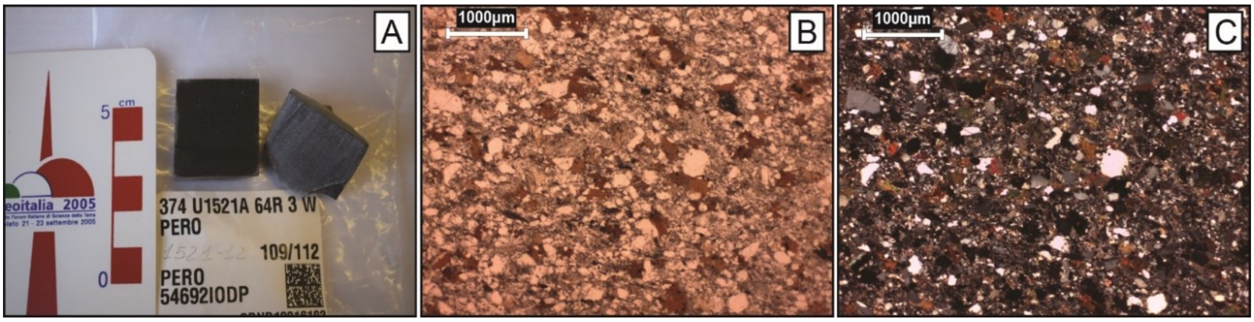

Figure 61 A) Macroscopic picture of the clast; B) PPL photomicrograph (2.5x); C) XPL photomicrograph (2.5x).

The clast is sub-rounded and represent a heterogranular, fine- to medium-grained, meta-sedimentary clastic rock that shows a weak foliation marked by the isorientation of biotite lepidoblasts. The rock has a high percentage of phyllosilicatic matrix. Clasts are mainly of quartz, biotite and feldspars replaced by sericite; zircons and white mica are accessory minerals.

Sample 374-U1521A-64R-6W, 20-24 cm - Biotite ± white mica gneiss

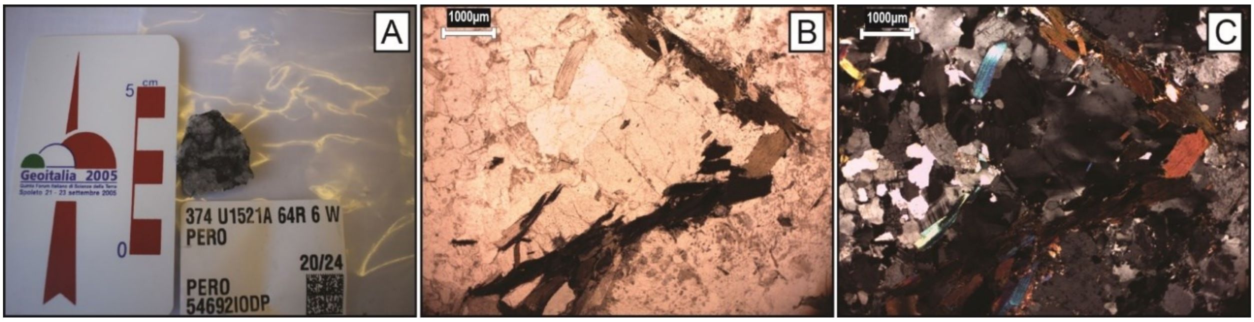

Figure 62 A) Macroscopic picture of the clast; B) PPL photomicrograph (1.6x); C) XPL photomicrograph (1.6x).

Sub-rounded clast of fine- to medium-grained metamorphic rock with gneissic texture; schistosity is defined by the isorientation of biotite and white mica, sometimes deformed. The main component is quartz, with wide grain size range and strong undulose extinction. The other components are K-feldspar (microcline) and altered plagioclase.

Sample 374-U1521A-66R-4W, 63-67 cm - Limestone

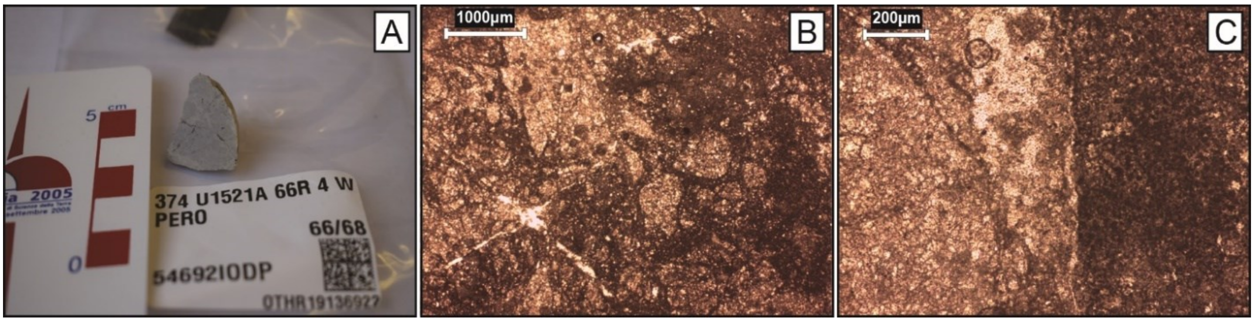

Figure 63 A) Macroscopic picture of the clast; B) PPL photomicrograph (2.5x); C) PPL photomicrograph (10x).

The sample is sub-rounded and made up of mud-supported, isotropic rock of carbonate composition that is mainly made up of micritic calcite. Allochems are rare and prevalently composed by altered peloids and rare bioclasts. The rock shows veins filled by coarse grained calcite crystals and quartz.

Sample 374-U1521A-67R-6W, 115-120 cm - Limestone

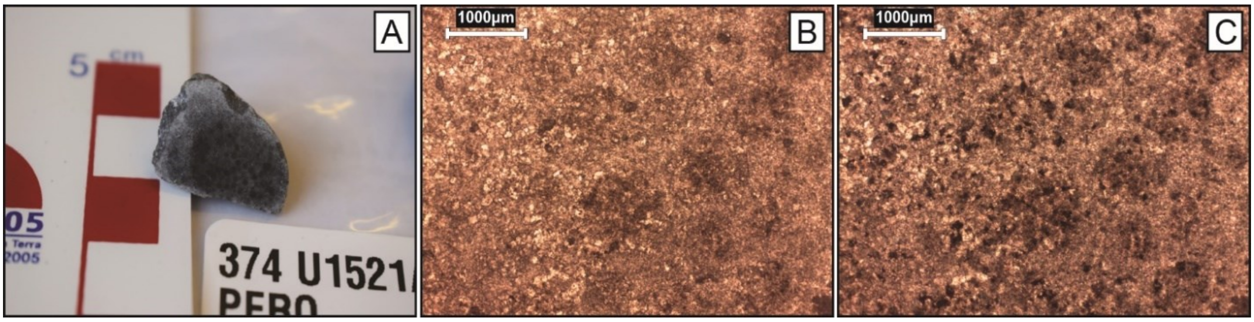

Figure 64 A) Macroscopic picture of the clast; B) PPL photomicrograph (2.5x); C) XPL photomicrograph (2.5x).

Sub-rounded clast of fine-grained carbonate rock with isotropic texture, made up of micritic to sparitic calcite crystals, sometimes with euhedral shape. In the mud-supported matrix there are rare peloids almost completely superimposed by a recrystallized microsparite texture.

Sample 374-U1521A-68R-2W, 58-61 cm - Biotite granite

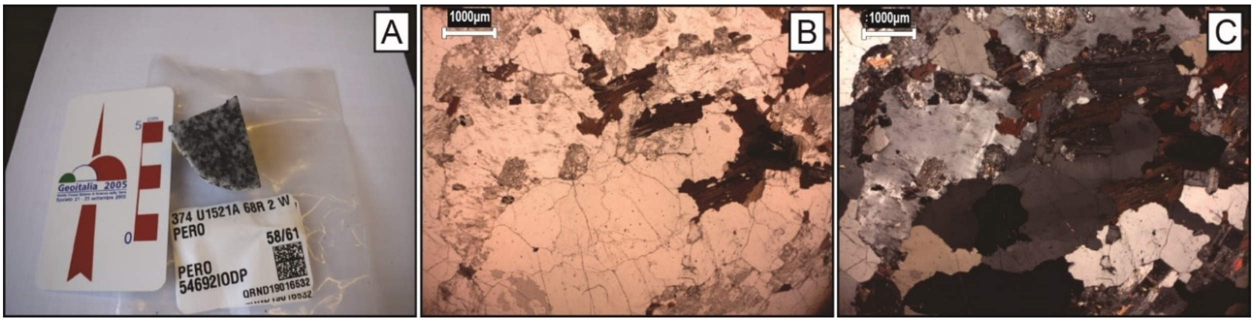

Figure 65 A) Macroscopic picture of the clast; B) PPL photomicrograph (1.6x); C) XPL photomicrograph (1.6x).

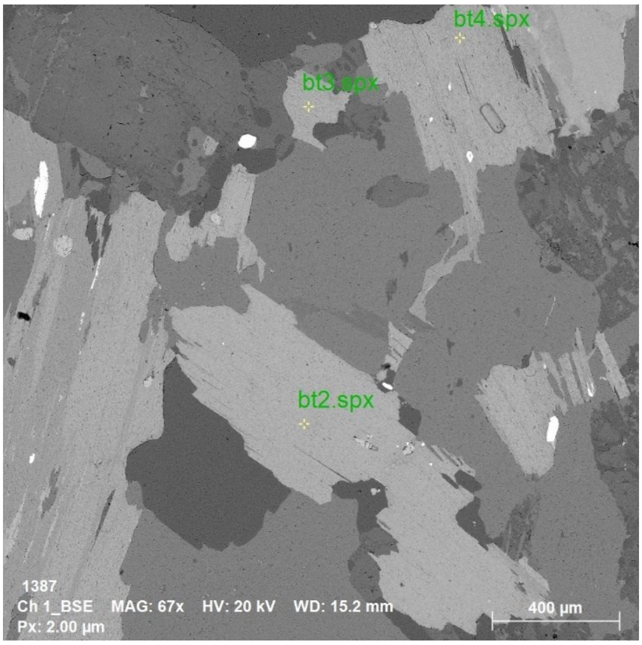

Figure 66 SEM images of some analyzed biotite crystals

Sub-rounded clast of holocrystalline, isotropic, medium-grained slightly heterogranular rock with hypidiomorphic texture. Quartz with homogeneous extinction is the main component (ca. 45%) and it is coarser than other mineralogical phases, sometimes with interlobate grain boundaries; plagioclase, partially replaced by sericite, constitutes ca. 37% of the rock, and sometimes forms mirmechitic structures with quartz. Less abundant is K-feldspar (ca. 10%). Biotite is the mafic mineral and constitutes ca. 8% of the whole rock and it is weakly replaced by chlorite.

Sample 374-U1521A-69R-1W, 120-125 cm - Chlorite Phyllite

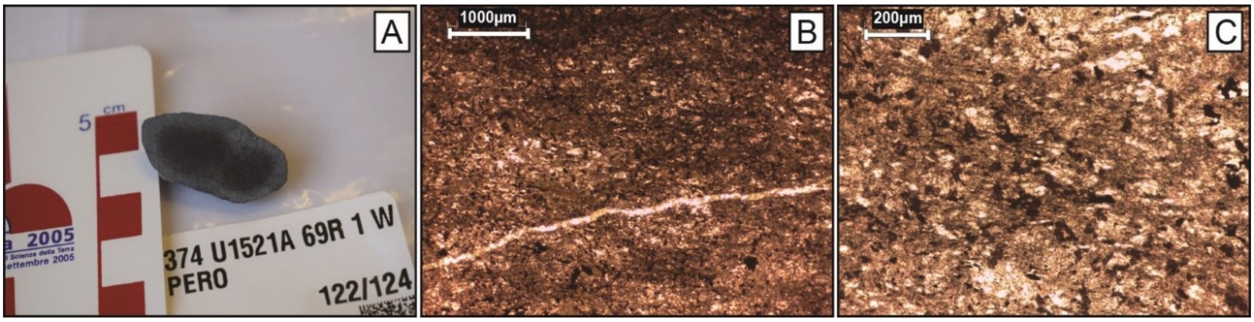

Figure 67 A) Macroscopic picture of the clast; B) PPL photomicrograph (2.5x); C) PPL photomicrograph (10x).

Rounded clast of very fine-grained metamorphic rock. The rock is mainly made up of thin lepidoblastic isoriented chlorite and quartz; opaque minerals are common. The rock is crossed by quartz veins. Mineral paragenesis suggests a low metamorphic grade.

Sample 374-U1521A-69R-5W, 109-112 cm - Granofels

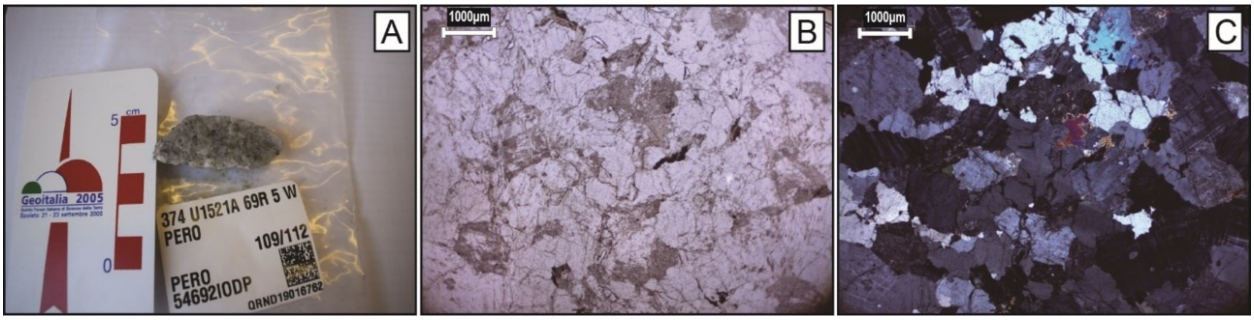

Figure 68 A) Macroscopic picture of the clast; B) PPL photomicrograph (1.6x); C) XPL photomicrograph (1.6x).

Medium-grained, slightly heterogranular, holocrystalline rock with isotropic texture. The main mineralogical phase is alkali feldspars: microcline forms anhedral crystals while orthoclase forms anhedral to subhedral crystals. Quartz shows strong undulose extinction. Plagioclase constitutes less than 10% of the whole volume. Large white mica crystals commonly occur within the sample.

Sample 374-U1521A-69R-6W, 40-45 cm - Biotite ± white mica schist

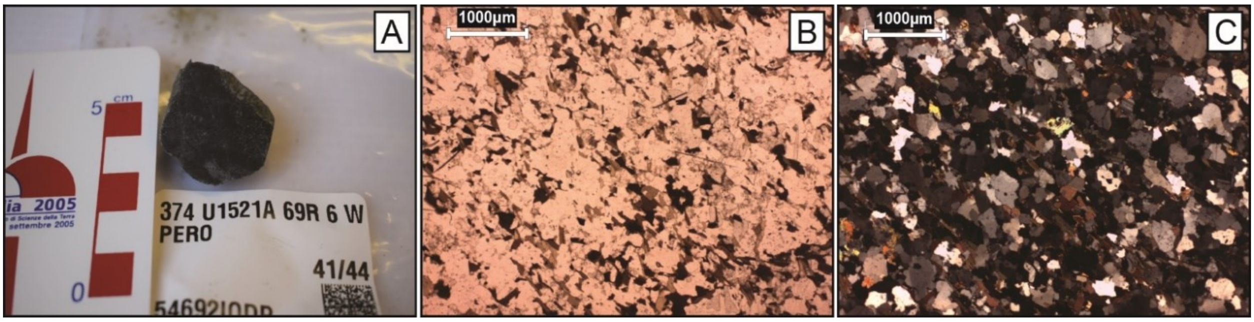

Figure 69 A) Macroscopic picture of the clast; B) PPL photomicrograph (2.5x); C) XPL photomicrograph (2.5x).

The sample is sub-angular. Heterogranular, fine- to medium-grained, metamorphic rock with weakly foliated texture marked by the isorientation of lepidoblastic biotite; the rock shows granulometric layering, with a fine-grained layer and a medium-grained one. The main component is quartz, secondly plagioclase; less common is white mica. The mineralogical association is typical of a medium-grade (amphibolitic) metamorphic facies.

Sample 374-U1521A-69R-6W, 63-66 cm - Foliated biotite granite

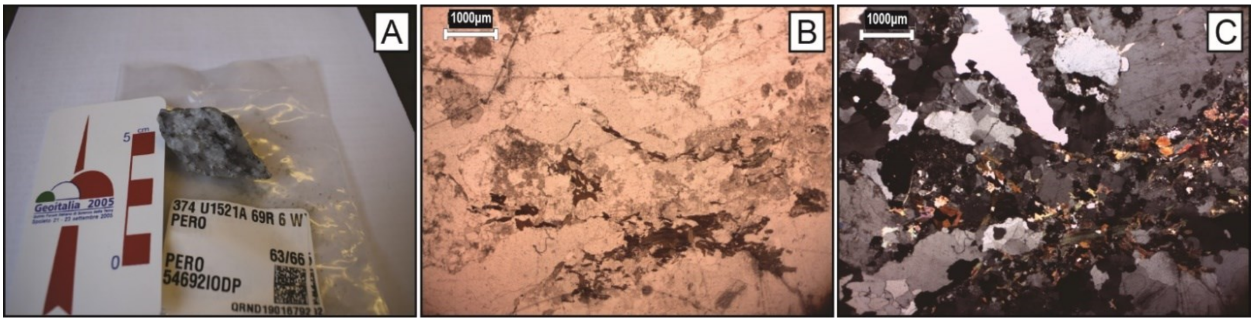

Figure 70 A) Macroscopic picture of the clast; B) PPL photomicrograph (1.6x); C) XPL photomicrograph (1.6x).

Sub-angular clast of medium-grained heterogranular igneous rock with weakly foliated and hypidiomorphic texture. The rock is leucocratic; the biotite, partially replaced by chlorite, is about 2%. The main component is quartz, sometimes with interlobate grain boundaries. K-feldspar, both orthoclase and microcline, represents ca. 38%; plagioclase is ca. 15%. Secondary white mica sometimes occurs.

Sample 374-U1521A-70R-1W, 55-58 cm - Mudstone

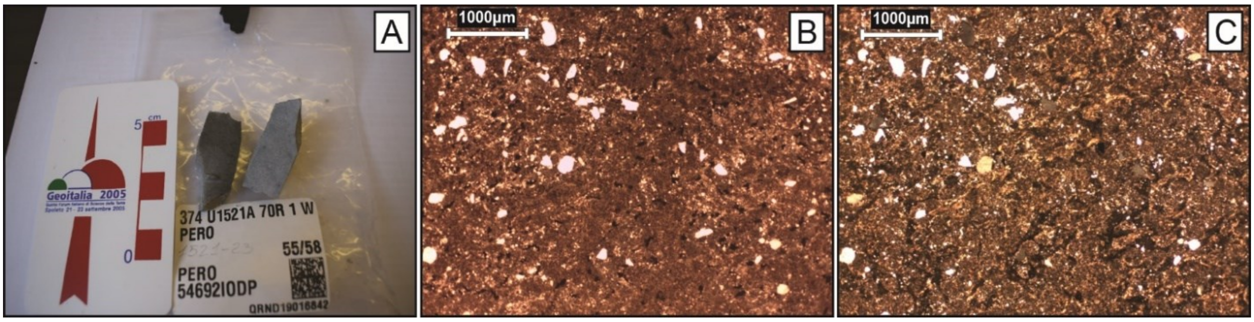

Figure 71 A) Macroscopic picture of the clast; B) PPL photomicrograph (2.5x); C) XPL photomicrograph (2.5x).

Sub-angular clast of very fine-grained, heterogranular clastic rock with isotropic texture. The rock is mainly constituted by mud-size matrix where scattered sand-size grains of sub-angular to well-rounded monocrystalline quartz occur.

Sample 374-U1521A-70R-4W, 120-125 cm - Biotite schist

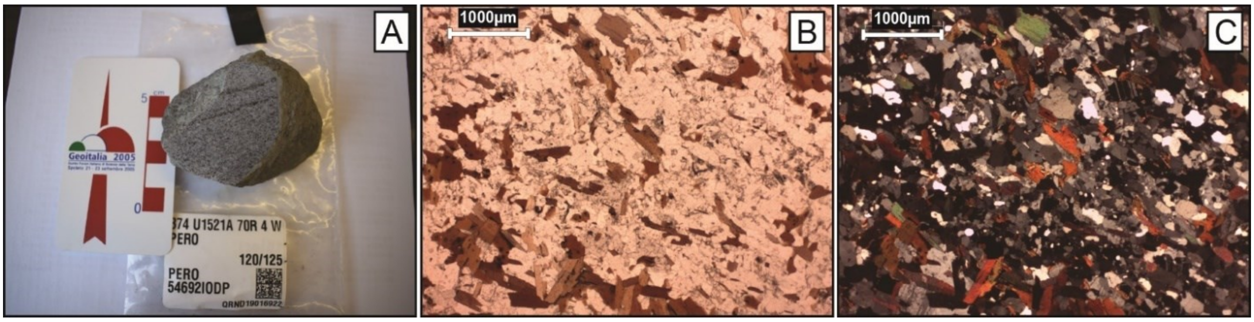

Figure 72 A) Macroscopic picture of the clast; B) PPL photomicrograph (2.5x); C) XPL photomicrograph (2.5x).

The sample has a sub-rounded shape and it is a fine- to medium-grained metamorphic rock with schistose granolepidoblastic texture. The main constituent is quartz with granoblastic polygonal to interlobate texture. Plagioclase is common. Biotite is more than 10% and defines schistosity; it is mainly iso-oriented, but some randomly oriented crystals show thermo-metamorphic overprint.

Sample 374-U1521A-71R-1W, 87-90 cm – Sandstone (arkose)

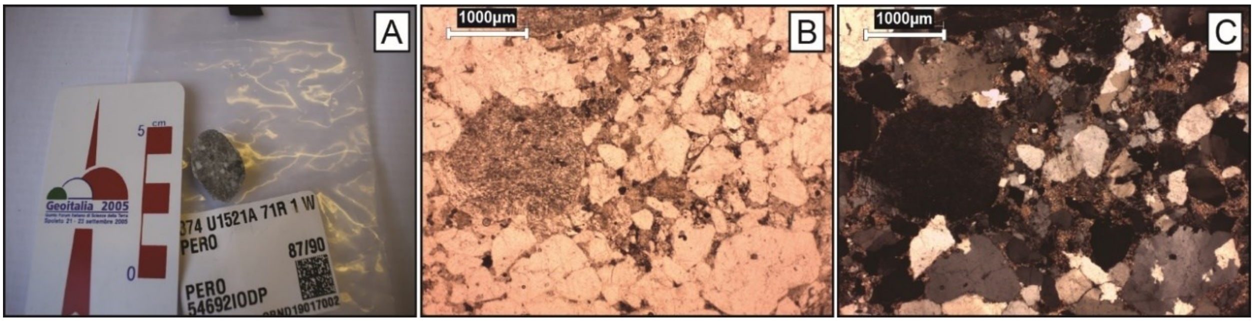

Figure 73 A) Macroscopic picture of the clast; B) PPL photomicrograph (2.5x); C) XPL photomicrograph (2.5x).

Rounded clast of siliciclastic rock with isotropic and heterogranular texture, medium- to coarse-grained; the phyllosilicate mud-grained matrix constitutes ca. 10-15% of the whole rock. Clasts are angular to sub-rounded and they are made up of mono- to poly-crystalline quartz showing marked undulose extinction; K-feldspar is common, with orthoclase more abundant than microcline, and is partially replaced by sericite aggregates; plagioclase grains are less common and less altered. Lithic fragments are rare and mainly made up of granitoid rocks.

Table 19 Summary of analyzed clasts, with sampling depth, clast shape and lithology. LSU – Lithostratigraphic Unit (from McKay et al., 2019)

Sample ID	LSU	Depth (m CSF-A)	Clast Shape	Lithology
374-U1521A-29R-6W, 59-63 cm	IV	272.77	sub-angular	(Meta-)granite
374-U1521A-30R-3W, 85-89 cm	IV	279.34	rounded	Basalt
374-U1521A-35R-3W, 65-72 cm	VI A	326.27	sub-rounded	Granite
374-U1521A-37R-3W, 110-113 cm	VI A	346.79	sub-rounded	Limestone
374-U1521A-38R-1W, 110-113 cm	VI A	353.61	rounded	Monzogranite
374-U1521A-38R-2W, 134-140 cm	VI A	355.34	sub-angular	(Meta-)greywacke
374-U1521A-38R-3W, 24-28 cm	VI A	355.72	sub-angular	Quartz-arenite
374-U1521A-39R-CCW, 10-12 cm	VIA	359.53	sub-rounded	Two micas granite
374-U1521A-44R-4W, 85-88 cm	VI B	386.46	rounded	Carbonate conglomerate
374-U1521A-48R-6W, 38-40 cm	VI B	427.30	sub-angular	Granodiorite
374-U1521A-50R-4W, 133-136 cm	VI C	444.55	sub-angular	Syenogranite
374-U1521A-55R-4W, 2-5 cm	VI C	491.04	sub-angular	Granite/Granodiorite
374-U1521A-60R-4W, 125-127 cm	VI C	539.85	sub-rounded	Rhyolitic porphyry
374-U1521A-60R-5W, 62-65 cm	VI C	541.08	sub-angular	Biotite gneiss
374-U1521A-60R-7W, 90-93 cm	VI C	543.64	angular	Greywacke
374-U1521A-61R-5W, 26-30 cm	VI C	550.17	rounded	Meta-granite
374-U1521A-62R-4W, 120-125 cm	VI C	559.14	rounded	Biotite phyllitic schist
374-U1521A-63R-5W, 8-17 cm	VII	568.89	sub-angular	Chlorite graphitic phyllite
374-U1521A-63R-CCW, 10-13 cm	VII	569.98	angular	Siltstone
374-U1521A-64R-3W, 28-31 cm	VII	576.32	sub-rounded	Meta-granite
374-U1521A-64R-3W, 109-112 cm	VII	577.18	sub-rounded	Biotite meta-greywacke
374-U1521A-64R-6W, 20-24 cm	VII	579.95	sub-rounded	Biotite ± white mica gneiss
374-U1521A-66R-4W, 63-67 cm	VII	597.03	sub-rounded	Limestone
374-U1521A-67R-6W, 115-120 cm	VII	610.17	sub-rounded	Limestone
374-U1521A-68R-2W, 58-61 cm	VII	613.70	sub-rounded	Biotite granite
374-U1521A-69R-1W, 120-125 cm	VII	622.50	rounded	Chlorite phyllite
374-U1521A-69R-5W, 109-112 cm	VII	627.96	rounded	Granofels
374-U1521A-69R-6W, 40-45 cm	VII	628.65	sub-angular	Biotite ± white mica schist
374-U1521A-69R-6W, 63-66 cm	VII	628.88	sub-angular	Foliated biotite granite
374-U1521A-70R-1W, 55-58 cm	VII	631.45	sub-angular	Mudstone
374-U1521A-70R-4W, 120-125 cm	VII	636.10	sub-rounded	Biotite schist
374-U1521A-71R-1W, 87-90 cm	VII	641.37	rounded	Sandstone (arkose)

Table 20 Occurrence in percentage of lithics the gravel from bulk diamictite matrix. Qtz - quartz; Fs - feldspars (plagioclase and alkali feldspar); Intr - intrusive rocks; Dol - dolerite; Meta - metamorphic rocks; Clastic sed - clastic sedimentary rocks; Carb sed - carbonate sedimentary rocks; Bas - basaltic rocks; F Porph - felsic porphyries; ND - Not Defined; Tot - total number of clasts counted in thin section.

Sample ID	Qtz	Fs	Intr	Dol	Meta	Clastic sed	Carb sed	Bas	F Porph	ND	Tot
374-U1521A-36R-1W, 67-70 cm	1%	2%	10%	22%	44%	4%	3%	2%	6%	4%	89
374-U1521A-36R-1W, 80-90 cm	2%	3%	17%	20%	43%	8%	2%	3%	3%	0%	65
374-U1521A-36R-3W, 45-55 cm	0%	8%	23%	18%	44%	3%	0%	5%	0%	0%	39
374-U1521A-43R-2W, 80-85 cm	5%	0%	14%	23%	50%	0%	5%	5%	0%	0%	22
374-U1521A-43R-2W, 94-98 cm	1%	3%	13%	10%	50%	8%	8%	1%	3%	5%	103
374-U1521A-43R-2W, 100-105 cm	3%	3%	8%	17%	41%	14%	7%	1%	1%	4%	71
374-U1521A-59R-8W, 31-36 cm	4%	20%	11%	1%	42%	7%	0%	3%	9%	2%	95

APPENDIX IV

Mineral chemistry analyses of IODP Site U1521 clasts

Chemical analysis of biotite crystals from seven metamorphic and intrusive pebbles. Analyses were carried out with an energy-dispersive X-ray system (Bruker Quantax 200 EDX) coupled with an Electron Scanning Microscope (Tescan Vega3) at the Department of Physical, Earth and Environmental Sciences - University of Siena. Analytical conditions were 20 kV of accelerating voltage, 15 µA of emission current, and a beam spot size of 0.2 µm. Natural mineral standards were used for calibration. Cations were recalculated on the basis of 22 oxygens. Crossed out data represent not valid analyses, and they were excluded from the interpretations.

Sample 374-U1521A-29R-6W, 59-63 cm

Table 21 Chemical analysis of biotite from Sample 374-U1521A-29R-6W, 59-63 cm

Wt%	Bt1	Bt2	Bt3	Bt4	Bt5	Bt6	Bt7	Bt8	Bt9	Bt10	Bt11	Bt12	Bt13
SiO_2	36.71	37.27	37.59	39.15	38.97	39.50	38.15	39.36	37.89	38.99	37.33	37.55	37.50
TiO_2	3.64	3.72	3.20	3.14	3.28	2.89	3.50	3.20	3.39	3.32	3.27	3.10	3.05
Al_2O_3	19.44	18.69	19.33	20.89	20.34	20.51	20.03	19.26	19.50	20.28	18.59	19.18	19.00
FeO	17.50	17.22	17.12	13.54	14.54	14.04	14.96	15.84	16.26	14.77	17.92	16.70	16.99
MnO													
MgO	10.20	10.28	10.38	11.60	10.95	11.66	10.90	10.60	10.63	10.66	10.30	10.88	10.95
CaO													
Na_2O													
K_2O	9.12	8.81	8.95	8.12	8.47	8.23	8.82	8.51	8.79	8.79	8.49	8.95	8.93
Cl													
F													
TOTAL	96.61	95.98	96.57	96.44	96.55	96.83	96.37	96.77	96.45	96.81	95.89	96.36	96.42
APFU													
Si	5.42	5.52	5.53	5.60	5.61	5.64	5.55	5.69	5.54	5.62	5.54	5.52	5.52
Al^{IV}	2.58	2.48	2.47	2.40	2.39	2.36	2.45	2.31	2.46	2.38	2.46	2.48	2.48
Al^{VI}	0.81	0.78	0.87	1.13	1.07	1.10	0.98	0.98	0.90	1.06	0.79	0.85	0.82
Ti	0.40	0.41	0.35	0.34	0.36	0.31	0.38	0.35	0.37	0.36	0.36	0.34	0.34
Fe(ii)	2.16	2.13	2.10	1.62	1.75	1.68	1.82	1.92	1.99	1.78	2.22	2.05	2.09
Mn	0.00	0.00	0.00	0.00	0.00	0.00	0.00	0.00	0.00	0.00	0.00	0.00	0.00
Mg	2.25	2.27	2.27	2.47	2.35	2.48	2.36	2.29	2.32	2.29	2.28	2.39	2.40
Ca	0.00	0.00	0.00	0.00	0.00	0.00	0.00	0.00	0.00	0.00	0.00	0.00	0.00
Na	0.00	0.00	0.00	0.00	0.00	0.00	0.00	0.00	0.00	0.00	0.00	0.00	0.00
K	1.72	1.66	1.68	1.48	1.56	1.50	1.64	1.57	1.64	1.62	1.61	1.68	1.68
Cl	0.00	0.00	0.00	0.00	0.00	0.00	0.00	0.00	0.00	0.00	0.00	0.00	0.00
F	0.00	0.00	0.00	0.00	0.00	0.00	0.00	0.00	0.00	0.00	0.00	0.00	0.00
TOTAL	15.34	15.27	15.29	15.04	15.08	15.07	15.17	15.10	15.22	15.11	15.27	15.31	15.33

Note: W% = percentage weight; APFU = atom per formula unit

Sample 374-U1521A-36R-1W, 67-70 cm

Table 22 Chemical analysis of biotite from clast n 18 in the Sample 374-U1521A-36R-1W, 67-70 cm

Wt%	**Bt18-1**	**Bt18-2**	**Bt18-3**	**Bt18-4**	**Bt18-5**	**Bt18-6**	**Bt18-7**	**Bt18-8**
SiO_2	40.89	41.02	40.18	~~39.92~~	40.53	41.16	40.51	40.34
TiO_2	2.37	2.62	2.87	~~2.82~~	1.80	1.58	3.02	2.52
Al_2O_3	15.63	16.11	15.60	~~15.29~~	17.15	16.00	16.61	16.47
FeO	18.68	18.01	19.16	~~19.00~~	18.91	18.31	18.63	18.99
MnO	0.59	0.40	0.41	~~0.41~~	0.45	0.36	0.38	0.36
MgO	13.94	14.27	13.92	~~13.54~~	15.28	14.96	14.22	14.78
CaO								
NaO				~~0.58~~				
K_2O	11.54	11.40	11.44	~~11.67~~	9.85	11.10	10.38	10.46
ClO								
F								
TOTAL	96.49	96.31	96.54	~~96.87~~	96.18	96.65	96.37	96.24
a.p.f.u.								
Si	5.72	5.70	5.64	~~5.65~~	5.60	5.73	5.62	5.60
Al^{IV}	2.28	2.30	2.36	~~2.35~~	2.40	2.27	2.38	2.40
Al^{VI}	0.30	0.33	0.22	~~0.19~~	0.39	0.36	0.33	0.30
Ti	0.25	0.27	0.30	~~0.30~~	0.19	0.17	0.32	0.26
Fe(ii)	2.19	2.09	2.25	~~2.25~~	2.18	2.13	2.16	2.20
Mn	0.07	0.05	0.05	~~0.05~~	0.05	0.04	0.04	0.04
Mg	2.91	2.95	2.91	~~2.86~~	3.15	3.11	2.94	3.06
Ca	0.00	0.00	0.00	~~0.00~~	0.00	0.00	0.00	0.00
Na	0.00	0.00	0.00	~~0.16~~	0.00	0.00	0.00	0.00
K	2.06	2.02	2.05	~~2.11~~	1.74	1.97	1.84	1.85
Cl	0.00	0.00	0.00	~~0.00~~	0.00	0.00	0.00	0.00
F	0.00	0.00	0.00	~~0.00~~	0.00	0.00	0.00	0.00
TOTAL	15.77	15.72	15.79	~~15.91~~	15.69	15.78	15.63	15.72

Note: Wt% = percentage weight; a.p.f.u. = atom per formula unit

Sample 374-U1521A-36R-1W, 80-90 cm

Table 23 Chemical analysis of biotite from clast n 36, 53, and 65 in the Sample 374-U1521A-36R-1W, 80-90 cm

Wt%	**Bt36-1**	**Bt36-2**	**Bt53-1**	**Bt53-2**	**Bt53-3**	**Bt53-4**	**Bt53-5**	**Bt53-6**	**Bt53-7**	**Bt53-8**	**Bt65-1**	**Bt65-2**
SiO_2	38.14	~~38.53~~	36.83	37.67	38.58	38.83	~~37.11~~	38.28	38.97	38.63	39.12	38.97
TiO_2	3.00	~~3.07~~	4.27	3.93	4.06	3.91	~~4.62~~	4.16	4.06	4.16	3.95	1.29
Al_2O_3	18.26	~~18.73~~	14.55	15.63	15.24	15.08	~~13.95~~	15.42	14.76	15.12	16.06	19.34
FeO	23.71	~~22.55~~	30.27	29.35	27.09	26.38	~~29.02~~	27.21	26.65	27.09	27.52	26.54
MnO	0.26	~~0.34~~	0.32	0.24	0.18	0.16	~~0.31~~	0.27	0.24	0.31	0.40	0.38
MgO	9.10	~~8.85~~	7.60	8.53	8.55	8.07	~~7.26~~	7.64	8.33	7.81	7.24	6.78
CaO		-										
NaO		-										
K_2O	11.34	~~11.58~~	9.71	8.66	9.58	10.99	~~11.63~~	10.78	10.62	10.81	9.52	10.30
ClO		-										
F		-										

TOTAL	96.33	~~96.49~~	96.56	96.14	96.83	96.69	~~96.25~~	96.37	96.5	96.22	96.34	96.53
a.p.f.u.		-										
Si	5.45	~~5.49~~	5.44	5.46	5.59	5.64	~~5.49~~	5.57	5.65	5.60	5.63	5.59
Al^{IV}	2.55	~~2.51~~	2.53	2.54	2.41	2.36	~~2.43~~	2.43	2.35	2.40	2.37	2.41
Al^{VI}	0.53	~~0.63~~	0.00	0.12	0.19	0.22	~~0.00~~	0.21	0.17	0.19	0.36	0.87
Ti	0.32	~~0.33~~	0.47	0.43	0.44	0.43	~~0.51~~	0.45	0.44	0.45	0.43	0.14
Fe(ii)	2.83	~~2.68~~	3.74	3.55	3.28	3.20	~~3.59~~	3.31	3.23	3.28	3.31	3.19
Mn	0.03	~~0.04~~	0.04	0.03	0.02	0.02	~~0.04~~	0.03	0.03	0.04	0.05	0.05
Mg	1.94	~~1.88~~	1.67	1.84	1.85	1.75	~~1.60~~	1.66	1.80	1.69	1.55	1.45
Ca	0.00	~~0.00~~	0.00	0.00	0.00	0.00	~~0.00~~	0.00	0.00	0.00	0.00	0.00
Na	0.00	~~0.00~~	0.00	0.00	0.00	0.00	~~0.00~~	0.00	0.00	0.00	0.00	0.00
K	2.07	~~2.10~~	1.83	1.60	1.77	2.04	~~2.20~~	2.00	1.96	2.00	1.75	1.89
Cl	0.00	~~0.00~~	0.00	0.00	0.00	0.00	~~0.00~~	0.00	0.00	0.00	0.00	0.00
F	0.00	~~0.00~~	0.00	0.00	0.00	0.00	~~0.00~~	0.00	0.00	0.00	0.00	0.00
TOTAL	15.72	~~15.66~~	15.73	15.58	15.55	15.66	~~15.87~~	15.66	15.63	15.65	15.45	15.57

Note: Wt% = percentage weight; a.p.f.u. = atom per formula unit

Table 24 Chemical analysis of amphibole from clast n 7 in the Sample 374-U1521A-36R-1W, 80-90 *cm*

Wt%	**Amp7-1**
SiO2	44.06
TiO2	1.25
Al2O3	12.05
FeO	23.85
MnO	0.69
MgO	5.77
CaO	11.31
NaO	1.53
K_2O	1.66
Cr_2O_3	
TOTAL	97.88
a.p.f.u.	
Si	0.72
Ti	0.02
Al	0.23
Fe	0.32
Mn	0.01
Mg	0.14
Ca	0.20
Na	0.05
K	0.03
Cr	0.00
TOTAl	22.82

Note: Wt% = percentage weight; a.p.f.u. = atom per formula unit

Sample 374-U1521A-38R-1W, 110-113 cm

Table 25 Chemical analysis of biotite from Sample 374-U1521A-38R-1W, 110-113 cm

Wt%	Bt1c	Bt1r	Bt2	Bt3	Bt4	Bt5	Bt6	~~Bt7~~	Bt8	Bt9	Bt10	Bt11	Bt12	Bt13	Bt14	Bt15
SiO_2	37.93	38.15	38.81	39.13	38.32	38.47	37.82	37.59	38.66	37.85	38.73	38.82	37.93	38.41	38.05	38.21
TiO_2	5.10	5.20	4.65	4.75	4.58	4.96	4.96	5.09	4.80	5.18	4.81	4.21	4.87	4.63	4.88	4.42
Al_2O_3	14.57	14.20	14.69	14.60	14.82	14.56	14.32	14.76	14.71	14.37	14.74	14.37	14.38	14.34	14.40	14.47
FeO	26.88	26.93	24.83	25.28	25.82	25.73	27.10	26.25	25.69	26.47	25.73	26.01	26.37	26.90	26.89	26.53
MnO	0.81	0.75	0.77	0.73	0.69	0.71	0.81	0.85	0.68	0.72	0.68	0.86	0.77	0.70	0.79	0.71
MgO	8.04	8.01	8.76	8.52	8.16	8.53	7.92	8.29	8.47	8.13	8.48	8.51	8.22	7.70	8.12	8.32
CaO																
NaO																
K_2O	10.69	10.45	11.05	11.04	10.88	10.79	10.28	10.63	10.88	10.74	10.90	10.86	10.77	10.55	10.66	10.93
ClO																
F																
TOTAL	96.13	96.44	96.57	96.11	96.84	96.39	96.5	96.38	96.26	96.66	96.09	96.49	96.81	96.88	96.34	96.53
a.p.f.u.																
Si	5.52	5.56	5.61	5.64	5.58	5.57	5.53	5.48	5.59	5.53	5.59	5.64	5.55	5.62	5.55	5.57
Al^{IV}	2.48	2.44	2.39	2.36	2.42	2.43	2.47	2.52	2.41	2.47	2.41	2.36	2.45	2.38	2.45	2.43
Al^{VI}	0.01	0.00	0.12	0.12	0.13	0.06	0.00	0.01	0.10	0.00	0.10	0.10	0.03	0.09	0.02	0.06
Ti	0.56	0.57	0.51	0.51	0.50	0.54	0.55	0.56	0.52	0.57	0.52	0.46	0.54	0.51	0.53	0.49
Fe(ii)	3.27	3.28	3.00	3.04	3.15	3.12	3.31	3.20	3.11	3.23	3.11	3.16	3.22	3.29	3.28	3.24
Mn	0.10	0.09	0.09	0.09	0.08	0.09	0.10	0.10	0.08	0.09	0.08	0.11	0.10	0.09	0.10	0.09
Mg	1.74	1.74	1.89	1.83	1.77	1.84	1.73	1.80	1.82	1.77	1.82	1.84	1.79	1.68	1.76	1.81
Ca	0.00	0.00	0.00	0.00	0.00	0.00	0.00	0.00	0.00	0.00	0.00	0.00	0.00	0.00	0.00	0.00
Na	0.00	0.00	0.00	0.00	0.00	0.00	0.12	0.09	0.00	0.00	0.00	0.00	0.00	0.00	0.00	0.00
K	1.98	1.94	2.04	2.03	2.02	1.99	1.92	1.97	2.01	2.00	2.01	2.01	2.01	1.97	1.98	2.03
Cl	0.00	0.00	0.00	0.00	0.00	0.00	0.00	0.00	0.00	0.00	0.00	0.00	0.00	0.00	0.00	0.00
F	0.00	0.00	0.00	0.00	0.00	0.00	0.00	0.00	0.00	0.00	0.00	0.00	0.00	0.00	0.00	0.00
TOTAL	15.67	15.62	15.65	15.62	15.65	15.64	15.71	15.73	15.64	15.67	15.64	15.68	15.68	15.62	15.67	15.71

Note: Wt% = percentage weight; a.p.f.u. = atom per formula unit

Table 26 Chemical analysis of amphibole from Sample 374-U1521A-38R-1W, 110-113 cm

Wt%	Amp1	Amp2	Amp3	Amp4	Amp5	Amp6	Amp7
SiO2	42.29	45.50	44.85	45.13	45.39	45.16	~~48.24~~
TiO2	2.27	1.62	1.48	1.77	1.60	2.22	~~1.86~~
Al2O3	10.26	9.62	9.39	9.38	9.45	9.37	~~7.32~~
FeO	24.71	22.82	23.11	23.23	22.24	22.27	~~25.20~~
MnO	1.18	1.17	1.13	1.14	1.07	0.91	~~1.27~~
MgO	6.52	7.67	7.66	7.58	8.28	8.11	~~4.51~~
CaO	12.01	10.93	11.26	11.10	11.07	11.13	~~12.21~~
NaO	1.68	1.89	1.79	1.86	1.61	2.02	~~0.00~~
K_2O	1.23	1.24	1.24	1.13	1.16	1.08	~~1.23~~
Cr_2O_3							
TOTAL	97.89	97.59	98.13	97.73	98.16	97.77	~~98.21~~
a.p.f.u.							
Si	0.70	0.76	0.75	0.75	0.76	0.75	~~0.80~~
Ti	0.03	0.02	0.02	0.02	0.02	0.03	~~0.02~~
Al	0.20	0.19	0.18	0.18	0.19	0.18	~~0.14~~

Fe	0.34	0.32	0.32	0.32	0.31	0.31	~~0.35~~
Mn	0.02	0.02	0.02	0.02	0.02	0.01	~~0.02~~
Mg	0.16	0.19	0.19	0.19	0.21	0.20	~~0.11~~
Ca	0.21	0.19	0.20	0.20	0.20	0.20	~~0.22~~
Na	0.05	0.06	0.06	0.06	0.05	0.07	~~0.00~~
K	0.03	0.03	0.03	0.02	0.02	0.02	~~0.03~~
Cr	0.00	0.00	0.00	0.00	0.00	0.00	~~0.00~~
TOTAl	22.71	22.68	22.68	22.68	22.62	22.74	~~23.12~~

Note: Wt% = percentage weight; a.p.f.u. = atom per formula unit

Sample 374-U1521A-39R-CCW, 10-12 cm

Table 27 Chemical analysis of biotite from Sample 374-U1521A-39R-CCW, 10-12 cm

Wt%	~~Bt1~~	Bt2	Bt3	~~Bt4~~	Bt5	Bt6	Bt7	~~Bt8~~	~~Bt9~~	~~Bt10~~	~~Bt11~~	Bt12	Bt13	Bt14
SiO_2	~~42.91~~	38.10	37.77	~~38.09~~	38.91	40.98	38.77	~~39.42~~	~~37.92~~	~~37.70~~	~~42.43~~	37.91	38.24	37.05
TiO_2	~~3.55~~	3.38	3.69	~~3.00~~	2.99	2.91	3.47	~~3.88~~	~~3.96~~	~~3.91~~	~~3.79~~	3.86	3.42	3.94
Al_2O_3	~~19.09~~	19.74	19.63	~~19.53~~	18.85	18.56	19.00	~~18.34~~	~~19.40~~	~~19.45~~	~~17.19~~	19.37	19.64	19.29
FeO	~~19.71~~	22.97	22.21	~~22.24~~	22.58	21.47	22.20	~~22.06~~	~~22.12~~	~~22.07~~	~~21.20~~	22.45	21.50	21.46
MnO	~~0.41~~	0.39	0.49	~~0.43~~	0.42	0.36	0.36	~~0.42~~	~~0.43~~	~~0.53~~	~~0.36~~	0.38	0.42	0.46
MgO	~~7.47~~	9.21	8.31	~~8.90~~	8.82	8.59	8.47	~~7.55~~	~~8.51~~	~~8.12~~	~~7.32~~	8.15	8.13	8.12
CaO														
NaO	~~1.02~~						0.60	~~0.66~~						
K_2O	~~9.92~~	9.77	11.65	~~11.53~~	10.69	10.95	11.05	~~10.91~~	~~11.59~~	~~11.66~~	~~11.12~~	11.51	11.24	11.23
ClO								~~0.62~~						
F														
TOTAL	~~96.08~~	96.56	96.39	~~96.41~~	96.84	96.31	96.24	~~96.29~~	~~96.22~~	~~96.67~~	~~96.71~~	96.48	97.48	98.48
a.p.f.u.														
Si	~~5.89~~	5.38	5.37	~~5.41~~	5.53	5.73	5.49	~~5.59~~	~~5.38~~	~~5.38~~	~~5.95~~	5.40	5.46	5.37
Al^{IV}	~~2.11~~	2.62	2.63	~~2.59~~	2.47	2.27	2.51	~~2.41~~	~~2.62~~	~~2.62~~	~~2.05~~	2.60	2.54	2.63
Al^{VI}	~~0.98~~	0.67	0.67	~~0.68~~	0.68	0.80	0.66	~~0.65~~	~~0.62~~	~~0.65~~	~~0.79~~	0.65	0.77	0.67
Ti	~~0.37~~	0.36	0.39	~~0.32~~	0.32	0.31	0.37	~~0.41~~	~~0.42~~	~~0.42~~	~~0.40~~	0.41	0.37	0.43
Fe(ii)	~~2.26~~	2.71	2.64	~~2.64~~	2.68	2.51	2.63	~~2.61~~	~~2.63~~	~~2.63~~	~~2.48~~	2.67	2.57	2.60
Mn	~~0.05~~	0.05	0.06	~~0.05~~	0.05	0.04	0.04	~~0.05~~	~~0.05~~	~~0.06~~	~~0.04~~	0.05	0.05	0.06
Mg	~~1.53~~	1.94	1.76	~~1.89~~	1.87	1.79	1.79	~~1.59~~	~~1.80~~	~~1.73~~	~~1.53~~	1.73	1.73	1.76
Ca	~~0.00~~	0.00	0.00	~~0.00~~	0.00	0.00	0.00	~~0.00~~	~~0.00~~	~~0.00~~	~~0.00~~	0.00	0.00	0.00
Na	~~0.27~~	0.00	0.00	~~0.00~~	0.00	0.00	0.16	~~0.18~~	~~0.00~~	~~0.00~~	~~0.00~~	0.00	0.00	0.00
K	~~1.74~~	1.76	2.11	~~2.09~~	1.94	1.95	1.99	~~1.97~~	~~2.10~~	~~2.12~~	~~1.99~~	2.09	2.05	2.08
Cl	~~0.00~~	0.00	0.00	~~0.00~~	0.00	0.00	0.00	~~0.15~~	~~0.00~~	~~0.00~~	~~0.00~~	0.00	0.00	0.00
F	~~0.00~~	0.00	0.00	~~0.00~~	0.00	0.00	0.00	~~0.00~~	~~0.00~~	~~0.00~~	~~0.00~~	0.00	0.00	0.00
TOTAL	~~15.20~~	15.49	15.64	~~15.68~~	15.54	15.41	15.64	~~15.47~~	~~15.62~~	~~15.62~~	~~15.23~~	15.61	15.54	15.59

Note: Wt% = percentage weight; a.p.f.u. = atom per formula unit

Sample 374-U1521A-43R-2W, 94-98 cm

Table 28 Chemical analysis of biotite from clasts n 27 and 51 in the Sample 374-U1521A-43R-2W, 94-98 cm

Wt%	Bt27-1	Bt27-2	Bt27-3	Bt27-4	Bt27-5	Bt27-6	Bt51-1	Bt51-2	Bt51-3	Bt51-4	Bt51-5
SiO_2	37.93	38.64	37.73	38.33	37.92	38.08	38.49	38.27	~~37.77~~	38.14	39.70

TiO_2	4.40	4.16	4.08	2.39	4.74	4.21	2.78	3.04	~~2.94~~	2.26	2.98
Al_2O_3	16.60	16.51	16.35	16.94	16.18	15.97	19.16	18.07	~~18.52~~	18.41	19.03
FeO	26.53	26.48	27.28	27.33	27.60	26.97	22.05	23.70	~~23.35~~	23.61	23.68
MnO	0.69	0.61	0.59	0.50	0.69	0.60	0.26	0.42	~~0.37~~	0.32	0.36
MgO	6.55	7.03	6.43	7.98	6.12	7.05	9.69	8.96	~~8.91~~	9.43	9.56
CaO											
NaO											
K_2O	10.59	10.32	11.13	10.03	10.61	11.06	11.11	11.25	~~11.46~~	11.22	11.52
ClO											
F											
TOTAL	96.81	96.39	96.54	96.63	96.29	96.21	96.58	96.44	~~96.8~~	96.72	93.61
a.p.f.u.											
Si	5.52	5.58	5.52	5.56	5.52	5.53	5.46	5.48	~~5.43~~	5.47	5.49
Al^{IV}	2.48	2.42	2.48	2.44	2.48	2.47	2.54	2.52	~~2.57~~	2.53	2.51
Al^{VI}	0.37	0.38	0.33	0.45	0.30	0.27	0.66	0.52	~~0.56~~	0.58	0.58
Ti	0.48	0.45	0.45	0.26	0.52	0.46	0.30	0.33	~~0.32~~	0.24	0.31
Fe(ii)	3.23	3.20	3.33	3.31	3.36	3.28	2.61	2.84	~~2.81~~	2.83	2.74
Mn	0.08	0.07	0.07	0.06	0.08	0.07	0.03	0.05	~~0.04~~	0.04	0.04
Mg	1.42	1.51	1.40	1.72	1.33	1.53	2.05	1.91	~~1.91~~	2.02	1.97
Ca	0.00	0.00	0.00	0.00	0.00	0.00	0.00	0.00	~~0.00~~	0.00	0.00
Na	0.00	0.00	0.00	0.00	0.00	0.00	0.00	0.00	~~0.00~~	0.00	0.00
K	1.97	1.90	2.08	1.85	1.97	2.05	2.01	2.05	~~2.10~~	2.05	2.03
Cl	0.00	0.00	0.00	0.00	0.00	0.00	0.00	0.00	~~0.00~~	0.00	0.00
F	0.00	0.00	0.00	0.00	0.00	0.00	0.00	0.00	~~0.00~~	0.00	0.00
TOTAL	15.55	15.52	15.67	15.66	15.56	15.66	15.65	15.70	~~15.74~~	15.76	15.67

Note: Wt% = percentage weight; a.p.f.u. = atom per formula unit

Table 29 Chemical analysis of amphibole from clasts n 8 and 80 in the Sample 374-U1521A-43R-2W, 94-98 cm

Wt%	Amp8-1	Amp8-2	Amp80-1
SiO2	45.22	45.33	46.12
TiO2	1.47	1.39	1.10
Al2O3	10.67	10.46	12.59
FeO	20.81	20.69	16.54
MnO	0.79	0.51	0.42
MgO	8.74	9.25	10.30
CaO	11.20	11.86	12.22
NaO	1.48	1.24	1.39
K_2O	1.35	1.38	1.56
Cr_2O_3			
TOTAL	98.31	97.94	97.79
a.p.f.u.			
Si	0.74	0.74	0.75
Ti	0.02	0.02	0.01
Al	0.21	0.20	0.24
Fe	0.28	0.28	0.23
Mn	0.01	0.01	0.01
Mg	0.21	0.22	0.25
Ca	0.20	0.21	0.21
Na	0.05	0.04	0.04
K	0.03	0.03	0.03
Cr	0.00	0.00	0.00

TOTAl	22.67	22.70	22.93

Note: Wt% = percentage weight; a.p.f.u. = atom per formula unit

Sample 374-U1521A-60R-4W, 125-128 cm

Table 30 Chemical analysis of biotite from Sample 374-U1521A-60R-4W, 125-128 cm

Wt%	Bt1	Bt2	Bt3	~~Bt4~~	~~Bt5~~	Bt6	Bt7	Bt8	Bt9	Bt10	Bt11	Bt12	Bt13	Bt14	Bt15
SiO_2	39.90	39.41	39.10	~~39.37~~	~~40.08~~	40.13	39.83	40.34	39.93	39.52	40.66	39.55	41.23	39.70	40.16
TiO_2	4.37	3.94	2.92	~~3.14~~	~~4.10~~	3.15	2.51	2.76	3.74	3.14	4.46	4.87	4.80	4.74	3.97
Al_2O_3	16.47	17.88	17.92	~~18.53~~	~~17.06~~	16.57	17.04	16.67	16.57	17.48	15.62	16.20	15.82	16.28	16.66
FeO	21.06	21.62	22.24	~~22.16~~	~~20.79~~	21.90	22.19	22.04	22.48	21.58	20.56	23.06	20.09	21.09	20.43
MnO	0.16	0.37	0.31	~~0.32~~	~~0.17~~	0.28	0.23	0.32	0.35	0.30	0.21	0.32	0.12	0.12	0.19
MgO	11.51	10.84	11.89	~~11.84~~	~~10.93~~	11.65	11.90	12.06	11.72	11.83	11.63	10.29	11.28	11.36	11.63
CaO															
NaO															
K_2O	10.32	9.57	8.88	~~8.61~~	~~10.70~~	9.90	9.65	9.64	8.85	9.64	10.28	9.67	10.56	10.37	10.50
ClO															
F															
TOTAL	96.35	96.49	96.84	~~96.17~~	~~96.31~~	96.54	96.77	96.32	96.49	96.63	96.7	96.19	96.25	96.46	96.58
a.p.f.u.															
Si	5.59	5.52	5.50	~~5.48~~	~~5.61~~	5.64	5.61	5.65	5.60	5.55	5.70	5.57	5.74	5.58	5.63
Al^{IV}	2.41	2.48	2.50	~~2.52~~	~~2.39~~	2.36	2.39	2.35	2.40	2.45	2.30	2.43	2.26	2.42	2.37
Al^{VI}	0.31	0.47	0.46	~~0.51~~	~~0.43~~	0.39	0.44	0.40	0.33	0.44	0.28	0.26	0.33	0.27	0.38
Ti	0.46	0.41	0.31	~~0.33~~	~~0.43~~	0.33	0.27	0.29	0.39	0.33	0.47	0.52	0.50	0.50	0.42
Fe(ii)	2.47	2.53	2.61	~~2.58~~	~~2.43~~	2.57	2.61	2.58	2.63	2.53	2.41	2.72	2.34	2.48	2.39
Mn	0.02	0.04	0.04	~~0.04~~	~~0.02~~	0.03	0.03	0.04	0.04	0.04	0.02	0.04	0.01	0.01	0.02
Mg	2.40	2.26	2.49	~~2.46~~	~~2.28~~	2.44	2.50	2.52	2.45	2.47	2.43	2.16	2.34	2.38	2.43
Ca	0.00	0.00	0.00	~~0.00~~	~~0.00~~	0.00	0.00	0.00	0.00	0.00	0.00	0.00	0.00	0.00	0.00
Na	0.00	0.00	0.00	~~0.00~~	~~0.00~~	0.00	0.00	0.00	0.00	0.00	0.00	0.00	0.00	0.00	0.00
K	1.84	1.71	1.59	~~1.53~~	~~1.91~~	1.78	1.73	1.72	1.58	1.73	1.84	1.74	1.87	1.86	1.88
Cl	0.00	0.00	0.00	~~0.00~~	~~0.00~~	0.00	0.00	0.00	0.00	0.00	0.00	0.00	0.00	0.00	0.00
F	0.00	0.00	0.00	~~0.00~~	~~0.00~~	0.00	0.00	0.00	0.00	0.00	0.00	0.00	0.00	0.00	0.00
TOTAL	15.51	15.44	15.51	~~15.44~~	~~15.50~~	15.54	15.58	15.55	15.43	15.54	15.46	15.43	15.40	15.50	15.52

Note: Wt% = percentage weight; a.p.f.u. = atom per formula unit

Sample 374-U1521A-60R-5W, 62-65 cm

Table 31 Chemical analysis of biotite from Sample 374-U1521A-60R-5W, 62-65 cm

Wt%	Bt1c	Bt2r	Bt2	Bt3	Bt4	Bt5	Bt6
SiO_2	35.43	35.72	35.40	36.40	36.69	36.21	35.92
TiO_2	3.53	3.20	3.27	2.87	3.30	3.35	3.36
Al_2O_3	18.06	18.89	18.35	18.98	18.87	18.07	18.58
FeO	22.14	21.52	21.59	20.63	21.08	21.50	21.73
MnO							
MgO	8.21	8.65	8.22	8.78	8.13	8.36	8.26
CaO							
Na_2O							

K_2O	9.16	8.49	9.16	8.60	8.80	8.90	8.97
Cl							
F							
TOTAL	96.53	96.48	95.99	96.26	96.87	96.39	96.81
APFU							
Si	5.39	5.38	5.40	5.47	5.49	5.47	5.42
Al^{IV}	2.61	2.62	2.60	2.53	2.51	2.53	2.58
Al^{VI}	0.62	0.74	0.69	0.83	0.82	0.69	0.72
Ti	0.40	0.36	0.37	0.32	0.37	0.38	0.38
Fe(ii)	2.82	2.71	2.75	2.59	2.64	2.72	2.74
Mn	0.00	0.00	0.00	0.00	0.00	0.00	0.00
Mg	1.86	1.94	1.87	1.97	1.81	1.88	1.86
Ca	0.00	0.00	0.00	0.00	0.00	0.00	0.00
Na	0.00	0.00	0.00	0.00	0.00	0.00	0.00
K	1.78	1.63	1.78	1.65	1.68	1.72	1.73
Cl	0.00	0.00	0.00	0.00	0.00	0.00	0.00
F	0.00	0.00	0.00	0.00	0.00	0.00	0.00
TOTAL	15.48	15.39	15.47	15.35	15.32	15.39	15.42

Note: c = core; r = rim; W% = percentage weight; APFU = atom per formula unit

Sample 374-U1521A-64R-3W, 109-112 cm

Table 32 Chemical analysis of biotite from Sample 374-U1521A-64R-3W, 109-112 cm

Wt%	bt3r	bt3c	bt4	bt5	bt6	bt7r	bt7c	bt8r	bt8c
SiO_2	37.18	37.85	37.21	37.36	37.57	37.42	37.31	37.98	37.35
TiO_2	2.30	2.29	1.95	2.09	2.17	2.41	2.39	2.02	2.01
Al_2O_3	20.56	19.05	20.36	20.31	20.00	19.38	19.22	20.26	19.78
FeO	15.50	15.45	15.67	15.67	15.82	15.83	15.91	14.79	15.92
MnO									
MgO	11.70	12.37	11.97	12.05	11.94	12.22	12.35	11.72	12.37
CaO									
Na_2O									
K_2O	9.38	8.85	8.97	8.96	9.07	9.12	9.31	9.19	8.83
Cl									
F									
TOTAL	96.62	95.85	96.13	96.44	96.57	96.38	96.49	95.97	96.26
APFU									
Si	5.43	5.56	5.46	5.46	5.49	5.49	5.48	5.55	5.48
Al^{IV}	2.57	2.44	2.54	2.54	2.51	2.51	2.52	2.45	2.52
Al^{VI}	0.97	0.85	0.98	0.96	0.93	0.84	0.80	1.04	0.89
Ti	0.25	0.25	0.22	0.23	0.24	0.27	0.26	0.22	0.22
Fe(ii)	1.89	1.90	1.92	1.92	1.93	1.94	1.95	1.81	1.95
Mn	0.00	0.00	0.00	0.00	0.00	0.00	0.00	0.00	0.00
Mg	2.55	2.71	2.62	2.62	2.60	2.67	2.70	2.55	2.70
Ca	0.00	0.00	0.00	0.00	0.00	0.00	0.00	0.00	0.00
Na	0.00	0.00	0.00	0.00	0.00	0.00	0.00	0.00	0.00
K	1.75	1.66	1.68	1.67	1.69	1.71	1.74	1.71	1.65
Cl	0.00	0.00	0.00	0.00	0.00	0.00	0.00	0.00	0.00
F	0.00	0.00	0.00	0.00	0.00	0.00	0.00	0.00	0.00

TOTAL	15.42	15.37	15.41	15.40	15.40	15.42	15.47	15.34	15.42

Note: c = core; r = rim; W% = percentage weight; APFU = atom per formula unit

Sample 374-U1521A-64R-6W, 20-24 cm

Table 33 Chemical analysis of biotite from Sample 374-U1521A-64R-6W, 20-24 cm

Wt%	Bt1	Bt2	Bt3	Bt4	Bt5	Bt6	Bt7	Bt8	Bt9	Bt10	Bt11	Bt12	Bt13
SiO_2	36.37	36.47	36.63	36.38	36.45	35.75	37.15	36.55	35.39	36.56	36.53	35.92	36.36
TiO_2	3.04	2.77	2.82	3.16	2.81	3.76	3.16	2.56	2.37	1.82	2.14	2.63	2.43
Al_2O_3	16.57	16.52	17.13	17.15	16.43	15.81	14.91	16.69	14.69	17.46	16.91	16.95	15.89
FeO	22.83	23.17	21.91	22.35	23.28	24.63	23.83	22.02	26.95	22.27	22.62	23.29	24.57
MnO													
MgO	8.83	8.50	9.01	8.87	8.69	7.82	7.84	9.28	7.66	8.97	9.44	8.74	8.10
CaO													
Na_2O													
K_2O	8.72	8.75	9.04	8.94	8.41	9.12	9.26	8.87	9.45	9.07	9.09	9.07	9.04
Cl													
F													
TOTAL	96.36	96.17	96.54	96.84	96.07	96.88	96.15	95.96	96.51	96.16	96.73	96.59	96.39
APFU													
Si	5.54	5.58	5.55	5.50	5.57	5.49	5.72	5.57	5.55	5.57	5.54	5.49	5.60
Al^{IV}	2.46	2.42	2.45	2.50	2.43	2.51	2.28	2.43	2.45	2.43	2.46	2.51	2.40
Al^{VI}	0.51	0.55	0.60	0.56	0.53	0.36	0.42	0.57	0.26	0.70	0.57	0.54	0.48
Ti	0.35	0.32	0.32	0.36	0.32	0.43	0.37	0.29	0.28	0.21	0.24	0.30	0.28
Fe(ii)	2.91	2.96	2.77	2.83	2.97	3.16	3.07	2.81	3.53	2.83	2.87	2.97	3.16
Mn	0.00	0.00	0.00	0.00	0.00	0.00	0.00	0.00	0.00	0.00	0.00	0.00	0.00
Mg	2.01	1.94	2.03	2.00	1.98	1.79	1.80	2.11	1.79	2.04	2.14	1.99	1.86
Ca	0.00	0.00	0.00	0.00	0.00	0.00	0.00	0.00	0.00	0.00	0.00	0.00	0.00
Na	0.00	0.00	0.00	0.00	0.00	0.00	0.00	0.00	0.00	0.00	0.00	0.00	0.00
K	1.69	1.71	1.75	1.72	1.64	1.79	1.82	1.72	1.89	1.76	1.76	1.77	1.78
Cl	0.00	0.00	0.00	0.00	0.00	0.00	0.00	0.00	0.00	0.00	0.00	0.00	0.00
F	0.00	0.00	0.00	0.00	0.00	0.00	0.00	0.00	0.00	0.00	0.00	0.00	0.00
TOTAL	15.47	15.47	15.48	15.47	15.45	15.53	15.47	15.50	15.76	15.54	15.58	15.57	15.57

Note: W% = percentage weight; APFU = atom per formula unit

Sample 374-U1521A-68R-2W, 58-61 cm

Table 34 Chemical analysis of biotite from Sample 374-U1521A-68R-2W, 58-61 cm

Wt%	Bt1	Bt2	Bt3	Bt4	Bt5	Bt6	Bt7	Bt8	Bt9	Bt10	Bt11	Bt12
SiO_2	35.54	34.98	35.71	35.43	35.63	35.31	35.94	35.42	35.86	34.97	35.68	35.29
TiO_2	3.68	3.45	3.69	3.47	3.43	3.90	3.64	3.70	3.59	3.49	3.68	3.47
Al_2O_3	18.69	18.65	18.55	18.98	18.84	17.92	18.77	17.31	18.49	19.01	18.38	19.03
FeO	22.05	23.20	22.10	22.29	21.67	23.30	21.57	24.16	22.36	23.10	22.81	22.08
MnO												
MgO	7.98	8.20	7.95	7.99	7.79	7.33	7.64	6.93	7.50	8.27	7.38	7.82
CaO												
Na_2O												

K_2O	9.07	8.01	8.86	8.53	9.00	9.06	8.92	9.20	8.89	8.12	8.95	8.83
Cl												
F												
TOTAL	97.01	96.48	96.85	96.69	96.37	96.81	96.48	96.73	96.69	96.96	96.88	96.52
APFU												
Si	5.36	5.31	5.39	5.35	5.40	5.38	5.43	5.43	5.43	5.28	5.41	5.35
Al^{IV}	2.64	2.69	2.61	2.65	2.60	2.62	2.57	2.57	2.57	2.72	2.59	2.65
Al^{VI}	0.69	0.65	0.69	0.73	0.76	0.60	0.77	0.56	0.73	0.67	0.69	0.75
Ti	0.42	0.39	0.42	0.39	0.39	0.45	0.41	0.43	0.41	0.40	0.42	0.40
Fe(ii)	2.78	2.95	2.79	2.82	2.75	2.97	2.72	3.10	2.83	2.92	2.89	2.80
Mn	0.00	0.00	0.00	0.00	0.00	0.00	0.00	0.00	0.00	0.00	0.00	0.00
Mg	1.80	1.86	1.79	1.80	1.76	1.66	1.72	1.59	1.69	1.86	1.67	1.77
Ca	0.00	0.00	0.00	0.00	0.00	0.00	0.00	0.00	0.00	0.00	0.00	0.00
Na	0.00	0.00	0.00	0.00	0.00	0.00	0.00	0.00	0.00	0.00	0.00	0.00
K	1.75	1.55	1.71	1.64	1.74	1.76	1.72	1.80	1.72	1.57	1.73	1.71
Cl	0.00	0.00	0.00	0.00	0.00	0.00	0.00	0.00	0.00	0.00	0.00	0.00
F	0.00	0.00	0.00	0.00	0.00	0.00	0.00	0.00	0.00	0.00	0.00	0.00
TOTAL	15.43	15.40	15.39	15.39	15.40	15.44	15.35	15.48	15.37	15.41	15.40	15.41

Note: W% = percentage weight; APFU = atom per formula unit

Sample 374-U1521A-69R-6W, 40-45 cm

Table 35 Chemical analysis of biotite from Sample 374-U1521A-69R-6W, 40-45 cm

Wt%	Bt1
SiO_2	36.47
TiO_2	3.27
Al_2O_3	17.38
FeO	19.19
MnO	
MgO	10.81
CaO	
Na_2O	
K_2O	9.01
Cl	
F	
TOTAL	96.12
APFU	
Si	5.48
Al^{IV}	2.52
Al^{VI}	0.55
Ti	0.37
Fe(ii)	2.41
Mn	0.00
Mg	2.42
Ca	0.00
Na	0.00
K	1.73
Cl	0.00
F	0.00

TOTAL	15.48

Note: W% = percentage weight; APFU = atom per formula unit

Sample 374-U1521A-70R-4W, 120-125 cm

Table 36 Chemical analysis of biotite from Sample 374-U1521A-70R-4W, 120-125 cm

Wt%	Bt1	Bt2	Bt3	Bt4	Bt5	Bt6	Bt7	Bt8	Bt10	Bt11	Bt12	Bt13	Bt14	Bt15
SiO_2	36.88	37.06	37.34	37.14	37.52	37.38	37.31	37.21	37.10	36.66	37.12	37.25	37.01	37.51
TiO_2	3.88	3.34	3.49	3.61	3.19	3.46	3.46	3.53	3.76	3.81	3.65	3.52	3.69	3.53
Al_2O_3	15.71	16.36	16.00	16.19	16.91	16.43	16.39	15.86	15.58	15.70	16.30	16.41	16.13	16.27
FeO	20.25	19.56	19.71	18.94	18.81	19.03	19.08	19.73	20.27	20.15	18.92	19.00	19.85	19.16
MnO														
MgO	10.81	10.87	11.24	11.16	11.19	11.40	11.06	10.88	10.54	10.90	11.27	10.99	10.98	10.83
CaO														
Na_2O														
K_2O	8.93	9.12	9.06	9.13	9.02	9.18	9.19	9.33	9.49	9.22	9.03	9.19	9.16	9.06
Cl														
F														
TOTAL	96.46	96.31	96.84	96.17	96.63	96.87	96.49	96.54	96.73	96.44	96.29	96.36	96.82	96.35
APFU														
Si	5.55	5.57	5.58	5.57	5.58	5.57	5.58	5.59	5.59	5.53	5.56	5.58	5.54	5.61
Al^{IV}	2.45	2.43	2.42	2.43	2.42	2.43	2.42	2.41	2.41	2.47	2.44	2.42	2.46	2.39
Al^{VI}	0.34	0.46	0.40	0.44	0.55	0.45	0.47	0.40	0.35	0.32	0.43	0.47	0.39	0.48
Ti	0.44	0.38	0.39	0.41	0.36	0.39	0.39	0.40	0.43	0.43	0.41	0.40	0.42	0.40
Fe(ii)	2.55	2.46	2.46	2.38	2.34	2.37	2.39	2.48	2.55	2.54	2.37	2.38	2.49	2.40
Mn	0.00	0.00	0.00	0.00	0.00	0.00	0.00	0.00	0.00	0.00	0.00	0.00	0.00	0.00
Mg	2.43	2.43	2.50	2.50	2.48	2.53	2.47	2.44	2.37	2.45	2.52	2.45	2.45	2.42
Ca	0.00	0.00	0.00	0.00	0.00	0.00	0.00	0.00	0.00	0.00	0.00	0.00	0.00	0.00
Na	0.00	0.00	0.00	0.00	0.00	0.00	0.00	0.00	0.00	0.00	0.00	0.00	0.00	0.00
K	1.72	1.75	1.73	1.75	1.71	1.74	1.75	1.79	1.82	1.77	1.72	1.76	1.75	1.73
Cl	0.00	0.00	0.00	0.00	0.00	0.00	0.00	0.00	0.00	0.00	0.00	0.00	0.00	0.00
F	0.00	0.00	0.00	0.00	0.00	0.00	0.00	0.00	0.00	0.00	0.00	0.00	0.00	0.00
TOTAL	15.47	15.48	15.48	15.46	15.44	15.48	15.46	15.50	15.52	15.53	15.45	15.46	15.49	15.42

Note: W% = percentage weight; APFU = atom per formula unit

APPENDIX V

Petrology of IODP Site U1522 clasts

This section shows petrographic descriptions of gravel-sized clasts sampled from Site U1522 core (Table 4). Petrographic analysis was carried out with a Leica DMLP polarizer microscopy equipped with a Leica ICC50 HD camera on polished thin sections. Each description is coupled with photomicrographs underlying representative features and microstructures. At the end of the figures and descriptions Table 37 summarizes clasts classification. Table 38 shows lithological percentages of lithic grains composing the > 2mm sieved fraction from bulk diamictite sample.

Sample 374-U1522A-55R-2W, 17-20 cm - Biotite meta-sandstone

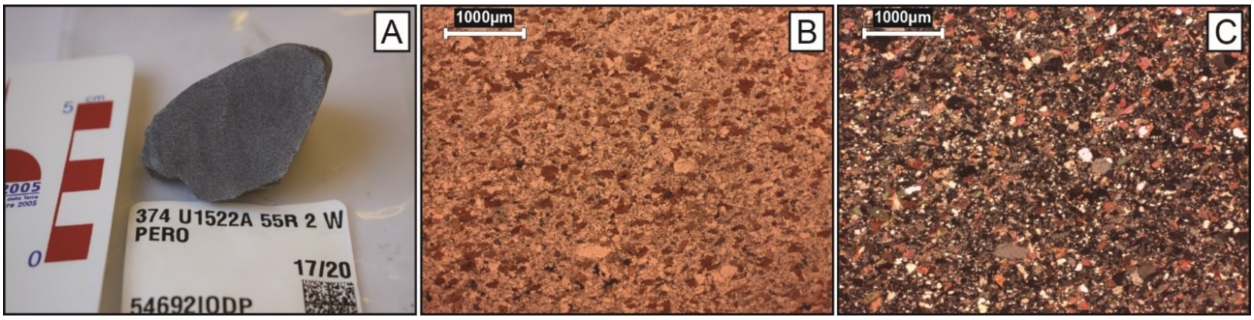

Figure 74 A) Macroscopic picture of the clast; B) PPL photomicrograph (2.5x); C) XPL photomicrograph (2.5x)

Hetero-granular, very fine to medium grained, lightly foliated meta-sedimentary rock. Quartz and plagioclase are the main components; they are mainly very fine grains and minor medium grained; biotite defines weak foliation. Calcite commonly occurs in the matrix. Accessory minerals are opaque, zircon, apatite, and titanite.

374-U1522A-55R-3W, 52-56 cm - (Meta-)limestone

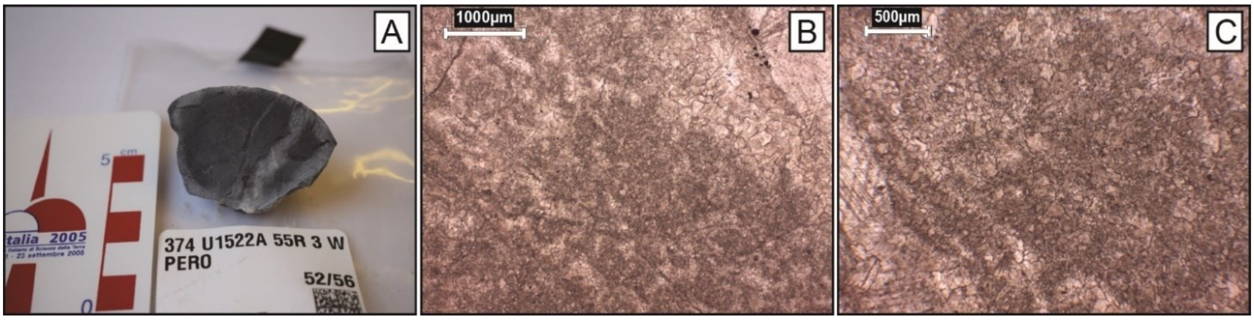

Figure 75 Macroscopic picture of the clast; B) PPL photomicrograph (2.5x); C) XPL photomicrograph (4x)

Heterogranular carbonate rock commonly crossed by veins filled by coarse-grained calcite and minor quartz. Rocks is completely constituted by calcite, weakly recrystallized, and rare quartz. Calcite crystals range from micro-sparite to sparite. Original bioclastsic structure is may recognizable.

374-U1522A-56R-1W, 48-51 cm - Biotite – White Mica meta-sandstone

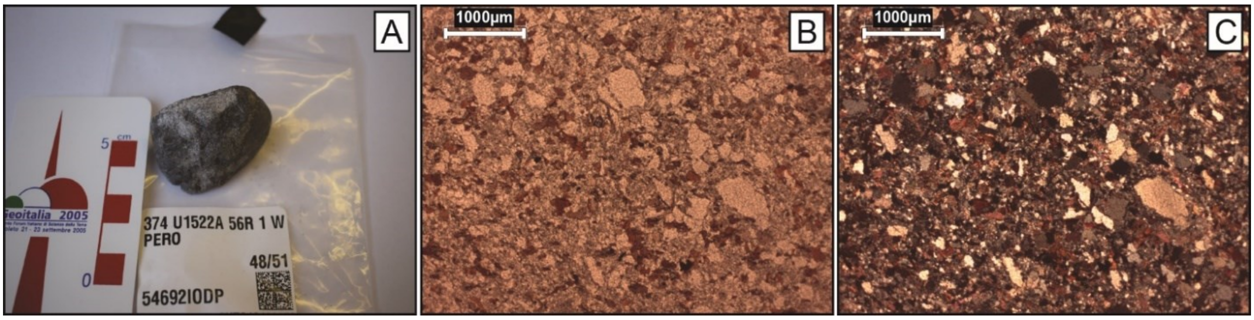

Figure 76 A) Macroscopic picture of the clast; B) PPL photomicrograph (2.5x); C) XPL photomicrograph (2.5x)

The rock is medium/fine-grained and weakly foliated. The protolith was of sedimentary origin (probably a greywacke). The rock is made up of quartz and minor feldspars crystals in a fine-grained matrix where calcite commonly occurs. Neoblastic biotite constituted ca. 20% of the whole. Accessory minerals are zircon, apatite, and opaque minerals. White mica is sometimes associated with biotite (secondary???).

374-U1522A-56R-4W, 44-46 cm – Volcanic rock

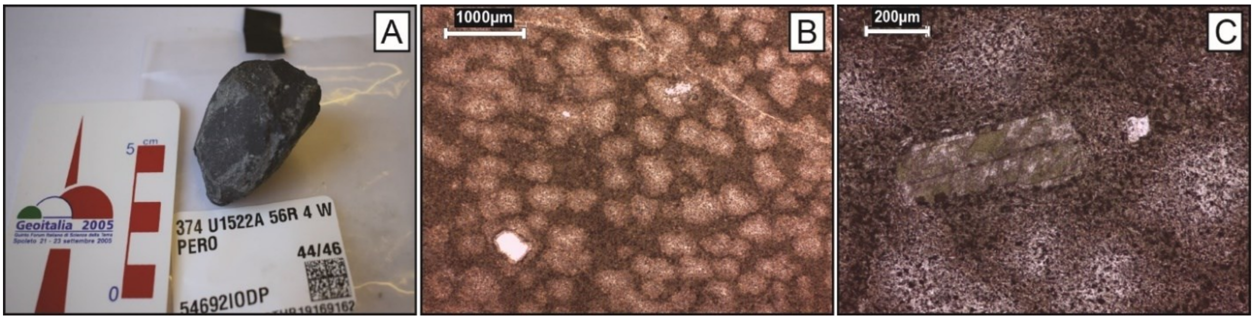

Figure 77 Macroscopic picture of the clast; B) PPL photomicrograph (2.5x); C) PPL photomicrograph (10x)

The rock is very fine grained, slightly porphyritic, and strongly altered. Scattered small porphyritic crystals occur within the groundmass; they are constituted by euhedral to subhedral feldspars (probably plagioclase), sometimes skeletal, which are strongly altered and quartz that has reaction crowns. The groundmass shows wide textural and compositional differences: it is mainly composed by feldspars, mainly isoriented, a green mineralogical phase (chlorite?) and calcite; in the groundmass subcircular spots are widely diffuse and they are constituted only by feldspars. Opaque minerals are common in the rock. The presence of feldspars, together with euhedral to subhedral phenocrystals indicate that the rock has volcanic origin.

374-U1522A-57R-1W, 0-3 cm - Biotite – White Mica meta-sandstone

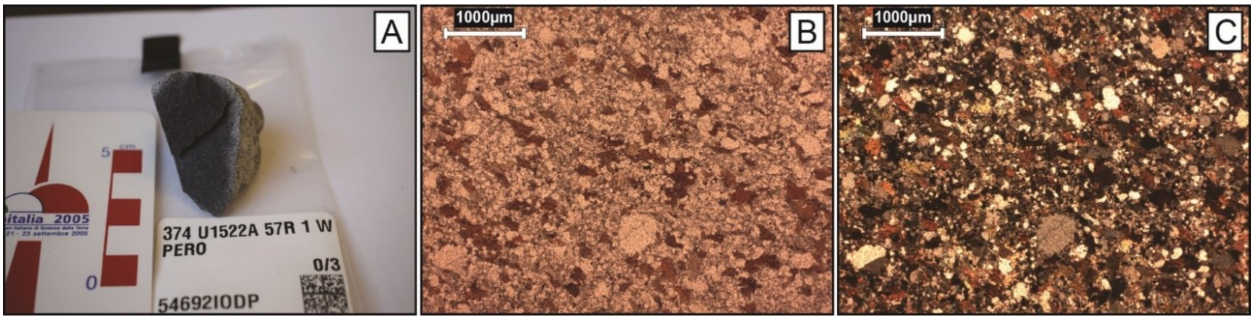

Figure 78 Macroscopic picture of the clast; B) PPL photomicrograph (2.5x); C) XPL photomicrograph (2.5x)

The rock is medium/fine-grained and weakly foliated. The protolith was of sedimentary origin (probably a greywacke). The rock is made up of quartz and minor feldspars crystals in a fine-grained matrix where calcite commonly occurs. Neoblastic biotite constituted ca. 20% of the whole. Accessory minerals are zircon, apatite, and opaque minerals. White mica is sometimes associated with biotite (secondary???).

374-U1522A-57R-2W, 120-123 cm – Felsic Porphyry

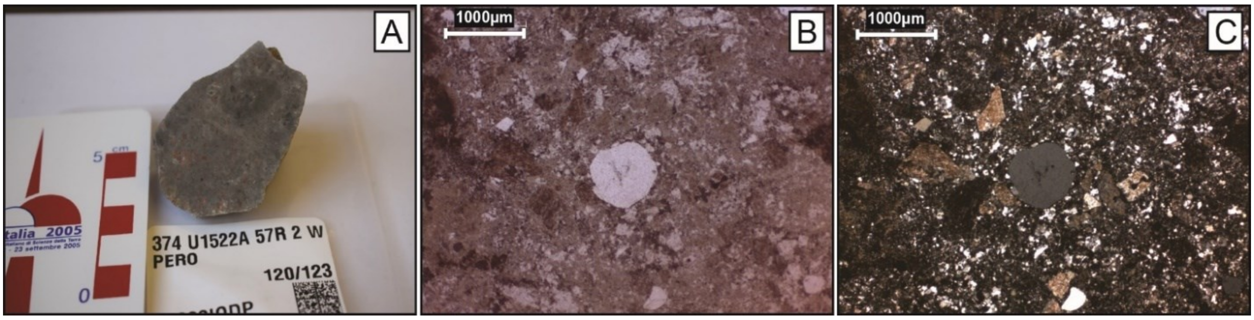

Figure 79 Macroscopic picture of the clast; B) PPL photomicrograph (2.5x); C) XPL photomicrograph (2.5x)

The rock has a holocrystalline porphyritic texture, with felsic composition. Phenocrystals, locally with glomeroporphyric texture, are millimetric, subhedral to euhedral, and they are mainly made up by feldspars, strongly replaced by sericite, and secondly by quartz, which shows reabsorption rims. Matrix is microcrystalline to very fine-grained, constituted by quartz and feldspar, that is partially replaced by sericite. In the rock portions where the matrix is microcrystalline, feldspars spherulites are common, sometimes with quartz crystals as core. Opaque minerals are common as accessory, zircons rarer. The rock is strongly altered.

374-U1522A-57R-5W, 1-6 cm – Foliated Granite/Meta-granite

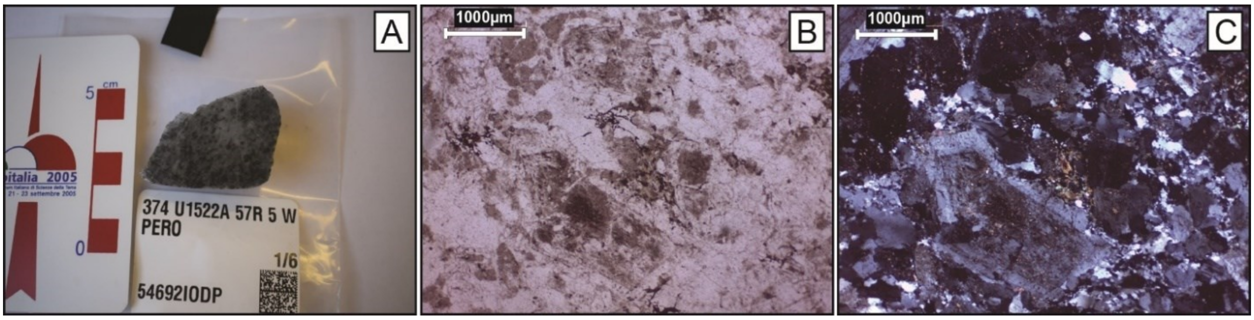

Figure 80 Macroscopic picture of the clast; B) PPL photomicrograph (2.5x); C) XPL photomicrograph (2.5x)

The rock is medium/fine grained and shows a slightly foliated/gneissic texture. The mineralogical composition is dominated by quartz, strongly recrystallized and with marked wavy extinction, plagioclase, which sometimes constitutes euhedral to subhedral shaped oversized crystals with chemical zonation, and alkali feldspar. Feldspars are strongly altered. Some rock portions show aggregates of biotite (2-3%), partially replaced by white mica and epidote.

374-U1522A-57R-5W, 37-41 cm – Biotite Orthogneiss

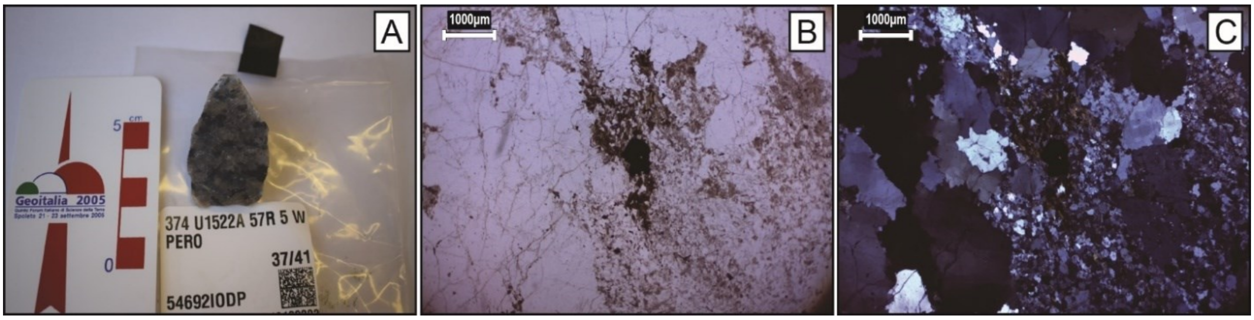

Figure 81 Macroscopic picture of the clast; B) PPL photomicrograph (1.6x); C) XPL photomicrograph (1.6x)

The rock shows gneissic texture. Mafic minerals represent about 5% of rock and are biotite, partially replaced by chlorite. The rock is composed by isolated, medium grained, orthoclase crystal, weakly altered; layers of medium/coarse grained quartz with strong wavy extinction; layers constituted by fine grained crystals of quartz, sometimes with granoblastic polygonal texture, and alkali feldspars, both orthoclase and microcline. Sub-euhedral prismatic opaque minerals are common; zircons are accessory minerals.

374-U1522A-58R-1W, 68-71 cm - Biotite Monzogranite

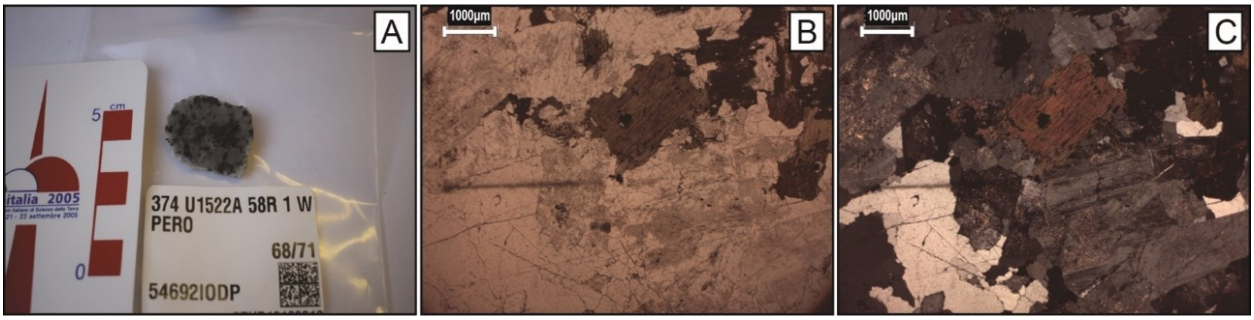

Figure 82 A) Macroscopic picture of the clast; B) PPL photomicrograph (1.6x); C) XPL photomicrograph (1.6x)

Holocrystalline, slightly hetero-granular, from fine/medium to coarse grained, rock with isotropic texture. Quartz, showing homogeneous extinction, constitutes about 30% of rock; alkali feldspars are about 25%, with orthoclase less common than microcline; euhedral to subhedral plagioclase, usually with chemical zonation, constitutes 35%. Feldspars are partially replaced by sericite; the biotite, weakly replaced by chlorite, represent 10% of the whole rock.

374-U1522A-58R-3W, 120-121 cm – Laminated Mudstone

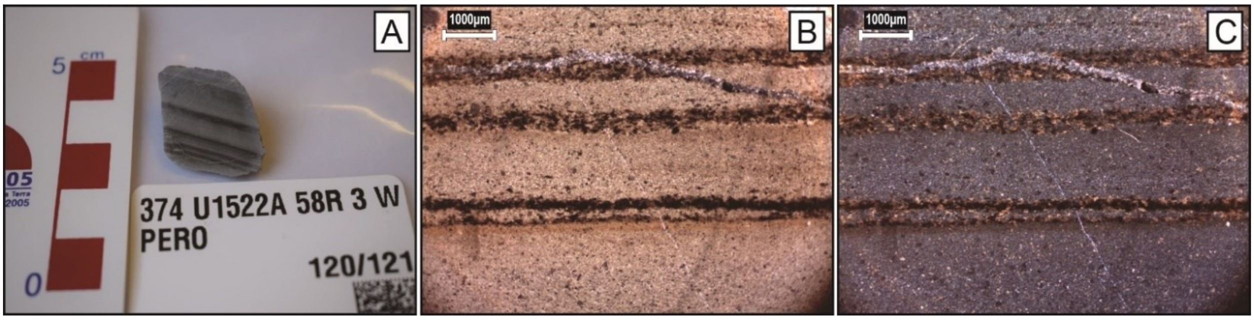

Figure 83 Macroscopic picture of the clast; B) PPL photomicrograph (1.6x); C) XPL photomicrograph (1.6x)

Equigranular, very fine grained, sedimentary rock with marked parallel lamination. The rock is mainly composed by very fine grained quartzo-feldspatic matrix; the lamination is marked by thin oxidised layers, associated with carbonates, probably calcite or siderite.

374-U1522A-58R-4W, 4-7 cm – Meta-granitoid

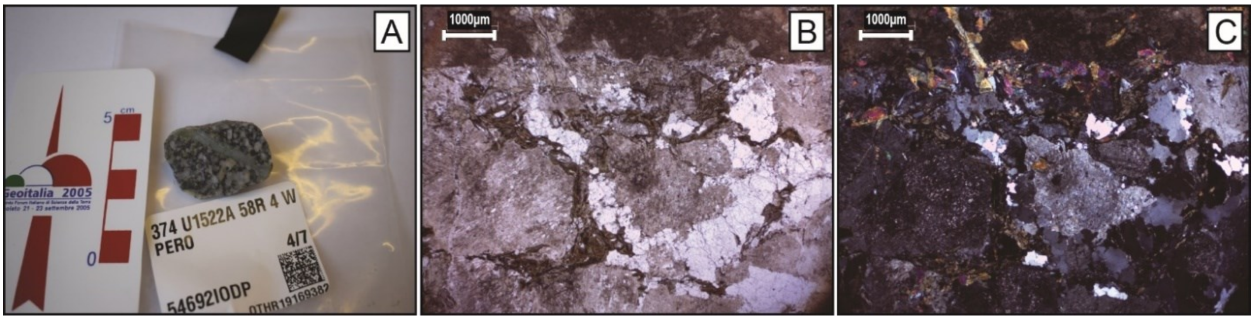

Figure 84 Macroscopic picture of the clast; B) PPL photomicrograph (1.6x); C) XPL photomicrograph (1.6x)

Medium grained, strongly hetero-granular, slightly foliated rock. The rock is cut by a ca. 4mm large vein/shear zone(??), made up of very fine grains. The rock is mainly constituted by feldspar, strongly altered but with most of them where twin geminations and chemical zonation of plagioclase are recognizable yet; may K-feldspar occurs. Quartz is minor and smaller; it shows wavy extinction and seems to be recrystallized. Mafic minerals are less than 10%; most of them is biotite, partially replaced by chlorite. Epidote is a common mineral phase, both in the rock and in the vein/shear zone.

374-U1522A-58R-6W, 131-133 cm – Micro leucogranite

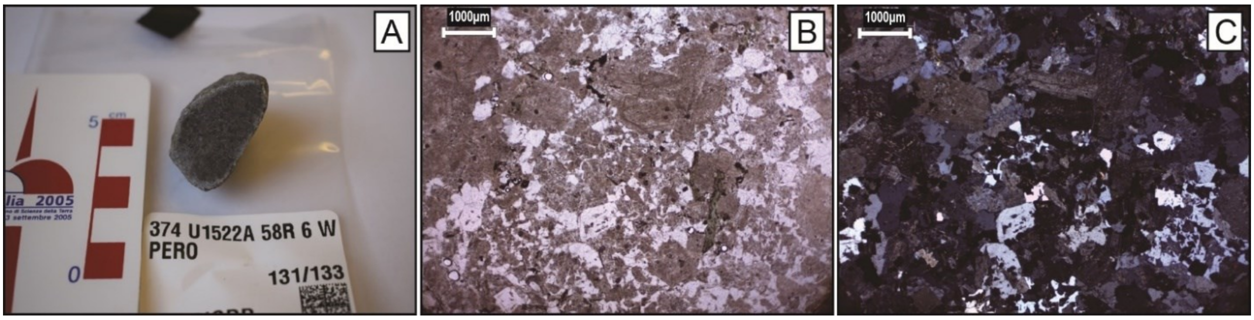

Figure 85 A) Macroscopic picture of the clast; B) PPL photomicrograph (1.6x); C) XPL photomicrograph (1.6x)

The rock is holocrystalline, fine grained, slightly porphyritic, with isotropic texture. The main constituents are feldspars, both plagioclase and orthoclase, and quartz. Plagioclase form anhedral to subhedral crystals which are almost completely replaced by sericite and clay mineral aggregates, although twinning and chemical zonation is frequently recognizable. Orthoclase is almost completely replaced by sericite and clay mineral aggregates. Quartz forms anhedral crystals with homogeneous extinction. Mafic minerals are ca. 5% of the whole and they were completely replaced by chlorite and white mica. Opaques are common accessory minerals.

374-U1522A-59R-7W, 22-24 cm - Granite

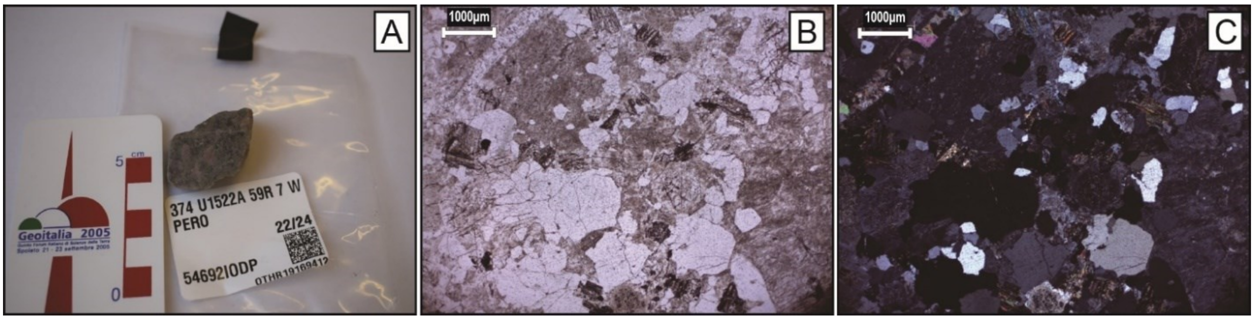

Figure 86 A) Macroscopic picture of the clast; B) PPL photomicrograph (1.6x); C) XPL photomicrograph (1.6x)

Holocrystalline, medium-grained, porphyritic rock with isotropic texture. Feldspars are the main mineralogical phase. Orthoclase forms both medium-grained anhedral to subhedral crystals and porphyritic subhedral to euhedral ones. Plagioclase is less common and usually form subhedral to anhedral crystals. Both feldspars are almost completely replaced by sericite, clay mineral aggregates, and calcite. Quartz, which forms anhedral crystals, shows homogeneous extinction. Mafic minerals were completely replaced by chlorite and white mica. Calcite vein cuts the sample.

374-U1522A-59R-7W, 91-93 cm – Basalt

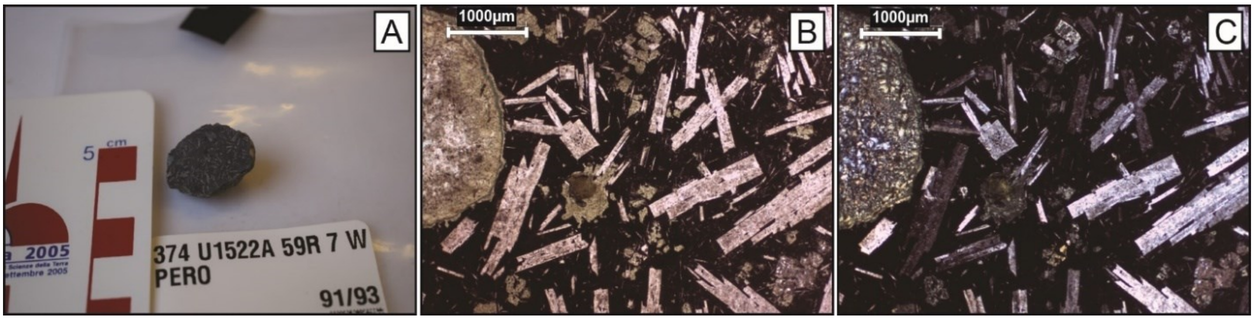

Figure 87 Macroscopic picture of the clast; B) PPL photomicrograph (2.5x); C) XPL photomicrograph (2.5x)

The rock has volcanic, isotropic, porphyritic texture. Millimetric-scale phenocrystals, euhedral to subhedral, are made up of twinned plagioclase; plagioclase is also present as skeletal fine-grained phenocrystals and as microliths. The rock also presents subhedral to euhedral hexagonal crystals totally replaced by alteration minerals (may olivine or pyroxene). Rounded vesicles are present and filled by chalcedony.

374-U1522A-60R-3W, 64-66 cm – Felsic Porphyry

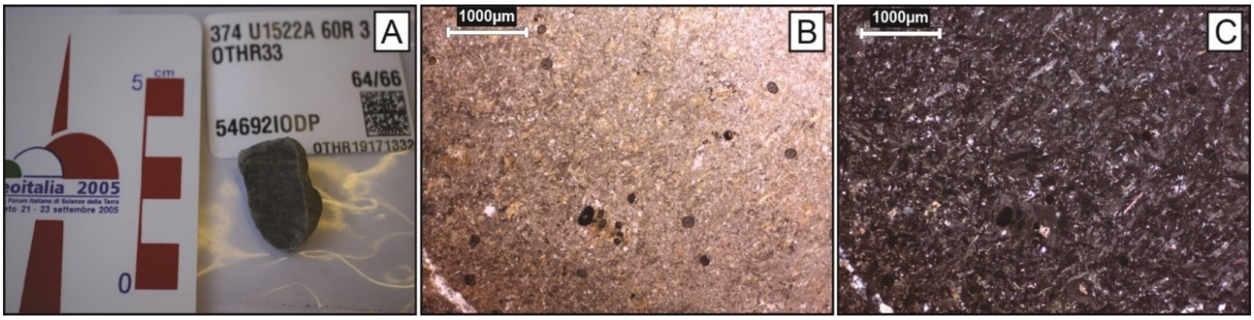

Figure 88 Macroscopic picture of the clast; B) PPL photomicrograph (2.5x); C) XPL photomicrograph (2.5x)

Holocrystalline rock with porphyritic, isotropic texture. Phenocrystals are rare, subhedral and made up of alkali feldspar(?), partially replaced by sericite. Groundmass is very fine grained and mainly constitute by feldspar, less common is quartz (<5%), that occupies interstitial position.

374-U1522A-60R-3W, 87-91 cm – Olivine Gabbro/Mafic Intrusive

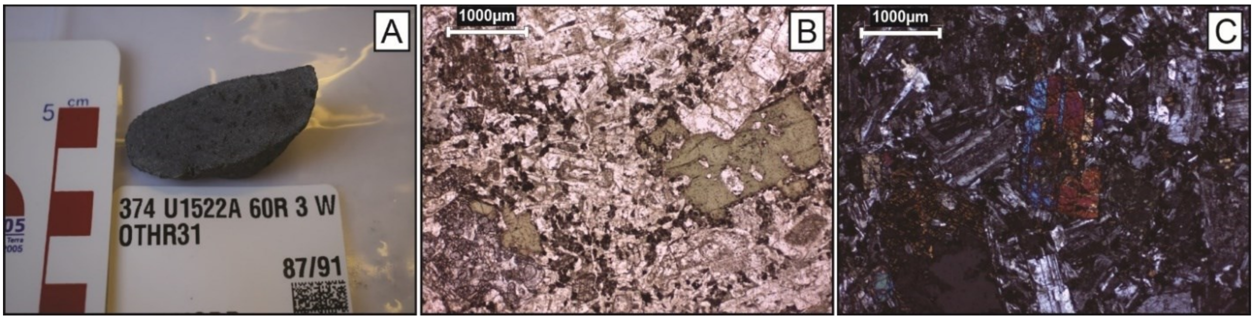

Figure 89 Macroscopic picture of the clast; B) PPL photomicrograph (2.5x); C) XPL photomicrograph (2.5x)

The rock is a medium to fine grained, hetero-granular mafic rock. The sub-ophitic texture, typical of dolerites, is not well developed. Some euhedral to subhedral, broadly hexagonal, grains occur which originally were constituted by olivine; those grains are completely replaced by serpentine. The rock composition is dominated by plagioclase, strongly replaced by sericite, and secondly by clinopyroxene, rims of which are partially replaced by serpentine.

374-U1522A-60R-5W, 36-40 cm - Meta-granite

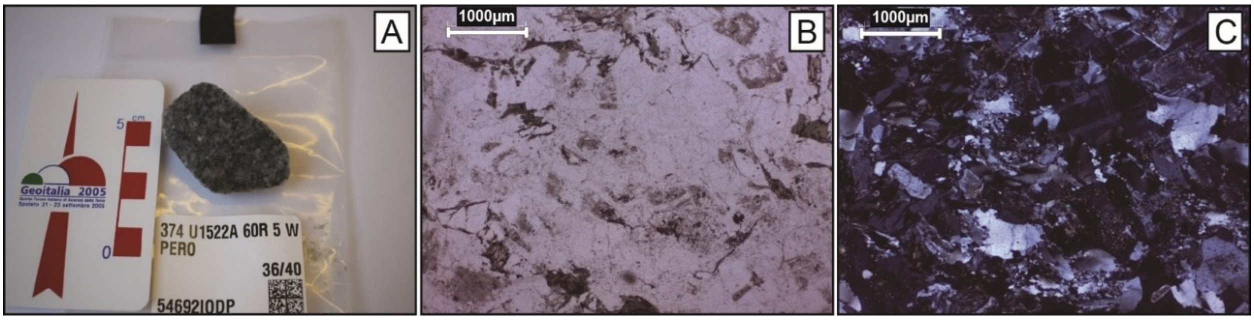

Figure 90 Macroscopic picture of the clast; B) PPL photomicrograph (2.5x); C) XPL photomicrograph (2.5x)

The rock show strongly heterogranular (very fine- to medium-grained) with a weak foliated texture. The main mineralogical phases are quartz and feldspar. Quartz is strongly recrystallized and usually shows marked mortar texture and undulose extinction. Feldspar is mainly alkali feldspar (pertite and microcline) and sometime forms porphyritic crystals; minor is plagioclase, sometimes zoned. Mafic mineral, that represent less than 5% of the whole, is secondary magnesian chlorite, sometimes associated with epidote.

374-U1522A-61R-1W, 0-2 cm – (Intermediate) Basalt

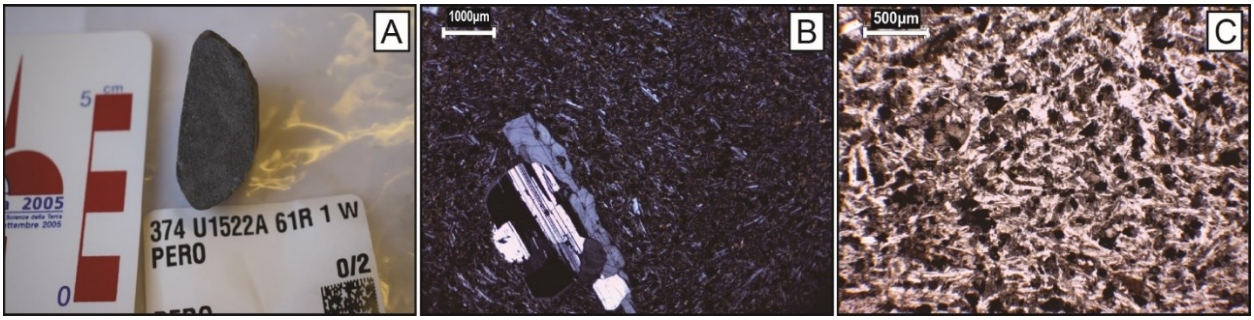

Figure 91 Macroscopic picture of the clast; B) XPL photomicrograph (1.6x); C) PPL photomicrograph (4x)

Hypocrystalline rock, non-vesicular, with fluidal, porphyritic texture. Phenocrystals are millimetric, subhedral with reabsorption rims, made up of zoned and twinned plagioclase. Groundmass is holocrystalline and constitute by tabular crystals of plagioclase, showing a fluidal orientation; less common are subhedral clinopyroxene crystals. Subhedral prismatic opaque minerals are widespread within the rock.

374-U1522A-61R-1W, 29-32 cm – Mafic Intrusive

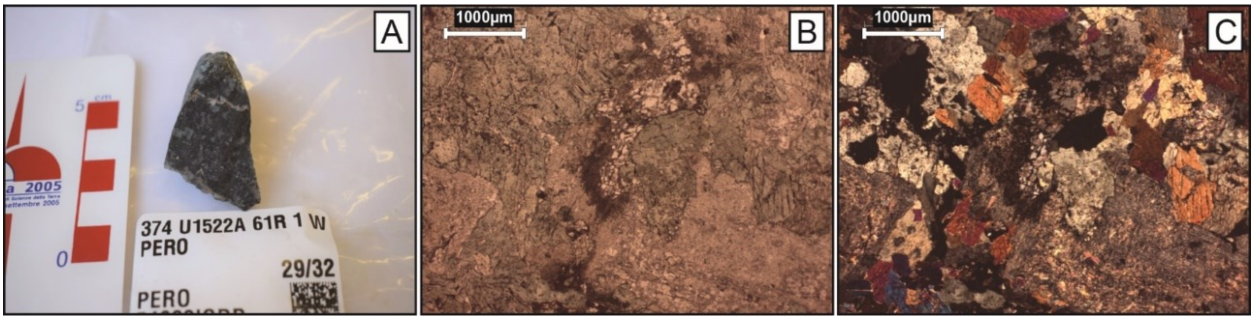

Figure 92 A) Macroscopic picture of the clast; B) PPL photomicrograph (2.5x); C) XPL photomicrograph (2.5x)

Holocrystalline, mafic intrusive rock, with equigranular, medium grained, isotropic texture. The main component is hornblende (green amphibole); feldspars are almost completely altered but they seem to be plagioclase because twinning is sometimes recognizable; alkali feldspar is also present. Quartz is rare and it occupy interstitial position. Secondary chlorite is common in the sample.

374-U1522A-61R-1W, 44-47 cm – Meta-porphyry

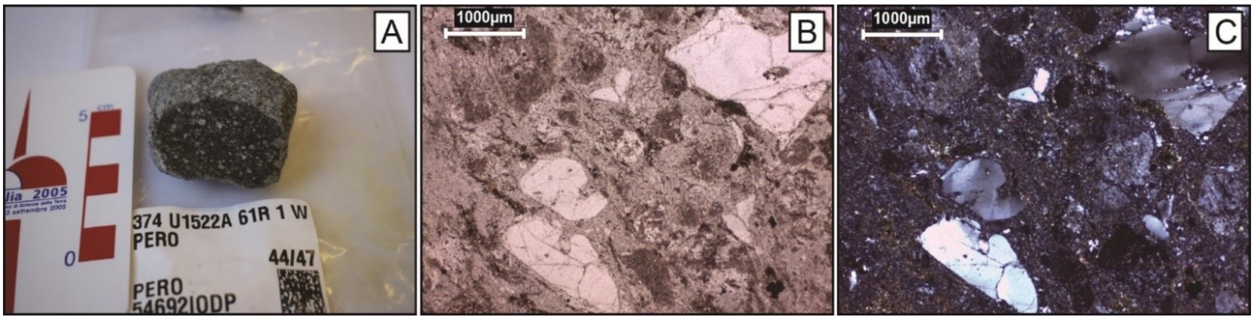

Figure 93 Macroscopic picture of the clast; B) PPL photomicrograph (2.5x); C) XPL photomicrograph (2.5x)

The rock is heterogranular and shows a broad schistosity. The matrix is very fine-grained, and it composed of quartz, feldspars, biotite and white mica. Quartz and feldspars are recrystallized; biotite is usually associated with white mica in lens-shaped agglomerates, partially with sheaf texture. Porphyritic clasts are mainly made up of quartz, plagioclase and alkali feldspar. Quartz, usually subhedral, seems to show reabsorption rims and it have strong wavy extinction and it is partially recrystallized. Plagioclase porphyritic clasts are subhedral, partially replaced by sericite; they usually maintain the chemical zonation. alkali feldspars are rare and strongly altered.

374-U1522A-61R-CCW, 38-40 cm – Biotite hornfels

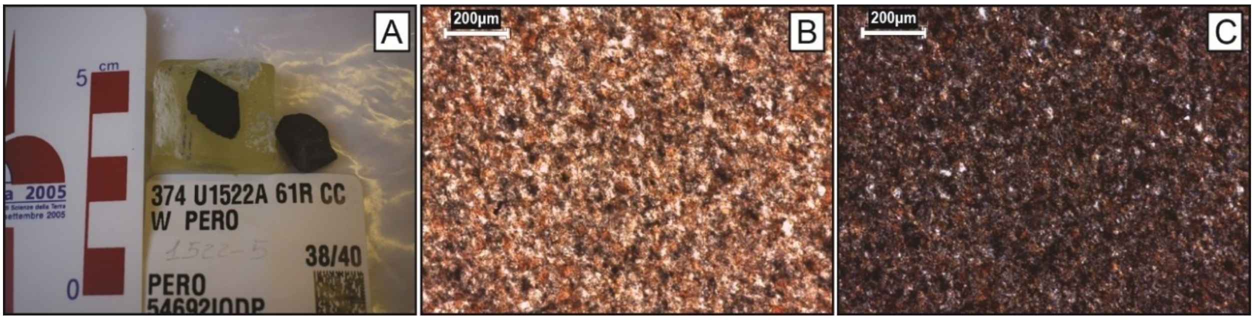

Figure 94 Macroscopic picture of the clast; B) PPL photomicrograph (10x); C) XPL photomicrograph (10x)

Very fine grained meta-sedimentary rock, with isotropic, equigranular texture. The rock is mainly quartzo-feldspatic (ca. 60%), and biotite constitutes ca. 40%.

374-U1522A-61R-CCW, 67-70 cm – Porphyry

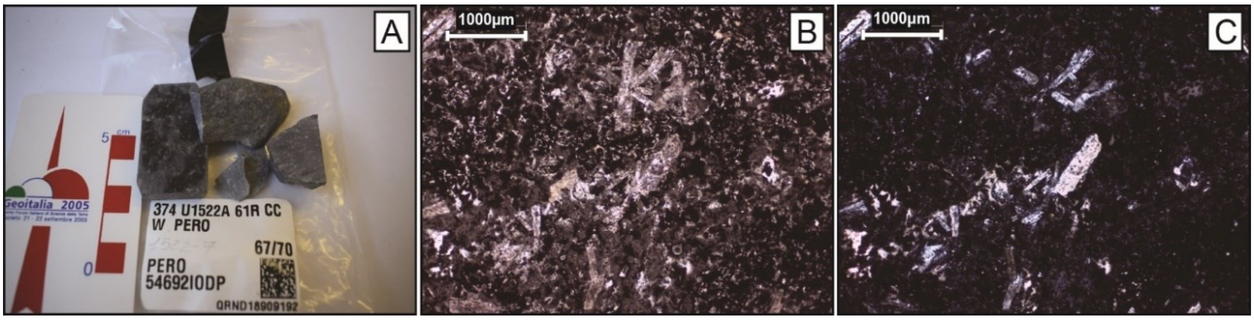

Figure 95 Macroscopic picture of the clast; B) PPL photomicrograph (2.5x); C) XPL photomicrograph (2.5x)

Holocrystalline, with isotropic texture, porphyritic rock. Phenocrystals are plurimillimetric, with subhedral tabular shape, made up of plagioclase; almost rare are quartz ones. Groundmass is mainly constituted by opaque minerals, forming ring shapes around feldspars rims; groundmass feldspars are almost completely replaced by sericite and calcite. Where the groundmass is finer (microcrystalline), feldspar spherulites are common. May mafic porphyritic crystals, completely altered, with elongated hexagonal shape.

374-U1522A-62R-1W, 12-15 cm – Basalt

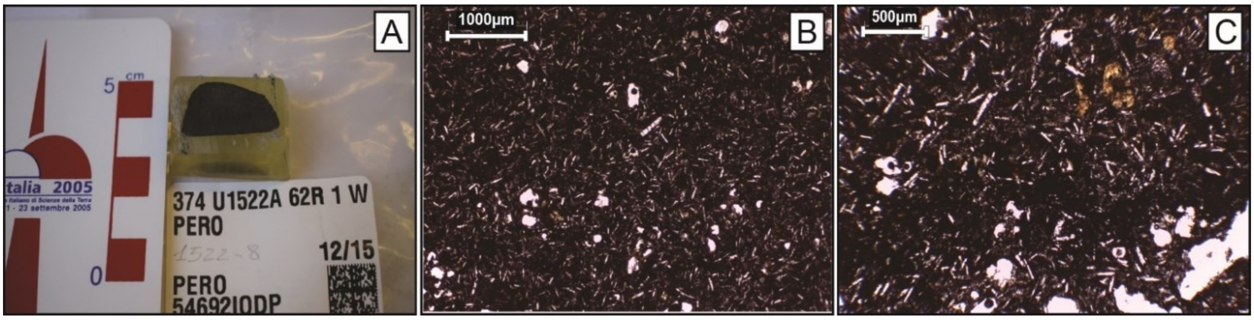

Figure 96 Macroscopic picture of the clast; B) PPL photomicrograph (2.5x); C) PPL photomicrograph (4x)

Volcanic rock, with isotropic, hypocrystalline, micro-porphyritic texture; micro-vesicles, unfilled, are present. Groundmass is made up of feldspar (probably plagioclase) microliths, tabular plagioclase, and pyroxene. Within the section, subhedral hexagonal micro-phenocrystals are common; they are made up of bowlingite(?), one of the alteration products of olivine.

374-U1522A-62R-1W, 65-68 cm - Micro-gabbro/Dolerite

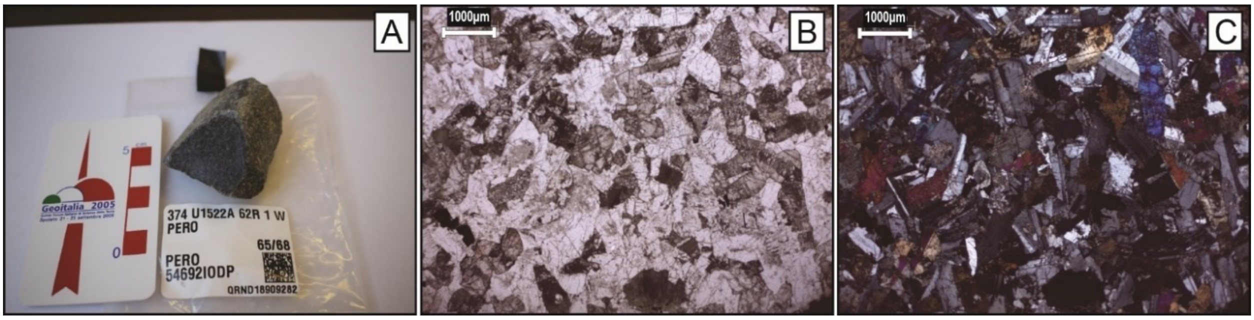

Figure 97 A) Macroscopic picture of the clast; B) PPL photomicrograph (1.6x); C) XPL photomicrograph (1.6x)

The rock is medium/fine-grained, equigranular, isotropic with slightly sub-ophitic texture. The rock is mainly composed by subhedral plagioclase and clinopyroxene. Interstitial quartz rarely occurs.

374-U1522A-62R-2W, 8-10 cm – Dolerite/Micro-gabbro

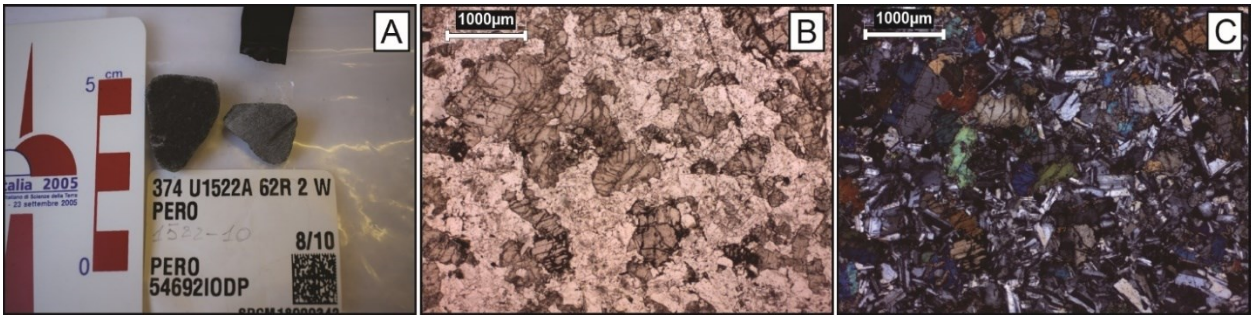

Figure 98 Macroscopic picture of the clast; B) PPL photomicrograph (2.5x); C) XPL photomicrograph (2.5x)

Holocrystalline mafic rock, with isotropic, equigranular, fine grained, texture. The main component is subhedral plagioclase, and both orthopyroxene and clinopyroxene; pyroxene is commonly twinned and minor with unmixing(?) lamellae. Quartz crystals are rare. Sub-ophitic texture is less developed.

374-U1522A-62R-2W, 49-52 cm - Micro-granite

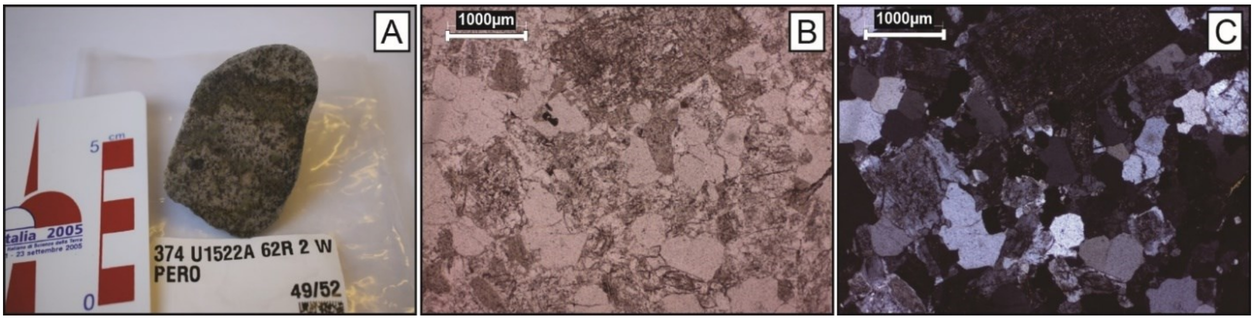

Figure 99 Macroscopic picture of the clast; B) PPL photomicrograph (2.5x); C) XPL photomicrograph (2.5x)

Fine-grained, quite equigranular, isotropic intrusive rock. The main mineralogical phase is feldspars, both plagioclase and alkali-feldspar. Plagioclase is partially replaced by sericite and clay mineral aggregates; plagioclase crystals are sometimes slightly porphyritic and with subhedral shape. Orthoclase is fine-grained and anhedral. Quartz is fine grained and constitute ca. 30% of the whole. Secondary white mica rarely occurs.

374-U1522A-62R-2W, 52-55 cm - Sandstone

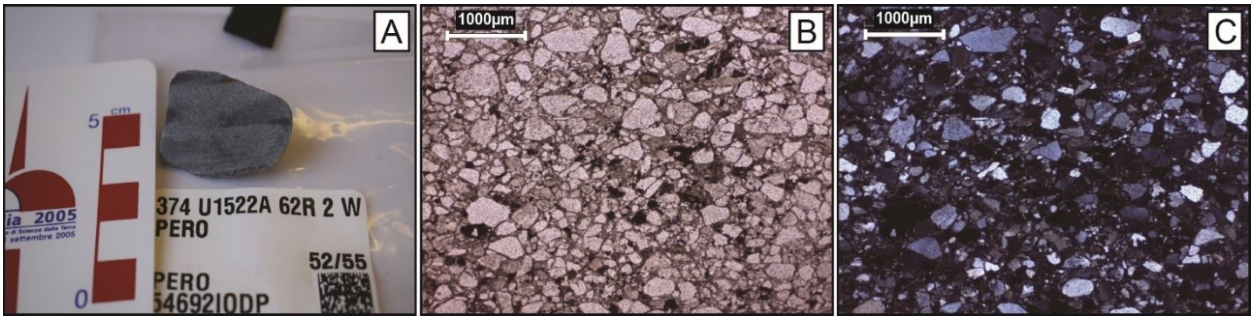

Figure 100 Macroscopic picture of the clast; B) PPL photomicrograph (2.5x); C) XPL photomicrograph (2.5x)

Medium-grained clastic sedimentary rock; the sample is clast-supported whereas fine-grained matrix occurs. Grains are broadly isoriented. Grains are rounded to sub-angular and made up of monocrystalline quartz and minorly plagioclase and alkali-feldspar. Lithic fragments rarely occur, and they are constituted by fine-grained metamorphic rocks and felsic volcanic rocks. Opaque minerals are common; other accessory minerals are brown to greenish tourmaline, zircon, and white mica.

374-U1522A-62R-CCW, 17-20 cm – Felsic Porphyry

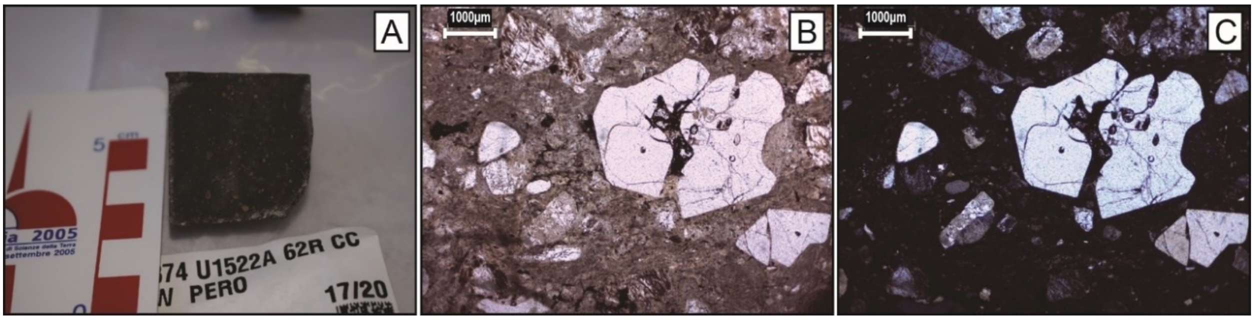

Figure 101 Macroscopic picture of the clast; B) PPL photomicrograph (1.6x); C) XPL photomicrograph (1.6x)

Porphyritic sub-volcanic rock with fluidal texture. Phenocrystals, that are up to 4 mm, constitute ca. 35% of the whole. They are made up of anhedral to subhedral crystals of quartz, usually showing embayed rims, subhedral crystals of plagioclase, usually zoned and partially replaced by sericite and clay mineral aggregates, and anhedral to subhedral crystals of alkali feldspar, sometimes strongly replaced by sericite and clay minerals aggregates. Scattered lamellae of mafic mineral occur within the sample whereas they are completely replaced by chlorite and white mica and the original mineralogy is not recognizable. The matrix is very fine-grained, quartzo-feldspatic, and with fluidal texture; sometimes spherulites occur. Opaque mineral are common accessories.

374-U1522A-63R-2W, 112-115 cm - White mica meta-siltstone

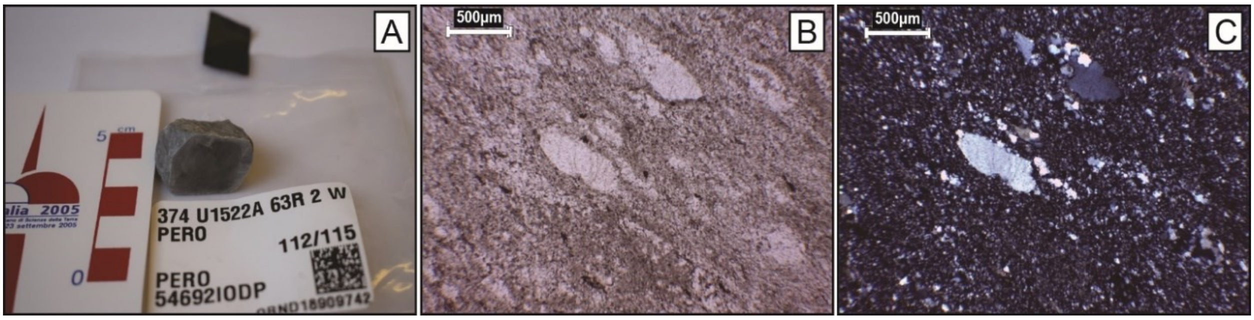

Figure 102 Macroscopic picture of the clast; B) PPL photomicrograph (4x); C) XPL photomicrograph (4x)

Very fine-grained schistose rock, weakly banded. The composition is dominated by fine grained quartz and minor feldspar, whereas some layers are richer in feldspar rather than others where quartz dominate. Sometimes porphyroblasts of quartz, with undulose extinction, occur. White mica fie-grained crystals are common, and they define the schistosity. Calcite is also common within the sample.

374-U1522A-64R-1W, 1-5 cm – Gneiss

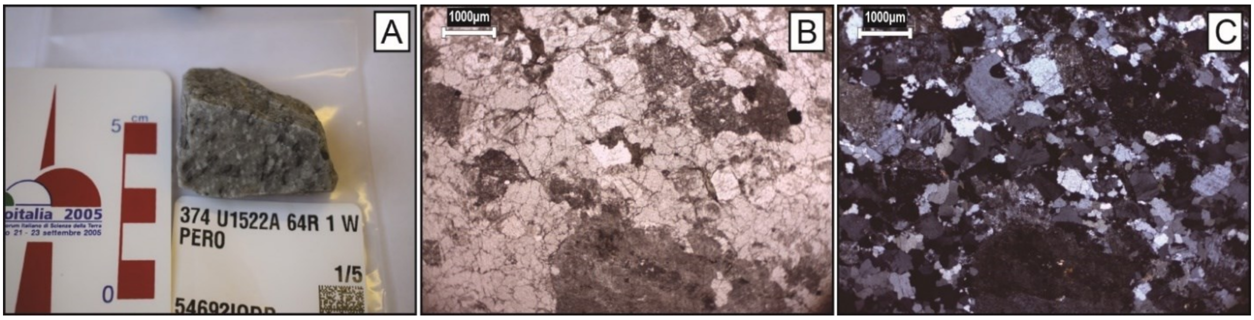

Figure 103 A) Macroscopic picture of the clast; B) PPL photomicrograph (1.6x); C) XPL photomicrograph (1.6x)

Heterogranular rock with schistose texture. The main constituent is quartz that shows undulose extinction. Alkali feldspars, both microcline and orthoclase, are the second mineralogical phase. Plagioclase commonly occurs and sometimes it forms porphyritic crystals. Biotite aggregates, almost completely replaced by chlorite, sometimes occur within the sample. Opaques are common accessory minerals.

374-U1522A-64R-4W, 86-89 cm – Intermediate Porphyry

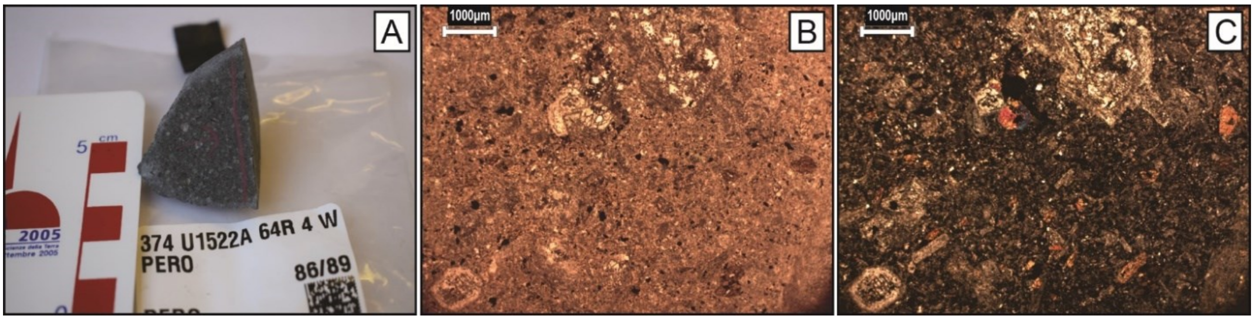

Figure 104 A) Macroscopic picture of the clast; B) PPL photomicrograph (1.6x); C) XPL photomicrograph (1.6x)

The sample is strongly altered. The rock is holocrystalline, porphyritic. The groundmass is very fine grained, constituted by feldspar. Brown amphibole, rhomboidal with euhedral to subhedral shape, occurs, as well as olivine. Chlorite (secondary??) is common; rare interstitial quartz occurs. Porphyritic crystals are euhedral to subhedral feldspar which is completely replaced by sericite whereas twinning of plagioclase is sometimes recognizable, brown amphibole (hornblende?), euhedral to subhedral. Alkali feldspars rarely occur in the groundmass. Small crystals of epidote sometimes occur. Opaque minerals are common.

374-U1522A-64R-4W, 89-92 cm - Meta-sandstone

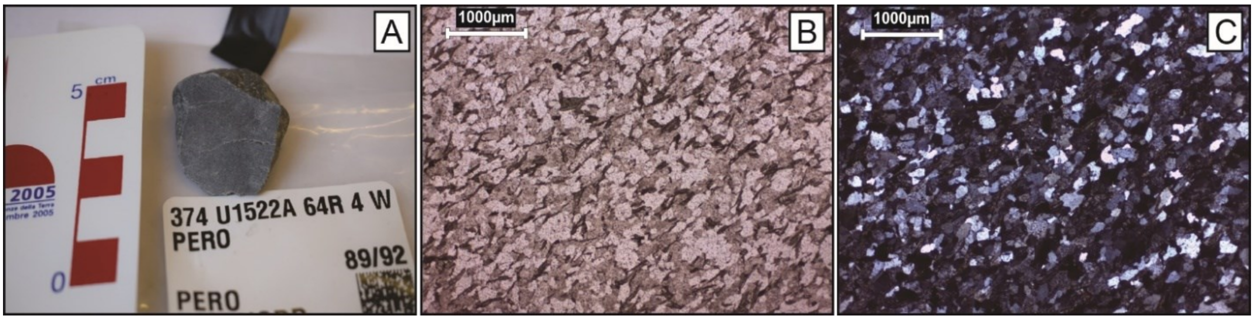

Figure 105 Macroscopic picture of the clast; B) PPL photomicrograph (2.5x); C) XPL photomicrograph (2.5x)

Very fine-grained, equigranular, slightly schistose metamorphic rock. The rock is mainly constituted by quartz, showing weak undulose extinction, and plagioclase, strongly replaced by sericite. Cordierite is common within the sample (ca. 10%). Chlorite crystals define the schistosity (secondary???). White mica is rare but recognizable (secondary???), as well as calcite. Accessory minerals are apatite, epidote and opaques.

374-U1522A-65R-3W, 77-80 cm – Sandstone

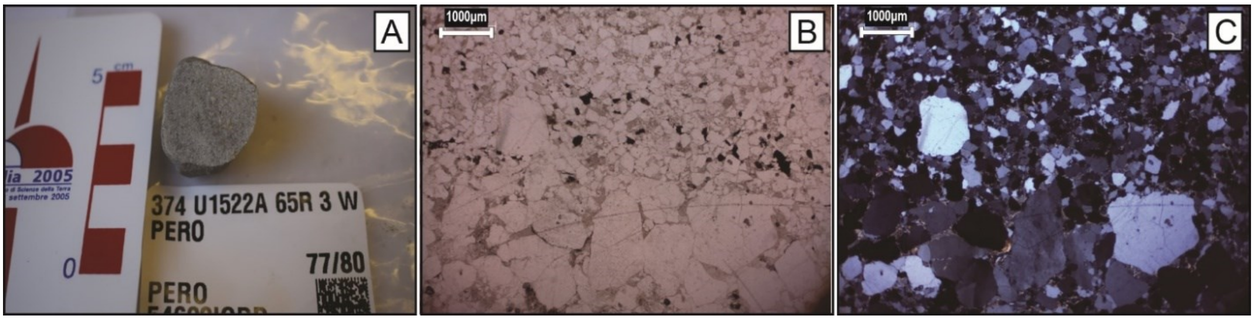

Figure 106 Macroscopic picture of the clast; B) PPL photomicrograph (1.6x); C) XPL photomicrograph (1.6x)

Siliciclastic rock with hetero-granular, fine to medium/coarse grained, layered texture. The fine-grained layer is isotropic, made up of sub-angular to sub-rounded quartz clasts, mainly mono-crystalline with homogeneous extinction, rarely with wavy one. Less common are microcline, orthoclase, and phyllosilicate lithics/pseudo-matrix; phyllosilicate matrix constitutes about 5-8% of the whole rock. Rutile, zircon, and opaques are common accessory minerals, while white mica is rarer. The coarser layer shows gradation from medium/coarse to medium/fine (or reverse); the clasts lithology is almost similar to the fine-grained portion but there are scattered felsitic lithics; the matrix is more abundant (5-10%). White mica is more common, instead rutile and zircon rarer; calcite is present.

374-U1522A-65R-3W, 89-92 cm - Granite

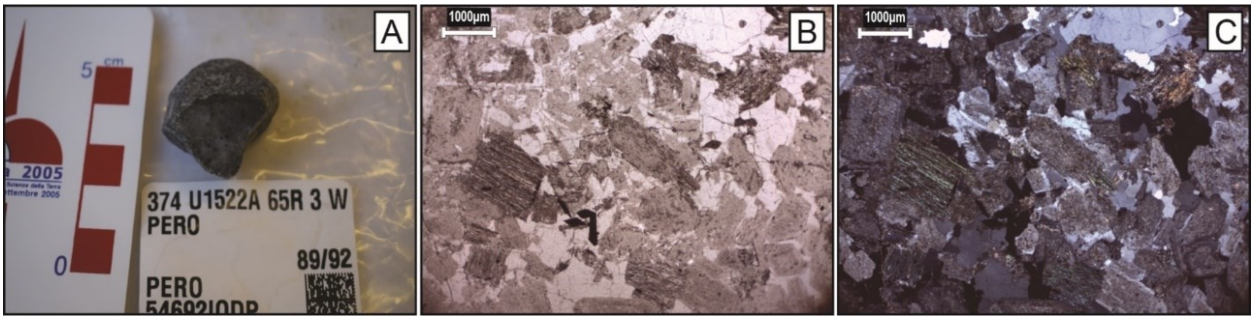

Figure 107 A) Macroscopic picture of the clast; B) PPL photomicrograph (1.6x); C) XPL photomicrograph (1.6x)

Holocrystalline, isotropic, medium/fine-grained rock. The main constituents are feldspars; however, they are almost completely replaced by sericite, white mica, and calcite. Sometimes the twinning typical of plagioclase is recognizable although the presence of alkali feldspars (likely orthoclase) can not be excluded. Poorly altered microcline sometimes occurs. Quartz forms anhedral crystals with homogeneous extinction. Biotite rarely occurs, while (secondary?) white mica is common. Opaque minerals are common. Calcite veins cut the rock.

374-U1522A-66R-1W, 56-59 cm – Biotite Gneiss

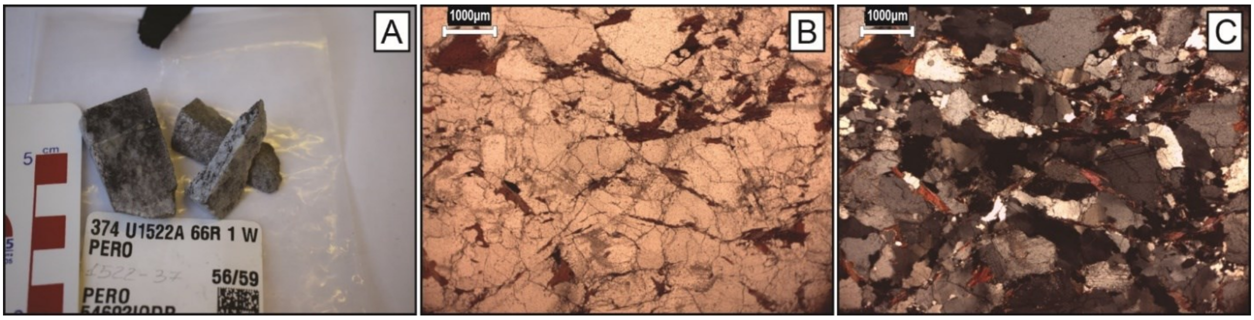

Figure 108 A) Macroscopic picture of the clast; B) PPL photomicrograph (1.6x); C) XPL photomicrograph (1.6x)

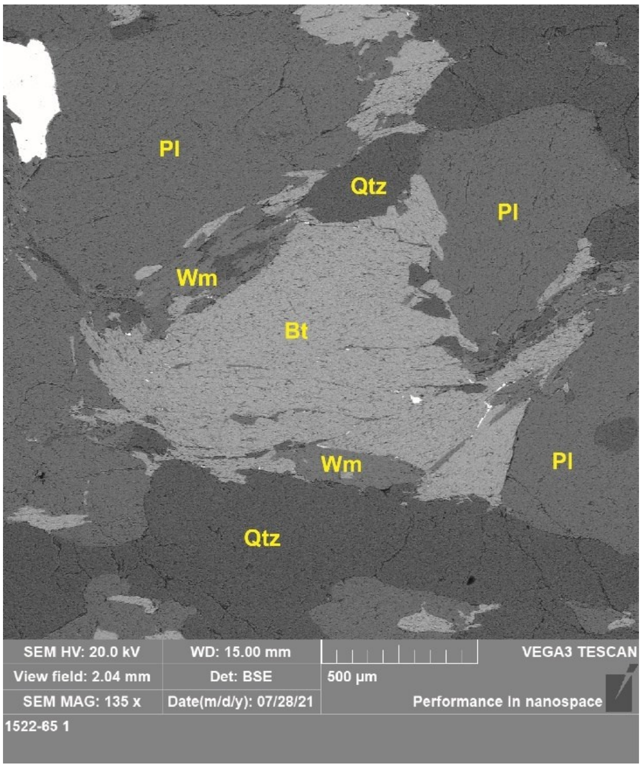

Figure 109 SEM - Back-Scattered Electrons image of the sample where identified mineralogical phases are reported. Bt – Biotite; Pl – Plagioclase; Qtz – Quartz; Wm – White Mica.

Metamorphic rock with hetero-granular gneissic texture. The leucosome is constitute mainly by quartz (60%), plagioclase (≈35%) and biotite (5%) and minor white mica (secondary?). The mesosome is dominated by biotite crystals. Apatite is a common accessory mineral, as well as zircon and opaques.

374-U1522A-66R-CCW, 19-22 cm – Biotite Schist

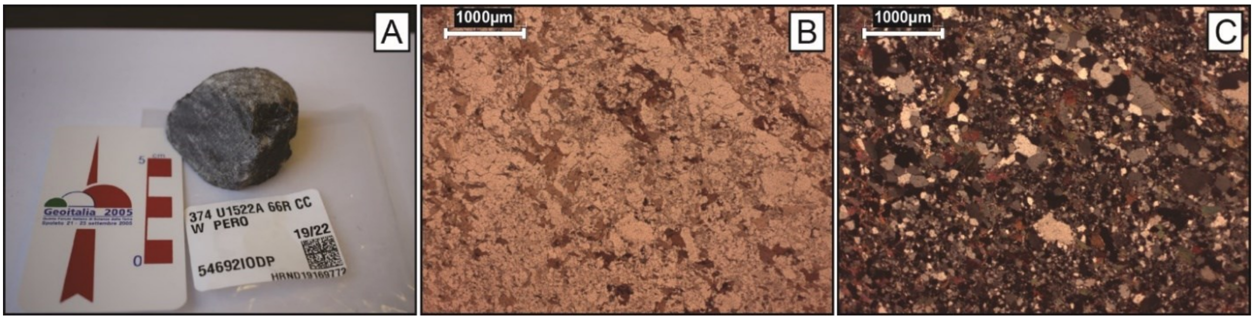

Figure 110 A) Macroscopic picture of the clast; B) PPL photomicrograph (2.5x); C) XPL photomicrograph (2.5x)

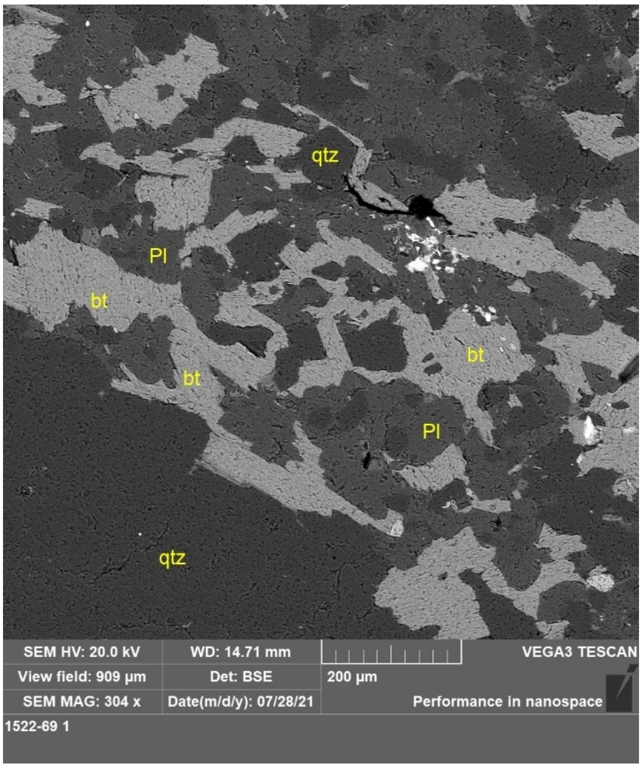

Figure 111 SEM - Back-Scattered Electrons image of the sample where identified mineralogical phases are reported. . Bt – Biotite; Pl – Plagioclase; Qtz – Quartz.

Hetero-granular, fine to medium grained, lightly foliated metamorphic rock. The main component is quartz; sometimes quartz forms medium grained lenticular layers where crystals have granoblastic polygonal texture. Biotite is abundant and isoriented. Accessory minerals are apatite, zircon and opaque.

374-U1522A-67R-2W, 72-75 cm - Lapilli Tuff

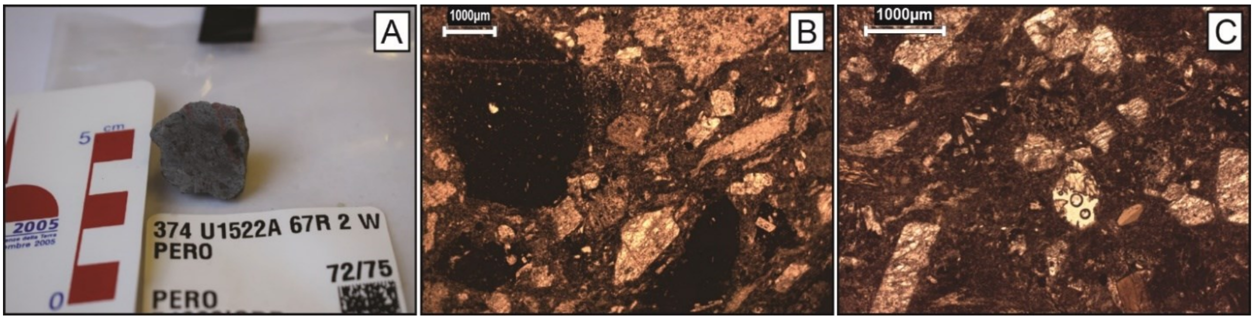

Figure 112 A) Macroscopic picture of the clast; B) PPL photomicrograph (1.6x); C) PPL photomicrograph (2.5x)

Volcanoclastic rock with fluidal texture; composed of lapilli and welded ash matrix. Lapilli are constituted of volcanic clasts and single crystals. Lithic fragments are: trachytic lava with porphyritic fluidal texture made up of hypocrystalline groundmass and euhedral feldspar phenocrystals and rarer and smaller opaque minerals and pyroxenes(?); isotropic lava with feldspar microliths and feldspar phenocrystals;

basalt with plagioclase microliths in the hypocrystalline matrix and plagioclase micro-phenocrystals. Singe crystals are euhedral and made up of feldspar, plagioclase, pyroxene, and brown amphibole. May completely altered olivine crystals occur.

374-U1522A-67R-2W, 105-108 cm – Hornblende and Biotite Granodiorite

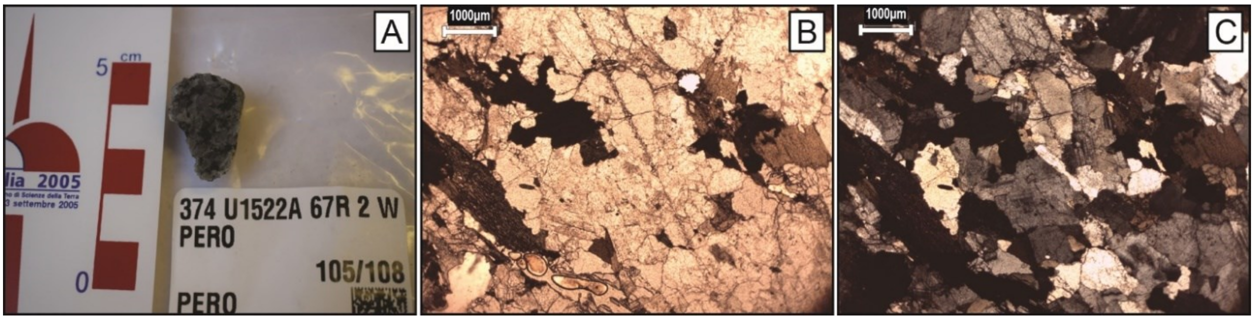

Figure 113 A) Macroscopic picture of the clast; B) PPL photomicrograph (1.6x); C) XPL photomicrograph (1.6x)

The rock is holocrystalline, medium-grained, isotropic to weakly foliated. The rock is mainly composed by plagioclase, sometimes chemically zoned, quartz, biotite, and green hornblende. Quartz shows undulose extinction. Mafic phases represent about 15% of volume. Alkali feldspars are rare. Titanite is an accessory mineral.

374-U1522A-67R-3W, 71-72 cm – Basalt

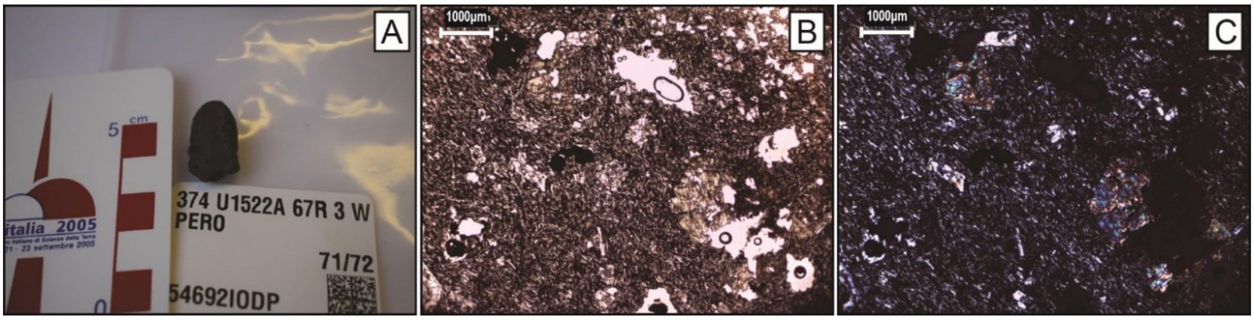

Figure 114 Macroscopic picture of the clast; B) PPL photomicrograph (1.6x); C) XPL photomicrograph (1.6x)

The sample is a porphyritic volcanic rock, with fluidal texture. The groundmass is made up of plagioclase and opaque minerals; olivine and/or pyroxene may occur in the groundmass. Porphyritic crystals are euhedral to subhedral clinopyroxene.

374-U1522A-67R-4W, 6-8 cm – Biotite and Clinopyroxene Gneiss

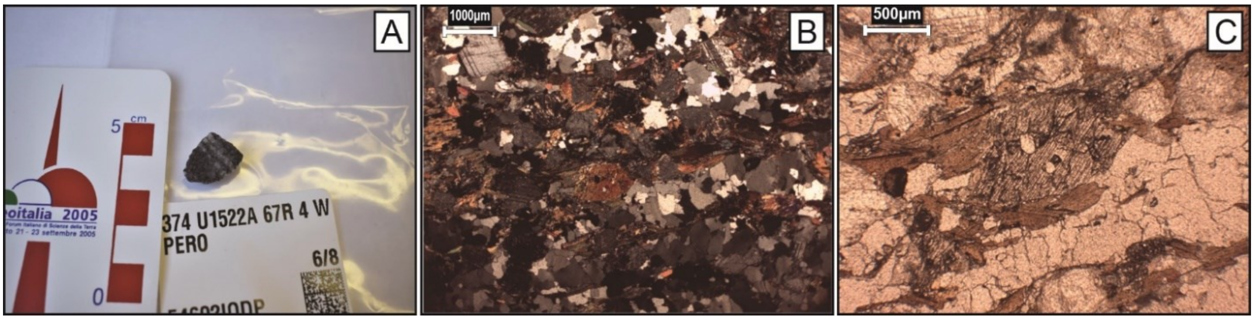

Figure 115 A) Macroscopic picture of the clast; B) XPL photomicrograph (1.6x); C) PPL photomicrograph (4x)

The rock has a gneissic structure. The rock is mainly composed by quartz and minor plagioclase. Biotite is common and it defines the schistosity. Calcic clinopyroxene crystals usually occur associated with biotite. Allanite and apatite are accessory minerals.

374-U1522A-67R-6W, 21-24 cm – Felsic Porphyry

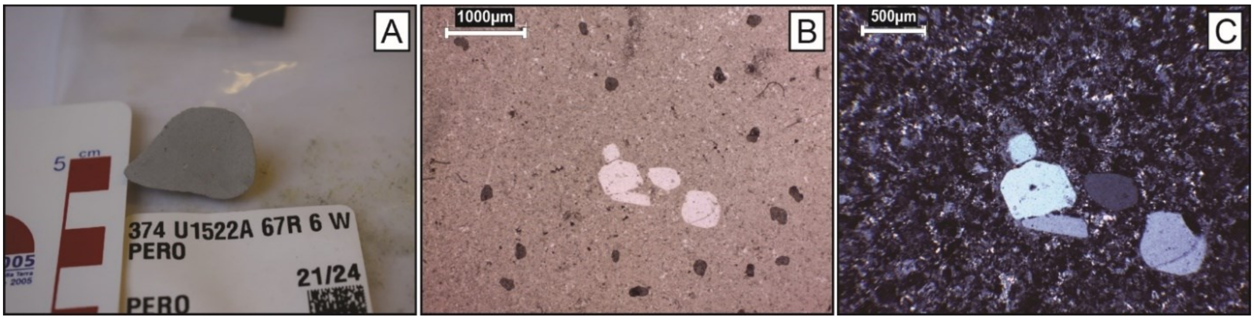

Figure 116 Macroscopic picture of the clast; B) PPL photomicrograph (2.5x); C) XPL photomicrograph (4x)

Holocrystalline rock with isotropic porphyritic texture. Groundmass is very fine grained to micro-crystalline, made up of feldspar and subsequently quartz; feldspars are partially replaced by sericite. Where the groundmass is microcrystalline, they have spherulitic structures. Phenocrystals are rare and small; they are made up mainly of subhedral quartz, showing reabsorption rims and reaction crowns; secondly of subhedral K-feldspar, partially replaced by sericite and oxides.

374-U1522A-68R-1W, 56-59 cm – Biotite, Amphibole and Calcite Schist

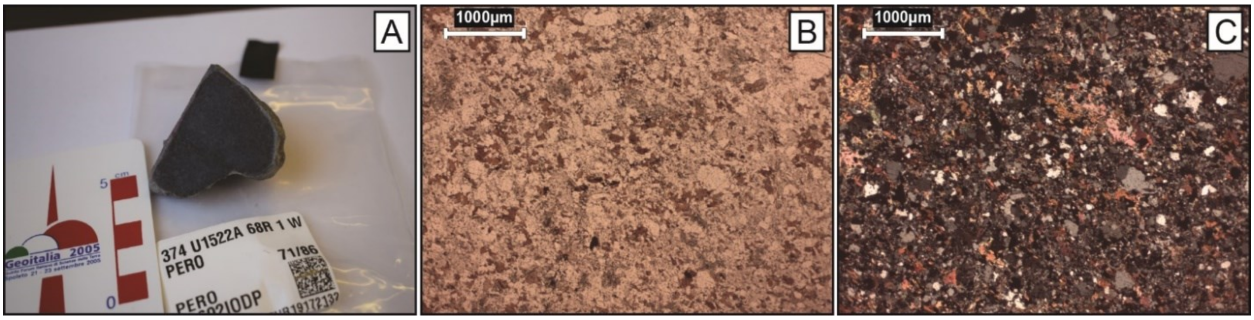

Figure 117 A) Macroscopic picture of the clast; B) PPL photomicrograph (2.5x); C) XPL photomicrograph (2.5x)

Lightly foliated, equigranular, fine-grained meta-sedimentary rock. The main component is quartz that sometimes shows granoblastic polygonal texture; biotite is abundant and isoriented. Green amphibole (hornblende) is common; crystals are usually altered and partially replaced by calcite. Opaque minerals and zircon are accessory.

374-U1522A-68R-2W, 78-80 cm – Al-silicate and Garnet Mica-schist

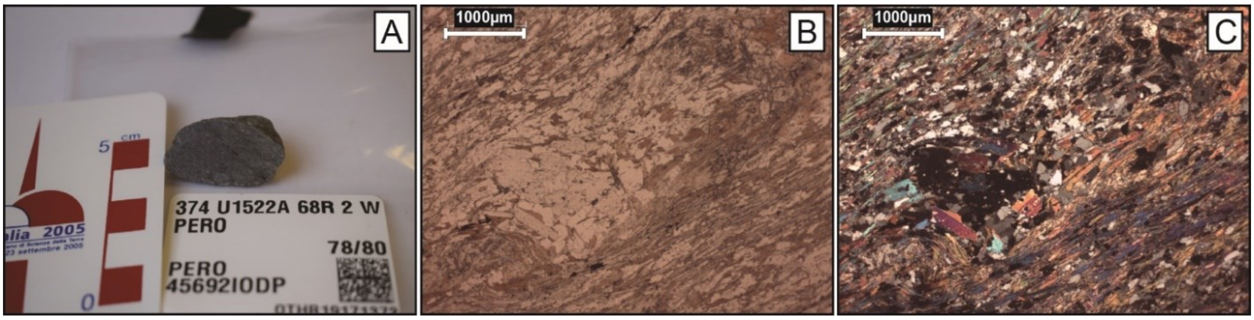

Figure 118 A) Macroscopic picture of the clast; B) PPL photomicrograph (2.5x); C) XPL photomicrograph (2.5x)

Fine grained, strongly foliated, metamorphic rock, with lepidoblastic texture. The main components are quartz, biotite, and white mica, both isoriented. The sample shows medium/coarse porphyroblasts of Al-silicate; the original Al-silicate is completely replaced by sericite and secondary Al-silicate (sillimanite) grew in the same portions. Garnet crystals rarely occur, as well as alkali feldspar. Accessory minerals are euhedral zoned tourmaline, apatite and opaques.

374-U1522A-68R-4W, 86-89 cm – (Meta-)sandstone

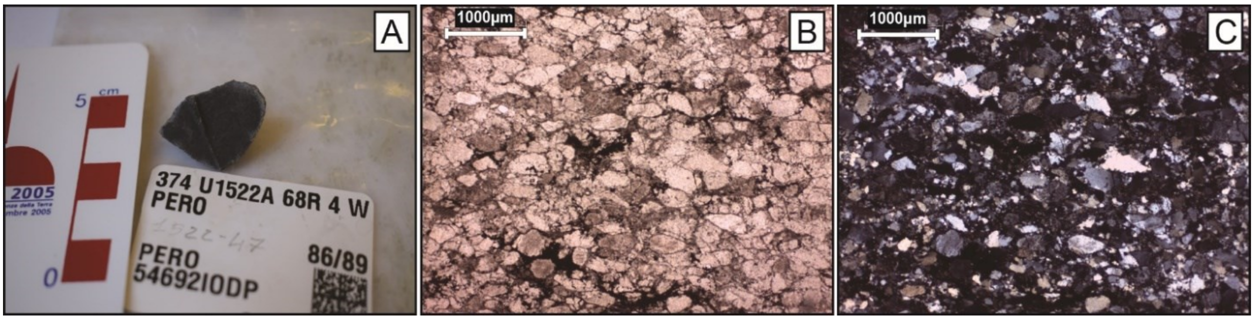

Figure 119 Macroscopic picture of the clast; B) PPL photomicrograph (2.5x); C) XPL photomicrograph (2.5x)

Hetero-granular, very fine to medium grained, slightly foliated, (meta-)sedimentary rock. Quartz is the main component, sometimes showing polygonal texture; K-feldspar, with orthoclase more abundant than microcline, and plagioclase are abundant. Fine grained meta-sedimentary lithics fragments are present. White mica, zircon and opaques are accessory minerals.

374-U1522A-68R-6W, 56-60 cm – Biotite schist

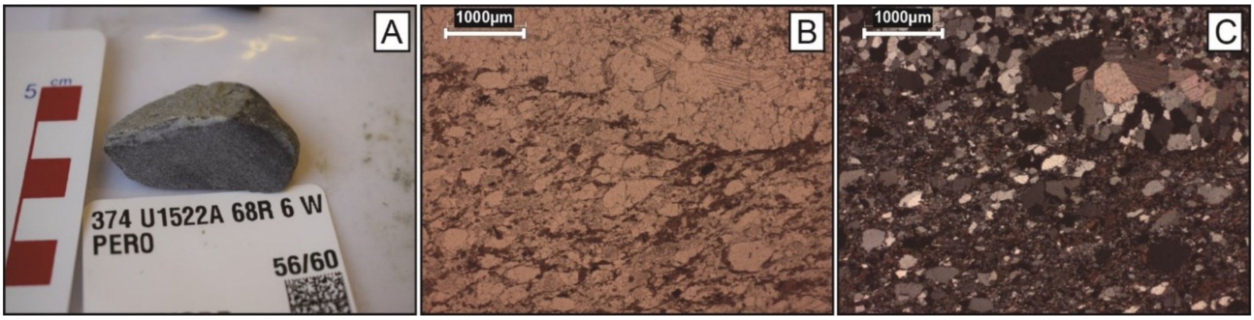

Figure 120 A) Macroscopic picture of the clast; B) PPL photomicrograph (2.5x); C) XPL photomicrograph (2.5x)

Fine-grained, hetero-granular schist. The rock shows compositional layering. The rock is mainly composed by quartz and feldspar (plagioclase?); calcite commonly occurs. Biotite defines the schistosity; epidote and apatite are accessory minerals. Some layers are solely constituted by polygonal quartz and calcite; white mica is rare.

374-U1522A-69R-1W, 0-4 cm – Hornblende and Biotite Granodiorite

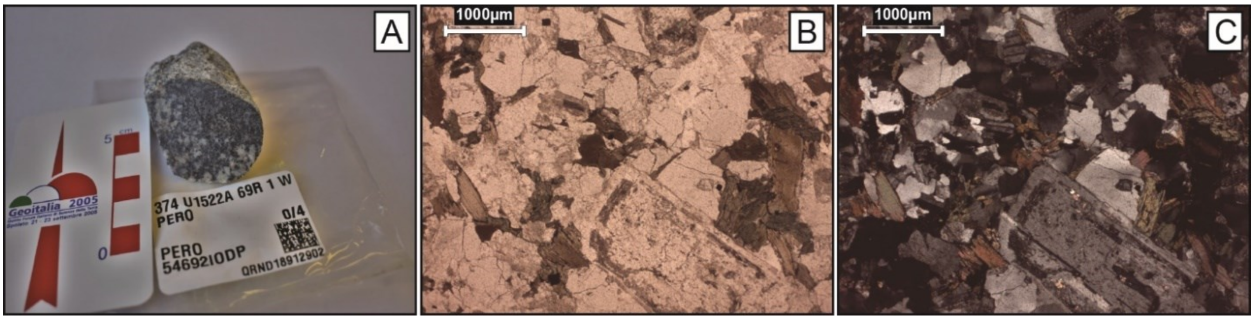

Figure 121 A) Macroscopic picture of the clast; B) PPL photomicrograph (2.5x); C) XPL photomicrograph (2.5x)

Holocrystalline, equigranular, slightly porphyritic, fine grained magmatic rock with isotropic texture. Quartz constitutes 30-35% of whole rock and shows wavy extinction; 40-45% is represented by feldspars, predominantly made up of plagioclase, secondly microcline. Plagioclase, partially altered, is twinned, zoned and with some euhedral crystals. Mafic minerals are ca. 15-20%, made up of biotite and hornblende; epidote is an accessory mineral.

374-U1522A-69R-1W, 3-5 cm – Mafic Intrusive

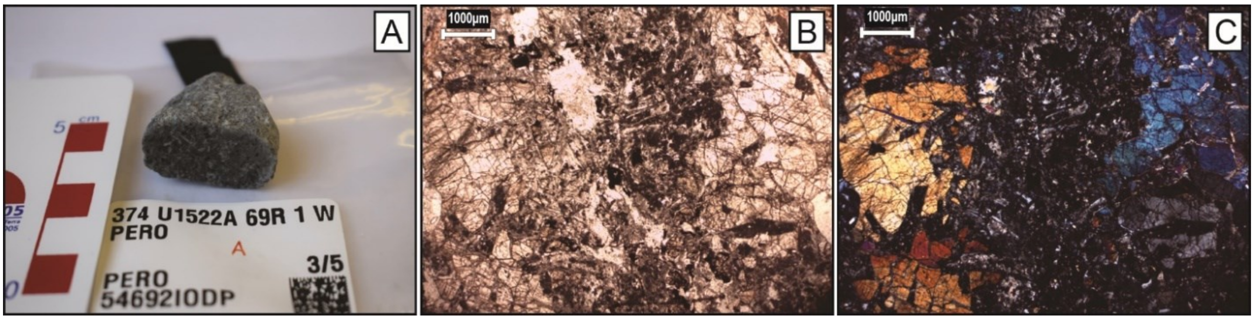

Figure 122 Macroscopic picture of the clast; B) PPL photomicrograph (1.6x); C) XPL photomicrograph (1.6x)

The rock is strongly affected by alteration, with a marked porphyritic structure. Pecilitic crystals of clinopyroxene represent ca. 50% of volume; rare orthopyroxene crystals occur. Feldspar constitutes the other part of the rocks; whereas almost completely altered (replaced by sericite and chlorite), chemical zonation and twinning sometimes are still recognizable. Pecilitic crystals are weakly aligned.

374-U1522A-70R-1W, 57-60 cm – Calcite Meta-sandstone

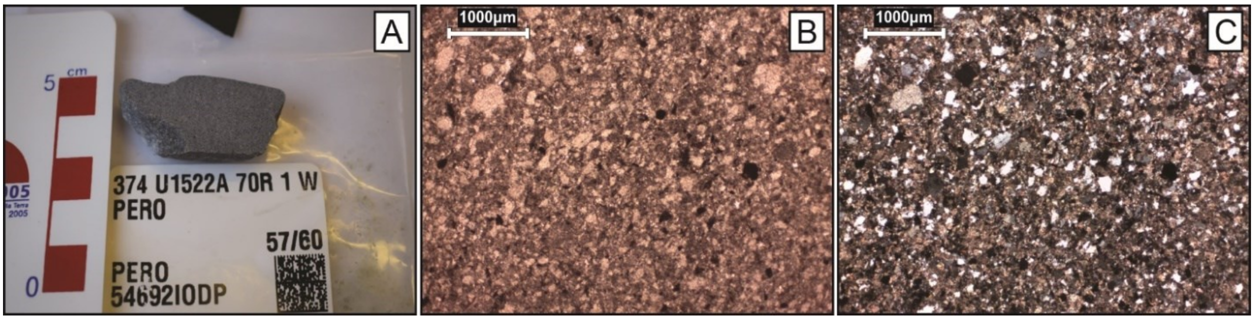

Figure 123 Macroscopic picture of the clast; B) PPL photomicrograph (2.5x); C) XPL photomicrograph (2.5x)

The sample is a fine-grained, slightly foliated metamorphic rock. The composition is ca. 50% calcite and 50% quartz and plagioclase; quartz is weakly recrystallized. White mica (detrital?) sometimes occurs, as well as biotite spots.

374-U1522A-70R-2W, 73-74 cm – Carbonate Breccia/Limestone

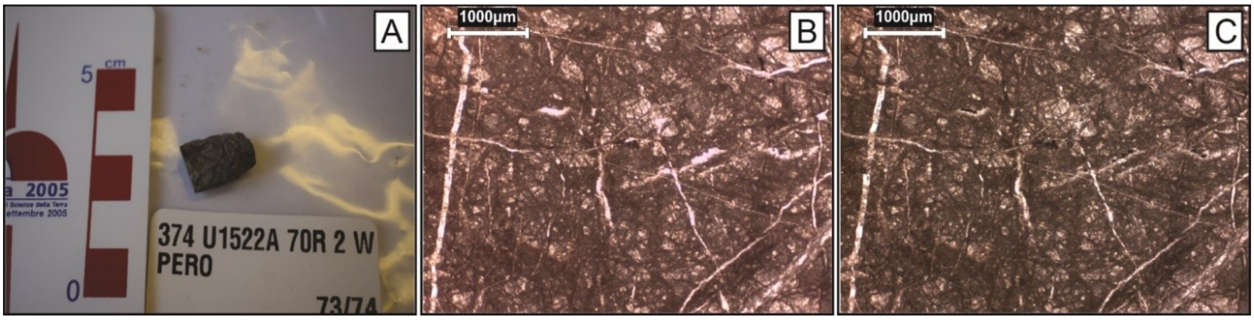

Figure 124 Macroscopic picture of the clast; B) PPL photomicrograph (2.5x); C) XPL photomicrograph (2.5x)

The rock is strongly fractured and crossed by some vein's patterns; it has a carbonate composition with isotropic texture. The limestone is mainly micrite; sparite is common as vein filling.

374-U1522A-70R-2W, 134-137 cm – Hornblende Granodiorite/Monzodiorite

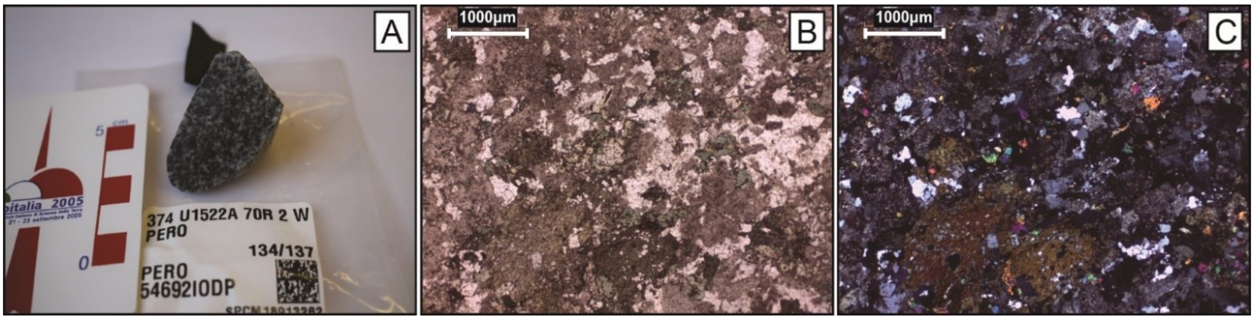

Figure 125 Macroscopic picture of the clast; B) PPL photomicrograph (2.5x); C) XPL photomicrograph (2.5x)

The rock is medium/fine-grained, holocrystalline, isotropic. The rock is mainly constituted by plagioclase, that is almost completely replaced by sericite but where twinning is recognizable yet; minor are alkali feldspar (microcline) and quartz, that shows granoblastic polygonal texture. Sometimes granophyric structures occur. More than 20% is green amphibole (hornblende). Epidote and chlorite are common secondary minerals.

374-U1522A-71R-4W, 45-48 cm - Chlorite Meta-sandstone

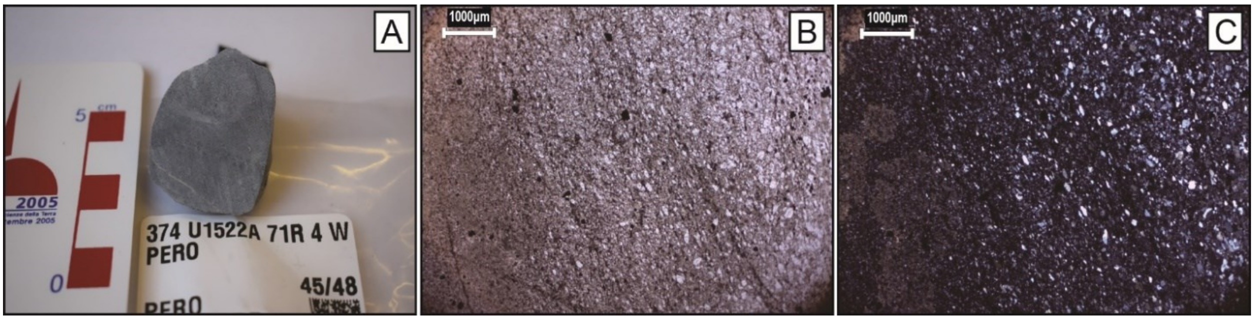

Figure 126 Macroscopic picture of the clast; B) PPL photomicrograph (1.6x); C) XPL photomicrograph (1.6x)

The rock is strongly heterogranular (very fine sand sized to fine silt sized) with gradational passages; moreover, compositional layering is recognizable. The coarser portion is dominated by quartz with granoblastic, quite polygonal, texture, and minor chlorite and calcite-rich matrix (?). Finer portions are dominated by quartzo-feldspatic fine-grained matrix, chlorite, and minorly quartz grains. Calcite-rich spots occurs within the samples, as well as calcite dominated layers. An epidote (???) and calcite layer is recognizable. Opaque minerals are common accessories.

374-U1522A-72R-1W, 34-37 cm - Porphyry

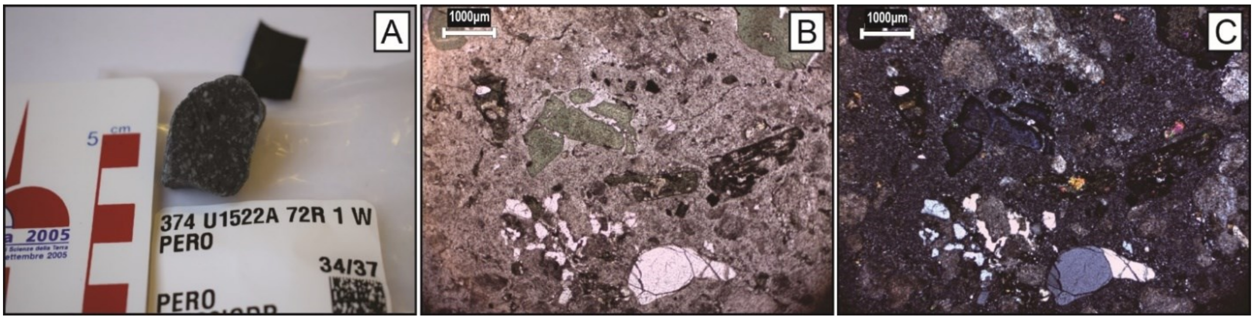

Figure 127 Macroscopic picture of the clast; B) PPL photomicrograph (1.6x); C) XPL photomicrograph (1.6x)

The sample is strongly altered. The rock has, isotropic, porphyritic texture; porphyritic crystals are ca. 30% of the whole. Crystals are mainly feldspar, whereas almost completely replaced by sericite and clay mineral aggregates; however, rarely plagioclase relicts are recognizable. Secondly phenocrystals are of quartz, that sometimes has embayed rims. Scattered mafic mineral porphyrocrystals occur, sometimes with euhedral hexagonal shape, whereas they are completely replaced by chlorite (???????). The groundmass is very fine-grained and with quartzo-feldspatic composition, whereas strongly replaced by sericite. Epidote is common within the rock. Opaque minerals are accessory.

374-U1522A-72R-1W, 108-111 cm – Meta-granite

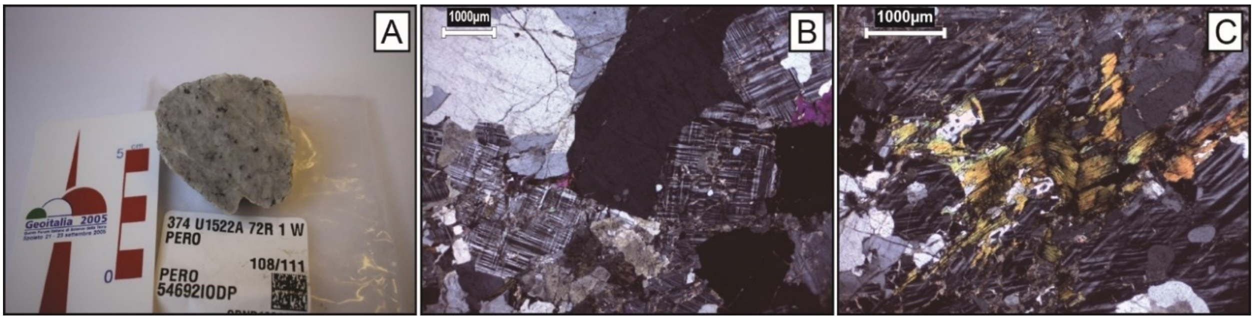

Figure 128 A) Macroscopic picture of the clast; B) PPL photomicrograph (1.6x); C) XPL photomicrograph (1.6x)

The rock is coarse-grained with slightly foliated texture. Some portions of the samples show cataclastic texture. Alkali feldspars, both microcline and pertitic orthoclase, are the main constituents; both are partially replaced by sericite and white mica. Plagioclase is strongly replaced by sericite. Quartz is concentrated in layers and crystals have undulose extinction. Deformed and altered biotite occurs, as well as deformed (secondary?) white mica.

374-U1522A-72R-3W, 71-74 cm Amphibole Meta-sediment

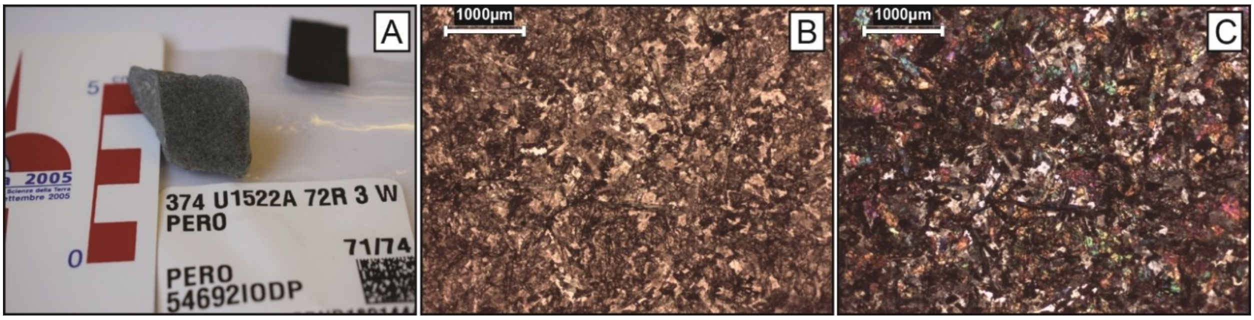

Figure 129 A) Macroscopic picture of the clast; B) PPL photomicrograph (2.5x); C) XPL photomicrograph (2.5x)

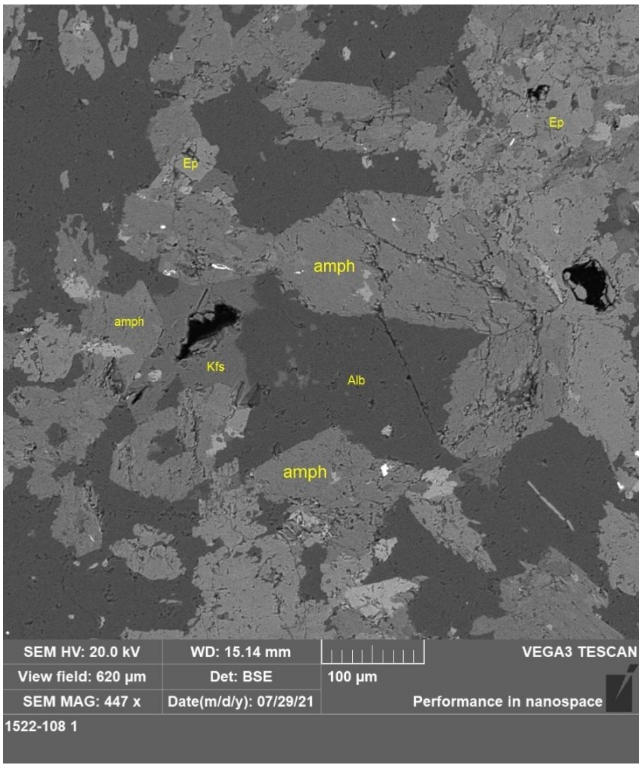

Figure 130 SEM - Back-Scattered Electrons image of the sample where identified mineralogical phases are reported. Alb – Albite; Amph – Amphibole; Ep – Epidote; Kfs – Alkali feldspar

The rock is fine-grained and isotropic. Mineralogical composition is >50% of green amphibole (actinolite), ca. 35% plagioclase, that is partially replaced by sericite, and epidote. Interstitial quartz and alkali feldspar occur.

374-U1522A-75R-1W, 25-28 cm – Felsic Porphyry

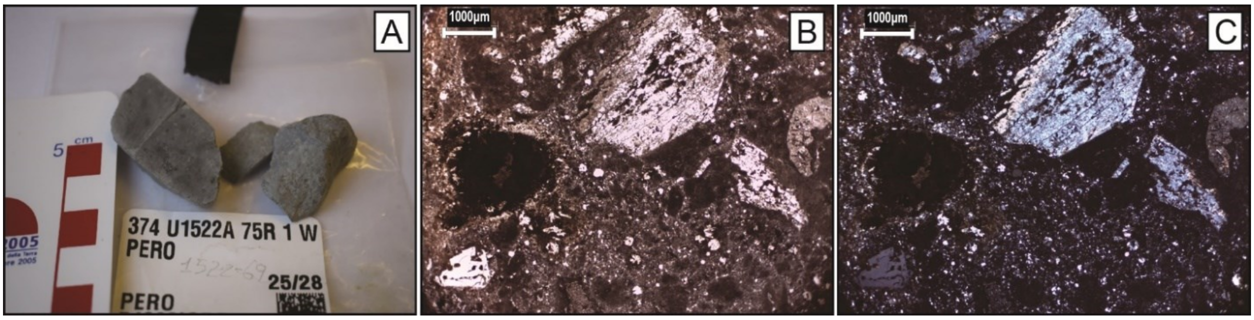

Figure 131 Macroscopic picture of the clast; B) PPL photomicrograph (1.6x); C) XPL photomicrograph (1.6x)

Holocrystalline rock, strongly altered, with isotropic and porphyritic texture. Groundmass is microcrystalline to very fine grained, made up of quartz and feldspars. Phenocrystals mainly are K-feldspar, with euhedral shape, almost completely replaced by calcite; secondly quartz, that shows marked reabsorption rims. Opaque minerals are common.

374-U1522A-75R-2W, 9-12 cm – Biotite and White Mica Schist

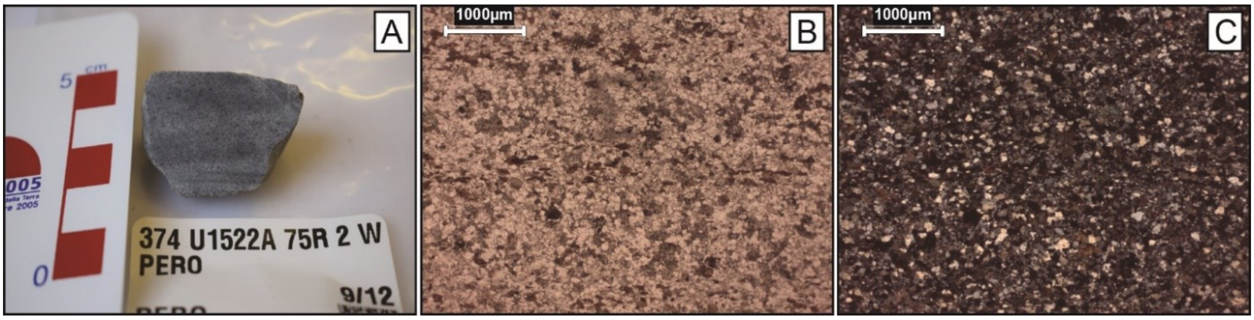

Figure 132 A) Macroscopic picture of the clast; B) PPL photomicrograph (2.5x); C) XPL photomicrograph (2.5x)

Fine grained, slightly schistose, meta-sedimentary rock. The main constituent is quartz. Biotite is abundant and sometimes replaced by chlorite; it defines the schistosity. Biotite is sometimes associate with white mica crystals. Alkali feldspar and calcite commonly occur in the sample, while plagioclase is rarer. Accessory minerals are epidote and opaques.

374-U1522A-75R-6W, 42-45 cm – Biotite Schist

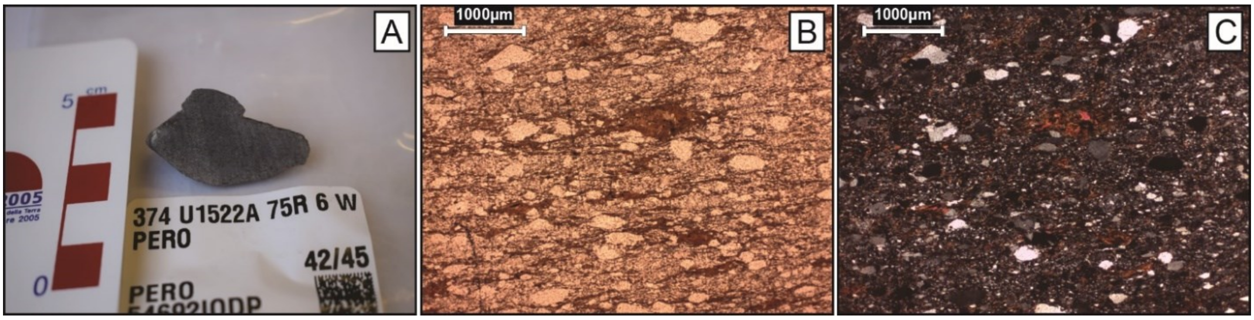

Figure 133 A) Macroscopic picture of the clast; B) PPL photomicrograph (2.5x); C) XPL photomicrograph (2.5x)

Very fine-grained, hetero-granular, foliated rock. The composition is quartz, plagioclase, and biotite, that defines the schistosity.

374-U1522A-76R-1W, 109-111 cm – Micro-granitoid

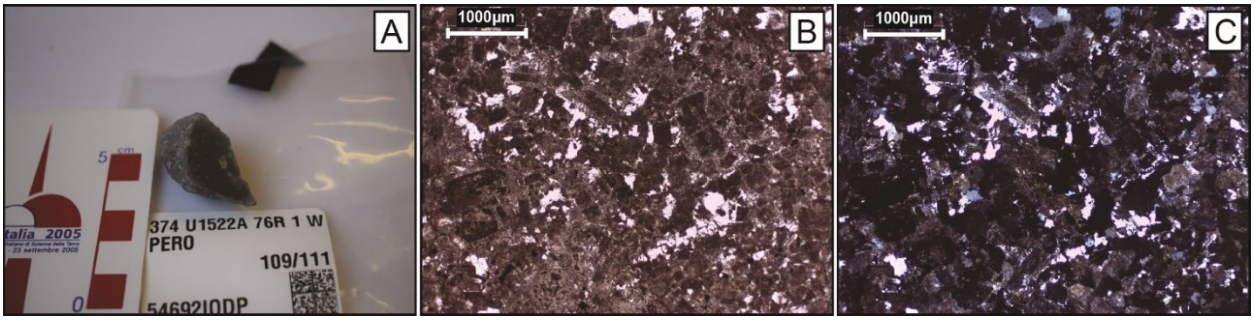

Figure 134 Macroscopic picture of the clast; B) PPL photomicrograph (2.5x); C) XPL photomicrograph (2.5x)

The sample is strongly altered. The sample is holocrystalline with slightly porphyritic texture. The main constituents are feldspars; thy are almost completely replaced by sericite and phyllosilicate aggregates and their recognizing is uncertain whereas plagioclase twinning is sometimes visible. Feldspar crystal are usually subhedral, sometimes show chemical zonation, and they form both fine grained and porphyritic crystals. Quartz, mainly interstitial, is secondly in abundance (ca. 10%). Where quartz and feldspar crystals are in contact, myrmekites usually develop. Chlorite replaced original mafic minerals, whereas they are rare.

374-U1522A-76R-2W, 7-10 cm - Meta-sandstone

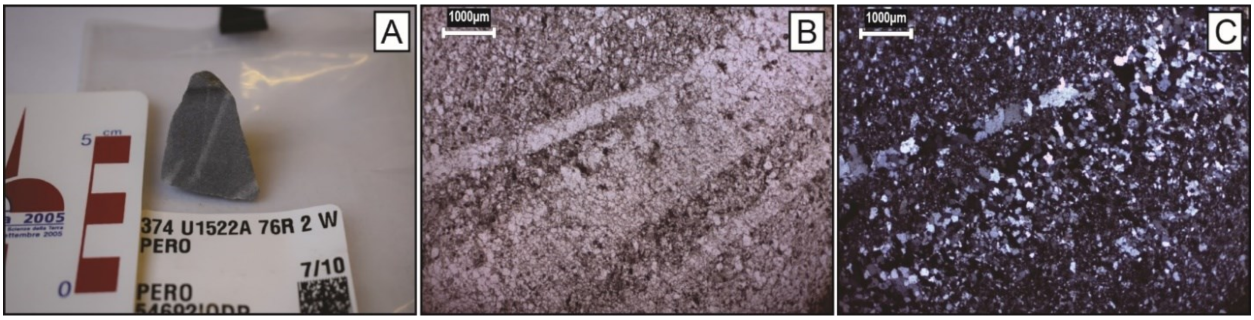

Figure 135 Macroscopic picture of the clast; B) PPL photomicrograph (1.6x); C) XPL photomicrograph (1.6x)

Very fine-grained, isotropic, meta-sedimentary rock. The sample is constituted by quartz grains in a fine-grained matrix. Plagioclase commonly occurs. The rock is crossed by zoned of granoblastic, quite polygonal, quartz.

374-U1522A-76R-3W, 42-45 cm – Dolerite/Micro-gabbro

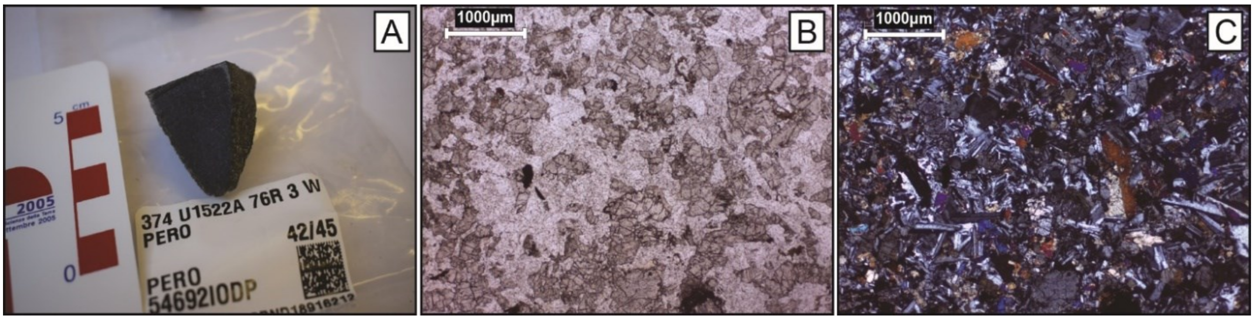

Figure 136 Macroscopic picture of the clast; B) PPL photomicrograph (2.5x); C) XPL photomicrograph (2.5x)

The sample is a mafic, fine-grained, rock with sub-ophitic texture. The composition is plagioclase and pyroxene.

Table 37 Summary of analyzed clasts, with sampling depth, clast shape and lithology. LSU – Lithostratigraphic Unit are from McKay et al. (2019)

Sample ID	LSU	Depth (m CSF-A)	Clast Shape	Lithology
374-U1522A-55R-2W, 17-20 cm	IIIB	493.29	sub-rounded	Biotite meta-sandstone
374-U1522A-55R-3W, 52-56 cm	IIIB	494.9	sub-angular	Meta-limestone
374-U1522A-56R-1W, 48-51 cm	IIIB	504.88	rounded	Meta-sandstone
374-U1522A-56R-4W, 44-46 cm	IIIB	504.83	sub-angular	Volcanic rock
374-U1522A-57R-1W, 0-3 cm	IIIB	510.91	sub-angular	Meta-sandstone
374-U1522A-57R-2W, 120-123 cm	IIIB	513.45	sub-rounded	Felsic Porphyry
374-U1522A-57R-5W, 1-6 cm	IIIB	516.52	angular	Foliated Granitoid/Meta-granite
374-U1522A-57R-5W, 37-41 cm	IIIB	516.88	sub-rounded	Biotite Orthogneiss
374-U1522A-58R-1W, 68-71 cm	IIIB	521.18	sub-angular	Monzogranite
374-U1522A-58R-3W, 120-121 cm	IIIB	524.51	sub-angular	Mudstone
374-U1522A-58R-4W, 4-7 cm	IIIB	524.78	rounded	Meta-granitoid
374-U1522A-58R-6W, 131-133 cm	IIIB	528.56	rounded	Micro leuco-granite
374-U1522A-59R-7W, 22-24 cm	IIIB	537.07	angular	Granite
374-U1522A-59R-7W, 91-93 cm	IIIB	537.86	sub-angular	Basalt
374-U1522A-60R-3W, 64-66 cm	IIIB	543.15	sub-rounded	Felsic Porphyry
374-U1522A-60R-3W, 87-91 cm	IIIB	543.38	sub-rounded	Mafic Intrusive
374-U1522A-60R-5W, 36-40 cm	IIIB	545.71	rounded	Meta-granite
374-U1522A-61R-1W, 0-2 cm	IIIC	549.3	sub-angular	Basalt
374-U1522A-61R-1W, 29-32 cm	IIIC	549.59	sub-angular	Mafic Intrusive
374-U1522A-61R-1W, 44-47 cm	IIIC	549.74	sub-rounded	Meta-porphyry
374-U1522A-61R-CCW, 38-40 cm	IIIC	550.9	sub-angular	Hornfels
374-U1522A-61R-CCW, 67-70 cm	IIIC	551.19	sub-angular	Porphyry
374-U1522A-62R-1W, 12-15 cm	IIIC	558.92	sub-rounded	Basalt
374-U1522A-62R-1W, 65-68 cm	IIIC	559.46	sub-angular	Micro-gabbro/Dolerite
374-U1522A-62R-2W, 8-10 cm	IIIC	560.1	rounded	Dolerite/Micro-gabbro
374-U1522A-62R-2W, 49-52 cm	IIIC	560.52	sub-rounded	Micro-granite
374-U1522A-62R-2W, 52-55 cm	IIIC	560.55	sub-rounded	Sandstone
374-U1522A-62R-CCW, 17-20 cm	IIIC	562.33	sub-rounded	Felsic Porphyry
374-U1522A-63R-2W, 112-115 cm	IIIC	570.79	sub-rounded	Meta-siltstone
374-U1522A-64R-1W, 1-5 cm	IIIC	557.83	sub-angular	Gneiss
374-U1522A-64R-4W, 86-89 cm	IIIC	582.95	sub-angular	Porphyry
374-U1522A-64R-4W, 89-92 cm	IIIC	583	sub-rounded	Meta-sandstone
374-U1522A-65R-3W, 77-80 cm	IIIC	590.9	sub-rounded	Sandstone
374-U1522A-65R-3W, 89-92 cm	IIIC	591.03	sub-rounded	Granite
374-U1522A-66R-1W, 56-59 cm	IIIC	597.36	ND	Biotite Gneiss
374-U1522A-66R-CCW, 19-22 cm	IIIC	601.19	sub-rounded	Biotite Schist
374-U1522A-67R-2W, 72-75 cm	IIIC	608.48	sub-rounded	Lapilli Tuff
374-U1522A-67R-2W, 105-108 cm	IIIC	608.81	sub-angular	Granodiorite
374-U1522A-67R-3W, 71-72 cm	IIIC	609.88	rounded	Basalt
374-U1522A-67R-4W, 6-8 cm	IIIC	610.45	rounded	Biotite and Clinopyroxene Gneiss
374-U1522A-67R-6W, 21-24 cm	IIIC	612.79	sub-rounded	Felsic Porphyry
374-U1522A-68R-1W, 56-59 cm	IIIC	616.51	sub-angular	Schist
374-U1522A-68R-2W, 78-80 cm	IIIC	617.81	rounded	Mica-schist
374-U1522A-68R-4W, 86-89 cm	IIIC	619.92	sub-rounded	(Meta-)sandstone
374-U1522A-68R-6W, 56-60 cm	IIIC	622.83	sub-rounded	Biotite Schist
374-U1522A-69R-1W, 0-4 cm	IIIC	625.33	sub-angular	Granodiorite
374-U1522A-69R-1W, 3-5 cm	IIIC	625.33	rounded	Mafic Intrusive
374-U1522A-70R-1W, 57-60 cm	IIIC	635.37	sub-rounded	Meta-sandstone
374-U1522A-70R-2W, 73-74 cm	IIIC	636.93	angular	Carbonate Breccia/Limestone
374-U1522A-70R-2W, 134-137 cm	IIIC	637.54	sub-angular	Granodiorite/Monzodiorite
374-U1522A-71R-4W, 45-48 cm	IV	648.86	sub-rounded	Meta-sandstone
374-U1522A-72R-1W, 34-37 cm	IV	654.15	sub-angular	Felsic Porphyry

374-U1522A-72R-1W, 108-111 cm	IV	654.9	angular	Meta-granite
374-U1522A-72R-3W, 71-74 cm	IV	657.24	sub-angular	Amphibole Meta-sediment
374-U1522A-75R-1W, 25-28 cm	IV	682.85	sub-rounded	Felsic Porphyry
374-U1522A-75R-2W, 9-12 cm	IV	684.11	rounded	Schist
374-U1522A-75R-6W, 42-45 cm	IV	690.18	sub-rounded	Schist
374-U1522A-76R-1W, 109-111 cm	IV	693.3	sub-angular	Micro-granitoid
374-U1522A-76R-2W, 7-10 cm	IV	693.78	sub-angular	Meta-sandstone
374-U1522A-76R-3W, 42-45 cm	IV	695.37	sub-angular	Dolerite/Micro-gabbro

Table 38 Occurrence in percentage of lithics the gravel from bulk diamictite matrix. Qtz - quartz; Fs - feldspars (plagioclase and alkali feldspar); Intr - intrusive rocks; Dol - dolerite; Meta - metamorphic rocks; Clastic sed - clastic sedimentary rocks; Carb sed - carbonate sedimentary rocks; Bas - basaltic rocks; F Porph - felsic porphyries; ND - Not Defined; Tot - total number of clasts counted in thin section.

Sample ID	**Qtz**	**Fs**	**Intr.**	**Dol.**	**Meta**	**Clastic sed.**	**Carb. sed.**	**Bas.**	**Fel. Porph.**	**ND**	**Tot (n)**
374-U1522A-67R-1W, 53-58 cm	14%	11%	20%	0%	32%	4%	0%	5%	11%	2%	207

APPENDIX VI

Mineral chemistry analyses of IODP Site U1522 clasts

Chemical analysis of biotite crystals from seven metamorphic and intrusive pebbles. Analyses were carried out with an energy-dispersive X-ray system (Bruker Quantax 200 EDX) coupled with an Electron Scanning Microscope (Tescan Vega3) at the Department of Physical, Earth and Environmental Sciences - University of Siena. Analytical conditions were 20 kV of accelerating voltage, 15 μA of emission current, and a beam spot size of 0.2 μm. Natural mineral standards were used for calibration. Cations of biotite and white mica were recalculated on the basis of 22 oxygens, of amphibole on the basis of 23 oxygens, of pyroxene based on 6 oxygens, and of garnet on the basis of 12 oxygens. Crossed out data represent not valid analyses, and they were excluded from the interpretations.

Sample 374-U1522A-55R-2W, 17-20 cm

Table 39 Chemical analysis of biotite

Wt%	**Bt1**	**Bt2**	**Bt3**	**Bt4**	**Bt5**	**Bt6**	**Bt7**	**Bt8**	**Bt9**	**Bt10**	**Bt11**	**Bt12**
SiO_2	37.93	37.73	38.10	38.27	38.20	37.62	37.99	37.83	~~37.58~~	36.73	37.42	38.17
TiO_2	2.80	2.52	2.63	2.55	2.79	2.48	2.12	2.71	~~2.46~~	2.72	2.81	2.71
Al_2O_3	15.72	17.55	16.43	17.21	16.22	17.09	16.67	16.89	~~16.73~~	16.24	16.90	16.29
FeO	17.71	15.58	16.40	16.18	16.85	16.97	17.58	16.49	~~17.52~~	16.29	16.25	15.82
MnO												
MgO	11.61	12.40	12.22	11.79	11.76	11.81	11.00	11.83	~~11.13~~	11.68	12.08	12.79
CaO												
NaO												
K_2O	10.84	10.70	10.63	10.76	10.52	10.88	10.82	10.80	~~11.48~~	10.56	10.93	10.65
ClO												
F												
TOTAL	96.6	96.48	96.41	96.77	96.32	96.85	96.18	96.54	~~96.91~~	94.24	96.39	96.42
a.p.f.u.												
Si	5.68	5.59	5.67	5.66	5.69	5.60	5.70	5.63	~~5.62~~	5.61	5.58	5.66
Al^{IV}	2.32	2.41	2.33	2.34	2.31	2.40	2.30	2.37	~~2.38~~	2.39	2.42	2.34
Al^{VI}	0.46	0.65	0.55	0.66	0.54	0.59	0.65	0.59	~~0.57~~	0.53	0.55	0.51
Ti	0.32	0.28	0.29	0.28	0.31	0.28	0.24	0.30	~~0.28~~	0.31	0.32	0.30
Fe^{2+}	2.22	1.93	2.04	2.00	2.10	2.11	2.21	2.05	~~2.19~~	2.08	2.03	1.96
Mn	0.00	0.00	0.00	0.00	0.00	0.00	0.00	0.00	~~0.00~~	0.00	0.00	0.00
Mg	2.59	2.74	2.71	2.60	2.61	2.62	2.46	2.62	~~2.48~~	2.66	2.69	2.83
Ca	0.00	0.00	0.00	0.00	0.00	0.00	0.00	0.00	~~0.00~~	0.00	0.00	0.00

Na	0.00	0.00	0.00	0.00	0.00	0.00	0.00	0.00	~~0.00~~	0.00	0.00	0.00
K	2.07	2.02	2.02	2.03	2.00	2.06	2.07	2.05	~~2.19~~	2.06	2.08	2.01
Cl	0.00	0.00	0.00	0.00	0.00	0.00	0.00	0.00	~~0.00~~	0.00	0.00	0.00
F	0.00	0.00	0.00	0.00	0.00	0.00	0.00	0.00	~~0.00~~	0.00	0.00	0.00
TOTAL	15.65	15.61	15.61	15.57	15.57	15.66	15.62	15.61	~~15.72~~	15.64	15.66	15.62

Note: Wt% = percentage weight; a.p.f.u. = atom per formula unit

Sample 374-U1522A-55R-3W, 52-56 cm

Table 40 Chemical analysis of biotite

Wt%	Bt1	Bt2	Bt3	Bt4	Bt5	Bt6	Bt7	Bt8	Bt9	Bt10
SiO_2	40.90	40.81	~~40.43~~	40.79	39.91	40.75	40.63	40.75	40.66	41.92
TiO_2	2.96	3.10	~~3.23~~	2.95	3.28	3.65	3.06	2.87	2.51	2.60
Al_2O_3	18.79	17.48	~~17.84~~	17.91	17.47	18.20	18.30	17.62	18.50	18.34
FeO	16.25	17.73	~~17.79~~	16.86	18.73	16.73	17.46	17.24	17.15	16.39
MnO										
MgO	13.42	12.69	~~12.31~~	13.56	13.05	13.04	13.11	13.67	12.99	13.26
CaO										
NaO										
K_2O	11.62	11.54	~~12.08~~	11.44	11.74	11.49	10.72	11.61	11.39	11.04
ClO										
F										
TOTAL	96.21	96.77	~~96.46~~	96.61	95.99	96.29	96.84	96.39	96.91	96.58
a.p.f.u.										
Si	5.61	5.67	~~5.62~~	5.63	5.55	5.61	5.62	5.63	5.64	5.74
Al^{IV}	2.39	2.33	~~2.38~~	2.37	2.45	2.39	2.38	2.37	2.36	2.26
Al^{VI}	0.64	0.54	~~0.55~~	0.55	0.41	0.56	0.60	0.50	0.66	0.70
Ti	0.31	0.32	~~0.34~~	0.31	0.34	0.38	0.32	0.30	0.26	0.27
Fe^{2+}	1.86	2.06	~~2.07~~	1.95	2.18	1.92	2.02	1.99	1.99	1.88
Mn	0.00	0.00	~~0.00~~	0.00	0.00	0.00	0.00	0.00	0.00	0.00
Mg	2.74	2.63	~~2.55~~	2.79	2.70	2.68	2.70	2.82	2.68	2.71
Ca	0.00	0.00	~~0.00~~	0.00	0.00	0.00	0.00	0.00	0.00	0.00
Na	0.00	0.00	~~0.00~~	0.00	0.00	0.00	0.00	0.00	0.00	0.00
K	2.03	2.05	~~2.14~~	2.02	2.08	2.02	1.89	2.05	2.01	1.93
Cl	0.00	0.00	~~0.00~~	0.00	0.00	0.00	0.00	0.00	0.00	0.00
F	0.00	0.00	~~0.00~~	0.00	0.00	0.00	0.00	0.00	0.00	0.00
TOTAL	15.59	15.60	~~15.65~~	15.61	15.72	15.55	15.52	15.66	15.60	15.48

Note: Wt% = percentage weight; a.p.f.u. = atom per formula unit

Sample 374-U1522A-57R-1W, 0-3 cm

Table 41 Chemical analysis of biotite

Wt%	Bt1	Bt2	Bt3	Bt4	Bt5	Bt6	Bt7	Bt8	Bt9	Bt10	Bt11
SiO_2	41.34	41.48	~~38.94~~	42.42	41.95	40.75	41.24	41.50	~~39.53~~	~~39.46~~	~~39.01~~

TiO_2	3.30	3.32	~~2.93~~	2.21	3.09	2.83	2.39	3.57	~~3.92~~	~~3.88~~	~~3.26~~
Al_2O_3	18.14	17.86	~~16.67~~	19.22	17.61	18.97	18.53	17.84	~~17.38~~	~~16.63~~	~~17.33~~
FeO	17.45	16.98	~~21.02~~	15.39	17.61	16.59	17.58	17.71	~~19.63~~	~~20.01~~	~~24.14~~
MnO											
MgO	12.89	12.61	~~11.38~~	14.64	12.38	13.43	12.39	12.10	~~11.30~~	~~11.85~~	~~11.90~~
CaO											
NaO											
K_2O	10.78	10.90	~~12.80~~	10.09	10.93	11.25	11.33	11.11	~~12.29~~	~~12.01~~	~~7.75~~
ClO											
F											
TOTAL	96.25	96.94	~~96.39~~	96.18	96.56	96.31	96.66	96.31	~~96.10~~	~~96.29~~	~~96.71~~
a.p.f.u.											
Si	5.67	5.72	~~5.55~~	5.72	5.77	5.59	5.70	5.71	~~5.55~~	~~5.56~~	~~5.49~~
Al^{IV}	2.33	2.28	~~2.45~~	2.28	2.23	2.41	2.30	2.29	~~2.45~~	~~2.44~~	~~2.51~~
Al^{VI}	0.60	0.63	~~0.34~~	0.77	0.63	0.66	0.72	0.61	~~0.42~~	~~0.32~~	~~0.36~~
Ti	0.34	0.34	~~0.31~~	0.22	0.32	0.29	0.25	0.37	~~0.41~~	~~0.41~~	~~0.34~~
Fe^{2+}	2.00	1.96	~~2.50~~	1.73	2.03	1.90	2.03	2.04	~~2.30~~	~~2.36~~	~~2.84~~
Mn	0.00	0.00	~~0.00~~	0.00	0.00	0.00	0.00	0.00	~~0.00~~	~~0.00~~	~~0.00~~
Mg	2.63	2.59	~~2.42~~	2.94	2.54	2.75	2.55	2.48	~~2.36~~	~~2.49~~	~~2.50~~
Ca	0.00	0.00	~~0.00~~	0.00	0.00	0.00	0.00	0.00	~~0.00~~	~~0.00~~	~~0.00~~
Na	0.00	0.00	~~0.00~~	0.00	0.00	0.00	0.00	0.00	~~0.00~~	~~0.00~~	~~0.00~~
K	1.89	1.92	~~2.33~~	1.73	1.92	1.97	2.00	1.95	~~2.20~~	~~2.16~~	~~1.39~~
Cl	0.00	0.00	~~0.00~~	0.00	0.00	0.00	0.00	0.00	~~0.00~~	~~0.00~~	~~0.00~~
F	0.00	0.00	~~0.00~~	0.00	0.00	0.00	0.00	0.00	~~0.00~~	~~0.00~~	~~0.00~~
TOTAL	15.47	15.44	~~15.90~~	15.40	15.44	15.57	15.54	15.45	~~15.70~~	~~15.73~~	~~15.43~~

Note: Wt% = percentage weight; a.p.f.u. = atom per formula unit

Sample 374-U1522A-61R-1W,29-32 cm

Table 42 Chemical analysis of amphibole

Wt%	Amp1	Amp2	Amp3	Amp4	Amp5	Amp6	Amp7	Amp8	Amp9
SiO2	49.00	52.55	56.94	61.83	52.14	56.53	54.50	54.36	54.23
TiO2	0.38	0.34			0.44				
Al2O3	11.35	7.41	3.52	4.10	7.10	3.54	6.05	5.44	5.88
FeO	11.52	10.43	8.91	10.44	11.15	9.06	10.12	10.47	10.50
MnO									
MgO	15.88	17.77	19.56	20.99	17.18	19.47	18.20	18.21	18.19
CaO	12.41	12.33	12.70	13.77	12.40	12.10	12.16	12.18	12.62
NaO	1.31	0.92	0.37	0.41	0.96	0.51	0.74	0.60	0.70
K_2O	0.67	0.29	0.17	0.00	0.45	0.00	0.38	0.30	0.28
Cr_2O_3									
TOTAL	97.54	98.01	97.87	89.65	98.21	98.79	97.92	98.46	97.65
a.p.f.u.									
Si	0.80	0.86	0.93	0.92	0.85	0.93	0.89	0.89	0.88
Ti	0.00	0.00	0.00	0.00	0.01	0.00	0.00	0.00	0.00
Al	0.22	0.14	0.07	0.07	0.14	0.07	0.12	0.11	0.11
Fe	0.16	0.14	0.12	0.13	0.15	0.12	0.14	0.14	0.14

Mn	0.00	0.00	0.00	0.00	0.00	0.00	0.00	0.00	0.00
Mg	0.38	0.43	0.48	0.47	0.42	0.48	0.44	0.44	0.44
Ca	0.22	0.22	0.22	0.22	0.22	0.21	0.21	0.21	0.22
Na	0.04	0.03	0.01	0.01	0.03	0.02	0.02	0.02	0.02
K	0.01	0.01	0.00	0.00	0.01	0.00	0.01	0.01	0.01
Cr	0.00	0.00	0.00	0.00	0.00	0.00	0.00	0.00	0.00

Sample 374-U1522A-64R-4W,86-89 cm

Table 43 Chemical analysis of amphibole

Wt%	Amp1	Amp2	Amp3	Amp4	Amp5	Amp6	Amp7	Amp8	Amp9	Amp10
SiO2	45.84	47.65	48.23	46.56	45.38	46.12	47.30	45.54	46.29	46.01
TiO2	3.28	2.64	1.81	3.30	3.31	3.25	3.18	3.44	3.20	3.38
Al2O3	11.71	10.88	9.77	12.04	11.31	12.65	12.02	12.50	12.01	12.28
FeO	11.34	11.97	14.66	10.87	13.86	10.87	10.43	11.08	11.27	11.06
MnO										
MgO	15.37	15.45	13.36	15.37	13.00	15.45	15.35	14.85	15.09	15.25
CaO	10.93	10.59	10.79	10.32	11.38	10.36	10.55	10.47	10.35	10.72
NaO	2.64	2.30	2.11	2.58	2.34	2.81	2.50	2.64	2.71	2.69
K_2O	0.72	0.69	0.73	0.65	0.71	0.69	0.57	0.68	0.54	0.62
Cr_2O_3										
TOTAL	98.21	97.88	98.56	98.34	98.72	97.86	98.15	98.81	98.56	98.03
a.p.f.u.										
Si	0.75	0.78	0.79	0.76	0.75	0.75	0.77	0.75	0.76	0.75
Ti	0.04	0.03	0.02	0.04	0.04	0.04	0.04	0.04	0.04	0.04
Al	0.23	0.21	0.19	0.23	0.22	0.24	0.23	0.24	0.23	0.24
Fe	0.15	0.16	0.20	0.15	0.19	0.15	0.14	0.15	0.15	0.15
Mn	0.00	0.00	0.00	0.00	0.00	0.00	0.00	0.00	0.00	0.00
Mg	0.37	0.38	0.33	0.38	0.32	0.38	0.37	0.36	0.37	0.37
Ca	0.19	0.18	0.19	0.18	0.20	0.18	0.18	0.18	0.18	0.19
Na	0.08	0.07	0.07	0.08	0.07	0.09	0.08	0.08	0.09	0.08
K	0.01	0.01	0.02	0.01	0.01	0.01	0.01	0.01	0.01	0.01
Cr	0.00	0.00	0.00	0.00	0.00	0.00	0.00	0.00	0.00	0.00

Note: Wt% = percentage weight; a.p.f.u. = atom per formula unit

Sample 374-U1522A-66R-1W,56-59 cm

Table 44 Chemical analysis of biotite

Wt%	Bt1	Bt2	Bt3	Bt4	Bt5	Bt6	Bt7	Bt8	Bt9	Bt10	Bt11	Bt12	Bt13
SiO_2	38.83	39.01	39.58	~~38.25~~	39.01	39.49	39.14	38.24	39.30	39.09	38.84	39.82	38.63
TiO_2	4.25	4.27	3.78	~~4.34~~	3.94	3.27	3.84	4.94	4.02	4.32	3.89	3.97	3.54
Al_2O_3	19.73	19.48	19.82	~~19.19~~	19.87	19.92	20.13	19.95	19.79	19.82	20.40	19.46	19.94
FeO	18.37	18.94	18.36	~~19.62~~	17.90	18.52	17.93	17.97	18.10	17.91	18.16	18.83	18.17
MnO													
MgO	10.90	10.80	11.27	~~10.61~~	11.25	11.35	11.10	11.14	11.06	11.20	10.69	10.52	10.94
CaO													

NaO													
K_2O	11.45	11.22	10.94	~~11.87~~	11.60	10.70	11.76	11.10	11.48	11.60	11.45	11.10	11.43
ClO													
F													
TOTAL	96.59	96.41	96.38	~~96.27~~	96.56	96.85	96.24	96.77	96.38	96.21	96.69	96.42	97.42
a.p.f.u.													
Si	5.41	5.43	5.48	~~5.37~~	5.42	5.49	5.43	5.33	5.45	5.42	5.41	5.53	5.43
Al^{IV}	2.59	2.57	2.52	~~2.63~~	2.58	2.51	2.57	2.67	2.55	2.58	2.59	2.47	2.57
Al^{VI}	0.65	0.63	0.71	~~0.54~~	0.68	0.75	0.71	0.60	0.69	0.65	0.75	0.71	0.73
Ti	0.45	0.45	0.39	~~0.46~~	0.41	0.34	0.40	0.52	0.42	0.45	0.41	0.41	0.37
Fe^{2+}	2.14	2.21	2.12	~~2.30~~	2.08	2.15	2.08	2.09	2.10	2.07	2.11	2.19	2.13
Mn	0.00	0.00	0.00	~~0.00~~	0.00	0.00	0.00	0.00	0.00	0.00	0.00	0.00	0.00
Mg	2.27	2.24	2.32	~~2.22~~	2.33	2.35	2.29	2.31	2.29	2.31	2.22	2.18	2.29
Ca	0.00	0.00	0.00	~~0.00~~	0.00	0.00	0.00	0.00	0.00	0.00	0.00	0.00	0.00
Na	0.00	0.00	0.00	~~0.00~~	0.00	0.00	0.00	0.00	0.00	0.00	0.00	0.00	0.00
K	2.04	1.99	1.93	~~2.13~~	2.06	1.90	2.08	1.97	2.03	2.05	2.03	1.97	2.05
Cl	0.00	0.00	0.00	~~0.00~~	0.00	0.00	0.00	0.00	0.00	0.00	0.00	0.00	0.00
F	0.00	0.00	0.00	~~0.00~~	0.00	0.00	0.00	0.00	0.00	0.00	0.00	0.00	0.00
TOTAL	15.54	15.52	15.48	~~15.65~~	15.56	15.49	15.57	15.50	15.53	15.54	15.53	15.45	15.57

Note: Wt% = percentage weight; a.p.f.u. = atom per formula unit

Table 45 Chemical analysis of white mica

Wt%	**Wm1**	**Wm2**
SiO_2	~~50.55~~	50.11
TiO_2	~~1.56~~	1.73
Al_2O_3	~~37.31~~	36.88
FeO	~~1.40~~	1.25
MnO		
MgO	~~0.84~~	0.79
CaO	~~0.01~~	
NaO	~~0.57~~	0.68
K_2O	~~12.78~~	12.25
ClO		
F		
TOTAL	~~95.21~~	96.44
a.p.f.u.		
Si	~~6.16~~	6.17
Al^{IV}	~~1.84~~	1.83
Al^{VI}	~~3.52~~	3.52
Ti	~~0.14~~	0.16
Fe^{2+}	~~0.14~~	0.13
Mn	~~0.00~~	0.00
Mg	~~0.15~~	0.15
Ca	~~0.00~~	0.00
Na	~~0.13~~	0.16
K	~~1.99~~	1.92

Cl	~~0.00~~	0.00
F	~~0.00~~	0.00
TOTAL	~~14.08~~	14.04

Note: Wt% = percentage weight; a.p.f.u. = atom per formula unit

Sample 374-U1522A-66R-CCW, 19-22 cm

Table 46 Chemical analysis of biotite

Wt%	Bt1	Bt2	Bt3	Bt4	Bt5	Bt6	Bt7	Bt8	Bt9	Bt10	Bt11	Bt12
SiO_2	40.22	40.16	39.61	40.23	~~38.97~~	~~41.12~~	39.37	40.11	38.99	39.46	39.54	42.88
TiO_2	2.94	3.04	3.04	3.03	~~3.29~~	~~3.38~~	3.26	3.05	3.51	2.73	3.35	2.97
Al_2O_3	18.69	18.38	18.78	18.94	~~18.23~~	~~17.12~~	18.31	18.41	18.55	19.01	18.28	17.24
FeO	19.16	19.39	19.97	19.25	~~19.69~~	~~21.62~~	20.19	19.35	20.45	19.43	19.48	19.09
MnO												
MgO	11.84	11.74	11.15	11.28	~~11.55~~	~~8.36~~	11.19	11.56	10.88	12.06	11.53	10.78
CaO												
NaO												
K_2O	10.90	10.84	11.63	11.07	~~11.73~~	~~12.42~~	11.37	11.10	11.50	10.74	11.45	10.76
ClO												
F												
TOTAL	96.39	96.57	95.98	96.34	~~96.67~~	~~96.13~~	96.44	96.54	96.26	96.68	96.51	96.42
a.p.f.u.												
Si	5.58	5.59	5.52	5.59	~~5.49~~	~~5.80~~	5.52	5.59	5.47	5.50	5.53	5.91
Al^{IV}	2.42	2.41	2.48	2.41	~~2.51~~	~~2.20~~	2.48	2.41	2.53	2.50	2.47	2.09
Al^{VI}	0.64	0.61	0.61	0.68	~~0.51~~	~~0.64~~	0.55	0.61	0.54	0.63	0.55	0.71
Ti	0.31	0.32	0.32	0.32	~~0.35~~	~~0.36~~	0.34	0.32	0.37	0.29	0.35	0.31
Fe^{2+}	2.22	2.26	2.33	2.23	~~2.32~~	~~2.55~~	2.37	2.25	2.40	2.27	2.28	2.20
Mn	0.00	0.00	0.00	0.00	~~0.00~~	~~0.00~~	0.00	0.00	0.00	0.00	0.00	0.00
Mg	2.45	2.44	2.32	2.33	~~2.42~~	~~1.76~~	2.34	2.40	2.28	2.51	2.40	2.22
Ca	0.00	0.00	0.00	0.00	~~0.00~~	~~0.00~~	0.00	0.00	0.00	0.00	0.00	0.00
Na	0.00	0.00	0.00	0.00	~~0.00~~	~~0.00~~	0.00	0.00	0.00	0.00	0.00	0.00
K	1.93	1.93	2.07	1.96	~~2.11~~	~~2.23~~	2.03	1.97	2.06	1.91	2.04	1.89
Cl	0.00	0.00	0.00	0.00	~~0.00~~	~~0.00~~	0.00	0.00	0.00	0.00	0.00	0.00
F	0.00	0.00	0.00	0.00	~~0.00~~	~~0.00~~	0.00	0.00	0.00	0.00	0.00	0.00
TOTAL	15.55	15.55	15.65	15.53	~~15.71~~	~~15.54~~	15.64	15.56	15.65	15.60	15.63	15.33

Note: Wt% = percentage weight; a.p.f.u. = atom per formula unit

Sample 374-U1522A-67R-1W, 53-58 cm

Table 47 Chemical analyses of biotite in clasts n 1, 2, 5, 6, and 7

Wt%	Bt1-1	Bt2-1	Bt5-1	Bt5-2	Bt5-3	Bt6-1	Bt6-2	Bt7-1
SiO_2	41.18	~~43.00~~	~~42.05~~	~~36.85~~	~~37.42~~	39.87	39.99	38.89
TiO_2	2.50	~~1.74~~	~~3.37~~	~~3.72~~	~~3.21~~	1.77	1.27	3.90

Al2O3	18.98	~~16.66~~	~~16.13~~	~~15.99~~	~~16.80~~	19.97	19.61	14.50
FeO	23.72	~~20.60~~	~~21.86~~	~~25.24~~	~~24.06~~	19.12	18.28	23.12
MnO	0.34	~~0.40~~	~~0.77~~	~~0.90~~	~~0.78~~	0.51	0.53	0.26
MgO	7.01	~~10.77~~	~~8.77~~	~~8.72~~	~~9.08~~	12.83	12.71	11.72
CaO		-			-			
NaO		-			-			
K2O	9.93	~~10.21~~	~~10.96~~	~~12.38~~	~~12.18~~	9.89	11.04	10.64
ClO		-			-			0.34
F		-			-			
TOTAL	96.48	~~96.73~~	~~96.24~~	~~96.33~~	~~96.59~~	96.19	96.68	96.75
a.p.f.u.		-	-		-			
Si	5.79	~~5.98~~	~~5.90~~	~~5.39~~	~~5.44~~	5.50	5.56	5.58
Al^{IV}	2.21	~~2.02~~	~~2.10~~	~~2.61~~	~~2.56~~	2.50	2.44	2.42
Al^{VI}	0.93	~~0.71~~	~~0.57~~	~~0.15~~	~~0.31~~	0.74	0.77	0.03
Ti	0.26	~~0.18~~	~~0.36~~	~~0.41~~	~~0.35~~	0.18	0.13	0.42
Fe(ii)	2.79	~~2.40~~	~~2.57~~	~~3.09~~	~~2.92~~	2.20	2.12	2.77
Mn	0.04	~~0.05~~	~~0.09~~	~~0.11~~	~~0.10~~	0.06	0.06	0.03
Mg	1.47	~~2.23~~	~~1.84~~	~~1.90~~	~~1.97~~	2.64	2.63	2.51
Ca	0.00	~~0.00~~	~~0.00~~	~~0.00~~	~~0.00~~	0.00	0.00	0.00
Na	0.00	~~0.00~~	~~0.00~~	~~0.00~~	~~0.00~~	0.00	0.00	0.00
K	1.78	~~1.81~~	~~1.96~~	~~2.31~~	~~2.26~~	1.74	1.96	1.95
Cl	0.00	~~0.00~~	~~0.00~~	~~0.00~~	~~0.00~~	0.00	0.00	0.08
F	0.00	~~0.00~~	~~0.00~~	~~0.00~~	~~0.00~~	0.00	0.00	0.00
TOTAL	15.27	~~15.38~~	~~15.39~~	~~15.97~~	~~15.90~~	15.57	15.68	15.71

Note: Wt% = percentage weight; a.p.f.u. = atom per formula unit

Table 48 Chemical analysis of amphibole from clast n. 7

Wt%	**Amp7-1**
SiO2	54.96
TiO2	1.00
Al2O3	4.64
FeO	16.63
MnO	0.55
MgO	11.73
CaO	11.93
NaO	
K_2O	0.52
Cr_2O_3	
TOTAL	98.08
a.p.f.u.	
Si	0.90
Ti	0.01
Al	0.09
Fe	0.23
Mn	0.01
Mg	0.29
Ca	0.21
Na	0.00

K	0.01
Cr	0.00

Note: Wt% = percentage weight; a.p.f.u. = atom per formula unit

Sample 374-U1522A-67R-2W, 72-75 cm

Table 49 Chemical analysis of amphibole

Wt%	Amp1	Amp2	Amp3	Amp5
SiO2	44.79	44.85	45.75	46.31
TiO2	3.94	4.10	4.18	3.66
Al2O3	11.35	10.38	10.00	9.82
FeO	12.70	12.15	12.22	12.91
MnO				
MgO	14.64	15.16	15.18	15.19
CaO	11.21	11.19	11.19	11.08
NaO	2.92	2.91	2.84	2.70
K_2O	0.50	0.62	0.55	0.61
Cr_2O_3				
TOTAL	97.99	98.65	98.13	97.78
a.p.f.u.				
Si	0.73	0.74	0.75	0.75
Ti	0.05	0.05	0.05	0.04
Al	0.22	0.20	0.19	0.19
Fe	0.17	0.17	0.17	0.18
Mn	0.00	0.00	0.00	0.00
Mg	0.36	0.37	0.37	0.37
Ca	0.20	0.20	0.20	0.19
Na	0.09	0.09	0.09	0.09
K	0.01	0.01	0.01	0.01
Cr	0.00	0.00	0.00	0.00

Note: Wt% = percentage weight; a.p.f.u. = atom per formula unit

Table 50 Chemical analysis of pyroxene

Wt%	Px0	Px1	Px2	Px3	Px4	Px5	Px6
SiO_2	53.26	53.90	53.49	53.74	52.58	~~54.68~~	53.90
TiO_2							
Al_2O_3	1.67	1.47	1.72	1.46	2.59	~~5.98~~	1.47
Cr_2O_3							
Fe_2O_3							
FeO	9.30	7.93	8.30	8.13	8.84	~~7.45~~	7.93
MnO							
MgO	15.66	16.10	15.85	15.85	15.98	~~12.80~~	16.10
CaO	20.10	20.60	20.65	20.82	20.01	~~17.10~~	20.60
Na_2O						~~0.70~~	
K_2O						~~1.28~~	
TOTAL	100.00	100.00	100.00	100.00	100.00	~~100.00~~	100.00
a.p.f.u.							
Si	1.97	1.99	1.98	1.99	1.94	~~2.05~~	1.99

Ti	0.00	0.00	0.00	0.00	0.00	~~0.00~~	0.00
Al	0.07	0.06	0.07	0.06	0.11	~~0.26~~	0.06
Cr	0.00	0.00	0.00	0.00	0.00	~~0.00~~	0.00
Fe^{3+}	0.00	0.00	0.00	0.00	0.00	~~0.00~~	0.00
Fe^{2+}	0.29	0.24	0.26	0.25	0.27	~~0.23~~	0.24
Mn	0.00	0.00	0.00	0.00	0.00	~~0.00~~	0.00
Mg	0.87	0.89	0.87	0.87	0.88	~~0.72~~	0.89
Ca	0.80	0.81	0.82	0.82	0.79	~~0.69~~	0.81
Na	0.00	0.00	0.00	0.00	0.00	~~0.05~~	0.00
TOTAL	6.01	6.02	6.01	6.02	6.00	~~6.16~~	6.02

Note: Wt% = percentage weight; a.p.f.u. = atom per formula unit

Sample 374-U1522A-67R-2W, 105-108 cm

Table 51 Chemical analysis of biotite

Wt%	Bt1	Bt2	Bt3	Bt4	Bt5	Bt6	Bt7	Bt8	Bt9	Bt10
SiO_2	39.68	40.18	39.03	39.75	43.30	40.24	39.98	~~39.72~~	39.96	40.58
TiO_2	4.08	3.77	4.73	3.45	3.05	3.78	3.12	~~3.30~~	3.67	2.67
Al_2O_3	15.94	16.33	14.93	15.44	14.50	16.06	16.76	~~16.52~~	16.10	16.62
FeO	20.61	19.49	21.38	20.80	21.30	20.00	19.38	~~19.84~~	19.62	19.30
MnO	0.00	0.00	0.00	0.00	0.00	0.00	0.00	~~0.00~~	0.00	0.00
MgO	12.05	12.92	11.75	12.60	10.06	12.57	13.01	~~12.44~~	13.22	13.31
CaO	0.00	0.00	0.00	0.00	0.00	0.00	0.00	~~0.00~~	0.00	0.00
NaO	0.00	0.00	0.00	0.00	0.00	0.00	0.00	~~0.00~~	0.00	0.00
K_2O	10.86	11.14	11.55	11.46	11.57	11.21	11.57	~~11.78~~	11.32	10.94
ClO										
F										
TOTAL	96.87	96.31	96.74	96.62	96.37	96.29	96.31	~~96.52~~	96.26	96.69
a.p.f.u.										
Si	5.60	5.61	5.56	5.62	6.07	5.63	5.59	~~5.59~~	5.59	5.67
Al^{IV}	2.40	2.39	2.44	2.38	1.93	2.37	2.41	~~2.41~~	2.41	2.33
Al^{VI}	0.26	0.30	0.07	0.20	0.46	0.28	0.36	~~0.33~~	0.25	0.40
Ti	0.43	0.40	0.51	0.37	0.32	0.40	0.33	~~0.35~~	0.39	0.28
Fe^{2+}	2.43	2.27	2.55	2.46	2.50	2.34	2.27	~~2.34~~	2.30	2.25
Mn	0.00	0.00	0.00	0.00	0.00	0.00	0.00	~~0.00~~	0.00	0.00
Mg	2.54	2.69	2.50	2.66	2.10	2.62	2.71	~~2.61~~	2.76	2.77
Ca	0.00	0.00	0.00	0.00	0.00	0.00	0.00	~~0.00~~	0.00	0.00
Na	0.00	0.00	0.00	0.00	0.00	0.00	0.00	~~0.00~~	0.00	0.00
K	1.96	1.98	2.10	2.07	2.07	2.00	2.06	~~2.12~~	2.02	1.95
Cl	0.00	0.00	0.00	0.00	0.00	0.00	0.00	~~0.00~~	0.00	0.00
F	0.00	0.00	0.00	0.00	0.00	0.00	0.00	~~0.00~~	0.00	0.00
TOTAL	15.62	15.64	15.72	15.75	15.45	15.65	15.73	~~15.75~~	15.71	15.66

Note: Wt% = percentage weight; a.p.f.u. = atom per formula unit

Table 52 Chemical analysis of amphibole

Wt%	Amp1	Amp2	Amp3	Amp4	Amp5	Amp6
SiO2	50.26	50.48	52.19	52.23	50.11	50.90
TiO2	1.07	1.38	1.12	1.09	1.28	1.25
Al2O3	7.76	7.83	6.80	7.47	6.29	6.46
FeO	14.34	14.06	13.68	13.37	16.92	15.32
MnO						
MgO	14.48	14.41	15.40	15.44	12.96	14.03
CaO	11.58	11.81	11.17	10.73	12.85	12.19
NaO	1.02	1.29	1.28	1.46	0.93	1.04
K_2O	0.66	0.54	0.46	0.51	0.52	0.46
Cr_2O_3						
TOTAL	98.84	98.23	97.95	97.76	98.19	98.39
a.p.f.u.						
Si	0.83	0.83	0.85	0.85	0.82	0.83
Ti	0.01	0.02	0.01	0.01	0.02	0.02
Al	0.15	0.15	0.13	0.14	0.12	0.12
Fe	0.20	0.19	0.19	0.18	0.23	0.21
Mn	0.00	0.00	0.00	0.00	0.00	0.00
Mg	0.36	0.35	0.37	0.37	0.32	0.34
Ca	0.20	0.21	0.20	0.19	0.22	0.21
Na	0.03	0.04	0.04	0.05	0.03	0.03
K	0.01	0.01	0.01	0.01	0.01	0.01
Cr	0.00	0.00	0.00	0.00	0.00	0.00

Note: Wt% = percentage weight; a.p.f.u. = atom per formula unit

Sample 374-U1522A-67R-4W, 6-8 cm

Table 53 Chemical analysis of biotite

Wt%	Bt1	Bt2	Bt3	Bt4	Bt5	Bt6	Bt7	Bt8	Bt9	Bt10	Bt11	Bt12	Bt13
SiO_2	40.88	41.07	41.17	40.68	~~35.60~~	~~39.86~~	41.54	42.56	42.06	40.84	42.27	42.04	43.64
TiO_2	2.68	2.48	2.85	1.50	~~2.91~~	~~2.53~~	1.74	1.62	1.85	2.76	2.59	2.01	2.40
Al_2O_3	18.16	17.74	17.31	17.63	~~14.83~~	~~16.36~~	18.63	18.56	18.04	18.28	18.08	17.15	16.52
FeO	16.74	17.68	18.29	18.48	~~25.29~~	~~20.60~~	15.83	15.62	16.11	16.74	16.09	17.85	17.70
MnO													
MgO	14.14	13.50	12.80	13.93	~~9.46~~	~~12.13~~	15.08	14.62	14.56	13.76	14.06	13.85	12.02
CaO													
NaO													
K_2O	11.13	11.02	11.39	11.69	~~15.28~~	~~12.47~~	10.92	10.49	10.57	11.25	10.31	10.64	11.58
ClO													
F													
TOTAL	96.41	96.64	96.33	96.24	~~96.74~~	~~96.19~~	96.39	96.65	96.91	96.50	96.71	96.57	96.29
a.p.f.u.													
Si	5.62	5.68	5.70	5.65	~~5.34~~	~~5.63~~	5.66	5.78	5.76	5.62	5.76	5.79	5.99
Al^{IV}	2.38	2.32	2.30	2.35	~~2.62~~	~~2.37~~	2.34	2.22	2.24	2.38	2.24	2.21	2.01
Al^{VI}	0.56	0.57	0.53	0.53	~~0.00~~	~~0.36~~	0.66	0.76	0.67	0.59	0.67	0.57	0.67
Ti	0.28	0.26	0.30	0.16	~~0.33~~	~~0.27~~	0.18	0.17	0.19	0.29	0.27	0.21	0.25
Fe^{2+}	1.92	2.04	2.12	2.15	~~3.17~~	~~2.43~~	1.81	1.77	1.84	1.93	1.83	2.06	2.03

Mn	0.00	0.00	0.00	0.00	~~0.00~~	~~0.00~~	0.00	0.00	0.00	0.00	0.00	0.00	0.00
Mg	2.90	2.78	2.64	2.88	~~2.11~~	~~2.56~~	3.07	2.96	2.97	2.82	2.86	2.84	2.46
Ca	0.00	0.00	0.00	0.00	~~0.00~~	~~0.00~~	0.00	0.00	0.00	0.00	0.00	0.00	0.00
Na	0.00	0.00	0.00	0.00	~~0.00~~	~~0.00~~	0.00	0.00	0.00	0.00	0.00	0.00	0.00
K	1.95	1.94	2.01	2.07	~~2.92~~	~~2.25~~	1.90	1.82	1.85	1.97	1.79	1.87	2.03
Cl	0.00	0.00	0.00	0.00	~~0.00~~	~~0.00~~	0.00	0.00	0.00	0.00	0.00	0.00	0.00
F	0.00	0.00	0.00	0.00	~~0.00~~	~~0.00~~	0.00	0.00	0.00	0.00	0.00	0.00	0.00
TOTAL	15.61	15.59	15.60	15.79	~~16.49~~	~~15.86~~	15.61	15.47	15.52	15.60	15.42	15.55	15.44

Note: Wt% = percentage weight; a.p.f.u. = atom per formula unit

Table 54 Chemical analysis of pyroxene

Wt%	Px1	Px2	Px3	Px4	Px5
SiO_2	54.52	54.45	~~55.58~~	54.56	~~55.81~~
TiO_2					
Al_2O_3	0.90	1.13	~~0.00~~	0.45	~~0.96~~
Cr_2O_3					
Fe_2O_3					
FeO	8.32	8.66	~~9.49~~	7.78	~~7.95~~
MnO					
MgO	13.71	13.48	~~9.67~~	13.88	~~13.88~~
CaO	22.55	22.29	~~25.26~~	23.32	~~21.40~~
Na_2O					
K_2O					
TOTAL	100.00	100.00	~~100.00~~	100.00	~~100.00~~
a.p.f.u.					
Si	2.04	2.04	~~2.12~~	2.03	~~2.08~~
Ti	0.00	0.00	~~0.00~~	0.00	~~0.00~~
Al	0.04	0.05	~~0.00~~	0.02	~~0.04~~
Cr	0.00	0.00	~~0.00~~	0.00	~~0.00~~
Fe^{3+}	0.00	0.00	~~0.00~~	0.00	~~0.00~~
Fe^{2+}	0.26	0.27	~~0.30~~	0.24	~~0.25~~
Mn	0.00	0.00	~~0.00~~	0.00	~~0.00~~
Mg	0.76	0.75	~~0.55~~	0.77	~~0.77~~
Ca	0.90	0.89	~~1.03~~	0.93	~~0.86~~
Na	0.00	0.00	~~0.00~~	0.00	~~0.00~~
TOTAL	6.06	6.06	~~6.12~~	6.04	~~6.10~~

Note: Wt% = percentage weight; a.p.f.u. = atom per formula unit

Sample 374-U1522A-68R-1W, 71-86 cm

Table 55 Chemical analysis of biotite

Wt%	Bt1	Bt2	Bt3	Bt4	Bt5	Bt6	Bt7	Bt8	Bt9	Bt10	Bt11	Bt12	Bt13
SiO_2	40.86	40.62	40.74	40.66	40.21	40.68	40.66	40.54	40.92	40.27	40.58	40.73	40.60
TiO_2	3.69	3.15	3.33	3.85	3.84	2.94	2.15	3.02	3.40	3.48	2.53	2.83	1.95

Al_2O_3	17.48	18.15	17.50	17.47	17.28	17.18	18.32	17.51	16.69	17.49	17.40	17.46	17.95
FeO	17.43	18.54	18.17	18.06	19.04	18.17	17.35	18.38	20.83	19.52	19.11	18.65	16.78
MnO													
MgO	13.00	12.97	12.99	12.34	12.40	13.93	13.89	13.09	10.28	12.52	13.40	13.10	15.45
CaO													
NaO													
K_2O	10.75	10.38	10.62	11.09	11.04	10.84	10.93	11.04	11.26	10.63	10.81	11.16	10.88
ClO													
F													
TOTAL	96.89	96.32	96.74	96.65	96.32	96.39	96.81	96.56	96.73	96.24	96.31	96.21	96.52
a.p.f.u.													
Si	5.65	5.60	5.65	5.64	5.59	5.63	5.62	5.63	5.76	5.59	5.63	5.64	5.59
Al^{IV}	2.35	2.40	2.35	2.36	2.41	2.37	2.38	2.37	2.24	2.41	2.37	2.36	2.41
Al^{VI}	0.50	0.55	0.50	0.50	0.42	0.43	0.61	0.49	0.52	0.45	0.48	0.49	0.50
Ti	0.38	0.33	0.35	0.40	0.40	0.31	0.22	0.31	0.36	0.36	0.26	0.30	0.20
Fe^{2+}	2.02	2.14	2.11	2.09	2.21	2.10	2.01	2.13	2.45	2.27	2.22	2.16	1.93
Mn	0.00	0.00	0.00	0.00	0.00	0.00	0.00	0.00	0.00	0.00	0.00	0.00	0.00
Mg	2.68	2.67	2.68	2.55	2.57	2.87	2.86	2.71	2.16	2.59	2.77	2.70	3.17
Ca	0.00	0.00	0.00	0.00	0.00	0.00	0.00	0.00	0.00	0.00	0.00	0.00	0.00
Na	0.00	0.00	0.00	0.00	0.00	0.00	0.00	0.00	0.00	0.00	0.00	0.00	0.00
K	1.90	1.83	1.88	1.96	1.96	1.91	1.93	1.95	2.02	1.88	1.91	1.97	1.91
Cl	0.00	0.00	0.00	0.00	0.00	0.00	0.00	0.00	0.00	0.00	0.00	0.00	0.00
F	0.00	0.00	0.00	0.00	0.00	0.00	0.00	0.00	0.00	0.00	0.00	0.00	0.00
TOTAL	15.49	15.51	15.52	15.51	15.57	15.62	15.63	15.60	15.51	15.56	15.64	15.62	15.71

Note: Wt% = percentage weight; a.p.f.u. = atom per formula unit

Table 56 Chemical analysis of amphibole

Wt%	Amp1	Amp2	Amp3	Amp4	Amp5	Amp6	Amp7	Amp8	Amp9	Amp10	Amp11
SiO2	55.95	54.45	57.63	54.46	51.76	~~53.73~~	55.98	53.01	58.15	52.43	55.99
TiO2					0.39						
Al2O3	3.31	5.27	1.98	5.75	7.28	~~4.84~~	4.76	6.53	1.75	7.25	3.30
FeO	15.31	15.75	12.92	15.64	15.71	~~14.31~~	14.55	15.66	14.13	16.22	14.26
MnO											
MgO	15.01	13.93	16.44	13.92	12.95	~~14.14~~	13.57	13.38	15.78	12.83	15.39
CaO	12.70	12.62	12.40	12.36	12.17	~~14.69~~	12.39	12.22	12.41	12.29	12.50
NaO					0.71			0.60		0.58	
K_2O					0.50			0.42		0.42	
Cr_2O_3											
TOTAL	97.76	98.02	98.65	97.91	98.54	~~98.33~~	98.76	98.21	97.82	98.03	98.58
a.p.f.u.											
Si	0.91	0.89	0.95	0.89	0.85	~~0.88~~	0.92	0.87	0.95	0.86	0.92
Ti	0.00	0.00	0.00	0.00	0.00	~~0.00~~	0.00	0.00	0.00	0.00	0.00
Al	0.06	0.10	0.04	0.11	0.14	~~0.09~~	0.09	0.13	0.03	0.14	0.06
Fe	0.21	0.21	0.18	0.21	0.22	~~0.20~~	0.20	0.21	0.19	0.22	0.20
Mn	0.00	0.00	0.00	0.00	0.00	~~0.00~~	0.00	0.00	0.00	0.00	0.00
Mg	0.36	0.34	0.40	0.34	0.32	~~0.34~~	0.33	0.33	0.38	0.31	0.38
Ca	0.22	0.22	0.22	0.22	0.21	~~0.26~~	0.22	0.21	0.22	0.21	0.22
Na	0.00	0.00	0.00	0.00	0.02	~~0.00~~	0.00	0.02	0.00	0.02	0.00
K	0.00	0.00	0.00	0.00	0.01	~~0.00~~	0.00	0.01	0.00	0.01	0.00

Cr	0.00	0.00	0.00	0.00	0.00	~~0.00~~	0.00	0.00	0.00	0.00	0.00

Note: Wt% = percentage weight; a.p.f.u. = atom per formula unit

Sample 374-U1522A-68R-2W, 78-80 cm

Table 57 Chemical analysis of biotite

Wt%	Bt1	Bt2	Bt3	Bt4	Bt5	Bt6	Bt7	Bt8	Bt9	Bt10	Bt11	Bt12
SiO_2	39.99	40.26	40.42	40.29	39.85	40.07	40.25	40.40	40.11	40.95	39.76	39.96
TiO_2	2.45	2.31	2.26	2.39	2.47	2.41	2.54	2.00	2.28	2.25	2.25	2.33
Al_2O_3	20.75	20.04	20.71	20.75	20.57	20.64	20.50	20.62	20.16	20.27	20.98	20.89
FeO	16.26	16.82	16.30	16.29	16.67	16.46	16.72	16.45	16.49	17.27	16.80	16.81
MnO												
MgO	13.22	13.32	13.16	12.84	13.15	12.90	12.98	13.10	13.29	12.26	12.86	12.85
CaO												
NaO												
K_2O	11.15	10.72	10.90	10.98	11.05	10.95	10.97	10.80	10.96	10.70	10.97	11.10
ClO												
F												
TOTAL	96.33	96.65	96.39	96.58	96.37	96.69	96.19	96.74	96.82	96.44	96.50	96.21
a.p.f.u.												
Si	5.47	5.53	5.52	5.52	5.47	5.50	5.50	5.54	5.52	5.61	5.46	5.47
Al^{IV}	2.53	2.47	2.48	2.48	2.53	2.50	2.50	2.46	2.48	2.39	2.54	2.53
Al^{VI}	0.82	0.77	0.86	0.87	0.79	0.84	0.81	0.87	0.79	0.88	0.86	0.84
Ti	0.25	0.24	0.23	0.25	0.26	0.25	0.26	0.21	0.24	0.23	0.23	0.24
Fe^{2+}	1.86	1.93	1.86	1.87	1.91	1.89	1.91	1.89	1.90	1.98	1.93	1.92
Mn	0.00	0.00	0.00	0.00	0.00	0.00	0.00	0.00	0.00	0.00	0.00	0.00
Mg	2.70	2.73	2.68	2.62	2.69	2.64	2.65	2.68	2.73	2.50	2.63	2.62
Ca	0.00	0.00	0.00	0.00	0.00	0.00	0.00	0.00	0.00	0.00	0.00	0.00
Na	0.00	0.00	0.00	0.00	0.00	0.00	0.00	0.00	0.00	0.00	0.00	0.00
K	1.95	1.88	1.90	1.92	1.93	1.92	1.91	1.89	1.92	1.87	1.92	1.94
Cl	0.00	0.00	0.00	0.00	0.00	0.00	0.00	0.00	0.00	0.00	0.00	0.00
F	0.00	0.00	0.00	0.00	0.00	0.00	0.00	0.00	0.00	0.00	0.00	0.00
TOTAL	15.58	15.55	15.53	15.52	15.58	15.54	15.54	15.53	15.57	15.46	15.57	15.57

Note: Wt% = percentage weight; a.p.f.u. = atom per formula unit

Table 58 Chemical analysis of white mica

Wt%	Wm1	Wm2	Wm3	Wm4	Wm5	Wm6	Wm7	Wm8	Wm9	Wm10	Wm11	Wm12
SiO_2	51.13	51.42	~~51.33~~	50.37	51.14	50.10	50.48	50.13	50.79	50.94	50.95	51.06
TiO_2				0.74	0.76	0.84	0.80	0.82	0.74	0.89	0.95	0.87
Al_2O_3	38.14	39.46	~~40.11~~	38.16	39.81	38.83	38.83	38.94	39.84	39.23	38.38	39.26
FeO	1.38	1.10	~~0.99~~	1.02	1.04	1.19	0.98	0.94	0.92	0.89	0.86	0.90
MnO												
MgO	1.39	0.64	~~0.62~~	0.76	0.69	0.83	0.76	0.69	0.54	0.76	0.82	0.76
CaO												
NaO	0.59	1.47	~~1.46~~	1.37	1.41	1.29	1.43	1.38	1.46	1.38	1.49	1.54

K_2O	12.22	11.41	~~11.59~~	11.14	11.39	11.46	11.17	11.16	11.39	11.18	10.82	11.15
ClO												
F												
TOTAL	95.37	94.78	~~94.25~~	96.56	94.12	95.65	95.73	96.11	94.62	94.99	95.89	94.76
a.p.f.u.												
Si	6.21	6.18	~~6.13~~	6.17	6.10	6.09	6.13	6.11	6.09	6.13	6.18	6.13
Al^{IV}	1.79	1.82	~~1.87~~	1.83	1.90	1.91	1.87	1.89	1.91	1.87	1.82	1.87
Al^{VI}	3.66	3.76	~~3.78~~	3.67	3.70	3.66	3.68	3.70	3.73	3.69	3.66	3.68
Ti	0.00	0.00	~~0.00~~	0.07	0.07	0.08	0.07	0.08	0.07	0.08	0.09	0.08
Fe^{2+}	0.14	0.11	~~0.10~~	0.10	0.10	0.12	0.10	0.10	0.09	0.09	0.09	0.09
Mn	0.00	0.00	~~0.00~~	0.00	0.00	0.00	0.00	0.00	0.00	0.00	0.00	0.00
Mg	0.25	0.11	~~0.11~~	0.14	0.12	0.15	0.14	0.13	0.10	0.14	0.15	0.14
Ca	0.00	0.00	~~0.00~~	0.00	0.00	0.00	0.00	0.00	0.00	0.00	0.00	0.00
Na	0.14	0.34	~~0.34~~	0.32	0.33	0.30	0.34	0.32	0.34	0.32	0.35	0.36
K	1.89	1.75	~~1.77~~	1.74	1.73	1.78	1.73	1.73	1.74	1.72	1.67	1.71
Cl	0.00	0.00	~~0.00~~	0.00	0.00	0.00	0.00	0.00	0.00	0.00	0.00	0.00
F	0.00	0.00	~~0.00~~	0.00	0.00	0.00	0.00	0.00	0.00	0.00	0.00	0.00
TOTAL	14.08	14.08	~~14.10~~	14.05	14.06	14.09	14.06	14.05	14.07	14.03	14.01	14.05

Note: Wt% = percentage weight; a.p.f.u. = atom per formula unit

Table 59 Chemical analysis of garnet

Wt%	Grt1	Grt2	Grt3	Grt4
SiO_2	38.21	38.30	38.30	38.45
TiO_2				
Al_2O_3	21.46	21.91	21.65	21.72
Cr_2O_3				
Fe_2O_3				
FeO	25.26	25.47	25.31	25.50
MnO	9.90	8.99	9.25	9.71
MgO	3.15	3.27	3.49	2.74
CaO	2.01	2.05	2.00	1.89
TOTAL	100	100	100	100
a.p.f.u.				
Si	3.06	3.06	3.06	3.08
Ti	0.00	0.00	0.00	0.00
Al	2.03	2.06	2.04	2.05
Cr	0.00	0.00	0.00	0.00
Fe^{3+}	0.00	0.00	0.00	0.00
Fe^{2+}	1.69	1.70	1.69	1.71
Mn	0.67	0.61	0.63	0.66
Mg	0.38	0.39	0.42	0.33
Ca	0.17	0.18	0.17	0.16
TOTAL	12.07	12.09	12.08	12.11

Note: Wt% = percentage weight; a.p.f.u. = atom per formula unit

Sample 374-U1522A-68R-6W, 56-60 cm

Table 60 Chemical analysis of biotite

Wt%	Bt1	Bt2	Bt3	Bt4	Bt5	Bt6	Bt7	Bt8	Bt9	Bt10	Bt11	Bt12	Bt13
SiO_2	39.56	39.08	39.23	39.51	39.84	40.45	39.50	39.33	39.48	39.59	39.40	39.57	39.57
TiO_2	3.12	3.31	3.32	3.56	3.24	3.17	3.21	3.38	3.39	3.46	3.27	3.41	3.41
Al_2O_3	19.73	19.24	19.32	18.68	18.52	18.67	18.86	19.21	19.06	19.04	18.78	18.53	18.53
FeO	20.13	20.52	20.59	20.21	20.24	20.18	20.52	20.60	20.52	19.88	20.32	20.39	20.39
MnO													
MgO	9.65	10.17	10.21	10.34	10.07	10.07	9.95	9.71	10.11	9.91	10.46	10.43	10.43
CaO													
NaO													
K_2O	11.26	11.26	11.30	11.51	11.32	11.22	11.66	11.39	11.26	11.39	11.66	11.42	11.42
ClO													
F													
TOTAL	96.66	96.54	96.18	96.32	96.87	96.36	96.42	96.51	96.33	96.84	96.24	96.39	96.39
a.p.f.u.													
Si	5.55	5.54	5.49	5.55	5.53	5.60	5.64	5.55	5.52	5.53	5.56	5.52	5.55
Al^{IV}	2.45	2.46	2.51	2.45	2.47	2.40	2.36	2.45	2.48	2.47	2.44	2.48	2.45
Al^{VI}	0.71	0.80	0.67	0.68	0.62	0.67	0.71	0.67	0.70	0.67	0.71	0.63	0.61
Ti	0.34	0.33	0.35	0.33	0.38	0.34	0.33	0.34	0.36	0.36	0.37	0.35	0.36
Fe^{2+}	2.35	2.36	2.41	2.37	2.37	2.38	2.35	2.41	2.42	2.40	2.33	2.38	2.39
Mn	0.00	0.00	0.00	0.00	0.00	0.00	0.00	0.00	0.00	0.00	0.00	0.00	0.00
Mg	2.15	2.01	2.13	2.16	2.16	2.11	2.09	2.08	2.03	2.11	2.07	2.19	2.18
Ca	0.00	0.00	0.00	0.00	0.00	0.00	0.00	0.00	0.00	0.00	0.00	0.00	0.00
Na	0.00	0.00	0.00	0.00	0.00	0.00	0.00	0.00	0.00	0.00	0.00	0.00	0.00
K	1.99	2.01	2.02	2.03	2.06	2.03	2.00	2.09	2.04	2.01	2.04	2.09	2.04
Cl	0.00	0.00	0.00	0.00	0.00	0.00	0.00	0.00	0.00	0.00	0.00	0.00	0.00
F	0.00	0.00	0.00	0.00	0.00	0.00	0.00	0.00	0.00	0.00	0.00	0.00	0.00
TOTAL	15.54	15.51	15.58	15.56	15.58	15.54	15.49	15.60	15.55	15.55	15.52	15.62	15.58

Note: Wt% = percentage weight; a.p.f.u. = atom per formula unit

Sample 374-U1522A-69R-1W, 0-4 cm

Table 61 Chemical analysis of biotite

Wt%	Bt1	Bt2	Bt3	Bt4	Bt5	Bt6	Bt7	Bt8	Bt9	Bt10
SiO_2	40.77	39.67	40.47	39.72	39.62	~~37.47~~	39.68	~~39.88~~	39.98	41.47
TiO_2	3.34	3.39	3.34	3.89	3.71	~~2.82~~	3.56	~~3.18~~	4.14	3.89
Al_2O_3	16.21	15.64	15.91	15.12	16.03	~~15.58~~	16.32	~~16.99~~	16.10	16.86
FeO	21.02	22.03	21.43	22.60	21.31	~~25.03~~	21.09	~~21.02~~	20.91	19.07
MnO										
MgO	11.17	11.64	11.52	10.72	11.78	~~10.80~~	11.58	~~11.21~~	11.29	11.12
CaO										
NaO										

K_2O	11.25	11.19	11.14	11.23	11.31	~~11.94~~	11.36	~~11.69~~	11.07	10.86
ClO										
F										
TOTAL	96.38	96.56	96.33	96.82	96.37	~~96.49~~	96.53	~~96.18~~	96.63	96.84
a.p.f.u.										
Si	5.73	5.63	5.70	5.67	5.60	~~5.45~~	5.61	~~5.61~~	5.64	5.77
AlIV	2.27	2.37	2.30	2.33	2.40	~~2.55~~	2.39	~~2.39~~	2.36	2.23
AlVI	0.41	0.25	0.34	0.22	0.26	~~0.11~~	0.32	~~0.43~~	0.31	0.54
Ti	0.35	0.36	0.35	0.42	0.39	~~0.31~~	0.38	~~0.34~~	0.44	0.41
Fe^{2+}	2.47	2.62	2.52	2.70	2.52	~~3.04~~	2.49	~~2.47~~	2.47	2.22
Mn	0.00	0.00	0.00	0.00	0.00	~~0.00~~	0.00	~~0.00~~	0.00	0.00
Mg	2.34	2.46	2.42	2.28	2.48	~~2.34~~	2.44	~~2.35~~	2.37	2.31
Ca	0.00	0.00	0.00	0.00	0.00	~~0.00~~	0.00	~~0.00~~	0.00	0.00
Na	0.00	0.00	0.00	0.00	0.00	~~0.00~~	0.00	~~0.00~~	0.00	0.00
K	2.02	2.03	2.00	2.05	2.04	~~2.21~~	2.05	~~2.10~~	1.99	1.93
Cl	0.00	0.00	0.00	0.00	0.00	~~0.00~~	0.00	~~0.00~~	0.00	0.00
F	0.00	0.00	0.00	0.00	0.00	~~0.00~~	0.00	~~0.00~~	0.00	0.00
TOTAL	15.59	15.71	15.63	15.66	15.69	~~16.02~~	15.68	~~15.69~~	15.58	15.40

Note: Wt% = percentage weight; a.p.f.u. = atom per formula unit

Table 62 Chemical analysis of amphibole

Wt%	Amp1	Amp2	Amp3	Amp4	Amp5	Amp6
SiO2	47.55	47.33	48.07	46.60	47.28	47.78
TiO2	1.04	1.15	1.17	1.09	0.95	1.05
Al2O3	9.77	9.15	8.99	10.07	9.27	9.54
FeO	17.75	18.18	18.12	18.78	18.57	18.20
MnO						
MgO	11.54	11.24	11.31	10.46	11.39	11.24
CaO	11.86	12.07	12.39	11.90	12.11	12.06
NaO	1.28	1.17	1.19	1.31	1.15	1.07
K_2O	1.16	1.18	1.09	1.16	1.02	1.18
Cr_2O_3						
TOTAL	98.09	98.56	97.73	98.65	98.27	97.92
a.p.f.u.						
Si	0.78	0.78	0.78	0.77	0.77	0.78
Ti	0.01	0.01	0.01	0.01	0.01	0.01
Al	0.19	0.18	0.17	0.19	0.18	0.18
Fe	0.24	0.25	0.25	0.26	0.25	0.25
Mn	0.00	0.00	0.00	0.00	0.00	0.00
Mg	0.28	0.27	0.27	0.26	0.28	0.27
Ca	0.21	0.21	0.22	0.21	0.21	0.21
Na	0.04	0.04	0.04	0.04	0.04	0.03
K	0.02	0.02	0.02	0.02	0.02	0.02
Cr	0.00	0.00	0.00	0.00	0.00	0.00

Note: Wt% = percentage weight; a.p.f.u. = atom per formula unit

Sample 374-U1522A-72R-3W, 71-74 cm

Table 63 Chemical analysis of amphibole

Wt%	Amp1	Amp2	Amp3	Amp4	Amp5	Amp6	Amp7	Amp8	Amp9	Amp10	Amp11
SiO2	56.63	56.43	56.49	57.37	57.39	56.88	54.62	56.78	57.06	56.80	57.13
TiO2											
Al2O3	2.34	2.88	2.73	2.25	2.58	2.51	4.75	2.55	2.28	2.43	2.40
FeO	11.35	11.30	11.70	11.70	11.50	11.81	12.29	11.02	11.14	11.66	11.70
MnO											
MgO	18.07	17.48	17.59	17.71	17.77	17.66	16.91	18.01	17.95	17.81	18.09
CaO	12.76	12.64	12.71	12.85	12.93	12.63	12.63	12.95	13.15	12.93	12.84
NaO	0.42	0.48	0.44				0.85				
K_2O											
Cr_2O_3											
TOTAL	98.46	98.81	98.36	98.14	97.87	98.53	97.99	98.71	98.44	98.39	97.89
a.p.f.u.											
Si	0.93	0.93	0.92	0.94	0.93	0.93	0.89	0.93	0.93	0.93	0.93
Ti	0.00	0.00	0.00	0.00	0.00	0.00	0.00	0.00	0.00	0.00	0.00
Al	0.05	0.06	0.05	0.04	0.05	0.05	0.09	0.05	0.04	0.05	0.05
Fe	0.16	0.16	0.16	0.16	0.16	0.16	0.17	0.15	0.15	0.16	0.16
Mn	0.00	0.00	0.00	0.00	0.00	0.00	0.00	0.00	0.00	0.00	0.00
Mg	0.44	0.43	0.43	0.43	0.43	0.43	0.41	0.44	0.44	0.43	0.44
Ca	0.22	0.22	0.22	0.22	0.23	0.22	0.22	0.23	0.23	0.23	0.22
Na	0.01	0.02	0.01	0.00	0.00	0.00	0.03	0.00	0.00	0.00	0.00
K	0.00	0.00	0.00	0.00	0.00	0.00	0.00	0.00	0.00	0.00	0.00
Cr	0.00	0.00	0.00	0.00	0.00	0.00	0.00	0.00	0.00	0.00	0.00

Note: Wt% = percentage weight; a.p.f.u. = atom per formula unit

Sample 374-U1522A-75R-2W, 9-12 cm

Table 64 Chemical analysis of biotite

Wt%	Bt1	Bt2	Bt3	Bt4	Bt5	Bt6	Bt7	Bt8	Bt9	Bt10	Bt11	Bt12
SiO_2	41.88	41.73	40.98	41.17	42.30	40.71	41.01	41.37	40.78	40.88	40.17	40.56
TiO_2	2.33	2.70	3.42	3.24	3.30	3.03	2.95	3.48	3.11	3.35	3.39	3.61
Al_2O_3	18.20	18.32	17.93	18.40	17.38	18.26	18.60	17.07	18.39	17.97	18.26	17.71
FeO	16.81	16.25	16.73	16.47	16.38	16.72	16.33	17.24	16.94	16.65	17.49	17.47
MnO												
MgO	12.85	13.36	12.69	12.69	13.19	13.39	13.19	12.66	13.07	13.28	12.81	12.73
CaO												
NaO												
K_2O	11.55	11.13	11.52	11.80	10.84	11.68	11.89	11.70	11.59	11.61	11.61	11.53
ClO												
F												
TOTAL	96.51	96.63	96.84	96.37	96.71	96.33	96.17	96.59	96.26	96.39	96.41	96.51
a.p.f.u.												
Si	5.76	5.72	5.67	5.66	5.80	5.61	5.63	5.73	5.61	5.63	5.56	5.62
AlIV	2.24	2.28	2.33	2.34	2.20	2.39	2.37	2.27	2.39	2.37	2.44	2.38

AlVI	0.71	0.68	0.59	0.64	0.60	0.57	0.64	0.51	0.60	0.55	0.54	0.51
Ti	0.24	0.28	0.36	0.34	0.34	0.31	0.30	0.36	0.32	0.35	0.35	0.38
Fe^{2+}	1.93	1.86	1.93	1.89	1.88	1.93	1.88	2.00	1.95	1.92	2.03	2.02
Mn	0.00	0.00	0.00	0.00	0.00	0.00	0.00	0.00	0.00	0.00	0.00	0.00
Mg	2.63	2.73	2.62	2.60	2.69	2.75	2.70	2.61	2.68	2.73	2.64	2.63
Ca	0.00	0.00	0.00	0.00	0.00	0.00	0.00	0.00	0.00	0.00	0.00	0.00
Na	0.00	0.00	0.00	0.00	0.00	0.00	0.00	0.00	0.00	0.00	0.00	0.00
K	2.02	1.95	2.03	2.07	1.90	2.05	2.08	2.07	2.04	2.04	2.05	2.04
Cl	0.00	0.00	0.00	0.00	0.00	0.00	0.00	0.00	0.00	0.00	0.00	0.00
F	0.00	0.00	0.00	0.00	0.00	0.00	0.00	0.00	0.00	0.00	0.00	0.00
TOTAL	15.54	15.49	15.53	15.55	15.41	15.62	15.60	15.55	15.59	15.58	15.62	15.58

Note: Wt% = percentage weight; a.p.f.u. = atom per formula unit

Table 65 Chemical analysis of white mica

Wt%	**Wm1**	**Wm2**	**Wm3**	**Wm4**	**Wm5**	**Wm6**	**Wm7**	**Wm8**	**Wm9**	**Wm10**
SiO_2	~~50.40~~	52.13	52.27	~~51.48~~	53.25	~~51.95~~	~~51.57~~	~~51.83~~	~~51.70~~	~~50.62~~
TiO_2							~~0.46~~			
Al_2O_3	~~36.82~~	36.11	37.02	~~35.83~~	36.46	~~36.09~~	~~35.96~~	~~36.27~~	~~34.75~~	~~39.31~~
FeO	~~1.66~~	1.57	1.16	~~1.77~~	1.48	~~1.28~~	~~1.92~~	~~1.83~~	~~1.86~~	~~0.98~~
MnO										
MgO	~~1.23~~	1.53	1.40	~~1.57~~	1.56	~~1.39~~	~~1.99~~	~~2.04~~	~~1.39~~	~~0.31~~
CaO										
NaO			0.34	~~0.39~~	0.36	~~0.40~~	~~0.42~~			
K_2O	~~13.95~~	12.79	12.55	~~13.12~~	12.34	~~13.53~~	~~13.24~~	~~13.16~~	~~14.38~~	~~13.64~~
ClO										
F										
TOTAL	~~96.11~~	96.03	95.48	~~95.99~~	94.83	~~95.56~~	~~94.73~~	~~95.12~~	~~96.08~~	~~95.37~~
a.p.f.u.										
Si	~~6.21~~	6.18	6.13	~~6.17~~	6.10	~~6.09~~	~~6.13~~	~~6.11~~	~~6.09~~	~~6.13~~
AlIV	~~1.79~~	1.82	1.87	~~1.83~~	1.90	~~1.91~~	~~1.87~~	~~1.89~~	~~1.91~~	~~1.87~~
AlVI	~~3.66~~	3.76	3.78	~~3.67~~	3.70	~~3.66~~	~~3.68~~	~~3.70~~	~~3.73~~	~~3.69~~
Ti	~~0.00~~	0.00	0.00	~~0.07~~	0.07	~~0.08~~	~~0.07~~	~~0.08~~	~~0.07~~	~~0.08~~
Fe^{2+}	~~0.14~~	0.11	0.10	~~0.10~~	0.10	~~0.12~~	~~0.10~~	~~0.10~~	~~0.09~~	~~0.09~~
Mn	~~0.00~~	0.00	0.00	~~0.00~~	0.00	~~0.00~~	~~0.00~~	~~0.00~~	~~0.00~~	~~0.00~~
Mg	~~0.25~~	0.11	0.11	~~0.14~~	0.12	~~0.15~~	~~0.14~~	~~0.13~~	~~0.10~~	~~0.14~~
Ca	~~0.00~~	0.00	0.00	~~0.00~~	0.00	~~0.00~~	~~0.00~~	~~0.00~~	~~0.00~~	~~0.00~~
Na	~~0.14~~	0.34	0.34	~~0.32~~	0.33	~~0.30~~	~~0.34~~	~~0.32~~	~~0.34~~	~~0.32~~
K	~~1.89~~	1.75	1.77	~~1.74~~	1.73	~~1.78~~	~~1.73~~	~~1.73~~	~~1.74~~	~~1.72~~
Cl	~~0.00~~	0.00	0.00	~~0.00~~	0.00	~~0.00~~	~~0.00~~	~~0.00~~	~~0.00~~	~~0.00~~
F	~~0.00~~	0.00	0.00	~~0.00~~	0.00	~~0.00~~	~~0.00~~	~~0.00~~	~~0.00~~	~~0.00~~
TOTAL	~~14.08~~	14.08	14.10	~~14.05~~	14.06	~~14.09~~	~~14.06~~	~~14.05~~	~~14.07~~	~~14.03~~

Note: Wt% = percentage weight; a.p.f.u. = atom per formula unit

Sample 374-U1522A-75R-6W, 42-45 cm

Table 66 Chemical analysis of biotite

Wt%	**Bt1**	**Bt2**	**Bt3**	**Bt4**	**Bt5**	**Bt6**	**Bt7**	**Bt8**	**Bt9**	**Bt10**	**Bt11**	**Bt12**
SiO_2	39.82	~~42.50~~	40.33	39.63	39.96	40.77	40.24	40.33	40.67	40.70	40.21	41.09
TiO_2	2.27	~~2.59~~	2.59	2.70	2.66	2.97	2.51	2.70	2.37	2.20	2.53	2.69
Al_2O_3	19.59	~~17.30~~	20.18	19.84	19.51	20.33	20.00	20.96	19.81	20.19	20.80	21.02
FeO	17.18	~~17.95~~	15.65	16.15	16.05	15.35	15.82	15.05	15.55	15.32	15.16	14.72
MnO												
MgO	13.91	~~11.37~~	13.88	13.68	13.48	12.28	13.35	12.88	13.76	13.88	13.20	12.89
CaO												
NaO												
K_2O	10.50	~~12.21~~	11.04	10.56	11.28	11.16	11.26	11.28	11.13	10.99	11.14	11.04
ClO												
F												
TOTAL	96.84	~~96.23~~	96.46	96.81	96.59	96.72	96.33	96.48	96.32	96.24	96.52	96.21
a.p.f.u.												
Si	5.49	~~5.87~~	5.51	5.46	5.51	5.58	5.52	5.51	5.56	5.55	5.50	5.57
Al^{IV}	2.51	~~2.13~~	2.49	2.54	2.49	2.42	2.48	2.49	2.44	2.45	2.50	2.43
Al^{VI}	0.68	~~0.69~~	0.76	0.68	0.68	0.86	0.75	0.88	0.75	0.79	0.85	0.92
Ti	0.24	~~0.27~~	0.27	0.28	0.28	0.31	0.26	0.28	0.24	0.23	0.26	0.27
Fe^{2+}	1.98	~~2.07~~	1.79	1.86	1.85	1.76	1.81	1.72	1.78	1.75	1.73	1.67
Mn	0.00	~~0.00~~	0.00	0.09	0.07	0.06	0.07	0.05	0.06	0.07	0.07	0.06
Mg	2.86	~~2.34~~	2.83	2.81	2.77	2.51	2.73	2.62	2.80	2.82	2.69	2.60
Ca	0.00	~~0.00~~	0.00	0.00	0.00	0.00	0.00	0.00	0.00	0.00	0.00	0.00
Na	0.00	~~0.00~~	0.00	0.00	0.00	0.00	0.00	0.00	0.00	0.00	0.00	0.00
K	1.85	~~2.15~~	1.92	1.86	1.98	1.95	1.97	1.96	1.94	1.91	1.94	1.91
Cl	0.00	~~0.00~~	0.00	0.00	0.00	0.00	0.00	0.00	0.00	0.00	0.00	0.00
F	0.00	~~0.00~~	0.00	0.00	0.00	0.00	0.00	0.00	0.00	0.00	0.00	0.00
TOTAL	15.60	~~15.53~~	15.56	15.58	15.62	15.45	15.59	15.51	15.57	15.56	15.54	15.43

Note: Wt% = percentage weight; a.p.f.u. = atom per formula unit

APPENDIX VII

Petrology of DSDP Site 270 clasts

This section shows petrographic descriptions of gravel-sized clasts sampled from DSDP Site 270 core (Table 5). Petrographic analysis was carried out with a Nikon Optiphot-Pol polarizer microscopy equipped with a Nikon Coolpix 990 camera on polished thin sections. Each description is coupled with photomicrographs underlying representative features and microstructures. At the end of the figures and descriptions Table 67 summarizes clasts classification and Table 68 shows lithological percentages of lithic grains composing the > 2mm sieved fraction from bulk diamictite samples.

28-270-1R-2W, 91-106 cm

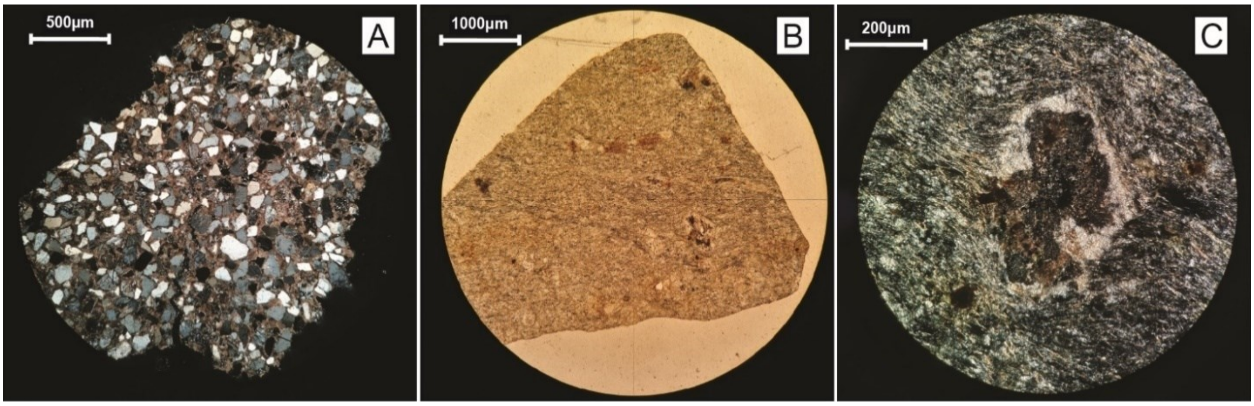

Figure 137 A) XPL photomicrograph (4X); B) PPL photomicrograph (2X); C) XPL photomicrograph (10X)

The sample include two pebbles which are treated separately:

i. **Sandstone** (Figure 137A) – The pebble is an isotropic, medium/fine-grained clastic sedimentary rock. Grains are angular to sub-rounded; abundant calcite cement occurs. Grains are composed by monocrystalline quartz, feldspar (alkali feldspar and plagioclase), that is it partially replaced by sericite and phyllosilicate aggregates, and lithic fragments (schists/phyllites). The sample is sandstone.

ii. **Meta-porphyry** (Figure 137B, C) – Fine-grained, foliated, metamorphic rock. The rock shows a well-defined foliation marked by green tabular minerals; quartz and feldspar commonly occur. Sometimes euhedral to subhedral shaped porphyroclasts of feldspar, strongly altered from the core toward rims, occurs.

28-270-13R-3W, 99-113 cm – Biotite Schist

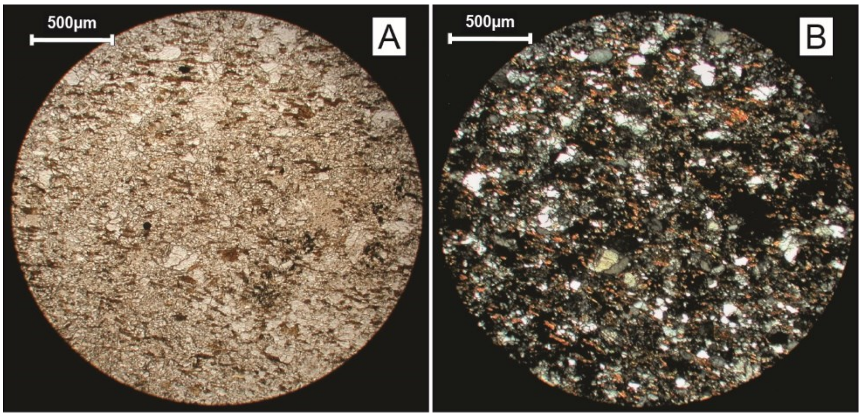

Figure 138 A) PPL photomicrograph (4X); B) XPL photomicrograph (4X)

Fine-grained metamorphic rock with grano-lepidoblastic texture. The sample is mainly composed by quartz, feldspar, and biotite; the latter define the weak schistosity.

28-270-14R-1W, 39-41 cm – White mica – Calcite Meta-sandstone

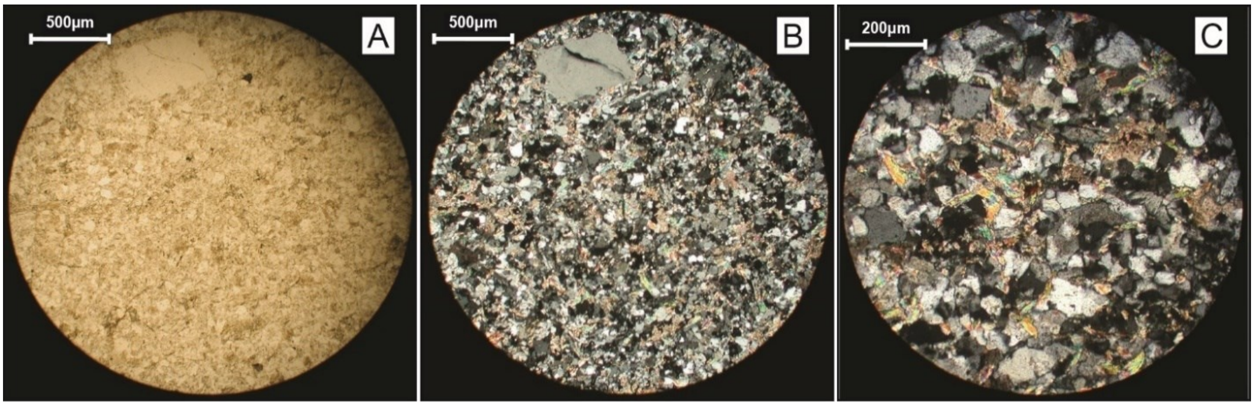

Figure 139 A) PPL photomicrograph (4X); B) XPL photomicrograph (4X); C) XPL photomicrograph (10X)

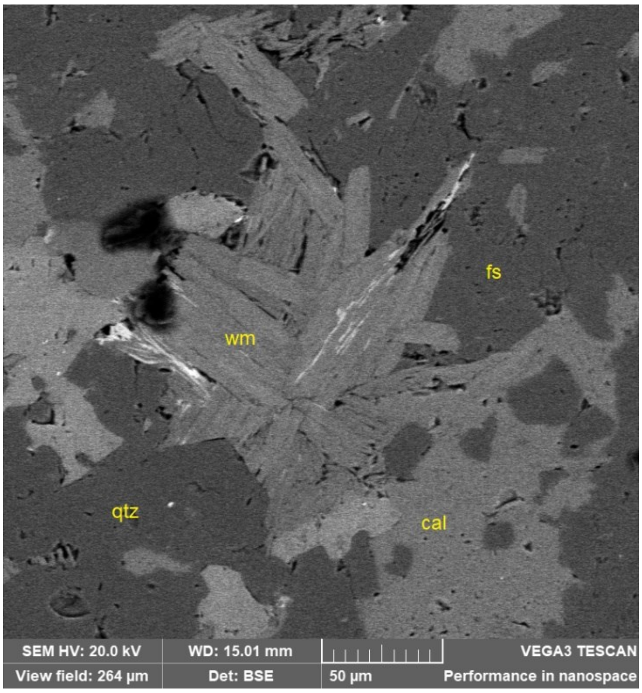

Figure 140 SEM – Back Scattered Electrons (BSE) images of the sample, with focus on the decussate texture of white mica crystals. Cal – calcite; fs – feldspar; qtz – quartz; wm – white mica

The sample is a fine-grained metamorphic rock. The texture is quite isotropic and no well-defined schistosity can be observed. Composition is quartz, feldspars, calcite, and white mica. White mica seems to show decussate structure. Calcite is common and it occurs in spots. Few oversized grains occur.

28-270-19R-2W, 50-54 cm - Basalt

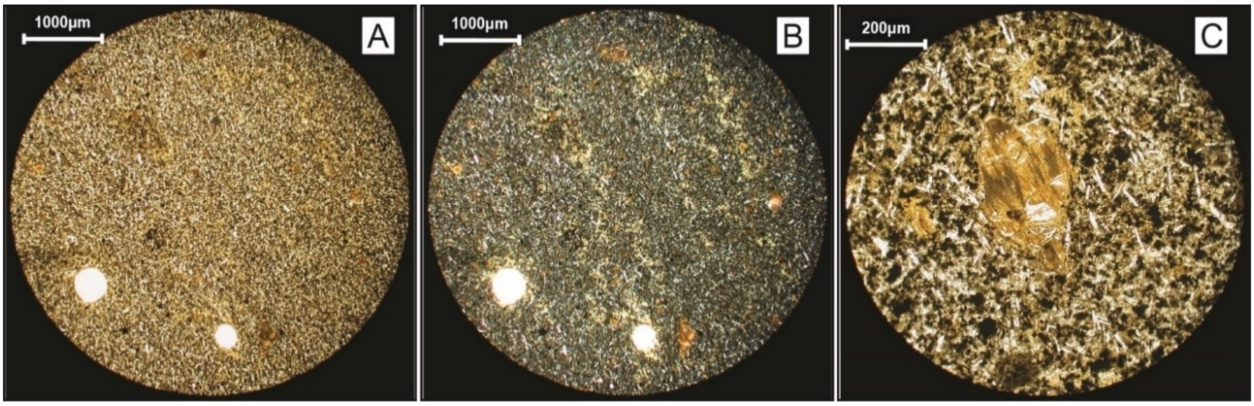

Figure 141 A) PPL photomicrograph (2X); B) XPL photomicrograph (2X); C) PPL photomicrograph (10X)

The sample is an isotropic, fine grained, slightly porphyritic volcanic rock. Groundmass is fine grained, and it is mainly constituted by feldspar crystals, opaque minerals, and probably interstitial glass; the matrix is isotropic. Scattered porphyritic crystals occur within the matrix. These crystals are euhedral to subhedral, with hexagonal-like shape; the original mineral was completely replaced by alteration phases (bowlingite).

On the basis of the shape and the replacing phase, possible original minerals were olivine. Scattered circular vesiculas occur.

28-270-27R-1W, 102-107 cm – Meta-sandstone

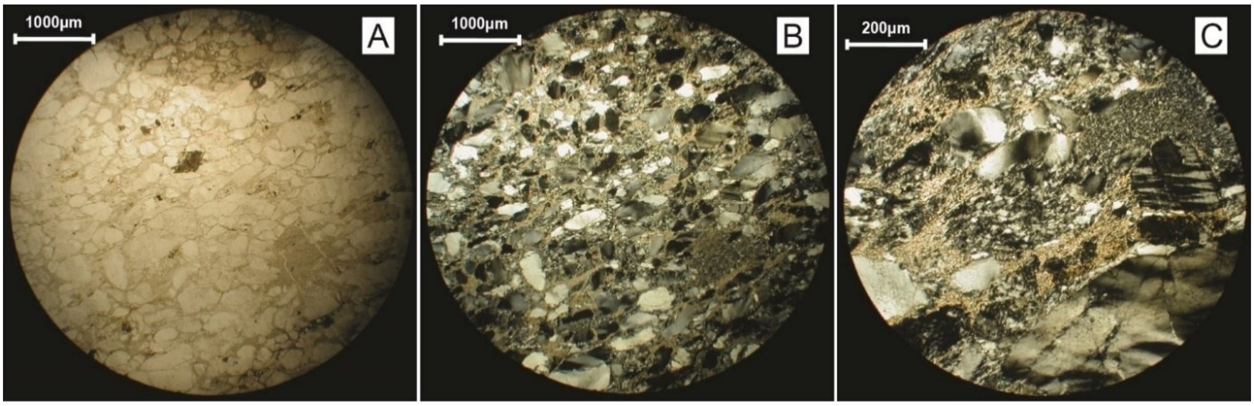

Figure 142 A) PPL photomicrograph (2X); B) XPL photomicrograph (2X); C) XPL photomicrograph (10X)

The clast is a foliated metamorphic rock; the grain size is strongly inhomogeneous. The matrix is constituted by fine-grained phyllosilicate crystals. Abundant deformed grains of quartz, that have strong wavy extinction and it is usually recrystallized with very fine-grained portions, microcline, and plagioclase.

28-270-27R-4W, 41-44 cm – Sandy mudstone

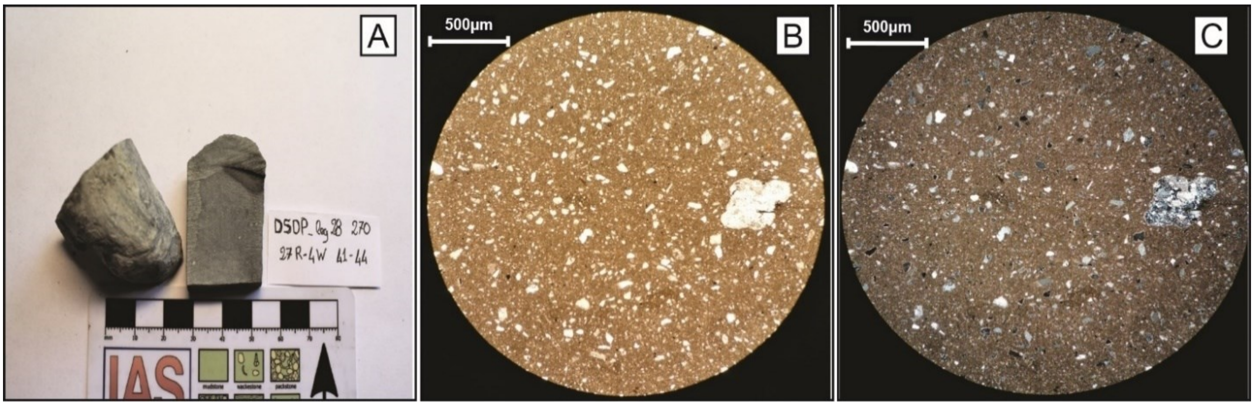

Figure 143 A) Macroscopic picture of the clast; B) PPL photomicrograph (4X); C) XPL photomicrograph (4X)

Hetero-granular sedimentary rock made up of abundant mud size matrix (>50%) with dispersed hetero-granular sand-size grains. The rock texture is isotropic. Most of the grains are angular to sub-angular and only few of them are sub-rounded. Grains are constituted by monocrystalline quartz, feldspar (both plagioclase and alkali feldspar), and minor lithic fragments. Feldspars are sometimes partially replaced by sericite and phyllosilicate aggregates. Lithic fragments are manly meta-sedimentary rocks (meta-sandstone and meta-siltstone), and minor magmatic (felsic intrusive and one grain of basaltic rock).

Zircon, white mica, and hornblende are common accessory minerals. One carbonate fossil occurs within the matrix.

28-270-27R-4W, 103-105 cm – Quartzite

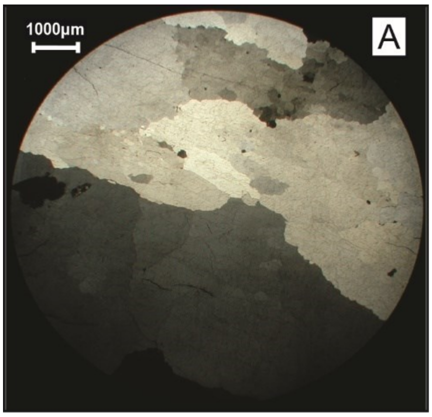

Figure 144 A) XPL photomicrograph (1X)

Very coarse-grained, hetero-granular metamorphic rock. The sample is exclusively composed by quartz crystals, that show undulose extinction.

28-270-38R-3W, 130-133 cm - Sandstone

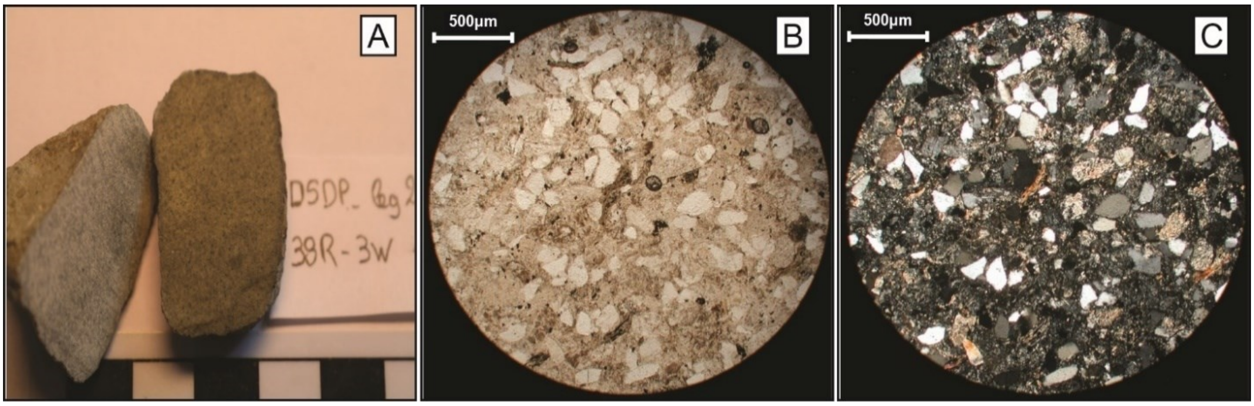

Figure 145 A) Macroscopic picture of the clast; B) PPL photomicrograph (4X); C) XPL photomicrograph (4X)

Isotropic, fine-grained sedimentary rock; grains are angular to sub-rounded and abundant quartzo-feldspatic matrix and pseudo-matrix occurs. Grains are mainly constituted by monocrystalline quartz, feldspar (alkali feldspar and plagioclase), and lithic fragments (mainly fine-grained metamorphic rocks). Accessory grains are biotite, usually decoloured, and white mica.

28-270-38R-3W, 141-143 cm – Biotite Schist

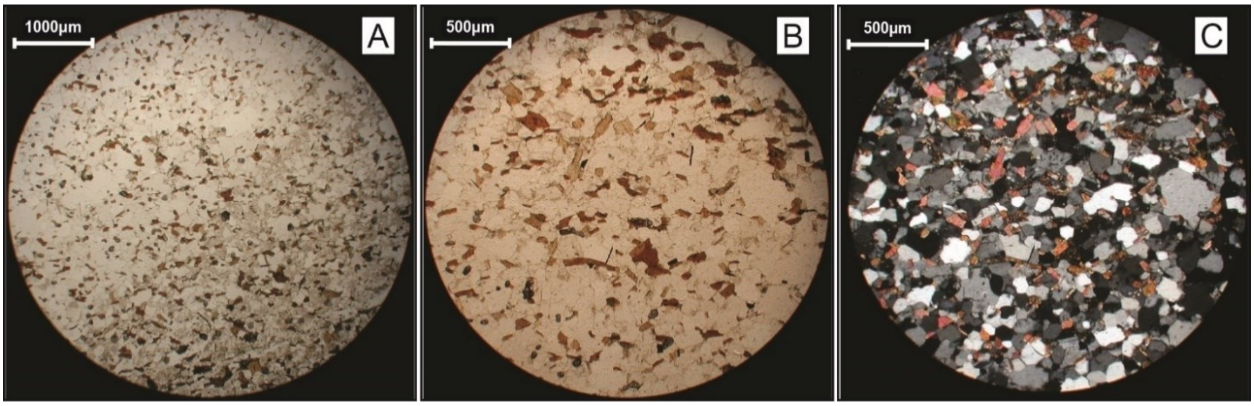

Figure 146 A) PPL photomicrograph (2X); B) PPL photomicrograph (4X); C) XPL photomicrograph (4X)

Fine-grained, foliated and compositionally layered metamorphic rocks. Layering is defined by the abundance of feldspar at the expense of quartz. Quartz is the main component, followed by feldspar (plagioclase and minorly alkali feldspar), that is usually altered, and biotite. Apatite is a common accessory mineral while zircons are rarer; white mica rarely occurs.

28-270-39R-1W, 122-123 cm – Sandstone

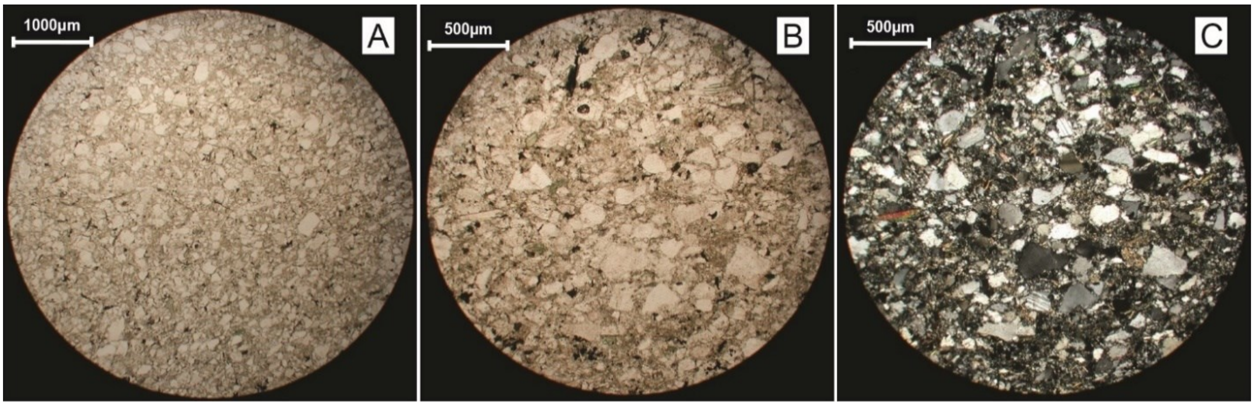

Figure 147 A) PPL photomicrograph (2X); B) PPL photomicrograph (4X); C) XPL photomicrograph (4X)

Fine-grained, slightly hetero-granular, isotropic or weakly structured sedimentary rock. Fine-grained quartzo-feldspatic matrix is common. Clasts are angular to sub-angular; they are mainly constituted by monocrystalline quartz and feldspar (K-feldspar), lithic fragments (fine-grained metamorphic rocks) are minor. White mica, and minor chlorite, are common accessory minerals.

28-270-47R-2W – Granite

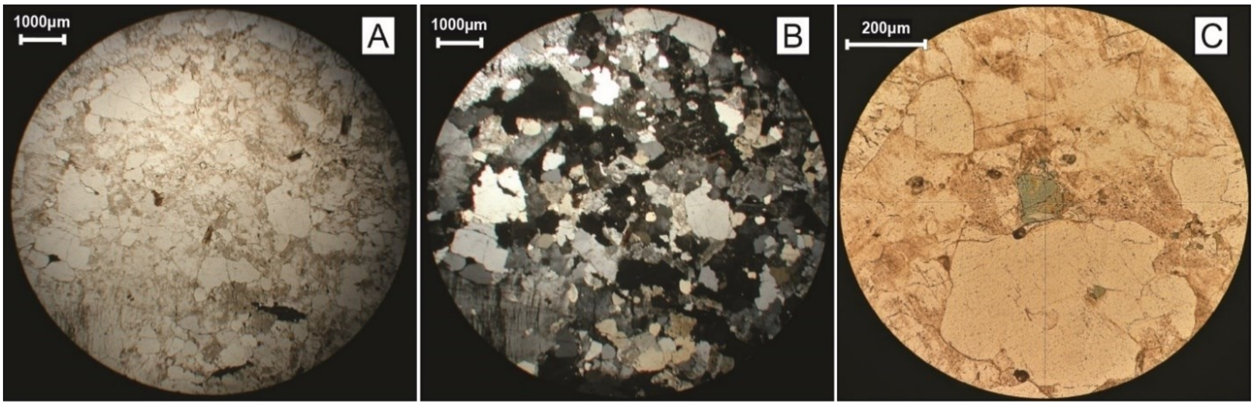

Figure 148 A) PPL photomicrograph (1X); B) XPL photomicrograph (1X); C) PPL photomicrograph (10X)

Fine grained, slightly hetero-granular (porphyritic), isotropic granitoid rock. The main components are quartz and feldspar (microcline, orthoclase, and plagioclase), that are partially altered and replaced by sericite and clay minerals aggregates. Biotite is the most common mafic minerals, but it represents less than 5%; it is partially replaced by chlorite. Blue tourmaline, sometimes with brown core, is an abundant accessory mineral; white mica, probably primary, sometimes occurs.

28-270-47R-3W, 110-116 cm; 48R-1W, 100-105 cm; 49R-1W – Calc-silicate Gneiss

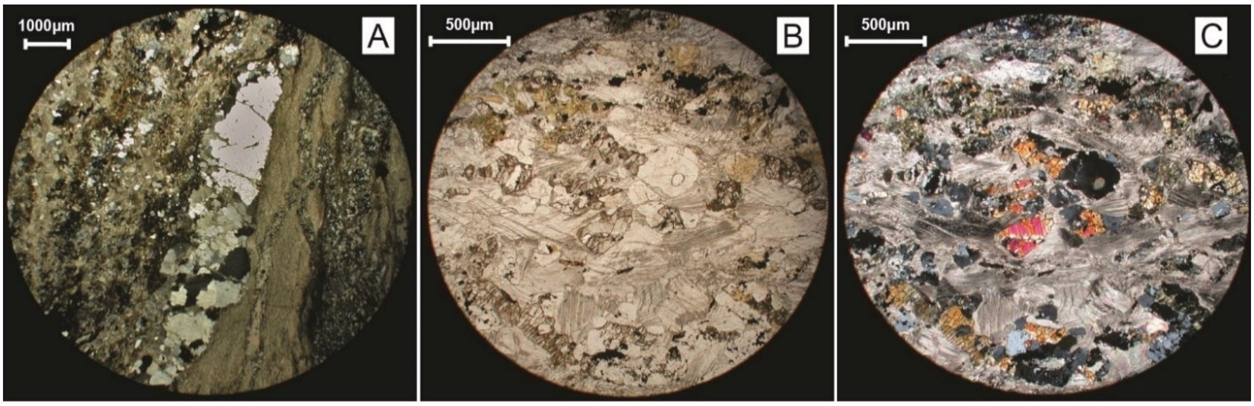

Figure 149 A) PPL photomicrograph (1X) from sample 28-270-48R-1W, 100-105 cm; B) PPL photomicrograph (4X) from sample 28-270-49R-1W; C) XPL photomicrograph (4X) from sample 28-270-49R-1W

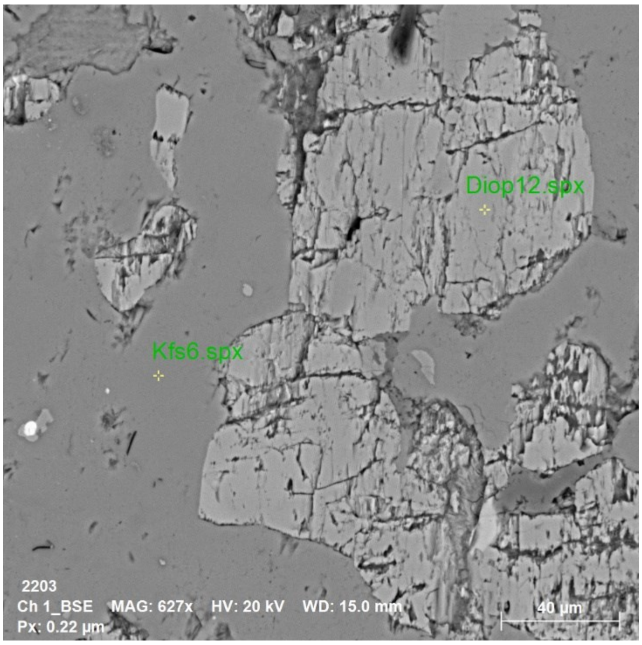

Figure 150 SEM – Back Scattered Electrons (BSE) image of the sample 28-270-49R-1W with a focus on the contact between diopside and alkali feldspar. EDS point analysis are shown (see Appendix VIII for chemical analysis)

Basement was sampled in three different portions along the core, but any significant compositional or textural difference can be observed; the three samples were described together.

The rock is characterized by compositional layering. Some layers are made up of hetero-granular marble, ranging from very fine to coarse. Other layers are dominated by quartz, alkali feldspar, diopside, and clinozoisite. Diopside are usually partially replaced by zeolite. Titanite is a common accessory mineral; apatite usually occurs.

Table 67 Summary of analyzed clasts, with sampling depth and lithology. LSU – Lithostratigraphic Unit are from Kraus (2016)

Sample ID	Leg	Site	Core	Type	Section	Sect. Half	Depth (m bsf)	LSU	Lithology
28-270-2R-2W,91-106 cm	28	270	2	R	2	W	2.50	I	sandstone + meta-porphyry
28-270-13R-3W, 99-113 cm	28	270	13	R	3	W	105.05	II	biotite schist
28-270-14R-1W, 39-41 cm	28	270	14	R	1	W	110.40	II	white mica meta-sandstone
28-270-19R-2W, 50-54 cm	28	270	19	R	2	W	160.00	III	basalt
28-270-24R-2W,	28	270	24	R	2	W		IV	
28-270-27R-1W, 102-107 cm	28	270	27	R	1	W	235.00	IV	meta-sandstone
28-270-27R-4W, 41-44 cm	28	270	27	R	4	W	238.90	IV	sandy mudstone/diamictite
28-270-27R-4W, 103-105 cm	28	270	27	R	4	W	239.50	IV	quartzite
28-270-27R-2W,	28	270	27	R	2	W		IV	
28-270-38R-3W, 130-133 cm	28	270	38	R	3	W	342.75	V	sandstone
28-270-38R-3W, 141-143 cm	28	270	38	R	3	W	342.85	V	biotite schist
28-270-39R-1W, 122-123 cm	28	270	39	R	1	W	349.20	VI	sandstone
28-270-47R-2W	28	270	47	R	2	W	411.50	-	biotite granite
28-270-47R-3W, 110-116 cm	28	270	47	R	3	W	413.60	-	cal silicate gneiss (basement)
28-270-48R-1W, 100-105 cm	28	270	48	R	1	W	415.50	-	cal silicate gneiss (basement)
28-270-49R-1W	28	270	49	R	1	W	422.70	-	cal silicate gneiss (basement)

Table 68 Occurrence in percentage of lithics the gravel from bulk diamictite matrix. Qtz - quartz; Fs - feldspars (plagioclase and alkali feldspar); Intr - intrusive rocks; Dol - dolerite; Meta - metamorphic rocks; Clastic sed - clastic sedimentary rocks; Carb sed - carbonate sedimentary rocks; Bas - basaltic rocks; F Porph - felsic porphyries; ND - Not Defined; Tot - total number of clasts counted in thin section.

Sample ID	Qtz	Fs	Intr.	Dol.	Meta	Clastic sed.	Carb. sed.	Bas.	Fel. Porph.	ND	Tot (n)
28-270-24R-2W,	5%	45%	0%	0%	5%	0%	0%	0%	40%	5%	20
28-270-27R-2W,	5%	0%	16%	0%	47%	11%	0%	5%	16%	0%	19

APPENDIX VIII

Mineral chemistry analyses of DSDP Site 270 clasts

The list of the analyzed samples is shown in Table 5. Analyses were carried out with an energy-dispersive X-ray system (Bruker Quantax 200 EDX) coupled with an Electron Scanning Microscope (Tescan Vega3) at the Department of Physical, Earth and Environmental Sciences - University of Siena. Analytical conditions were 20 kV of accelerating voltage, 15 μA of emission current, and a beam spot size of 0.2 μm. Natural mineral standards were used for calibration. Cations were recalculated on the basis of 22 oxygens (biotite and white mica), and on the basis of 6 oxygens (pyroxene). Crossed out data represent not valid analyses, and they were excluded from the interpretations.

Sample 28-270-13R-3W, 99-113 cm

Table 69 Chemical analysis of biotite

Wt%	Bt1	Bt2	Bt3	Bt4	Bt5	Bt6	Bt7	Bt8	Bt9	Bt10	Bt11	Bt12
SiO_2	39.73	40.28	~~39.75~~	39.73	~~42.16~~	39.92	40.20	39.60	40.07	39.14	39.77	39.80
TiO_2	2.45	2.26	~~2.00~~	2.17	~~2.25~~	2.41	2.19	2.40	2.44	2.27	2.39	2.06
Al_2O_3	19.59	19.69	~~20.02~~	19.67	~~17.85~~	19.53	19.88	19.60	19.39	19.02	18.83	19.46
FeO	20.35	19.61	~~20.69~~	20.12	~~20.75~~	19.63	19.50	20.32	20.47	20.59	20.93	20.65
MnO		0.42	~~0.41~~		~~0.48~~	0.43		0.42		0.40	0.38	
MgO	10.81	11.10	~~11.67~~	11.19	~~9.72~~	10.95	11.04	10.97	10.71	10.71	10.33	10.93
CaO												
Na_2O												
K_2O	11.10	10.83	~~9.07~~	10.44	~~10.75~~	10.95	10.88	10.78	10.69	11.28	11.11	10.96
Cl												
F												
TOTAL	96.13	95.98	~~96.52~~	96.79	~~96.19~~	96.33	96.43	96.08	96.37	96.71	96.40	96.29
a.p.f.u.												
Si	5.53	5.57	~~5.51~~	5.54	~~5.86~~	5.56	5.58	5.51	5.58	5.52	5.58	5.55
Al^{IV}	2.47	2.43	~~2.49~~	2.46	~~2.14~~	2.44	2.42	2.49	2.42	2.48	2.42	2.45
Al^{VI}	0.75	0.79	~~0.78~~	0.78	~~0.78~~	0.76	0.83	0.73	0.76	0.68	0.70	0.75
Ti	0.26	0.23	~~0.21~~	0.23	~~0.24~~	0.25	0.23	0.25	0.26	0.24	0.25	0.22
Fe^{2+}	2.37	2.27	~~2.40~~	2.35	~~2.41~~	2.28	2.26	2.36	2.38	2.43	2.46	2.41
Mn	0.00	0.05	~~0.05~~	0.00	~~0.06~~	0.05	0.00	0.05	0.00	0.05	0.05	0.00
Mg	2.24	2.29	~~2.41~~	2.33	~~2.01~~	2.27	2.28	2.28	2.22	2.25	2.16	2.27
Ca	0.00	0.00	~~0.00~~	0.00	~~0.00~~	0.00	0.00	0.00	0.00	0.00	0.00	0.00
Na	0.00	0.00	~~0.00~~	0.00	~~0.00~~	0.00	0.00	0.00	0.00	0.00	0.00	0.00
K	1.97	1.91	~~1.60~~	1.86	~~1.90~~	1.94	1.93	1.91	1.90	2.03	1.99	1.95
Cl	0.00	0.00	~~0.00~~	0.00	~~0.00~~	0.00	0.00	0.00	0.00	0.00	0.00	0.00
F	0.00	0.00	~~0.00~~	0.00	~~0.00~~	0.00	0.00	0.00	0.00	0.00	0.00	0.00
TOTAL	15.59	15.54	~~15.45~~	15.54	~~15.40~~	15.56	15.53	15.59	15.52	15.67	15.60	15.60

Note: Wt% = percentage weight; a.p.f.u. = atom per formula unit

Sample 28-270-14R-1W, 39-41 cm

Table 70 Chemical analysis of white mica

Wt%	**Wm1**	**Wm2**	**Wm3**	**Wm4**	**Wm5**	**Wm6**	**Wm7**	**Wm8**	**Wm9**	**Wm10**	**Wm11**	**Wm12**	**Wm13**
SiO_2	~~52.11~~	52.66	53.22	~~52.08~~	51.08	~~52.16~~	50.84	51.69	52.82	~~51.03~~	~~52.88~~	~~51.31~~	51.94
TiO_2													
Al_2O_3	~~34.69~~	34.05	34.07	~~34.48~~	36.53	~~35.89~~	34.01	36.30	34.63	~~37.00~~	~~32.43~~	~~33.08~~	35.71
FeO	~~5.22~~	5.05	4.74	~~4.47~~	4.62	~~3.82~~	7.29	3.37	4.52	~~2.89~~	~~6.41~~	~~7.19~~	3.90
MnO													
MgO													
CaO													
Na_2O													
K_2O	~~13.37~~	13.23	13.08	~~13.56~~	12.99	~~13.41~~	13.28	13.33	13.11	~~13.66~~	~~13.40~~	~~13.48~~	13.31
Cl													
F													
TOTAL	~~94.89~~	95.25	95.13	~~95.61~~	95.03	~~94.99~~	94.86	95.52	95.16	~~95.63~~	~~95.14~~	~~95.19~~	95.37
a.p.f.u.													
Si	~~6.42~~	6.50	6.54	~~6.45~~	6.28	~~6.39~~	6.34	6.36	6.49	~~6.29~~	~~6.57~~	~~6.42~~	6.39
Al^{IV}	~~1.58~~	1.50	1.46	~~1.55~~	1.72	~~1.61~~	1.66	1.64	1.51	~~1.71~~	~~1.43~~	~~1.58~~	1.61
Al^{VI}	~~3.47~~	3.46	3.48	~~3.49~~	3.58	~~3.58~~	3.34	3.62	3.51	~~3.66~~	~~3.32~~	~~3.31~~	3.57
Ti	~~0.00~~	0.00	0.00	~~0.00~~	0.00	~~0.00~~	0.00	0.00	0.00	~~0.00~~	~~0.00~~	~~0.00~~	0.00
Fe^{2+}	~~0.54~~	0.52	0.49	~~0.46~~	0.48	~~0.39~~	0.76	0.35	0.46	~~0.30~~	~~0.67~~	~~0.75~~	0.40
Mn	~~0.00~~	0.00	0.00	~~0.00~~	0.00	~~0.00~~	0.00	0.00	0.00	~~0.00~~	~~0.00~~	~~0.00~~	0.00
Mg	~~0.00~~	0.00	0.00	~~0.00~~	0.00	~~0.00~~	0.00	0.00	0.00	~~0.00~~	~~0.00~~	~~0.00~~	0.00
Ca	~~0.00~~	0.00	0.00	~~0.00~~	0.00	~~0.00~~	0.00	0.00	0.00	~~0.00~~	~~0.00~~	~~0.00~~	0.00
Na	~~0.00~~	0.00	0.00	~~0.00~~	0.00	~~0.00~~	0.00	0.00	0.00	~~0.00~~	~~0.00~~	~~0.00~~	0.00
K	~~2.10~~	2.08	2.05	~~2.14~~	2.04	~~2.10~~	2.11	2.09	2.06	~~2.15~~	~~2.12~~	~~2.15~~	2.09
Cl	~~0.00~~	0.00	0.00	~~0.00~~	0.00	~~0.00~~	0.00	0.00	0.00	~~0.00~~	~~0.00~~	~~0.00~~	0.00
F	~~0.00~~	0.00	0.00	~~0.00~~	0.00	~~0.00~~	0.00	0.00	0.00	~~0.00~~	~~0.00~~	~~0.00~~	0.00
TOTAL	~~14.11~~	14.06	14.02	~~14.10~~	14.09	~~14.06~~	14.21	14.06	14.03	~~14.10~~	~~14.11~~	~~14.21~~	14.06

Note: Wt% = percentage weight; a.p.f.u. = atom per formula unit

Sample 28-270-27R-2W

Table 71 Chemical analyses of biotite

Wt%	**Bt15-1**	**Bt15-2**	**Bt15-3**	**Bt15-4**	**Bt15-5**	**Bt15-6**	**Bt15-7**	**Bt15-8**	**Bt15-9**	**Bt15-10**	**Bt15-11**	**Bt15-12**	**Bt15-13**
SiO_2	40.37	40.38	40.94	42.50	39.55	~~38.84~~	39.02	40.73	39.71	39.47	41.15	41.53	40.09
TiO_2	2.94	2.61	3.29	3.00	3.40	~~3.42~~	3.22	2.59	2.77	2.98	2.14	2.87	2.93
Al_2O_3	16.90	17.78	17.20	18.20	16.14	~~16.41~~	16.05	16.60	16.95	16.66	17.49	18.49	16.95
FeO	22.14	21.80	22.47	19.25	22.91	~~23.09~~	23.82	21.98	21.94	23.01	20.90	19.90	22.43
MnO	0.85	0.85	0.82	0.66	0.88	~~0.84~~	0.88	0.85	0.77	0.93	0.70	0.70	0.86
MgO	9.52	9.82	9.33	10.07	9.70	~~9.20~~	9.27	10.37	10.54	9.34	11.13	10.58	9.41
CaO													
Na_2O													

K_2O	11.05	10.30	9.91	9.69	11.12	~~11.42~~	11.23	10.71	10.71	11.26	10.12	9.79	10.74
Cl													
F													
TOTAL	96.36	96.58	96.19	96.74	96.44	~~96.89~~	96.62	96.31	96.73	96.48	96.51	96.28	96.69
a.p.f.u.													
Si	5.71	5.68	5.74	5.86	5.64	~~5.59~~	5.61	5.74	5.63	5.64	5.75	5.74	5.69
Al^{IV}	2.29	2.32	2.26	2.14	2.36	~~2.41~~	2.39	2.26	2.37	2.36	2.25	2.26	2.31
Al^{VI}	0.53	0.63	0.58	0.82	0.36	~~0.37~~	0.34	0.50	0.47	0.44	0.62	0.74	0.53
Ti	0.31	0.28	0.35	0.31	0.36	~~0.37~~	0.35	0.27	0.30	0.32	0.22	0.30	0.31
Fe^{2+}	2.62	2.57	2.63	2.22	2.73	~~2.78~~	2.87	2.59	2.60	2.75	2.44	2.30	2.66
Mn	0.10	0.10	0.10	0.08	0.11	~~0.10~~	0.11	0.10	0.09	0.11	0.08	0.08	0.10
Mg	2.01	2.06	1.95	2.07	2.06	~~1.97~~	1.99	2.18	2.23	1.99	2.32	2.18	1.99
Ca	0.00	0.00	0.00	0.00	0.00	~~0.00~~	0.00	0.00	0.00	0.00	0.00	0.00	0.00
Na	0.00	0.00	0.00	0.00	0.00	~~0.00~~	0.00	0.00	0.00	0.00	0.00	0.00	0.00
K	1.99	1.85	1.77	1.70	2.02	~~2.10~~	2.06	1.93	1.94	2.05	1.80	1.73	1.95
Cl	0.00	0.00	0.00	0.00	0.00	~~0.00~~	0.00	0.00	0.00	0.00	0.00	0.00	0.00
F	0.00	0.00	0.00	0.00	0.00	~~0.00~~	0.00	0.00	0.00	0.00	0.00	0.00	0.00
TOTAL	15.56	15.49	15.38	15.20	15.65	~~15.70~~	15.71	15.57	15.62	15.67	15.49	15.32	15.55

Note: Wt% = percentage weight; a.p.f.u. = atom per formula unit

Sample 28-270-38R-3W, 141-143 cm

Table 72 Chemical analysis of biotite

Wt%	Bt1	Bt2	Bt3	Bt4	Bt5	Bt6	Bt7	Bt8	Bt9	Bt10	Bt11	Bt12
SiO_2	38.58	38.52	38.26	38.77	37.78	38.29	38.16	38.43	38.75	38.26	38.69	39.07
TiO_2	2.87	2.58	2.88	2.54	2.83	3.51	3.32	3.28	3.29	3.16	3.01	3.27
Al_2O_3	20.63	20.61	20.48	20.82	20.33	20.28	20.00	20.05	19.77	19.98	20.02	20.21
FeO	19.67	19.76	20.38	20.00	21.37	20.70	20.26	20.58	20.41	20.35	20.29	19.64
MnO			0.37	0.00	0.46		0.44	0.41		0.39		
MgO	10.32	10.26	10.16	10.47	10.84	9.61	9.99	10.09	10.16	10.42	10.53	10.34
CaO												
Na_2O												
K_2O	11.48	11.48	11.26	11.36	10.09	11.53	11.24	11.27	11.23	11.22	11.40	11.24
Cl												
F												
TOTAL	96.57	96.89	96.34	96.19	96.44	96.23	96.71	96.06	96.52	96.36	96.22	96.38
a.p.f.u.												
Si	5.40	5.41	5.37	5.41	5.31	5.38	5.38	5.38	5.44	5.37	5.41	5.45
Al^{IV}	2.60	2.59	2.63	2.59	2.69	2.62	2.62	2.62	2.56	2.63	2.59	2.55
Al^{VI}	0.81	0.83	0.76	0.83	0.67	0.73	0.70	0.70	0.71	0.68	0.72	0.77
Ti	0.30	0.27	0.30	0.27	0.30	0.37	0.35	0.35	0.35	0.33	0.32	0.34
Fe^{2+}	2.30	2.32	2.39	2.33	2.51	2.43	2.39	2.41	2.39	2.39	2.37	2.29
Mn	0.00	0.00	0.04	0.00	0.05	0.00	0.05	0.05	0.00	0.05	0.00	0.00
Mg	2.15	2.15	2.13	2.18	2.27	2.01	2.10	2.11	2.12	2.18	2.20	2.15
Ca	0.00	0.00	0.00	0.00	0.00	0.00	0.00	0.00	0.00	0.00	0.00	0.00
Na	0.00	0.00	0.00	0.00	0.00	0.00	0.00	0.00	0.00	0.00	0.00	0.00
K	2.05	2.06	2.02	2.02	1.81	2.06	2.02	2.02	2.01	2.01	2.03	2.00
Cl	0.00	0.00	0.00	0.00	0.00	0.00	0.00	0.00	0.00	0.00	0.00	0.00

F	0.00	0.00	0.00	0.00	0.00	0.00	0.00	0.00	0.00	0.00	0.00	0.00
TOTAL	15.62	15.64	15.64	15.63	15.62	15.61	15.62	15.62	15.59	15.64	15.64	15.55
Note: Wt% = percentage weight; a.p.f.u. = atom per formula unit												

Sample 28-270-47R-2W

Table 73 Chemical analysis of biotite

Wt%	Bt1	Bt2	Bt3	Bt4	Bt5	Bt6	Bt7	Bt8	Bt9
SiO_2	39.90	38.13	38.23	38.75	38.24	~~35.76~~	38.74	38.47	38.02
TiO_2		2.23	2.18	1.86	1.95	~~2.46~~	1.60	2.29	2.20
Al_2O_3	18.91	19.26	18.49	18.78	18.82	~~17.45~~	19.77	18.19	18.97
FeO	24.07	24.70	25.04	24.80	24.85	~~31.23~~	22.13	24.95	24.15
MnO	0.77	0.51	0.63	0.61	0.69	~~0.53~~	1.03	0.59	0.63
MgO	8.92	7.93	8.04	8.47	8.40	~~8.09~~	9.25	8.24	8.54
CaO									
Na_2O									
K_2O	10.87	10.75	11.08	10.31	10.35	~~7.98~~	10.87	11.35	11.18
Cl									
F									
TOTAL	96.41	96.37	96.16	96.29	96.56	~~96.42~~	96.71	96.08	96.44
a.p.f.u.									
Si	5.69	5.47	5.50	5.54	5.49	~~5.25~~	5.50	5.52	5.45
Al^{IV}	2.31	2.53	2.50	2.46	2.51	~~2.75~~	2.50	2.48	2.55
Al^{VI}	0.87	0.72	0.63	0.70	0.68	~~0.27~~	0.81	0.59	0.65
Ti	0.00	0.24	0.24	0.20	0.21	~~0.27~~	0.17	0.25	0.24
Fe^{2+}	2.87	2.96	3.01	2.96	2.98	~~3.84~~	2.63	2.99	2.89
Mn	0.09	0.06	0.08	0.07	0.08	~~0.07~~	0.12	0.07	0.08
Mg	1.90	1.70	1.72	1.80	1.80	~~1.77~~	1.96	1.76	1.82
Ca	0.00	0.00	0.00	0.00	0.00	~~0.00~~	0.00	0.00	0.00
Na	0.00	0.00	0.00	0.00	0.00	~~0.00~~	0.00	0.00	0.00
K	1.98	1.97	2.03	1.88	1.90	~~1.50~~	1.97	2.08	2.04
Cl	0.00	0.00	0.00	0.00	0.00	~~0.00~~	0.00	0.00	0.00
F	0.00	0.00	0.00	0.00	0.00	~~0.00~~	0.00	0.00	0.00
TOTAL	15.71	15.65	15.72	15.62	15.65	~~15.71~~	15.66	15.74	15.73
Note: Wt% = percentage weight; a.p.f.u. = atom per formula unit									

Sample 28-270-49R-1W, 100-105 cm

Table 74 Chemical analysis of pyroxene

Wt%	Cpx1	Cpx2	Cpx3	Cpx4	Cpx5	Cpx6	Cpx7	Cpx8	Cpx9	Cpx10	Cpx11	Cpx12	Cpx13	Cpx14	Cpx15
SiO_2	53.66	53.15	53.43	53.95	53.80	53.98	53.27	53.91	53.83	54.27	53.94	54.18	53.83	54.31	54.06
TiO_2															
Al_2O_3															
Cr_2O_3															
FeO	9.30	12.55	9.71	9.08	8.39	8.96	11.27	9.11	8.41	7.54	8.81	7.27	9.62	7.80	8.23
MnO															
MgO	13.21	10.65	12.58	12.92	13.37	13.21	11.38	12.70	13.28	13.74	13.29	14.38	12.77	13.55	13.57

CaO	23.83	23.65	24.28	24.05	24.43	23.85	24.08	24.28	24.47	24.45	23.95	24.16	23.78	24.35	24.14
Na_2O															
K_2O															
TOTAL	100	100	100	100	100	100	100	100	100	100	100	100	100	100	100
a.p.f.u.															
Si	2.01	2.02	2.01	2.02	2.01	2.02	2.01	2.02	2.01	2.02	2.01	2.01	2.02	2.02	2.01
Al^{IV}	-0.01	-0.02	-0.01	-0.02	-0.01	-0.02	-0.01	-0.02	-0.01	-0.02	-0.01	-0.01	-0.02	-0.02	-0.01
Al^{VI}	0.01	0.02	0.01	0.02	0.01	0.02	0.01	0.02	0.01	0.02	0.01	0.01	0.02	0.02	0.01
Fe^{3+}	0.00	0.00	0.00	0.00	0.00	0.00	0.00	0.00	0.00	0.00	0.00	0.00	0.00	0.00	0.00
Cr	0.00	0.00	0.00	0.00	0.00	0.00	0.00	0.00	0.00	0.00	0.00	0.00	0.00	0.00	0.00
Ti	0.00	0.00	0.00	0.00	0.00	0.00	0.00	0.00	0.00	0.00	0.00	0.00	0.00	0.00	0.00
Fe^{2+}	0.29	0.40	0.31	0.29	0.26	0.28	0.36	0.29	0.26	0.24	0.28	0.23	0.30	0.24	0.26
Mn	0.00	0.00	0.00	0.00	0.00	0.00	0.00	0.00	0.00	0.00	0.00	0.00	0.00	0.00	0.00
Mg	0.74	0.60	0.70	0.72	0.74	0.74	0.64	0.71	0.74	0.76	0.74	0.80	0.71	0.75	0.75
Ca	0.96	0.96	0.98	0.96	0.98	0.95	0.98	0.97	0.98	0.97	0.96	0.96	0.95	0.97	0.96
Na	0.00	0.00	0.00	0.00	0.00	0.00	0.00	0.00	0.00	0.00	0.00	0.00	0.00	0.00	0.00
K	0.00	0.00	0.00	0.00	0.00	0.00	0.00	0.00	0.00	0.00	0.00	0.00	0.00	0.00	0.00
TOTAL	3.99	3.98	3.99	3.98	3.99	3.99	3.99	3.98	3.99	3.99	3.99	3.99	3.99	3.98	3.99
Wo	48.16	48.97	49.18	48.94	49.25	48.44	49.41	49.46	49.40	49.41	48.53	48.45	48.44	49.37	48.80
En	37.15	30.67	35.45	36.58	37.52	37.31	32.48	36.00	37.31	38.64	37.48	40.14	36.20	38.23	38.17
Fs	14.70	20.36	15.37	14.48	13.24	14.25	18.11	14.54	13.29	11.95	13.99	11.41	15.36	12.40	13.03

Note: Wt% = percentage weight; a.p.f.u. = atom per formula unit; Wo = Wollastonite; En = Enstatite; Fs = Ferrosilite

APPENDIX IX

Mineral chemistry analyses of PRR samples

The list of the analyzed samples is shown in Table 6; samples were stored at the Polar Rock Repository (PRR) at Byrd Polar and Climate Research Centre of the Ohio State University. Analyses were carried out with an energy-dispersive X-ray system (Bruker Quantax 200 EDX) coupled with an Electron Scanning Microscope (Tescan Vega3) at the Department of Physical, Earth and Environmental Sciences - University of Siena. Analytical conditions were 20 kV of accelerating voltage, 15 µA of emission current, and a beam spot size of 0.2 µm. Natural mineral standards were used for calibration. Cations were recalculated on the basis of 22 oxygens (biotite), on the basis of 6 oxygens (pyroxene), on the basis of 23 oxygens (amphibole), and on the basis of 12 oxygens (garnet). Crossed out data represent not valid analyses and they were excluded from the interpretations.

PRR-18760 - Byrd Coast Granite

Table 75 Chemical analysis of biotite

Wt%	Bt1c	Bt1r	Bt2c	Bt2r	Bt3c	Bt3r	Bt4c	~~Bt4r~~	Bt5c	Bt5r	Bt6c	Bt6r	Bt7c	Bt7r	Bt8c
SiO_2	38.72	~~41.97~~	39.00	38.77	39.31	40.42	39.32	~~43.69~~	38.88	38.87	39.02	39.10	39.75	39.23	39.24
TiO_2	2.54	~~2.14~~	2.71	2.59	2.83	2.56	2.75	~~2.50~~	2.45	2.61	2.70	2.59	2.38	2.11	2.64
Al_2O_3	20.27	~~19.81~~	20.35	21.36	20.86	20.27	21.41	~~19.35~~	20.83	20.76	20.80	20.57	20.91	21.31	20.69
FeO	27.15	~~26.34~~	28.65	26.33	25.04	25.67	25.70	~~24.83~~	26.71	26.74	26.49	26.59	26.21	26.33	26.64
MnO	0.50	~~0.57~~	0.69	0.53	0.47	0.62	0.59	~~0.47~~	0.57	0.59	0.50	0.56	0.55	0.54	0.61
MgO	2.90	~~2.25~~	2.72	2.99	3.27	3.08	3.06	~~2.71~~	3.00	3.19	3.01	3.17	3.16	2.97	3.11
CaO	0.00	~~0.00~~	0.00	0.00	0.00	0.00	0.00	~~0.00~~	0.00	0.00	0.00	0.00	0.00	0.00	0.00
NaO	0.00	~~0.00~~	0.00	0.00	0.00	0.00	0.00	~~0.00~~	0.00	0.00	0.00	0.00	0.00	0.00	0.00
K_2O	11.18	~~10.51~~	11.27	11.15	11.33	11.02	11.03	~~10.25~~	10.89	11.08	10.99	10.68	10.46	10.81	10.74
ClO	0.00	~~0.00~~	0.36	0.00	0.00	0.00	0.00	~~0.00~~	0.00	0.00	0.00	0.00	0.00	0.00	0.00
F	0.00	~~0.00~~	0.00	0.00	0.00	0.00	0.00	~~0.00~~	0.00	0.00	0.00	0.00	0.00	0.00	0.00
TOTAL	96.84	~~96.53~~	94.56	96.42	96.99	96.49	96.28	~~96.34~~	96.77	96.29	96.61	96.84	96.69	96.81	96.47
a.p.f.u.															
Si	5.62	~~5.97~~	5.57	5.57	5.65	5.77	5.61	~~6.12~~	5.61	5.59	5.61	5.63	5.69	5.64	5.63
Al^{IV}	2.38	~~2.03~~	2.43	2.43	2.35	2.23	2.39	~~1.88~~	2.39	2.41	2.39	2.37	2.31	2.36	2.37
Al^{VI}	1.08	~~1.29~~	0.99	1.18	1.18	1.18	1.21	~~1.31~~	1.15	1.10	1.14	1.13	1.21	1.25	1.13
Ti	0.28	~~0.23~~	0.29	0.28	0.31	0.27	0.29	~~0.26~~	0.27	0.28	0.29	0.28	0.26	0.23	0.28
Fe(ii)	3.29	~~3.13~~	3.42	3.16	3.01	3.06	3.07	~~2.91~~	3.22	3.21	3.19	3.20	3.14	3.16	3.20
Mn	0.06	~~0.07~~	0.08	0.06	0.06	0.07	0.07	~~0.06~~	0.07	0.07	0.06	0.07	0.07	0.07	0.07
Mg	0.63	~~0.48~~	0.58	0.64	0.70	0.65	0.65	~~0.57~~	0.64	0.68	0.65	0.68	0.67	0.64	0.67
Ca	0.00	~~0.00~~	0.00	0.00	0.00	0.00	0.00	~~0.00~~	0.00	0.00	0.00	0.00	0.00	0.00	0.00
Na	0.00	~~0.00~~	0.00	0.00	0.00	0.00	0.00	~~0.00~~	0.00	0.00	0.00	0.00	0.00	0.00	0.00

K	2.07	~~1.91~~	2.05	2.04	2.07	2.01	2.01	~~1.83~~	2.00	2.03	2.02	1.96	1.91	1.98	1.97
Cl	0.00	~~0.00~~	0.09	0.00	0.00	0.00	0.00	~~0.00~~	0.00	0.00	0.00	0.00	0.00	0.00	0.00
F	0.00	~~0.00~~	0.00	0.00	0.00	0.00	0.00	~~0.00~~	0.00	0.00	0.00	0.00	0.00	0.00	0.00
TOTAL	15.41	~~15.10~~	15.41	15.37	15.32	15.25	15.30	~~14.94~~	15.36	15.39	15.34	15.32	15.25	15.32	15.32

Note: Wt% = percentage weight; a.p.f.u. = atom per formula unit

PRR-18768 - Byrd Coast Granite

Table 76 Chemical analysis of biotite

Wt%	Bt1c	Bt1r	Bt2c	Bt2r	Bt3c	Bt3r	Bt4	Bt5c	Bt5r	Bt6c	Bt6r	Bt7
SiO_2	~~43.08~~	~~45.33~~	~~42.73~~	~~42.47~~	~~41.32~~	~~42.25~~	~~41.96~~	~~40.16~~	~~40.22~~	~~41.37~~	~~42.44~~	~~41.89~~
TiO_2	~~1.93~~	~~0.64~~	~~1.27~~	~~1.33~~	~~1.65~~	~~1.54~~	~~1.36~~	~~1.75~~	~~1.46~~	~~0.85~~	~~0.87~~	~~0.87~~
Al_2O_3	~~22.15~~	~~21.92~~	~~21.24~~	~~20.83~~	~~21.54~~	~~21.34~~	~~21.29~~	~~21.19~~	~~21.29~~	~~21.64~~	~~21.26~~	~~21.95~~
FeO	~~24.94~~	~~24.63~~	~~27.08~~	~~27.19~~	~~27.04~~	~~27.10~~	~~27.34~~	~~28.32~~	~~28.60~~	~~27.81~~	~~27.33~~	~~27.09~~
MnO	~~0.34~~	~~0.46~~	~~0.48~~	~~0.51~~	~~0.53~~	~~0.49~~	~~0.48~~	~~0.60~~	~~0.54~~	~~0.34~~	~~0.47~~	~~0.45~~
MgO	~~0.28~~	~~0.19~~	~~0.28~~	~~0.21~~	~~0.21~~	~~0.27~~	~~0.29~~	~~0.22~~	~~0.27~~	~~0.28~~	~~0.23~~	~~0.19~~
CaO												
NaO												
K_2O	~~10.88~~	~~10.29~~	~~10.82~~	~~10.80~~	~~10.94~~	~~10.77~~	~~11.00~~	~~11.11~~	~~11.19~~	~~10.89~~	~~11.15~~	~~11.14~~
ClO												
F												
TOTAL	~~96.52~~	~~96.64~~	~~96.24~~	~~96.77~~	~~96.89~~	~~96.37~~	~~96.4~~	~~96.76~~	~~96.55~~	~~96.92~~	~~96.38~~	~~96.53~~
a.p.f.u.												
Si	~~6.05~~	~~6.30~~	~~6.05~~	~~6.06~~	~~5.92~~	~~6.00~~	~~5.98~~	~~5.81~~	~~5.81~~	~~5.94~~	~~6.04~~	~~5.97~~
Al^{IV}	~~1.95~~	~~1.70~~	~~1.95~~	~~1.94~~	~~2.08~~	~~2.00~~	~~2.02~~	~~2.19~~	~~2.19~~	~~2.06~~	~~1.96~~	~~2.03~~
Al^{VI}	~~1.71~~	~~1.90~~	~~1.60~~	~~1.57~~	~~1.56~~	~~1.57~~	~~1.56~~	~~1.43~~	~~1.44~~	~~1.60~~	~~1.61~~	~~1.66~~
Ti	~~0.20~~	~~0.07~~	~~0.14~~	~~0.14~~	~~0.18~~	~~0.16~~	~~0.15~~	~~0.19~~	~~0.16~~	~~0.09~~	~~0.09~~	~~0.09~~
Fe(ii)	~~2.93~~	~~2.86~~	~~3.21~~	~~3.25~~	~~3.24~~	~~3.22~~	~~3.26~~	~~3.43~~	~~3.46~~	~~3.34~~	~~3.25~~	~~3.23~~
Mn	~~0.04~~	~~0.05~~	~~0.06~~	~~0.06~~	~~0.06~~	~~0.06~~	~~0.06~~	~~0.07~~	~~0.07~~	~~0.04~~	~~0.06~~	~~0.05~~
Mg	~~0.06~~	~~0.04~~	~~0.06~~	~~0.04~~	~~0.04~~	~~0.06~~	~~0.06~~	~~0.05~~	~~0.06~~	~~0.06~~	~~0.05~~	~~0.04~~
Ca	~~0.00~~	~~0.00~~	~~0.00~~	~~0.00~~	~~0.00~~	~~0.00~~	~~0.00~~	~~0.00~~	~~0.00~~	~~0.00~~	~~0.00~~	~~0.00~~
Na	~~0.00~~	~~0.00~~	~~0.00~~	~~0.00~~	~~0.00~~	~~0.00~~	~~0.00~~	~~0.00~~	~~0.00~~	~~0.00~~	~~0.00~~	~~0.00~~
K	~~1.95~~	~~1.83~~	~~1.95~~	~~1.97~~	~~2.00~~	~~1.95~~	~~2.00~~	~~2.05~~	~~2.06~~	~~2.00~~	~~2.03~~	~~2.03~~
Cl	~~0.00~~	~~0.00~~	~~0.00~~	~~0.00~~	~~0.00~~	~~0.00~~	~~0.00~~	~~0.00~~	~~0.00~~	~~0.00~~	~~0.00~~	~~0.00~~
F	~~0.00~~	~~0.00~~	~~0.00~~	~~0.00~~	~~0.00~~	~~0.00~~	~~0.00~~	~~0.00~~	~~0.00~~	~~0.00~~	~~0.00~~	~~0.00~~
TOTAL	~~14.89~~	~~14.75~~	~~15.02~~	~~15.03~~	~~15.08~~	~~15.02~~	~~15.08~~	~~15.22~~	~~15.24~~	~~15.13~~	~~15.09~~	~~15.10~~

Note: Wt% = percentage weight; a.p.f.u. = atom per formula unit

PRR-18783 - Byrd Coast Granite

Table 77 Chemical analysis of biotite

Wt%	Bt1c	Bt1r	Bt2	Bt3	Bt4c	Bt4r	Bt5c	Bt5r	Bt6	Bt7	Bt8	Bt9
SiO_2	~~39.97~~	~~40.77~~	~~40.31~~	~~40.84~~	~~40.40~~	~~40.35~~	~~41.36~~	~~42.28~~	~~40.92~~	~~42.21~~	~~42.00~~	~~42.12~~
TiO_2	~~2.60~~	~~1.47~~	~~1.83~~	~~0.98~~	~~1.08~~	~~1.09~~	~~0.78~~	~~0.92~~	~~1.00~~	~~0.66~~	~~0.91~~	~~0.57~~
Al_2O_3	~~18.55~~	~~19.79~~	~~19.87~~	~~20.23~~	~~20.25~~	~~20.36~~	~~20.28~~	~~20.39~~	~~20.45~~	~~20.80~~	~~19.93~~	~~20.87~~
FeO	~~30.87~~	~~29.39~~	~~29.68~~	~~29.79~~	~~29.49~~	~~30.18~~	~~29.48~~	~~27.77~~	~~28.67~~	~~27.89~~	~~28.44~~	~~28.20~~
MnO	~~0.53~~	~~0.56~~	~~0.47~~	~~0.66~~	~~0.46~~	~~0.53~~	~~0.45~~	~~0.50~~	~~0.52~~	~~0.49~~	~~0.41~~	~~0.29~~
MgO	~~0.27~~	~~0.05~~	~~0.04~~	~~0.09~~	~~0.16~~	~~0.06~~	~~0.21~~	~~0.15~~	~~0.23~~	~~0.19~~	~~0.10~~	~~0.17~~

CaO												
NaO												
K_2O	~~10.69~~	~~11.09~~	~~11.09~~	~~11.00~~	~~10.91~~	~~10.59~~	~~10.90~~	~~11.05~~	~~11.19~~	~~11.05~~	~~11.05~~	~~11.20~~
ClO	~~0.44~~	~~0.36~~	~~0.44~~	~~0.44~~	~~0.36~~	~~0.39~~	~~0.33~~	~~0.55~~	~~0.48~~	~~0.35~~	~~0.45~~	~~0.44~~
F												
TOTAL	~~96.24~~	~~96.63~~	~~96.41~~	~~96.14~~	~~96.98~~	~~96.57~~	~~96.35~~	~~96.52~~	~~96.66~~	~~96.48~~	~~96.81~~	~~96.29~~
a.p.f.u.												
Si	~~5.84~~	~~5.93~~	~~5.87~~	~~5.91~~	~~5.90~~	~~5.87~~	~~5.97~~	~~6.07~~	~~5.93~~	~~6.05~~	~~6.07~~	~~6.03~~
Al^{IV}	~~2.16~~	~~2.07~~	~~2.13~~	~~2.09~~	~~2.10~~	~~2.13~~	~~2.03~~	~~1.93~~	~~2.07~~	~~1.95~~	~~1.93~~	~~1.97~~
Al^{VI}	~~1.04~~	~~1.32~~	~~1.27~~	~~1.37~~	~~1.38~~	~~1.36~~	~~1.43~~	~~1.51~~	~~1.42~~	~~1.56~~	~~1.46~~	~~1.56~~
Ti	~~0.29~~	~~0.16~~	~~0.20~~	~~0.11~~	~~0.12~~	~~0.12~~	~~0.09~~	~~0.10~~	~~0.11~~	~~0.07~~	~~0.10~~	~~0.06~~
Fe(ii)	~~3.77~~	~~3.58~~	~~3.61~~	~~3.61~~	~~3.60~~	~~3.67~~	~~3.56~~	~~3.33~~	~~3.47~~	~~3.34~~	~~3.43~~	~~3.38~~
Mn	~~0.07~~	~~0.07~~	~~0.06~~	~~0.08~~	~~0.06~~	~~0.07~~	~~0.05~~	~~0.06~~	~~0.06~~	~~0.06~~	~~0.05~~	~~0.03~~
Mg	~~0.06~~	~~0.01~~	~~0.01~~	~~0.02~~	~~0.03~~	~~0.01~~	~~0.05~~	~~0.03~~	~~0.05~~	~~0.04~~	~~0.02~~	~~0.04~~
Ca	~~0.00~~	~~0.00~~	~~0.00~~	~~0.00~~	~~0.00~~	~~0.00~~	~~0.00~~	~~0.00~~	~~0.00~~	~~0.00~~	~~0.00~~	~~0.00~~
Na	~~0.00~~	~~0.00~~	~~0.00~~	~~0.00~~	~~0.00~~	~~0.00~~	~~0.00~~	~~0.00~~	~~0.00~~	~~0.00~~	~~0.00~~	~~0.00~~
K	~~1.99~~	~~2.06~~	~~2.06~~	~~2.03~~	~~2.03~~	~~1.96~~	~~2.01~~	~~2.02~~	~~2.07~~	~~2.02~~	~~2.04~~	~~2.05~~
Cl	~~0.11~~	~~0.09~~	~~0.11~~	~~0.11~~	~~0.09~~	~~0.10~~	~~0.08~~	~~0.13~~	~~0.12~~	~~0.08~~	~~0.11~~	~~0.11~~
F	~~0.00~~	~~0.00~~	~~0.00~~	~~0.00~~	~~0.00~~	~~0.00~~	~~0.00~~	~~0.00~~	~~0.00~~	~~0.00~~	~~0.00~~	~~0.00~~
TOTAL	~~15.22~~	~~15.20~~	~~15.21~~	~~15.22~~	~~15.22~~	~~15.20~~	~~15.18~~	~~15.06~~	~~15.19~~	~~15.09~~	~~15.10~~	~~15.11~~

Note: Wt% = percentage weight; a.p.f.u. = atom per formula unit

PRR-18792 – unnamed metamorphic rocks

Table 78 Chemical analysis of biotite

Wt%	Bt1	Bt2	Bt3	Bt4	Bt5	Bt6	Bt7	Bt8	Bt9	Bt10	Bt11
SiO_2	39.01	38.80	38.63	39.17	39.16	38.87	39.41	38.97	38.93	39.22	38.59
TiO_2	3.45	3.07	3.46	3.23	2.99	3.24	3.57	3.29	3.70	3.78	3.74
Al2O3	18.49	18.23	18.42	18.41	18.58	17.81	18.84	18.45	18.43	18.25	18.45
FeO	19.35	19.73	19.87	19.45	19.47	19.42	18.47	19.41	19.33	19.32	19.72
MnO	0.33	0.37	0.36	0.27	0.34	0.47	0.31	0.32	0.35	0.34	0.36
MgO	11.88	11.93	11.63	11.72	11.84	12.14	11.54	11.80	11.19	11.56	11.35
CaO											
NaO											
K2O	11.39	11.29	11.44	11.34	11.69	11.42	11.49	11.70	11.37	11.50	11.67
ClO											
F											
TOTAL	96.23	96.69	96.31	96.54	96.08	96.75	96.49	96.2	96.81	96.17	96.26
a.p.f.u.											
Si	5.45	5.46	5.43	5.49	5.48	5.48	5.50	5.46	5.48	5.48	5.42
Al^{IV}	2.55	2.54	2.57	2.51	2.52	2.52	2.50	2.54	2.52	2.52	2.58
Al^{VI}	0.50	0.49	0.48	0.53	0.54	0.44	0.59	0.50	0.53	0.49	0.48
Ti	0.36	0.32	0.37	0.34	0.31	0.34	0.37	0.35	0.39	0.40	0.40
Fe(ii)	2.26	2.32	2.33	2.28	2.28	2.29	2.15	2.27	2.27	2.26	2.32
Mn	0.04	0.04	0.04	0.03	0.04	0.06	0.04	0.04	0.04	0.04	0.04
Mg	2.48	2.50	2.44	2.45	2.47	2.55	2.40	2.46	2.35	2.41	2.38
Ca	0.00	0.00	0.00	0.00	0.00	0.00	0.00	0.00	0.00	0.00	0.00
Na	0.00	0.00	0.00	0.00	0.00	0.00	0.00	0.00	0.00	0.00	0.00
K	2.03	2.03	2.05	2.03	2.09	2.05	2.04	2.09	2.04	2.05	2.09
Cl	0.00	0.00	0.00	0.00	0.00	0.00	0.00	0.00	0.00	0.00	0.00

F	0.00	0.00	0.00	0.00	0.00	0.00	0.00	0.00	0.00	0.00	0.00
TOTAL	15.68	15.71	15.71	15.66	15.72	15.73	15.60	15.72	15.62	15.64	15.70

Note: Wt% = percentage weight; a.p.f.u. = atom per formula unit

PRR-18812 – unnamed metamorphic rocks

Table 79 Chemical analysis of biotite

Wt%	Bt1	Bt2	Bt3	Bt4	Bt5	Bt6	Bt7	Bt8	Bt9	Bt10	Bt11
SiO_2	39.30	39.50	40.19	38.99	40.42	39.36	~~38.78~~	39.90	40.12	39.08	40.65
TiO_2	2.88	2.99	3.08	3.42	3.41	3.72	~~3.99~~	3.65	3.33	3.59	3.29
Al2O3	17.33	17.94	18.05	16.13	17.97	17.53	~~16.37~~	17.34	18.24	17.14	18.12
FeO	20.27	20.10	19.05	22.68	18.08	19.50	~~21.05~~	19.45	19.12	20.51	18.09
MnO	0.24	0.24	0.17	0.35	0.22	0.32	~~0.28~~	0.24	0.32	0.36	0.22
MgO	12.18	12.06	12.78	10.45	13.14	12.39	~~11.12~~	11.67	12.11	11.37	12.97
CaO											
NaO											
K2O	11.20	11.18	10.44	11.27	10.66	11.13	~~12.12~~	11.20	10.84	11.16	10.48
ClO											
F											
TOTAL	96.71	96.14	96.38	96.81	96.25	96.19	~~96.43~~	96.67	96.07	96.88	96.31
a.p.f.u.											
Si	5.54	5.52	5.57	5.58	5.58	5.50	~~5.52~~	5.59	5.56	5.53	5.60
Al^{IV}	2.46	2.48	2.43	2.42	2.42	2.50	~~2.48~~	2.41	2.44	2.47	2.40
Al^{VI}	0.42	0.48	0.52	0.30	0.50	0.39	~~0.26~~	0.46	0.54	0.39	0.55
Ti	0.31	0.31	0.32	0.37	0.35	0.39	~~0.43~~	0.38	0.35	0.38	0.34
Fe(ii)	2.39	2.35	2.21	2.72	2.09	2.28	~~2.50~~	2.28	2.22	2.43	2.09
Mn	0.03	0.03	0.02	0.04	0.03	0.04	~~0.03~~	0.03	0.04	0.04	0.03
Mg	2.56	2.51	2.64	2.23	2.70	2.58	~~2.36~~	2.44	2.50	2.40	2.67
Ca	0.00	0.00	0.00	0.00	0.00	0.00	~~0.00~~	0.00	0.00	0.00	0.00
Na	0.00	0.00	0.00	0.00	0.00	0.00	~~0.00~~	0.00	0.00	0.00	0.00
K	2.01	1.99	1.85	2.06	1.88	1.98	~~2.20~~	2.00	1.92	2.02	1.84
Cl	0.00	0.00	0.00	0.00	0.00	0.00	~~0.00~~	0.00	0.00	0.00	0.00
F	0.00	0.00	0.00	0.00	0.00	0.00	~~0.00~~	0.00	0.00	0.00	0.00
TOTAL	15.72	15.68	15.56	15.72	15.55	15.66	~~15.78~~	15.59	15.56	15.66	15.51

Note: Wt% = percentage weight; a.p.f.u. = atom per formula unit

PRR-18853 – unnamed metamorphic rocks

Table 80 Chemical analysis of biotite

Wt%	Bt1	Bt2	Bt3	Bt4c	Bt4r	Bt5	Bt6c	Bt6r	Bt7	Bt8	Bt9	Bt10	Bt11c	Bt11r	Bt12	Bt13
SiO_2	40.58	39.88	39.74	39.63	39.45	39.73	39.83	41.10	39.68	39.55	39.86	39.64	39.52	39.74	39.68	41.01
TiO_2	2.54	2.72	2.68	2.81	2.67	2.83	2.54	2.33	2.77	2.67	2.73	2.66	2.62	2.37	2.51	2.50
Al2O3	21.27	21.07	21.18	20.20	21.29	21.00	20.88	21.82	21.58	20.91	21.56	21.17	21.65	21.14	20.56	21.05
FeO	15.61	16.83	16.27	18.50	16.75	16.79	16.91	15.56	16.47	17.11	16.27	16.52	16.67	16.99	17.34	16.41
MnO	0.17	0.22	0.32	0.25	0.18	0.25	0.19	0.12	0.17	0.22	0.17	0.17	0.21	0.24	0.21	0.14
MgO	12.36	12.06	12.12	11.13	12.08	11.76	12.11	12.56	11.99	11.76	12.00	11.96	12.00	11.84	12.10	11.34
CaO																
NaO																

K2O	10.74	11.28	11.06	11.31	11.15	11.14	10.79	10.58	11.08	11.31	11.17	11.23	11.32	11.47	11.11	11.13
ClO																
F																
TOTAL	96.83	96.11	96.74	96.32	96.56	96.61	96.84	96.09	96.39	96.58	96.40	96.76	96.17	96.35	96.61	96.53
a.p.f.u.																
Si	5.54	5.47	5.47	5.50	5.43	5.47	5.49	5.55	5.44	5.46	5.46	5.46	5.42	5.47	5.48	5.61
Al^{IV}	2.46	2.53	2.53	2.50	2.57	2.53	2.51	2.45	2.56	2.54	2.54	2.54	2.58	2.53	2.52	2.39
Al^{VI}	0.97	0.87	0.90	0.80	0.88	0.88	0.88	1.03	0.92	0.86	0.94	0.90	0.92	0.90	0.83	1.00
Ti	0.26	0.28	0.28	0.29	0.28	0.29	0.26	0.24	0.29	0.28	0.28	0.28	0.27	0.25	0.26	0.26
Fe(ii)	1.78	1.93	1.87	2.14	1.93	1.93	1.95	1.76	1.89	1.98	1.86	1.90	1.91	1.96	2.00	1.88
Mn	0.02	0.03	0.04	0.03	0.02	0.03	0.02	0.01	0.02	0.03	0.02	0.02	0.02	0.03	0.02	0.02
Mg	2.52	2.46	2.49	2.30	2.48	2.41	2.49	2.53	2.45	2.42	2.45	2.46	2.45	2.43	2.49	2.31
Ca	0.00	0.00	0.00	0.00	0.00	0.00	0.00	0.00	0.00	0.00	0.00	0.00	0.00	0.00	0.00	0.00
Na	0.00	0.00	0.00	0.00	0.00	0.00	0.00	0.00	0.00	0.00	0.00	0.00	0.00	0.00	0.00	0.00
K	1.87	1.97	1.94	2.00	1.96	1.96	1.90	1.82	1.94	1.99	1.95	1.97	1.98	2.01	1.96	1.94
Cl	0.00	0.00	0.00	0.00	0.00	0.00	0.00	0.00	0.00	0.00	0.00	0.00	0.00	0.00	0.00	0.00
F	0.00	0.00	0.00	0.00	0.00	0.00	0.00	0.00	0.00	0.00	0.00	0.00	0.00	0.00	0.00	0.00
TOTAL	15.42	15.54	15.51	15.56	15.55	15.51	15.50	15.39	15.50	15.56	15.50	15.53	15.55	15.58	15.56	15.41

Note: Wt% = percentage weight; a.p.f.u. = atom per formula unit

PRR-33917 – Fosdick Migmatite

Table 81 Chemical analysis of biotite

Wt%	Bt1	Bt2	Bt3	Bt4	Bt5	Bt6	Bt7	Bt8	Bt9	Bt10	Bt11	Bt12	Bt13
SiO_2	38.04	37.80	38.41	37.89	37.74	38.53	37.91	37.81	38.29	38.45	38.44	38.23	38.08
TiO_2	3.41	3.69	3.85	3.83	3.88	3.72	3.75	3.74	3.84	3.04	3.92	3.96	4.11
Al2O3	19.89	20.14	20.16	19.69	19.83	19.64	19.41	19.59	19.61	20.23	19.93	20.12	19.68
FeO	21.37	21.35	21.08	21.39	21.91	21.34	21.14	21.11	21.04	20.15	20.69	20.70	21.13
MnO	0.24	0.17	0.31	0.23	0.24	0.22	0.17	0.31	0.16	0.14	0.23	0.34	0.22
MgO	9.27	8.88	8.90	8.89	8.61	9.00	9.43	9.26	9.51	10.17	9.16	9.09	9.11
CaO													
NaO													
K2O	11.47	11.53	11.33	11.47	11.34	11.46	11.48	11.49	11.63	11.62	11.26	11.44	11.41
ClO													
F													
TOTAL	96.44	96.56	96.12	96.71	96.58	96.23	96.82	96.79	96.08	96.34	96.51	96.27	96.39
a.p.f.u.													
Si	5.38	5.35	5.40	5.38	5.36	5.43	5.38	5.37	5.39	5.40	5.41	5.38	5.38
Al^{IV}	2.62	2.65	2.60	2.62	2.64	2.57	2.62	2.63	2.61	2.60	2.59	2.62	2.62
Al^{VI}	0.69	0.71	0.73	0.67	0.68	0.69	0.63	0.65	0.64	0.74	0.72	0.71	0.65
Ti	0.36	0.39	0.41	0.41	0.41	0.39	0.40	0.40	0.41	0.32	0.41	0.42	0.44
Fe(ii)	2.53	2.53	2.48	2.54	2.60	2.51	2.51	2.51	2.48	2.37	2.43	2.43	2.49
Mn	0.03	0.02	0.04	0.03	0.03	0.03	0.02	0.04	0.02	0.02	0.03	0.04	0.03
Mg	1.95	1.88	1.86	1.88	1.82	1.89	1.99	1.96	2.00	2.13	1.92	1.91	1.92
Ca	0.00	0.00	0.00	0.00	0.00	0.00	0.00	0.00	0.00	0.00	0.00	0.00	0.00
Na	0.00	0.00	0.00	0.00	0.00	0.00	0.00	0.00	0.00	0.00	0.00	0.00	0.00
K	2.07	2.08	2.03	2.08	2.05	2.06	2.08	2.08	2.09	2.08	2.02	2.05	2.05
Cl	0.00	0.00	0.00	0.00	0.00	0.00	0.00	0.00	0.00	0.00	0.00	0.00	0.00
F	0.00	0.00	0.00	0.00	0.00	0.00	0.00	0.00	0.00	0.00	0.00	0.00	0.00
TOTAL	15.64	15.61	15.54	15.61	15.60	15.58	15.63	15.63	15.62	15.65	15.53	15.56	15.58

Note: Wt% = percentage weight; a.p.f.u. = atom per formula unit

PRR-33918 – Fosdick Migmatite

Table 82 Chemical analysis of biotite

Wt%	Bt1	Bt2	Bt3	Bt4	Bt5	Bt6	Bt7	Bt8	Bt9	Bt10	Bt11	Bt12	Bt13
SiO_2	39.26	39.62	39.74	39.37	39.03	40.08	39.68	39.34	39.27	39.33	39.99	39.05	39.08
TiO_2	4.21	4.06	3.99	3.91	3.86	3.60	3.59	3.68	3.69	3.87	3.84	3.71	3.96
Al2O3	20.62	20.51	20.35	19.91	20.10	20.55	19.60	20.37	20.18	20.83	19.64	20.23	20.12
FeO	19.34	19.40	19.60	20.17	20.35	19.34	20.75	19.85	20.18	19.41	20.88	20.40	20.49
MnO	0.19	0.26	0.17	0.27	0.22	0.21	0.22	0.31	0.25	0.20	0.19	0.22	0.22
MgO	8.99	9.03	9.02	9.42	8.89	9.01	9.14	8.92	9.00	8.98	8.46	9.01	8.59
CaO													
NaO													
K2O	11.24	11.29	10.89	10.97	11.05	10.49	10.83	10.94	10.77	10.99	10.85	10.94	10.95
ClO													
F													
TOTAL	96.29	95.99	96.38	96.14	96.63	96.84	96.33	96.71	96.77	96.51	96.30	96.57	96.69
a.p.f.u.													
Si	5.46	5.49	5.52	5.48	5.47	5.57	5.54	5.50	5.50	5.47	5.58	5.47	5.48
Al^{IV}	2.54	2.51	2.48	2.52	2.53	2.43	2.46	2.50	2.50	2.53	2.42	2.53	2.52
Al^{VI}	0.84	0.84	0.85	0.75	0.79	0.93	0.77	0.86	0.83	0.89	0.81	0.81	0.81
Ti	0.44	0.42	0.42	0.41	0.41	0.38	0.38	0.39	0.39	0.40	0.40	0.39	0.42
Fe(ii)	2.25	2.25	2.28	2.35	2.39	2.25	2.42	2.32	2.36	2.26	2.44	2.39	2.40
Mn	0.02	0.03	0.02	0.03	0.03	0.02	0.03	0.04	0.03	0.02	0.02	0.03	0.03
Mg	1.86	1.87	1.87	1.96	1.86	1.87	1.90	1.86	1.88	1.86	1.76	1.88	1.80
Ca	0.00	0.00	0.00	0.00	0.00	0.00	0.00	0.00	0.00	0.00	0.00	0.00	0.00
Na	0.00	0.00	0.00	0.00	0.00	0.00	0.00	0.00	0.00	0.00	0.00	0.00	0.00
K	1.99	2.00	1.93	1.95	1.98	1.86	1.93	1.95	1.92	1.95	1.93	1.95	1.96
Cl	0.00	0.00	0.00	0.00	0.00	0.00	0.00	0.00	0.00	0.00	0.00	0.00	0.00
F	0.00	0.00	0.00	0.00	0.00	0.00	0.00	0.00	0.00	0.00	0.00	0.00	0.00
TOTAL	15.41	15.41	15.36	15.45	15.45	15.30	15.43	15.41	15.41	15.39	15.37	15.45	15.42

Note: Wt% = percentage weight; a.p.f.u. = atom per formula unit

PRR-33926 – Byrd Coast Granite

Table 83 Chemical analysis of biotite

Wt%	Bt1c	Bt1r	Bt2c	Bt2r	Bt3c	Bt3r	Bt4c	Bt4r	Bt5c	Bt5r	Bt6c	Bt6r
SiO_2	40.42	41.93	42.92	44.05	43.39	44.73	418.31	40.98	44.26	42.89	42.95	42.70
TiO_2	3.25	2.76	2.28	2.69	2.24	2.39	27.64	3.15	2.33	2.59	2.46	2.58
Al2O3	14.91	15.98	15.08	13.27	14.44	13.19	152.20	14.77	14.34	15.76	14.64	15.25
FeO	20.17	16.91	15.05	15.12	15.47	14.65	163.57	17.99	14.27	14.72	16.00	15.03
MnO	2.24	2.10	1.83	1.99	1.92	1.83	21.14	2.36	1.99	1.86	1.96	1.98
MgO	11.73	13.00	14.48	14.30	14.34	14.92	133.11	12.69	15.86	14.64	13.49	13.86
CaO												
NaO	0.40		0.53	0.58	0.45			0.38		0.43	0.63	0.53
K2O	10.56	11.13	11.06	11.85	11.53	11.91	113.89	11.77	10.89	10.70	11.51	11.11
ClO											0.40	0.51

F												
TOTAL	96.44	96.32	96.87	96.29	96.36	96.5	9.71	96.07	96.22	96.53	96.11	96.57
a.p.f.u.												
Si	5.72	5.81	5.93	6.08	5.99	6.15	5.85	5.76	6.03	5.88	5.94	5.90
Al^{IV}	2.28	2.19	2.07	1.92	2.01	1.85	2.15	2.24	1.97	2.12	2.06	2.10
Al^{VI}	0.21	0.43	0.39	0.24	0.34	0.29	0.36	0.20	0.33	0.43	0.33	0.39
Ti	0.35	0.29	0.24	0.28	0.23	0.25	0.29	0.33	0.24	0.27	0.26	0.27
Fe(ii)	2.39	1.96	1.74	1.75	1.79	1.68	1.91	2.11	1.62	1.69	1.85	1.74
Mn	0.27	0.25	0.21	0.23	0.22	0.21	0.25	0.28	0.23	0.22	0.23	0.23
Mg	2.47	2.69	2.98	2.94	2.95	3.06	2.78	2.66	3.22	2.99	2.78	2.86
Ca	0.00	0.00	0.00	0.00	0.00	0.00	0.00	0.00	0.00	0.00	0.00	0.00
Na	0.11	0.00	0.14	0.15	0.12	0.00	0.00	0.10	0.00	0.11	0.17	0.14
K	1.91	1.97	1.95	2.09	2.03	2.09	2.03	2.11	1.89	1.87	2.03	1.96
Cl	0.00	0.00	0.00	0.00	0.00	0.00	0.00	0.00	0.00	0.00	0.09	0.12
F	0.00	0.00	0.00	0.00	0.00	0.00	0.00	0.00	0.00	0.00	0.00	0.00
TOTAL	15.70	15.58	15.65	15.68	15.68	15.58	15.62	15.80	15.53	15.57	15.66	15.58

Note: Wt% = percentage weight; a.p.f.u. = atom per formula unit

PRR-33991 – Ford Granodiorite

Table 84 Chemical analysis of biotite

Wt%	Bt1	~~Bt2c~~	Bt2r	Bt3c	Bt3r	Bt4	Bt5	Bt6	Bt7	Bt8
SiO_2	39.87	~~38.93~~	39.28	42.14	40.54	41.56	39.33	42.60	39.48	40.30
TiO_2	4.71	~~5.12~~	4.83	4.47	4.33	4.25	4.56	4.37	4.68	4.24
Al_2O_3	14.79	~~14.12~~	14.51	13.94	15.16	14.47	15.04	13.88	14.63	14.89
FeO	22.20	~~23.20~~	22.65	22.23	21.21	22.26	22.94	21.65	22.66	21.74
MnO	0.34	~~0.32~~	0.27	0.34	0.33	0.43	0.41	0.33	0.39	0.36
MgO	11.01	~~10.12~~	10.52	10.37	11.12	10.48	10.03	9.76	10.38	11.03
CaO										
NaO										
K_2O	10.85	~~11.59~~	11.37	10.40	10.89	9.97	11.21	10.68	11.30	11.21
ClO										
F										
TOTAL	96.36	~~96.71~~	96.68	96.26	96.54	96.69	96.6	96.83	96.59	96.37
a.p.f.u.										
Si	5.65	~~5.61~~	5.63	5.92	5.72	5.86	5.63	6.01	5.65	5.71
Al^{IV}	2.35	~~2.39~~	2.37	2.08	2.28	2.14	2.37	1.99	2.35	2.29
Al^{VI}	0.12	~~0.01~~	0.08	0.23	0.24	0.26	0.16	0.31	0.11	0.19
Ti	0.50	~~0.56~~	0.52	0.47	0.46	0.45	0.49	0.46	0.50	0.45
Fe(ii)	2.63	~~2.80~~	2.71	2.61	2.50	2.62	2.74	2.55	2.71	2.57
Mn	0.04	~~0.04~~	0.03	0.04	0.04	0.05	0.05	0.04	0.05	0.04
Mg	2.33	~~2.17~~	2.25	2.17	2.34	2.20	2.14	2.05	2.21	2.33
Ca	0.00	~~0.00~~	0.00	0.00	0.00	0.00	0.00	0.00	0.00	0.00
Na	0.00	~~0.00~~	0.00	0.00	0.00	0.00	0.00	0.00	0.00	0.00
K	1.96	~~2.13~~	2.08	1.86	1.96	1.79	2.05	1.92	2.06	2.03
Cl	0.00	~~0.00~~	0.00	0.00	0.00	0.00	0.00	0.00	0.00	0.00
F	0.00	~~0.00~~	0.00	0.00	0.00	0.00	0.00	0.00	0.00	0.00
TOTAL	15.59	~~15.70~~	15.67	15.39	15.54	15.39	15.64	15.34	15.65	15.61

Note: Wt% = percentage weight; a.p.f.u. = atom per formula unit

Table 85 Chemical analysis of amphibole

Wt%	Amp1	Amp2	Amp3c	Amp3r	Amp4	Amp5	Amp6	Amp7	Amp8
SiO_2	49.51	48.17	48.86	48.63	50.73	50.84	50.22	50.54	~~50.20~~
TiO_2	1.44	1.96	1.37	1.48	1.01	1.17	1.19	1.20	~~1.63~~
Al_2O_3	7.75	8.44	7.43	7.89	5.96	7.31	6.63	6.61	~~7.08~~
FeO	18.03	18.84	18.86	19.02	18.70	17.76	18.26	18.22	~~18.22~~
MnO	0.42	0.54	0.57	0.64	0.71	0.62	0.55	0.55	~~0.57~~
MgO	11.28	10.34	10.89	10.90	11.38	10.93	11.75	11.71	~~10.18~~
CaO	11.34	11.39	11.37	11.40	11.28	11.04	11.73	11.55	~~11.32~~
NaO	1.71	1.61	1.33	1.53	1.12	1.60	1.07	1.23	~~1.64~~
K_2O	0.73	0.73	0.88	0.88	0.60	0.62	0.65	0.67	~~0.70~~
Cr_2O_3									
TOTAL	97.84	98.03	98.46	97.69	98.52	98.17	97.99	97.76	~~98.48~~
a.p.f.u.									
Si	0.81	0.79	0.80	0.79	0.83	0.83	0.82	0.82	~~0.82~~
Ti	0.02	0.02	0.02	0.02	0.01	0.01	0.01	0.01	~~0.02~~
Al	0.15	0.16	0.14	0.15	0.12	0.14	0.13	0.13	~~0.14~~
Fe	0.25	0.26	0.26	0.26	0.26	0.24	0.25	0.25	~~0.25~~
Mn	0.01	0.01	0.01	0.01	0.01	0.01	0.01	0.01	~~0.01~~
Mg	0.27	0.25	0.27	0.26	0.28	0.27	0.29	0.28	~~0.25~~
Ca	0.20	0.20	0.20	0.20	0.20	0.19	0.20	0.20	~~0.20~~
Na	0.05	0.05	0.04	0.05	0.04	0.05	0.03	0.04	~~0.05~~
K	0.02	0.02	0.02	0.02	0.01	0.01	0.01	0.01	~~0.01~~
Cr	0.00	0.00	0.00	0.00	0.00	0.00	0.00	0.00	~~0.00~~
TOTAL									

Note: Wt% = percentage weight; a.p.f.u. = atom per formula unit

Table 86 Chemical analysis of pyroxene

Wt%	Px1	Px2	Px3	Px4	Px5	Px6	Px7	Px8	Px9	Px10	Px11	Px12
SiO_2	48.21	49.72	50.00	47.80	48.46	49.21	51.46	48.98	49.61	49.27	48.92	48.92
TiO_2	2.13	1.49	1.75	1.95	2.14	1.80	0.95	2.14	1.79	1.89	1.80	1.84
Al_2O_3	5.58	5.12	5.35	5.64	5.44	5.09	2.44	4.55	4.49	4.82	5.17	4.89
Cr_2O_3												
FeO	9.37	7.79	8.40	9.22	9.77	8.84	8.63	9.60	9.17	9.11	8.57	8.60
MnO	0.25	0.08	0.16	0.38	0.16	0.16	0.25	0.22	0.25	0.14	0.10	0.25
MgO	13.70	14.37	13.70	13.22	13.43	13.52	15.30	13.34	13.83	13.91	14.18	13.99
CaO	20.27	21.09	20.26	21.27	20.11	20.89	20.60	20.67	20.41	20.47	20.82	21.11
NaO	0.48	0.31	0.40	0.43	0.49	0.49	0.36	0.50	0.45	0.39	0.45	0.39
K_2O	0.00	0.03	0.00	0.08	0.00	0.00	0.00	0.00	0.00	0.00	0.00	0.02
TOTAL	100	100	100	100	100	100	100	100	100	100	100	100
a.p.f.u.												
Si	1.81	1.85	1.85	1.80	1.82	1.84	1.91	1.84	1.85	1.84	1.83	1.83
Al^{IV}	0.19	0.15	0.15	0.20	0.18	0.16	0.09	0.16	0.15	0.16	0.17	0.17
Al^{VI}	0.05	0.07	0.09	0.05	0.06	0.06	0.02	0.04	0.05	0.05	0.05	0.04
Fe(iii)	0.08	0.04	0.00	0.12	0.06	0.05	0.06	0.06	0.04	0.05	0.08	0.08
Cr	0.00	0.00	0.00	0.00	0.00	0.00	0.00	0.00	0.00	0.00	0.00	0.00
Ti	0.06	0.04	0.05	0.06	0.06	0.05	0.03	0.06	0.05	0.05	0.05	0.05
Fe(ii)	0.21	0.20	0.26	0.17	0.24	0.22	0.21	0.24	0.24	0.24	0.18	0.19
Mn	0.01	0.00	0.00	0.01	0.01	0.01	0.01	0.01	0.01	0.00	0.00	0.01
Mg	0.77	0.80	0.76	0.74	0.75	0.75	0.85	0.75	0.77	0.77	0.79	0.78
Ca	0.81	0.84	0.81	0.86	0.81	0.84	0.82	0.83	0.82	0.82	0.83	0.85

Na	0.03	0.02	0.03	0.03	0.04	0.04	0.03	0.04	0.03	0.03	0.03	0.03
K	0.00	0.00	0.00	0.00	0.00	0.00	0.00	0.00	0.00	0.00	0.00	0.00
TOTAL	4.03	4.01	3.99	4.04	4.02	4.02	4.02	4.02	4.01	4.01	4.03	4.02
Wo	43%	44%	43%	44%	42%	44%	42%	43%	43%	43%	43%	44%
En	40%	42%	41%	38%	39%	40%	43%	39%	40%	41%	41%	40%
Fs	16%	13%	14%	16%	16%	15%	14%	16%	15%	15%	14%	14%
Ac	2%	1%	2%	2%	2%	2%	1%	2%	2%	1%	2%	1%

Note: Wt% = percentage weight; a.p.f.u. = atom per formula unit. Wo: Wollastonite; En: Enstatite; Fs: Ferrosilite; Ac: Acmite

PRR-34146 – Ford Granodiorite

Table 87 Chemical analysis of biotite

Wt%	Bt1	Bt2	Bt3	Bt4	Bt5	Bt6	Bt7	Bt8	Bt9	Bt10	Bt11	Bt12	Bt13
SiO_2	38.24	37.96	37.75	37.92	38.04	37.75	38.22	37.55	37.70	37.70	38.00	38.44	37.98
TiO_2	3.41	3.01	2.93	3.09	5.74	5.85	5.53	5.64	5.63	4.67	2.53	4.14	2.14
Al2O3	19.14	18.99	19.40	19.37	19.32	19.17	19.53	19.42	19.64	19.24	19.70	19.78	19.58
FeO	20.76	21.19	21.27	20.83	18.78	19.18	18.39	19.62	19.55	19.80	20.62	16.48	21.38
MnO	0.13	0.19	0.02	0.17	0.06	0.00	0.00	0.12	0.09	0.11	0.20	0.04	0.06
MgO	11.16	11.17	11.49	11.04	10.02	10.06	10.06	9.90	9.68	10.38	10.66	13.70	11.50
CaO													
NaO													
K2O	11.30	11.08	10.96	11.22	11.42	11.46	11.68	11.54	11.58	11.58	11.54	11.36	11.11
ClO													
F													
TOTAL	96.03	96.54	96.32	96.49	96.72	96.64	96.69	96.35	96.28	96.63	96.85	96.21	96.38
a.p.f.u.													
Si	5.37	5.37	5.32	5.35	5.34	5.31	5.35	5.28	5.29	5.32	5.38	5.30	5.36
Al^{IV}	2.63	2.63	2.68	2.65	2.66	2.69	2.65	2.72	2.71	2.68	2.62	2.70	2.64
Al^{VI}	0.53	0.53	0.54	0.57	0.53	0.48	0.57	0.49	0.54	0.52	0.67	0.51	0.61
Ti	0.36	0.32	0.31	0.33	0.61	0.62	0.58	0.60	0.59	0.50	0.27	0.43	0.23
Fe(ii)	2.44	2.51	2.51	2.46	2.20	2.25	2.15	2.31	2.29	2.34	2.44	1.90	2.52
Mn	0.02	0.02	0.00	0.02	0.01	0.00	0.00	0.01	0.01	0.01	0.02	0.00	0.01
Mg	2.34	2.35	2.41	2.32	2.10	2.11	2.10	2.07	2.02	2.18	2.25	2.82	2.42
Ca	0.00	0.00	0.00	0.00	0.00	0.00	0.00	0.00	0.00	0.00	0.00	0.00	0.00
Na	0.00	0.00	0.00	0.00	0.00	0.00	0.00	0.00	0.00	0.00	0.00	0.00	0.00
K	2.02	2.00	1.97	2.02	2.04	2.05	2.09	2.07	2.07	2.08	2.08	2.00	2.00
Cl	0.00	0.00	0.00	0.00	0.00	0.00	0.00	0.00	0.00	0.00	0.00	0.00	0.00
F	0.00	0.00	0.00	0.00	0.00	0.00	0.00	0.00	0.00	0.00	0.00	0.00	0.00
TOTAL	15.70	15.73	15.74	15.72	15.48	15.52	15.50	15.55	15.53	15.63	15.74	15.66	15.79

Note: Wt% = percentage weight; a.p.f.u. = atom per formula unit

PRR-34164 – Fosdick Migmatite

Table 88 Chemical analysis of garnet

Wt%	Grn1c	Grn1r	Grn2	Grn3	Grn4	Grn5	Grn6	Grn7	Grn8	Grn9	Grn10
SiO_2	37.33	37.51	37.38	37.13	37.19	36.79	37.24	37.32	37.06	37.34	37.23
TiO_2	0.03	0.00	0.10	0.00	0.01	0.02	0.00	0.00	0.00	0.01	0.04
Al_2O_3	21.20	21.26	21.59	21.20	21.08	21.11	21.53	21.24	21.19	21.24	21.08

Cr_2O_3											
Fe_2O_3											
FeO	33.27	33.44	32.09	34.25	34.43	34.82	33.42	33.14	33.94	33.38	33.60
MnO	1.84	2.01	1.51	2.29	2.54	2.38	1.72	1.97	2.03	1.68	1.82
MgO	5.04	4.54	6.01	3.75	3.56	3.64	4.95	5.15	4.56	5.11	4.90
CaO	1.19	1.12	1.16	1.28	1.09	1.10	1.07	1.12	1.11	1.13	1.21
TOTAL	99.91	99.88	99.84	99.91	99.89	99.86	99.93	99.93	99.89	99.89	99.88
a.p.f.u.											
Si	2.97	2.99	2.95	2.98	2.99	2.96	2.96	2.97	2.96	2.97	2.97
Ti	0.00	0.00	0.01	0.00	0.00	0.00	0.00	0.00	0.00	0.00	0.00
Al	1.99	2.00	2.01	2.01	2.00	2.00	2.02	1.99	2.00	1.99	1.98
Cr	0.00	0.00	0.00	0.00	0.00	0.00	0.00	0.00	0.00	0.00	0.00
Fe(iii)	0.07	0.01	0.07	0.03	0.02	0.08	0.05	0.07	0.08	0.06	0.08
Fe(ii)	2.15	2.22	2.05	2.27	2.30	2.27	2.17	2.13	2.19	2.16	2.16
Mn	0.12	0.14	0.10	0.16	0.17	0.16	0.12	0.13	0.14	0.11	0.12
Mg	0.60	0.54	0.71	0.45	0.43	0.44	0.59	0.61	0.54	0.61	0.58
Ca	0.10	0.10	0.10	0.11	0.09	0.09	0.09	0.10	0.10	0.10	0.10
TOTAL	8.00	8.00	8.00	8.00	8.00	8.00	8.00	8.00	8.00	8.00	8.00
Almandine	72.89	74.32	70.05	76.29	76.96	77.15	73.69	72.45	74.52	73.15	73.49
Pyrope	19.70	17.97	23.36	14.90	14.18	14.38	19.45	20.06	17.83	19.94	19.08
Grossular	3.33	3.19	3.26	3.64	3.12	3.12	3.02	3.13	3.13	3.18	3.40
Spessartine	4.08	4.52	3.33	5.17	5.75	5.35	3.85	4.37	4.52	3.72	4.03

Note: Wt% = percentage weight; a.p.f.u. = atom per formula unit

PRR-34188 – Ford Granodiorite

Table 89 Chemical analysis of biotite

Wt%	**Bt1c**	**Bt1r**	**Bt2**	**Bt3c**	**Bt3r**	**Bt4c**	**Bt4r**	**Bt5**	**Bt6c**	**Bt6r**	**Bt7c**	**Bt7r**	**Bt8c**	**Bt8r**	**Bt9c**	**Bt9r**
SiO_2	40.90	~~39.77~~	39.67	40.97	39.43	~~36.46~~	~~38.94~~	40.37	39.83	42.56	40.73	~~38.92~~	~~36.58~~	~~38.91~~	39.68	40.26
TiO_2	4.31	~~4.65~~	4.21	4.34	4.25	~~4.75~~	~~3.73~~	3.08	4.56	3.29	3.75	~~4.45~~	~~5.64~~	~~4.75~~	4.71	4.32
Al_2O_3	15.16	~~14.51~~	15.05	14.99	14.62	~~12.51~~	~~14.15~~	15.04	13.71	16.14	14.90	~~14.26~~	~~12.62~~	~~14.14~~	14.26	14.75
FeO	19.27	~~20.49~~	19.99	19.17	21.60	~~25.83~~	~~21.97~~	20.27	21.70	16.94	19.54	~~21.56~~	~~25.03~~	~~21.01~~	20.65	19.88
MnO	0.33	~~0.31~~	0.29	0.29	0.35	~~0.48~~	~~0.26~~	0.31	0.36	0.13	0.32	~~0.33~~	~~0.43~~	~~0.32~~	0.34	0.36
MgO	13.05	~~12.17~~	12.64	13.33	11.90	~~10.61~~	~~12.20~~	13.55	12.41	14.75	13.47	~~12.03~~	~~10.92~~	~~12.68~~	12.65	12.95
CaO																
NaO																
K_2O	10.88	~~11.64~~	11.41	10.91	11.75	~~12.87~~	~~12.07~~	11.35	11.50	10.00	10.89	~~12.19~~	~~12.71~~	~~11.77~~	11.43	11.23
ClO																
F																
TOTAL	96.24	~~96.59~~	96.84	96.16	96.25	~~96.61~~	~~96.78~~	96.18	96.09	96.33	96.52	~~96.4~~	~~96.22~~	~~96.53~~	96.41	96.38
a.p.f.u.																
Si	5.70	~~5.64~~	5.62	5.70	5.61	~~5.41~~	~~5.60~~	5.67	5.65	5.81	5.70	~~5.57~~	~~5.38~~	~~5.55~~	5.62	5.66
Al^{IV}	2.30	~~2.36~~	2.38	2.30	2.39	~~2.19~~	~~2.40~~	2.33	2.29	2.19	2.30	~~2.40~~	~~2.19~~	~~2.38~~	2.38	2.34
Al^{VI}	0.19	~~0.07~~	0.13	0.16	0.06	~~0.00~~	~~0.00~~	0.16	0.00	0.40	0.16	~~0.00~~	~~0.00~~	~~0.00~~	0.00	0.10
Ti	0.45	~~0.50~~	0.45	0.45	0.46	~~0.53~~	~~0.40~~	0.33	0.49	0.34	0.40	~~0.48~~	~~0.62~~	~~0.51~~	0.50	0.46
Fe(ii)	2.25	~~2.43~~	2.37	2.23	2.57	~~3.21~~	~~2.64~~	2.38	2.57	1.93	2.29	~~2.58~~	~~3.08~~	~~2.51~~	2.45	2.34
Mn	0.04	~~0.04~~	0.03	0.03	0.04	~~0.06~~	~~0.03~~	0.04	0.04	0.01	0.04	~~0.04~~	~~0.05~~	~~0.04~~	0.04	0.04
Mg	2.71	~~2.57~~	2.67	2.77	2.52	~~2.35~~	~~2.62~~	2.84	2.62	3.00	2.81	~~2.57~~	~~2.39~~	~~2.70~~	2.67	2.71
Ca	0.00	~~0.00~~	0.00	0.00	0.00	~~0.00~~	~~0.00~~	0.00	0.00	0.00	0.00	~~0.00~~	~~0.00~~	~~0.00~~	0.00	0.00
Na	0.00	~~0.00~~	0.00	0.00	0.00	~~0.00~~	~~0.00~~	0.00	0.00	0.00	0.00	~~0.00~~	~~0.00~~	~~0.00~~	0.00	0.00
K	1.93	~~2.10~~	2.06	1.94	2.13	~~2.44~~	~~2.21~~	2.03	2.08	1.74	1.95	~~2.22~~	~~2.38~~	~~2.14~~	2.06	2.01

Cl	0.00	~~0.00~~	0.00	0.00	0.00	~~0.00~~	~~0.00~~	0.00	0.00	0.00	0.00	~~0.00~~	~~0.00~~	~~0.00~~	0.00	0.00
F	0.00	~~0.00~~	0.00	0.00	0.00	~~0.00~~	~~0.00~~	0.00	0.00	0.00	0.00	~~0.00~~	~~0.00~~	~~0.00~~	0.00	0.00
TOTAL	15.57	~~15.70~~	15.71	15.58	15.78	~~16.18~~	~~15.91~~	15.77	15.76	15.43	15.64	~~15.86~~	~~16.10~~	~~15.82~~	15.72	15.67

Note: Wt% = percentage weight; a.p.f.u. = atom per formula unit

PRR-34205 – Fosdick Migmatite

Table 90 Chemical analysis of biotite

Wt%	Bt1	Bt2	Bt3	Bt4	Bt5	Bt6	Bt7	Bt8c	Bt8r	Bt9c	Bt9r	Bt10c	Bt10r	Bt11	Bt12	Bt13
SiO_2	38.86	38.54	39.28	38.79	40.19	39.49	~~37.94~~	38.01	39.02	38.50	38.41	39.98	38.69	39.50	38.50	39.66
TiO_2	4.22	4.29	4.33	4.10	4.27	3.93	~~4.48~~	4.53	4.10	4.16	4.44	4.07	4.28	3.45	3.97	3.48
Al_2O_3	19.86	18.99	18.19	19.04	21.18	20.57	~~18.22~~	18.78	19.76	20.03	19.15	20.12	19.09	20.56	18.90	19.37
FeO	18.45	19.52	20.62	19.79	16.60	17.75	~~21.25~~	20.31	18.68	18.38	20.13	17.62	19.91	17.32	20.11	18.24
MnO	0.16	0.23	0.25	0.23	0.22	0.24	~~0.31~~	0.25	0.21	0.17	0.22	0.21	0.21	0.15	0.33	0.23
MgO	10.69	10.46	9.63	10.74	10.24	11.09	~~9.72~~	10.10	10.57	10.85	10.37	10.75	10.44	11.83	10.28	11.55
CaO																
NaO																
K_2O	11.16	11.46	11.38	11.23	10.56	10.98	~~11.82~~	11.62	11.17	11.25	11.30	10.90	11.23	10.67	11.55	10.77
ClO																
F																
TOTAL	96.71	96.63	96.44	96.23	96.84	96.11	~~96.39~~	96.52	96.59	96.76	96.14	96.5	96.28	96.65	96.48	96.8
a.p.f.u.																
Si	5.42	5.42	5.53	5.42	5.52	5.44	~~5.39~~	5.37	5.44	5.38	5.38	5.51	5.42	5.45	5.42	5.51
Al^{IV}	2.58	2.58	2.47	2.58	2.48	2.56	~~2.61~~	2.63	2.56	2.62	2.62	2.49	2.58	2.55	2.58	2.49
Al^{VI}	0.68	0.56	0.55	0.56	0.94	0.77	~~0.44~~	0.50	0.69	0.67	0.54	0.78	0.57	0.79	0.56	0.68
Ti	0.44	0.45	0.46	0.43	0.44	0.41	~~0.48~~	0.48	0.43	0.44	0.47	0.42	0.45	0.36	0.42	0.36
Fe(ii)	2.15	2.29	2.43	2.31	1.91	2.04	~~2.52~~	2.40	2.18	2.15	2.36	2.03	2.33	2.00	2.37	2.12
Mn	0.02	0.03	0.03	0.03	0.03	0.03	~~0.04~~	0.03	0.03	0.02	0.03	0.02	0.03	0.02	0.04	0.03
Mg	2.22	2.19	2.02	2.24	2.10	2.27	~~2.06~~	2.13	2.20	2.26	2.17	2.21	2.18	2.43	2.16	2.39
Ca	0.00	0.00	0.00	0.00	0.00	0.00	~~0.00~~	0.00	0.00	0.00	0.00	0.00	0.00	0.00	0.00	0.00
Na	0.00	0.00	0.00	0.00	0.00	0.00	~~0.00~~	0.00	0.00	0.00	0.00	0.00	0.00	0.00	0.00	0.00
K	1.98	2.06	2.04	2.00	1.85	1.93	~~2.14~~	2.09	1.99	2.00	2.02	1.92	2.01	1.88	2.08	1.91
Cl	0.00	0.00	0.00	0.00	0.00	0.00	~~0.00~~	0.00	0.00	0.00	0.00	0.00	0.00	0.00	0.00	0.00
F	0.00	0.00	0.00	0.00	0.00	0.00	~~0.00~~	0.00	0.00	0.00	0.00	0.00	0.00	0.00	0.00	0.00
TOTAL	15.50	15.58	15.53	15.58	15.26	15.45	~~15.68~~	15.63	15.50	15.54	15.58	15.39	15.56	15.46	15.62	15.49

Note: Wt% = percentage weight; a.p.f.u. = atom per formula unit

PRR-34207 – Fosdick Migmatite

Table 91 Chemical analysis of biotite

Wt%	Bt1	Bt2	Bt3	Bt4	Bt5	Bt6	Bt7	Bt8	Bt9	Bt10	Bt11	Bt12	Bt13
SiO_2	38.75	38.39	38.49	38.28	38.18	37.90	38.12	38.68	37.91	38.12	38.69	38.95	38.65
TiO_2	3.29	3.79	3.61	3.79	3.78	4.07	3.81	3.58	3.57	3.57	3.15	3.71	3.54
Al_2O_3	20.47	20.44	20.18	20.39	20.04	20.06	20.40	20.64	20.42	20.28	20.56	20.98	20.09
FeO	19.35	19.16	19.27	19.16	19.66	19.43	19.31	19.23	19.22	19.15	19.19	19.69	19.24
MnO	0.21	0.20	0.18	0.23	0.25	0.24	0.24	0.22	0.27	0.16	0.22	0.18	0.22
MgO	10.60	10.39	10.45	10.35	10.49	10.22	10.23	10.09	10.35	10.53	10.56	10.77	10.48
CaO													

NaO													
K_2O	11.37	11.45	11.37	11.44	11.37	11.57	11.61	11.63	11.47	11.47	11.34	11.81	11.60
ClO													
F													
TOTAL	96.12	96.33	96.57	96.49	96.38	96.63	96.42	96.08	96.9	96.81	96.43	94.26	96.31
a.p.f.u.													
Si	5.39	5.36	5.39	5.36	5.35	5.33	5.34	5.39	5.33	5.35	5.40	5.33	5.40
Al^{IV}	2.61	2.64	2.61	2.64	2.65	2.67	2.66	2.61	2.67	2.65	2.60	2.67	2.60
Al^{VI}	0.75	0.72	0.72	0.72	0.66	0.65	0.71	0.77	0.72	0.71	0.78	0.71	0.71
Ti	0.34	0.40	0.38	0.40	0.40	0.43	0.40	0.38	0.38	0.38	0.33	0.38	0.37
Fe(ii)	2.25	2.24	2.25	2.24	2.30	2.28	2.26	2.24	2.26	2.25	2.24	2.25	2.25
Mn	0.02	0.02	0.02	0.03	0.03	0.03	0.03	0.03	0.03	0.02	0.03	0.02	0.03
Mg	2.20	2.16	2.18	2.16	2.19	2.14	2.14	2.09	2.17	2.21	2.20	2.20	2.18
Ca	0.00	0.00	0.00	0.00	0.00	0.00	0.00	0.00	0.00	0.00	0.00	0.00	0.00
Na	0.00	0.00	0.00	0.00	0.00	0.00	0.00	0.00	0.00	0.00	0.00	0.00	0.00
K	2.02	2.04	2.03	2.04	2.03	2.08	2.07	2.07	2.06	2.06	2.02	2.06	2.07
Cl	0.00	0.00	0.00	0.00	0.00	0.00	0.00	0.00	0.00	0.00	0.00	0.00	0.00
F	0.00	0.00	0.00	0.00	0.00	0.00	0.00	0.00	0.00	0.00	0.00	0.00	0.00
TOTAL	15.59	15.58	15.58	15.59	15.61	15.62	15.61	15.58	15.62	15.62	15.59	15.63	15.61

Note: Wt% = percentage weight; a.p.f.u. = atom per formula unit

PRR-34241 – Swanson Formation

Table 92 Chemical analysis of biotite

Wt%	Bt1	Bt2	Bt3	Bt4	Bt5	Bt6	Bt7	Bt8	Bt9	Bt10	Bt11	Bt12	Bt13
SiO_2	39.69	39.49	39.89	40.21	39.27	39.39	39.74	40.62	39.98	39.58	40.42	40.00	39.50
TiO_2	2.72	2.55	2.69	2.69	2.75	2.62	2.37	2.49	2.75	3.05	2.87	2.78	3.08
Al_2O_3	20.09	19.58	19.51	19.05	20.13	19.98	20.20	20.87	20.12	20.33	18.98	19.58	20.23
FeO	16.92	17.52	17.19	17.13	16.85	17.30	17.11	16.10	17.00	17.00	16.86	16.65	16.51
MnO	0.49	0.60	0.47	0.51	0.50	0.48	0.46	0.44	0.52	0.45	0.52	0.43	0.50
MgO	12.87	13.43	12.96	13.11	12.93	13.28	13.40	12.30	12.51	12.52	12.97	12.82	12.62
CaO													
NaO													
K_2O	11.11	10.46	11.13	10.57	10.92	10.89	10.76	10.92	10.68	11.15	10.79	10.94	11.18
ClO													
F													
TOTAL	96.25	96.49	96.31	96.84	96.76	96.23	96.11	96.41	96.56	96.09	96.71	96.89	96.51
a.p.f.u.													
Si	5.46	5.45	5.50	5.56	5.43	5.43	5.45	5.55	5.50	5.44	5.58	5.53	5.45
Al^{IV}	2.54	2.55	2.50	2.44	2.57	2.57	2.55	2.45	2.50	2.56	2.42	2.47	2.55
Al^{VI}	0.72	0.64	0.67	0.66	0.72	0.67	0.72	0.91	0.77	0.73	0.66	0.72	0.73
Ti	0.28	0.26	0.28	0.28	0.29	0.27	0.24	0.26	0.28	0.31	0.30	0.29	0.32
Fe(ii)	1.95	2.02	1.98	1.98	1.95	1.99	1.96	1.84	1.96	1.95	1.94	1.92	1.90
Mn	0.06	0.07	0.05	0.06	0.06	0.06	0.05	0.05	0.06	0.05	0.06	0.05	0.06
Mg	2.64	2.77	2.66	2.70	2.67	2.73	2.74	2.50	2.57	2.56	2.67	2.64	2.59
Ca	0.00	0.00	0.00	0.00	0.00	0.00	0.00	0.00	0.00	0.00	0.00	0.00	0.00
Na	0.00	0.00	0.00	0.00	0.00	0.00	0.00	0.00	0.00	0.00	0.00	0.00	0.00
K	1.95	1.84	1.96	1.86	1.93	1.91	1.88	1.90	1.88	1.95	1.90	1.93	1.97
Cl	0.00	0.00	0.00	0.00	0.00	0.00	0.00	0.00	0.00	0.00	0.00	0.00	0.00
F	0.00	0.00	0.00	0.00	0.00	0.00	0.00	0.00	0.00	0.00	0.00	0.00	0.00

TOTAL	15.60	15.61	15.61	15.54	15.60	15.64	15.61	15.46	15.52	15.58	15.53	15.55	15.57

Note: Wt% = percentage weight; a.p.f.u. = atom per formula unit

PRR-34385 – Swanson Formation

Table 93 Chemical analysis of biotite

Wt%	Bt1c	Bt1r	Bt2	Bt3	Bt4	Bt5	Bt6	Bt7	Bt8	Bt9	Bt10	Bt11	Bt12	Bt13
SiO_2	38.95	38.73	39.28	38.86	38.91	39.41	38.66	39.36	39.51	38.79	39.38	39.05	38.67	38.51
TiO_2	3.39	3.36	3.19	3.43	3.23	3.55	3.32	3.03	3.23	3.59	3.19	3.35	3.33	3.36
Al_2O_3	19.83	19.60	19.57	19.38	19.41	18.40	19.32	19.65	19.53	19.29	19.50	19.97	20.04	20.19
FeO	18.47	19.24	18.19	19.04	18.79	20.04	19.41	18.79	18.84	18.67	18.61	18.49	18.41	18.38
MnO	0.18	0.19	0.21	0.23	0.11	0.15	0.19	0.19	0.13	0.21	0.13	0.08	0.14	0.17
MgO	11.79	11.39	11.84	11.39	11.56	10.96	11.64	12.12	12.01	11.66	11.41	11.47	11.64	11.57
CaO														
NaO														
K_2O	11.32	11.22	11.14	11.19	11.35	11.34	11.15	10.93	10.76	11.28	11.05	11.25	11.73	11.64
ClO														
F														
TOTAL	96.23	96.41	96.69	96.59	96.74	96.29	96.44	96.09	96.13	96.64	96.83	96.47	96.19	96.33
a.p.f.u.														
Si	5.41	5.41	5.47	5.43	5.44	5.52	5.41	5.45	5.47	5.42	5.49	5.43	5.38	5.36
Al^{IV}	2.59	2.59	2.53	2.57	2.56	2.48	2.59	2.55	2.53	2.58	2.51	2.57	2.62	2.64
Al^{VI}	0.65	0.63	0.68	0.62	0.64	0.55	0.59	0.65	0.65	0.60	0.70	0.70	0.67	0.68
Ti	0.35	0.35	0.33	0.36	0.34	0.37	0.35	0.32	0.34	0.38	0.33	0.35	0.35	0.35
Fe(ii)	2.15	2.25	2.12	2.23	2.20	2.35	2.27	2.18	2.18	2.18	2.17	2.15	2.14	2.14
Mn	0.02	0.02	0.03	0.03	0.01	0.02	0.02	0.02	0.02	0.02	0.02	0.01	0.02	0.02
Mg	2.44	2.37	2.46	2.37	2.41	2.29	2.43	2.50	2.48	2.43	2.37	2.38	2.41	2.40
Ca	0.00	0.00	0.00	0.00	0.00	0.00	0.00	0.00	0.00	0.00	0.00	0.00	0.00	0.00
Na	0.00	0.00	0.00	0.00	0.00	0.00	0.00	0.00	0.00	0.00	0.00	0.00	0.00	0.00
K	2.00	2.00	1.98	2.00	2.03	2.02	1.99	1.93	1.90	2.01	1.97	1.99	2.08	2.07
Cl	0.00	0.00	0.00	0.00	0.00	0.00	0.00	0.00	0.00	0.00	0.00	0.00	0.00	0.00
F	0.00	0.00	0.00	0.00	0.00	0.00	0.00	0.00	0.00	0.00	0.00	0.00	0.00	0.00
TOTAL	15.62	15.63	15.58	15.61	15.63	15.60	15.65	15.60	15.56	15.62	15.55	15.58	15.67	15.66

Note: Wt% = percentage weight; a.p.f.u. = atom per formula unit

PRR-4604 – Granite Harbour Intrusive Complex

Table 94 Chemical analysis of biotite

Wt%	Bt1	Bt2	Bt3
SiO_2	~~41.19~~	41.22	41.74
TiO_2	~~2.03~~	2.91	2.66
Al_2O_3	~~18.40~~	17.86	17.60
FeO	~~19.42~~	18.07	18.56
MnO	~~0.26~~	0.22	0.27
MgO	~~13.25~~	12.38	12.33
CaO			
NaO			
K_2O	~~9.47~~	10.92	10.61

ClO			
F			
TOTAL	~~96.14~~	96.55	96.37
a.p.f.u.			
Si	~~5.66~~	5.70	5.76
Al^{IV}	~~2.34~~	2.30	2.24
Al^{VI}	~~0.63~~	0.61	0.62
Ti	~~0.21~~	0.30	0.28
Fe(ii)	~~2.23~~	2.09	2.14
Mn	~~0.03~~	0.03	0.03
Mg	~~2.71~~	2.55	2.54
Ca	~~0.00~~	0.00	0.00
Na	~~0.00~~	0.00	0.00
K	~~1.66~~	1.93	1.87
Cl	~~0.00~~	0.00	0.00
F	~~0.00~~	0.00	0.00
TOTAL	~~15.47~~	15.51	15.47

Note: Wt% = percentage weight; a.p.f.u. = atom per formula unit

Table 95 Chemical analysis of amphibole

Wt%	Amp1	Amp2	Amp3
SiO2	~~48.51~~	48.28	49.48
TiO2	~~1.32~~	1.02	1.15
Al2O3	~~10.07~~	10.78	9.40
FeO	~~16.16~~	16.80	16.11
MnO	~~0.53~~	0.36	0.37
MgO	~~11.22~~	10.67	11.57
CaO	~~11.37~~	11.35	11.25
NaO	~~1.14~~	1.39	1.20
K_2O	~~1.18~~	1.26	1.02
Cr_2O_3			
TOTAL	~~98.51~~	98.13	98.48
a.p.f.u.			
Si	~~0.80~~	0.79	0.81
Ti	~~0.02~~	0.01	0.01
Al	~~0.19~~	0.21	0.18
Fe	~~0.22~~	0.23	0.22
Mn	~~0.01~~	0.00	0.01
Mg	~~0.27~~	0.26	0.28
Ca	~~0.20~~	0.20	0.20
Na	~~0.04~~	0.04	0.04
K	~~0.02~~	0.03	0.02
Cr	~~0.00~~	0.00	0.00

Note: Wt% = percentage weight; a.p.f.u. = atom per formula unit

PRR-21042 – Granite Harbour Intrusive Complex

Table 96 Chemical analysis of biotite

Wt%	Bt1	Bt2	Bt3	Bt4	Bt5	Bt6	Bt7	Bt8	Bt9	Bt10
SiO_2	39.64	~~40.09~~	~~39.48~~	39.43	39.63	~~39.18~~	~~39.56~~	~~39.72~~	~~39.59~~	39.32
TiO_2	2.95	~~2.14~~	~~2.66~~	2.73	2.52	~~2.64~~	~~2.97~~	~~1.99~~	~~2.84~~	2.71

Al_2O_3	17.08	~~17.90~~	~~17.09~~	17.46	17.56	~~17.26~~	~~17.22~~	~~17.43~~	~~17.35~~	17.60
FeO	20.94	~~20.15~~	~~20.95~~	21.36	21.53	~~21.77~~	~~21.20~~	~~20.95~~	~~21.31~~	21.35
MnO	0.40	~~0.33~~	~~0.41~~	0.26	0.37	~~0.34~~	~~0.39~~	~~0.40~~	~~0.35~~	0.38
MgO	11.15	~~11.39~~	~~11.03~~	10.77	10.76	~~11.19~~	~~10.80~~	~~11.34~~	~~10.70~~	10.55
CaO										
NaO										
K_2O	11.32	~~11.72~~	~~11.59~~	11.57	11.37	~~11.68~~	~~11.74~~	~~11.80~~	~~11.89~~	11.50
ClO										
F										
TOTAL	96.63	~~96.41~~	~~96.89~~	96.54	96.39	~~96.09~~	~~96.27~~	~~96.49~~	~~96.12~~	96.7
a.p.f.u.										
Si	5.60	~~5.63~~	~~5.61~~	5.58	5.60	~~5.54~~	~~5.59~~	~~5.62~~	~~5.59~~	5.58
Al^{IV}	2.40	~~2.37~~	~~2.39~~	2.42	2.40	~~2.46~~	~~2.41~~	~~2.38~~	~~2.41~~	2.42
Al^{VI}	0.45	~~0.59~~	~~0.47~~	0.50	0.52	~~0.42~~	~~0.46~~	~~0.52~~	~~0.48~~	0.52
Ti	0.31	~~0.23~~	~~0.28~~	0.29	0.27	~~0.28~~	~~0.32~~	~~0.21~~	~~0.30~~	0.29
Fe(ii)	2.48	~~2.37~~	~~2.49~~	2.53	2.54	~~2.58~~	~~2.50~~	~~2.48~~	~~2.52~~	2.53
Mn	0.05	~~0.04~~	~~0.05~~	0.03	0.04	~~0.04~~	~~0.05~~	~~0.05~~	~~0.04~~	0.05
Mg	2.35	~~2.39~~	~~2.33~~	2.27	2.27	~~2.36~~	~~2.28~~	~~2.39~~	~~2.25~~	2.23
Ca	0.00	~~0.00~~	~~0.00~~	0.00	0.00	~~0.00~~	~~0.00~~	~~0.00~~	~~0.00~~	0.00
Na	0.00	~~0.00~~	~~0.00~~	0.00	0.00	~~0.00~~	~~0.00~~	~~0.00~~	~~0.00~~	0.00
K	2.04	~~2.10~~	~~2.10~~	2.09	2.05	~~2.11~~	~~2.12~~	~~2.13~~	~~2.14~~	2.08
Cl	0.00	~~0.00~~	~~0.00~~	0.00	0.00	~~0.00~~	~~0.00~~	~~0.00~~	~~0.00~~	0.00
F	0.00	~~0.00~~	~~0.00~~	0.00	0.00	~~0.00~~	~~0.00~~	~~0.00~~	~~0.00~~	0.00
TOTAL	15.68	~~15.71~~	~~15.73~~	15.71	15.70	~~15.79~~	~~15.72~~	~~15.78~~	~~15.73~~	15.70

Note: Wt% = percentage weight; a.p.f.u. = atom per formula unit

Table 97 Chemical analysis of amphibole

Wt%	Amp1	Amp2	Amp3	Amp4	Amp5	Amp6	Amp7	Amp8	Amp9
SiO2	~~50.82~~	46.31	46.43	43.66	44.52	47.51	47.05	46.75	47.88
TiO2	~~1.11~~	1.35	0.85	0.81	0.75	1.04	1.27	1.19	1.41
Al2O3	~~8.65~~	10.39	11.89	13.09	12.37	11.10	9.84	9.63	8.68
FeO	~~18.89~~	18.82	18.44	20.36	20.15	18.77	19.06	19.13	18.36
MnO	~~0.46~~	0.51	0.47	0.50	0.49	0.52	0.50	0.49	0.54
MgO	~~7.74~~	10.01	9.16	8.45	8.47	8.65	10.02	10.03	10.60
CaO	~~12.00~~	12.12	11.57	12.11	12.21	11.59	12.28	11.97	12.18
NaO	~~0.75~~	1.13	1.24	1.40	1.08	1.17	1.04	1.16	0.95
K_2O	~~1.23~~	1.33	1.35	1.69	1.46	1.35	1.15	1.22	1.06
Cr_2O_3									
TOTAL	~~98.39~~	98.07	98.63	97.98	98.51	98.33	97.85	98.44	98.36
a.p.f.u.									
Si	~~0.83~~	0.76	0.76	0.71	0.73	0.78	0.77	0.77	0.78
Ti	~~0.01~~	0.02	0.01	0.01	0.01	0.01	0.02	0.01	0.02
Al	~~0.17~~	0.20	0.23	0.25	0.24	0.21	0.19	0.19	0.17
Fe	~~0.26~~	0.26	0.25	0.28	0.28	0.26	0.26	0.26	0.25
Mn	~~0.01~~	0.01	0.01	0.01	0.01	0.01	0.01	0.01	0.01
Mg	~~0.19~~	0.24	0.22	0.21	0.21	0.21	0.24	0.25	0.26
Ca	~~0.21~~	0.21	0.20	0.21	0.21	0.20	0.21	0.21	0.21
Na	~~0.02~~	0.04	0.04	0.04	0.03	0.04	0.03	0.04	0.03
K	~~0.03~~	0.03	0.03	0.04	0.03	0.03	0.02	0.03	0.02
Cr	~~0.00~~	0.00	0.00	0.00	0.00	0.00	0.00	0.00	0.00

Note: Wt% = percentage weight; a.p.f.u. = atom per formula unit

PRR-15282 – Granite Harbour Intrusive Complex

Table 98 Chemical analysis of biotite

Wt%	Bt1c	Bt1r	Bt2	Bt3	Bt4	Bt5	Bt6	Bt7	Bt8	Bt9	Bt10
SiO_2	39.38	38.89	39.41	39.04	39.76	39.42	41.89	39.30	39.46	39.42	39.54
TiO_2	3.64	3.45	3.64	3.69	3.58	3.50	3.42	3.54	3.43	3.57	3.53
Al_2O_3	18.29	18.41	17.85	17.98	18.31	17.90	17.57	18.13	18.25	17.93	18.54
FeO	22.85	23.11	23.22	22.67	23.03	22.68	22.04	22.85	22.89	23.59	22.01
MnO	0.48	0.52	0.53	0.51	0.52	0.55	0.40	0.56	0.48	0.56	0.48
MgO	8.15	8.56	8.09	8.39	8.53	8.31	8.21	8.23	8.26	8.15	8.51
CaO											
NaO											
K_2O	11.12	10.48	10.97	11.06	10.24	11.20	10.41	11.13	10.87	10.69	10.90
ClO											
F											
TOTAL	96.24	96.69	96.42	96.77	96.19	96.56	96.21	96.39	96.48	96.25	96.61
a.p.f.u.											
Si	5.58	5.53	5.60	5.56	5.60	5.61	5.85	5.58	5.60	5.59	5.59
Al^{IV}	2.42	2.47	2.40	2.44	2.40	2.39	2.15	2.42	2.40	2.41	2.41
Al^{VI}	0.63	0.61	0.59	0.58	0.64	0.61	0.74	0.61	0.65	0.59	0.68
Ti	0.39	0.37	0.39	0.40	0.38	0.37	0.36	0.38	0.37	0.38	0.38
Fe(ii)	2.71	2.75	2.76	2.70	2.71	2.70	2.57	2.71	2.71	2.80	2.60
Mn	0.06	0.06	0.06	0.06	0.06	0.07	0.05	0.07	0.06	0.07	0.06
Mg	1.72	1.81	1.71	1.78	1.79	1.76	1.71	1.74	1.75	1.72	1.79
Ca	0.00	0.00	0.00	0.00	0.00	0.00	0.00	0.00	0.00	0.00	0.00
Na	0.00	0.00	0.00	0.00	0.00	0.00	0.00	0.00	0.00	0.00	0.00
K	2.01	1.90	1.99	2.01	1.84	2.03	1.85	2.02	1.97	1.93	1.97
Cl	0.00	0.00	0.00	0.00	0.00	0.00	0.00	0.00	0.00	0.00	0.00
F	0.00	0.00	0.00	0.00	0.00	0.00	0.00	0.00	0.00	0.00	0.00
TOTAL	15.51	15.51	15.51	15.54	15.42	15.54	15.28	15.53	15.50	15.49	15.47

Note: Wt% = percentage weight; a.p.f.u. = atom per formula unit

PRR-15321 – Granite Harbour Intrusive Complex

Table 99 Chemical analysis of biotite

Wt%	Bt1	Bt2	Bt3	Bt4	Bt5	Bt6	Bt7	Bt8	Bt9
SiO_2	39.78	40.27	41.63	38.74	39.94	38.39	38.96	40.63	39.21
TiO_2	3.33	3.10	3.13	3.34	3.61	3.54	3.19	3.18	2.87
Al_2O_3	19.42	20.86	18.32	19.43	19.21	19.62	19.69	19.71	19.70
FeO	23.05	21.75	23.38	23.71	23.78	24.10	23.48	22.55	23.88
MnO	0.87	0.74	0.63	0.70	0.71	0.86	0.85	0.72	0.62
MgO	6.19	5.49	5.78	6.44	5.66	5.79	6.20	6.20	6.39
CaO									
NaO									
K_2O	11.18	11.08	10.65	11.22	11.06	11.45	11.32	10.43	11.35
ClO									
F									
TOTAL	96.33	96.82	96.61	96.54	96.19	96.38	96.44	96.69	96.14

a.p.f.u.									
Si	5.64	5.67	5.88	5.53	5.66	5.50	5.55	5.72	5.57
Al^{IV}	2.36	2.33	2.12	2.47	2.34	2.50	2.45	2.28	2.43
Al^{VI}	0.88	1.14	0.92	0.80	0.87	0.81	0.86	0.99	0.87
Ti	0.35	0.33	0.33	0.36	0.38	0.38	0.34	0.34	0.31
Fe(ii)	2.73	2.56	2.76	2.83	2.82	2.89	2.80	2.66	2.84
Mn	0.10	0.09	0.08	0.09	0.08	0.10	0.10	0.09	0.07
Mg	1.31	1.15	1.22	1.37	1.19	1.24	1.32	1.30	1.35
Ca	0.00	0.00	0.00	0.00	0.00	0.00	0.00	0.00	0.00
Na	0.00	0.00	0.00	0.00	0.00	0.00	0.00	0.00	0.00
K	2.02	1.99	1.92	2.04	2.00	2.09	2.06	1.87	2.06
Cl	0.00	0.00	0.00	0.00	0.00	0.00	0.00	0.00	0.00
F	0.00	0.00	0.00	0.00	0.00	0.00	0.00	0.00	0.00
TOTAL	15.40	15.26	15.23	15.49	15.35	15.51	15.48	15.24	15.50

Note: Wt% = percentage weight; a.p.f.u. = atom per formula unit

PRR-15790 – Granite Harbour Intrusive Complex

Table 100 Chemical analysis of biotite

Wt%	Bt1	Bt2	Bt3	Bt4	Bt5	Bt6	Bt7	Bt8	Bt9	Bt10
SiO_2	39.18	39.17	38.79	39.14	39.35	39.39	39.74	38.56	39.40	38.52
TiO_2	2.23	2.25	2.37	2.12	2.64	3.07	2.35	4.09	4.03	3.96
Al_2O_3	17.97	17.10	17.60	17.29	16.96	17.19	17.24	16.67	16.70	16.30
FeO	25.13	25.86	25.43	25.40	25.09	24.80	24.61	25.56	25.18	25.82
MnO	0.35	0.57	0.57	0.43	0.46	0.50	0.53	0.59	0.50	0.53
MgO	7.93	7.75	7.94	8.27	7.56	8.10	8.46	7.45	7.08	7.38
CaO										
NaO										
K_2O	11.17	11.04	10.89	10.72	11.28	10.87	10.51	11.01	10.92	11.17
ClO										
F										
TOTAL	96.18	96.39	96.54	96.73	96.78	96.23	96.68	96.22	96.33	96.45
a.p.f.u.										
Si	5.61	5.65	5.59	5.63	5.68	5.63	5.68	5.55	5.65	5.58
Al^{IV}	2.39	2.35	2.41	2.37	2.32	2.37	2.32	2.45	2.35	2.42
Al^{VI}	0.64	0.55	0.57	0.57	0.56	0.52	0.59	0.38	0.47	0.36
Ti	0.24	0.24	0.26	0.23	0.29	0.33	0.25	0.44	0.44	0.43
Fe(ii)	3.01	3.12	3.06	3.06	3.03	2.96	2.94	3.08	3.02	3.12
Mn	0.04	0.07	0.07	0.05	0.06	0.06	0.06	0.07	0.06	0.06
Mg	1.69	1.67	1.70	1.78	1.63	1.73	1.80	1.60	1.51	1.59
Ca	0.00	0.00	0.00	0.00	0.00	0.00	0.00	0.00	0.00	0.00
Na	0.00	0.00	0.00	0.00	0.00	0.00	0.00	0.00	0.00	0.00
K	2.04	2.03	2.00	1.97	2.08	1.98	1.92	2.02	2.00	2.06
Cl	0.00	0.00	0.00	0.00	0.00	0.00	0.00	0.00	0.00	0.00
F	0.00	0.00	0.00	0.00	0.00	0.00	0.00	0.00	0.00	0.00
TOTAL	15.66	15.67	15.66	15.65	15.63	15.58	15.57	15.60	15.50	15.63

Note: Wt% = percentage weight; a.p.f.u. = atom per formula unit